University of Nottingham
UK | CHINA | MALAYSIA
Faculty of Engineering
Department of Architecture and Built Environment

A Novel Integrated Daylighting System for Optimal Daylight Performance in Office Buildings

Fawzan Mohammed Aljudaiy

B.Arch., MSc

Thesis submitted to the University of Nottingham for the degree of Doctor of Philosophy

September 2021

Abstract

The thesis assessed the potential of optimising the daylight performance for an office building in Riyadh city, Saudi Arabia, by means of a novel passive daylighting system that can achieve balanced daylighting performance. The function of the proposed system is to prevent and mitigate the negative impact of direct sunlight inside the building by reducing the illuminance level in the front area while increasing it in the deep area of the space. The aim was to reduce the annual level of sunlight exposure (ASE) while increasing the daylight autonomy (DA), the useful daylight illuminance (UDI) and the daylighting uniformity at the work plane. This aim was achieved through four objectives, to assess the current situation of the daylighting performance for typical office space, to invent a novel integrated daylighting system that can enhance the daylighting performance, to optimise the design of the proposed system and finally to assess the daylighting performance of the proposed system.

A novel integrated daylighting system that consist of a perforated solar screen (PSS) and daylight-redirecting devices (DRDs) was designed. The PSS was optimised by examining the effect of the perforation percentage on the daylighting performance. Next, the impact of the DRD on the daylighting performance was investigated. The tested parameters include the position, per unit area ratio, material, geometry, tilt angle and truncation. Finally, a prismatic lens was integrated within the DRD and its impact was evaluated.

The daylighting performance of the case study was evaluated for Riyadh city, Saudi Arabia. First, the redirection of the sunbeams was analysed through a raytracing study. Afterwards, the illuminance levels at the workplane were assessed using climate-based daylight modelling. The annual daylighting performance was evaluated for the whole year and each season. Furthermore, the hourly daylighting performance was assessed between 8 am and 4 pm on the summer solstice, autumn equinox and winter solstice days at 2-hour intervals. Later, experimental tests for a prototype model under an artificial sun simulator were conducted. Finally, the simulation modelling results were validated against the outputs of the experimental test for a prototype-scale model under real sky conditions.

The results of the study revealed that the daylight uniformity was enhanced by the proposed system compared to the base case and the perforated screen. The daylight uniformity was enhanced by case DRSS11-B for most of the tested hours. A significant improvement was

recorded on 21 December. The daylight uniformity was increased from 2% to 22% compared to the base case. In addition, the daylight uniformity on 21 June and 21 September reached up to 32% whereas the highest uniformity was19% and 28% for the base case and the PSS, respectively.

Furthermore. the annual analysis of the daylighting performance indicates that the proposed system reduced the negative impact of direct sunlight. The ASE value was reduced from 381 hours to 121 hours by case DRSS11-B and 186 hours by case PSS5 compared to the base case. On the other hand, the DA value analysis showed that at daylighting zones Z1 and Z2 the performance was similar among the tested cases, namely, the base case, case PSS5 and case DRSS11-B. The DA value was 100% at Z1 and 97 to 98% at Z2. However, the highest DA values at Z3 was 72% for case PSS5 with an increase of 3% and 6% compared to the base case and case DRSS11-B, respectively. Nevertheless, the UDI values revealed that the at daylight zones Z1 and Z4, case DRSS11-B increased the UDI values from 1% and 3% to 5% at Z1, and 5% and 15% to 17% compared to the base case and case PSS5, respectively.

Acknowledgement

First and foremost I am extremely grateful to my supervisor, Dr Siddig Omer for his invaluable advice, scientific insight, continuous support, and patience during my PhD study. His immense knowledge and plentiful experience have encouraged me in all the time of my academic research. I also thank Professor Jo Darkwa for his advice.

I would also like to thank the technicians at the Department of Architecture and Built Environment for their technical support on my study. My appreciation also goes out to my friends and colleagues for their support all through my studies.

Last but not least, I would like to express my gratitude to my parents, my wife and my children, my brothers and sisters for their support and encouragement in the past few years.

Table of Contents

Abstract i

Acknowledgement iii

Table of Contents iv

List of figures xi

List of tables xxi

Chapter 1. Introduction 1

1.1. Introduction 1

1.2. Aims and objectives 3

1.3. Statement of the problem 4

1.4. The novelty of the research 5

1.5. Research hypothesis 5

1.6. Thesis structure 6

1.7. Background 7

1.7.1. Overview of daylight in low latitude regions 7

1.7.2. Nature of light 9

1.7.3. Daylighting metrics 11

1.7.4. Definitions associated with glazing. 18

1.7.5. Energy status 19

Chapter 2. Literature review in daylighting technologies 25

2.1. Introduction 25

2.2. Daylighting systems 26

2.2.1. Daylight redirection systems 26

2.2.2. Daylight filtration systems 45

2.2.3. Daylight transport systems 53

2.2.4. Skylight systems 56
2.3. Comparison of Daylighting Systems 58
Chapter 3. Literature review in innovative glazing 62
3.1. Introduction 62
3.2. Types of smart glazing 64
3.2.1. Active smart glazing 65
3.2.2. Passive smart glazing 71
3.3. Daylight assessment tools 76
3.3.1. Daylighting simulation software 76
Chapter 4. Research methodology 80
4.1. Research methodology 80
4.1.1. Location of the study 81
4.1.2. Case study 81
4.1.3. Literature review 83
4.1.4. Research hypothesis 84
4.1.5. Daylight simulation 85
4.1.6. Experimental investigations 86
4.2. Design and operation principles of the proposed system 88
4.3. Summary 89
Chapter 5. Computer modelling of the base case 91
5.1. Introduction 91
5.2. Procedure 91
5.2.1. Location of the study 91
5.2.2. Case study description 93
5.2.3. Daylight zones 95
5.2.4. Daylighting performance metrics 96

5.3. Computer modelling set up. 97
5.3.1. Computer modelling set up for the raytracing study 98
5.3.2. Computer modelling set up for the daylight intensity study 99
5.3.3. Summary 110
5.4. Base case 111
5.4.1. Overall evaluation by an annual daylight study 111
5.4.2. Analysis of the sunray's reflection behaviour 117
5.4.3. Hourly evaluation through a point-in-time daylight study 119
.5.4.4 Daylight uniformity 132
5.4.5. Analysis of daylight glare probability 133
5.5. Discussion and Summary 135
Chapter 6. Computer modelling of the proposed daylighting system 138
6.1. Introduction 138
6.2. Perforated Solar Screen 138
6.2.1. Overall evaluation by an annual daylight study 139
6.2.2. Hourly evaluation through a point-in-time daylight study 146
6.2.3. Analysis of daylight glare probability 153
6.3. Daylight-redirecting device 155
6.3.1. Design of the proposed daylight-redirecting device 156
6.3.2. Optimisation by raytracing 158
6.3.3. Hourly evaluation through a point-in-time daylight study 167
6.3.4. Overall evaluation by an annual daylight study 173
6.3.5. Analysis of daylight glare probability 176
6.4. Discussion and Summary 179
Chapter 7. Fabrication of the rig 185
7.1. Experimental design and procedure 185

7.1.1. Simple parallax error (SPE) 186
7.1.2. Measurements and calibrations 187
7.2. Results 199
7.2.1. Results of luminance-meter calibration 199
7.2.2. Results of materials reflectance measurements 202
7.2.3. Results of illuminance-meters calibration 203
7.3. Fabrication of the rig 205
7.3.1. Fabrication of the room 205
7.3.2. Fabrication of the PSS 208
7.3.3. Fabrication of the DRD 210
7.4. Daylight measurement tools 214
Chapter 8. Test under the direct-light simulator 217
8.1. Procedure 217
8.1.1. Location and time 217
8.1.2. Test Process 217
8.1.3. The uniformity of the light source 218
8.1.4. The setting of the solar altitude and azimuth 219
8.1.5. Elimination of the external light reflection 221
8.2. Investigation of daylight performance 222
8.2.1. Effect of position 224
8.2.2. Effect of unit per area ratio 225
8.2.3. Effect of material 225
8.2.4. Effect of geometry 226
8.2.5. Effect of truncation 226
.8.2.6 Effect of prismatic lens 226
8.3. Results 227

8.3.1. Comparison of PSS5 and DRSS1 227
8.3.2. Test effect of significant parameters of DRDs 228
8.4. Discussion and Conclusions 234
Chapter 9. Test under the diffuse-light sky dome 237
9.1. Test Procedure 238
9.1.1. Location and time 238
9.1.2. The sky dome 238
9.1.3. The position of the sun and sky elements 239
9.1.4. Tests process 242
9.2. Results 243
9.2.1. Comparison of PSS5 and DRSS1 244
9.2.2. Effect of position 245
9.2.3. Effect of unit per area ratio 247
9.2.4. Effect of material 248
9.2.5. Effect of geometry 251
9.2.6. Effect of truncation 254
9.2.7. Effect of prismatic lens 255
9.3. Discussion and Conclusions 256
Chapter 10. Test under real sky 258
10.1. Introduction 258
10.2. Purpose of the experiment 258
10.3. Experiment setup and procedure 258
10.4. Results 260
10.4.1. Comparison of PSS5 and DRSS1 260
10.4.2. Effect of position 261
10.4.3. Effect of unit per area ratio 262

10.4.4. Effect of material 262
10.4.5. Effect of geometry 263
10.4.6. Effect of truncation 264
10.4.7. Effect of prismatic lens 264
10.5. Validation of the simulation model 265
10.6. Discussion and Conclusions 266
Chapter 11. Simulation of the final design 269
11.1. Introduction 269
11.2. Optimisation process 269
11.3. Results 271
11.3.1. Optimisation of the geometry 271
11.3.2. Optimisation of the tilt angle 280
11.3.3. Integration of the prismatic lens 291
11.4. Comparison of case DRSS11-B performance with the base case and PSS5 298
11.5. Discussion and Conclusions 300
Chapter 12. Conclusions 303
12.1. Summary 303
12.2. Key findings 305
Base case performance 305
The performance of the perforated solar screen (PSS) 306
The performance of Case PSS5 306
The performance of case DRSS1 (normal mode) 307
Experimental tests 308
Test under diffuse-light simulator 308
Test under real sky 309
Final simulation 309

12.3. Limitations 310
12.4. Future works.....311
References 312
Appendices 322

List of figures

Figure 1.1: Thesis Outline 7
Figure 1.2 Range of low, middle and high latitude regions 8
Figure 1.3 Sun altitude and azimuth for northern latitudes (mpoweruk.com, 2005) 9
Figure 1.4 Electromagnetic radiation spectrum (Szokolay, 2014) 9
Figure 1.5 The daylight components [A] (Mardaljevic, 1999) [B] (skylineroofing.co.uk 2017). [C] Light characteristics (tpub.com 2017) 10
Figure 1.6 The photometric quantities of the light (Robertson, 2003) 11
Figure 1.7 Relation of daylight components to DF and CBDM approaches (Mardaljevic et al., 2009) 13
Figure 1.8: Daylight factor 13
Figure 1.9 Equation of daylight glare index (Boubekri, 2014) 17
Figure 1.10 The luminance of the source (Boubekri, 2014). 17
Figure 1.11 Solar Heat Gain Coefficient (Petermann, 2008) 19
Figure 1.12: Annual energy consumption in Saudi Arabia, from 2000 to 2018 (above), and 2014 to 2018 (below) (CEIC Data, 2020). 21
Figure 1.13 Energy Consumption due to lighting in Saudi Arabia from 2000 to 2014 23
Figure 2.1 External louvres system, Traffic Control Headquarters, Spain (Tectonica-online.com 2009) 28
Figure 2.2 Internal Venetian blinds for office buildings (dolsoninteriors.com 2017) 29
Figure 2.3 Optical louvres system applied in the top of the window (Boubekri, 2014) 30
Figure 2.4 OLS system and its interior view [A] and [B], Venetian blinds [C] (Konis and Lee, 2015) 30
Figure 2.5 Edgework detail of a micro sun-shielding louvre (Eckelt.at 2017) 31
Figure 2.6 Shutter (Knoop et al., 2016) 31
Figure 2.7 Light shelves made out of semi-transparent reflective glass (Littlefair, 1996, Ruck et al., 2000) 32
Figure 2.8 External light shelf characteristics and concept (left) (Lee et al., 2017). External light shelves at the University of Oregon (right) (tboake.com 2017) 33
Figure 2.9 Top section of interior/exterior light shelf (Ruck et al., 2000) 33
Figure 2.10 Internal/external-light shelves, SMUD Head Quarters, California (Ruck et al., 2000) 34
Figure 2.11: Winter and summer operation of the VALRA (Ruck et al., 2000, Littlefair, 1996, Howard et al., 1986) (left), and (Boubekri, 2014) (right) 34
Figure 2.12: Section of testbed [A], and a non-perforated and a perforated light shelf [B] and [C](Lee et al., 2017) 35
Figure 2.13 Light-redirecting louvres [A], and light- redirecting glazing [B] (Klammt et al., 2012) 35
Figure 2.14 Prismatic sheets (uk.archello.com 2004) 36
Figure 2.15 The function of a light redirecting system (Mashaly et al., 2017) 36
Figure 2.16 Prism structures are used in daylighting applications (microsharp.co.uk 2011) 36
Figure 2.17 External and internal view of Rutec tower (Subtilitas.site 2017) 37
Figure 2.18 Microscopic pictures of PMMA sheets (left), and double-sided and single-sided prisms (right) (Mashaly et al., 2017) 37
Figure 2.19 Variation between simulation results in Radiance and real measurements (Mashaly et al., 2017) ... 38
Figure 2.20 The basic optical principle of LCP (Boubekri, 2014) 38

Figure 2.21 View through a laser-cut panel (Boubekri, 2014) 39
Figure 2.22 Light incident geometry received from obstruction angle (Edmonds, 2005) 39
Figure 2.23 MicroShade, (baulinks.de 2017) (left) and (saint-gobain-lounge.de 2017) (right)..... 40
Figure 2.24 Magnification of prismatic film (2.5X) (left) and (57X) (right) (Vázquez-Moliní et al., 2012)..... 41
Figure 2.25 Cross-section of LUMITOP (left), Ray tracing results for a PMMA (right) (Klammt et al., 2012).. 41
Figure 2.26 Layer without (left) and with PMMA (right) (Klammt et al., 2012). 41
Figure 2.27 Compound Parabolic Concentrators (CPCs) (edmundoptics.com 2017) 42
Figure 2.28 Anidolic lighting systems, Compound Parabolic Concentrator (CPC) (edmundoptics.com 2017)... 42
Figure 2.29 The components of dCPC coated with PV cell (left), and the ray-tracing results from 10^{o} angle (Yu et al., 2014). 42
Figure 2.30 Section of the computer model (left) and photograph of physical components (right) of anidolic solar blinds (Ruck et al., 2000)..... 43
Figure 2.31 Anidolic solar blinds installed on the exterior of a mockup building, and the luminance measured inside the model (LESO website). 44
Figure 2.32 The maximum input and the design angle of the CPC (left), 3D hollow HCPC (middle), experimental prototype (right) (Vázquez-Moliní et al., 2012) 44
Figure 2.33 Concept of the system (above), and computer model and prototype of T-CPC (below) (Vázquez-Moliní et al., 2013) 45
Figure 2.34 Interior (left) and exterior (right) views of Mashrabiya (Sherif et al., 2012a)..... 46
Figure 2.35 Contemporary solar screens in the American University (left) (Sherif et al., 2012a), metal solar screens at Tampa Museum of Art (right) (archdaily.com 2017) 46
Figure 2.36 Perforated skin façade, Kanazawa Umimirai Library (archdaily.com 2017) 47
Figure 2.37 Exterior and interior of Arab World Institute kinetic screen facade in Paris (aedesign.files.wordpress.com 2017)..... 47
Figure 2.38 [A] expanded metal mesh, [B] tubular shading structure, and [C] micro-perforated screen (Fernandes et al., 2015) 47
Figure 2.39 Perforation and depth of solar screens (left), shading percentages of screens with different depth ratios (right) (Sherif et al., 2012a) 48
Figure 2.40 Opened (left) and closed SVM (right) (Giovannini et al., 2015)..... 49
Figure 2.41 Optimized perforated screens for each case (Lavin and Fiorito, 2017)..... 50
Figure 2.42 Close-up view of the complex geometry (left) and the whole screen (right) (Omidfar, 2011) 51
Figure 2.43 View through MSPSS (left), unobstructed view (right) (Appelfeld et al., 2012) 51
Figure 2.44 The configuration of the double skin perforated screen (Blanco et al., 2016)..... 52
Figure 2.45 MicroShade® layer (Rasmussen 2013)..... 52
Figure 2.46 Coordinate measuring machine (left), the scanning result of the mesh(right) (Fernandes et al., 2015) 52
Figure 2.47 Light Pipe system (durlum.de 2017) 54
Figure 2.48 The components of the system (Aizenberg, 2013) 54
Figure 2.49 Sunlight collector (left) (buildings.com 2017,) fibre optics cables (middle) (e3tnw.org 2017), and light diffusers (right) (buildinggreen.com 2017)..... 55
Figure 2.50 Proposed model of the integrated daylighting system (Al-Obaidi et al., 2017)..... 55
Figure 2.51 Optical light rod shows the illumination of the end of the rod (Callow and Shao, 2003) 56
Figure 2.52 Skylight systems (flickr.com 2017)..... 56

Figure 3.1 Wavelength range from Universe by Freedman and Kaufmann, left (nasa.gov 2017), and wavelength range, right (thiesclima.com 2017) 63
Figure 3.2 Ideal glazing façade in summer (left) and winter (right) (Long and Ye, 2014a) 63
Figure 3.3 Sequence of an electrochromic laminated glass switching process (Gesimat, 2017) 66
Figure 3.4 Electrochromic technology in clear and tinted states (Sbar et al., 2012). 67
Figure 3.5 Schematic multilayer structure of an SPD in OFF (right) and ON (left) states (Barrios et al., 2015) . 68
Figure 3.6 An opaque (right) and a transparent state (left) of SPD glazing (Ghosh et al., 2016) 69
Figure 3.7 LC Privacy Glass, the translucent mood on the right and transparent mood on the left (Innovative Glass Corporation, 2017) 69
Figure 3.8 Illustration of the OFF and ON mood of the LC device (Dream Glass Group, 2017) 69
Figure 3.9 Crystalline silicon PV glazing, Berlin Hauptbahnhof (Casini, 2016) 70
Figure 3.10 Generated power and transparency of PV panels (Casini, 2016) 71
Figure 3.11 Thermochromic glazing (middle room). Surface temperature (left) (Lee et al., 2013) 72
Figure 3.12 Thermochromic glazing lower (a) and higher than the transition temperature (b) (Silva et al., 2016) 72
Figure 3.13 Thermotropic glazing: transparent on the left and translucent on the right, Configuration of window unit consists of low-emissivity and thermotropic glass (Inoue et al., 2008) 73
Figure 3.14: [A] Aerogel glazing applied on the façade (Reim et al., 2005), and [B] a monolithic aerogel sample (Buratti and Moretti, 2012) 74
Figure 3.15 PCM internal shading devices (Sharma et al., 2009) 75
Figure 3.16 Ladybug plug-in (grasshopper3d.com 2017) 78
Figure 3.17 Honeybee plug-in (grasshopper3d.com 2017) 78
Figure 4.1: Flowchart of research methodology 81
Figure 4.2: Plan (above) and section (below) of the room 83
Figure 4.3: Light ray reflection by concave shape (Boubekri, 2014) 84
Figure 4.4 Law of reflection (above), and Specular, diffuse, and spread reflection from a surface (below) (Ryer 1997), pp. 13. 85
Figure 5.1: Flow chart of the computer modelling study procedure 91
Figure 5.2 Location of the case study City (Riyadh) 92
Figure 5.3: Illumination Range 92
Figure 5.4 Radiation Range 93
Figure 5.5: Occupation schedule component in HoneybeePlus 95
Figure 5.6: Daylight zones, section (above) and perspective (below) 96
Figure 5.7: Computer modelling set up (Raytracing Process) 97
Figure 5.8: GRASSHOPPER components that were used to run the raytracing study in RADIANCE 98
Figure 5.9: Sun path, 21 June at solar noon, Riyadh city, from A to D, top, side, perspective, and front views .. 99
Figure 5.10 Daylight simulation requirements (Reinhart, 2010) 99
Figure 5.11: Workflow to conduct CBDM modelling (Brembilla, 2017) 101
Figure 5.12: Six methods used to conduct a daylighting simulation by Radiance, Credit: Mostapha Sadeghipour (Subramaniam, 2018) 102
Figure 5.13: The total sensor illuminance, E(x), (Bourgeois et al., 2008) 103
Figure 5.14: Front and perspective views show the tested room. 104

Figure 5.15: Illuminance values (above), and the minimum, the maximum, and the mean (below) base case on December 21st at solar noon in Riyadh city 105
Figure 5.16: Standard deviation between the 10-simulation runs 106
Figure 5.17: Tregenza (145 divisions) [left], and Reinhart (581 divisions) [right] (Ward et al., 2011) 107
Figure 5.18 Tregenza Sky matrix for Riyadh city, [A] total, [B] diffuse, and [C] direct radiation (kWh/m^2) 107
Figure 5.19: Illuminance values (above), and the minimum, the maximum, and the mean (below) 108
Figure 5.20: Standard deviation between the 10 simulation runs 108
Figure 5.21 Reinhart Sky matrix (fine density, 580 sky patches) 109
Figure 5.22: Illuminance values (above), and the minimum, the maximum, and the mean (below) 110
Figure 5.23: Standard deviation between the 10 110
Figure 5.24: Front and perspective views of the base case, left to right, respectively 111
Figure 5.25: The DA (left) and the ASE (right) for the base case 112
Figure 5.26: The DA (left) and ASE (right) for the whole year 113
Figure 5.27: $UDI_{(300\text{-}1000\ lux)}$ (left), and $UDI_{(300\text{-}500\ lux)}$ (right), for the base case 113
Figure 5.28: The daylight simulation outputs, $UDI_{300\text{-}500lx}$ (left) and $UDI_{300\text{-}1000lx}$ (right). 114
Figure 5.29: The DA for each season 115
Figure 5.30: The ASE for each season, for the base case 116
Figure 5.31: The UDI for each season, for the base case 117
Figure 5.32: The daylight simulation outputs for spring, DA (left), ASE (middle), and UDI (right). 117
Figure 5.33: Raytracing of direct sunlight at 12 pm on 21 June (above), 21 September (middle) and 21 December (below) 119
Figure 5.34: Total illuminance for the base case 120
Figure 5.35: Daylight distribution within the four zones at 8 am, for the base case 121
Figure 5.36: Total illuminance at 8 am on 21 June (left), 21 September (middle) and 21 December (right) 121
Figure 5.37: Total illuminance for the base case 122
Figure 5.38: Daylight distribution within the four zones at 10 am 123
Figure 5.39: Total and direct illuminance at Z1 on 21 December at 10 am 123
Figure 5.40: Total illuminance at 10 am on the 21st of June, September and December (from left to right) 124
Figure 5.41: Total illuminance for the base case at Z1, Z2, Z3 and Z4. 125
Figure 5.42: Total illuminance for the base case at Z2, Z3 and Z4 125
Figure 5.43: Total and direct illuminance at Z1 on 21 December at 12 pm 125
Figure 5.44: Total illuminance at 12 pm on 21 June (left), 21 September (middle) and 21 December (right). (Below) the high bound of scale is set to 2000 lux 126
Figure 5.45: Daylight distribution within the four zones at 12 pm on the 21st of June, September and December 127
Figure 5.46: Total illuminance at 2 pm for the base case 128
Figure 5.47: Total and direct illuminance at Z1 on 21 December at 2 pm 128
Figure 5.48: Daylight distribution within the four zones at 2 pm 129
Figure 5.49: Total illuminance at 2 pm on 21 June (left), 21 September (middle) and 21 December (right) 130
Figure 5.50: Total illuminance for the base case 131
Figure 5.51: Daylight distribution within the four zones at 4 pm 131

Figure 5.52: Total illuminance at 4 pm on 21 June (left), 21 September (middle) and 21 December (right)..... 132
Figure 5.53: The DUWP for the base case 133
Figure 5.54: The luminance, on 21 December at 8 am, Base case, Riyadh 134
Figure 5.55: The luminance, on 21 December at 10 am, Base case, Riyadh 134
Figure 5.56: The luminance, on 21 December at 12 pm, Base case, Riyadh 134
Figure 5.57: The luminance, on 21 December at 2 pm, Base case, Riyadh 135
Figure 5.58: The luminance, on 21 December at 4 pm, Base case, Riyadh 135
Figure 6.1: Front and perspective views of case PSS5 (A) and (B), respectively 139
Figure 6.2: ASE at Z1 for Riyadh city 140
Figure 6.3: UDI at Z1 for Riyadh city 140
Figure 6.4: UDI at Z2 for Riyadh city 141
Figure 6.5: UDI at Z3 for Riyadh city 141
Figure 6.6: UDI at Z4 for Riyadh city 142
Figure 6.7: The DA for Riyadh city 142
Figure 6.8: The ($UDI_{(300\text{-}1000\ lux)}$) for Riyadh city 143
Figure 6.9: The ($UDI_{(300\text{-}500\ lux)}$) for Riyadh city 144
Figure 6.10: The DA during each season for case PSS5, in Riyadh 144
Figure 6.11: The ASE for case PSS5 in Riyadh 145
Figure 6.12: The UDI for case PSS5 in Riyadh 146
Figure 6.13: Total illuminance. Case PSS5 in Riyadh 147
Figure 6.14: Total and direct illuminance at Z1 on 21 December at 8 am. Case PSS5, in Riyadh 147
Figure 6.15: Total illuminance Case PSS5 in Riyadh 148
Figure 6.16: Total and direct illuminance at Z1 on 21 December at 10 am. Case PSS5, in Riyadh 149
Figure 6.17: Total illuminance for case PSS5 in Riyadh City 150
Figure 6.18: Total illuminance on 21 June, 21 September and 21 December at 2 pm. Case PSS5 in Riyadh..... 151
Figure 6.19: Total illuminance. Case PSS5 in Riyadh 151
Figure 6.20: DUWP for the optimum PSS (PSS5), for Riyadh 152
Figure 6.21: Comparison of DUWP between BCWRR25 and PSS5, for Riyadh 153
Figure 6.22: The luminance, on 21 December at 8 am, Case PSS5, Riyadh 154
Figure 6.23: The luminance, on 21 December at 10 am, Case PSS5, Riyadh 154
Figure 6.24: The luminance, on 21 December at 12 pm, Case PSS5, Riyadh 154
Figure 6.25: The luminance, on 21 December at 2 pm, Case PSS5, Riyadh 155
Figure 6.26: The luminance, on 21 December at 4 pm, Case PSS5, Riyadh 155
Figure 6.27: Front (A) and perspective (B) views of case PSS5 156
Figure 6.28: DRD views, side view (A), top view (B), 3D view (left C) and front view (D), dimensions in centimetres 157
Figure 6.29: Front view shows the position and dimensions of the DRDs ..... **Error! Bookmark not defined.**
Figure 6.30: Cases DRSS. The dimensions are in meters 158
Figure 6.31: 21 December at 8am, 10am, 12pm, 2pm and 4pm [from above to below], CPC in normal mode 161
Figure 6.32: 21 December at 4 pm, CPC in normal mode 161

Figure 6.33: The drawings of the DRD after the elimination of the upper part 162
Figure 6.34: Raytracing of sun paths for developed CPC in normal mode. 21 December at 8am, 10am, 12pm, 2pm and 4pm [from above to below] 167
Figure 6.35: Total illuminance. Case DRSS1 in Riyadh 168
Figure 6.36: Total and direct illuminance at Z1 on 21 December at 8 am. Case DRSS1, in Riyadh 168
Figure 6.37: Total illuminance. Case DRSS1 in Riyadh 169
Figure 6.38: Total illuminance for case DRSS1 in Riyadh 170
Figure 6.39: Total illuminance on 21 June, 21 September and 21 December at 2 pm. Case DRSS1 in Riyadh 171
Figure 6.40: Total illuminance. Case DRSS1 in Riyadh 171
Figure 6.41: DUWP for Case DRSS1 in Riyadh 173
Figure 6.42: Daylight autonomy $DA_{300\ lux\ (50\%)}$ (%), case DRSS1, Riyadh 174
Figure 6.43: The ASE at Z1, case DRSS1, Riyadh 174
Figure 6.44: The UDI for case DRSS1 in Riyadh 175
Figure 6.45: (A) the DA, and (B) the ASE for case DRSS1 in Riyadh 175
Figure 6.46: (A) the $UDI_{300\text{-}1000\ lux}$, and (B) the $UDI_{300\text{-}500\ lux}$, for case DRSS1 in Riyadh 176
Figure 6.47: The luminance, 21 December at 8 am. Case DRSS1, Riyadh 177
Figure 6.48: The luminance, 21 December at 10 am. Case DRSS1, Riyadh 177
Figure 6.49: The luminance, 21 December at 12 pm. Case DRSS1, Riyadh 178
Figure 6.50: The luminance, 21 December at 2 pm. Case DRSS1, Riyadh 178
Figure 6.51: The luminance, 21 December at 4 pm. Case DRSS1, Riyadh 178
Figure 6.52: Comparison of DGP for the base case, PSS5 and DRSS1, for Riyadh 179
Figure 7.1: Hemispherical fish-eye views of the CIE clear sky distribution (Mardaljevic, 2002) 187
Figure 7.2: GPM designed by [A] Coburn and Peddle (2006), and [B and C] by Biliouris et al. (2007) 188
Figure 7.3: The GPM used in the research 189
Figure 7.4: Sliding support for the photosensor 189
Figure 7.5: Front, side and top view of the GPM, (from above to below), dimensions in mm and degrees 190
Figure 7.6: Lightbulb used in the GPM (EN-DGU1024) 190
Figure 7.7: Photos inside the laboratory 191
Figure 7.8: Luminance calibration setup by LRS (Nikolova et al., 2018) 194
Figure 7.9: The process of the luminance meter calibration and the reflectance measurements 194
Figure 7.10: Front view shows the measuring angle (2 degrees) and the measuring area at 0.5-meter (0.0003 m^2), dimension in meter 195
Figure 7.11: Law of reflection (left), and specular, diffuse, and spread reflection from a surface (right) (Ryer 1997) pp. 13 196
Figure 7.12: Basic principles of surface reflectance (Nayar et al., 2009) 196
Figure 7.13: Setting of the angle between the light source and the photosensor of the GPM (Author) 196
Figure 7.14: Photo of luminance measurement, the GPM is set on a 15-degree 196
Figure 7.15: The setting of the goniophotometer for the normal reflectance angle 198
Figure 7.16: The installation of the illuminance meters and the setting of the light source angle 199
Figure 7.17: Comparison of luminance emitted by the small sample and by the GPM platform surface 200
Figure 7.18: Measured luminance at the 18%-Reflectance-Grey Card 201

Figure 7.19: Comparison of the typical and the calculated reflectance of the 18%-Reflectance-Grey Card..... 201
Figure 7.20: Luminance emitted by the GPM platform surface without and with the black-matt fabric 201
Figure 7.21: Measured luminance of room materials (left), and typical and calculated reflectance (right) 202
Figure 7.22: Measured luminance of DRD (left), and typical and calculated reflectance (right)..... 203
Figure 7.23: Front view (top left), side view (top right), floor plan (middle) of the room, and 3D views (below) 207
Figure 7.24: Coating (A) and polishing (B) of the model interior surfaces..... 208
Figure 7.25: Apply vinyl film on the room surfaces..... 208
Figure 7.26: The interior of the room painted with white primer (left) and with vinyl film (right)..... 208
Figure 7.27: Fabrication of the PSS by a laser cut machine using AutoCAD 209
Figure 7.28: Multiple layers of filler primer paint and grey acrylic spray..... 209
Figure 7.29: Groove in the wall to insert the PSS (bottom, left) and thickness of perforated screen (bottom, right), exterior view (left) and interior view (right)..... 209
Figure 7.30: Exterior (left) and interior (right) of the PSS 209
Figure 7.31: Rhinoceros interface (left), the exported STL file in Ultimaker^3 software (middle) and HIPS material (right)..... 210
Figure 7.32: 3D-Printing process of the DRD units (left), and the fabricated DRD (right)..... 211
Figure 7.33: Mirror effect paint (A), DRDs with different coatings, from left to right, HIPS, PLA, foil sheet-1, foil sheet-2, and mirror-effect paint (B)..... 211
Figure 7.34: Forming HIPs on negative DRD mould by the Vacuum machine 211
Figure 7.35: Positive moulds of DRD made by the 3D printer (left). DRD sanding before the vacuuming (right) 212
Figure 7.36: The enhanced positive DRD mould 212
Figure 7.37: Vacuuming and finishing of the HIP sheet on the positive mould of the DRD..... 213
Figure 7.38: The installation of the DRDs within the PSS 213
Figure 7.39: The cutting process by the laser-cut machine (left) and prism lens (right) 214
Figure 7.40: Single-point illuminance meter (uk.rs-online.com)..... 214
Figure 7.41: Connection sequence of the measurement equipment..... 214
Figure 7.42: Floor plan (top) and details drawing (below) of the model show the light sensors position 215
Figure 7.43: Installation of light sensors inside the model 215
Figure 8.1**:** Flowchart of the daylight tests procedure 218
Figure 8.2: The light bulb used for the DRLS 219
Figure 8.3: Turntable used for Riyadh city test 220
Figure 8.4: DRLS (left) and adjustable tilt angle (right)..... 220
Figure 8.5: Model and sun position setup..... 220
Figure 8.6: Model was set for Riyadh 21st June at solar noon 221
Figure 8.7: The interior (left) and the exterior (right) of the model, for Nottingham, 21 October at 12 pm..... 221
Figure 8.8: Opening for the camera (left) and the illuminance with and without the camera (right) 222
Figure 8.9: The external ground with black plastic (A) and with matt-black fabric (B), and luminance levels (C and D), for Riyadh on 21Jun at 12 pm..... 222
Figure 8.10: Exterior view of tested cases..... 224
Figure 8.11: Drawings of cases DRSS1, DRSS2 and DRSS3, dimensions are in meters. 224

Figure 8.12: Cases DRSS1, DRSS4 and DRSS5, dimensions are in meters 225
Figure 8.13: Case DRSS5, DRSS6, DRSS7, and DRSS8, dimensions are in meters 226
Figure 8.14: Illuminance (left) and DUWP (right) under DRLS at solar noon 228
Figure 8.15: Illuminance (left) and DUWP (right) under DRLS at solar noon 229
Figure 8.16: Illuminance (left) and DUWP (right) under DRLS at solar noon 229
Figure 8.17: Illuminance (left) and DUWP (right) under DRLS at solar noon 230
Figure 8.18: Illuminance (left) and DUWP (right) under DRLS at solar noon 231
Figure 8.19: Illuminance (left) and DUWP (right) under DRLS at solar noon 232
Figure 8.20: Illuminance (left) and DUWP (right) under DRLS at solar noon 232
Figure 8.21: Illuminance (left) and DUWP (right) under DRLS at solar noon 233
Figure 8.22: Illuminance (left) and DUWP (right) under DRLS at solar noon 234
Figure 9.1: The interior of the prototype 237
Figure 9.2: The interior of the sky dome at the IEDE 239
Figure 9.3: Sun and sky elements positions and the angular distance (x) between them 240
Figure 9.4**:** Sun and sky element position at solar noon in Riyadh on the 21 June (above) 21 December (below) 241
Figure 9.5: The sun and sky positions at solar noon in Riyadh 242
Figure 9.6: Flowchart of the test process 242
Figure 9.7: The DFLS setting 243
Figure 9.8: The installation of the sample screen 243
Figure 9.9: The illuminance (left) and DUWP (right) under the DFLS 245
Figure 9.10: The illuminance (left) and DUWP (right) under the DFLS 246
Figure 9.11: Case DRSS1, DRSS4 and DRSS5, from left to right 247
Figure 9.12: The illuminance (left) and DUWP (right) under the DFLS 248
Figure 9.13: The illuminance (left) and DUWP (right) under the DFLS 249
Figure 9.14: External photographs show the used material for the proposed system. White gloss HIPS material on the left and Mirror HIPS material on the right 250
Figure 9.15: The illuminance (left) and DUWP (right) under the DFLS 251
Figure 9.16: External photographs of DRSS5 (left) and DRSS7 (right) 252
Figure 9.17: The illuminance (left) and DUWP (right) under the DFLS 252
Figure 9.18: The illuminance (left) and DUWP (right) under the DFLS 253
Figure 9.19: The illuminance (left) and DUWP (right) under the DFLS 254
Figure 9.20: The illuminance (left) and DUWP (right) under the DFLS 255
Figure 10.1: The sun azimuth was 180 degrees from the north. A clear sunny day in Nottingham on 21st Oct at solar noon 259
Figure 10.2: Exterior view of the model under the real sky in Nottingham on 21 October at solar noon 260
Figure 10.3: Daylight factor (%) at light sensor Z1 and P2 for Case PSS5 and DRSS1 261
Figure 10.4: Daylight factor at light sensor Z1 and P2 262
Figure 10.5: Daylight factor at light sensor P1 and P2 262
Figure 10.6: Daylight factor at light sensor P1 and P2 263
Figure 10.7: Daylight factor at light sensor P1 and P2 264

Figure 10.8: Daylight factor at light sensor P1 and P2 264
Figure 10.9: Daylight factor at light sensor P1 and P2 264
Figure 10.10: Luminance distribution and Sky patch and sun position for Nottingham city, 21st October at solar noon. Tregenza sky division. 265
Figure 10.11: Daylight factor values of case DRSS5 in Nottingham on 21st October at solar noon 266
Figure 10.12: Daylight uniformity values of case DRSS5 in Nottingham on 21st October at solar noon..... 266
Figure 11.1: Integration of prismatic lens within the DRD units..... 271
Figure 11.2: Sun rays reflection with the initial CPC in a reverse mode, Riyadh at 12 pm..... 272
Figure 11.3: Sun rays reflection with the developed CPC in a reverse mode, Riyadh at 12 pm..... 274
Figure 11.4: Total illuminance for case DRSS11 275
Figure 11.5: Total illuminance for case DRSS11 275
Figure 11.6: Direct illuminance, diffuse illuminance, and total illuminance at Z1 on 21 December at 8 am..... 275
Figure 11.7: Total illuminance for case DRSS11 276
Figure 11.8: Total illuminance for case DRSS11 276
Figure 11.9: Total illuminance for case DRSS11 277
Figure 11.10: Total illuminance for case DRSS11 278
Figure 11.11: DUWP for case DRSS11..... 278
Figure 11.12: The daylight autonomy for case DRSS11 279
Figure 11.13: Annual sunlight exposure for case DRSS11 279
Figure 11.14: Useful daylight illuminance for case DRSS11..... 280
Figure 11.15: Raytracing of sun paths at solar noon on 21st June, from above to below, the tilt angle of the DRD is 0, 5, 10, 15, 20, 25 and 30 degrees..... 282
Figure 11.16: Total illuminance at Z4 as a function of DRDs tilt angle from zero to 30 degrees with a 5-degree step..... 284
Figure 11.17: Total illuminance at Z4 as a function of DRDs tilt angle from zero to 30 degrees with a 5-degree step..... 284
Figure 11.18: Total illuminance at the work plane at Z4 as a function of DRDs tilt angle from zero to 30 degrees with a 5-degree step..... 285
Figure 11.19: Total illuminance at the work plane at Z4 as a function of DRDs tilt angle from zero to 30 degrees with a 5-degree step..... 285
Figure 11.20: Total illuminance at the work plane at Z4 as a function of DRDs tilt angle from zero to 30 degrees with a 5-degree step..... 286
Figure 11.21: DUWP as a function of DRDs tilt-angle from zero to 30 degrees with a 5-degree step 287
Figure 11.22: DUWP as a function of DRDs tilt-angle from zero to 30 degrees with a 5-degree step 287
Figure 11.23: DUWP as a function of DRDs tilt-angle from zero to 30 degrees with a 5-degree step 288
Figure 11.24: DUWP as a function of DRDs tilt-angle from zero to 30 degrees with a 5-degree step 288
Figure 11.25: DUWP as a function of DRDs tilt-angle from zero to 30 degrees with a 5-degree step 289
Figure 11.26: Comparison of DUWP between case DRSS11 and DRSS11-B..... 289
Figure 11.27: Direct illuminance, diffuse illuminance, and total illuminance at Z1 on 21 December at 8 am for case DRSS1-B 290
Figure 11.28: The DA for case DRSS11-B (5-deg. tilt) 290
Figure 11.29: Annual sunlight exposure for case DRSS11-B..... 291

Figure 11.30: Useful daylight illuminance for case DRSS11-B 291
Figure 11.31: Total illuminance at Z1, Z2, Z3 and Z4 for case DRSS12 292
Figure 11.32: Total illuminance at Z2, Z3 and Z4 for case DRSS12 293
Figure 11.33: Direct illuminance, diffuse illuminance, and total illuminance at Z1 on 21 December at 8 am, case DRSS12 293
Figure 11.34: Total illuminance for case DRSS12 293
Figure 11.35: Total illuminance for case DRSS12 294
Figure 11.36: Interior view of the room at solar noon on 21 June, case DRSS12 294
Figure 11.37: Total illuminance for case DRSS12 295
Figure 11.38: Total illuminance for case DRSS12 295
Figure 11.39: DUWP for case DRSS12 296
Figure 11.40: Daylight autonomy for case DRSS12 296
Figure 11.41: Annual sunlight exposure for case DRSS12 297
Figure 11.42: Useful daylight illuminance for case DRSS12 297
Figure 11.43: DA (left) and ASE (right) for the whole year for case DRSS12 298
Figure 11.44: $UDI_{300\text{-}1000lx}$ (left) and $UDI_{300\text{-}500lx}$ (right) for the whole year for case DRSS12 298
Figure 11.45: Comparison of the daylight uniformity 299
Figure 11.46: Comparison of annual sunlight exposure (ASE) 299
Figure 11.47: Comparison of daylight autonomy (DA) 300
Figure 11.48: Comparison of useful daylight illuminance (UDI) 300

List of tables

Table 1.1: The position index of the window (Boubekri, 2014).....17

Table 1.2: Energy Consumption due to lighting in Saudi Arabia from 2000 to 2014.....24

Table 2.1 Comparison of daylighting systems.....58

Table 4.1: Prosperities of the tested room 82

Table 5.1: BREAM requirements for daylighting in office buildings (BREEAM, 2016).....94

Table 5.2: Properties of the surface's material 95

Table 5.3: Radiance parameters for the point-in-time simulation 104

Table 5.4: The Radiance parameters for the annual daylight simulation for the daylight matrix (dmtxPar) and the direct sun matrix (smtxPar) calculations.....107

Table 5.5: Glare study results of daylight redirecting solar screen the base case.....133

Table 6.1: Tested parameters of the Perforated Screens.....139

Table 6.2: Glare study results of daylight-redirecting solar screen case PSS5.....153

Table 6.3: Glare study results of daylight-redirecting solar screen case DRSS1 177

Table 7.1: Specifications of the lightbulb used in the GPM.....191

Table 7.2: The materials were tested utilising the Goniophotometer.....197

Table 7.3: Calibration results of lux meter-1 (LM1) by RS Components LTD. 203

Table 7.4: Calibration results of lux meter-2 (LM2) by RS Components LTD. 203

Table 7.5: Calibration results of lux meter-3 (LM3) by RS Components LTD. 204

Table 7.6: Calibration results of lux meter-4 (LM4) by RS Components LTD. 204

Table 7.7: Calibration of the Lux meters by the GPM at range 40 lux.....204

Table 7.8: Calibration of Lux meters LM2 by the GPM at range 400 lux. 205

Table 7.9: Calibration of Lux meters LM2 by the GPM at range 4000 lux. 205

Table 7.10: Calibration of Lux meters LM2 by the GPM at range 40 Klux.....205

Table 7.11: Dimensions of the main elements of the model (mm).....206

Table 7.12: Components of the model.....206

Table 8.1: The specifications of the light bulb used for the DRLS (Lamp, 2018) 219

Table 8.2: Conditions of the DRLS test, the dimensions in mm and degree.....222

Table 8.3: Main parameters and their properties 223

Table 9.1: The properties of the tested scenarios.....238

Table 9.2: Standard parameters of the CIE Standard Clear Sky (ISO, 2004).....239

Table 10.1: Main parameters and their properties 259

Table 11.1: Cases names and tilt angles in degree.....270

Table 11.2: Total illuminance levels angle at the work plane at Z4 as a function of DRDs tilt angle.....283

Table 11.3: DUWP at the work plane as a function of DRDs tilt angle.....286

Chapter 1. Introduction

This chapter introduces the aims and objectives of this study and presents the problem statement, the novelty of the study, and the structure of the thesis.

1.1. Introduction

Adequate daylighting performance is significantly important because it not only reduces the extent of lighting energy consumption but also serves to improve the quality of the indoor environment. A number of studies (Anstead and Franta, 1994, Edwards and Torcellini, 2002) have found that an adequate daylighting level in working environments leads to improvements in the health and productivity of the building occupants.

The utilisation of artificial lighting consumes a large portion of the available energy globally. This account for around 20% of the generated energy. Furthermore, the production of this energy emits a significant amount of CO2 (Dubois et al., 2016). The energy consumption in the building section in the majority of countries is about one-fifth to two-fifths of the final energy consumption (DOE, 2005, Janda, 2009, Pérez-Lombard et al., 2008). Additionally, 40% of materials are used by the building industry and there are emissions of approximately half of the greenhouse gasses (Prasad and Hall, 2005). The increase in the staying period and comfort inside indoor spaces increases energy demands (Pérez-Lombard et al., 2008). As a result, the need to reduce energy consumption by harnessing the available solar energy for daylighting applications became a significant goal.

Previous studies have reported the benefits of daylighting on occupants. It was found that people in office spaces that are illuminated by daylight recorded an increase in general well-being. The benefits include improving the health and productivity of occupants in addition to reducing the rates of absence among the employees (Anstead and Franta, 1994, Edwards and Torcellini, 2002).

Research has also shown that occupants prefer office spaces with windows. A survey of employees working in office spaces by Collins (1975) reported that over a third of the occupants stated that windowless space is the main disadvantage of a work environment. According to Finnegan and Solomon (1981), this was mainly due to the lack of daylight and

natural ventilation, which influences visual and thermal comfort and prevents interaction with the outdoor environment (Edwards and Torcellini, 2002).

Although studies have indicated that daylighting provides numerous benefits to occupants, inadequate daylighting design can lead to indoor discomfort. As a result, daylight has to be appropriately utilised in order to increase the occupants' level of comfort while reducing its negative impact. For instance, the inadequate daylighting level can lead to glare and overheating. This could increase the rate of employees absence (Edwards and Torcellini, 2002).

Daylight is a combination of direct sunlight and diffuse skylight (Baker and Steemers, 2014, Wong, 2017, Alrubaih et al., 2013). It accesses a building through horizontal or vertical openings, and it is an alternative to artificial lighting (Alrubaih et al., 2013, Manning, 2006). The daylighting performance is influenced by a number of different factors, such as location, latitude and climate, conditions of the sky, time, and building design (Wong, 2017, Baker and Steemers, 2014).

The amount of potential daylight in low and intermediate latitude regions is significant. However, the capacity for daylight harvesting is limited. The issues of heat gain and glare are the main obstacles that prevent designers from effectively and consistently using daylighting in buildings. Many studies have been undertaken in order to eliminate the negative effect of the use of sunlight in buildings; however, it has been found that further studies are required in order to produce effective daylighting systems for low latitude regions.

As a result, the author has conducted a critical review to evaluate the current daylighting and glazing technologies in order to investigate their development status, limitations and obstacles, and the lack of knowledge regarding these technologies. It was found that a potential solution could be achieved by integrating different daylighting technologies. Therefore, the author proposed a novel integrated daylighting system which consists of daylight redirection methods and a daylight filtration system.

The proposed novel daylighting system is intended to provide a building with an adequate daylighting level without compromising the degree of visual comfort. This study aimed to optimise the daylighting performance of office buildings in low latitude regions by enhancing the daylight illumination in deep, dark areas, enhancing the daylighting distribution uniformity, and reducing the glare while providing a visual connection with the outdoor environment.

The study proposed a novel daylighting system that can be utilised in low and high latitude regions. The latitude region includes countries located in the range of 0^{o} to 30^{o} degrees north

and south from the equator. These areas are defined as tropical and subtropical climates with hot summers, clear sky conditions and high solar altitudes. On the other hand, in the high latitude regions located in the range of 30^{o} to 60^{o} degrees north and -30^{o} to -60^{o} south from the equator, the solar altitude is low, and the sky conditions for most of the year are overcast or partially clouded.

The proposed system is based on the potentiality and certain limitations were identified in previous subject-related literature. A comparison was conducted to select the most effective daylighting technology to improve the daylighting performance inside buildings.

The proposed system is a daylight-redirecting perforated solar screen (DRSS). It is an integration of a daylight filtration system, namely, a perforated solar screen (PSS) and a daylight redirection device (DRDs). The DRD is a developed design of a compound parabolic concentrator (CPC) integrated with prism lenses. The interior of the DRD is a hollow parabolic integrated with a prismatic lens in the inlet and outlet, see Figure 4.3.

The two components (PSS and DRD) are embedded between two layers of single glazing. The purpose of the glass is to prevent undesirable air from accessing the interior spaces and keeping the daylighting system clean and protected from any source of pollution such as dust particles. However, the glass coating was not included in the modelling in this study to avoid its transmittance or refraction effect on the sunray's behaviour.

1.2. Aims and objectives

The study aims to achieve a balanced daylighting performance that mitigates the negative impact of direct sunlight on the front area while increasing the employment of daylight in the deep area of a room. It particularly aims to reduce the annual level of sunlight exposure (ASE) while increasing the daylight autonomy (DA) and the useful daylight illuminance (UDI). Furthermore, the daylighting performance of an office building was enhanced by increasing the daylighting uniformity at the work plane. At the same time, it allows a visual connection with the outdoor environment.

The study begins with a literature review in daylighting followed by an investigation of the daylighting performance of the proposed system. The investigations were conducted via computer simulation and physical experimental studies. The outputs were validated, and a further investigation study was conducted. The aim of the study was achieved through the completion of five tasks. The objectives of these tasks are described as follows:

Literature review

- To conduct a critical literature review in daylighting technologies and innovative glazing systems

The design of the proposed system

- To invent a novel integrated daylighting system.

Parametric study via computer simulation

- To investigate the significant parameters that can influence the performance of visual comfort inside buildings.
- To optimise the design of the PSS
- To test the proposed daylight-redirecting system (DRSS)

Parametric study via physical experimental studies

The experimental studies were subdivided into four tasks: rig fabrication, test under direct-light solar simulator (DRLS), test under diffuse-light sky dome (DFLS), and test under a real sky (RSK).

- To investigate the performance of the proposed system in reality
- To find the uncertainty between the outputs of the computer-based simulation and the physical model tests
- To investigate the DRDs influence on the daylighting illumination level in deep areas, an increase of the distribution uniformity and glare reduction.
- To investigate the influence of the geometry, material and vertical position of the DRDs
- To investigate the influence of prismatic lens on the performance of the DRDs

Final simulation

- To optimise the design of the proposed system
- To provide criteria and recommendations for daylighting practices

1.3. Statement of the problem

Whilst the daylight availability is sufficient in low latitude regions, it was found that inadequate employment of the daylight can produce overlit areas and glare in the front half of the interior space. Thus, shading systems are applied to avoid direct sunlight and reduce the daylight level in the front areas. However, this may lead to a diminishment in the daylight level in the back half of the room.

While the solar altitude in low latitude regions is high, the conventional daylighting system does not provide the deeper areas within the room with an adequate daylight level which is comparable to the front areas. Furthermore, in some cases, the areas near the window can be excessively overlit. This can result in glare which is undesirable for the occupants.

Although many studies have intended to increase the daylighting level in deep areas inside buildings, most of these studies focused on high latitude regions. A number of studies have attempted to solve the problem in the low latitude regions. However, such systems are not available commercially. As a result, a novel daylighting system that can enhance the daylighting uniformity by enhancing the daylighting level in the deep areas while reducing the glare is required.

The daylight-redirecting systems are one of the methods that are applied to increase the daylight level in the rear area of the interior spaces. In this study, we proposed a new daylight-redirecting system that can increase daylight uniformity by obstructing the direct sunlight, reducing the level of daylight in the front areas of the room while increasing it in the back of the room.

1.4. The novelty of the research

The study proposed the introduction of a novel integrated daylighting-redirecting system. It is a combination of a daylight filtration system (perforated solar screen) and a daylight redirection system (a compound parabolic concentrator working in reverse mode (CPC), integrated with a prismatic lens. The system can filter and redirect the daylight, which leads to an enhancement in the daylighting performance.

It was found that the CPC has not yet been applied in low latitude regions as a daylight-redirection system that redirects the daylight directly through the external façade towards the interior ceiling. Although the CPC in a reverse mode has been utilised for daylighting purposes, it was employed indirectly by integrating it with a light pipe system. Another study proposed that anidolic blinds should be placed on the façade of the building for the purpose of daylight redirection. The geometry of its units consists of two parabolic elements arranged in a grid. Nevertheless, the proposed system was designed for high latitude regions. Furthermore, the geometry and the configuration of the proposed system are quite different from the anidolic blinds.

1.5. Research hypothesis

When daylight strikes the DRD, the internal surface of the concave shape will redirect the daylight towards the internal ceiling. The ceiling will then redirect it to the deeper areas of the room. This behaviour is described in Chapter 4 on page 84, and it is illustrated in Figure 4.3.

The level of daylight redirection is enhanced due to the “deflecting position” of the concave shape and the reflective coating inside the element (Boubekri, 2014).

1.6. Thesis structure

The thesis is divided into twelve chapters as follows:

Chapter 1 is the introduction, which outlines the aim and objectives of the study. It highlights the research gap and explains the research problem which has been investigated through the previous related studies. It presents the research hypothesis based on the scientific knowledge of daylighting and the findings of the previous studies. In addition, the novelty of the research is presented and explained in relation to related proposed systems found in previous studies.

Following this, it provides an overview of the science of daylight and daylighting and its characteristics in low latitude regions. In addition, it shows the energy consumption due to artificial lighting use in Saudi Arabia.

Chapter 2 illustrates an extensive literature review in daylighting technologies, and *Chapter 3* provides a review of smart glazing technologies.

Chapter 4 describes the proposed methodology and the design of the proposed daylighting system.

Computer modelling for the base case in *Chapter 5* and for the proposed system in *Chapter 6* are presenting the procedure, results and discussion of annul and hourly daylighting evaluations.

Chapter 7 addresses the fabrication of the rig. It illustrates the fabrication of the rig and the calibration of the daylight measurement tools.

Chapter 8 is a test under a direct-light solar simulator. The procedure, results and discussion were presented. Similarly, *Chapter 9* describes the daylight tests under a diffuse-light sky dome.

Chapter 10 presents the daylight study that was conducted under an actual sky and a validation study compared to the simulation results.

Chapter 11 represents alternative DRD design and further investigation study.

Finally, *Chapter 12* provides the reader with the recommendations, limitations and conclusions of the research. It is followed with the expected future works. The thesis structure is outlined in the flow chart presented in Figure 1.1.

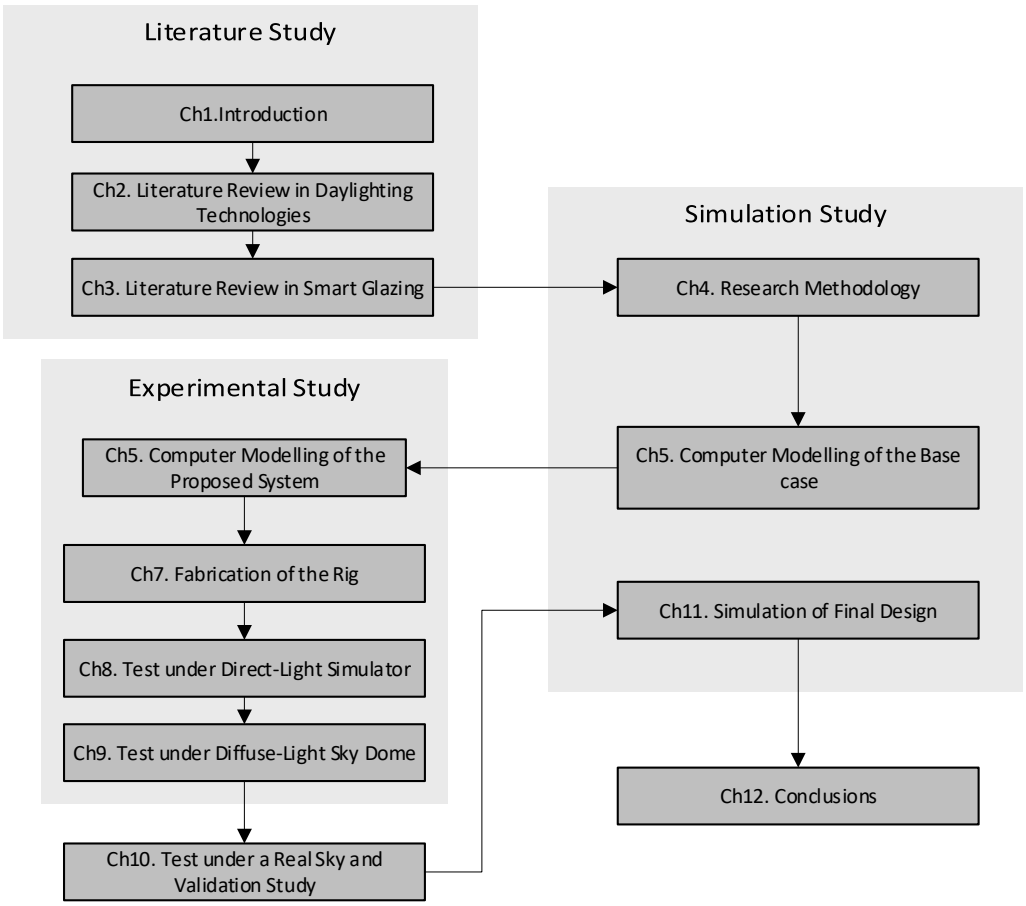


Figure 1.1: Thesis Outline

1.7. Background

The main aims of daylighting systems are the enhancement of the uniformity of daylight, the reduction of glare, controlling direct daylight, and improving daylight illumination in deep areas within the building (Littlefair et al., 1994). This section provides the reader with an overview of daylight science and daylighting technologies, particularly in low latitude regions. It includes definitions of basic daylighting terms, in addition to an overview of indoor visual comfort in office buildings and daylighting metrics.

1.7.1. Overview of daylight in low latitude regions

The amount of potential daylight in low and intermediate latitude regions is significant. However, the extent of the daylight harvest is limited. The heat gains and the glare are the main obstacles that prevent the designer from effectively implementing daylighting in buildings. A balance between indoor visual and thermal comfort is therefore required.

1.7.1.1. The climate in low latitude regions

The low latitude region includes tropical and subtropical climates. The tropical climate is the climate of the territories that are located within the latitude of 10 to 23 degrees north (Cancer) and south (Capricorn) (Edmonds and Greenup, 2002). The subtropical climate is higher where it is located within the latitude of 10 to 35 degrees north and south from the equator. The annual average direct sun component in the sub tropic and many of the tropical regions is around 240 days per year, and the sky is clear most of the year (Edmonds and Greenup, 2002). The range of the low latitude regions is displayed in Figure 1.2 below.

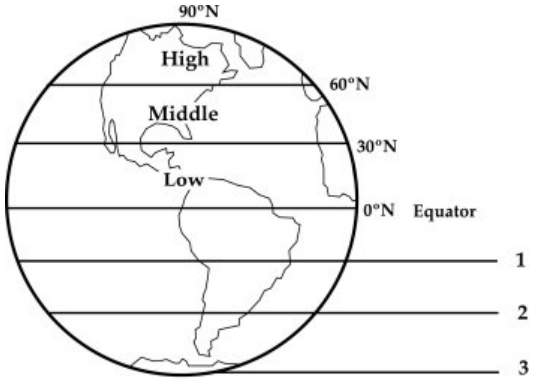


Figure 1.2 Range of low, middle and high latitude regions

1.7.1.2. Sun altitude, azimuth and zenith

In order to design a sustainable building concerning solar energy, two important angles have to be considered: sun altitude and azimuth. Sun altitude is the angle between the sun and the horizon, assuming there are no surrounding buildings or landscape. It is within the range from 0^o to 90^o. The zenith angle is the altitude angle at 90^o. Azimuth is the angular distance between the sun's projection onto the horizon and due south (Reinhart, 2014), Figure 1.3.

The sun altitude increases when the latitude of the location decreases. The sun altitude in low latitude is high compared with high latitude regions. It is 90^o at the equator and around 80^o at a latitude of 30^o north and south of the equator. The sky has three main conditions, clear, partly overcast and overcast. The sky conditions in low latitude regions are clear for the majority of the year.

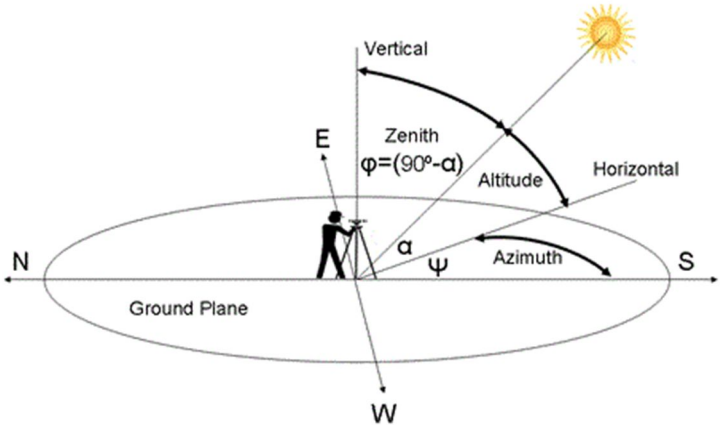


Figure 1.3 Sun altitude and azimuth for northern latitudes (mpoweruk.com, 2005)

1.7.2. Nature of light

Human eyes observe light from a wavelength of electromagnetic radiation from 380 nm to 780 nm, Figure 1.4 (Szokolay, 2014). The illumination of natural daylight can range from 5000 lux under an overcast sky to 4000 lux in direct sunlight. However, the required illumination in an office building is lower than this amount, at typically 500 lux (Robertson, 2003).

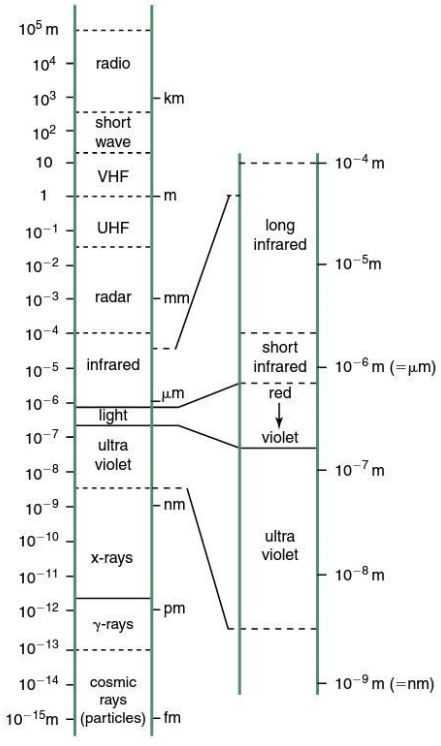
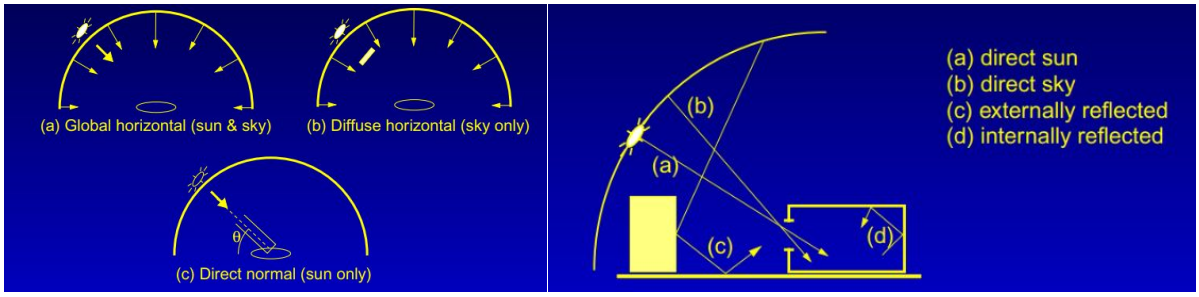


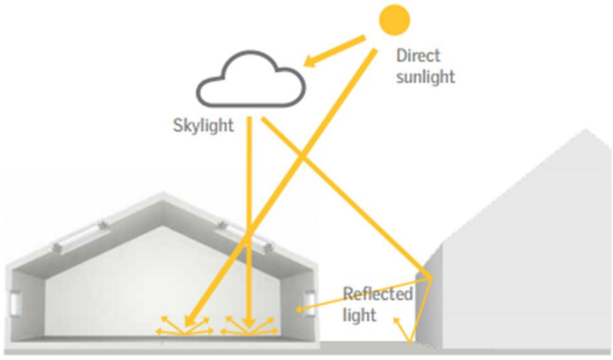
Figure 1.4 Electromagnetic radiation spectrum (Szokolay, 2014)

1.7.2.1. Daylight components

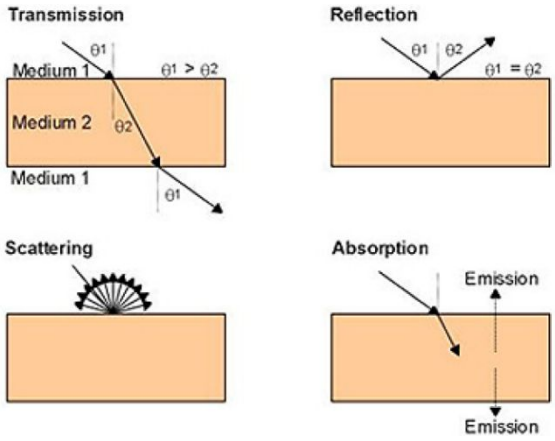
Daylight is a combination of direct sunlight and diffuse skylight (Baker and Steemers, 2014, Wong, 2017, Alrubaih et al., 2013). The direct sunlight comes from the sun directly, while the diffuse skylight is daylight that is reflected from the clouds and the surroundings. It is known as diffuse daylight, as illustrated in Figure 1.5 [A, B]. The characteristics of light are presented in Figure 1.5 [C]. When a light ray strikes a surface, the ray can be transmitted, reflected, scattered or absorbed by that surface.



[A]



[B]



[C]

Figure 1.5 The daylight components [A] (Mardaljevic, 1999) [B] (skylineroofing.co.uk 2017). [C] Light characteristics (tpub.com 2017)

1.7.2.2. The photometric quantities of the light

The photometric quantities of the light are illustrated in Figure 1.6. **Luminance** is defined as the brightness of a surface, and its unit is candela per square meter (cd/m^2). The light is observed in a logarithmic manner over a vertical scale, where humans observe the increase of 100% in the luminance level as a 50% increase. **Illuminance** is defined as the quantity of light exposed to a plane. The preferred illuminance level of a work plane in an office building is 500 lux. One lux is equal to one lumen per square meter (Robertson, 2003), Figure 1.6.

Luminous intensity is defined as the intensity of the light source. The luminous intensity that is emitted can be concentrated in one beam or be dispersed in many directions. The quantity of the light would be changed while its intensity would be not. Luminous intensity also is known as Candela (cd). **Luminous flux** is defined as the quantity of light which is generated by a light source. A 60-watt incandescent bulb can generate 900 lumens, while 3000 lumens can be generated by a 36-watt fluorescent tube (Robertson, 2003). Luminous flux is also described in lumens. **Luminous efficacy** is applied to compare different light sources, and it is the number of lumens generated for each watt of the overall degree of radiation or electrical power. The peak value of the luminous efficacy is 683 lumen/watt (Reinhart, 2014).

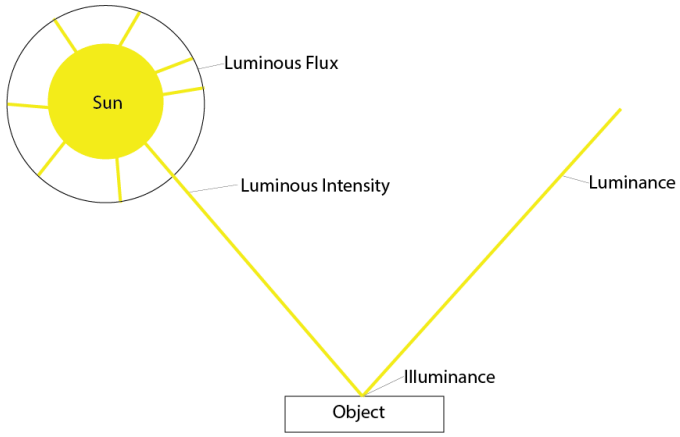


Figure 1.6 The photometric quantities of the light (Robertson, 2003)

1.7.2.3. Glare

Glare can lead to visual discomfort and cause harm to human vision. It occurs when the eye is directly exposed to the light source or by a reflected surface in a room (Robertson, 2003). Glare is divided into two types based on its intensity, namely, disability glare and discomfort glare. Disability glare reduces visibility while discomfort glare leads to discomfort. Headaches or eye pain are examples of the negative impact of glare on occupants (Osterhaus, 2005, Galatioto and Beccali, 2016).

1.7.3. Daylighting metrics

Different metrics have been utilised to measure daylighting performance in previous studies. Researchers evaluated these metrics in order to define their limitations. For instance, daylight factor (DF) is one of the widespread daylighting metrics that have been used for a long period. However, it was found that the application of DF is limited to overcast sky conditions. Therefore, a new method was developed in the late 1990s by Mardaljevic and Reinhart. This

was based on the climatic data of the building, and it is known as climate-based daylight modelling (CBDM).

Other widely utilised daylighting metrics to assess the annual daylighting performance based on the CBDM method are the annual daylight autonomy (DA), useful daylight illuminance (UDI), annual sunlight exposure (ASE). In addition, daylight uniformity is also employed to assess the daylight distribution (illuminance levels) within the interior spaces. On the other hand, the daylight glare index (DGI) and the daylight glare probability (DGP) are used to assess visual comfort.

1.7.3.1. Climate-based modelling

CBDM is a climate-based metric that is defined as the prediction of different luminous or radiant amounts, for instance, illuminance, radiance and luminance, or irradiance. CBDM utilises sky conditions obtained from standardised annual meteorological datasets. The calculated amount of, for example, illuminance, depends on the climate data of the tested location, the orientation of the fenestrations, and the material properties and geometry of the space (Mardaljevic et al., 2009).

Furthermore, the shading devices and their operation method can be modelled, for instance, luminaire operated automatically, or Venetian blinds operated by occupants. The CBDM has many advantages over the daylight factor that is limited to overcast sky conditions. The daylight components and their relation to the CBDM and DF are illustrated in Figure 1.7 below (Mardaljevic et al., 2009).

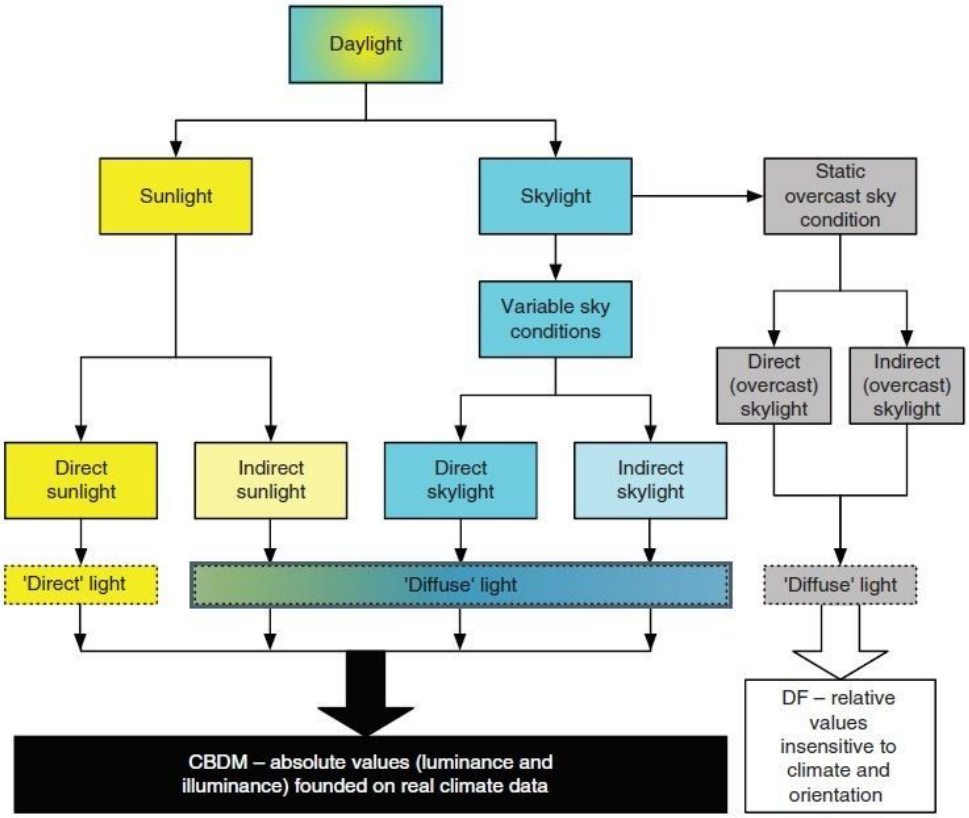


Figure 1.7 Relation of daylight components to DF and CBDM approaches (Mardaljevic et al., 2009)

1.7.3.2. Daylight factor

Daylight Factor (DF) is used to measure the level of daylight inside a room. It is defined as the quantity of light in a given point inside the indoor space in relation to the available daylight in the outdoor (Robertson, 2003), specifically under an overcast sky (Galatioto and Beccali, 2016), as illustrated in Figure 1.8. The formula of the DF is given as:

$$\mathbf{DF = E_{in} / E_{out}}$$

Equation 1

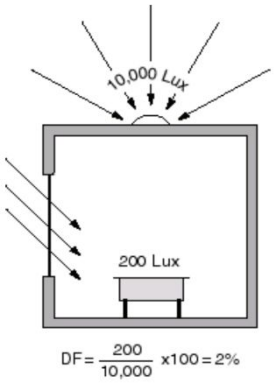


Figure 1.8: Daylight factor

1.7.3.3. Daylight autonomy

Daylight Autonomy (DA) is defined as the percentage of time when space is daylit only by means of daylight (Galatioto and Beccali, 2016).

$$DA = \frac{\sum_i (wf_i t_i)}{\sum_i t_i} \in [0, 1] \qquad wf_i = \begin{cases} 1 & \text{if} \quad E_{Daylight} \geq E_{lim} \\ 0 & \text{if} \quad E_{Daylight} \leq E_{lim} \end{cases}$$

Continuous daylight autonomy

Continuous Daylight Autonomy (cDA) was developed based on the daylight autonomy (DA) that cannot give relevance to lighting levels lower or higher than the threshold of the established lighting. Continuous Daylight Autonomy (cDA) has been developed by Rogers (2006). It defines the threshold value of selected tasks, for instance, an illuminance level below 500 lux. Furthermore, it offers time step values when the illuminance decreases less under the lowest level (Galatioto and Beccali, 2016).

Spatial daylight autonomy

Daylight Autonomy (sDA) is applied to evaluate if the received daylight inside the space during the year is adequate (Galatioto and Beccali, 2016). It is the percentage of floor area when at least 50% of the annual occupied hours obtain a minimum of 300 lux.

1.7.3.4. Useful daylight illuminance

Useful daylight illuminance (UDI) is a daylight measurement system that was developed by Nabil and Mardaljevic (2006). The UDI assess the issue of daylight performance through ranges of illuminance values to indicate if the level of indoor visual comfort is effectively maintained. The UDI is based on real weather data from a specific period of the year. Its parameters are divided into three steps: UDI fell-short, UDI achieved and UDI exceed. Their values are lower than 100lx (insufficient daylight), 100lx to 2000lx (useful daylight) and higher than 2000lx (visual discomfort) (Galatioto and Beccali, 2016).

Nabil and Mardaljevic (2006) found that the UDI is insufficient if it is less than 100 lx, effective if it is in the range of 100–500 lx, desirable or at least tolerable in the range of 500–2000 lx, and it produces visual or thermal discomfort when it exceeds 2000 lx. Therefore, the author used the range of 300-1000 lx in this study as an optimum UDI.

1.7.3.5. Annual Sunlight Exposure

Annual Sunlight Exposure (ASE) is applied to ascertain whether space is subject to overheating (Galatioto and Beccali, 2016), causing visual discomfort or increased cooling load as a result of receiving too much direct light. It is defined as the percentage of floor area when 1000 lux or higher is received for a minimum of 250 hours for the whole year. The utilisation of the ASE metric is necessary with the DA to investigate the percentage of the overlit areas, which is not considered in the DA as it does not have a high threshold. The ASE is useful to indicate if space is receiving excessive direct sunlight which could result in glare or increased cooling loads (Sterner, 2017).

1.7.3.6. Daylight uniformity

Daylight uniformity measures the quality of the light distribution within a space. It can be utilised to measure the distribution of illuminance level (lux or lm/m^2) and luminance (candela/m^2). The daylight uniformity has been defined by a number of different formulas. In order to assess the improvement of the daylight performance, the daylight uniformity at the work plane (DUWP) can be calculated. This can be accomplished by means of three methods. The first calculation method is defined in Equation 2 below. It is the result of the minimum illuminance value divided by the maximum illuminance value. In this calculation method, only two values are considered. It can be given as:

$$\mathbf{U1 = E_{min} / E_{max}}$$

Equation 2

where:
E_{min} is the minimum illuminance value (lux)
E_{max} is the maximum illuminance value (lux)

The contrast ratio is another calculation method that considers only the maximum and minimum values. However, it is more complicated than the ratio between the minimum to the maximum that has been mentioned previously. It can be defined as follows:

$$\mathbf{U2 = (E_{max} - E_{min}) / (E_{max}\ E_{min})}$$

Equation 3

On the other hand, the second calculation method considers the illuminance values for all the test points in the room, as described in Equation 4 below. It is the result of the minimum illuminance value (E_{min}) dividing by the mean of all points (E_{mean}). In this method, outputs that

are more reliable can be achieved compared with the first method mentioned above. Therefore, the second method has been utilised for the comparisons of the cases (Galatioto and Beccali, 2016). It is given as:

$$U3 = \frac{E_{min}}{E_{mean}}$$

Equation 4

$$U3 = E_{mean}\left(\frac{1}{N}\sum_{i=1}^{N} E_i\right)^{-1}$$

where:
E_{mean} is the mean illuminance value (lux) over a number of points (N).
(Moreno, 2010)

Finally, the non-uniformity, which is the opposite of the uniformity, has also been calculated. Non-uniformity is used to investigate the decrease in the quality of the light distribution inside the space. It is defined in Equation 5 below. It can be obtained by finding the difference between the minimum and maximum illuminance values then dividing the result into the maximum illuminance value. It is crucial to clarify that the non-uniformity equation addresses only the minimum and maximum illuminance values. Therefore, it does not consider the other illuminance values within the space leading to an inaccurate understanding of the light distribution quality inside the room.

The no uniformity metric (NU) can be used to avoid the errors that occur because of the local variations. It can be defined as the ratio of standard deviation to the mean, which is named by IESNA as coefficient variation, and it can be given as (Moreno, 2010):

$$NU = {}^{\sigma}E / E_{mean}$$

Equation 5

$$NU = \frac{\sigma E}{E_{mean}} = \left(\frac{1}{N-1}\sum_{i=1}^{N}\left[\frac{(E_i - E_{mean})}{E_{mean}}\right]\right)$$

where:
${}^{\sigma}E$ is the standard deviation.

In addition, there is another daylight uniformity metric (U4) that use the standard deviation and the mean of the values, which is defined as (Moreno, 2010):

$$U4 = E_{mean} \quad X \quad (E_{mean} + {}^{\sigma}E)^{-1}$$

Equation 6

1.7.3.7. Daylight glare index

Glare can be measured by daylight glare index (DGI). It is defined as a function of the source luminance, its background luminance, the source size and the location of the light source, and the viewing direction in relation to the window, as illustrated in Figure 1.10. Table 1.1 shows the acceptance level of the DGI (Boubekri, 2014). The equation of DGI is given as:

$$DGI = 10Log0.478\sum_{i=1}^{n}\frac{L_s^{1.6}\Omega^{0.8}}{L_b + 0.07\omega^{0.5}L_w}$$

Figure 1.9 Equation of daylight glare index (Boubekri, 2014)

where:

L_s: is the average luminance of each glare source in the field of view (candela/m 2)

L_b and L_w: is the background excluding the glare source (candela/m 2) and the window (cd/m 2) treated same as L_s, respectively.

ω: is the solid angle of the source seen from the point of observation (sr)

Ω: is the solid angle in steradians subtended by the source, modified for the effect of the position of the observer in relation to the source

n: is the number of glare sources

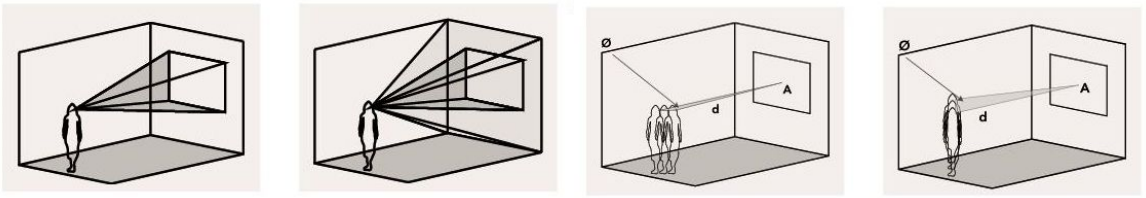


Figure 1.10 The luminance of the source (Boubekri, 2014).

Table 1.1: The position index of the window (Boubekri, 2014)

Zone	Acceptance level	DGI
Discomfort zone	Intolerable	>28
	Just tolerable	28
	Uncomfortable	26
	Just uncomfortable	24
Comfort zone	Acceptable	22
	Just acceptable	20
	Noticeable	18
	Just perceptible	16

1.7.3.8. Daylight glare probability

The daylight glare probability (DGP) is a functional index that is applied to measure discomfort. DGP was obtained by Guth (1963) through an experimental comparison of an office room. DGP considers the influence of subjects (Guth, 1963, Schiler, 2009, Luckiesh and Guth, 1949, Galatioto and Beccali, 2016). DGP is linked to the lighting perception of the users due to its dependence on vertical eye illuminance. It is applied to compare daylighting design options, and it can be calculated by means of DAYSIM (daysim.ning.com 2017). However, Galatioto and Beccali (2016) found that the equation does not take into account the glare that is produced by individual sources. In addition, Konstantzos et al. (2015) showed that when the sun is within the view level, the DGP is not precise.

However, Jakubiec and Reinhart (2010) recommended that the DGP is the most reliable metric that can provide the most possible outputs with fewer errors. This is due to its predictable response to most daylight situations with solid angle direct or specular luminance sources. The DGP has four levels, Imperceptible Glare (0.35 > DGP), Perceptible Glare (0.40 > DGP >= 0.35), Disturbing Glare (0.45 > DGP >= 0.40), and Intolerable Glare (DGP >= 0.45).

1.7.4. Definitions associated with glazing.

Glazing is a primary element of most daylighting systems that directly deliver daylight to a building through its facade or roof. The following points define a number of thermal and visible significant properties of glazing.

Solar heat gain coefficient (SHGC) is defined as the quantity of solar gain that passes the glazing area divided by the total solar energy on its external surface. Its value ranges from 0 for the opaque wall to 1 for a fully glazed façade. (Robertson, 2003). While it is desirable to have a high SHGC in a cool climate to allow more solar heating (AWS, 2015), in a hot climate, low SHGC is required to reduce heat gain, particularly in summer (Robertson, 2003).

Visible light transmittance (VT) is defined as the measurement of the visible spectrum passed through the glazed facade. High VT increases the daylight penetration. However, the SGHC value has to be considered to avoid overheating, Figure 1.11.

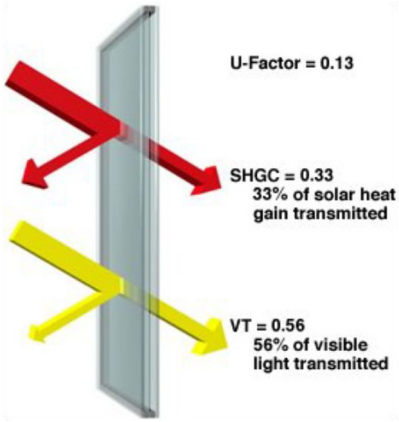


Figure 1.11 Solar Heat Gain Coefficient (Petermann, 2008)

The thermal transmittance (U-value) is defined as the measurement of heat transfer through the object. Tied insulation for window frame can provide a low U-value, leading to a decrease in heat loss and gain (AWS, 2015).

Low-emissivity (low-E) is the type of coating embedded between two or three layers of glass to reduce heat loss and gain (Robertson, 2003).

Switchable glazing is smart glazing that can be changed under specific impacts. Electrochromic glazing is changed by applying an electric current. Thermochromic glazing is changed by heat while photochromic glazing is influenced by light (Robertson, 2003).

1.7.5. Energy status

The energy consumption in the building section in most countries is about one-fifth to two-fifths of the final energy consumption (DOE, 2005, Janda, 2009, Pérez-Lombard et al., 2008). Additionally, the building industry uses 40% of materials, which emits about half of the greenhouse gasses (Prasad and Hall, 2005).

A review by the international energy agency concluded that, in non-residential buildings, the growth in the energy demand is increasing rapidly (Dubois et al., 2016). Furthermore, it is expected to rise by 26% in 2030 while the increase in residential buildings may rate at approximately 12% (Capros et al., 2008, Boyano et al., 2013). Another study by Pérez-Lombard et al. (2008) predicted that among the non-developed countries, the growth in the energy demand would increase by 100% over the next two decades. The usage of electricity among commercial buildings in some of economically wealthy countries in the global south, Japan and the USA is reaching an extremely high demand. According to Janda (2009), the

improvement in the quality of living and the development in the service sector causes an increase in demand for electricity, particularly in non-residential buildings.

Through the life of a building, 80% of the final energy is consumed during the operation stage (Sisson and Van Aerschot, 2007). Artificial lighting is one of the major factors which could account for 15% to 60% of the final amount of energy used in the building (Spyropoulos and Balaras, 2011). Therefore, energy policy at regional, national and international levels currently considers energy efficiency in buildings to be a prime objective (Pérez-Lombard et al., 2008).

The office building envelope in a cooling-dominated climate is regarded as a major source that influences the energy consumption of a building (Fasi and Budaiwi, 2015). The typical office building consumes about one-third to half of the energy used for the purpose of lighting (Crawley et al., 2008). On the other hand, some of the developing countries, which include 25% of the globe's population, have to use environmentally unsound energy sources such as kerosene (Mills, 2005, Bhusal et al., 2007) due to the lack of electric energy available in those regions. Jomoah et al. (2013) stated that lighting and air-condition consume the majority of the electrical energy in buildings located in Saudi Arabia.

1.7.5.1. Energy consumption in Saudi Arabia

The electricity consumption in Saudi Arabia has increased significantly throughout the last two decades. The statistical data provided by the Saudi Electricity Company (SEC) shows that electricity consumption increased by 91% from 2000 to 2014. The average growth rate from 2000 to 2014 was 6.5 % 11.5 TWh (SEC, 2015). The total annual energy consumption was 114 TWh in 2000. It increased rapidly to reach 274.5 TWh in 2014, and the average annual consumption was 181 TWh. The residential sector has recorded the highest total energy consumption among the other sectors in 2014 and during the whole period. Detailed total energy consumption in Saudi Arabia by sectors is presented in Appendix 1.

The tables illustrate the sold energy in GWh by consumption types in Saudi Arabia from 2000 to 2014. It is apparent that the degree of consumption has increased significantly over the last 15 years by around 160 GWh from 114.161 GWh to 274.502 GWh. The growth rate in energy consumption recorded a very high percentage which reached 140.5% for the total period, while the average annual growth rate was 6.5% (SEC, 2015). See Appendix 1.

Although the residential sector consumes the highest amount of energy, the potentiality of saving energy by utilising daylight is higher in the non-residential sector, specifically in

educational and office buildings. This is due to the operation period of these buildings. Educational and office buildings are part of the governmental and commercial building sectors. Detailed data of the sold energy and the number of customers by consumption types (GWh) in Saudi Arabia from 2000 to 2014 is shown in Appendix 1.

The pattern of the energy consumption for the residential building shows that the high demand for electricity consumption exists during the early morning and the late evening periods where the availability of daylight generally is limited. On the other hand, in the office and educational buildings, the operation period starts typically after sunrise and ends prior to sunset, particularly in regions with hot climates such as Saudi Arabia, where the earliest sunset time in winter is 17:00.

Data on electricity consumption in Saudi Arabia from 2000 to 2018 was published by the Ministry of Environment, Water and Agriculture in Saudi Arabia. The lower electricity consumption was 114 TWh in 2000, while the peak consumption was 290 TWh in 2018. The increase in consumption from 2017 to 2018 was 28807 TWh. The average consumption over 18 years was 193.5 TWh, as shown in Figure 1.12 (CEIC Data, 2020).

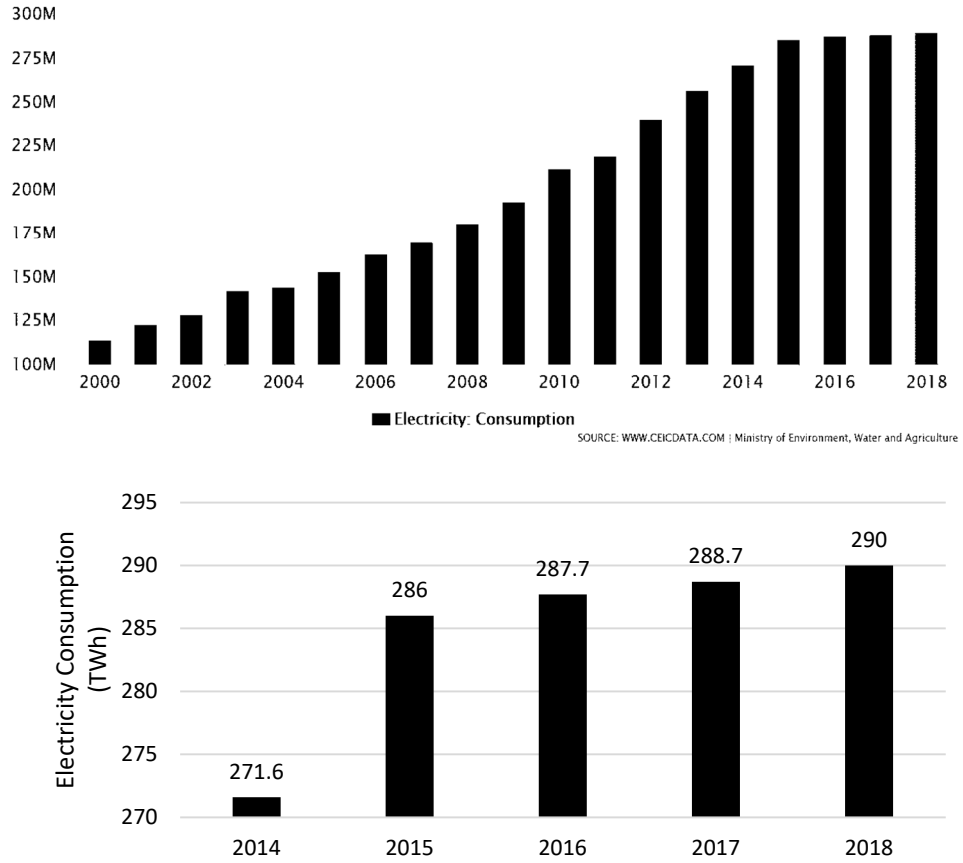


Figure 1.12: Annual energy consumption in Saudi Arabia, from 2000 to 2018 (above), and 2014 to 2018 (below) (CEIC Data, 2020).

The brief procedure of the energy calculations

In order to investigate the importance of saving energy due to artificial lighting, the energy consumption of this factor was calculated. Although many studies have been conducted in the field of daylighting in buildings, there is a lack of knowledge regarding the total annual energy consumption due to lighting in office buildings in Saudi Arabia. The previous studies have calculated the energy due to lighting for a limited number of buildings, and the published data by the SECC for the energy consumption is the total consumption, which is based in the building sector regardless of the type of consumption. Therefore, the energy consumption due to lighting was calculated based on the published data by the SEC for the total energy consumption through the following procedure:

1. To find the total energy consumption in Saudi Arabia from Saudi Electricity Company (SEC) data
2. To obtain the average energy consumption due to lighting through the previous studies
3. To calculate the energy consumption due to lighting in Saudi Arabia

Previous studies (Mohammed and Budaiwi, 2013) and (Altan and Alshareef, 2015) have calculated the energy consumption due to lighting for different buildings in hot climates. They found that lighting could consume from 11 to 14 per cent of the total energy consumption. Another study reported that the global average energy consumption due to lighting in buildings is 20 per cent (Dubois et al., 2016).

The estimated energy consumption due to lighting is less than the global average by about 6%. The variation in the estimation may be due to the variation of the daylighting availability between the low and the high latitude regions. The length of the day is longer at low latitude regions. Furthermore, the sky condition is clear for most of the year.

Based on the annual growth in energy consumption over the previous 14 years, it can be predicted that the energy consumption due to lighting has also increased. Therefore, the percentage of the consumed energy due to lighting was estimated as 15% of the total annual energy consumption.

Energy Consumption due to Lighting in Saudi Arabia

The energy consumption from artificial lighting was calculated for Saudi Arabia as a reference. The calculation utilized the data published by the Saudi Electricity Company (SEC), the only company providing electricity in Saudi Arabia. The data covers the electricity consumption over 14 years for all building sectors.

As mentioned previously, it was found that the minimum energy consumption due to lighting in buildings is approximately 15%. According to SBC data (2015), the total energy consumption in Saudi Arabia from 2000 to 2014 was 2,716.5 TWh. As a result, the energy consumption due to lighting was approximately 407.5 TWh.

As the average annual consumption was 181 TWh, then the average annual consumption due to lighting can be calculated using the following equation:

Annual Average Energy Consumption due to Lighting = Annual Average Energy Consumption X Percentage of Annual Average Energy Consumption due to Lighting

Equation 7

Annual Average Energy Consumption due to Lighting = 181 TWh X 0.15

Annual Average Energy Consumption due to Lighting = 27 TWh

The annual average energy consumption due to Lighting for all sectors was 27 TWh. The highest energy consumption due to lighting was consumed by the residential sector by 20.4 TWh in 2014, and the average annual consumption was 13.8 TWh. On the other hand, the lowest average annual consumption was 516 GWh by the agricultural sector.

However, the highest growth rate during the 15-year period was recorded by the commercial sector by 330%, with an 11 % average annual growth rate. While the industrial sector recorded the lowest growth rate by 86%, with a 4.5 % average annual growth rate. Detailed energy consumption due to lighting in Saudi Arabia was calculated and is illustrated in Figure 1.13 and Table 1.2.

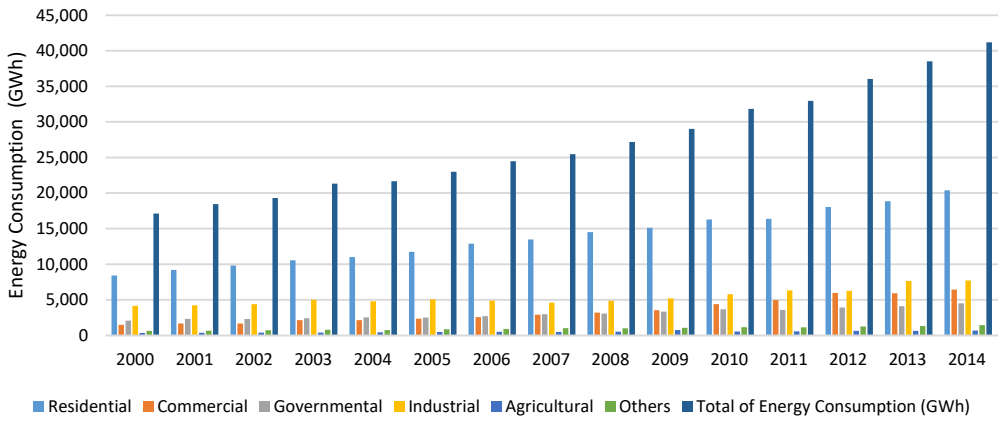


Figure 1.13 Energy Consumption due to lighting in Saudi Arabia from 2000 to 2014

Table 1.2: Energy Consumption due to lighting in Saudi Arabia from 2000 to 2014

		Sector						Total of Energy Consumption (GWh)
		Residential	Commercial	Governmental	Industrial	Agricultural	Others	
Year	2000	8,409	1,495	2,084	4,149	340	647	17,124
	2001	9,201	1,672	2,319	4,235	357	658	18,442
	2002	9,819	1,667	2,300	4,398	396	715	19,294
	2003	10,556	2,147	2,420	5,007	400	799	21,329
	2004	11,005	2,145	2,516	4,796	438	758	21,658
	2005	11,746	2,337	2,501	5,070	475	864	22,993
	2006	12,904	2,561	2,701	4,882	507	917	24,473
	2007	13,485	2,916	2,970	4,595	475	1,025	25,467
	2008	14,503	3,205	3,069	4,863	519	1,006	27,165
	2009	15,125	3,541	3,337	5,198	759	1,061	29,021
	2010	16,294	4,397	3,677	5,785	543	1,143	31,839
	2011	16,389	4,951	3,588	6,319	568	1,134	32,949
	2012	18,037	5,971	3,913	6,257	629	1,236	36,043
	2013	18,852	5,925	4,108	7,662	644	1,313	38,503
	2014	20,386	6,428	4,502	7,725	687	1,448	41,175
Total of Energy Consumption for 15 Years (GWh)		206,711	51,359	46,004	80,942	7,736	14,724	407,475
Average Annual Consumption (GWh)		13,781	3,424	3,067	5,396	516	982	27,165
Growth Rate During Period (%)		142.4	329.9	116.0	86.2	102.1	123.9	
Average Annual Growth rate (%)		6.5	11.0	5.7	4.5	5.2	5.9	
							Average Growth rate during period (%)	140.5
							Average annual growth rate during period (%)	6.5

Chapter 2. Literature review in daylighting technologies

This study was initiated with an extensive review in two areas, daylighting technologies and innovative glazing. Firstly, the search covered most of the available daylighting technologies found in the previous studies. This chapter provides a review and discusses the state-of-the-art daylighting technologies. It shows the availability of daylighting products and the limitations of the implementation of these technologies. Lastly, it concludes with a comparison that shows the advantages and disadvantages of the different systems.

2.1. Introduction

Daylight is a clean source that can be employed through affordable costs to illuminate the interior built environment. In low latitude regions with clear sky conditions, there is a sufficient amount of sunlight to provide daylight within buildings. However, the main obstacle is that the direct solar radiation of a clear sky can cause glare and overheating, hence, this may lead to high cooling load and thus increase energy consumption (Sherif et al., 2012a). In order to achieve sustainable building's interior, daylight technologies should be optimised by employing suitable solar daylighting devices in low latitude regions. Nevertheless, various obstacles hinder the utilisation of the sunlight in these regions. One of the main challenges is high solar irradiance level and the fact that the sun light strikes the building from the zenith (Al-Obaidi et al., 2017).

Fenestration systems significantly influence energy consumption and occupant comfort due to the amount of heat and solar gain that pass through their transparent materials (Appelfeld et al., 2012). In low latitude regions, the impact of the glazed facades is notable. It has been found that many office buildings have a medium to a high window to wall ratio (WWR). This consequently impacts strongly on heat gain in addition to the internal heat gain that is produced by the artificial lighting and the amount of required office appliances (Mainini et al., 2015). Therefore, the design of a fenestration system must meet the balanced performance of daylighting and thermal comfort (Mainini et al., 2015, Giovannini et al., 2015).

According to (ASHRAE Handbook) 1997, if the glazed façade is shaded adequately, a significant reduction of solar heat gain can be obtained. Many studies have been done in daylighting for high latitude regions. These have led to the production of well-developed

commercial daylighting products, yet they are suitable for only high latitude regions. On the other hand, the availability of sufficient commercial daylighting systems for low latitude regions is quite limited. Therefore, this review aims to evaluate the current daylighting technologies to investigate the amount of knowledge in the field in order to conclude the research gap that should be investigated to provide adequate indirect daylight without compromising on either the visual or the thermal comfort as well as reducing the cooling load and therefore to enhancing energy and building performance.

2.2. Daylighting systems

Daylighting systems can be categorised, based on their function, into four main categories: daylight redirection systems, daylight filtration systems, daylight transport systems and skylights systems.

2.2.1. Daylight redirection systems

The main function of the daylight redirection systems is to redirect direct sunlight and to diffuse skylight into the interior spaces. The redirection of daylight can be obtained by the reflection and refraction of the sunlight beam by means of different technologies, for instance, prismatic elements, concave geometries, or metallic coated surfaces. The daylight redirection systems include three sub-categories, namely, louvres, light shelves and light-redirecting elements.

2.2.1.1. Louvres

As a sub-category of the daylight-redirection systems, Louvres can be divided into five types of devices: external louvres, blinds, optical louvre systems (OLSs), and micro sun-shading louvres or shutters.

External louvres:

Louvres are a daylighting system utilized as shading devices to redirect daylight and reduce glare (Palmero-Marrero and Oliveira, 2010, Knoop et al., 2016, Ruck et al., 2000). They have various configurations, and they can be arranged horizontally, vertically or at sloping angles.

External louvres and internal blinds can be made from various materials (Ruck et al., 2000, Knoop et al., 2016). External louvres are typically made of painted aluminium or coating steel, and in order to increase the durability and reduce the required maintenance, they are fabricated from PVC (Ruck et al., 2000). They often are utilized as external shading devices, and they

influence the architectural and structural design of the building. Figure 2.1 shows an example of an external louvre shading system.

In addition, they require frequent maintenance in polluted climates, particularly if they are operated automatically. Their influence depends on the orientation of the façade, the tilt angle of the slats, and their reflected surface characteristics. Depending on their tilt, louvres can decrease the direct incident light by 60% to 90%. As a result, they can contribute to an approximate energy-saving rate of 20% in summer and 80% in the winter (Knoop et al., 2016). The applications of louvre systems are spread for the purpose of solar protection, which can lead to cooling load reduction (Palmero-Marrero and Oliveira, 2010).

Their influence on the level of the illuminance depends on the tilt of the slat and the altitude of the sun. For instance, the light transmission is 60% to 80% if the tilt of the slat is 30 degrees and the solar altitude is 30 degrees as well, while it decreases to 50% to 75% and 45% to 60% when the solar altitude increases to 45 degrees and 60 degrees, respectively. The light transmission when the tilt of the slat is 45 degrees, and the solar altitude is 45 degrees. It is approximately 30% to 50%, while it decreases to 20% to 40% and 30% to 50% at the same slat slope when the solar altitude increases to 60 degrees. The light transmission can be even decreased more to 10% to 25% if the tilt of the slat and the solar altitude are both at 60 degrees. Louvres can be made from glass, which can provide higher light transmittance. However, in order to control the solar gain and the glare, the utilisation of diffuse glass is required. In addition, this shading system can be integrated with PV systems (Knoop et al., 2016).

Palmero-Marrero and Oliveira (2010) carried out a study on the impact of the louvre shading system for different facades and different latitudes, namely, Mexico in Mexico, Cairo in Egypt, Lisbon in Portugal, Madrid in Spain and London in the UK. The study focused on the impact of the horizontal and vertical louvre on energy consumption and indoor thermal comfort. It was found that this shading system leads to indoor thermal comfort and may decrease the energy consumption compared to a building without a shading system.

Hammad and Abu-Hijleh (2010) investigated the impact of external dynamic louvres with a light dimming strategy on the energy performance of an office building in Abu Dhabi in the UAE. Simulation by IES-VR software was utilised for the prediction of energy consumption. Their results showed that the dynamic louvres with light dimming strategies archived energy saving by 30% to 34% compared with a daylighting system using a light dimming strategy which achieved saving energy by 24% to 25 %. In addition, they found that the optimal angle

for the static louvres for the south facade is -20 degrees while it is 20 degrees for the east and west facades.

(Freewan et al., 2009) studied the influence of the ceiling geometries on the performance of louvres through an experiment and computer simulation using Radiance for a room in a low latitude region. The tested daylighting variables were the illumination level and the distribution uniformity. They found that the illumination level increased in the back of the room and decreased in the front of the room when the ceiling geometry was changed, compared to a room with a flat ceiling. The best geometry of the ceiling was the chamfered shape in the front and back area of the room. On the other hand, Knoop et al. (2016) stated that louvres could provide good daylighting distribution, increase thermal and visual comfort, and contribute to energy saving. However, the payback period of the system is long.

Huang et al. (2014) analysed the thermal and daylighting performance of low-emissivity glazing, internal blinds, and overhang shading devices for an office building in four cities in low latitude regions Singapore, Hong Kong, Miami and Houston. Another study focused on the visual connection with the outdoor environment through tilted louvres, and it was compared to three other shading devices, namely, overhang, blind and light shelf (Lavin and Fiorito, 2017).



Figure 2.1 External louvres system, Traffic Control Headquarters, Spain (Tectonica-online.com 2009)

***Blinds**:*

Blinds are solar shading systems applied to block or redirect the daylight based on their angle of slope. They are made of a number of lamellas arranged horizontally or vertically, as shown in Figure 2.2. The size, properties of the material, such as the reflectivity and the colour of the surface, can influence their performance. Blinds are often placed in the internal façade, and they can be placed as external shading devices. However, it is important to take into

consideration their limited resistance to the wind and the required frequent cleaning if applied as an external shading system in high-rise buildings (Knoop et al., 2016).

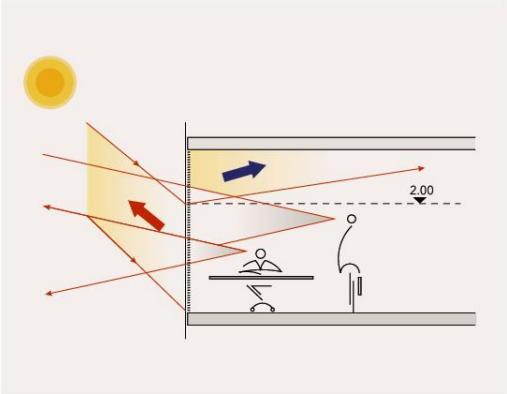
Blinds are retractable so that occupants can adjust their slope based on the incident slope; however, this can be one of the downsides of this shading system where the preference of the occupants varies. If blinds are placed in the external facades, they could perform better in reducing heat gain. However, the control is more complicated. Nevertheless, moderate energy-saving and glare protection can be achieved by utilising a blinds system (Knoop et al., 2016).



Figure 2.2 Internal Venetian blinds for office buildings (dolsoninteriors.com 2017)

Optical louvre system:

The optical louvre system (OLS) is a commercial product produced by LightLouver LLC, known as LightLouver™. It is fabricated in a concave shape with a highly reflective material. The principles of the OLS are to redirect the daylight to the deep areas of the room while blocking the direct sunlight on the front area. It is notable that the view toward the outside is fully obstructed by the system, as illustrated in Figure 2.3



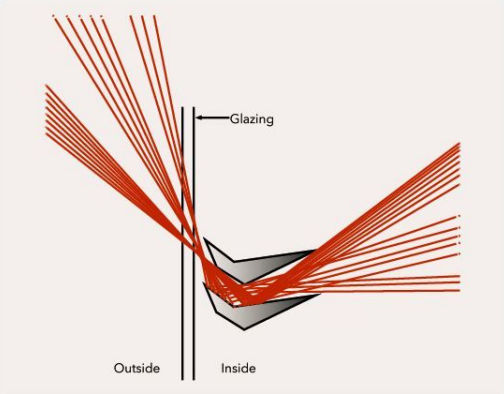




Figure 2.3 Optical louvres system applied in the top of the window (Boubekri, 2014)

A study on an optical louvre system (OLS) was conducted by Konis and Lee (2015) through an experimental test in Berkeley, California (latitude 37°N). The OLS was placed on top of the window "clerestory". The geometry of the OLS was developed and compared with conventional Venetian blinds (VB) that were utilised as a reference condition, as shown in Figure 2.4. The study used daylight autonomy (DA), window luminance and ceiling luminance uniformity as daylighting performance indicators. The results showed that under the sunny sky conditions, the OLS compared with the Venetian blinds improved the daylight level in the deep area of the room while reducing glare. However, it was found that the Venetian blinds produced higher daylight autonomy, but caused discomfort by producing glare. Notably, a sessional variation was recorded for both systems.



[A] [B] [C]

Figure 2.4 OLS system and its interior view [A] and [B], Venetian blinds [C] (Konis and Lee, 2015)

Micro sun-shading louvres:

Micro sun-shading louvres are daylighting systems that consist of a high specular micro geometry coating between two pans of glazing. This daylighting system is applied for top-lighting purposes in a horizontal orientation or with a slight slope. The solar heat gain coefficient (SHGC) of the micro sun-shading louvres is low, about 10% to 15% (Knoop et al.,

2016). However, the variation in the SHGC of this system is not available (Knoop et al., 2016), as shown in Figure 2.5.

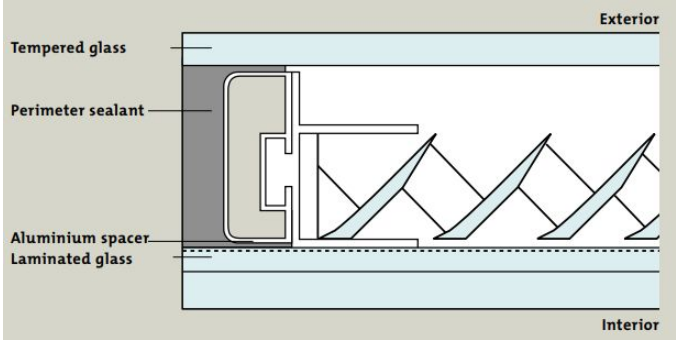


Figure 2.5 Edgework detail of a micro sun-shielding louvre (Eckelt.at 2017)

Shutters:

Shutters are shading devices that can provide buildings with essential solutions in terms of daylight control, solar shading, dynamic façade U-value, natural ventilation and noise reduction. They can be turned on the horizontal or vertical axial of the façade; however, they cannot be applied to a wholly glazed façade, as illustrated in Figure 2.6 (Knoop et al., 2016).

A study compared the shutter system with double and triple low-emissivity glazing. It was found that the transmission heat loss is reduced by 30% when the shutter is in the closed mode, while it allows 85% and 34% of the solar gain when it is in the withdrawn mode for the shutter with double and triple glazing, respectively (Knoop et al., 2016).

The energy performance of the shutter system can be enhanced by utilising an automated operation. In addition, it can improve the thermal and visual indoor environment. Shutters can be applied for flat vertical facades of all orientations. Shutters have relatively high initial and running costs; however, they can provide many benefits that double-skin facades can provide (Knoop et al., 2016).



Figure 2.6 Shutter (Knoop et al., 2016)

2.2.1.2. Light Shelfs

A light shelf is a daylighting system with a typically horizontal orientation, and it can be an internal or an external shading system. The light shelf can be built within the façade or be attached to it afterwards. The light shelf, in general, is located over the level of vision, where it allows the occupant to have an external view through the lower part while it redirects the daylight to the internal ceiling through the top side, as shown in Figure 2.7. In order to optimise the performance of a light shelf, advanced optical systems are employed, to enhance the redirection of the daylight to reach deeper spaces. The purpose of the light shelf is to avoid glare and send the daylight to the deep area inside the space while allowing the occupant to have a view toward the outdoor environment. The selection of a light shelf position depends on several factors, namely, the height of the ceiling, the eye level of a standing person and the configuration of the interior space. However, it is recommended that the position of a light shelf set at a low level. It has been found that, in general, the glare and the amount of daylight reflected by the ceiling increases when the level of the light shelf decreases (Ruck et al., 2000).



Figure 2.7 Light shelves made out of semi-transparent reflective glass (Littlefair, 1996, Ruck et al., 2000)

External light shelf:

Full-scale and small-scale model measurements have shown that the daylight factor is less in a space that is daylit by a window with an internal light shelf compared to that without a shading system (Aiziewood, 1993, Christoffersen, 1995, Michel, 1998, Ruck et al., 2000, Littlefair, 1996). On the other hand, the utilisation of an external light shelf in some cases can provide the interior space with a daylight level equivalent to that in a daylit space that has a window without a shading system. In addition, the external light shelf can provide higher illuminance uniformity distribution compared to the conventional window with the same area depending on its geometry (Ruck et al., 2000).

However, it was found that a light shelf can increase the uniformity of daylight distribution but it could not reduce glare on the vertical façade when a direct sunlight incident is received. As a result, the system requires integration with another shading system to provide the occupant with glare protection. Blinds set at 45 degrees have been integrated with a light shelf, and the result has shown improvements in the performance of the glare protection (Ruck et al., 2000). An example of external light selves and their concept is illustrated in Figure 2.8 below.

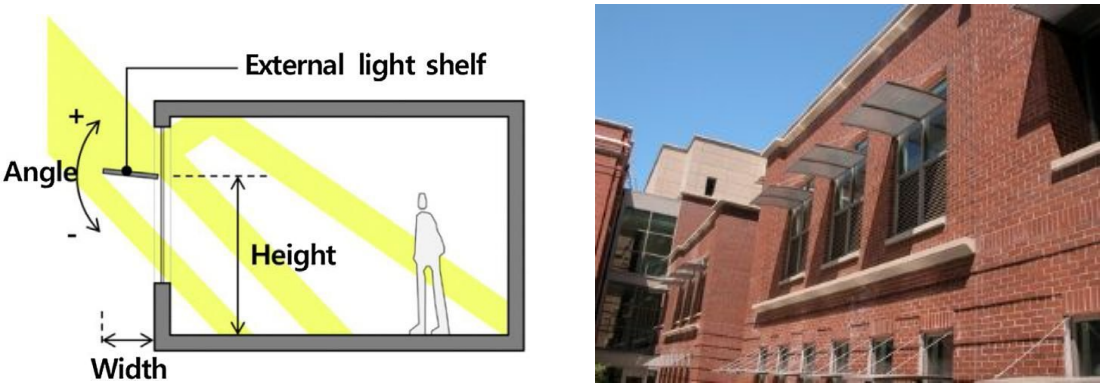


Figure 2.8 External light shelf characteristics and concept (left) (Lee et al., 2017). External light shelves at the University of Oregon (right) (tboake.com 2017)

Internal light shelf:

In tropical and sub-tropical regions where the latitude is low, direct sunlight can be prevented by increasing the depth of internal light shelves. It can be noted that, in winter, the light shelf alone does not adequately control glare, as shown in Figure 2.9. Figure 2.10 shows an interior view of an office with internal/external-light shelves. Figure 2.11 shows a sun-tracking light shelf system called the VALRA (Variable area light-reflecting assembly) that reflects the daylight through the ceiling (Howard et al., 1986, Ruck et al., 2000).

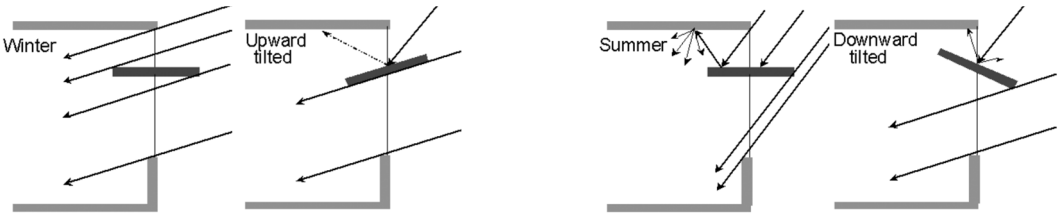


Figure 2.9 Top section of interior/exterior light shelf (Ruck et al., 2000)



Figure 2.10 Internal/external-light shelves, SMUD Head Quarters, California (Ruck et al., 2000)

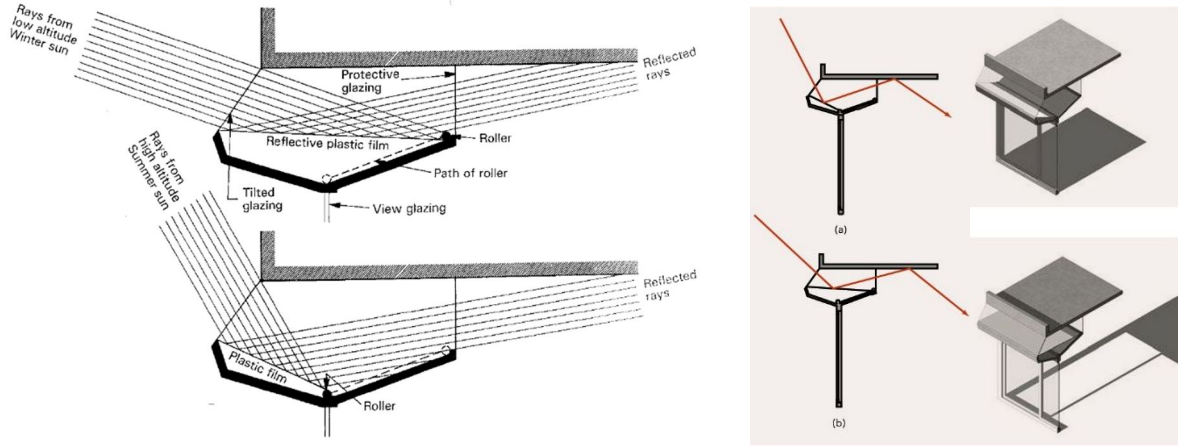


Figure 2.11: Winter and summer operation of the VALRA (Ruck et al., 2000, Littlefair, 1996, Howard et al., 1986) (left), and (Boubekri, 2014) (right).

Perforated light shelf:

However, light shelves could redirect the daylight into the deep area of the building. The risk of destruction by high wind pressure is possible, particularly if applied on high-rise buildings. Therefore, Lee et al. (2017) have proposed a perforated light shelf that may reduce the impact of wind pressure, as shown in Figure 2.12.

It was found that the lighting energy consumption was reduced by 51% to 74% comparing with a non-perforated light shelf. Thus, the increase in the width of the light shelf might enhance its performance. However, this study did not indicate the influence of wind pressure on the perforated light shelf due to limitations on the wind tunnel test (Lee et al., 2017).

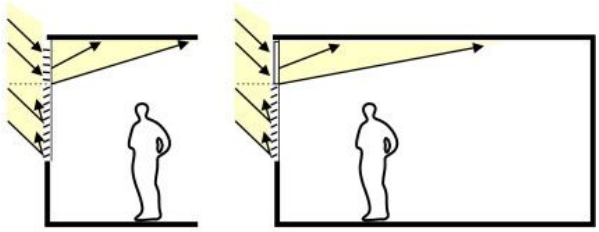


[A] [B] [C]

Figure 2.12: Section of testbed [A], and a non-perforated and a perforated light shelf [B] and [C](Lee et al., 2017)

2.2.1.3. Light-redirecting glazing

Light-redirecting glazing is a daylighting system that redirects the received sunlight incident to the deep areas inside the building to enhance the illumination level and uniformity of the daylighting distribution within the interior environment as illustrated in Figure 2.13. This comes in different configurations and materials, and can be non-sun tracking or sun-tracking systems. The angle of reflection is the most significant factor that influences the performance of a light-redirecting element. They include prismatic panels, anidolic lighting systems, laser cut panels, micro lamellae, and microstructured glazing.



[A] [B]

Figure 2.13 Light-redirecting louvres [A], and light- redirecting glazing [B] (Klammt et al., 2012)

Prismatic panels

Prismatic panels are redirection daylight devices that consist of thin clear acrylic in a serrated shape, which reflect direct sunlight but transmit other forms of light, as illustrated in Figure 2.14. They are typically coated by two panes of glass for protection against mechanical damage or dust. However, in some recent projects, prismatic panels have been used without protection, where the problem of dust and dirt collection was minimized by orienting the prisms downwards (Laar and Grimme, 2002).

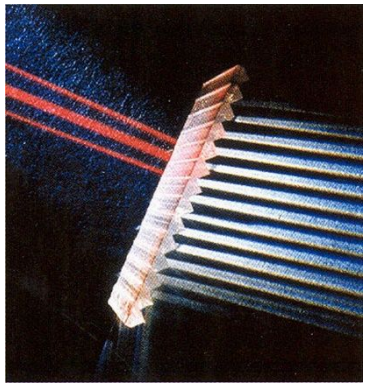


Figure 2.14 Prismatic sheets (uk.archello.com 2004)

Prismatic glazing is made to redirect the received incident by means of refraction and reflection (Boubekri, 2008). As aforementioned, the principles of prismatic panels are to provide shading and redirect sunlight to reach the depth of the room. Part of the daylight is reflected when it hits the ceiling to reach the deep areas in the room, while the other part is reflected downwards to the front of the room. As a result, daylight distribution uniformity can be enhanced (Shi and Chew, 2012, Mashaly et al., 2017), as shown in Figure 2.15. Prism structures that are used in daylighting applications are illustrated in Figure 2.16 below.

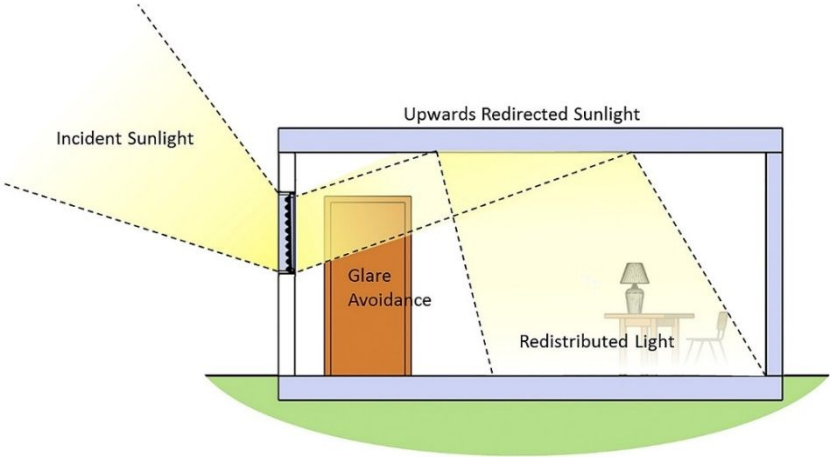


Figure 2.15 The function of a light redirecting system (Mashaly et al., 2017)

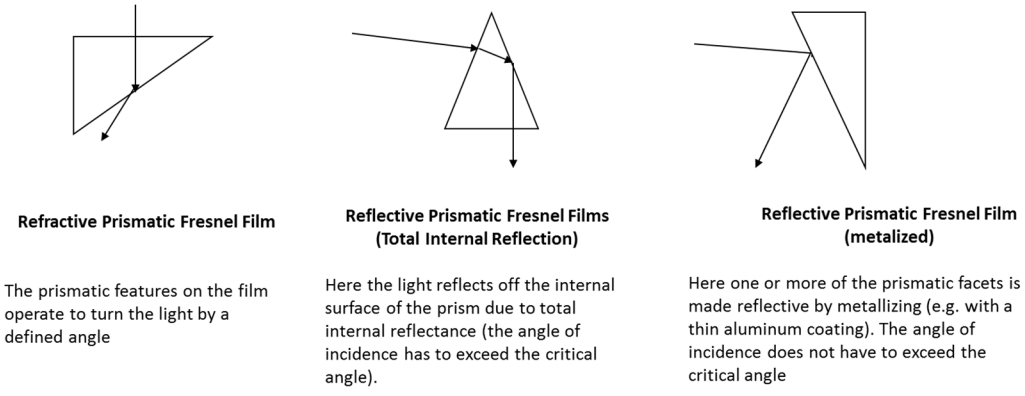


Figure 2.16 Prism structures are used in daylighting applications (microsharp.co.uk 2011)

Prism panels can be applied as shading devices on all façade orientations as well as top lighting and could improve lighting uniformity and thermal comfort and reduce energy consumption by reducing the cooling and heating load and use of artificial lighting. This daylighting system is transparent; however, it does not allow a view of the outside, as shown in Figure 2.17 (Knoop et al., 2016, Ruck et al., 2000). One of the technical obstacles of prismatic panels is that some of the redirected sunlight may be reflected downwards, causing glare. Furthermore, due to the high coefficient of expansion, prismatic panels have the required thermal expansion. Moreover, an awareness of fire regulations is necessary when such a system is applied (Ruck et al., 2000).



Figure 2.17 External and internal view of Rutec tower (Subtilitas.site 2017)

Mashaly et al. (2017) conducted a study of two types of prism panels; both comprised a Poly-methyl-meth-acrylate (PMMA) layer, single-sided and double-sided prisms, as illustrated in Figure 2.18. It was found that the single-sided prism performed better in redirecting the daylight to the deep areas without causing glare. However, it is essential to note that a significant variation was recorded between the simulation results in RADIANCE and real measurements due to external environmental factors (Mashaly et al., 2017), as shown in the graphs in Figure 2.19.

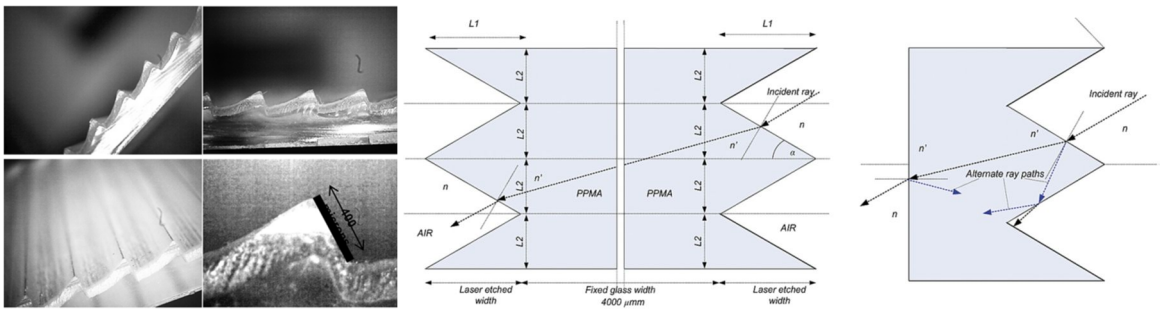


Figure 2.18 Microscopic pictures of PMMA sheets (left), and double-sided and single-sided prisms (right) (Mashaly et al., 2017)

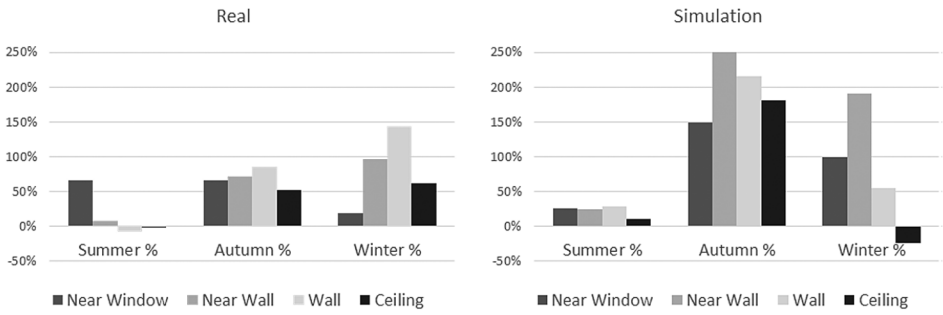


Figure 2.19 Variation between simulation results in Radiance and real measurements (Mashaly et al., 2017)

A study by McNeil et al. (2017) analysed the lighting energy saving and glare protection of a prismatic film compared with Vientiane blind in an office building in four climates, namely, Houston (29°N latitude), Chicago (41°N latitude), Sacramento (38°N latitude) and Burbank (34°N latitude). The performance of the system in a deep open office (12m) was evaluated for the south and east facades through goniophotometric measurements and a ray-tracing simulation in Radiance. It was found that the optimal angle for the prismatic film was between 18 and 35 degrees and within 45 degrees plus or minus the angle of the normal incidence to the window plane. Further, results showed that a lighting energy saving of 39 to 43 % was achieved by means of the prismatic film. In addition, the system controlled glare occurring in parallel to the window; however, it produced glare for occupants at seat level (McNeil et al., 2017). Klammt et al. (2012) stated that discomfort that occurs through the use of pure prisms could be averted through the utilisation of lens-like geometries.

Laser-cut panels

Laser-cut panels (LCPs) are thin acrylic panels divided into rectangular laser cuts. The cuts make a surface like a small internal mirror that redirects daylight into the depth of the room (Ruck et al., 2000, Knoop et al., 2016). LCPs have a similar optical principle to that of other daylight redirecting devices. The received daylight is reflected by the LCP toward the ceiling while sun rays from an undesirable angle are rejected, as illustrated in Figure 2.20 (Boubekri, 2014).

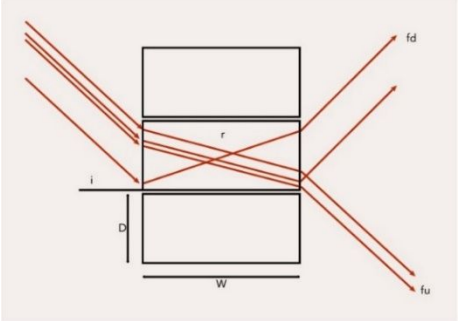


Figure 2.20 The basic optical principle of LCP (Boubekri, 2014)

The performance of laser cut panels is better under sunny sky conditions and with direct sunlight. Laser-cut panels should ideally be placed in the upper part of the window to redirect daylight toward the ceiling. The daylight from an angle lower than 30 degrees will pass through the panel (Knoop et al., 2016). Therefore, protection from glare needs integration with another daylighting system. Knoop et al. (2016) stated that utilising LCPs can enhance the daylight distribution uniformity by increasing the daylighting level in the deeper areas by 10% to 30%. Nevertheless, it was indicated that LCPs distort the view toward the outside. However, Ruck et al. (2000) showed that LCPs can maintain a connection with the outdoor environment, as shown in Figure 2.21.

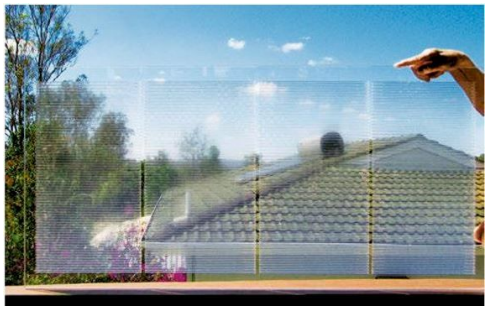


Figure 2.21 View through a laser-cut panel (Boubekri, 2014)

The laser-cut panel is easy to be installed between two layers of glasses. However, mechanical control may be required due to the significant impact of the panel position on the daylighting performance, which may lead to higher maintenance requirements (Knoop et al., 2016).

Edmonds (2005) studied the impact of daylight redirecting panels on daylighting performance in an obstructed room within the lower level of a high-density building in a dense urban area of Hong Kong (22° N latitude). It was found that the daylight factor in the deep areas of the room may be increased by three times if the tilt angle of the daylight redirecting panels equals half the obstruction angle. The geometry of light incident from obstruction angle ΘL is illustrated in Figure 2.22, where β is the tilt angle of the panel, NN is the normal of the panel and light is redirected horizontally into the room.

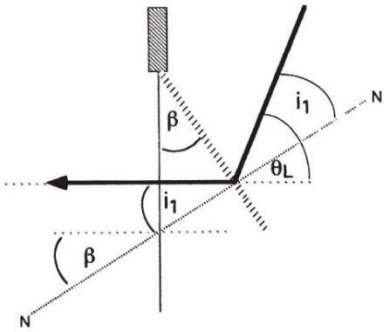


Figure 2.22 Light incident geometry received from obstruction angle (Edmonds, 2005)

Micro lamellae

Micro lamellae are strips with small perforations, made from stainless steel mounted between two low-emissivity layers of glass (Knoop et al., 2016). MicroShade is a commercial product of the micro lamellae daylighting system, as shown in Figure 2.23 (left). Micro lamellae block the sunlight from high altitude sun and provide a visual connection with the outdoor environment, as can be seen in Figure 2.23 (right). However, this system cannot protect from glare. Micro lamellae do not require maintenance, and can be applied in horizontal or vertical windows and large scale glazing facades (Knoop et al., 2016).

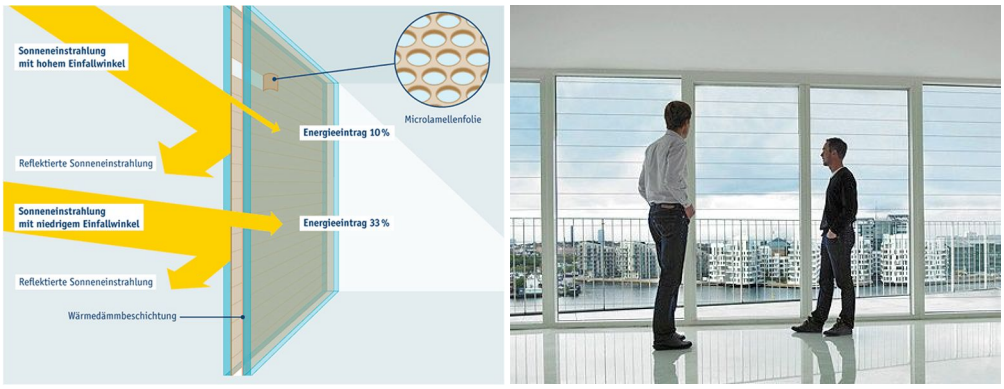


Figure 2.23 MicroShade, (baulinks.de 2017) (left) and (saint-gobain-lounge.de 2017) (right)

Microstructured glazing

Microstructured glazing is the type of daylight redirection element whereby film with microscopic structures is applied between two panels of glass or to the inner surface of the daylighting device. The main principle of microstructured glazing is similar to that of other redirecting elements, where its function is to redirect the daylight to the ceiling and then to deep areas while rejecting the undesired direct sunlight. The main advantage of this daylighting system is its microscale size which is around 20 to 500 micrometres (Knoop et al., 2016).

Microstructured glazing provides bidirectional scattering distribution functions. Many types of microstructured glazing has been researched, and a number of commercial products are available. The efficiency of microstructured glazing is influenced by a number of factors, namely, transmittance, sky conditions, climate, orientation, size of window and lighting requirements (Knoop et al., 2016).

Several microstructured glazing systems apply a prismatic film. A prismatic film is a thin layer made from plastic the structure of which has optical principles of prisms, specifically, total internal reflection (TIR). Figure 2.24 shows an example of a prismatic film with an inclined angle at 45 degrees. The light angular acceptance is 30 degrees, which is identified by the

refractive index. The prismatic film rejects the daylight beam that does not meet that angle. Further, the prismatic film can be made from a mirror or transparent material (Vázquez-Moliní et al., 2012).

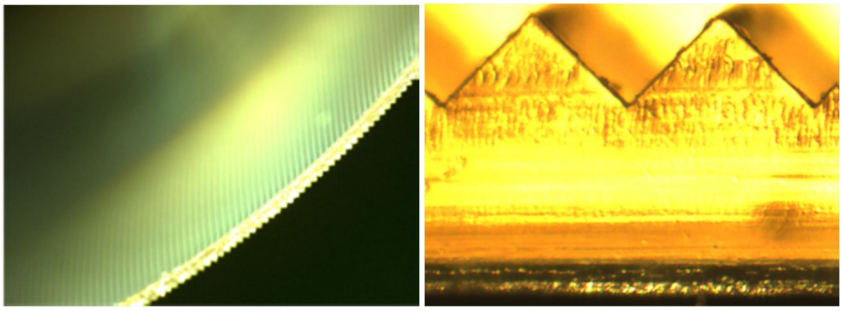


Figure 2.24 Magnification of prismatic film (2.5X) (left) and (57X) (right) (Vázquez-Moliní et al., 2012).

Another type of microstructured glazing is LUMITOP, proposed by Klammt et al. (2012), as illustrated in Figure 2.25 (left). LUMITOP can be integrated into glazing on the upper part of the window. Their findings showed that the room was illuminated by redirecting the daylight from a sun altitude of 15 to 65 degrees without producing glare, as shown in Figure 2.25 (right) and Figure 2.26.

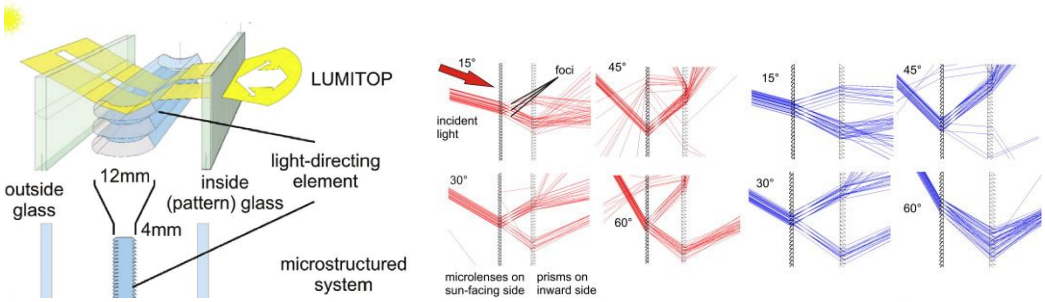


Figure 2.25 Cross-section of LUMITOP (left), Ray tracing results for a PMMA (right) (Klammt et al., 2012)



Figure 2.26 Layer without (left) and with PMMA (right) (Klammt et al., 2012).

2.2.1.4. Anidolic lighting systems

Anidolic lighting systems are non-imaging optical lighting systems that typically use parabolic mirrors to receive the sunlight and redirect it to the deep areas inside the buildings while diffusing the direct sunlight to reduce glare (Chaves, 2015). Anidolic systems are also known

as non-imaging optical systems because their purpose is to enhance the daylighting performance instead of forming an image of the light source as in the imaging-optical system. Figure 2.27 shows a sample of a compound parabolic concentrator that is used for daylight concentration.

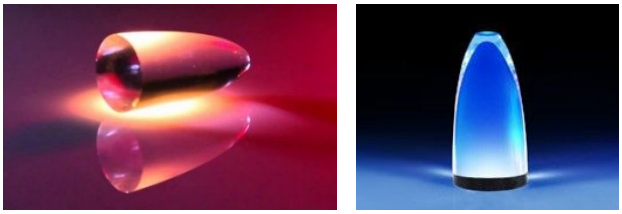


Figure 2.27 Compound Parabolic Concentrators (CPCs) (edmundoptics.com 2017)

A compound parabolic concentrator (CPC) is a non-imaging optical element in parabolic geometry. It has been applied for sunlight concentration for solar energy generation purposes where its efficiency has been approved (Welford and Winston, 1978). It has an internal reflected surface that redirects the sunlight through a selected range of angles toward the exit of the device (Vázquez-Moliní et al., 2012). The daylight enters the CPC through the large cross, and it is reflected towards the smaller one, as illustrated in Figure 2.28.

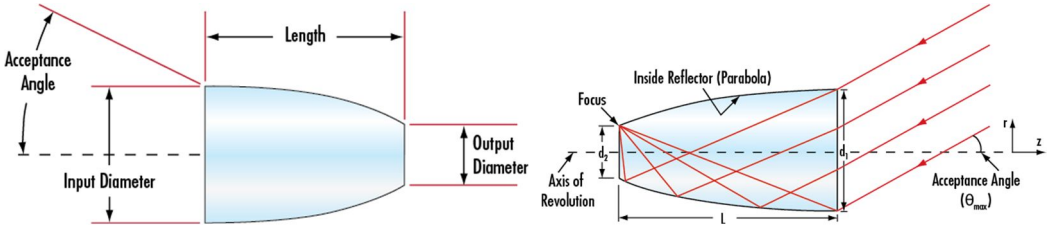


Figure 2.28 Anidolic lighting systems, Compound Parabolic Concentrator (CPC) (edmundoptics.com 2017)

Yu et al. (2014) evaluated the daylight transmittance performance of a dielectric compound parabolic concentrator (dCPC) compared with prismatic structures under standard and real sky conditions. The CPC unit is coated with a PV cell on the smaller side, where the large section is the daylight receiver. The results showed that the dCPC exceeded the performance of common prismatic structures due to the wide acceptance angle that the dCPC provides, as shown in Figure 2.29.

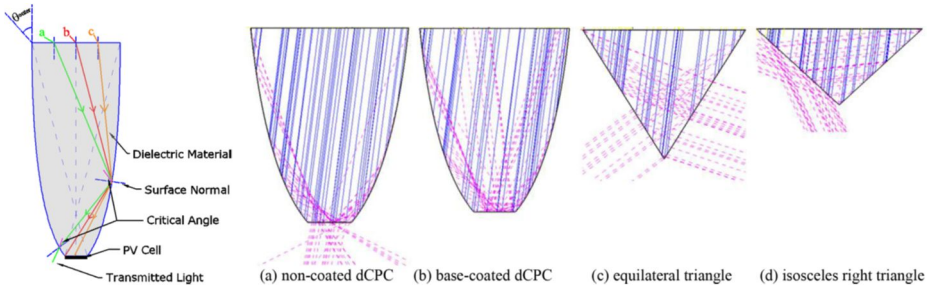


Figure 2.29 The components of dCPC coated with PV cell (left), and the ray-tracing results from 10 ° angle (Yu et al., 2014).

In addition, the CPCs can be applied in a reverse mode for direct use as a daylighting system, where the daylight is received through the small side and is then reflected toward the large side. The function of using the CPCs as a daylighting system is to receive daylight from a specific angle and then redirecting toward the interior ceiling to send the daylight to the deep areas of the room.

Ruck et al. (2000) presented an anidolic solar blinds system constructed by a grid of double hollow three-dimensional compound parabolic concentrators in an asymmetrical arrangement and had an internal reflective surface shown in Figure 2.30. A prototype was built; however, the system has not been used in buildings. The principle of the anidolic blinds was to reject the direct sunlight from the high solar latitude while transmitting the diffuse daylight from the low solar latitude. The system was applied only on a south façade in the high latitude region (latitude 47°N). Therefore, an optimisation based on the orientation and the latitude is required. Theoretically, the elements of the anidolic solar blinds can be produced in any size larger than the daylight wavelength.

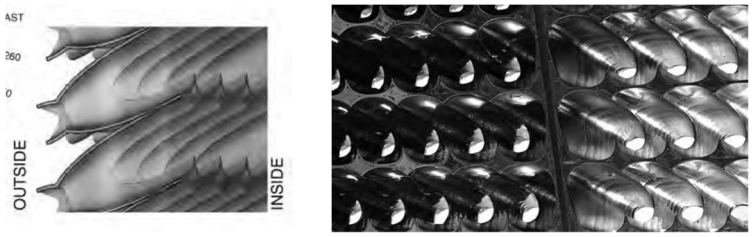


Figure 2.30 Section of the computer model (left) and photograph of physical components (right) of anidolic solar blinds (Ruck et al., 2000)

Another study showed anidolic solar blinds that have a geometry similar to the previous study mentioned above. This system consists of 48 elements placed on a plane with an 18-degree tilt angle, as shown in Figure 2.31. To obtain mirrored surfaces, aluminium layers in addition to several coatings of varnish were utilised. It was found that the adjustment of the vertical inclination can improve the performance of the system. Furthermore, to achieve better performance an integration in the façade and interior ceiling is necessary (d-lite.org 2017).

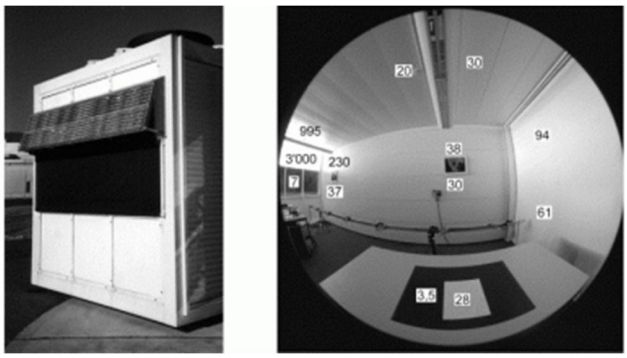


Figure 2.31 Anidolic solar blinds installed on the exterior of a mockup building, and the luminance measured inside the model (LESO website).

A three-dimensional hollow prismatic compound parabolic concentrator (PCPC) in reverse mode was proposed by Vázquez-Moliní et al. (2012). In order to enhance its efficiency, the PCPC was made of a prismatic dielectric material. The concept of the system was to apply the shape of the compound parabolic concentrator (CPC) in a hollow prismatic light guide. The system was compared with a CPC made of aluminium. Figure 2.32 illustrates the design of the CPC unit that works in a reverse mode where the small section is the input (Entry 1) in addition to the surface of the CPC (Entry 2). The system was evaluated through ray-tracing software in addition to an experiment on a prototype.

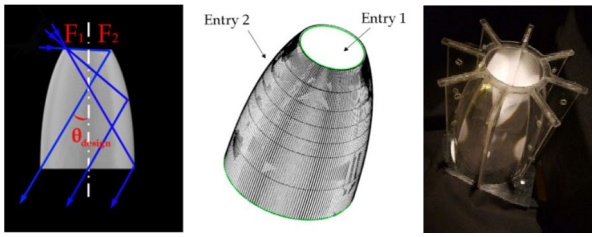


Figure 2.32 The maximum input and the design angle of the CPC (left), 3D hollow HCPC (middle), experimental prototype (right) (Vázquez-Moliní et al., 2012)

It was found that the efficiency of the PCPC, in the case of using entry 1 and entry 2, increased at an 85º incidence angle by six times, and the average increase from 0º to 85º incidence angle was three times compared with standard aluminium. In contrast, the performance of the aluminium CPC (ACPC) is higher in the case of using entry 1 only. As a result, further investigations are required for high incident angles, particularly those higher than 35º (Vázquez-Moliní et al., 2012).

A study by Vázquez-Moliní et al. (2013) presented an anidolic daylight collecting system based on a truncated compound parabolic concentrator (T-CPC) for nonresidential buildings, Figure 2.33. The optimised parameters were the truncation angle (α), the tilt angle (β), the compaction

ratio (dx, dy), the radiation angle Θ. The result showed that the system obtained improvement in the light flux uniformity. In addition, it reduced the dependence on the solar incidence angle.

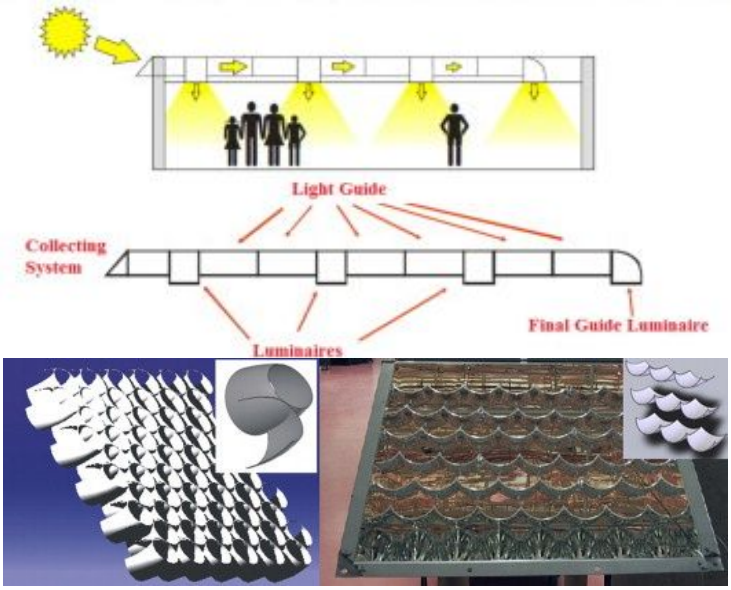


Figure 2.33 Concept of the system (above), and computer model and prototype of T-CPC (below) (Vázquez-Moliní et al., 2013)

2.2.2. Daylight filtration systems

Perforated solar screens were used in traditional architecture, particularly in hot climates. Today, their applications have become a trend as a skin for many contemporary commercial or institutional buildings (Hoffmann et al., 2016). However, the main concern for most of these implementations was the aesthetical aspect. Therefore, essential principles such as occupant comfort, including daylighting performance and energy efficiency (Bakker et al., 2014), have not been considered.

Perforated solar screens are some of the promising shading systems that can allow the daylight to access the building while balancing the received solar radiation. They have been found to be effective shading devices through the history of traditional architecture in desert climates. However, there is a lack of knowledge regarding their performance as a daylighting system in contemporary buildings (Sherif et al., 2012b).

2.2.2.1. Traditional perforated solar screens

In traditional architecture, perforated solar screens were made from wood with a thick section with desirable characteristics as a shading device. If this shading system is developed, it could contribute to significant energy-saving (Sherif et al., 2012a). This shading system is known as

"Mashrabeya", "Rawshan", or "Shanshūl". Figure 2.34 shows an example of a traditional Mashrabiya made of wood.

Geometric patterns have been utilised in different types of traditional buildings. In addition, these patterns have been employed in solar perforated screens. The purpose of these screens is not only ornamental, but it has a main function as a daylighting element that enhances the daylight performance inside the building (Emami and Giles, 2016).



Figure 2.34 Interior (left) and exterior (right) views of Mashrabiya (Sherif et al., 2012a)

2.2.2.2. Contemporary perforated solar screens

Perforated solar screens have been developed and utilised in the facades of contemporary buildings by different means. They have been applied as a wooden solar screen similar to the traditional Mashrabiya, as shown in Figure 2.35 (left), while in other buildings, they were applied as a double skin made of metal as shown in Figure 2.35 (right) or made of concrete as shown in Figure 2.36. Further developments have been made on the perforated solar screen where they have been integrated with a kinetic control system to be adapted to outdoor conditions as found at the Institut du Monde Arabe building in Paris, as illustrated in Figure 2.37.

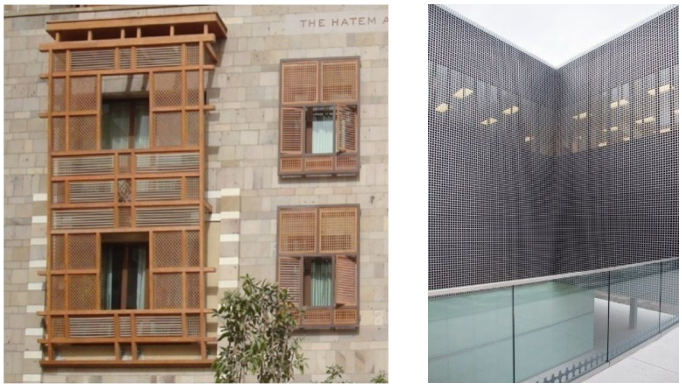


Figure 2.35 Contemporary solar screens in the American University (left) (Sherif et al., 2012a), metal solar screens at Tampa Museum of Art (right) (archdaily.com 2017)

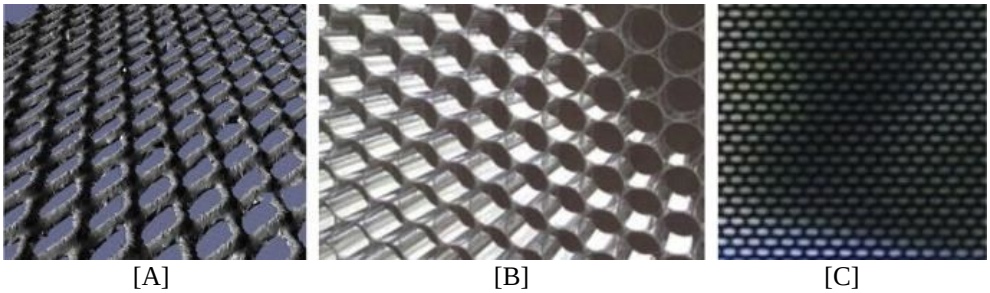


Figure 2.36 Perforated skin façade, Kanazawa Umimirai Library (archdaily.com 2017)



Figure 2.37 Exterior and interior of Arab World Institute kinetic screen facade in Paris (aedesign.files.wordpress.com 2017).

Perforated solar screens use the principles of static angular selective shading systems, which allow diffuse daylight while obstructing direct sunlight (Fernandes et al., 2015). One of the perforated solar screen types that have widespread application is the double-skin perforated façades. Their component consists of a glass pane and metallic layer with an air cavity in the middle (Blanco et al., 2016). They are applied as daylight filtration, solar gain protection, and designed to improve the architectural design of the building. Their performance as shading devices is influenced by their geometry, surface and implementation (Mainini et al., 2014). Figure 2.38 shows three examples of double-skin perforated façades.



[A] [B] [C]

Figure 2.38 [A] expanded metal mesh, [B] tubular shading structure, and [C] micro-perforated screen (Fernandes et al., 2015)

Sherif et al. (2012b) examined the daylight performance of solar screens in a residential building in a desert climate by investigating the impact of the perforation percentage to find the minimum size of perforations that can provide the space with an adequate level of illuminance around the year. They stated that the impact of the screen on the daylighting

performance depends mainly on the time and the orientation of the fenestration. It was found that the perforated screen can decrease the glare and provide the space with an adequate illuminance level while maintaining indoor thermal comfort by controlling the heat gain. The results showed the satisfaction rate with the illuminance levels was 83%, 53%, and 40% for the front, middle, and rear zones.

They recommended that higher perforation percentages are required to enhance the illumination level in the deep areas of the room. In addition, they suggested that future studies should take into consideration the non-uniform distribution of the perforations. It was found that the southern and western screens perform adequately; however, the northern screen provided an insufficient illuminance level.

Sherif et al. (2012a) examined the energy saving of a solar screen system located within low latitude desert climates at the Kharga Oasis in Egypt by investigating the impact of different depths and perforation percentages, as shown in Figure 2.39. They concluded that energy consumption could be reduced by 30% by applying an external fixed deep perforated solar screen in the south and west facades. The results showed that the optimum depth is 1:1 and the optimum perforation percentages are 80% to 90%. In addition, it was found that higher energy performance can be achieved by applying lighter and deeper solar screen configurations (Sherif et al., 2012a).

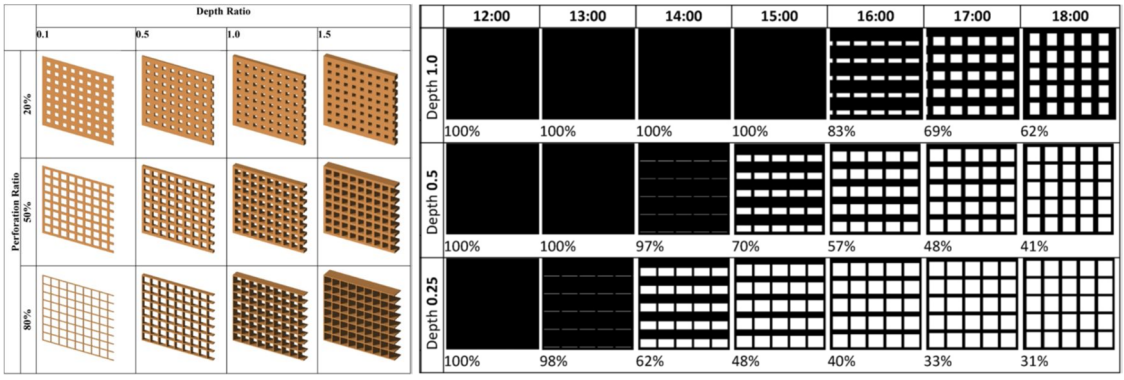


Figure 2.39 Perforation and depth of solar screens (left), shading percentages of screens with different depth ratios (right) (Sherif et al., 2012a)

Giovannini et al. (2015) developed a shading and a daylighting system called “Shape Variable Mashrabiya (SVM)”, which is developed using a perforated screen shading system as it is known in the vernacular architecture as Mashrabiya. The SVM is an adaptive shading system consisting of three similar opaque layers with a backscattering pattern inspired by the traditional Mashrabiya. They stated that the system could adapt to the sunlight by switching it off and on as desired. Figure 2.40 shows a configuration of an opened (left) and closed SVM

(right). This system was applied to the east and west facades of an office building in Abu Dhabi in UAE (24.4°N, 54.7°E) to analyse its influence on the annual lighting and primary energy performance.

They claimed that the performance of SVM exceeds the performance of the current control solar systems that are used in Middle Eastern regions. This is due to the ability of SVM to reduce the heat gain, control the glare, and then enhance the energy performance and visual comfort. However, the SVM was compared only with three systems: external Venetian blind systems and reflective and selective glazing types.

The results showed that SVM could reduce overheating, which reduces the cooling load, and hence, energy saving by 17.2% and 9.9% compared to the special glazing and the Venetian blinds, respectively. In addition, it reduced the glare; however, the view to the outside was limited to the closed configuration of the system. Furthermore, energy consumption was reduced by 65.7% and 30.7% for lighting and by 27% and 16.3% for glass as compared to special glazing and the Venetian blinds, respectively (Giovannini et al., 2015).

However, it is significant to note that the results of their study are underestimated in terms of illuminance values due to the setting of the bounces, which was equal to eight. Furthermore, the time-step of the weather file was set for one hour. In addition, the Venetian blinds were set on the external side while it could perform better in terms of the reduction of overheating if put on the interior side (Giovannini et al., 2015).

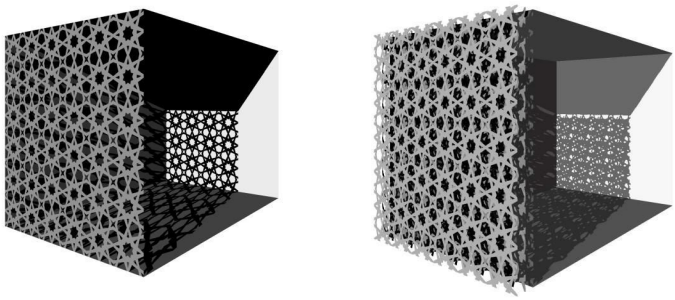


Figure 2.40 Opened (left) and closed SVM (right) (Giovannini et al., 2015)

Mainini et al. (2015) analysed the performance of a static metal mesh shading system applied in an office building in Italy. They evaluated the primary energy consumption of the lighting, cooling and heating. Different geometries and openness factor values were studied for two locations, orientations and window to wall ratio values (WWRs), Milan (45° N, 9° E) and Palermo (38° N, 13° E), south and west, and 33% and 100%, respectively. This was then compared to Venetian blinds and sun control windows.

The analysis showed that the metal mesh performed worse than the glazing systems with a 33% window to wall ratio (WWR). However, with 100% WWR, the metal mesh with a high value of wire diameter (d)/ space between wires (D) (d/D) for the south façade in Milan was the optimum solar control. On the other hand, the Venetian blinds are the best alternative for west elevation exposure, showing low cooling energy and high values of lighting energy, due to their self-shading effect, due to their equal spacing and width. However, this study did investigate the performance of the metal mesh on glare reduction (Mainini et al., 2015).

Sherif et al. (2012c) investigated the influence of the opening aspect ratio and the axial rotation angle of a solar screen on the daylighting performance of a residential building in a desert climate. Their study aimed to find an optimal design that works appropriately within different orientations. They found that the solar screen performs better in the horizontal aspect ratios rather than the vertical one. Particularly, 12:1 and 18:1 (H:V), where the screens obtained the highest performance by providing daylight for 92% of the space compared with 53% of the reference. However, for the south façade, the recommended ratio is 3:1 (H:V) due to the ability to reduce the annual transmitted solar radiation by 60% while providing the space with an acceptable daylight level.

A study by Lavin and Fiorito (2017) attempted to improve Useful Daylight Illuminance (UDI), energy-saving and to decrease the glare by means of shading devices with a perforated screen in an office building in Australia (Southern hemisphere). The screen was applied to the north and west facades. They investigated the impact of the size and distribution of the perforation of the solar screen with space without shading devices, as shown in Figure 2.41. The results showed that the solar screen could significantly improve the UDI level, energy-saving and also reduce the glare.

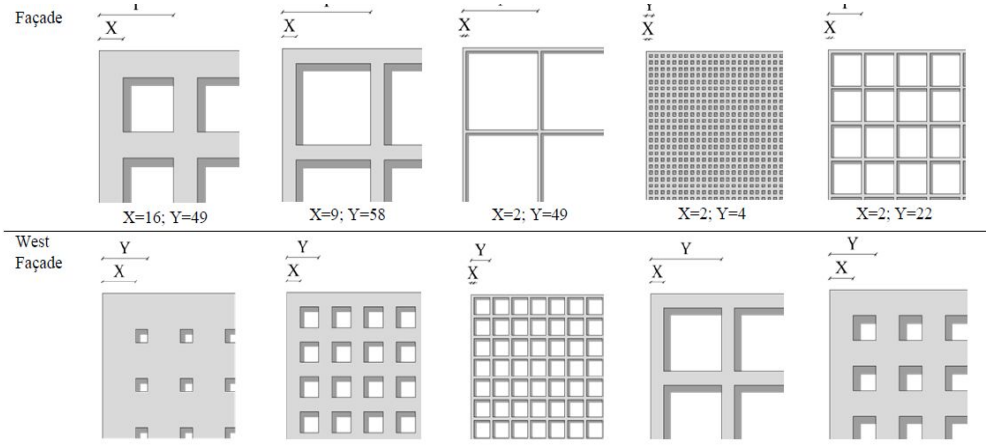


Figure 2.41 Optimized perforated screens for each case (Lavin and Fiorito, 2017)

Omidfar (2011) optimized a complex geometry sun-shading screen to enhance daylighting and energy performance as illustrated in Figure 2.42. This study showed that a reduction in annual energy consumption could be obtained at 35% and 42 %.

The performance of a micro structural perforated shading screen (MSPSS) was assessed by Appelfeld et al. (2012). The bi-directional transmittance properties of the system and the influence on daylight performance and indoor thermal comfort were determined. The results were compared to three different static complex fenestration systems (CFSs). They stated that MSPSS was found to control the solar gain, reduce glare from high sun altitude. In addition, it provides a view to the outside, as shown in Figure 2.43.

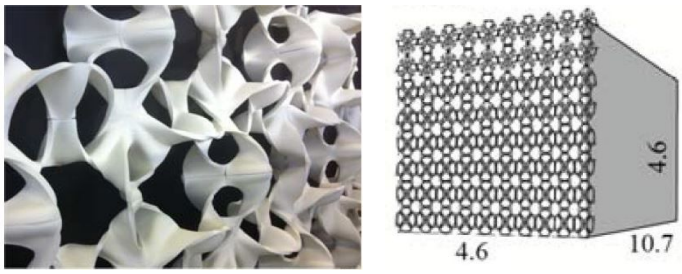


Figure 2.42 Close-up view of the complex geometry (left) and the whole screen (right) (Omidfar, 2011)

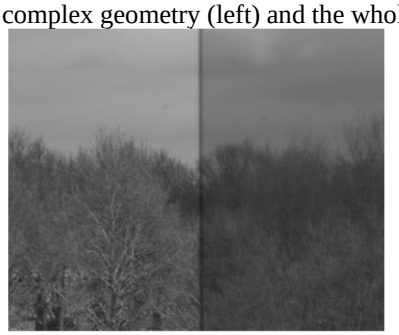


Figure 2.43 View through MSPSS (left), unobstructed view (right) (Appelfeld et al., 2012)

(Blanco et al., 2016) have built a theoretical model through Energyplus® (Design Builder) to predict the thermal performance of double skin perforated screens, as illustrated in Figure 2.44. The results showed that the application of a perforated metal screen with different perforation rates is appropriate in hot climate zones. However, this study did not consider the details of the perforations due to the limitation of the software that was used (Design Builder). Furthermore, the study considers only the south facade. On the other hand, Sherif et al. (2012b) state that the openness factor of perforated solar screens is not an adequate parameter to identify the performance of such a shading system. Other parameters, for instance, geometry and distance between openness as well as layer thickness, can influence its performance.

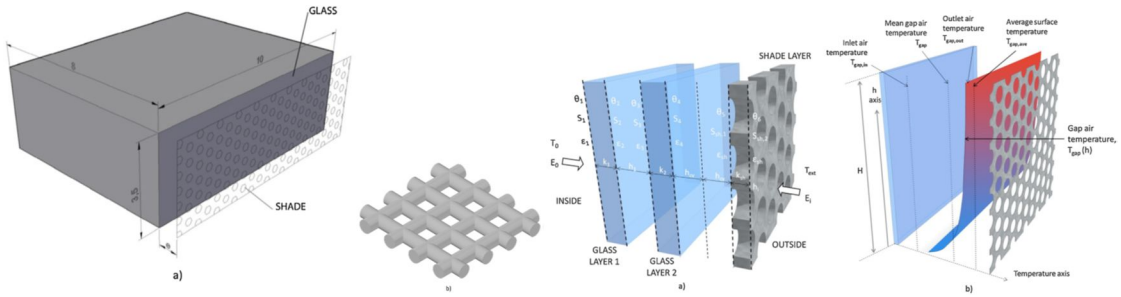


Figure 2.44 The configuration of the double skin perforated screen (Blanco et al., 2016).

A study by Fernandes et al. (2015) investigated the potential energy-saving properties of three perforated metal screens in commercial buildings: a micro-perforated screen, a tubular shading structure, and an expanded metal mesh. The micro-perforated screen was available commercially as MicroShade by Photosolar, placed between two layers of clear low-emissivity glass, Figure 2.45. The metal mesh was fabricated and scanned by a coordinate measuring machine where the information of the detailed geometry was not available, as shown in Figure 2.46.

The analysis was done through a computer simulation by EnergyPlus, Radiance and Window simulation tools for two locations, Chicago, Illinois 41° N, 87° W and Houston, Texas 29° N, 95° W. It was found that energy saving, by 28% to 47%, can be achieved. In addition, it was identified that the spectral selectivity of low-emissivity glazing has a significant influence on the performance.

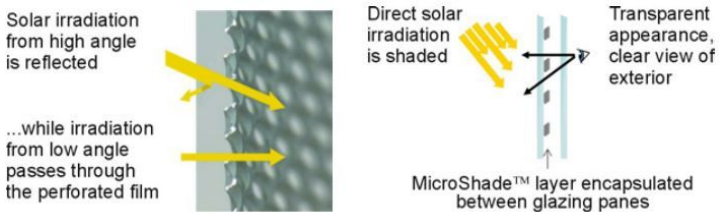


Figure 2.45 MicroShade® layer (Rasmussen 2013)

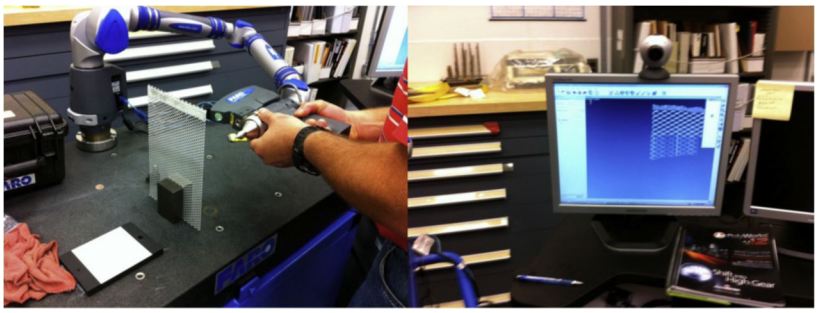


Figure 2.46 Coordinate measuring machine (left), the scanning result of the mesh(right) (Fernandes et al., 2015)

Another study by Mayhoub and Labib (2015) evaluated the thermo-visual performance of glazing for buildings in Egypt. Five glazing types were tested, and then perforated double skin facades and light shelves were combined. The light shelf with clear glass performed best in

terms of daylighting uniformity and thermal comfort. However, the enhancement in the daylighting availability was insignificant.

A study by Mainini et al. (2014) compared the cooling loads of two facades, one with low-emissivity glazing and another with a clear glazing and perforated metal mesh. The results showed that the clear glass with a perforated metal mesh reduced the cooling load by 40% and the mean radiant temperature was 3-4 ^{o}C.

Sherif et al. (2014) studied the effectiveness of applying different glazing and shading systems on the lighting, cooling, and heating for a hospital in Cairo, Egypt. The evaluation was done by simulation in EnergyPlus. The results showed that the energy-saving, by applying the shading systems, was higher than all the glazing types, and particularly, the perforated solar screens achieved the highest energy saving properties among the other systems.

2.2.3. Daylight transport systems

The main function of the transport systems is to transport direct sunlight and to diffuse daylight through the system to reach the deep areas in the interior space. Daylight transport systems include light pipes, fibre optics and light rods. They are a useful solution for windowless spaces such as basements or deep rooms within buildings if the connection with the outdoor environment is not required (Knoop et al., 2016).

2.2.3.1. Light Pipes

Light pipes are daylight guiding systems that transport daylight into the deep area of the building by collecting, redirecting (CIE, 2012) or concentrating the sunlight (Aizenberg, 2013). They have a light transport channel connecting two devices, the outer collector and the inner diffuser devices. The operation of the collector can be active or passive. The transport channel typically comes as a linear tube coated with a material that has high reflectivity properties, prismatic material or other daylight redirecting elements. Additionally, the inner diffusers distribute the daylight inside the room. These diffusers are usually made of prismatic material or opal (CIE, 2012). Figure 2.47 shows an example of a light pipe system.

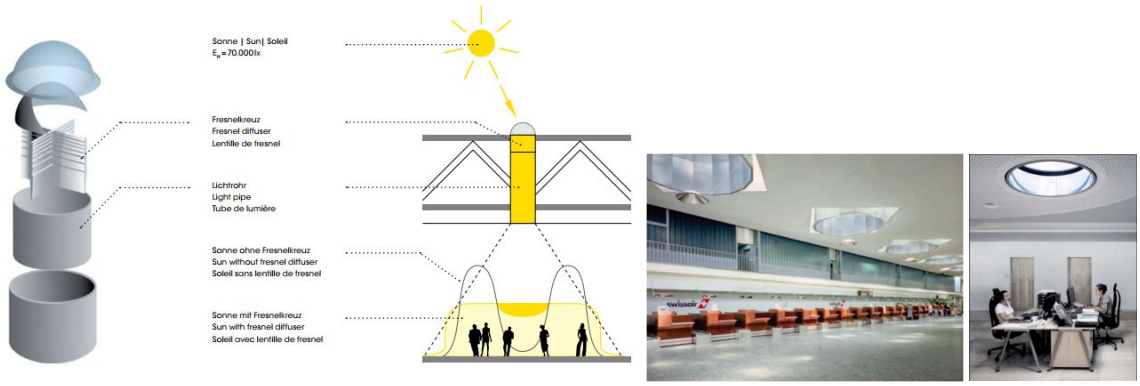


Figure 2.47 Light Pipe system (durlum.de 2017)

A light pipe device with a flat captation system was proposed by Aizenberg (2013). The application of the device does not require modifications to the building envelope. Two light pipe devices were placed in parallel, and the opening made transparent by 30%. The area of the window was 1/8 the floor area. Figure 2.48 shows the components of the system.

They reported that their proposed light pipe device improved the uniformity of the daylighting distribution and the illuminance level on the deep areas and the work plane. In addition, it reduced the glare, overheating and lighting and cooling energy. Nevertheless, Knoop et al. (2016) stated that light pipes can increase the daylight contribution without producing glare; however, they are not suitable when a visual connection with the outdoor environment is one of the purposes that the daylighting system is intended.

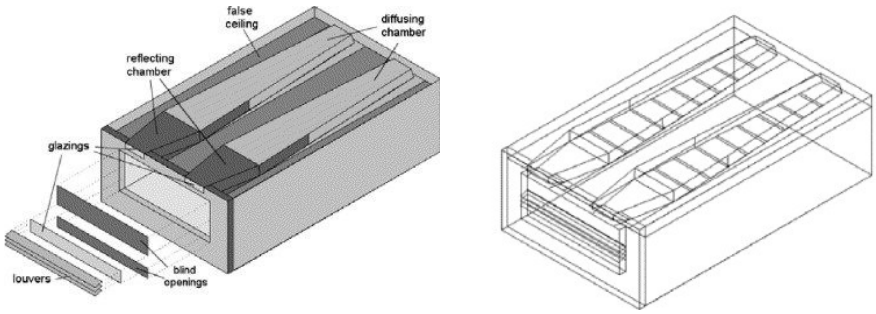


Figure 2.48 The components of the system (Aizenberg, 2013)

2.2.3.2. Fibre optics

Fibre optics, also known as optical fibres, are a new daylighting technology that uses the properties of transferring daylight through the optical fibre cables from outdoors towards the indoor spaces. Like light pipes, the fibre optics system consists of three main components, a solar collector placed on the top of the building, optical fibre cables as a transport channel and an internal diffuser to distribute the daylight inside the room. Fibre optics are applied typically when a direct side light is not available or is unable to send an adequate daylight level to the deep area of the interior. Figure 2.49 shows the three main components of a fibre optics system.

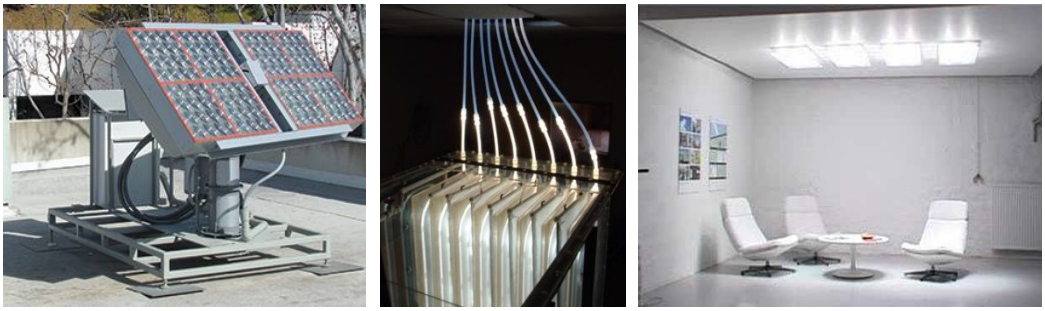


Figure 2.49 Sunlight collector (left) (buildings.com 2017,) fibre optics cables (middle) (e3tnw.org 2017), and light diffusers (right) (buildinggreen.com 2017)

A study by Al-Obaidi et al. (2017) proposed a daylighting system by integrating fibre optics with roof light and a dynamic shading system, as shown in Figure 2.50. The proposed system was evaluated through an empirical experiment in Malaysia. Their findings showed that the daylighting could be provided by the proposed system from 8 am to 6 pm, and the fibre optics system could provide daylighting at an adequate level by 300 to 680 lx, with an average of 492 lx, and the functionality range was from 44% to 54%. In addition, it was found that a uniform illuminance can be obtained at a solar irradiance higher than 500 W/m^2.

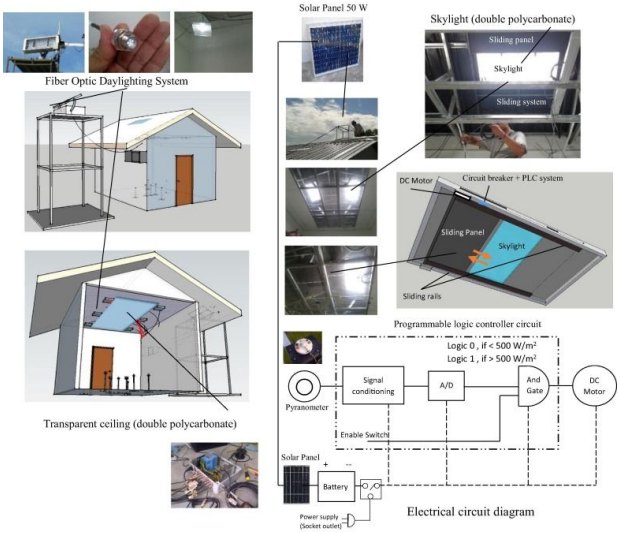


Figure 2.50 Proposed model of the integrated daylighting system (Al-Obaidi et al., 2017).

2.2.3.3. Optical light rods

Optical light rods are daylight transport systems that transfer the sunlight through small tubular rods with high transmittance efficiency. The principle of the system is to employ the properties of the Polymethyl methacrylate material (PMMA) transmittance possesses (Liu et al., 1998). Figure 2.51 illustrates an optical light rod showing the illumination at the end of the rod and light rods with 40, 60 and 90-degree bends.

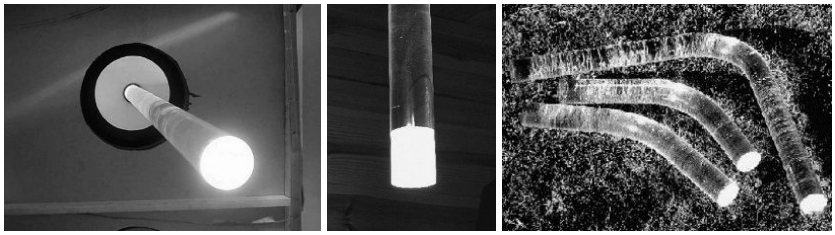


Figure 2.51 Optical light rod shows the illumination of the end of the rod (Callow and Shao, 2003)

2.2.4. Skylight systems

Skylight systems can provide a significant amount of daylight depending on their size. The optimal performance of the skylight can be achieved with a diffuse skylight. In addition, sunscreening or proper orientation is required in order to prevent glare and heat gain. That can be obtained using translucent glazing; however, the level of light transmission will be reduced.

Skylights may cause a fluctuation in the lighting level; thus, it is not the preferred solution if the function of the space requires constant light levels (Knoop et al., 2016), such as office and education buildings. Furthermore, the cost of the installation and the maintenance of the skylight system is relatively high. In addition, frequent surface cleanliness is required to provide optimum daylighting performance (Knoop et al., 2016).

The best orientation for the skylight system in the northern hemisphere can be obtained by facing the north façade. A Northern skylight can provide illumination while minimizing the heat gain. On the other hand, a southern skylight can increase the heat gain, which may negatively influence thermal comfort and energy performance. In the case of the horizontal skylight, the area of glazing should be minimized in order to reduce the heat gain. It is important to note that the skylight system cannot provide a view toward the outside, recommended in workplace environments especially in office buildings (Knoop et al., 2016). Figure 2.52 shows two examples of skylight systems; a skylight system illuminates the atrium of a building (left), a skylight system with deep depth to provide shading while lighting the interior (right).

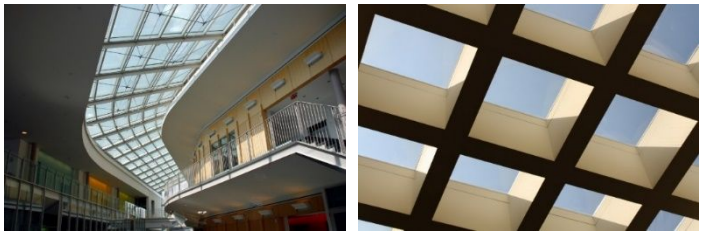


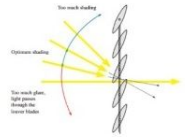
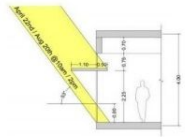
Figure 2.52 Skylight systems (flickr.com 2017)

A study on skylight systems by Al-Obaidi et al. (2014) found that the direct application of the skylight daylighting system in low latitudes regions is an inappropriate method for achieving a balance between lighting and thermal performance. However, the performance of these

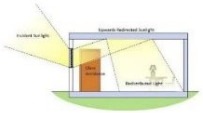
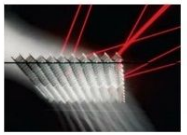
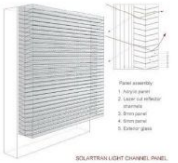
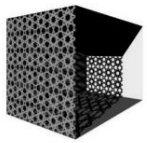
systems can be enhanced if other technologies are integrated, for instance, shading devices, smart glazing, glare protection and prism elements. In addition, a skylight system can provide daylight for only the spaces that have an external roof.

2.3. Comparison of Daylighting Systems

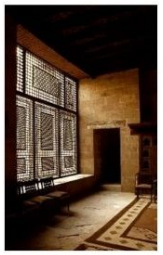
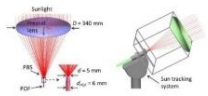
Table 2.1 Comparison of daylighting systems

Code	Name	Graph	Advantages	Disadvantages	Position	Degree of Daylighting enhancement	Degree of Glare Protection	Degree of Overheating Reduction	Indication Cost	Suitable for Low Latitude Regions	Commercially Available	Example Product	References
Category A- Daylight Redirection Systems													
A1- Louvers													
A1a	External louvers		Better daylighting distribution. Increase of visual and thermal comfort. Reduce cooling loads. Significant energy saving. Glare protection. 70% additional illuminance at the workplane level under clear sky conditions	Long payback period. Glare possibility through reflected surfaces (Slats)	ES	4	3	3	3	Y	Y		[1] [2] [3] [4] [5]
A1b	Blinds		High energy saving potential. Optimal daylight utilization. Retractable. Reduce solar gain Increase thermal comfort.	Limited resistance to high wind pressure and risk of dirty if they place on the external façade. Long payback period. Glare possibility through reflected surfaces (Slats)	ES/IS	3	4	4	4	Y	Y		[1]
A2-Light shelfs													
A2a	Light shelfs		Provide sufficient daylight level in deep areas. Higher illuminance uniformity distribution.	Do not protect from glare when sun altitude is low (winter). Internal lightshelf have lower daylight availability comparing with external light shelf. Requires high roof/ceiling to perform efficiently. Performance is reduced in west and east facades (Vertical shading is required).	ES	3	1	2	3	Y	Y		[6] [7] [8]

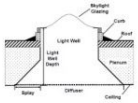
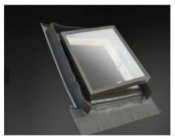
Key: E= External device. I= Internal device, B= Between two layers of glazing, S= Sid lighting, T= Top lighting, Y=Yes, N=No, 1 = Extremely Ineffective, 2= Ineffective, 3= Moderate, 4= Effective 5 = Extremely Effective.

Code	Name	Graph	Advantages	Disadvantages	Position	Degree of Daylighting enhancement	Degree of Glare Protection	Degree of Overheating Reduction	Indication Cost	Suitable for Low Latitude Regions	Commercially Available	Example Product	References
A3-Light-redirecting elements													
A3a	**Prismatic panels**		Increase daylight uniformity. Increase light level in deep areas.	Does not protect from glare at medium solar sun altitude in September in low latitude regions May require sun tracking.	**ES/T/B**	**4**	**2**	**2**	**2**	**Y**	**Y**		[9] [1]
A3b	**Laser cut panels**		Perform best under sunny conditions. Allowing diffuse daylight. Increases daylight level in deep areas (10-30%). Improve light distribution and uniformity. View out Increase energy saving.	Redirects light only from 30° and higher. Does not protect from glare if light incident lower 30°.	**ES/B**	4	3	3	**2**	**Y**	**Y**		[1] [6] [10] [11]
Category B- Daylight Filtration Systems													
A4- **Perforated shading screens**													
B1	**Contemporary perforated solar screens**		Reduce overheating. Higher energy saving from cooling load compare with special glazing and Venetian blinds, 17.2% and 9.9%, lighting load 65.7% and 30.7%, respectively. Enhance building's aesthetics. Can be applied to new build and refurbishment project. Easy to be formed, and shaped.	In closed configuration, view to outside is not available.	**ES/B**	**4**	**4**	**4**	**3**	**Y**	**Y**		[12]

Key: E= External device. I= Internal device, B= Between two layers of glazing, S= Sid lighting, T= Top lighting, Y=Yes, N=No, 1 = Extremely Ineffective, 2= Ineffective, 3= Moderate, 4= Effective 5 = Extremely Effective.

Code	Name	Graph	Advantages	Disadvantages	Position	Degree of Daylighting enhancement	Degree of Glare Protection	Degree of Overheating Reduction	Indication Cost	Suitable for Low Latitude Regions	Commercially Available	Example Product	References
B2	Traditional perforated solar screens		Reduce overheating. Higher energy saving from cooling load compare with special glazing and Venetian blinds, 17.2% and 9.9%, lighting load 65.7% and 30.7%, respectively. Enhance building's aesthetics. Can be applied to new build and refurbishment project. Easy to be formed, and shaped.	In closed configuration, view to outside is not available.	ES	4	4	4	3	Y	Y		[13]
Category C-Daylight Transport Systems													
C1	Light pipes		Performance is enhanced if prismatic elements is integrated.	Performance is significantly influenced by orientation, solar azimuth angle, incident light angle.	T	4	4	3	3	Y	Y		[14]
C2	Fibre optics		Better daylight uniformity distribution. Can be hybrid with LED lighting system to achieve better performance of daylighting and energy saving.	Possibility of fire due to the concentrated heat from the fibre optics.	T	4	4	3	1	Y	Y		

Key: E= External device. I= Internal device, B= Between two layers of glazing, S= Sid lighting, T= Top lighting, Y=Yes, N=No, 1 = Extremely Ineffective, 2= Ineffective, 3= Moderate, 4= Effective 5 = Extremely Effective.

Code		Name	Graph	Advantages	Disadvantages	Position	Degree of Daylighting enhancement	Degree of Glare Protection	Degree of Overheating Reduction	Indication Cost	Suitable for Low Latitude Regions	Commercially Available	Example Product	References
Category D- Skylights systems														
D1	Skylights			Longer daylighting period compare with side lighting if not blocked (shaded) by surrounding buildings.	High possibility of overheating. Inappropriate to obtain balance of thermal comfort and lighting level. To avoid overheating it requires integration with other technologies such as special glazing, prisms, glare protection or shading. High possibility of glare.	T	4	3	1	3	N	Y		[15] [16]

Key: E= External device. I= Internal device, B= Between two layers of glazing, S= Sid lighting, T= Top lighting, Y=Yes, N=No, 1 = Extremely Ineffective, 2= Ineffective, 3= Moderate, 4= Effective 5 = Extremely Effective.

Sources:

1. Knoop, M., et al., *Daylighting and electric lighting retrofit solutions*. 2016, Universitätsverlag der TU Berlin.
2. Palmero-Marrero, A.I. and A.C. Oliveira, *Effect of louver shading devices on building energy requirements.* Applied Energy, 2010. **87**(6): p. 2040-2049.
3. Hammad, F. and B. Abu-Hijleh, *The energy savings potential of using dynamic external louvers in an office building.* Energy and Buildings, 2010. **42**(10): p. 1888-1895.
4. Freewan, A.A., L. Shao, and S. Riffat, *Interactions between louvers and ceiling geometry for maximum daylighting performance.* Renewable Energy, 2009. **34**(1): p. 223-232.
5. Leung, T.C.Y., P. Rajagopalan, and R. Fuller, *Performance of a daylight guiding system in an office building.* Solar Energy, 2013. **94**: p. 253-265.
6. Ruck, N., et al., *Daylight in Buildings: A source book on daylighting systems and components*. 2000, International Energy Agency, Lawrence Berkeley National Laboratory: Berkeley (USA).
7. Lee, H., et al., *Effectiveness of a perforated light shelf for energy saving.* Energy and Buildings, 2017. **144**: p. 144-151.
8. Lim, Y.-W., et al., *Building façade design for daylighting quality in typical government office building.* Building and Environment, 2012. **57**: p. 194-204.
9. Mashaly, I.A., et al., *A prismatic daylight redirecting fenestration system for southern skies.* Renewable Energy, 2017. **109**: p. 202-212.
10. Shah, A., et al., *DAYLIGHT PERFORMANCE EVALUATION OF LASER CUT PANELS IN OFFICE BUILDINGS-A CASE OF INDIAN CITIES*. 2015.
11. Edmonds, I., *Daylighting high-density residential buildings with light redirecting panels.* Lighting Research & Technology, 2005. **37**(1): p. 73-84.
12. Giovannini, L., et al., *Lighting and Energy Performance of an Adaptive Shading and Daylighting System for Arid Climates.* Energy Procedia, 2015. **78**: p. 370-375.
13. Sherif, A., H. Sabry, and T. Rakha, *External perforated Solar Screens for daylighting in residential desert buildings: Identification of minimum perforation percentages.* Solar Energy, 2012. **86**(6): p. 1929-1940.
14. Aizenberg, J.B., *Hollow light guides: 50 years of research, development, manufacture and application-a retrospective and looking to the future.* Light & Engineering, 2013. **21**(4).
15. Al-Obaidi, K.M., M. Ismail, and A.M. Abdul Rahman, *A study of the impact of environmental loads that penetrate a passive skylight roofing system in Malaysian buildings.* Frontiers of Architectural Research, 2014. **3**(2): p. 178-191.
16. Lawrence, T. and K.W. Roth, *Commercial building toplighting: energy saving potential and potential paths forward*. 2008, EERE Publication and Product Library, Washington, DC (United States).

Chapter 3. Literature review in innovative glazing

This chapter presents a review on the innovative glazing technologies and their application in building facades. It provides a description of each type with the aid of graphical presentation, highlighting their advantages and disadvantages in addition to their availability and limitations. It focuses on the potential of smart glazing in improving visual comfort inside a building. Further, it provides a brief review of a number of daylight simulation tools.

3.1. Introduction

This review includes current knowledge on new and innovative technologies and materials of smart glazing. It highlights the characteristics of innovative glazing in relation to visual comfort through analysis of previous studies and focuses on the type of innovative glazing that can enhance daylighting performance while increasing energy saving.

Windows have a number of purposes, and their impact on building performance is significant. It can influence the thermal and visual comfort as well as the health quality of the occupant. Furthermore, windows impact the psychological behaviour of people (Chabane and Bensalem, 2006, Rezaei et al., 2017). Moreover, windows provide the space with natural ventilation, a view and better acoustic performance (Park and Kim, 2015). Therefore, due to these factors, utilization of the window in building facades is more significant, alongside the importance of taking into account visual comfort and energy efficiency of the design and windows selection (Rezaei et al., 2017).

Window glazing is one of the most significant components of a building that influences its performance in visual and thermal comfort. Solar radiation comes at a variety of wavelengths that have different thermal and optical properties. The visible wavelength ranges from red (650 nm) to violet (400 nm), as shown in Figure 3.1. The ideal glazing façade must perform optimally in both winter and summer, by transmitting the desirable radiations while reflecting those of undesirable wavelength.

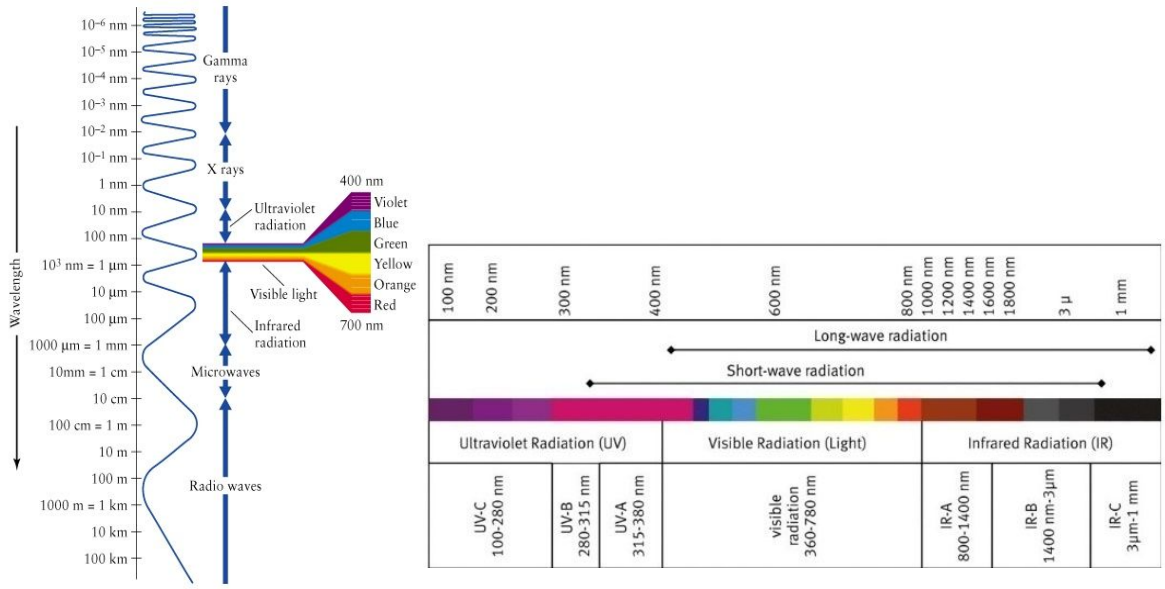


Figure 3.1 Wavelength range from Universe by Freedman and Kaufmann, left (nasa.gov 2017), and wavelength range, right (thiesclima.com 2017)

The behaviour of ideal glazing is illustrated in Figure 3.2 below. As shown, part of the longwave thermal radiation is emitted by the glazing surface while others are reflected. In summer conditions, the visible light accesses the space through the glazing to illuminate the indoor environment while the infrared radiation is rejected to reduce solar heat gain. In contrast, it allows most of the solar radiation to reduce the requirement for space heating in winter (Long and Ye, 2014a).

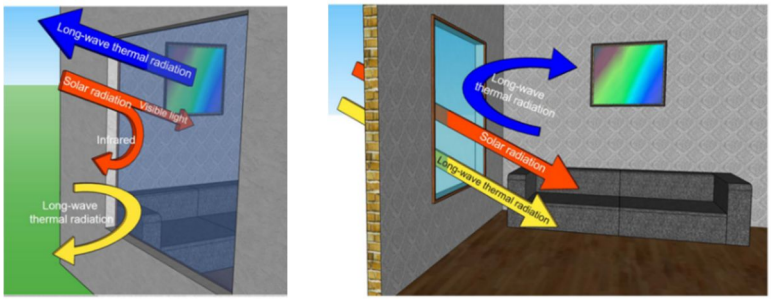


Figure 3.2 Ideal glazing façade in summer (left) and winter (right) (Long and Ye, 2014a)

While previous studies such as (Chow et al., 2010, Cuce and Cuce, 2016, Ascione, 2017) have focused on advanced glazing technologies, their utilisation and manufacturing specifications, limited studies have indicated glazing issues in terms of their influence on the performance of daylighting and energy efficiency. Previous researches have covered several glazing types that are either under development or available commercially, and the innovative glazing was classified under different categories [Sadineni et al. (2011); Hee et al. (2015); and Ghosh et al. (2015)].

A review of the impact of glazing on daylighting and energy saving by Hee et al. (2015) highlighted several glazing technologies and their applications. This investigated the effect of glazing on thermal energy performance, daylighting level and total energy performance. Glazing types were classified into five categories: static windows, dynamic windows, thermotropic windows, PV windows and innovative glazing. Innovative glazing technologies include aerogel glazing, phase change materials (PCM), prismatic glazing, and vacuum glazing. It was concluded that more validation is needed regarding the performance of PCM glazing in terms of visible transmittance (Tvis) and aerogel glazing in terms of its solar control.

Technologies and materials that aim to provide enhanced performance in daylighting solutions, thermal insulation or solar gain or that aim to enhance the performance of a combination of several factors were presented by Sadineni et al. (2011). Technologies and materials were classified into five types: aerogel glazing, vacuum glazing, switchable reflective glazing, suspended particle devices (SPD), and film and holographic optical elements.

The performance of smart glazing in terms of solar modulation, insulation properties, glare control, infrared (IR) reflectance, and visibility enhancement was investigated by Rezaei et al. (2017). Glazing technologies were classified into three categories, static, smart and electrical power generating and included the materials and technologies of conventional, advanced and smart glazing.

Another example of classification of glazing technologies was conducted by Ghosh et al. (2015), based on the switching method from transparent to translucent state, and inversely. Glazing that controls solar heat gain was defined under two categories: switchable transparency glazing and constant transparency glazing. Further, Ghosh and Norton (2017) introduced smart glazing types that can control daylight, alongside the inclusion of properties of heat loss and heat gain.

To conclude, it has been found that previous reviews of smart glazing have concentrated on two aspects, namely, energy-saving and thermal comfort. However, while some studies have attempted to investigate the optical properties of smart glazing in high latitudes, knowledge about the influence of smart glazing on visual comfort, particularly in low latitudes, is limited.

3.2. Types of smart glazing

This section provides definitions and descriptions of smart glazing that can be applied for daylighting purposes. Smart glazing types are classified in this review based on their operation method as either passive or active.

3.2.1. Active smart glazing

Active smart glazing requires external control by the user to change its status, for instance, electrical voltage or gas and includes electrochromic glazing, gasochromic glazing, suspended particle device (SPD), liquid crystal glazing (LC) and photovoltaic-powered (PV) glazing.

3.2.1.1. Electrochromic glazing

The phenomenon of electrochromism is the reversible conversion of the characteristics of optical properties of the material when external power is applied while the ion is inserting or releasing (Kalagi et al., 2011, Baetens et al., 2010, Piccolo et al., 2009); this process changes the colour of the glass which can be seen macroscopically (Piccolo et al., 2009). The majority of electrochromic glazing (EC) contains more than one layer. Glass or plastic is the basic material covered by a transparent conducting film. By switching between their oxidised and reduced form, the optical properties of electrochromic glazing are changed.

However, electrochromics reflecting in their coloured state instead of absorbing are the most favourable; most electrochromics are absorbing, as that has been found exceedingly difficult. Instead of the material property, the phenomenon of electrochromism could therefore be defined as a feature of the window component. Optimisation of the switching speed, durability and modulation range can be achieved by combining two types of electrochromic devices, for instance, ion conductors and ion-storage films (Baetens et al., 2010).

A study by (Piccolo et al., 2009) found that suitability to the latitude and orientation of the site within local climate conditions can be achieved by changing the angle of the glazing that has an active switching impact. In addition, it was concluded that a high level of constant illuminance can be obtained by means of electrochromic glass if operated using a dynamic control approach. However, this is not possible in the case where the daylighting beam enters the building directly. The major finding of the study was that though glare caused by direct daylight cannot be entirely resolved utilising switchable glazing, glare emanating from diffused sunlight occurring through significantly reflected glazing can be minimised by the use of switchable glazing. Figure 3.3 below shows a switching sequence of electrochromic laminated glass, with the colour darkness of the glass increasing from right to left.



Figure 3.3 Sequence of an electrochromic laminated glass switching process (Gesimat, 2017)

Moeck et al. (1998) conducted a computer simulation by means of RADIANCE for the west façade of an office building in Phoenix, Arizona, in the USA, which is located in a hot climate zone within a mid-latitude region with a latitude of 33 North. It was concluded that a constant illumination level of 500 lux (IES-recommended levels) could be met under the conditions of the Arizona climate under an overcast and a clear sky using electrochromic devices that could provide a visible transmittance range of 0.08-0.88, except if the building received direct sunlight, where a visible transmittance range of 0.01 is required to achieve an illumination level of 500 lux.

In order to investigate the performance of electrochromic glazing in commercial buildings, large-area electrochromic glazing was examined through a full-scale field test by Lee and DiBartolomeo (2002). Monitored outputs were produced showing that a new level of dynamic illumination control and transparency could be achieved by electrochromic glazing devices. Energy-saving from the lighting was achieved from 6 to 24% and 3 to 13% compared to 11 and 38% via glazing, with an improvement in brightness level inside the space and respective improved window brightness control. The study concluded that visual comfort and energy efficiency might not be maintained by means of EC devices if direct daylight enters the space during winter, where the altitude of the sunbeam is low. Moreover, the application of ECs for nonresidential projects will be limited during winter if the architectural improvement of the façade and window in addition to the dynamic control does not apply due to the slow speed of the switching process.

To maintain visual comfort, the current switching speeds of EC require an enhancement if the glazing area is larger than $0.1m^2$ when the ambient temperature ranges from -20 to 80 ^oC. However, that enhancement should not reduce the durability of the window, which seems to be the major obstacle facing the application of large-area EC glazing in the future (Lee and DiBartolomeo, 2002).

A lighting energy monitoring and control system development of ceramic thin-film EC devices were initiated at Lawrence Berkeley National Laboratory in Berkeley, CA, United States. The

study measured the performance of the EC window-lighting control system during the equinox under overcast, partly cloudy and clear sky conditions. It was found that energy consumption for the lighting was reduced by 44% to 59% and 8% to 23% compared to the referenced glazing with visible transmittance of 0.15 and 0.50, respectively. The setpoint range of 510-700 lux could be obtained for 89 to 99% of the day within a 10% increase or decrease of the illuminance level, if an integrated window-lighting control system was utilised (Lee et al., 2006).

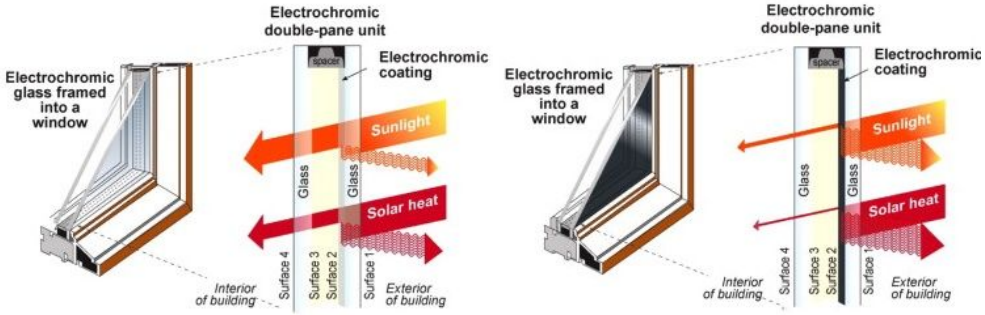


Figure 3.4 Electrochromic technology in clear and tinted states (Sbar et al., 2012).

3.2.1.2. Gasochromic glazing

Gasochromic glazing has similar principles to electrochromic glazing. While electrical voltage is required to change the colour of the glazing in the electrochromic device, gasochromic glazing can change colour by applying hydrogen gas H_2. One of the significant advantages of gasochromic devices is that in the bleached state, they have a high solar transmittance (Wittwer et al., 2004). In addition, the cost of gasochromic glazing is low (Baetens et al., 2010), and they have a simple configuration due to the absence of transparent electrical layers, where one electrochromic layer is enough to change the colour state of the glazing (Wittwer et al., 2004, Baetens et al., 2010). Finally, it has been concluded that, if the gas exchange of the gasochromic device (GD) has good control processes, this can be an option for glazing applications (Baetens et al., 2010).

Gasochromic devices have a varied transmittance range. The principle factor for the change in transmittance is based on a thin tungsten oxide layer (WO_3) that is shielded by a very thin platinum layer. When a gas of diluted hydrogen is applied to the coating, the tungsten oxide reduces, hence, the colour changes (Wittwer et al., 2004). Applying diluted oxygen will have the opposite effect of the hydrogen. The required amount of gas to switch the colour status is exceptionally low, where an electrolyser is responsible for producing hydrogen and oxygen.

The gasochromic device contains a gasochromic layer. The transparency and colour of the glazing are changed when the GC layer is exposed to diluted hydrogen. The volume of the

hydrogen is responsible for the transparency level of the gasochromic glazing, and therefore, to change the GC to a transparent state, diluted oxygen gas is applied (Rezaei et al., 2017). This make possible that the performance of most of the conventional glazing systems to be enhanced by integrating a gasochromic coating. New applications of gasochromic devices are available due to the use of metal hydrides in switchable mirrors (Wittwer et al., 2004).

3.2.1.3. Suspended particle device

Suspended particle device (SPD), also known as electrophoretic glazing, is a smart glazing that has a double layer of glass with a gap filled with a plastic film. The glass itself has a herapathite suspended particle device or suspended dihydrocinchonidine bisulfite polyiodide (Ghosh and Norton, 2017). The first suspended particle device, known as the “light valve”, was invented by Dr Edwin Land in the 1930s (Vergaz et al., 2008). The SPD has an active layer with spherical or needle-shaped particles suspended in a gel or an organic fluid. The fluid is filled or coated between two transparent electrodes. During the state of voltage absence, particles are suspended; hence, they do not allow the light to pass through where they have a random orientation (Vergaz et al., 2008, Ghosh and Norton, 2017) due to Brownian movement (Ghosh and Norton, 2017). In contrast, the internal charges of the particles are moved to a minimum energy state when a single alternate voltage is applied, where the particles have a rotation movement that sets them within alignment lines, and this process allows light to pass through the window, as shown in Figure 3.5 (Vergaz et al., 2008).

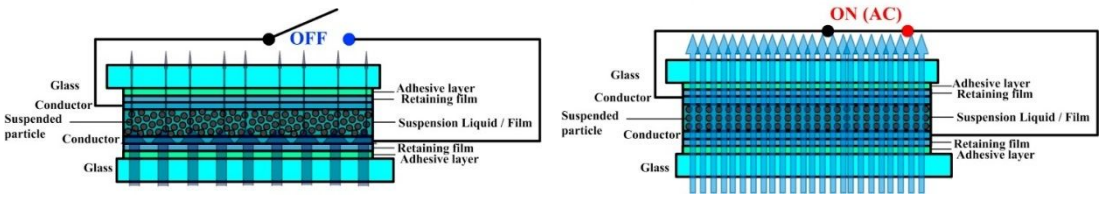


Figure 3.5 Schematic multilayer structure of an SPD in OFF (right) and ON (left) states (Barrios et al., 2015)

In order to keep the SPDs film transparent, an electric field is necessary, while this is not required for electrochromics devices. SPDs typically require a voltage of 20-150 V RMS (root mean square) to be operated, which depends on the thickness of the device. With a switching speed of hundreds of milliseconds, the typical transmission range of the SPD is from 20 to 60% (Vergaz et al., 2008). SPDs have many advantages, and it is simple to control their electrical power (Ghosh et al., 2016). Figure 3.6 illustrates the operation of a suspended particle device.

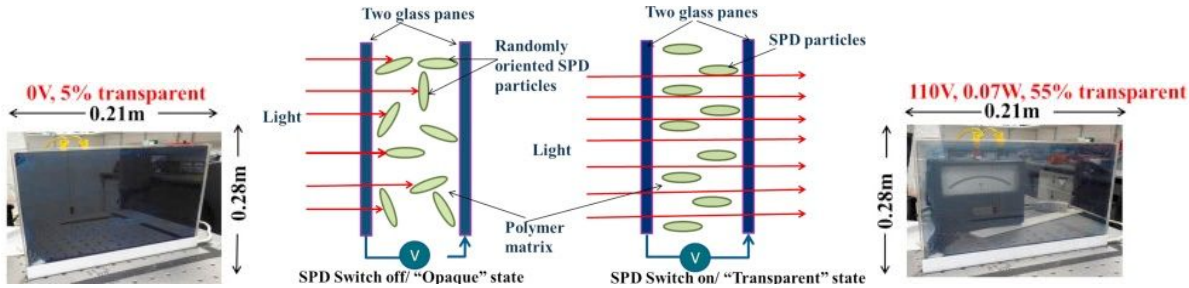


Figure 3.6 An opaque (right) and a transparent state (left) of SPD glazing (Ghosh et al., 2016)

3.2.1.4. Liquid Crystal glazing

Liquid crystal glazing (LC) is a type of electroactive glazing that turns to a transparent state if an alternative voltage power (AC) is applied. Due to the application of the electrical power inside the particles, the liquid crystal device is set in an alignment arrangement instead of random orientation, which allows the light to pass through the window (Rezaei et al., 2017). Most liquid crystal devices turn into a translucent state, and are white in colour if the application of electrical power is absent (Rezaei et al., 2017). Figure 3.7 and Figure 3.8 below illustrate the translucent state (OFF mood) and transparent state (ON mood) of LC glazing. Liquid crystal glazing is a preferred option to provide privacy for the occupant (Rezaei et al., 2017). However, the switching process requires electrical voltage to turn on the ON mood (Transparent state). Recent studies have attempted to reverse the operation process to make the LC require the power to switch to a translucent state instead (Rezaei et al., 2017, Kim et al., 2015, Yamaguchi and Takasu, 2015).



Figure 3.7 LC Privacy Glass, the translucent mood on the right and transparent mood on the left (Innovative Glass Corporation, 2017)

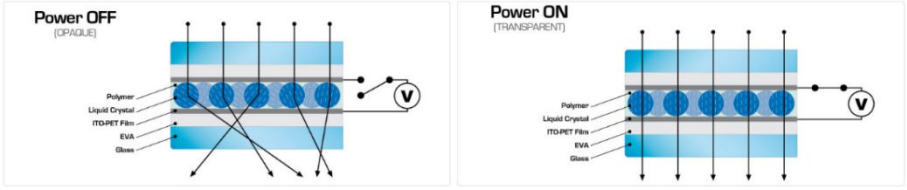


Figure 3.8 Illustration of the OFF and ON mood of the LC device (Dream Glass Group, 2017)

3.2.1.5. Photovoltaic-powered glazing

Photovoltaic-powered (PV) glazing is most desirable among electrochromic devices where it does not require exterior wiring, primarily due to the compatibility in operation of electrochromic and photovoltaic glazing. Self-powered PV electrochromic devices have been built by the National Renewable Energy Laboratory of Golden, USA (Bullock et al., 1996). Future research for large-scale implementations of PV electrochromic glazing is focused on the energy loss generated by the PV for large areas. In addition, the low transmission in the transparent condition and limited range of optical modulation are also among the significant focuses (Baetens et al., 2010). Semi-transparent PV systems have been utilised for daylighting purposes. They were applied on walls, windows and rooves (Casini, 2016), as shown in Figure 3.9.



Figure 3.9 Crystalline silicon PV glazing, Berlin Hauptbahnhof (Casini, 2016)

The potential of utilizing PV for energy generation and daylighting became possible due to the transparent solar cell being integrated into glazing. However, the high cost of this technology challenges its application in the building sector (Jelle et al., 2012). Furthermore, the balance between the performance of the daylighting and the energy generation is a challenge (Chow et al., 2010, Jelle et al., 2012). A comparison of the generated power and transparency percentage of thin-film and crystalline silicon PV panels was conducted by Casini (2016) and it is shown in Figure 3.10.

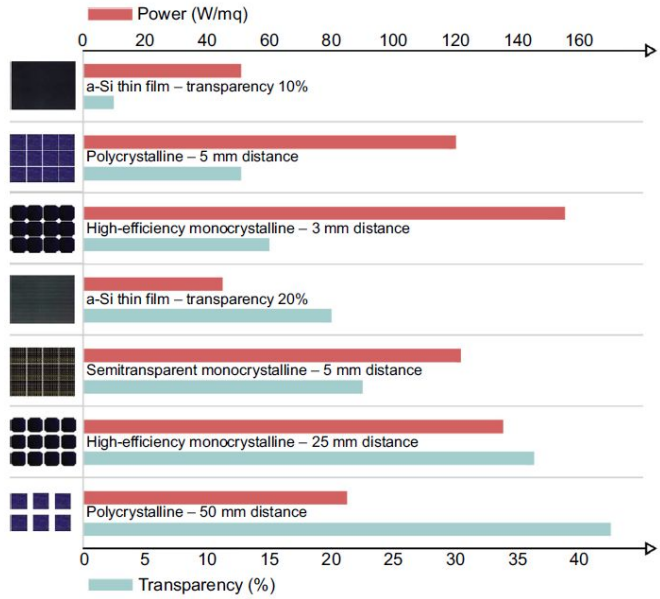


Figure 3.10 Generated power and transparency of PV panels (Casini, 2016)

3.2.2. Passive smart glazing

Passive smart glazing can change its status through the effect of natural sources, for instance, a change in heat or light intensity. Passive smart glazing includes thermochromic glazing, photochromic glazing, thermotropic glazing, aerogel glazing, PCM glazing and light-redirecting glazing.

3.2.2.1. Thermochromic glazing

Thermochromic is intelligent glazing that changes its properties at a critical temperature (Tc), as shown in Figure 3.11. The cooling loads may be reduced where the device allows solar energy to pass through space when the temperature is below Tc, and this reflects the infra-red portion of solar energy when the temperature is higher than Tc, as illustrated in Figure 3.12 (Parkin et al., 2008, Long and Ye, 2014b, Konstantoglou and Tsangrassoulis, 2016)

Parkin et al. (2008) concluded that intelligent thermochromic glazing could be switched at a temperature of 25-30 ^{o}C, which can be specified by the tungsten doping level. However, in order to produce thermochromic glazing commercially, there are three main challenges: to change the colour of the film (yellow/brown); to enlarge the size; to be able to protect the coating from external environmental conditions due to thermal cycling (Parkin et al., 2008).

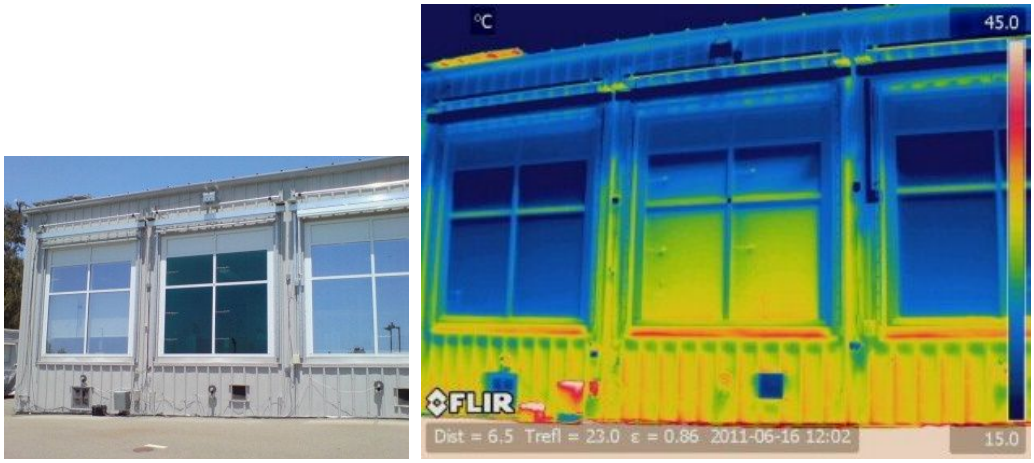


Figure 3.11 Thermochromic glazing (middle room). Surface temperature (left) (Lee et al., 2013)

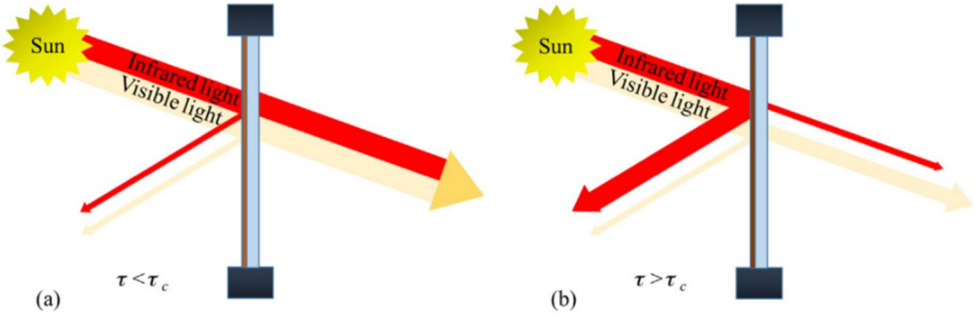


Figure 3.12 Thermochromic glazing lower (a) and higher than the transition temperature (b) (Silva et al., 2016)

3.2.2.2. Photochromic glazing

Photochromic glazing was referenced for the first time at the end of the 1980s (Mohelnikova, 2007). Photochromic and thermochromic devices are types of smart gazing; however, they cannot be controlled in the same way as electrochromic devices, due to the switching in both of these technologies, with the switching in colour of the glazing being based on temperature and solar radiation, respectively (Jelle et al., 2012). Furthermore, photochromic and thermochromic devices are not able to control external environmental conditions. As a result, they cannot control the properties of the photo (Baetens et al., 2010).

The transparency of photochromic glazing changes when the ambient solar radiation, which depends on the light intensity, faces the window, (Ascione, 2017, Mohelnikova, 2007). Therefore, the daylighting performance and energy efficiency can be enhanced by utilising photochromic glazing to reduce glare and heat gain, hence reducing the cooling (Ascione, 2017).

3.2.2.3. Thermotropic glazing

Thermotropic glazing possesses a polymer gel that is sandwiched between two layers of glass (Inoue et al., 2008). In order to utilise the thermotropic materials in the glazing application with extended stability, protection for their layers is required. As a result, two transparent glass panes are typically used to cover the active thermotropic layer and seal the edges (Nitz and Hartwig, 2005).

The optical properties of the thermotropic and thermochromic devices change when they reach a specific threshold temperature (Nitz and Hartwig, 2005). The polymer gel inside the thermochromic glazing is converted from a transparent to translucent state at a threshold temperature (Inoue et al., 2008). Thermotropic devices have the propensity to scatter daylight through the material when the temperature changes, while thermochromic devices change the colour of the material given the same effect (Nitz and Hartwig, 2005).

The dimming of thermotropic glass can be prevented by the low temperature during the cold season, where solar shading may be needed. By using a suitable control for the heating layer, however, the thermotropic layer can perform better for shading purposes in office buildings with the absence of a heating layer despite the simple configuration of the system. In addition to the utilisation of solar radiation, low voltage electric power is required to maintain the translucent state of the glass (Inoue et al., 2008). Figure 3.13 shows two thermotropic glazing types in transparent and translucent states [A] and [B]. In addition, it illustrates the configuration of a window unit consisting of low-emissivity and thermotropic glass [C] (Inoue et al., 2008).



Figure 3.13 Thermotropic glazing: transparent on the left and translucent on the right, Configuration of window unit consists of low-emissivity and thermotropic glass (Inoue et al., 2008)

3.2.2.4. Aerogel glazing

Aerogels are lightweight porous dried gel (Baetens et al., 2011, Rezaei et al., 2017, Hüsing and Schubert, 1998, Bahaj et al., 2008), and can be made from different materials such as silica, alumina, metal chalcogenides, carbon, inorganic and organic polymers and metal oxides (Bahaj et al., 2008, Jelle et al., 2012, Cuce and Riffat, 2015). However, they typically possess air and silica (Rezaei et al., 2017, Jelle et al., 2012, Cuce and Riffat, 2015), and have at least 50% porosity (Bahaj et al., 2008).

Aerogels were invented in the 1930s by Kistler (Baetens et al., 2011, Kistler, 1931, NASA, 2011). They are insulation materials with high performance in thermal insulation and light transmission (Rezaei et al., 2017) and were developed as an insulation material by NASA (Bahaj et al., 2008, Jelle et al., 2012, NASA, 2011). Aerogel glazing can diffuse the daylight due to the use of translucent aerogel particles (Jelle et al., 2012). Aerogels materials have been applied for daylighting solutions in current buildings with a large glazing area (Baetens et al., 2011). In 2006 aerogel material was used in the market extensively as a translucent curtain wall (Bahaj et al., 2008, Granqvist, 1995), as shown in Figure 3.14 [A].

Commercial aerogel has a low thermal conductivity as low as 0.013 W m^{-1} K^{-1} (Baetens et al., 2011, Rezaei et al., 2017) and 1 to 150 kg/m^3 density that consists of 90-99.8% air (Bahaj et al., 2008). Aerogel can improve the solar, daylight and thermal performance of windows in buildings. The U-value of aerogel glazing can be as low as 0.1 W/m^2 however, improvement is required to enhance its visible transmittance property (Jelle et al., 2012). A view through a monolithic aerogel sample is shown in Figure 3.14 [B].



[A] [B]

Figure 3.14: [A] Aerogel glazing applied on the façade (Reim et al., 2005), and [B] a monolithic aerogel sample (Buratti and Moretti, 2012)

3.2.2.5. PCM glazing

Phase change materials (PSMs) are materials that store heat during the latent heat stage. PCMs gain or lose thermal energy when the state of the material is converted from liquid to solid and vice versa. The recommended deliquesce point of PCMs for thermal storage for heating and cooling purpose is within the range of 20 to 32 ^{o}C (Tyagi and Buddhi, 2007).

While the need for heat energy is greater during cold nights, the peak of heat energy from solar radiation is during the daytime; hence, energy storage is necessary to resolve this issue. Through the transition of the material, PCMs can store a large amount of energy. The state of PCMs in the liquid phase has high transparency, and they do not scatter the daylight (Weinlader et al., 2005).

Mehling (2004) tested PCMs integrated with a glazing system for heating and cooling purposes and daylighting enhancement. The PCMs were applied as internal louvres, as shown in Figure 3.15 (Sharma et al., 2009). Another study by Alawadhi (2012) evaluated an internal shading device made from PCM material to reduce heat gain through fenestrations in a hot climate region (Kuwait). The study found that heat gain can be reduced by 23.29%.

A further study by Goia et al. (2012) investigated the performance of a PCM glazing system compared with a conventional reference double window. It was concluded that the performance of PCM glazing was improved, and the indoor thermal environment can be enhanced through PCM glazing.



Figure 3.15 PCM internal shading devices (Sharma et al., 2009)

3.3. Daylight assessment tools

The daylight study can be assessed using daylight simulation's software, a daylight scale model, or a daylight measurement in a real case study.

3.3.1. Daylighting simulation software

This section discusses the various software used for daylighting simulation.

RADIANCE

RADIANCE software is a tool that analyses and helps to visualises the lighting for design and research purposes. Scene geometry, luminaires, date, time, materials and sky conditions are specified by input files. It calculates spectral radiance, irradiance and glare. Its outputs can be visualised as colour images, contour plots and numerical values (radiance-online.org 2016). RADIANCE is a validated ray-tracing software used by many specialists in the daylighting field, including designers, engineers, and researchers (Reinhart and Fitz, 2006).

DAYSIM

DAYSIM is a dynamic daylight simulation tool based on RADIANCE. It calculates the daylight in the building during the whole year. It can model different daylighting systems controlled automatically or by occupants, for instance, redirecting elements, switchable glazing or a combination of different systems. Many daylighting performance outputs can be obtained using DAYSIM. For instance, it can provide useful daylight illuminance, daylight autonomy and annual glare (daysim.ning.com 2017). Prediction of the short-time stem enhancement of illuminances inside the space can be obtained by DAYSIM, which applies the concept of the daylight coefficient and Perez sky model, as validated by Reinhart and Walkenhorst (2001).

Desktop RADIANCE

Desktop RADIANCE is a simulation tool that links AutoCAD with RADIANCE. It uses AutoCAD to build the geometry and RADIANCE to analyse the daylighting performance. RADOUT is the link tool with AutoCAD (Kota et al., 2014).

ECOTECT to RADIANCE and DAYSIM

ECOTECT has been used widely in previous studies for daylighting analysis. The model is built in ECOTECT and then exported to RADIANCE and DAYSIM.

EnergyPlus

EnergyPlus is a simulation tool for energy analysis, HVAC (heating, ventilation, and air conditioning) and lighting (energy.gov 2016). Through its radiosity daylighting engine, EnergyPlus is capable of daylighting simulation (Motamedi and Liedl, 2017).

RHINOCEROS

RHINOCEROS 3D is a modelling program based on the non-uniform rational basis spline (NURBS) method. Furthermore, it is a visualization tool that is linked with GRASSHOPPER, RADIANCE and DAYSIM. Finally, it provides daylighting simulation through its toolbar (Lagios et al., 2010).

DIVA for RHINOCEROS 3D to DAYSIM

DIVA is a plug that links RHINOCEROS 3D with RADIANCE and DAYSIM. It allows users to use the interface of RHINOCEROS and the engine of RADIANCE and DAYSIM for daylighting simulation (Kota et al., 2014) and performs climate-based daylighting metrics (CBDM) and glare analysis (diva4rhino.com 2017).

GRASSHOPPER

GRASSHOPPER is a plugin for RHINOCEROS. It is a graphical algorithm editor used for parametric studies, and can be used without experience of scripting (Day, 2010). It is integrated with RHINOCEROS software, where it is used to visualize the outputs of its algorithmic formula (grasshopper3d.com 2017).

LADYBUG and HONEYBEE

LADYBUG and HONEYBEE are plugins for GRASSHOPPER for environmental design (grasshopper3d.com 2017). LADYBUG reads IDF (Intermediate Data Format) files (Motamedi and Liedl, 2017) and visualises the weather data by importing the (.epw) files into GRASSHOPPER (grasshopper3d.com 2017), as presented in Figure 3.16. LADYBUG links daylighting engines such as RADIANCE, DAYSIM and EnergyPlus with GRASSHOPPER (Roudsari and Pak, 2013).

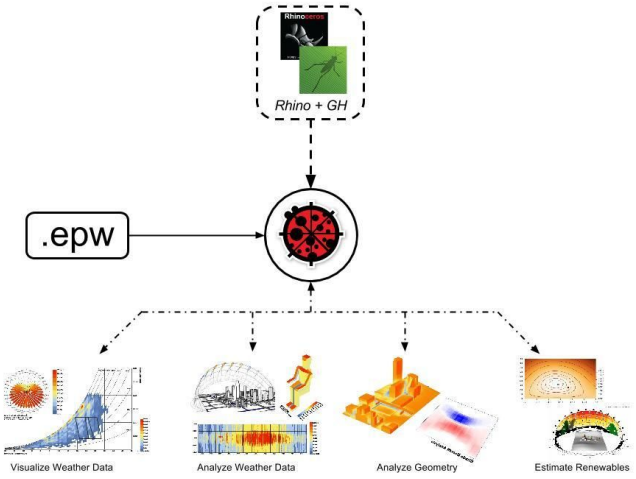


Figure 3.16 Ladybug plug-in (grasshopper3d.com 2017).

HONEYBEE is a plug-in that links GRASSHOPPER with daylighting and building energy simulation engines, namely, RADIANCE, DAYSIM, EnergyPlus and OpenStudio. By linking GRASSHOPPER with daylighting engines through HONEYBEE, daylighting analysis can be conducted using a parametric method (grasshopper3d.com 2017), as shown in Figure 3.17. Thus, HONEYBEE, as an extension of LADYBUG, allows users to do more advanced analysis than LADYBUG (Roudsari and Pak, 2013).

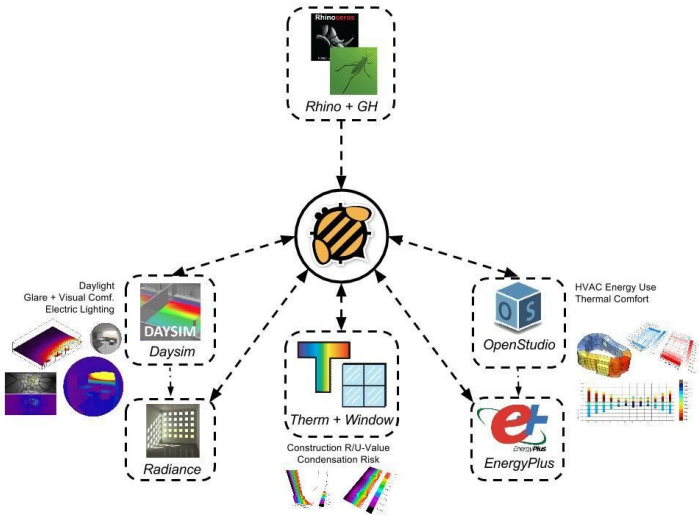


Figure 3.17 Honeybee plug-in (grasshopper3d.com 2017).

OpenStudio

OpenStudio® is a cross-platform that works with different operating systems, namely, Windows, Mac, and Linux and support software to conduct daylighting analysis by RADIANCE and build energy model by EnergyPlus. OpenStudio is an open-source (LGPL) project for building sector community and has a graphical interface through Software Development Kit (SDK) (openstudio.net 2017).

PHOTOPIA

PHOTOPIA is a simulation software for non-imaging optical systems such as compound parabolic concentrator (CPC) and concave reflected surfaces. This 3D CAD simulation software is widely applied, and has been validated in previous studies. Furthermore, PHOTOPIA can simulate daylighting by means of the sky model, which is based on the IES-PR21 document (Yu and Su, 2015). PHOTOPIA includes a built-in CAD system or is available as an add-in for SOLIDWORKS® (ltioptics.com 2017).

Autodesk 3dsMax Design

Autodesk 3dsMax Design is used mainly for rendering and animation purposes. Daylighting design and analysis can be conducted in 3dsMax via a module called Exposure and a daylighting engine called mental ray (Kota et al., 2014).

ADELINE

ADELINE (Advanced Daylight and Electric Lighting Integrated New Environment) is software for daylighting and artificial lighting simulation. It is connected with RADIANCE and energy simulation by SUPERLINK. The geometry is built in SCRIBE-Modeller, and the materials are provided by PLINK, which assists in doing daylighting simulation by defining the climate data (Kota et al., 2014).

VELUX

VELUX is software for lighting simulation that analyses and visualizes daylight inside buildings providing users with daylight levels and appearance (velux.com 2017).

Chapter 4. Research methodology

This chapter describes the methodology of the research and the design of the proposed system. It briefly explains each part of the study; however, an in-depth description and illustration of the procedure of each part of the system design is shown at the beginning of the relevant chapters. This research is based on a quantitative approach with data obtained mainly through computer modelling and experimental tests. The objective of the study was to enhance the daylighting performance at the work plane level. The study examined a typical office with a south façade in low and high latitude regions. The effect of sun altitude and azimuth angles has been tested.

4.1. Research methodology

The data collection in this study was conducted through three main phases: an extensive literature review, a computer simulation, and physical experimental studies. The research methods relied on an extensive review of literature relating to daylighting given in Chapter 2 and Chapter 3. Thereafter a hypothesis is presented, which is delivered from the conclusions of the literature review study. Then, the design of the daylight-redirection device (DRD) was enhanced through an optimisation process using a parametric computer tool.

The simulation comprises two stages: early optimisation and futher investigation. Experimental tests were carried out after the early optimisation stage with the purpose of observing the performance of the proposed system in reality and validating the outputs of the daylight simulation. The chapter concludes with a discussion of the limitations, recommendations, and conclusions of the research methods. An outline of the research methodology is illustrated in Figure 4.1.

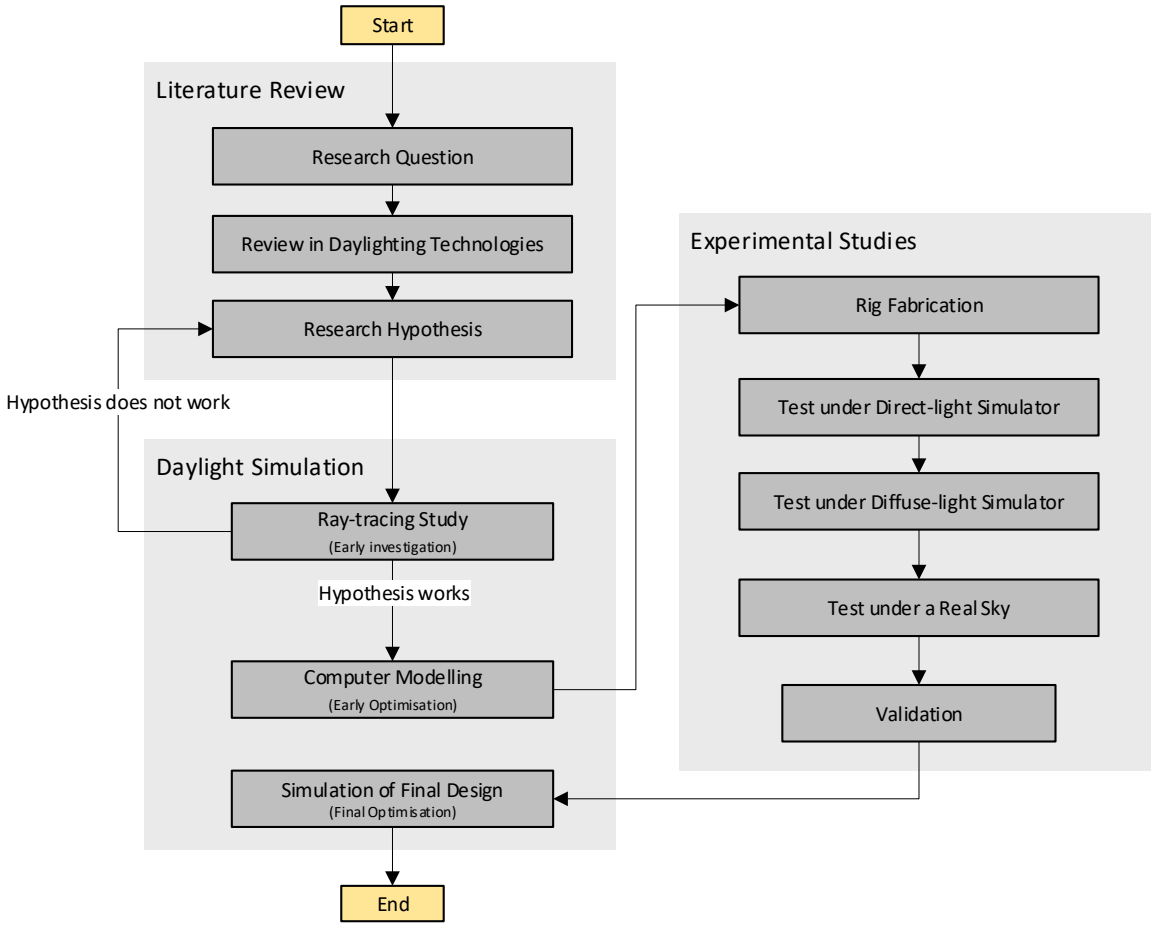


Figure 4.1: Flowchart of research methodology

4.1.1. Location of the study

The study was conducted using two specific locations: Riyadh, Saudi Arabia (low latitude) and Nottingham, United Kingdom (high latitude). These two locations were chosen to investigate the performance of the proposed system in the booth latitudes, to reflect low and high latitude regions, where the solar altitude is high and low, respectively.

4.1.2. Case study

The case study is a room within an office building. The main characteristics of the room and the window are typical for office buildings, as commonly found in previous studies. The initial window to wall ratio (WWR) is calculated based on the recommended window to floor ratio (WFR) found on the Saudi Building Codes-General document (SBC 201), 2018.

The applied perforated solar screen (PSS) is found extensively on vernacular architecture in hot climates and applied globally in contemporary buildings. Currently, building designers attempt to employ PSS as a feature for better daylighting practice, as many studies claim that

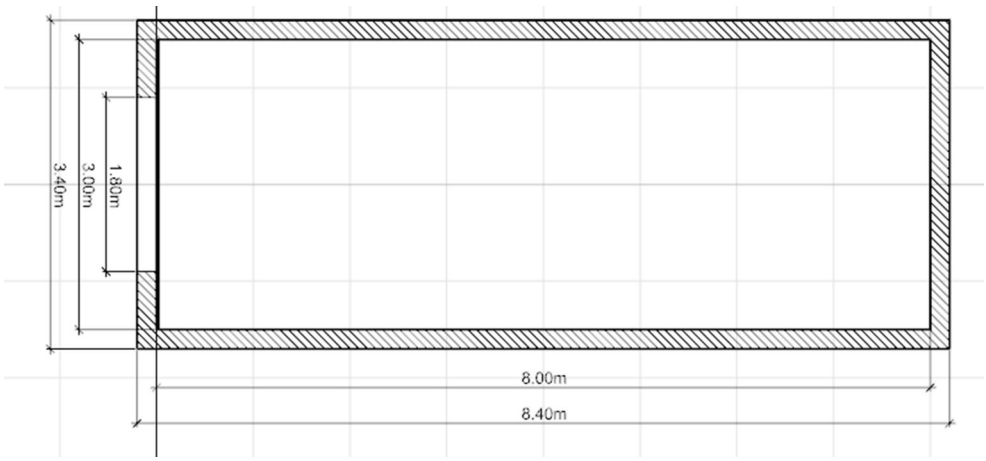
PSSs can provide occupants with balanced daylighting while allowing a view out of the outdoor environment.

In this study, PSS is applied to an office building with a south façade and tested for two aforementioned locations of Riyadh and Nottingham, representative of low and high latitude regions, respectively. The purpose was to investigate the ability of the proposed system to enhance daylighting performance under different sky conditions. The PSS was integrated with the daylight-redirecting device DRD as previously described. The development of the proposed DRD was informed by the findings and science around daylight and daylighting. Further, it is integrated with the suggested PSS to produce a novel daylighting system that can improve the performance of daylight uniformity at the work plane (DUWP).

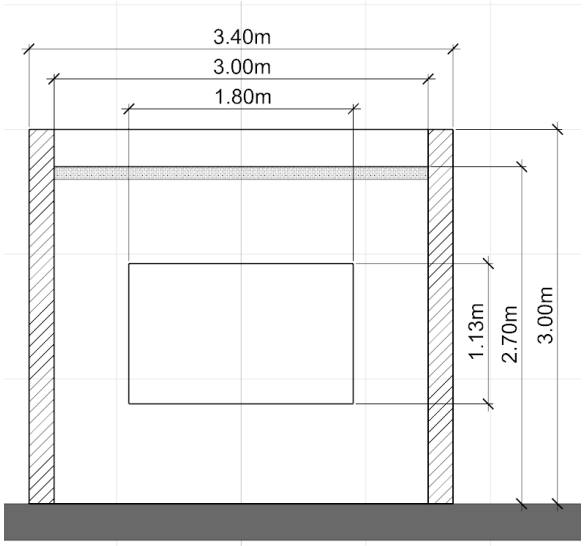
The case study used a single space typical office room, with a rectangular plan that has one external façade facing south. The width, depth and height of the room are 3 x 8 x 3 meters, respectively and the net height from floor to ceiling is 2.70m. The window to floor ratio (WFR) is 0.084 %, which equates to a 25% window to wall ratio (WWR). The window area is 2.01 m^2, the windowsill is 0.80 m from floor level, with dimensions of 1.8 width x 1.13-meter height, as shown in Table 4.1and Figure 4.2 below.

Table 4.1: Prosperities of the tested room

Room						**Window**			
Orientation	Width	Depth	Height	WFR	WWR	Area	Sill	Width	Height
South	3 m	8 m	3 m	0.084 %	25%	2.01 m^2	0.80 m	1.8 m	1.13 m



[A]



[B]

Figure 4.2: [A] Plan, and [B] section of the room

4.1.3. Literature review

First, an extensive literature review in three primary areas of daylighting, namely daylighting technologies (Chapter 2), innovative glazing, and daylight assessment tools (Chapter 3), was conducted to identify the research gap and to build the research hypothesis.

i) Daylighting technologies

The review was expanded to cover most of the new daylighting technologies to investigate the strengths and weaknesses of each system. This comprised three main types: daylighting redirecting technologies, daylighting transporting technologies, and daylighting filtration technologies, with categorisation based on the purpose of this study and the operation principles of the technologies.

ii) Innovative glazing

Glazing, in general, plays a crucial role in daylighting performance of buildings. In this review, the focus was on smart glazing, which could be employed to enhance the performance of the proposed system. Several glazing technologies were included, categorised under two main types: active and passive smart glazing.

Finally, the hypothesis was developed based on the findings and the principles of daylight science. A proposed novel daylighting system was designed based on the potential daylighting improvement of selected daylighting technology and the related knowledge gap found in previous studies.

4.1.4. Research hypothesis

When daylight strikes the inner surface of a redirecting device, its concave surface redirects the daylight towards the ceiling, at which point the ceiling redirects it to the deeper areas of the room. The reflection of the daylight is expanded by the reflected material of the inner surface of the device. This process is shown in Figure 4.3. The daylight redirection is enhanced due to the “deflecting position” of the concave shape and the reflective coating inside the element (Boubekri, 2014).

The angle of the sunbeams is increased before it hits the inner surface of the DRD by means of a prism layer which is integrated into the inlet of the DRD (top of the device); at the same time, in the outlet of the DRD, the angle of the reflected beam incident is increased. The purpose of increasing the sunbeams angle is twofold; first, the prism lens in the inlet allows the sunbeam to reach deeper inside the truncated redirecting device. Secondly, the prism lens in the outlet sends the reflected daylight to a deeper area inside the room.

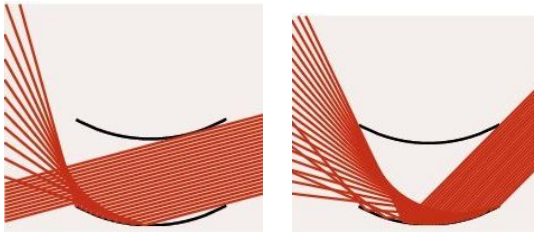


Figure 4.3: Light ray reflection by concave shape (Boubekri, 2014)

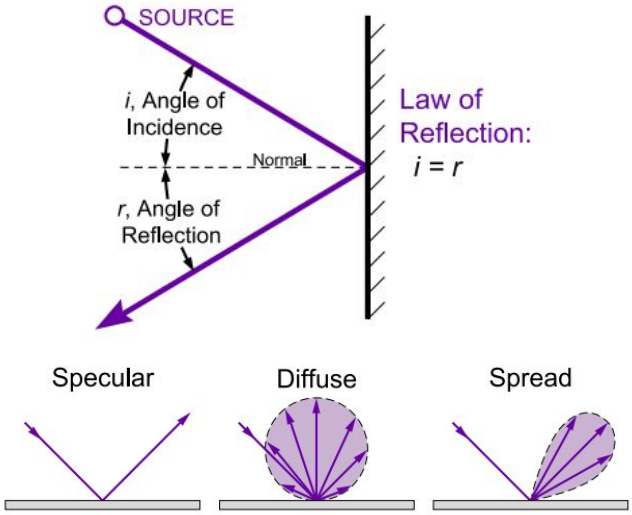


Figure 4.4 Law of reflection (above), and Specular, diffuse, and spread reflection from a surface (below) (Ryer 1997), pp. 13.

4.1.5. Daylight simulation

A daylight simulation in RADIANCE software was conducted through LADYBUG tools in GRASSHOPPER, the plugin of RHINOCEROS software. The simulation began with a ray-tracing study to analyse the sunrays behaviour to test the research hypothesis. Later, the model was set up for a daylight intensity simulation and the accuracy of the outputs was tested through three stages. The main factors tested were the Radiance parameters, simulation method, and sky type. These processes are significant to enhance the accuracy of the simulation results. Moreover, to assess the effect of high and low complexity of Radiance parameters, two types of simulation methods, and two types of the sky were investigated.

Outputs of the model with acceptable (low) and accurate (complex) Radiance parameters were compared. Next, daylight simulation by point-in-time (PIT) and annual daylight studies was conducted. The outputs of the two methods were then compared. Finally, the effect of sky type on the accuracy of the outputs was investigated. The model was simulated with the Tregenza and Reinhart sky matrices.

The room was tested with the minimum WFR recommended by SBC for a room that is daylit by means of daylight only. Then the illuminance levels were measured at the work plane as a function of 6 different perforation percentages, namely, 25, 27, 29, 31, 33 and 35%. Annual dynamic daylight metrics of daylight autonomy, useful daylight illuminance and annual sunlight exposure were used to assess the daylighting performance.

The aim of the early investigation was to test the research hypothesis with the focus on the DRD's lower-inner surface installed on the top third of the façade. A ray-tracing study was run to test the reflection behaviour of the sunrays in a complex method using raytracing by means of RADIANCE. This study revealed an understanding of the sunrays' behaviour during the daylight-redirection process made by the DRD.

The second step was then conducted to investigate the significant parameters of the proposed system. This study revealed the effect of the reflected sunrays on daylight intensity. Based on the investigation, the most significant parameters were carefully selected. The procedure of this study is described in more detail in Chapter 5.

4.1.5.1. Further investigation by simulation

The further investigationwas conducted after the experimental studies to optimise system design and included four main tests: a whole-CPC in reverse mode, a half-CPC in reverse mode, an optimisation of DRD tilt angle, and the effect of prismatic lens integration. The prismatic lens was applied to the inlet and outlet of the DRD to enhance the receiving of sunrays and the redirection process.

4.1.5.2. Limitations

The point-in-time daylight test (PIT) was limited to the following solar times: 8 am, 10 am, 12 pm, 2 pm and 4 pm. On the other hand, the annual daylight simulation includes the whole year. The system was tested in two locations only, Riyadh and Nottingham; however, the proposed system should work with similar performance if the location has the same sky conditions. Two types of materials were applied for the DRD: aluminium and high-reflective white paint. In addition, the materials of the interior elements of the room were limited to the specifications in Table 5.2.

4.1.6. Experimental investigations

After the computer modelling, three experimental studies were conducted to measure and observe the influence of different parameters on the daylighting performance of the proposed system under laboratory and real conditions. The physical model was tested under a direct-light solar simulator (DRLS), under a diffuse-light solar simulator (DFLS), and under UK climate (under a real sky in Nottingham [RSK]). These tests were conducted parallel with the design optimisation, specifically between the early optimisation and the further investigationstages.

The experimental studies had two primary purposes. The first purpose was to assess the accuracy of each method as a tool of daylight assessment, including the computer simulation. The second purpose was to observe and understand the behaviour of the daylight inside the room under real physical conditions.

First, it was important to measure the reflectivity of the applied materials. Therefore, a goniophotometer (GPM) was designed and built for this purpose. In addition, the lux meters were calibrated under the same GPM. Second, the physical scale model was fabricated on a scale of 1:10, based on the recommendations found in previous research for detailed daylight studies (Bodart et al., 2006)**.** Different machines and technologies were utilised to produce an accurate physical daylight model, including a 3D printer, laser cut machine, vacuum machine. Third, the model was tested under two types of solar simulators and real sky conditions. The first and second tests were conducted under the DRLS and DLFS, while the third test was conducted under a real sky in Nottingham (RSK). DRLS represents direct sunbeam only; DFLS represents the diffused daylight, while RSK represents both the direct and the diffused daylight. Finally, uncertainty among the outputs of the experimental tests was compared with the results obtained by the computer simulation for validation purposes.

4.1.6.1. Limitations

The experimental tests of the scale model were limited to the south orientation. In addition, the material applied in the model and the proposed system was limited to what is specified in Table 5.2. With regards to the reflectivity study, reflection angles were calculated for the normal reflection angle only. The surface can distribute the light and hence, reflect it with different angles; however, if the surface is smooth (roughness of the surface is exceptionally low), most of the reflected light should come from a given angle from the normal. The tested material under the GPM is listed in Table 6.2.

The test under the DRLS was conducted for solar noontime only for two dates in two locations only, Riyadh and Nottingham. The simulator utilised the direct light beam while the diffused sky components were applied in the following test. On the other hand, the test under the DFLS focused on diffused daylight only. The test utilised CIE sky (clear with low turbidity) for Riyadh and Nottingham and was limited to south orientation at solar noontime.

4.2. Design and operation principles of the proposed system

The proposed system comprises two types of daylighting technologies integrated with smart glazing, specifically, integration of daylight-redirection and daylight-filtration technologies and a prismatic lens. The name of the daylighting technologies is based on the proposed classification in Chapter 2.

The proposed system integrates a perforated solar screen (PSS) and daylight-redirecting devices (DRDs). The DRD consists of two parts: the redirecting device and the prismatic lens. The selected PSS is used in contemporary and traditional architecture to enhance daylighting inside buildings. The design of the DRD is based on that of a developed compound parabolic concentrator (CPC) that operates in reverse mode. While the initial purpose of a CPC is to concentrate the sunlight to produce thermal energy, the CPC in reverse mode aims to distribute the sunlight to produce uniform daylighting inside buildings. The reverse CPC was applied in previous studies as described in 3.2.1.3.2 Anidolic lighting systems on page 35 above.

The CPC has been tested in previous studies. In Vázquez-Moliní et al. (2013) the application of the system was integrated with transporting daylight technology (light pipes). Another study by Gong et al. (2018) applied it as a micro-light shelf embedded inside two layers of glass. Therefore, the integration of the device within a PSS on the building's façade is a novel idea.

The DRD is a hollow half CPC made from aluminium integrated with two prismatic lenses, installed in the inlet and outlet of the DRD. These prisms have two functions; the inlet prism lens ($Prism_{inlet}$) aims to redirect the sunlight from low solar altitude toward the ceiling. The purpose is to prevent direct sunlight from accessing the DRD without passing through the redirection process by the lower inner surface of the device. In contrast, the outlet prism lens ($Prism_{outlet}$) aims to redirect sunlight from an extreme high solar altitude to reach the deep inner surface of the DRD, which will redirect it toward the ceiling (as shown in Figures 4.4 and 4.5). The design of the proposed system is illustrated in Figure 4.6 and shows the front view, section, and top view with the dimensions in meters.

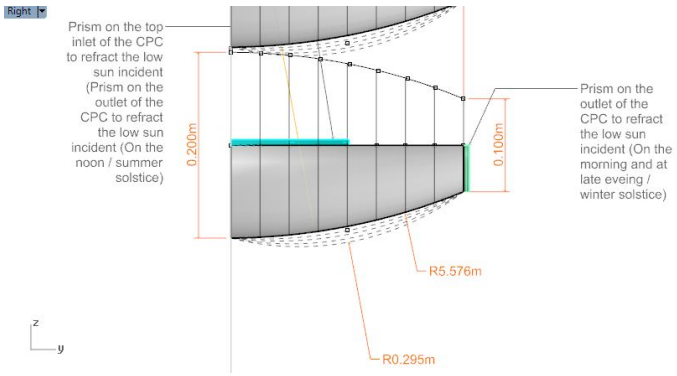


Figure 4.4: The integrated prism lens on the top (DRD $_{inlet}$) and the side (DRD $_{outlet}$) of the DRD

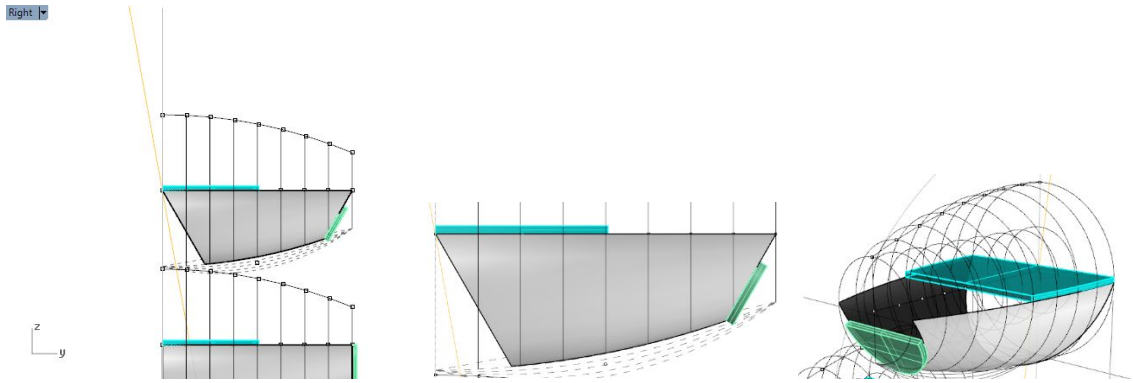


Figure 4.5. DRD with a 30-degrees (inward) truncation

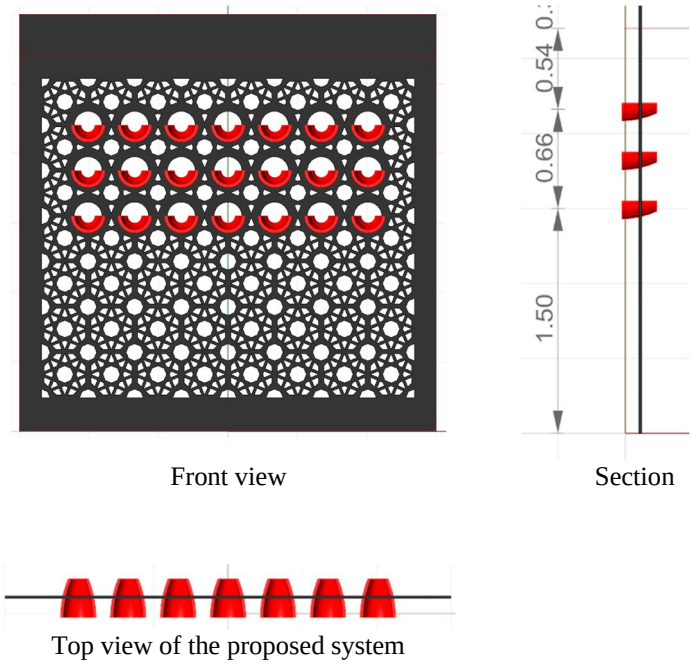


Figure 4.6: The front, section and top views of the proposed system, dimensions are in meters

4.3. Summary

The study included a review of previous research in daylighting and their related applications, including existing daylighting technologies and related smart glazing systems. A research hypothesis was created based on the findings and the potentiality of these technologies to

enhance the daylighting performance inside buildings. This was then followed by a review of daylight assessment tools. Next, an investigation of the reliability of the hypothesis using RADIANCE software was conducted. A raytracing of the sunrays was modelled in RADIANCE software to develop the design of the proposed system. The inner surface reflection was studied through a raytracing complex method. Later, the design was optimised through three main phases: early optimisation, experimental studies. A validation study was conducted after the experimental tests to compare the outputs of the simulation and experimental tests. Finally, an alterantive DRD design was proposed and developed and further investigation was conucted.

Chapter 5. Computer modelling of the base case

5.1. Introduction

The design of the proposed system was optimised by means of computer modelling using Radiance simulation software. The optimisation was accomplished in two main phases. The first phase was completed in four steps. First, it was necessary to set up the computer model accurately. Second, the daylight performance of the base case was conducted. Third, the PSS was optimised and assessed. Fourth, the design of the DRD was optimised, and the daylight performance was evaluated. In this phase, the daylight performance was evaluated for Riyadh City, Saudi Arabia.

5.2. Procedure

The daylight modelling started with a description of the case study and the test location. These data were provided to the simulation software. Next, the light sensor's location and the daylight zones were illustrated. These are used to collect the daylight simulation outputs. Next, the daylight metrics that were used to assess the daylight performance was described. After completing the model setup, an accuracy test was conducted to guarantee the reliability of the simulation outputs. Later the daylight studies were conducted for the base case, the PSS and the daylight-redirecting perforated solar screen (DRSS) sequentially. Finally, the results are discussed and conclusions were drawn to summarise the main findings of these studies. The flow chart in Figure 5.1 shows the main procedure followed in conducting the computer modelling study.

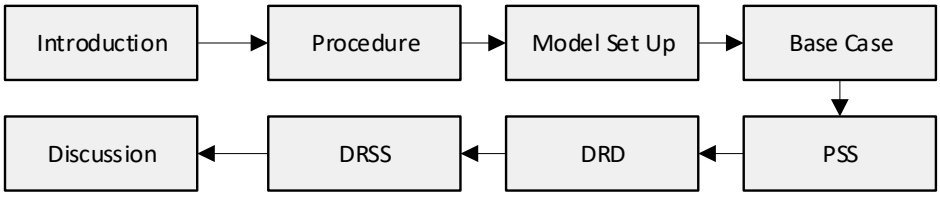


Figure 5.1: Flow chart of the computer modelling study procedure

5.2.1. Location of the study

The study was conducted for Riyadh City, Saudi Arabia, to investigate the performance of the proposed system in the low latitude region. Riyadh City has a latitude and a longitude of 24.7 north and 46.8 east, respectively, see Figure 5.2. The highest sun altitude at solar noon in Riyadh is 88.73 degrees in summer solstice (June 21st), and the lowest is 41.86 degrees in

winter solstice (December 21st) while it is 66.96 degrees in the equinoxes (September 21st and March 21st), as shown in Figure 5.3.



Figure 5.2 Location of the case study City (Riyadh)

The condition of the weather in Riyadh is sunny during most of the year. The illumination and radiation ranges for Riyadh were obtained using CLIMATE CONSULTANT software through an EPW (EnergyPlus Weather Format) climate data. The highest average daily total direct normal radiation is 7,612 Wh/m^2 and occurs in June, while the lowest is 4,592 Wh/m^2 and occurs in December. The highest average daily total diffuse radiation is 2,378 Wh/m^2 and occurs in May, while the lowest is 1,235 Wh/m^2 and occurs in December. The highest average hourly direct normal illumination is 74,369 lux and occurs in October, while the lowest is 46,765 lux and occurs in December, as presented in Figure 5.3 and Figure 5.4.

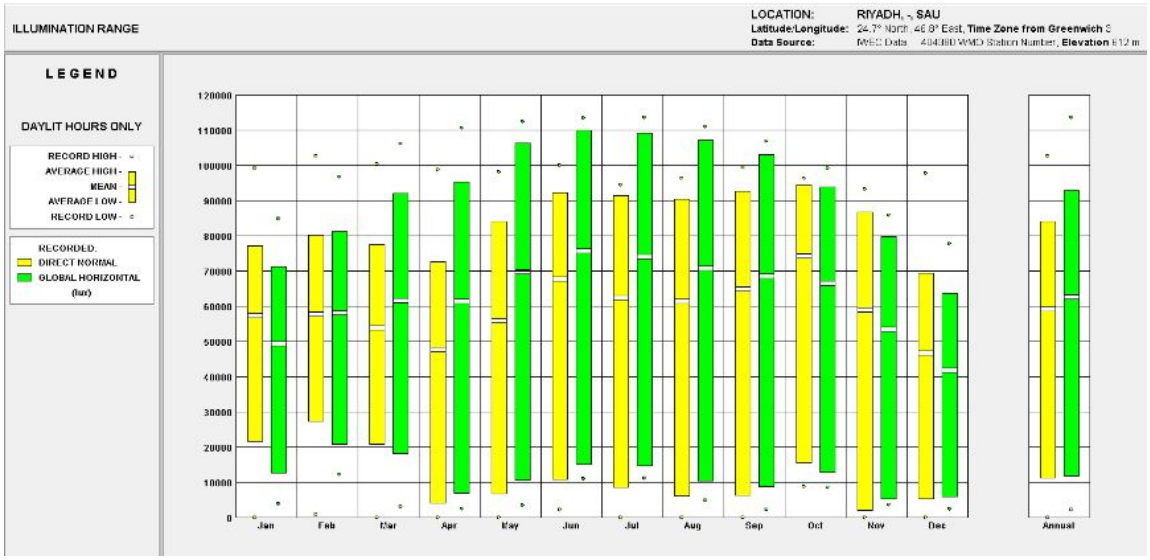


Figure 5.3: Illumination Range

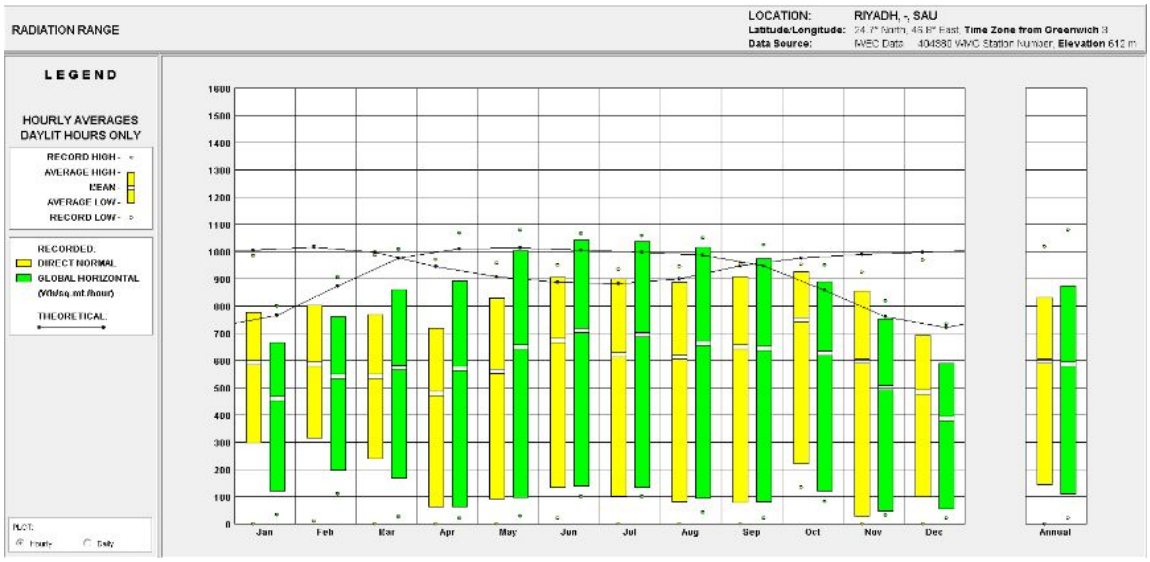


Figure 5.4 Radiation Range

5.2.2. Case study description

The case study was described in Chapter 4, and is using a single space typical office room. The room of the reference case is an office with a rectangular plan. It has one external façade toward the south. The width, depth and height of the room are 3 x 8 x 3 meters, respectively. The net height from the floor to the ceiling is 2.70 m. The window to floor ratio (WFR) is 0.084 %, which equals a 25% window to wall ratio (WWR).

According to SBC 201 (2007) section 7.5.2 and SBC 201 (2018), the net area of glazing for a room should not be less than 8% of the floor area (regardless of the room orientation); this percentage is known as WFR. It was found in the previous studies that the optimum WWR for the south façade is less than other orientations. If the width and depth of the room are 3m X 8m, respectively, hence, the floor area is 24 m^2, and then, the glazed area can be found as follows:

Window area = Minimum WFR*floor area = 0.08 X floor area

Equation 8

$$\text{Window area} = 24\ m^2 \text{ X } 0.08 = 1.92\ m^2$$

In order to convert the WFR to the window to wall ratio, the following equation need to be utilised:

Minimum WWR = Window area / Façade area

Equation 9

Knowing that the net height from the floor level to the ceiling is 2.70 m, then the area of the façade is 2.70 m X 3 m, which equal 8.10 m^2. Therefore:

$$\text{Minimum WWR} = 1.92\ m^2 / 8.10\ m^2 = 0.237$$

According to the Saudi Building Code, an occupiable space must be lit by means of natural light (with minimum WFR equals 8 %) or by artificial light at 107 lux at the level of the work plane (at 760 mm height above the floor level) (Section 7.5, SBC201, 2007, 2018). In addition, the minimum width of habitable space is 2.2 meters except for kitchens, and the minimum ceiling height of an occupiable space is 2.3 meters (SBC 201 Section 7.8.1 and 7.8.2, 2007).

The Saudi Building Code for Green Buildings (SBC 1001) (2018) requires that at least 50% of the floor area must be located within the daylit area for buildings with height up to two stories and 25% for buildings three stories or higher.

According to BREEAM (2016), the average daylight illuminance at common areas and offices within multi-story buildings should meet at least 300 lux for 2650 hours per year or more. The minimum daylight illuminance at the worst lit point is 90 lux for 2560 hours per year. Furthermore, at least 80% of the area should have a 3% average daylight factor.

On the other hand, the average daylight illuminance at common areas and offices within single-story buildings should meet at least 300 lux for 3000 hours per year or more. The minimum daylight illuminance at the worst lit point is 120 lux for 3000 hours per year. Furthermore, at least 80% of the area should have a 4% average daylight factor.

Table 5.1: BREAM requirements for daylighting in office buildings (BREEAM, 2016)

Area type	**Average daylight factor required**	**Minimum area (m2) to comply**	**Average daylight illuminance (averaged over entire space)**	**Minimum daylight illuminance at worst lit point**
Common areas and offices (multi-storey buildings)	3%	80%	At least 300 lux for 2650 hours per year or more	At least 90 lux for 2650 hours per year or more
Common areas and offices (single-storey buildings)	4%	80%	At least 300 lux for 3000 hours per year or more	At least 120 lux for 3000 hours per year or more

- **Surface's materials**

The properties of the model materials are shown in Table 5.2. The reflectivity values of the materials were obtained from the previous studies and the recommended reflectance for office

building interiors as described in (Appelfeld et al., 2012). The ceiling and daylight-redirecting devices should have the highest reflectivity value, 70% to 90%. The interior walls should be from 30% to 60%. Finally, the floor should have a low reflectivity value, namely, 20% to 30%.

Table 5.2: Properties of the surface's material

Surface	**Properties**		
	Reflectance	Specularity	Roughness
Walls	50%	0	0
Floor	20%	0	0
Ceiling	80%	0	0
External Ground	20%	0	0
PSS	50%	0	0
DRD	80%	0	0

- **Operation hours**

The occupation hours are required to run an annual daylight simulation, as shown in Figure 5.5. The operation hours of the case study are the typical working hours of office buildings. They started at 8 am and end at 5 pm. The office is occupied during this period five days a week. As a result, the total occupation hour for the whole year is 2,200 hours. The annual daylight simulation was run for the whole year then the daylight outputs for the operation hours were extracted and analysed.

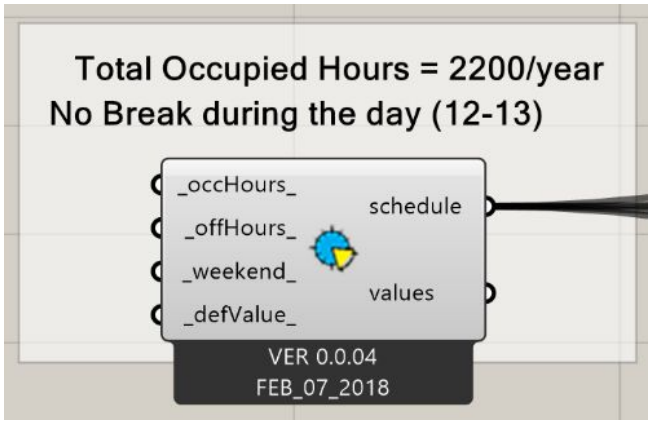


Figure 5.5: Occupation schedule component in HoneybeePlus

5.2.3. Daylight zones

The illuminance values were calculated at the work plane level (0.76 meters from the floor level) (Nabil and Mardaljevic, 2005). This height is identified as a standard height of the working level for work desks in office buildings. The illuminance level at the work plane was measured at 4 points inside the room as a function of distance from the external façade. The test point names are Z1, Z2, Z3 and Z4.

The distance between Z1 and the external façade, and from Z4 to the back wall, is one meter. It was recommended in previous studies that a 0.5-meter perimeter from the walls around the work plane should be kept. The distance between every two light sensors is 2 meters apart. That could produce reliable illuminance values that can be utilised to calculate the DUWP within the room. Each test point is located within the middle of each zone, which can be helpful to measure the improvement of the light intensity for each zone individually, as illustrated in Figure 5.6.

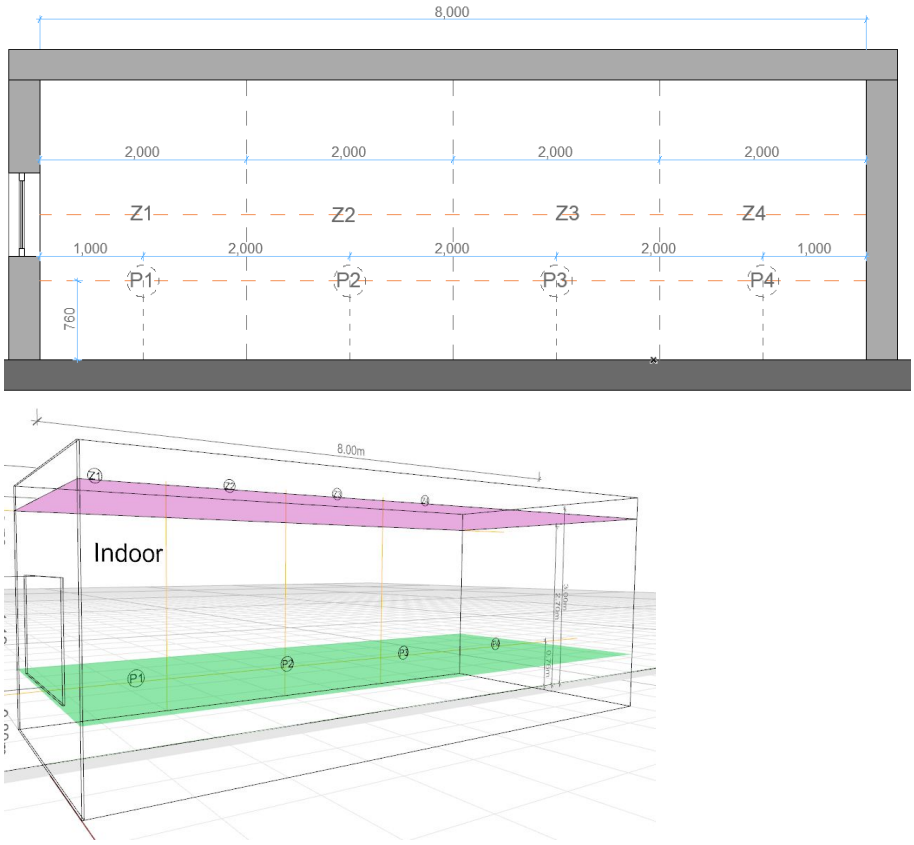


Figure 5.6: Daylight zones, section (above) and perspective (below)

5.2.4. Daylighting performance metrics

The daylighting performance was assessed through an annual daylight study and a point-in-time study (PIT). For the annual study, the obtained values can be presented as several dynamic daylight metrics, for example, daylight autonomy (DA), annual sunlight exposure (ASE), useful daylight illuminance (UDI), and daylight factor (DF). In this stage, three dynamic daylight metrics were utilised to assess the annual daylighting performance, namely, DA, ASE and UDI.

Then, for the PIT study, the illuminance values were compared, and the daylight uniformity at the work plane (DUWP) was assessed based on Equation 4. In addition, the daylight glare probability (DGP) was evaluated for the worst day of the year that recorded the highest AES value. The daylight metrics were described previously in Chapter 1.

On the other hand, three dynamic daylight metrics were used to evaluate the annual daylight performance at the work plane. The daylight autonomy $DA_{300lx/50\%}$ was utilised to assess the total illuminance values that reached the low threshold. The annual sunlight exposure ($ASE_{1000lx/250hr}$) was utilised to assess the direct illuminance that exceeded the high threshold. Finally, the useful daylight illuminance (UDI-$a_{300\text{-}1000lx}$) was utilised to assess the illuminance level with a low and high threshold.

5.3. Computer modelling set up.

The procedures of the computer modelling set up for the raytracing and the daylight intensity studies are described below. It provides detailed information about the utilised software tools and the inputs of the model. In addition, it shows illustrations from the software that shows the process of modelling, as illustrated in Figure 5.7 and Figure 5.8.

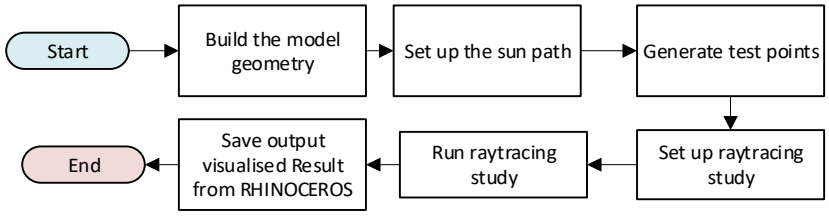
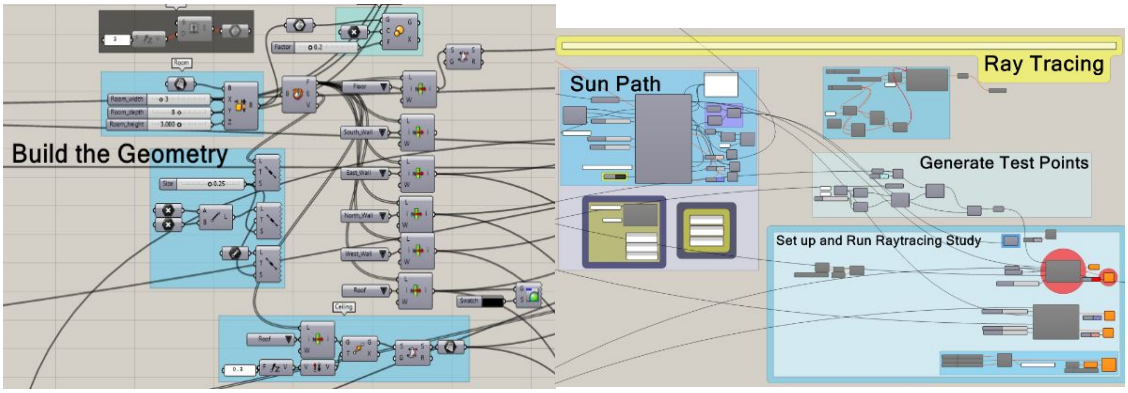


Figure 5.7: Computer modelling set up (Raytracing Process)



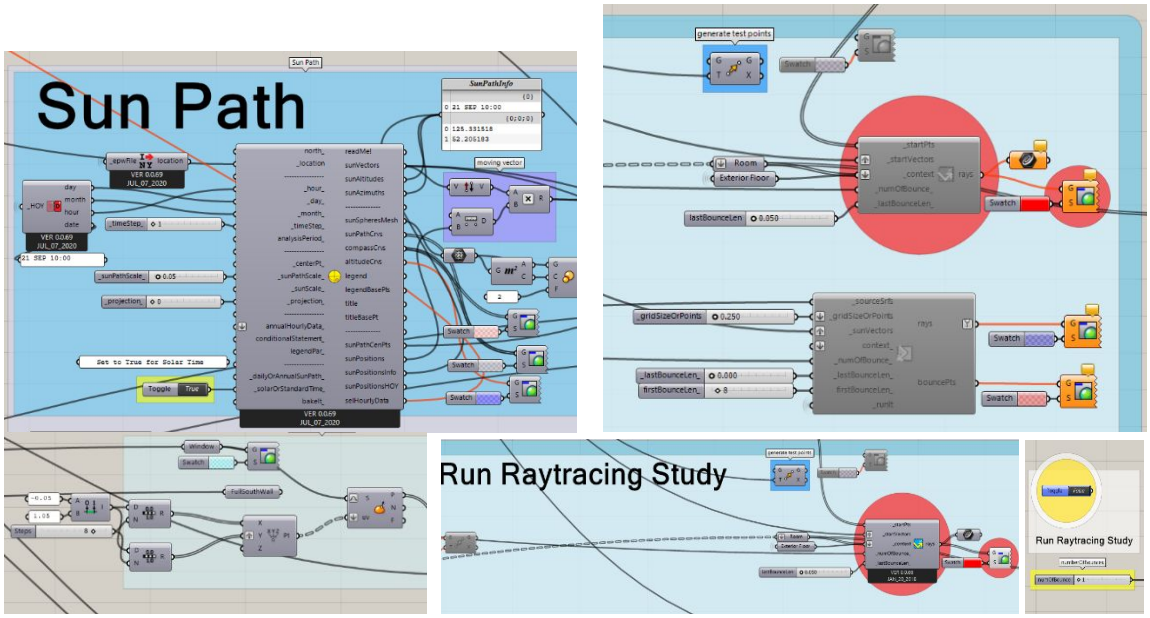
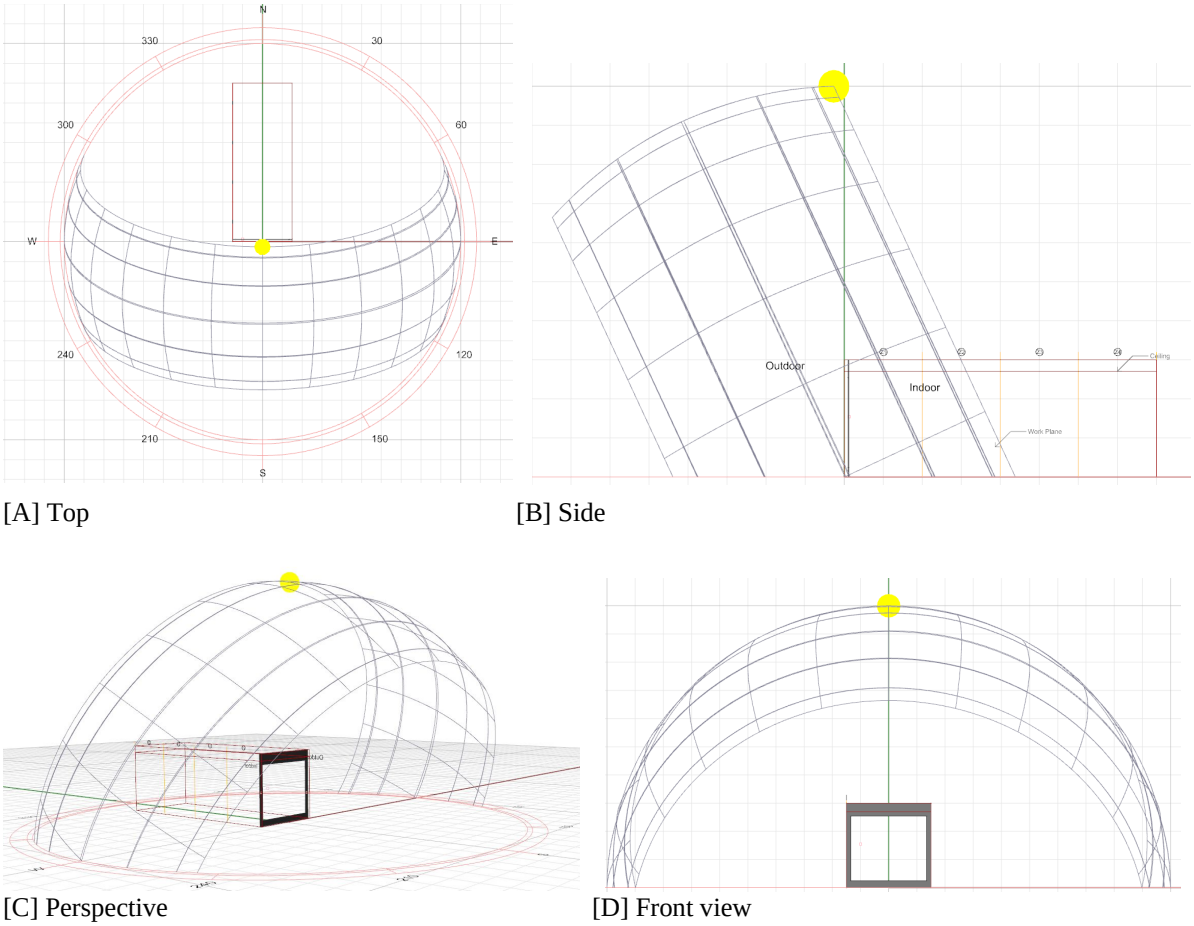


Figure 5.8: GRASSHOPPER components that were used to run the raytracing study in RADIANCE

5.3.1. Computer modelling set up for the raytracing study

In order to conduct the sunrays raytracing study, the model was created inside GRASSHOPPER, the plugin of RHINOCEROS software. GRASSHOPPER allows users to make a parametric study of multiple parameters simultaneously. GRASSHOPPER and RHINOCEROS were utilised to create the geometry of the test room and daylighting system. The raytracing model was created by the LADYBUG tools, which includes HONEYBEE, the plugin of GRASSHOPPER for daylighting studies. The main work of the daylight simulation is done by Radiance engine, the validate daylighting software. RADIANCE is linked with GRASSHOPPER by the LADYBUG and HONEYBEE.

The outputs of the simulation were obtained as numerical values and as visual mesh maps with colour keys. The numerical values were exported to Excel for analysis. Tables and charts for the results were produced by Excel. The sun path is for Riyadh city on the 21st of June at solar noon is illustrated in Figure 5.9.



[A] Top [B] Side

[C] Perspective [D] Front view

Figure 5.9: Sun path, 21 June at solar noon, Riyadh city, from A to D, top, side, perspective, and front views

5.3.2. Computer modelling set up for the daylight intensity study

In order to run the daylight simulation, two main components need to be set, namely, the building data and the sky condition, which create a simulation algorithm that feeds the analysis recipe component, as illustrated in Figure 5.10.

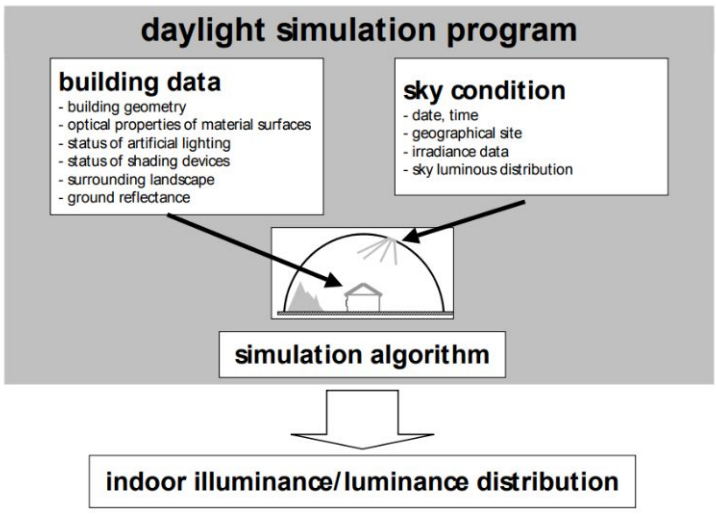


Figure 5.10 Daylight simulation requirements (Reinhart, 2010)

After creating the geometry in RHINOCEROS and GRASSHOPPER, the first step to set up the daylighting model is to add two main components to GRASSHOPPER canvas, namely, Ladybug-Ladybug and Honeybee-Honeybee, “these components carry all of LADYBUG and HONEYBEE main classes" (Roudsari, 2018).

Next, all RHINOCEROS components were converted and internalised into GRASSHOPPER components. Then, each surface inside GRASSHOPPER has been converted to a HONEYBEE surface and was assigned material with a specific name, reflectivity, specularity and roughness values as described in Table 5.2 above. The HONEYBEE surfaces create HONEYBEE zones or objects fed to the analysis recipe (HONEYBEE component) to be supplied to run a daylight simulation inside Radiance.

This component requires three necessary inputs to run, the analysis recipe, the HONEYBEE object and the *Radiance seen* component. The analysis recipe is a HONEYBEE component that has two main types, *image-based* and *grid-based recipes*. The image-based produce a three-dimensional view with colour code or HDR image, while the grid-based provide a two-dimensional grid view for the values.

The analysis recipe component is a component in HONEYBEE that is run inside the engine of RADIANCE for the point-in-time daylight study (PIT) and inside DAYSIM to run an annual daylight study. However, the annual daylight by HoneybeePlus utilised the RADIANCE engine for both the PIT and the annual simulation.

It is essential to mention that HoneybeePlus is using the RADIANCE engine for annual study. The advantages of using the RADIANCE engine instead of the DAYSIM engine are that RADIANCE uses all the weather data from the *epw* file for the tested location. In contrast, DAYSIM extracts only the location from the *epw* file without considering the weather data for the tested location.

The advantage of RADIANCE is that an accurate sun position is defined for direct sun calculation. On the other hand, in DAYSIM, a simplified method is used; the sun position is defined by the nearest sun from about 65 sun positions (Reinhart and Walkenhorst, 2001).

In other words, RADIANCE is more accurate than DAYSIM because it considers the specific weather data for each location, while DAYSIM uses uniform weather data for all locations. The output of the simulation can provide illuminance (lux), luminance (cd/m^2) and solar radiation (kWh/m^2) values.

Image-based and grid-based recipes require four inputs. The two recipes require the sky data, the RADIANCE parameters, and the analysis type (illuminance, luminance, or radiation). The last input is different for each recipe, for the image-based recipe requires a views component while the grid-based recipe requires an analysis grid component.

The grid size for the test is 0.4 X 0.4 meter, and the height of the work plane is 0.76m from the floor level. The RADIANCE parameters are shown in Table 5.3. The sky type was selected based on the simulation accuracy test below. RADIANCE parameters are based on the recommended values by the developer of RADIANCE software and previous studies. Furthermore, the model was tested with the acceptable and accurate RADIANCE parameter to show their effect on the reliability of the results. Figure 5.11 illustrates the workflow to conduct CBDM modelling. The highlighted inputs are provided by the user, while the other work is completed by the software (Brembilla, 2017).

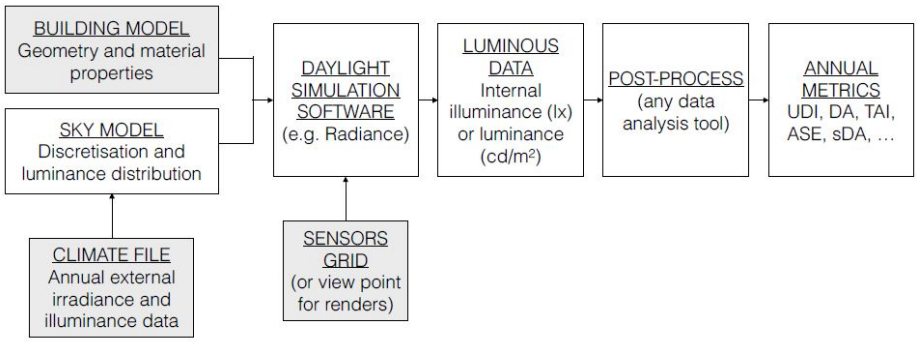


Figure 5.11: Workflow to conduct CBDM modelling (Brembilla, 2017)

A process to find a proper RADIANCE simulation method for accurate daylight results was proposed by Subramaniam (2018), as illustrated in Figure 5.12. The daylight coefficient (DC) method (the 2-phase method) was utilised in this study. The DC method is an accurate daylight simulation method to perform an annual daylight illuminance simulation (Laouadi et al., 2008).

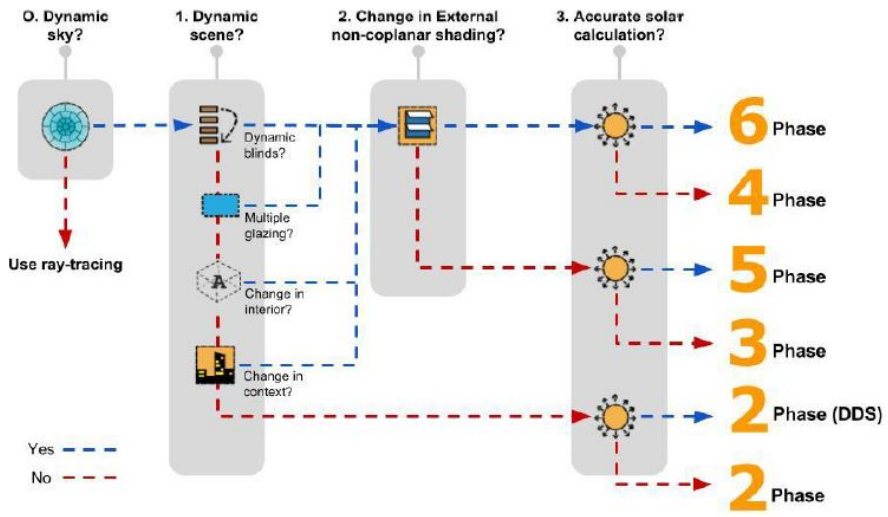


Figure 5.12: Six methods used to conduct a daylighting simulation by Radiance, Credit: Mostapha Sadeghipour (Subramaniam, 2018)

The concept of daylight coefficients originally proposed by Tregenza and Waters (1983), theoretically divides the celestial hemisphere into disjointed parts of the sky and then calculates the contribution of each part of the sky at each sensor point in the building to the total illuminance based on each sensor. Position (for example, on a table) and orientation (for example, facing the ceiling) in a given environment (Bourgeois et al., 2008).

According to Bourgeois et al. (2008), for light sensor X, a daylight coefficient DC α(X) that related to the sky segment S α can be defined as the illuminance, E, at sensor X that occurred by the sky segment S α, divided by luminance L α and the angular size ΔS of the segment:

$$\mathbf{DC_{\alpha}(x) = E_{\alpha}(x) / L_{\alpha} \Delta S_{\alpha}}$$

Equation 10

where:

x is sensor point.
S_{α} is sky segment
ΔS_{α} is angular size of S_{α}
$E_{\alpha}(x)$ is illuminance at x due to S_{α}
L_{α} is luminance of S_{α}

The total illuminance E (x) of the sensor, as illustrated in Figure 5.13, is obtained by linearly superimposing each daylight coefficient DCα with the luminance Lα of the part of the sky Sα that coincides. Using Equation 11, accurate annual daylight simulations can be performed for any climate and scene direction in minutes (Bourgeois et al., 2008).

$$\mathbf{E(x)} = \sum_{\alpha=1}^{\mathbf{N}} \mathbf{DC_\alpha(x) L_\alpha \Delta S_\alpha}$$

Equation 11

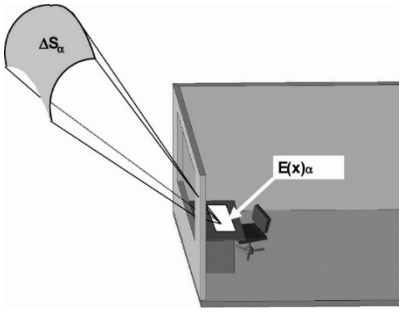


Figure 5.13: The total sensor illuminance, E(x), (Bourgeois et al., 2008)

5.3.2.1. Effect of RADIANCE simulation parameters

The Radiance parameters influence the simulation time and its accuracy (Reinhart and Walkenhorst, 2001). The influence of two settings of RADIANCE simulation parameters on the accuracy of the simulation were tested, an *Acceptable* and an *Accurate* setting. LADYBUG tools, by default, provide three pre-set levels of accuracy, low, medium and complex. The low level is fast but not reliable; however, it is helpful during the model creation process. On the other hand, the *Acceptable* and the *Accurate* settings are used for the daylight analysis. The *Acceptable* Radiance parameters can be adequate if the daylighting system is not included in the geometry. Finally, the *Accurate* Radiance parameters need a longer time to run, but their outputs are reliable.

However, the software provides the user with pre-set Radiance parameters options; the parameters can be modified separately based on the nature of the daylight study. The complexity of the daylight system is one of the main factors that can require higher accuracy. The values of the default *Acceptable* and an *Accurate* setting of RADIANCE parameters that were utilised in this test are shown in Table 5.3 below. For further information about RADIANCE parameters refer to Larson and Shakespeare (1998) and Larson and Shakespeare (2021).

Table 5.3: Radiance parameters for the point-in-time simulation

Parameter	Abbreviation	Value	
		Acceptable	Accurate
Limit weight	-lw	0.01	0.005
Direct certainty	-dc	0.5	0.75
Ambient resolution	-ar	64	128
Specular jitter	-ss	0.7	1
Direct pretest density	-dp	256	512
Direct relays	-dr	1	3
Direct threshold	-dt	0.25	0.15
Ambient bounces	-ab	3	6
Ambient super samples	-as	2048	4096
Direct sampling	-ds	0.25	0.05
Ambient accuracy	-aa	0.2	0.1
Limit reflection	-lr	6	8
Ambient divisions	-ad	2048	4096
Direct jitter	-dj	0.5	1
Specular threshold	-st	0.5	0.15

A comparison was made between the *Accepted* and the *Accurate* Radiance parameters to observe the range of variation between the two settings. The comparison was conducted at solar noon on the 21st of December for the base case, as shown in Figure 5.14. The illuminance value was measured at light sensor Z4. A PIT simulation method with a climate-based sky was utilised, the study conducted for Riyadh City, Saudi Arabia.

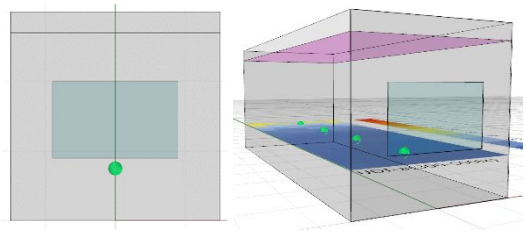
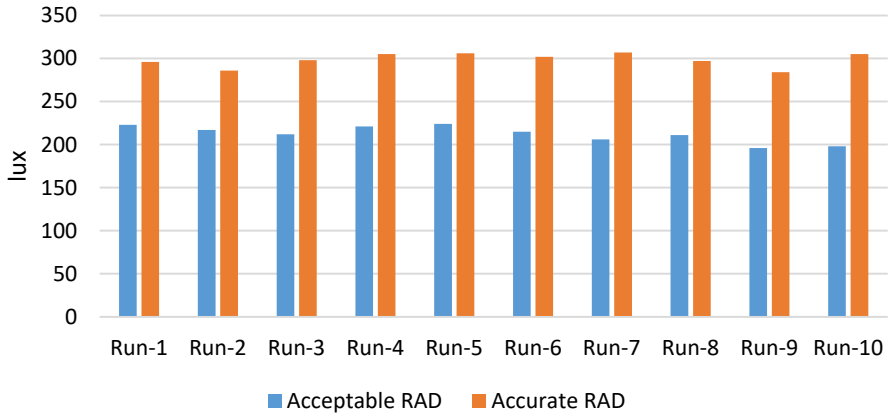
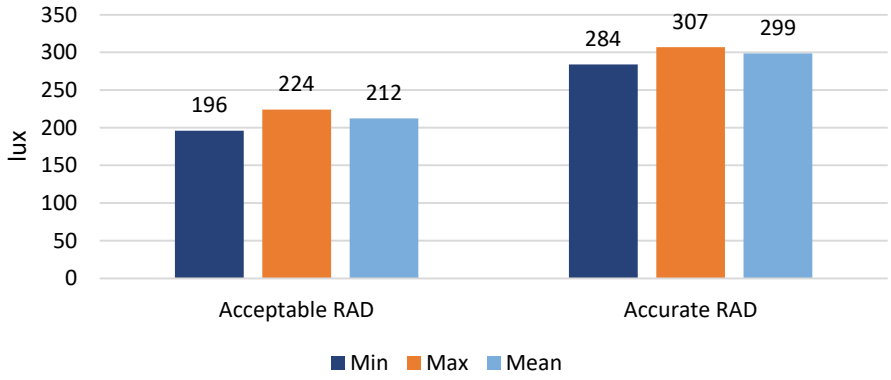


Figure 5.14: Front and perspective views show the tested room.

Ten simulations were run ten times with the *Acceptable* then with *Accurate* Radiance parameters. Then, the illuminance values were exported to Microsoft Excel to calculate the minimum, maximum and mean values, as shown in Figure 5.15. The lowest illuminance value with the *Acceptable* Radiance parameters was 196 lux, the highest was 224 lux, and the mean was 212 lux. On the other hand, the minimum illuminance value with the *Accurate* Radiance parameters was 284 lux, the maximum was 307 lux, and the average was 299 lux. It can be seen that the illuminance values among the simulation scenarios that used an accurate radiance parameter produced higher illuminance reading. The difference between the two minimum, maximum and average values was 88 lux and 83 lux and 87 lux, respectively.



(a)



(b)

Figure 5.15: (a) Illuminance values (above), and (b) the minimum, the maximum, and the mean (below) base case on December 21st at solar noon in Riyadh city

In order to determine the range of variance among the 10-simulation runs, the standard deviation (SD) was calculated based on Equation 12. The SD values were 8.17 and 9.82 with the *Accurate* and the *Acceptable* Radiance parameters, respectively. The simulation with the *Accurate* Radiance parameters was recorded an SD value lower than the *Acceptable* Radiance Parameter by 1.65, as shown in Figure 5.16. The SD was obtained by the following formula:

$$SD = \sqrt{\frac{\sum |x-\mu|^2}{N}}$$

Equation 12

where:

SD = population standard deviation
N = the size of the population
× = each value from the population
μ = the population mean

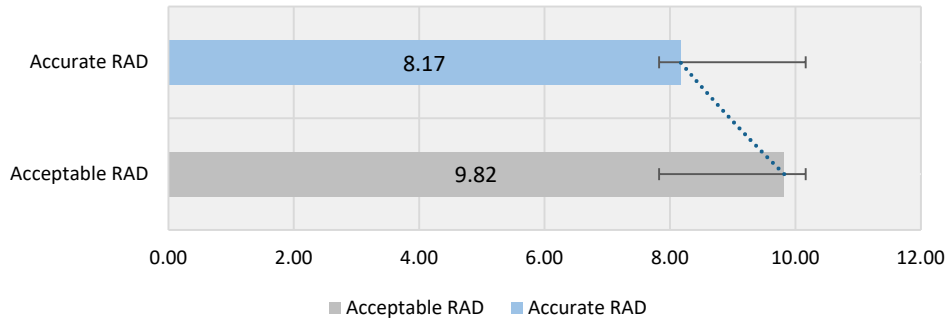


Figure 5.16: Standard deviation between the 10-simulation runs

5.3.2.2. Effect of the daylight simulation method

The daylight study can be conducted by means of Radiance through two main methods, a PIT or an annual daylight simulation. Each method utilises a different type of skies. One of the most validated sky types for the PIT simulation is the climate-based sky, which depends on the sun position and the weather data obtained from the "*epw*" file for the test time location. On the other hand, the annual daylight simulation can utilise different sky matrixes representing the whole year hours. These sky matrixes use a "*wea*" file, which is generated from an "*epw*". Both methods are considered as climate-based daylight modelling (CBDM).

To optimise the daylight system or to analyse the daylight performance for a specific hour, the annual daylight simulation can be used. The target hour can be extracted from the annual results for these purposes. The occupation hours can also be used with the annual daylight simulation for the daylight performance analysis. Furthermore, the annual results can be divided into shorter periods, for example, based on seasons or months.

A comparison was conducted to investigate the reliability of using the annual daylight simulation for the optimisation stage, where a specific hour needs to be analysed separately. The base case was assessed through a PIT and an annual daylight simulation. The first method utilised a climate-based sky, while the second method utilised the Tregenza sky matrix. Tregenza sky matrix is a sky matrix representing the whole year, and it is divided into 145 sky patches, as shown in Figure 5.17.

The test compared ten daylight simulation runs for each method. Accurate Radiance parameters were applied for both methods; the Radiance parameters are shown in Table 5.3 and Table 5.4. The Ambient divisions' parameter (*-ad*) for the annual daylight simulation is higher compared with the PIT simulation because the annual simulation is modelled 8760 hours while the point-in-time simulation run the model for one hour. Consequently, the Limit weight's parameter *(-lw*) is lower for the annual simulation because (*-lw)* is dependent on *–ad* value.

For the PIT study, a climate-based sky was utilised, and for the annual study, the Tregenza sky matrix was used. Figure 5.18 shows a model of the Tregenza Matrix sky for Riyadh city. The total radiation, diffuse radiation and direct radiation (kWh/m^2) are shown from left to right.

Table 5.4: The Radiance parameters for the annual daylight simulation for the daylight matrix (dmtxPar) and the direct sun matrix (smtxPar) calculations.

Parameter	Abbreviation	Value	
		dmtxPar	**smtxPar**
Limit weight	-lw	4e-07	0.05
Direct certainty	-dc	0.75	1
Ambient resolution	-ar	128	16
Specular jitter	-ss	1	0
Direct pretest density	-dp	512	64
Direct relays	-dr	3	0
Direct threshold	-dt	0.15	0
Ambient bounces	-ab	6	0
Ambient super samples	-as	4096	128
Direct sampling	-ds	0.05	0.5
Ambient accuracy	-aa	0.1	0.25
Limit reflection	-lr	8	4
Ambient divisions	-ad	25000	512
Direct jitter	-dj	1	0
Specular threshold	-st	0.15	0.85

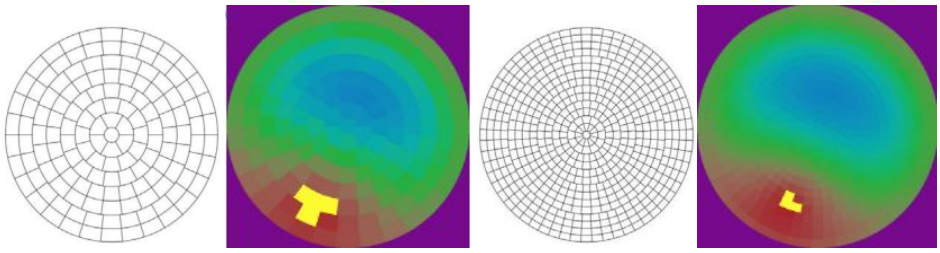
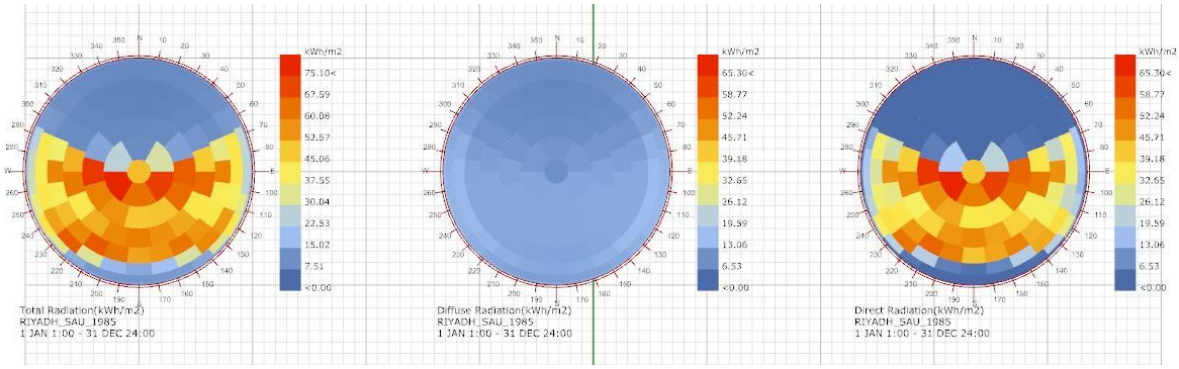


Figure 5.17: Tregenza (145 divisions) [left], and Reinhart (581 divisions) [right] (Ward et al., 2011)



[A] [B] [C]

Figure 5.18 Tregenza Sky matrix for Riyadh city, [A] total, [B] diffuse, and [C] direct radiation (kWh/m^2)

The results of the PIT and the annual simulations are shown in Figure 5.19 below. It was found that the minimum, maximum, and mean illuminance values for the annual daylight simulation with a Tregenza sky matrix was 246 lux, 271 lux and 258 lux, respectively. It was found that the annual simulation with a Tregenza sky matrix recorded lower illuminance values compared with the PIT method. The difference between the minimums, maximums and means were 38 lux, 36 lux and 41 lux, respectively. The standard deviation among the results of the annual simulation with Tregenza sky was 7.47, which is lower than the PIT simulation by 0.5, as shown in Figure 5.20.

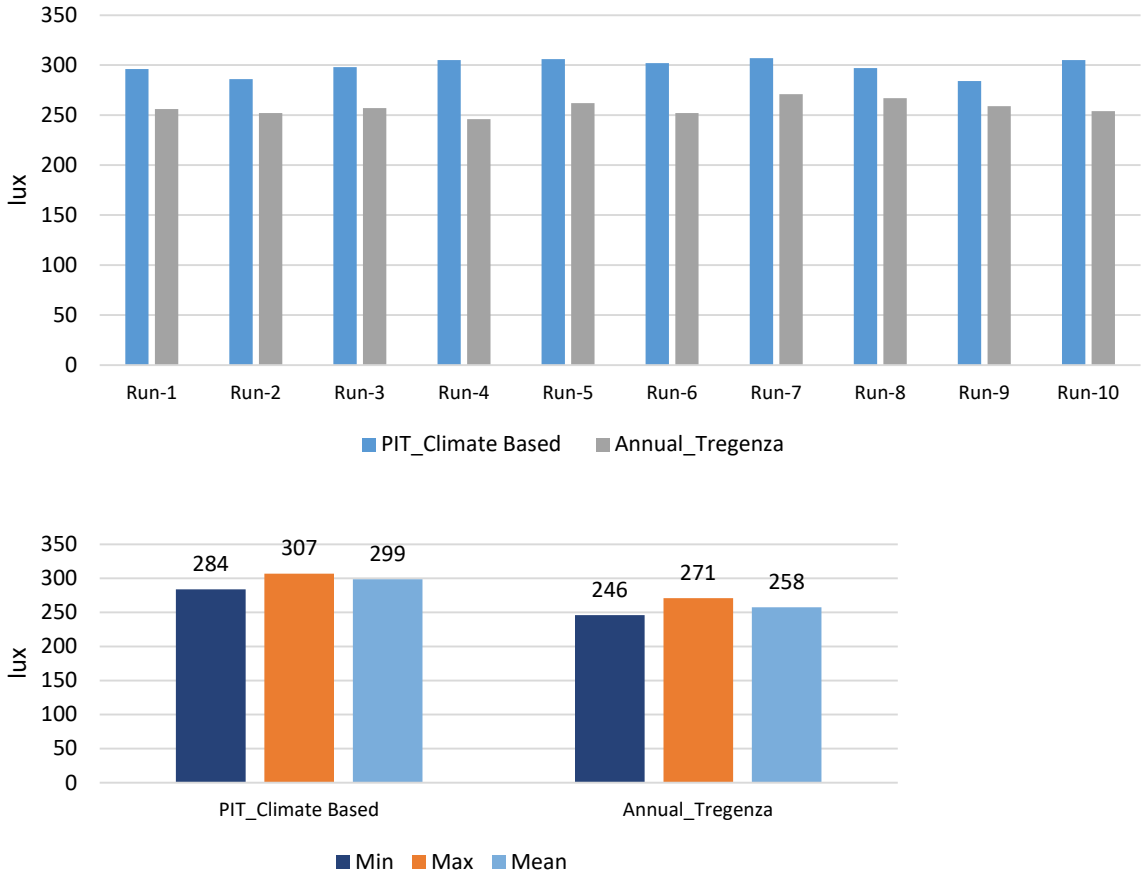


Figure 5.19: Illuminance values (above), and the minimum, the maximum, and the mean (below)

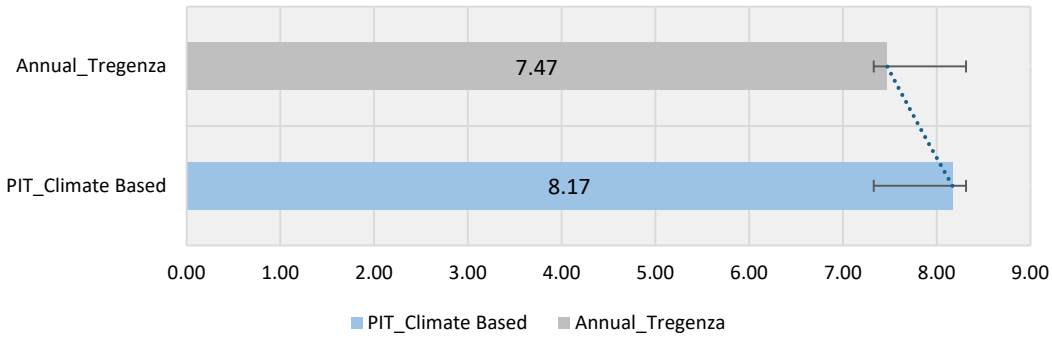


Figure 5.20: Standard deviation between the 10 simulation runs

5.3.2.3. Effect of the sky matrix type

The effect of the sky matrix type on the variation range among the simulation scenarios was analysed for the base case at the solar noon on the 21st of December for Riyadh city, Saudi Arabia. Two types of sky matrixes were tested: the Tregenza sky matrix and the Reinhart sky matrix. Reinhart sky matrix is a refined version of the Tregenza sky matrix. It is divided into 580 sky patches, 300% higher than the Tregenza sky matrix, as illustrated in Figure 5.21. Ten simulation runs were compared and analysed through the minimum, maximum and mean illuminance values at the work plane for light sensor Z4. Then, the standard deviation was calculated for each sky matrix.

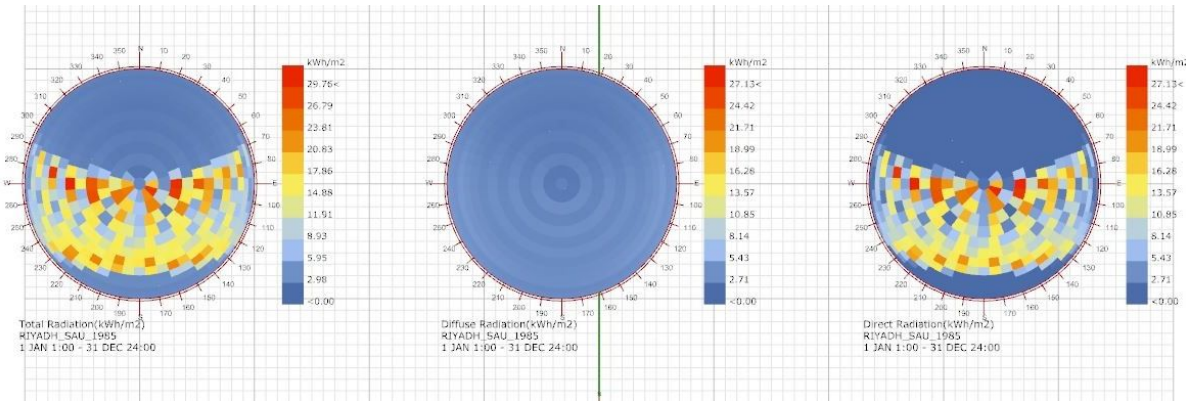


Figure 5.21 Reinhart Sky matrix (fine density, 580 sky patches)

The illuminance values for the 10 simulation runs with the annual daylight simulation using a Reinhart sky matrix are shown in Figure 5.22. The minimum, maximum and mean values were 241 lux, 271 lux and 262 lux, respectively. It was found that the annual daylight simulation with Reinhart sky matrix and with Tregenza sky matrix recorded the same maximum illuminance value. On the other hand, the minimum value was lower with Reinhart sky by 5 lux while the mean was higher by 3 lux than Tregenza sky.

The standard deviation among the 10-illuminance values for the annual simulation with Reinhart sky matrix was 8.83, which is 1.36 higher than the SD of the simulation results with the Tregenza sky matrix, as presented in Figure 5.23.

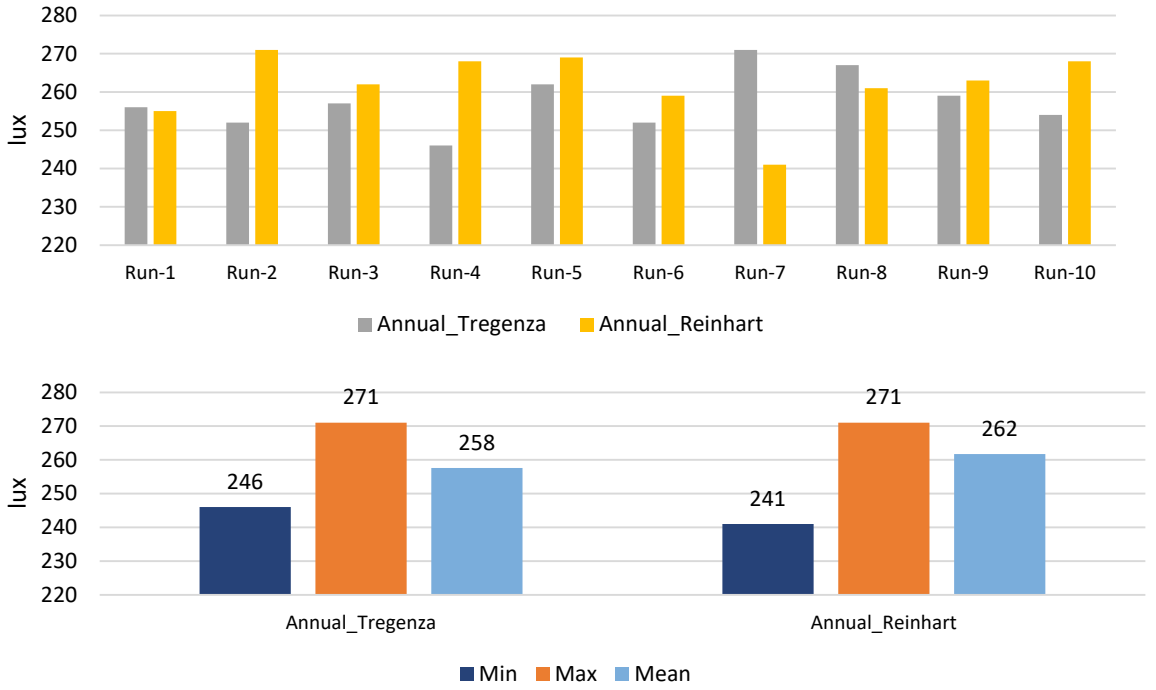


Figure 5.22: Illuminance values (above), and the minimum, the maximum, and the mean (below)

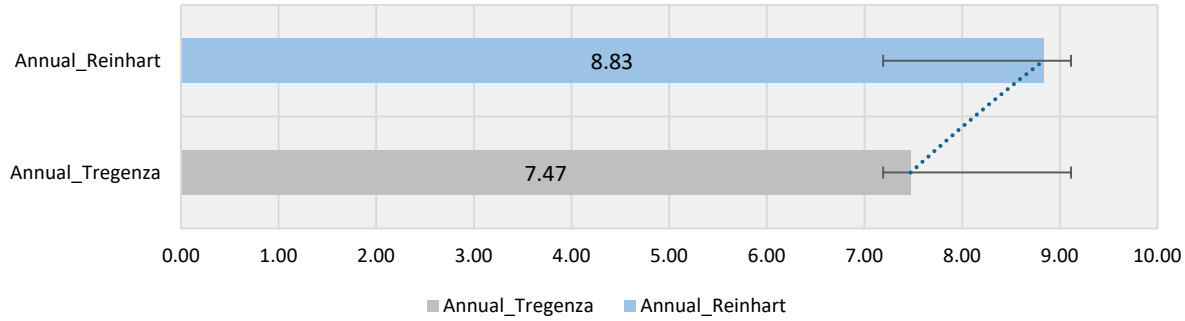


Figure 5.23: Standard deviation between the 10

5.3.3. Summary

To sum up, the most reliable simulation setting was obtained from the analysis of the four tests above. These are the PIT simulation with climate-based sky with *Accurate* and *Acceptable* Radiance parameters and an annual simulation with *Tregenza* and *Reinhart* sky matrixes. It was found that the *Accurate* Radiance parameters are more reliable compared with the *Acceptable* Radicle parameters. In terms of the simulation methods, the annual simulation with *Tregenza* recorded a lower SD value than the PIT simulation. Similarly, for the sky matrixes comparison, the SD value of the simulation with the *Tregenza* sky matrix was lower than the simulation with the *Reinhart* sky matrix. Therefore, the case study modelling was simulated through an annual simulation method using the *Tregenza* sky matrix with *Accurate* Radiance parameters.

5.4. Base case

The base case, which has a window with a 25% WWR without any daylighting devices, was modelled and analysed. This investigation stage achieved two objectives. First, it evaluated the overall daylighting performance through an annual study method for the whole year. Then the data of the daylight performance that was obtained for the whole year was analysed for each season separately to investigate the performance during the selected periods. Second, it analysed the direct sunlight behaviour inside the room through a raytracing simulation. This stage was to visualise the sun paths to assess the behaviour of the sun rays inside the room. Third, it evaluated the hourly daylighting performance through a PIT study for the summer and winter solstice days and the equinox day. This stage shows the illuminance values at the work plane as a function of different solar altitude angles.

5.4.1. Overall evaluation by an annual daylight study

The overall daylight performance was assessed through two methods, an annual and a seasonal evaluation. The annual evaluation was conducted for the whole year to analyse the daylight performance to observe the overall performance, while the second was to analyse the performance within each season individually.

The objective of the illuminance level assessment at the work plane for the base case was to investigate the daylight performance in the current situation. Therefore, it was crucial to determine the areas out of the acceptable illuminance level. The inadequate daylight level can be either above (over-daylit) or lower (not-daylit) than the high and the low threshold of the optimum daylight level.

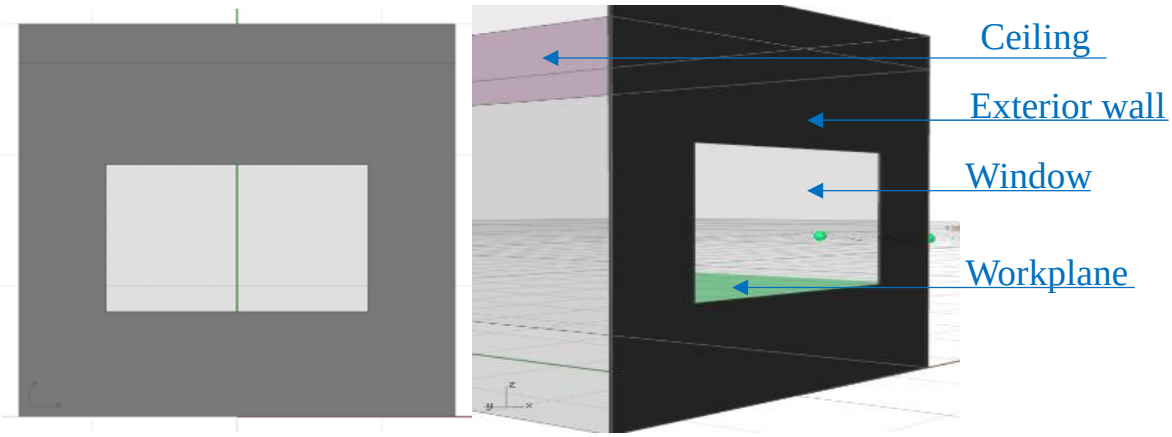


Figure 5.24: Front and perspective views of the base case, left to right, respectively

5.4.1.1. Annual daylight evaluation

In order to assess the overall daylight performance of the base case, annual daylight dynamic metrics were utilised. In addition, the daylight performance for the occupation hours of the year was evaluated through daylight autonomy (DA), the annual sunlight exposure (ASE) and useful daylight illuminance (UDI).

It was found that the DA was achieved by 100%, 98%, and 96% at Z1, Z2 and Z3, respectively; however, the DA at Z4 was exceptionally low, which only met the requirement at 5%. On the other hand, the ASE was within the acceptable range at all the zones except Z1, where the ASE was occurred 381 hours during the year, as shown in Figure 5.25 and Figure 5.26.

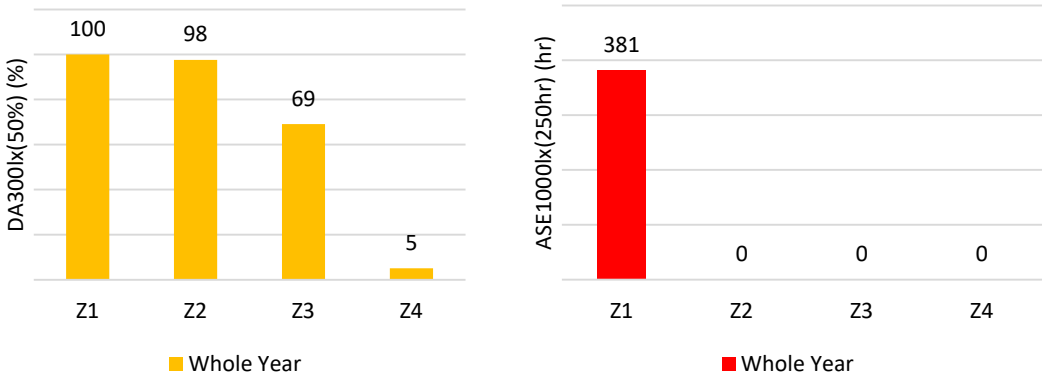
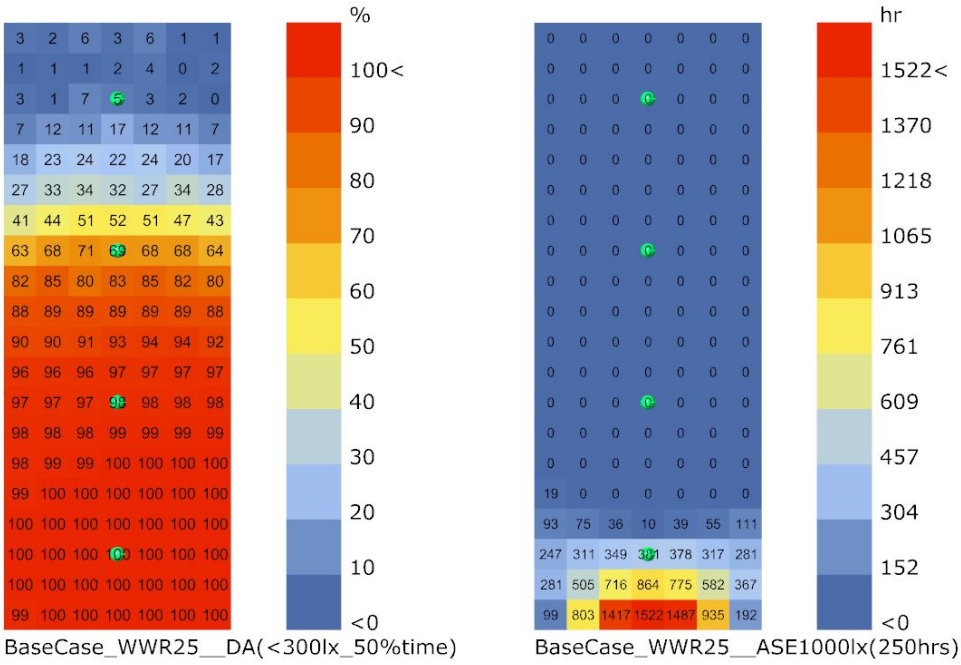


Figure 5.25: The DA (left) and the ASE (right) for the base case



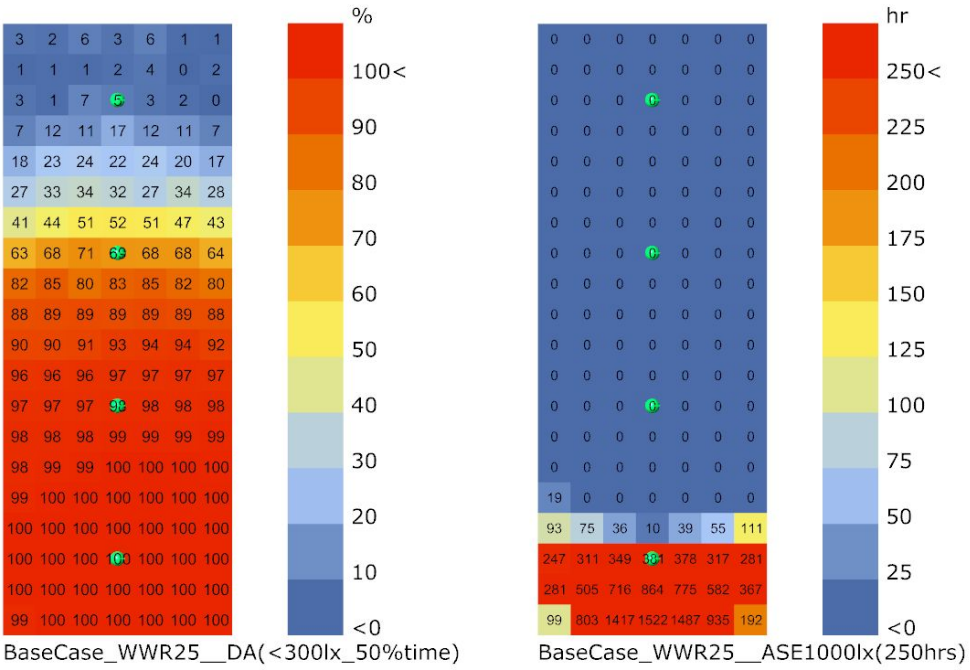


Figure 5.26: The DA (left) and ASE (right) for the whole year

The DA does not have a maximum threshold, which means that it does not consider the occurrence of excessive light intensity. Furthermore, the ASE does not consider the diffuse illuminance; therefore, it was essential to evaluate the daylight performance by the UDI. Two UDI scales were used in this study, 300-500 lux and 300-1000 lux. Both of the UDI indicators have a 300-lux low threshold. The maximum thresholds are 500 lux and 1000 lux.

The chart in Figure 5.27 and the visualisation of the simulation output in Figure 5.28 below show that the illuminance levels at Z2 and Z3 met the $UDI_{300\text{-}1000\ lux}$ at 59% and 69%, respectively. On the other hand, the front and rear zones, which are Z1 and Z4, were recorded a low percentage at only 1% and 5%, respectively. Nevertheless, by utilising the 300-500 lux threshold, the $UDI_{300\text{-}500\ lux}$ at Z2 was dropped by 51%, and Z3 was decreased by 14%, while the value at Z4 remains the same.

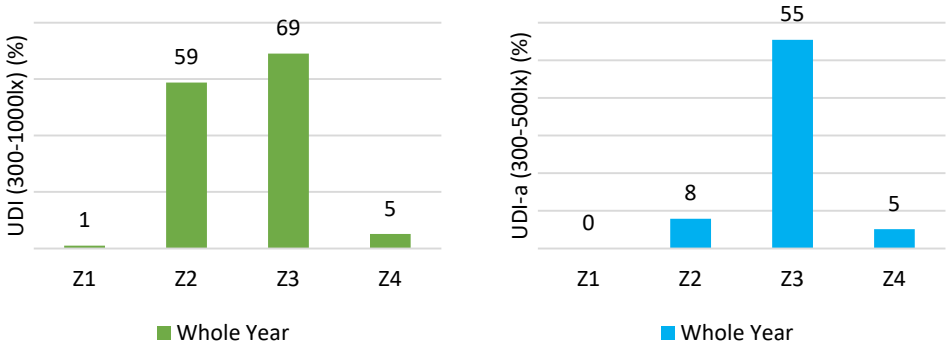


Figure 5.27: $UDI_{(300\text{-}1000\ lux)}$ (left), and $UDI_{(300\text{-}500\ lux)}$ (right), for the base case

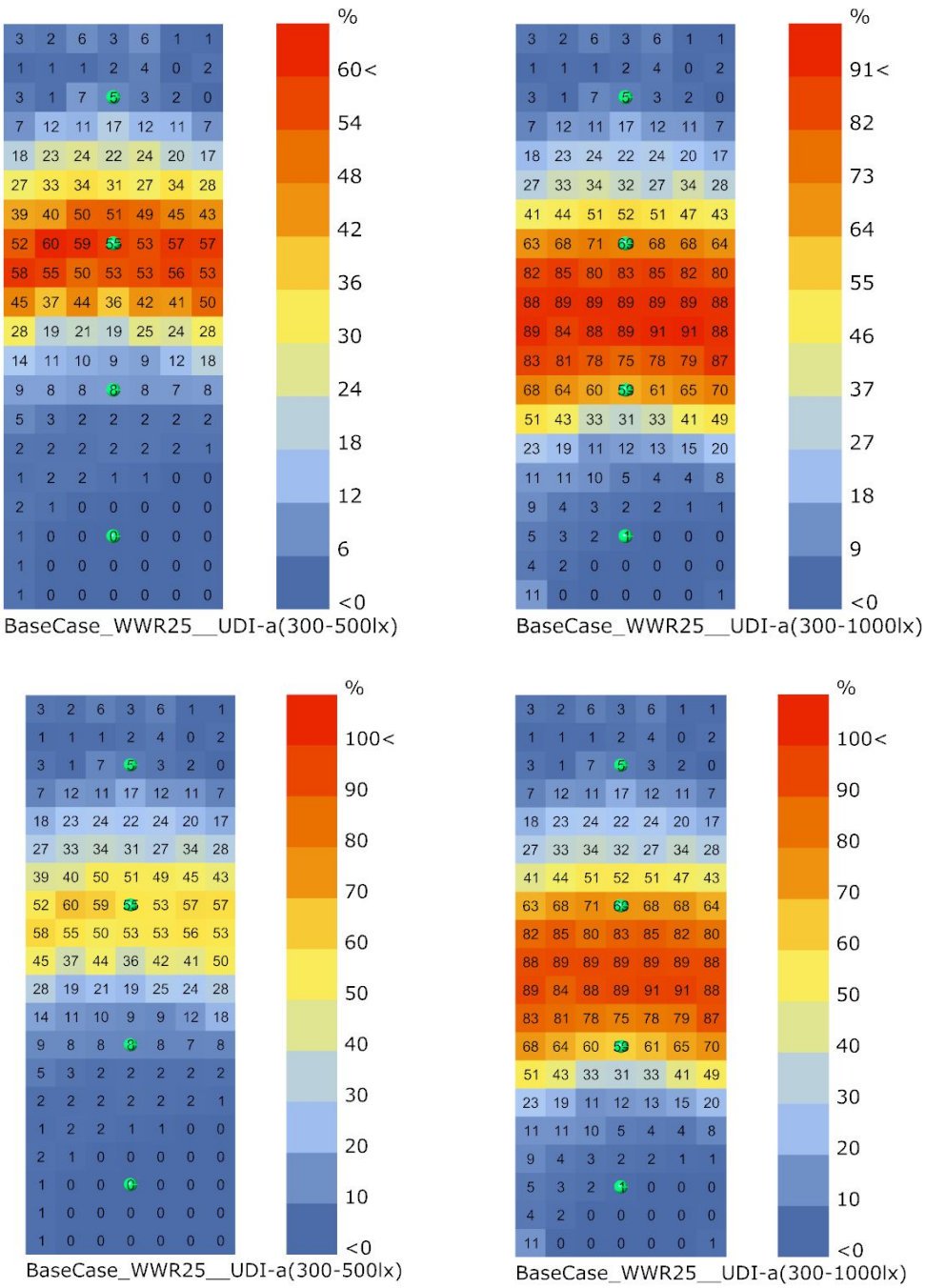


Figure 5.28: The daylight simulation outputs, $UDI_{300\text{-}500lx}$ (left) and $UDI_{300\text{-}1000lx}$ (right).

5.4.1.2. Seasonal daylight evaluation

The second step of the evaluation was a seasonal evaluation based on the available monthly range of solar radiation during the year. Each period consists of three months, start from the first day of month-1 and end on the last day of month-3. The first period includes February, March and April, the second period includes May, June and July, the third period includes August, September and October, and finally, the fourth period includes November, December and January. The four periods will be referred to as spring, summer, autumn and winter,

respectively. The first and second periods represent the medium and peak solar radiation months, respectively. The lowest solar radiation months occurred in the fourth period (winter).

In order to assess the annual daylight performance during these periods, dynamic daylight metrics were utilised, namely, the DA, the ASE and the UDI. The DA has a minimum threshold, a 300-lux threshold that should be met for at least 50% of the occupational time. ASE has a maximum threshold, a 1000-lux maximum threshold for at least 250 hours of occupational time. Finally, the optimum UDI for this study has a minimum threshold of 300 lux and a maximum threshold of 1000 lux.

The DA assesses the minimum daylight performance where it does not have a maximum threshold. The ASE, on the other hand, assesses the maximum direct illuminance and does not consider the diffuse illuminance. Furthermore, it does not have a minimum threshold. However, it is a helpful indicator to investigate the amount of direct solar radiation at the work plane. Therefore, it was necessary to use an additional dynamic daylight metric to investigate the optimum daylight performance. This metric is the UDI, which has a minimum and maximum threshold, and it measures the total illuminance.

As shown in the chart below in Figure 5.29, the DA was calculated for the four seasons at the work plane at daylight zone Z1, Z2, Z3 and Z4. It was found that the DA was achieved at Z1 during the four periods with a high percentage ranging from 90% in winter to 98% in spring. Similarly, at Z2, the DA was obtained at least at 83% in winter, and the highest DA was achieved at 90% in spring and summer. In contrast, the DA was lower at Z3, which was dropped to 45% in summer, while the highest DA value at Z3 was in winter at 74%. Finally, the worst scenario was at Z4, where the DA was not met during all the seasons except in winter, which was 18%.

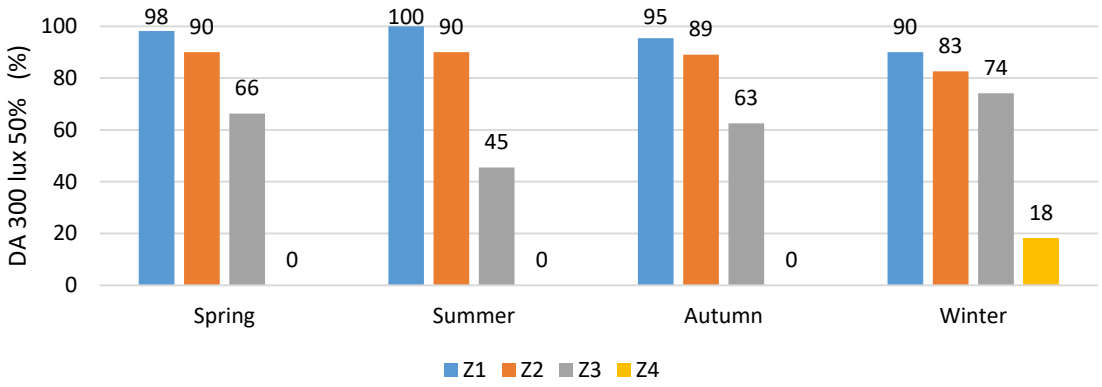


Figure 5.29: The DA for each season

ASE was calculated at the work plane at daylight zone Z1, Z2, Z3 and Z4. It was found that the ASE is exceeded 1,000 lux for more than 250 hours at Z1 during the whole year except in summer. The ASE was particularly high in winter, where it reached 338 hours. On the other hand, the ASE was much lower in spring and autumn; it was 20 hours and 3 hours, respectively, as shown in Figure 5.30.

ASE failed area for the whole room in winter, spring and autumn was 10.7%, 3.57% and 2.85%, respectively. On the other hand, the whole room met the target in summer (no area higher than 1,000 lux from direct sunlight for more than 250 hours at more than 10% of the space).

At daylight zone Z1, more than 10 per cent of the area was received direct sunlight that produces an illuminance value higher than 1,000 lux for more than 250 hours during occupational hours.

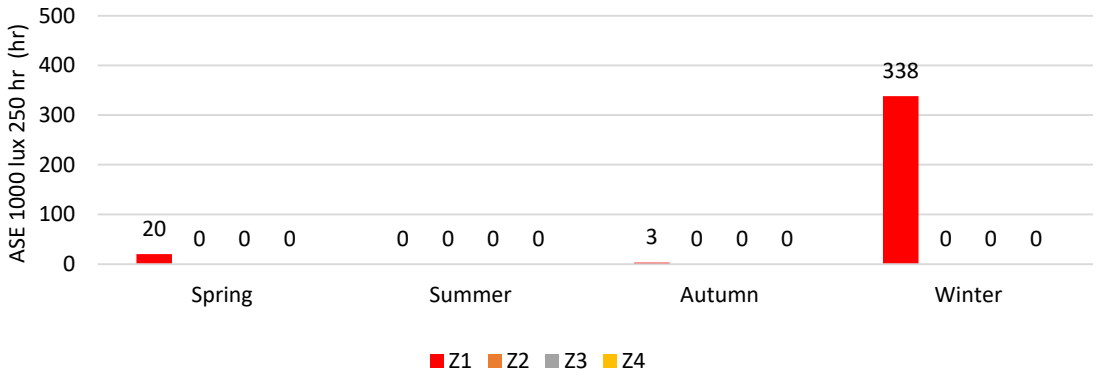


Figure 5.30: The ASE for each season, for the base case

The results of the $UDI_{300\text{-}1000\ lux}$ showed that the best performance was achieved at daylight zone Z2 in summer at 90%. On the other hand, the worst scenarios, where the $UDI_{300\text{-}1000\ lux}$ was not met completely, were recorded at daylight zone Z1 and summer and Z4 in spring, summer and autumn. In general, Z3 was recorded more constant $UDI_{300\text{-}1000\ lux}$, ranging from 45.5% in summer to 74.4% in winter. At Z2, the $UDI_{300\text{-}1000\ lux}$ was low in winter at 20.9%; however, it was better in spring and autumn at 46.7% and 52.1%, respectively. At Z1, the nearest area towards the window, the $UDI_{300\text{-}1000\ lux}$ was extremely low in most seasons, the highest UDI was 7.6% in spring, and the lowest was in summer at 0%. Similarly, it was 2.9% and 3.3% in autumn and winter, respectively. The worst scenario among the daylight zones was Z4, where the UDI was not met except in winter with a low percentage, 17.7%, as shown in Figure 5.31 and Figure 5.32.

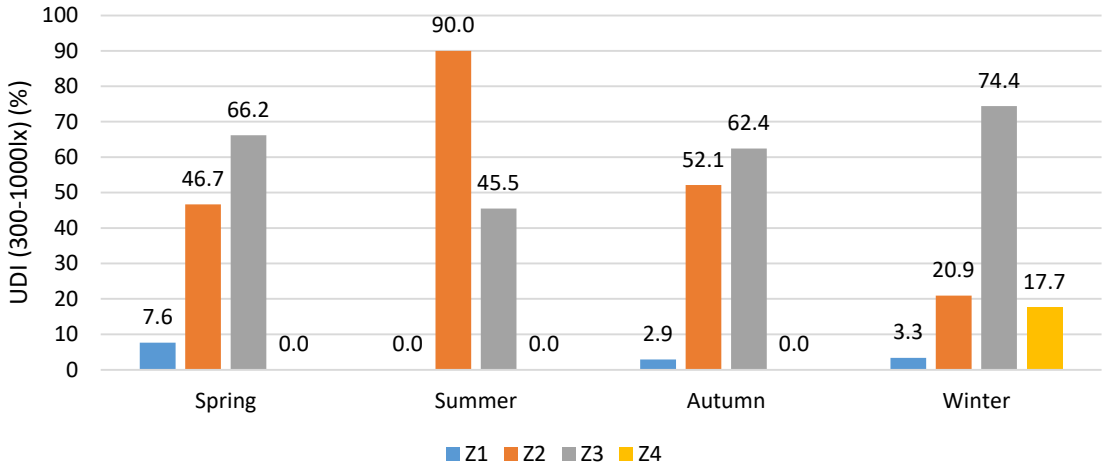


Figure 5.31: The UDI for each season, for the base case

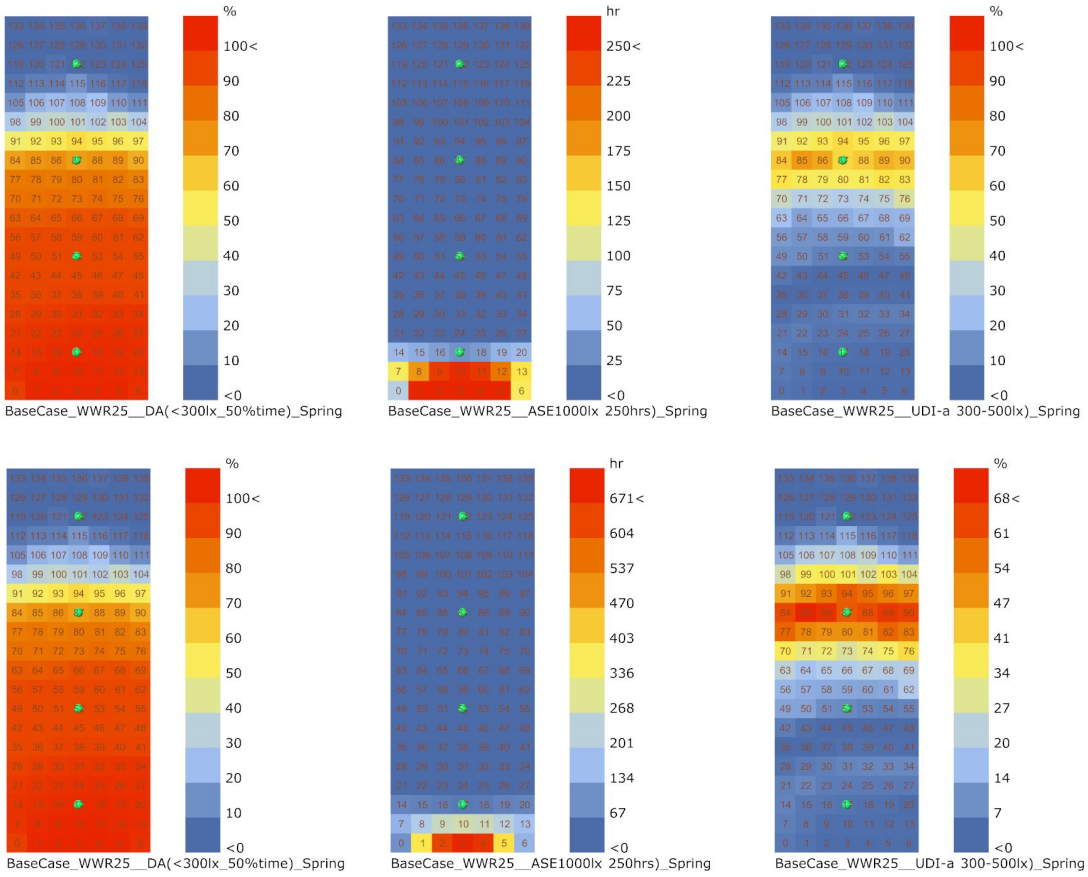


Figure 5.32: The daylight simulation outputs for spring, DA (left), ASE (middle), and UDI (right).

5.4.2. Analysis of the sunray's reflection behaviour

The objective of the raytracing study of the direct sun paths for the base case was to investigate the amount of direct sunlight that accesses the room towards the work plane in the current situation.

The sunrays were modelled for the 21st of June, September and December, representing the summer and winter solstices and autumn equinox. They were modelled at the solar noon when the sun azimuth is 180 degrees. The objective of utilising the forward-raytracing method was to visualise the sunrays to observe their behaviour (sunbath behaviour). From the raytracing of the sunrays, we can see only the direct sun components. They were modelled for five solar hours of the day, 8 am, 10 am, 12 pm, 2 pm and 4 pm. These hours represent the early morning, the midday and the evening time. The selected times can cover most of the common scenarios of the sun movement during the operation hours of the building during g the whole year.

5.4.2.1. Results

Figure 5.33 shows the sun paths at solar noon in Riyadh city for the base case on the 21st of June, September and December. The solar altitude angle (α) on 21 June is 88 degrees, and the solar azimuth angle (γ) is 180 degrees. It found that the direct sun rays access a minimal area next to the window, precisely 0.01 meter from the façade. As a result, it can be appreciated that the daylighting in the room during these times obtains mainly from the diffuse daylight.

On the 21st of September at solar noon, when α is 66 degrees and γ is 180 degrees, the sun can access a deeper area than the 21st of June. It can be seen that the direct sunrays can access the room through the south façade. The area received a direct sunray on 21 September was a 0.47-meter length, and the distance between the first ray and the window was 0.01 meter.

On the other hand, on the 21st of December at solar noon, when α is 42 degrees and γ is 180 degrees, the direct sunlight can reach a deeper distance inside the room. The direct sunbeams reached the nearest point at the work plane next to the window, and the last beam reached about 1.16-meter depth.

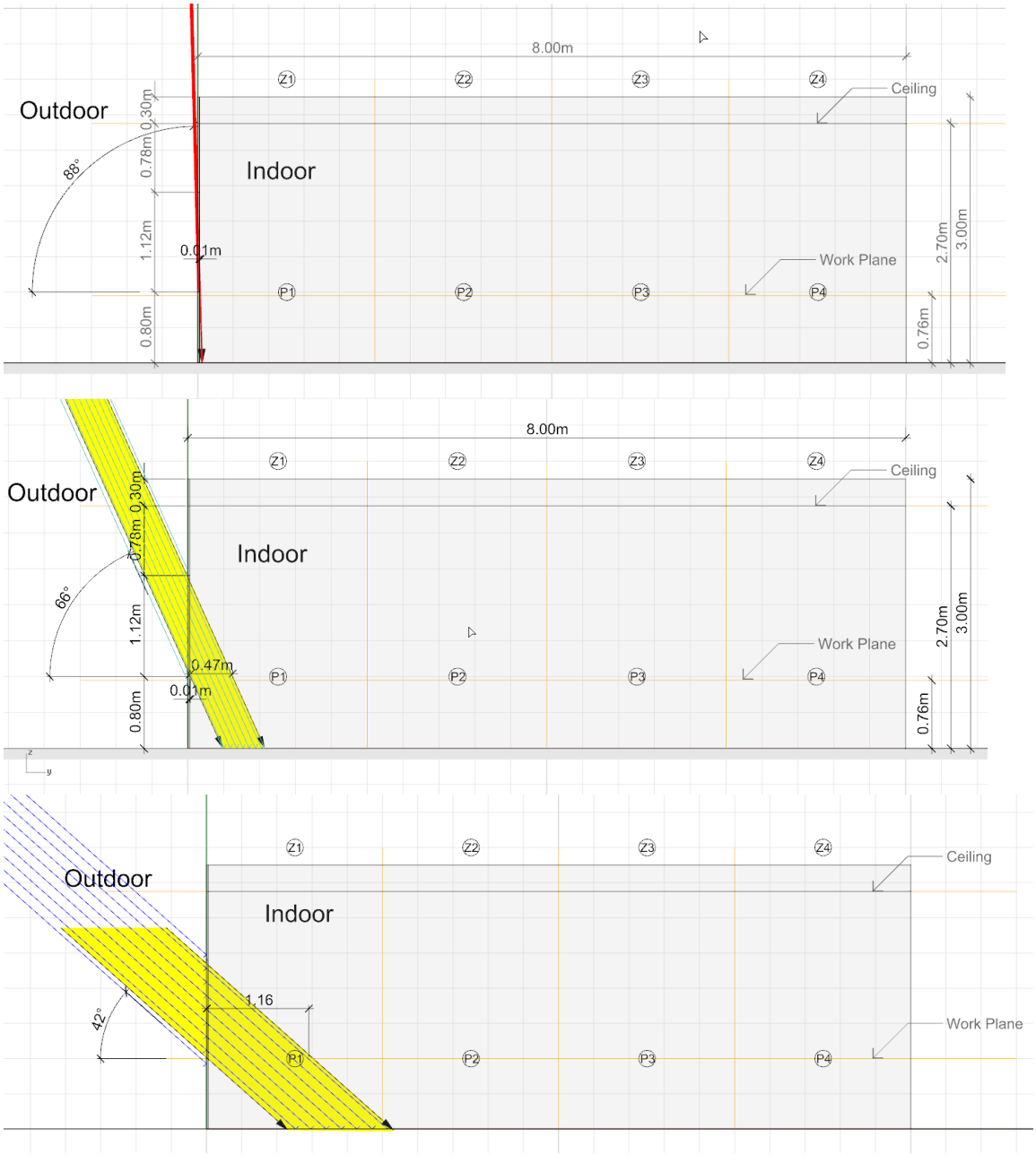


Figure 5.33: Raytracing of direct sunlight at 12 pm on 21 June (above), 21 September (middle) and 21 December (below)

5.4.3. Hourly evaluation through a point-in-time daylight study

The daylight performance of the base case was analysed between 8 am and 4 pm on 21 June, 21 September, and 21 December at 2-hour intervals. The results were obtained for solar time through an annual daylight simulation. The selected days represent the summer and winter solstices and autumn equinox. At solar noon during these three days, the sun position reached its highest, lowest and average solar altitude.

The illuminance values at the work plane were measured at the four daylight zones. Then the DUWP was calculated for the entire area. While the illuminance level at the test point gives an

indicator about the quantity of the light intensity at that point, the DUWP can be considered as a reliable indicator that can provide a clear conclusion about the quality of the illuminance distribution, and hence the visual comfort level in the interior space.

5.4.3.1. Daylight performance during morning hours

The illuminance at the work plane was calculated at the five test hours that were mentioned previously. The chart in Figure 5.34 shows the illuminance values at 8 am on the 21st of June, September, and December. The illuminance values from Z1 to Z4 in June were 2,871, 651, 250 and 149 lux. In September, they were 3,723, 824, 297 and 180 lux, and in December, they were 4,610, 906, 342 and 188 lux, respectively. The outputs of the simulation are presented in Figure 5.36.

It can be seen that the drop in total illuminance value between the daylight zones was relatively more significant on December 21st, while the lowest difference was recorded on June 21st. The decrease in the illuminance value from Z1 to Z4 was 4,422 lux, 3,543 lux and 2,722 lux on December 21st, September 21st and June 21st.

The ratio of daylight distribution within the room was calculated for the four lighting zones. The chart in Figure 5.35 shows that the daylight distribution ratio variance among the three tested hours was insignificant. The daylight percentage was 73%, 17%, 6% and 4% in June, and it was 74%, 17%, 6% and 4%, in September, and it was 76%, 15%, 6% and 3% in December, from Z1 to Z4, respectively.

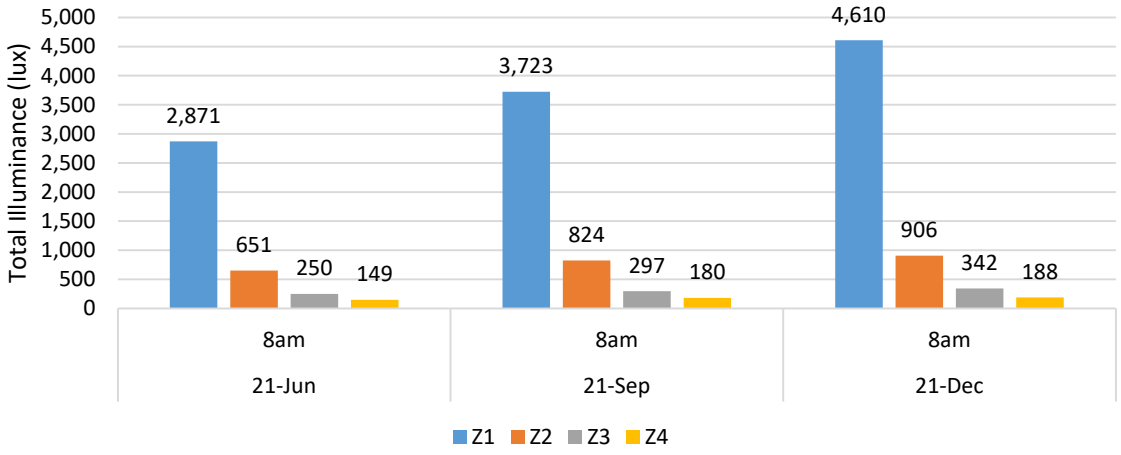
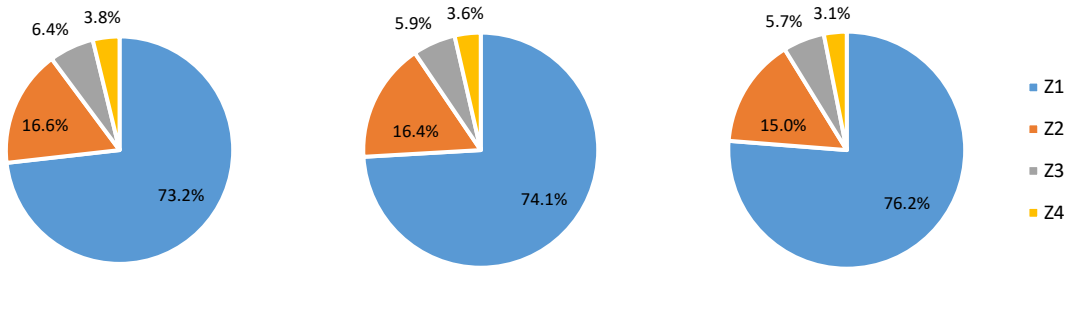
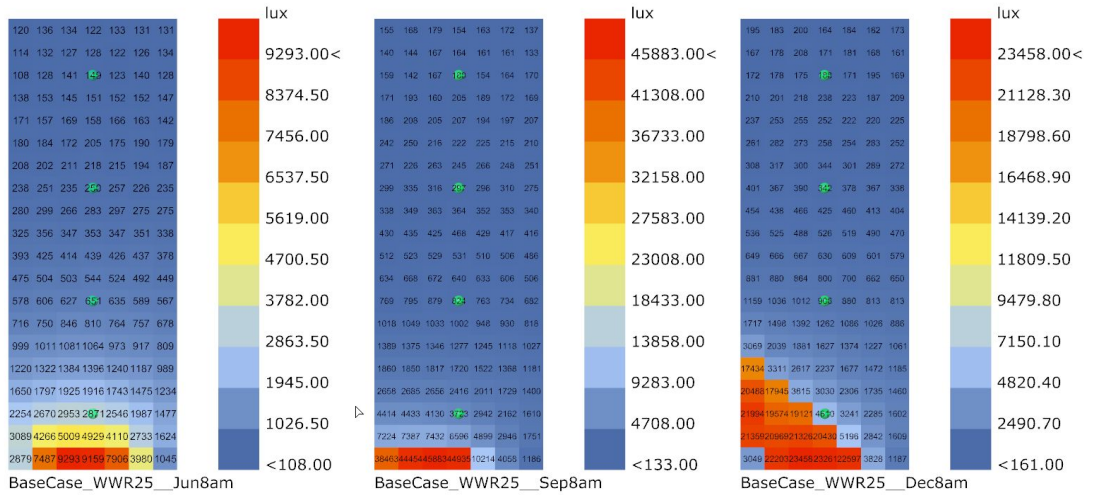


Figure 5.34: Total illuminance for the base case



21 Jun 21 Sep 21 Dec

Figure 5.35: Daylight distribution within the four zones at 8 am, for the base case



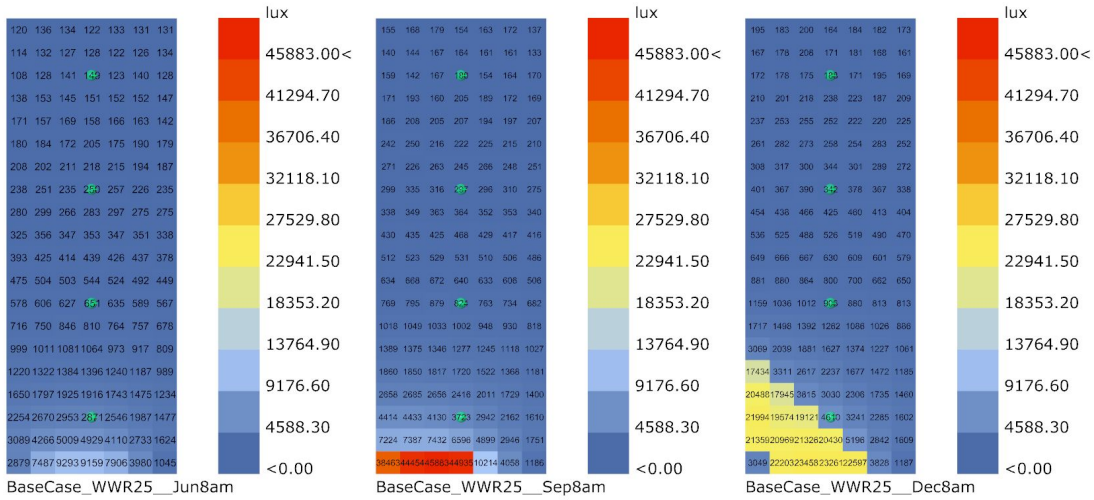


Figure 5.36: Total illuminance at 8 am on 21 June (left), 21 September (middle) and 21 December (right)

In order to investigate the daylight performance at the work plane (DLPWP) after the early morning hours and before the solar noontime, the illuminance level was assessed at 10 am on the 21st of Jun, September and December. It was found that the DLPWP on Jun 21st was within the range from 2,782 lux to 190 lux from Z1 to Z4, respectively. On September 21st, the illuminance was relatively higher, it was 5,452 lux at Z1 with an increase of 2,671 lux, and the lowest was 233 lux at Z4 with an increase of 43 lux compared against June 21st. On the other

hand, on December 21st, the illuminance at Z1 was extremely high, which reached 44,002 lux. However, the increase of the illuminance values at Z2, Z3 and Z4 was much lower than Z1. The illuminance at Z2, Z3 and Z4 was 1,550 lux, 601 lux and 301 lux. The increase in the illuminance from Z1 to Z4 on 21 December compared with 21 September was 38,549, 433, 140 and 68 lux, respectively, as shown in Figure 5.37 and Figure 5.40.

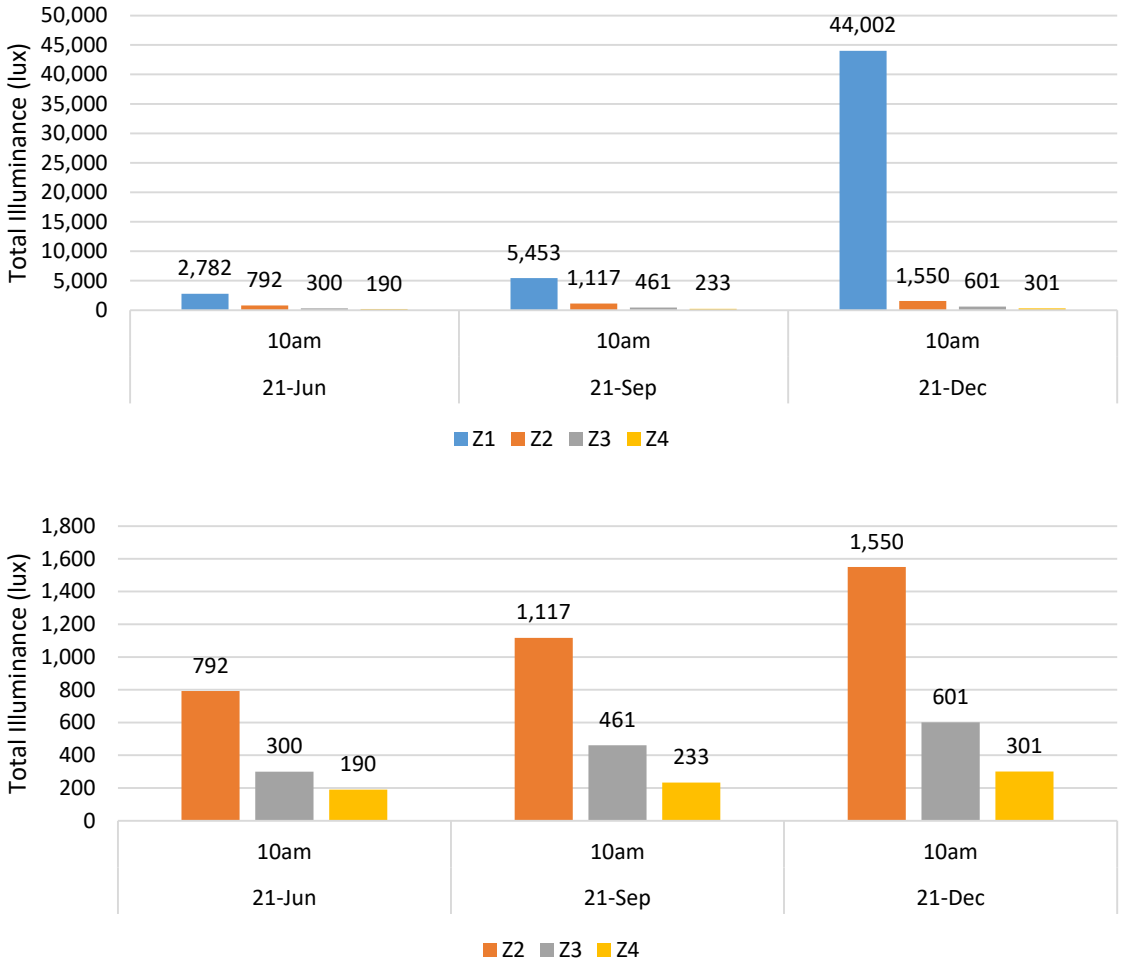


Figure 5.37: Total illuminance for the base case

The ratio of the daylight distribution between the daylight zones within the room was calculated for the three test hours. It was found that Z1 has a large quantity of daylight for the three scenarios while the daylight at Z4 is the lowest. On June 21st, the daylight distribution percentage was 68%, 20%, 7% and 5% from Z1 to Z4, respectively. Similarly, on September 21st, it was 75%, 16%, 6% and 3%. Finally, on December 21st it was 95%, 3%, 1.3% and 0.6%.

It can be seen that the worst balance in the daylight distribution between the front and the rear area of the room was in December, and the best was in June. However, the three scenarios are lower than the standard requirements of the daylight interior office spaces. The maximum

daylight availability at Z4 was in June at 5% and similarly on Z3, 7%. The daylight distribution percentage at Z2 was promising on June 21st, 20%, and acceptable on September 21st, 16 %. On the other hand, it was inadequate at Z3 on December 21st, only 3%, as illustrated in Figure 5.38.

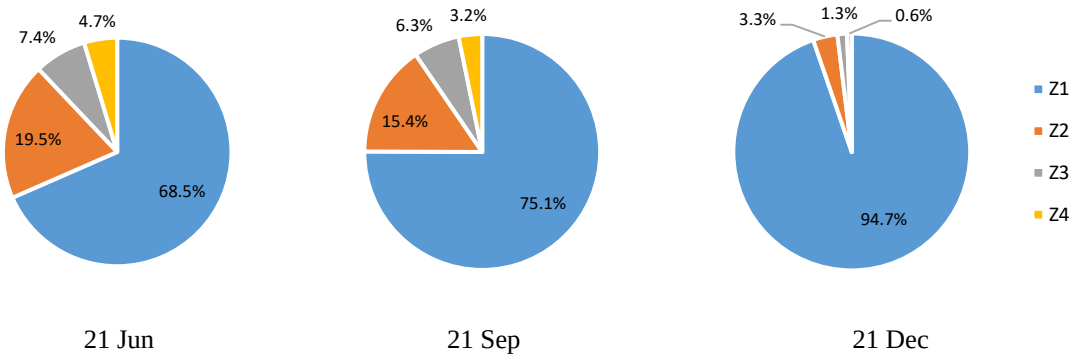


Figure 5.38: Daylight distribution within the four zones at 10 am

The direct illuminance at the work plane was calculated to investigate the penetration of the direct solar radiation. It can be seen that the direct illuminance at 10 am was recorded only at Z1 on December 21st. The 44,002 lux total illuminance was obtained mainly from the direct solar radiation, which produced 35,405 lux, as shown in Figure 5.39. Hence, the diffuse illuminance at this point was 8,597 lux.

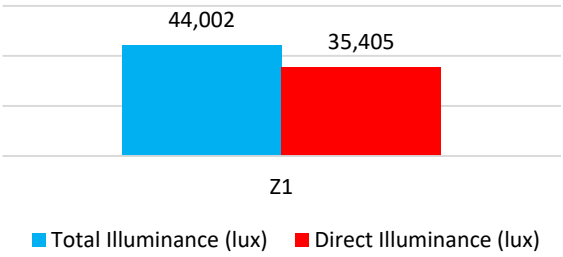


Figure 5.39: Total and direct illuminance at Z1 on 21 December at 10 am

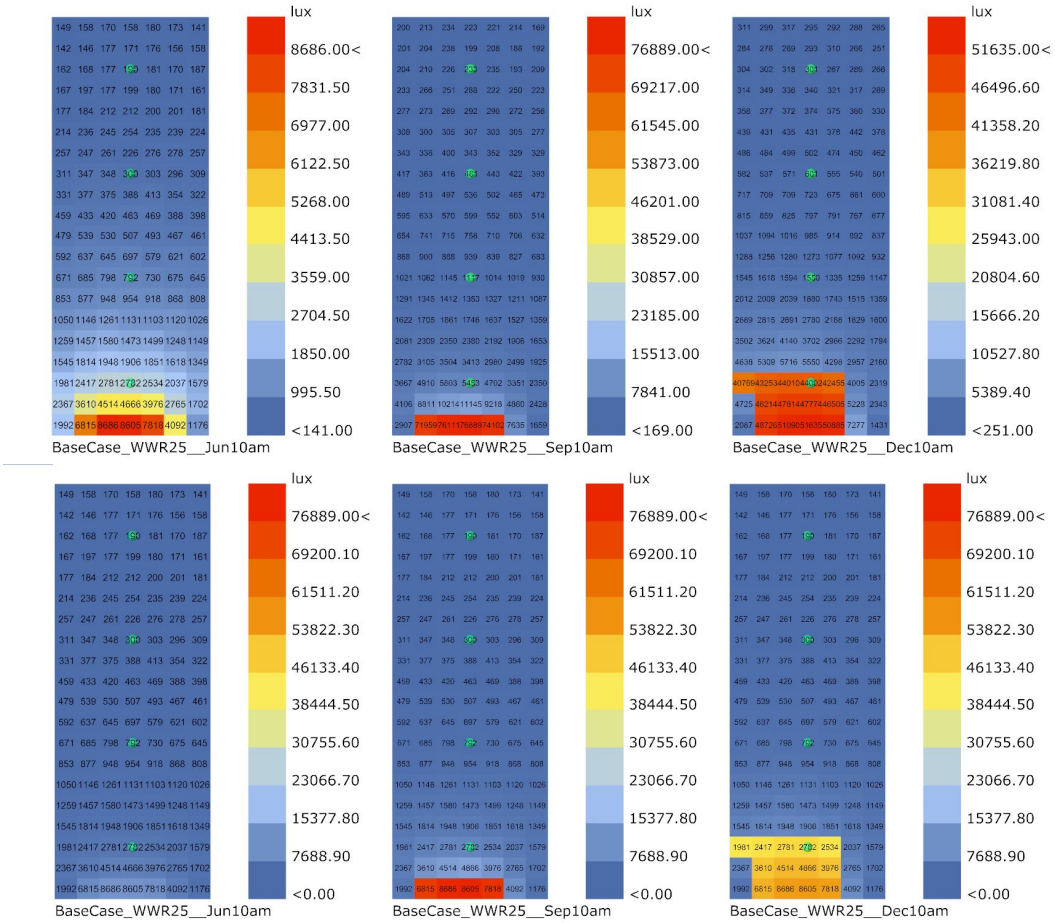


Figure 5.40: Total illuminance at 10 am on the 21st of June, September and December (from left to right)

5.4.3.2. Daylight performance at solar noon

The four zones (Z1 to Z4) were assessed by a PIT study from an annual simulation in RADIANCE. The room was tested at solar noon on the 21st day of June (summer solstice), September (autumn equinox) and December (winter solstice), as illustrated in Figure 5.6 above.

It was found that the total illuminance value at Z4 was the lowest among the four zones. The highest total illuminance for Z4 was recorded on December 21st at 315 lux, then on September 21st at 222 lux, while the lowest illuminance value was on June 21st at 197 lux. On the other hand, the highest total illuminance values among the zones were recorded at Z1. The peak value was recorded on December 21st at 48,460 lux while it was lower in September at 5,718 lux, and the lowest illuminance at Z1 was recorded in June at 2,938 lux.

The reduction in the total illuminance level from Z1 to Z4 during the same test hour was analysed. It was found that on December 21st, the highest difference was recorded; the total illuminance was dropped by 48,145 lux. The lowest reduction was recorded on June 21st by 2,741 lux. On September 21st, a decrease in the total illuminance by 5,496 lux was recorded, as shown in Figure 5.41 and Figure 5.42.

The remarkably high total illuminance value at Z1 on December 21st is due to the high value of the direct illuminance. The direct illuminance was 3,9258 lux, while the diffuse illuminance was 9,202 lux, as shown in Figure 5.43.

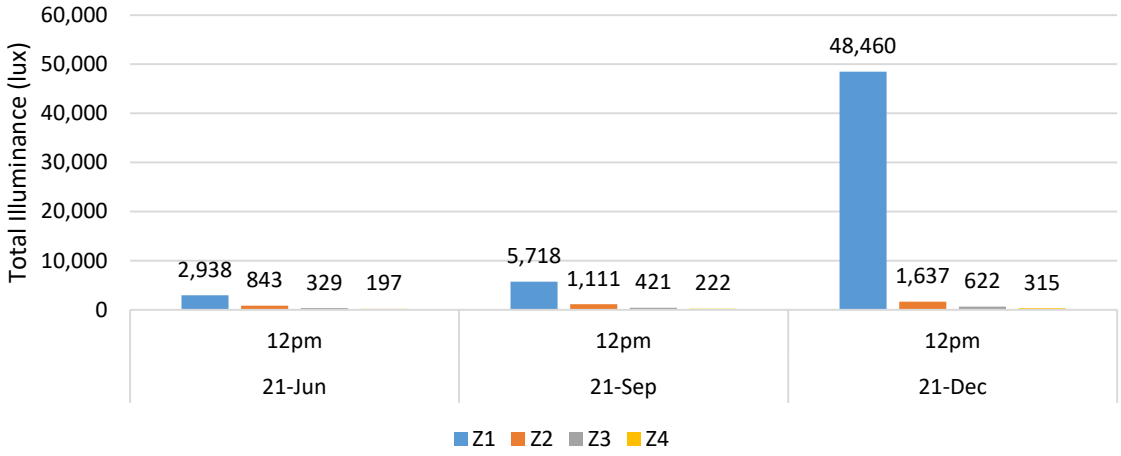


Figure 5.41: Total illuminance for the base case at Z1, Z2, Z3 and Z4.

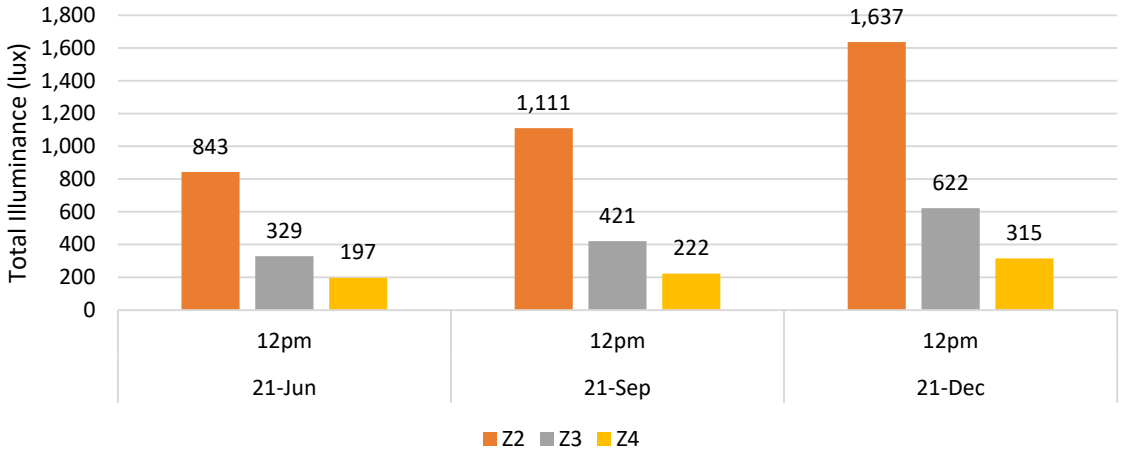


Figure 5.42: Total illuminance for the base case at Z2, Z3 and Z4

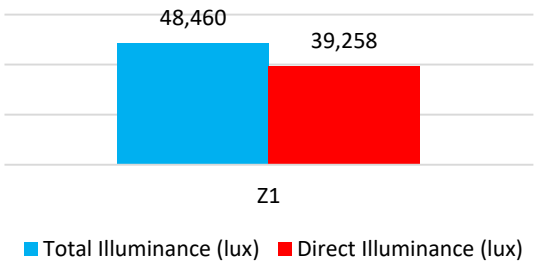


Figure 5.43: Total and direct illuminance at Z1 on 21 December at 12 pm

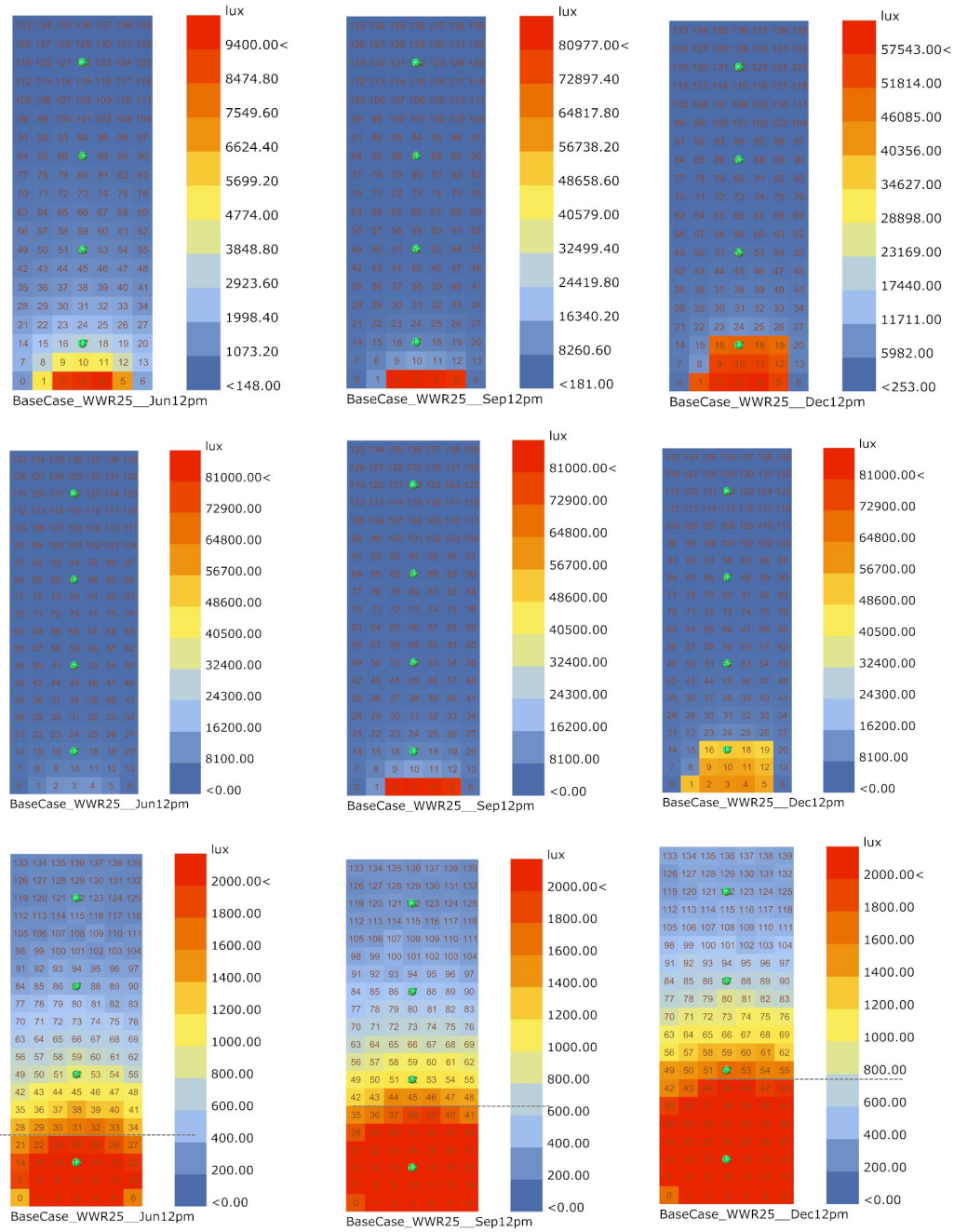
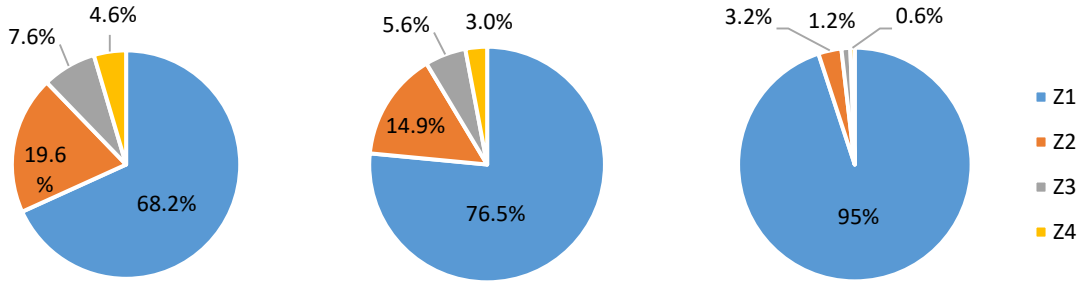


Figure 5.44: Total illuminance at 12 pm on 21 June (left), 21 September (middle) and 21 December (right). (Below) the high bound of scale is set to 2000 lux

The percentage of the daylight distribution among the four zones was calculated. In general, it can be seen that the balance of daylight distribution for the three cases was extremely low. Z1 has obtained a high percentage of daylight compared with the other three zones. The worst scenario was in December, with a 94% drop from Z1 to Z4. In December, the daylight distribution percentage was 95%, 3.21%, 1.22% and 0.62% at Z1, Z2, Z3 and Z4.

In September and June, the drop of the daylight percentage was better than in December, by 21% and 31%, respectively. In September, the daylight distribution was 76%, 15%, 6% and 3

% at Z1, Z2, Z3 and Z4, respectively. While in June, it was 68%, 19%, 8% and 5 % at Z1, Z2, Z3 and Z4, respectively, as shown in Figure 5.45.



21 Jun 21 Sep 21 Dec

Figure 5.45: Daylight distribution within the four zones at 12 pm on the 21st of June, September and December

5.4.3.3. Daylight performance during evening hours

The illuminance at the work plane was assessed at 2 pm on the 21st of June, September and December. The purpose was to investigate the daylight performance between the solar noon and the late operation hours of the building. It was found that the total illuminance at the work plane was extremely high at Z1 on 21 December. In contrast, the total illuminance was lower than the required minimum threshold at Z4 for all scenarios. At Z3, the total illuminance was above the minimum threshold on 21 September and 21 December but was lower on 21 June.

From the charts in Figure 5.46, it can be seen that the total illuminance on 21 June was 3,039 lux, 741 lux, 286 lux and 173 lux at Z1, Z2, Z3 and Z4, respectively. Similarly, on 21 September, it was 4,520 lux, 917 lux, 351 lux and 211 lux. Finally, on 21 December, it was 38,065 lux, 1,323 lux, 526 lux, 299 lux.

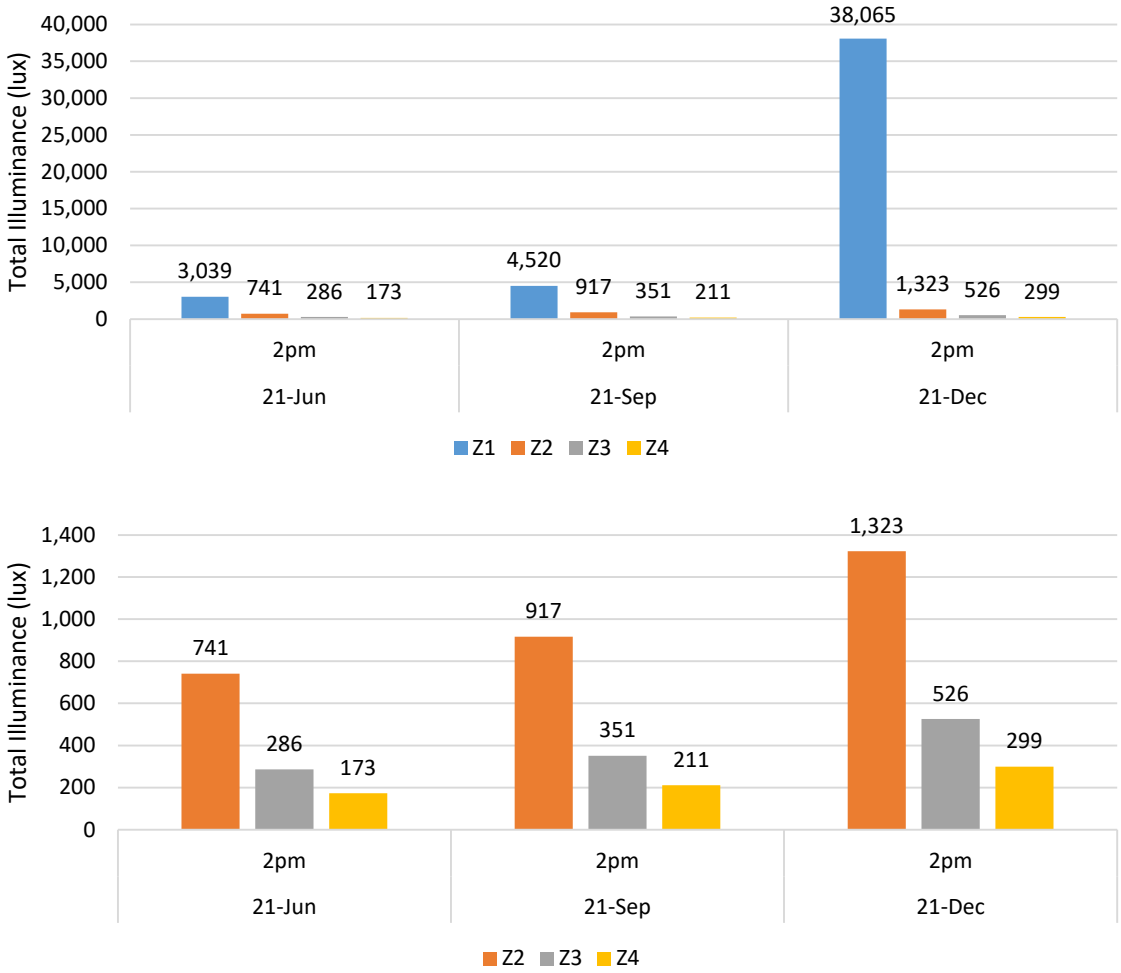


Figure 5.46: Total illuminance at 2 pm for the base case

The total illuminance and the direct illuminance at the four daylight zones were measured separately to investigate the penetration of the direct solar ratio at the work plane. It was found that the direct illuminance was recorded only at Z1. As seen on the chart in Figure 5.47, the total illuminance was 38,065 lux, consisting of 32,169-lux direct illuminance. Thus, the diffuse illuminance was 5,896 lux, which is relatively higher than the illuminance at the same point on the 21st of June (3,039 lux) and September (4,520 lux).

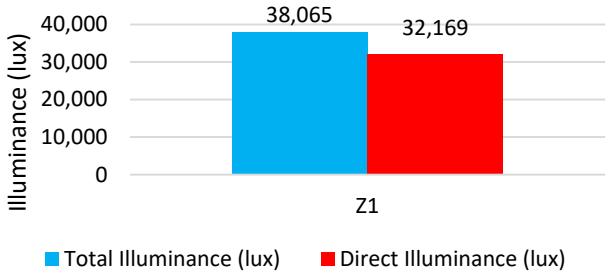


Figure 5.47: Total and direct illuminance at Z1 on 21 December at 2 pm

The daylight percentage at each daylight zone was calculated to investigate the equality of the daylight distribution within the room. It was found that the best quality of the daylight distribution was on 21 June and then 21 September. On the other hand, the worst scenario was on 21 December. However, the minimum requirement of an adequate daylight distribution was not met for all scenarios.

The percentage of the daylight distribution on 21 June was 71.1%, 17.5%, 6.7% and 4.1% at Z1, Z2, Z3 and Z4, respectively. Similarly, on 21 September, it was 75.3%, 15.3%, 5.9% and 3.5%. Finally, on 21 December, it was 94.7%, 3.3%, 1.3% and 0.7%.

From the pie chart below in Figure 5.48, it can be seen that Z1 dominated most of the daylight availability inside the room. In contrast, a low percentage of daylight reached Z3 and Z4. The situation at Z2 on the 21st of June and September was better than Z4; however, on 21 December at the same zone, the available daylight percentage was inadequate.

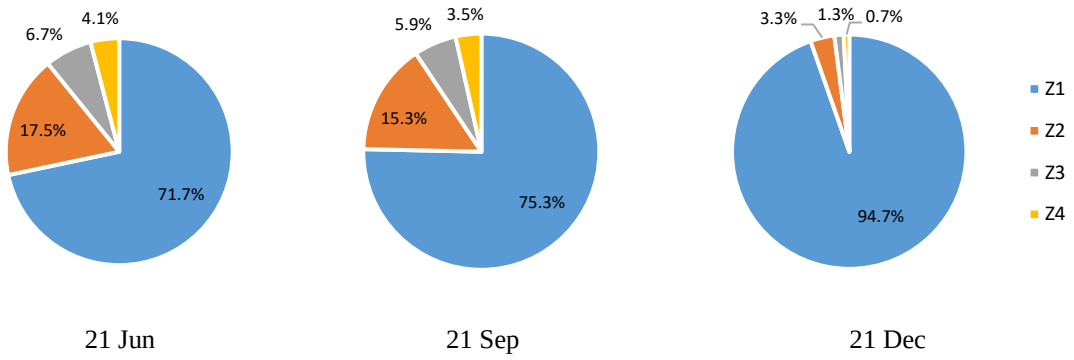


Figure 5.48: Daylight distribution within the four zones at 2 pm

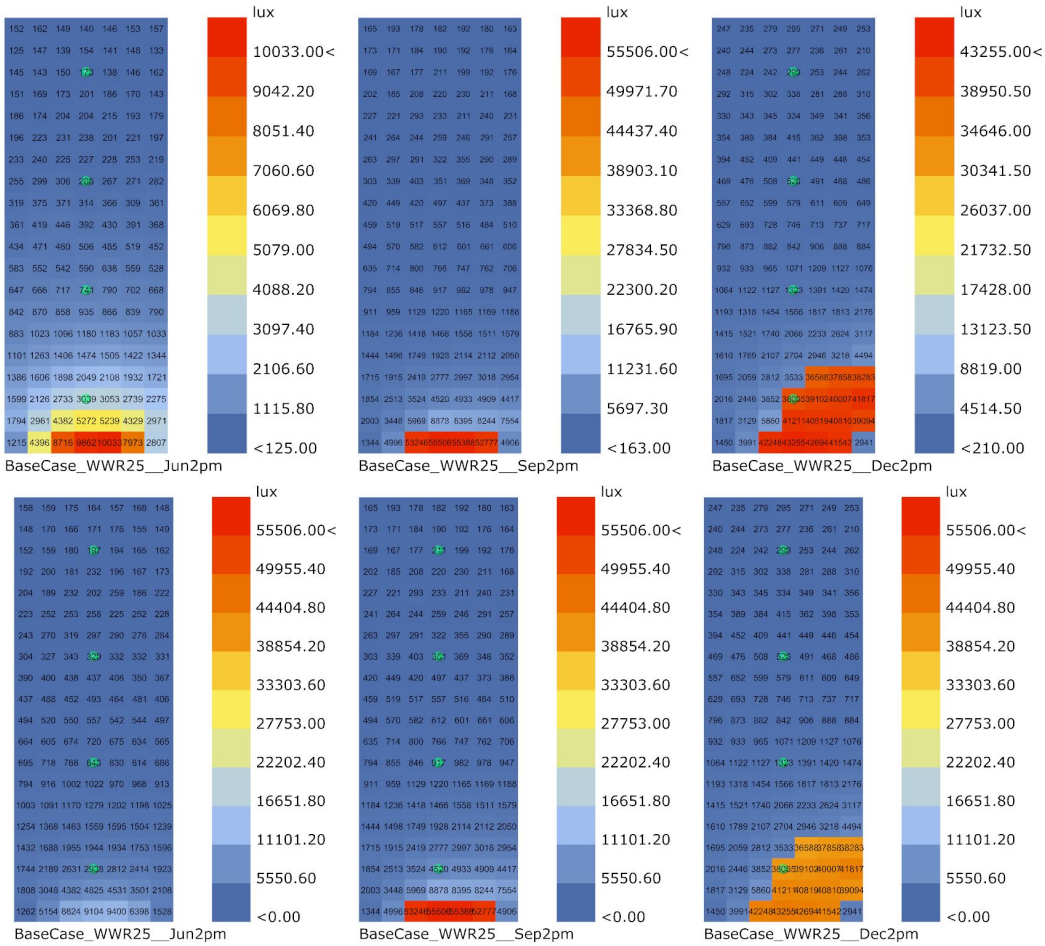


Figure 5.49: Total illuminance at 2 pm on 21 June (left), 21 September (middle) and 21 December (right)

The daylight illuminance at the work plane was measured at 4 pm to investigate the daylight performance during the late occupation hours, from 8 am to 5 pm. During that hour, the total illuminance does not have a direct illuminance for all scenarios. In contrast with the previous test hour (2 pm), it was noticed that the daylight pattern between the three months had been changed.

It can be seen from the chart in Figure 5.50 that the illuminance at the work plane on 21 June has recorded the highest values at the four daylight zones. On the other hand, the lowest illuminance values were recorded on 21 December. The illuminance on 21 June was 2,324 lux, 470 lux, 169 lux and 104 lux at Z1, Z2, Z3 and Z4, respectively. Similarly, on 21 September, it was 2,148 lux, 401 lux, 165 lux, and 84 lux. Finally, on 21 December, it was 1,279 lux, 278 lux, 106 lux, and 52 lux.

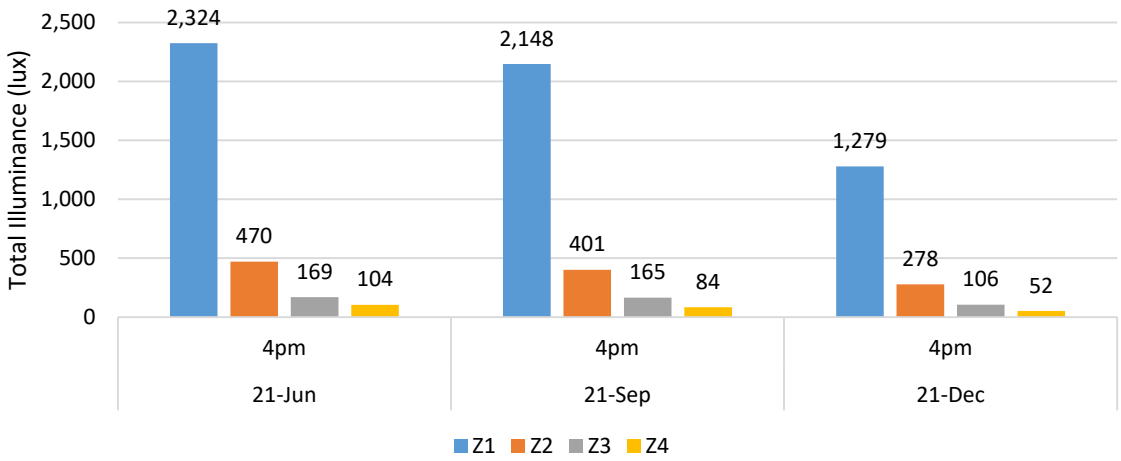


Figure 5.50: Total illuminance for the base case

The quality of the daylight distribution was relatively similar among the three test hours. Z1 dominated most of the available illuminance like the previously tested scenarios, while Z4 and Z3 were not provided with sufficient daylight. The percentage of daylight at Z2 was better than Z3 and Z4, but it was lower than the desirable level.

From the pie chart in Figure 5.51, it can be seen that the difference in the daylight distribution weight between the three scenarios for the same daylight zone is insignificant. For example, at Z1, the difference between the highest daylight distribution percentage (on 21 September) and the lowest (on 21 December) was 2.2%. Similarly, at Z2, it decreased by 1.9% from 16.2% on 21 December to 14.3% on 21 September. The lowest percentages were at Z3 and Z4 at 5.5% and 3.4% on 21 June, 5.9% and 3.0% on 21 September, and 6.2% and 3.0% on 21 December.

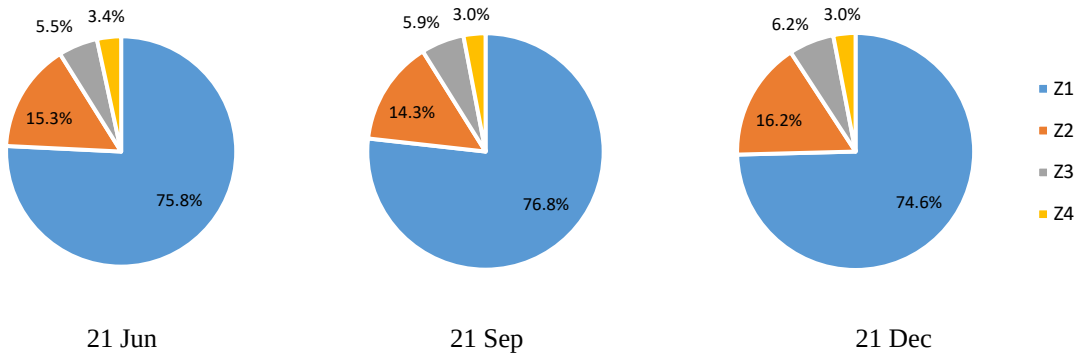


Figure 5.51: Daylight distribution within the four zones at 4 pm

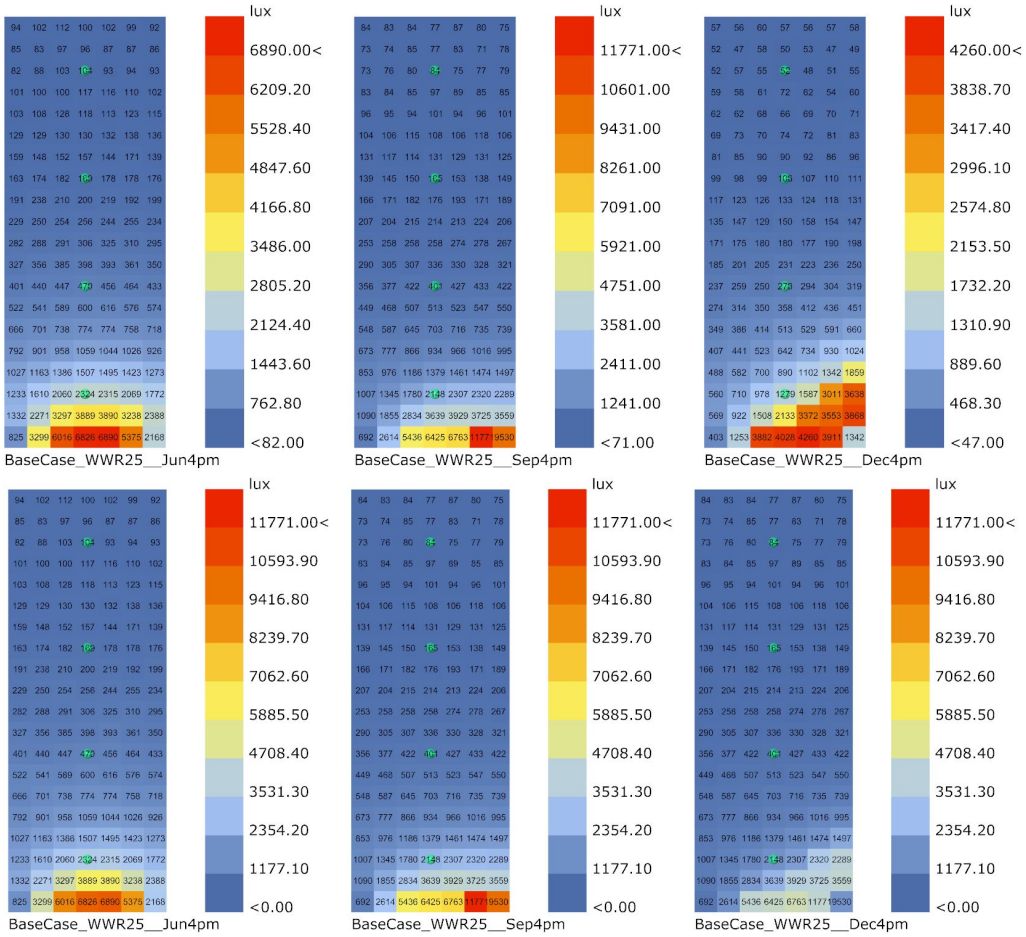


Figure 5.52: Total illuminance at 4 pm on 21 June (left), 21 September (middle) and 21 December (right)

5.4.4. Daylight uniformity

The daylight uniformity of the total illuminance at the work plane (DUWP) was calculated to investigate the overall performance for each test hour. It was calculated based on Equation 4. It was found that the best DUWP value among the three months, namely June, September and December, was recorded in June. In contrast, the worst DUWP was found in December. Regarding the hourly performance, it was found that the peak DUWP performance was achieved for each month at a different hour. For example, it can be seen from the chart in Figure 5.53 below that the peak DUWP performance was obtained at 10 am on 21 June, at 8 am and 2 pm on 21 September, and at 8 am and 4 pm on 21 December.

However, as overall performance, the DUWP changes during the day were constant. The DUWP on 21 September was between 12% (at noon) to 14% (at 8 am and 2 pm), with a 2% change. Similarly, on 21 June, the variance in the DUWP was 5%, which is low but slightly higher than 21 September. On the other hand, the DUWP on 21 December was the worst, where the decrease was by 10%, from 12% to 2%. The DUWP was 12% in the early morning (8 am)

and the late evening (4 pm). However, it was dropped to 3% at 10 am and 2 pm, while the lowest was at noon at 2%.

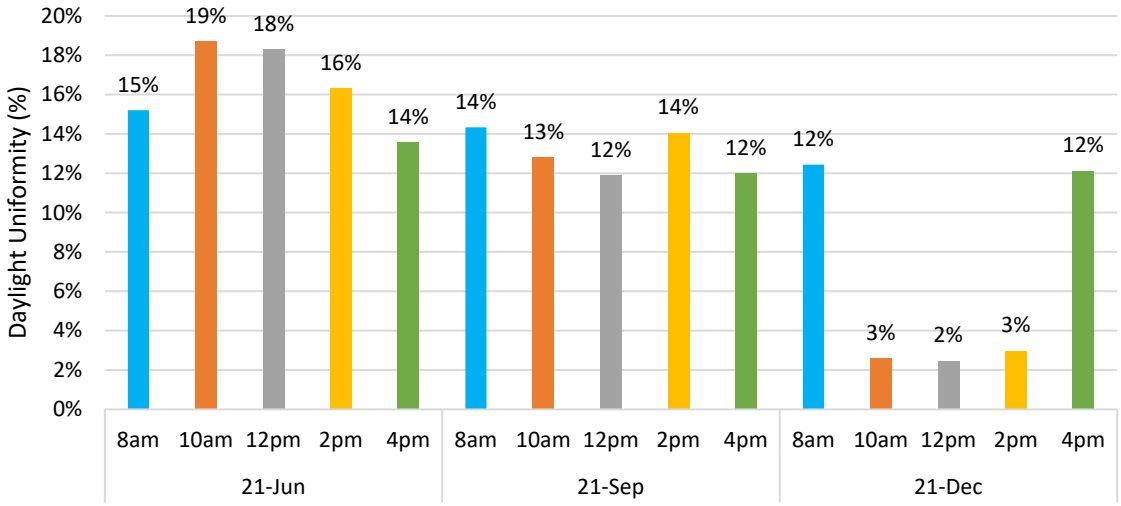


Figure 5.53: The DUWP for the base case

5.4.5. Analysis of daylight glare probability

Another significant aspect of visual comfort is glare. The daylight glare probability (DGP) was analysed for the worst day that recorded the highest ASE. As was mentioned in the previous chapters, ASE represents the direct illuminance occurrence during the year. The previous illuminance assessments found that the highest ASE among the tested days was recorded on the 21st of December.

Glare may cause discomfort for occupants; therefore, it was necessary to analyse the DGP after assessing the illuminance. It was found that the glare comfort range was within the intolerable glare for all the tested hours except at 8 am, which was a disturbing glare, as shown in Table 5.5. The DGP values were above the maximum threshold of the disturbing glare, which is 0.45. The DGP values were 0.82, 0.94, 0.83 and 0.47 at 10 am, 12 pm, 2 pm and 4 pm, respectively, while it was 0.42 at 8 am. The visualisation of the luminance values at 8 am, 10 am, 12 pm, 2 pm and 4 pm are illustrated in the fish-eye images from Figure 5.54 to Figure 5.58.

Table 5.5: Glare study results of daylight redirecting solar screen the base case

Date	Time	DGP	Glare Comfort Range
21 December	8 am	0.42	Disturbing Glare
	10 am	0.82	Intolerable Glare
	12 pm	0.94	Intolerable Glare
	2 pm	0.83	Intolerable Glare
	4 pm	0.47	Intolerable Glare

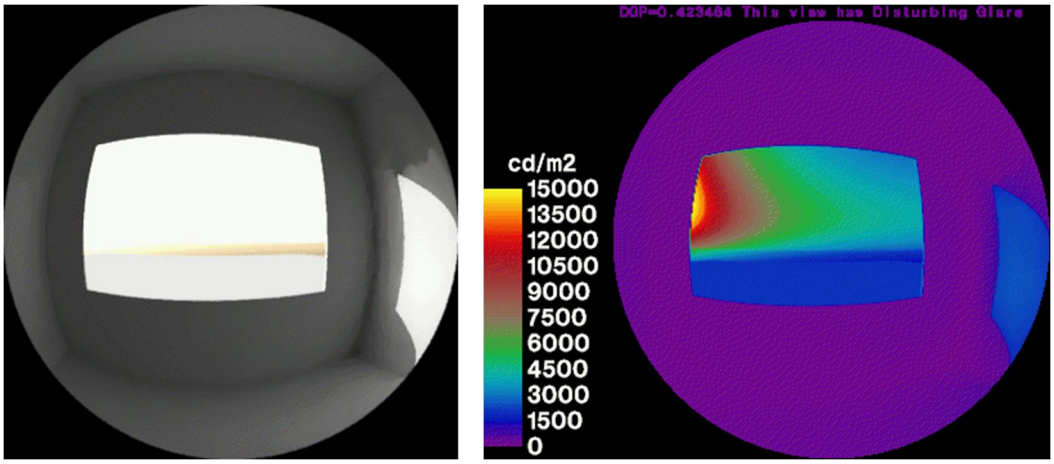


Figure 5.54: The luminance, on 21 December at 8 am, Base case, Riyadh

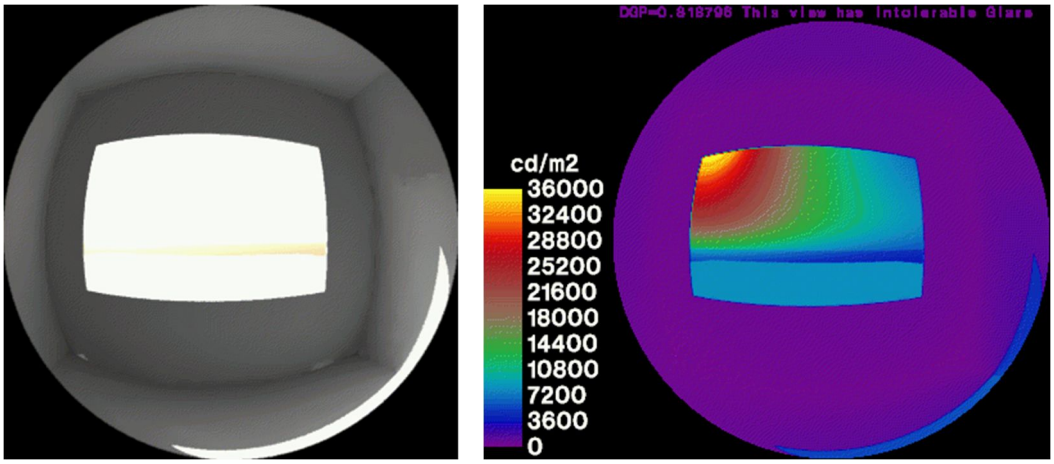


Figure 5.55: The luminance, on 21 December at 10 am, Base case, Riyadh

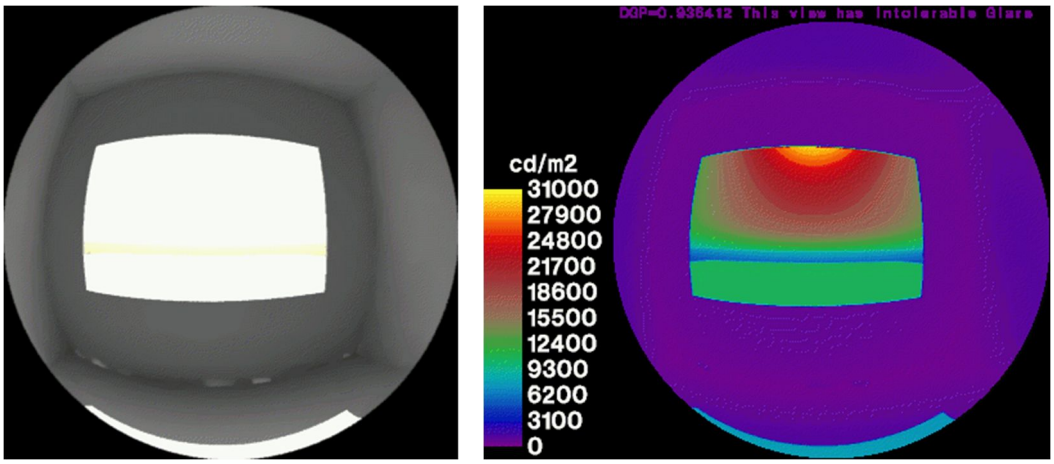


Figure 5.56: The luminance, on 21 December at 12 pm, Base case, Riyadh

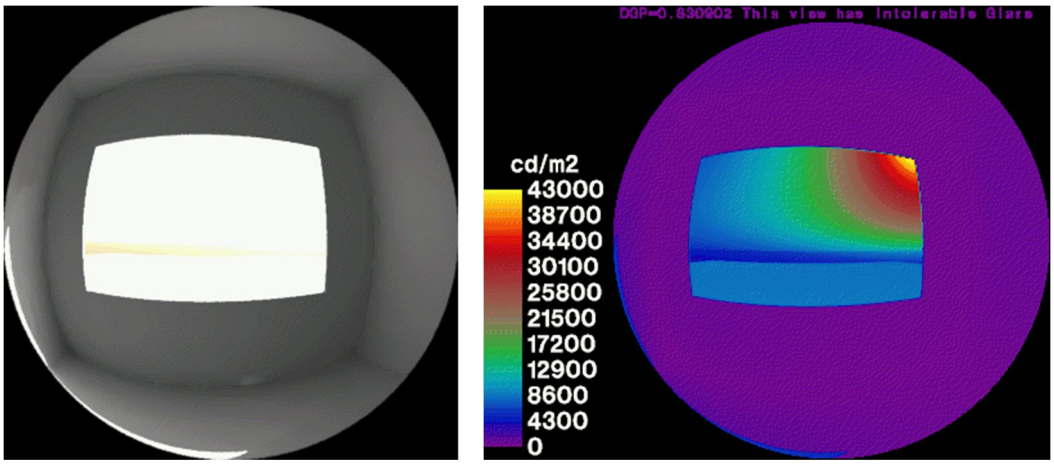


Figure 5.57: The luminance, on 21 December at 2 pm, Base case, Riyadh

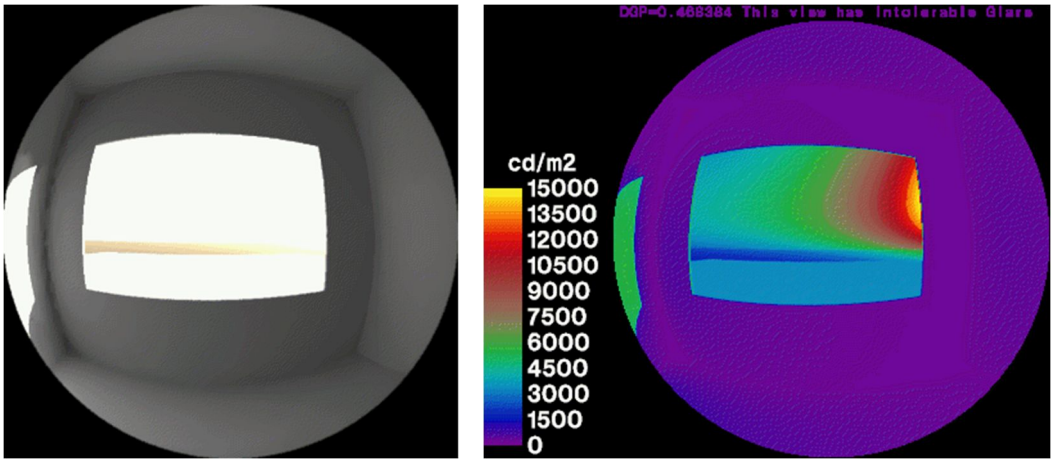


Figure 5.58: The luminance, on 21 December at 4 pm, Base case, Riyadh

5.5. Discussion and Summary

On base case

The results of the computer modelling were shown and analysed in this chapter. The daylight intensity was obtained for the 21st of June, September and December at solar noon in Riyadh. The illuminance values were calculated at the work plane level (0.76 meters from the floor level) (Nabil and Mardaljevic, 2005). This height is identified as a standard height of the working level for work desks in office buildings. The room has been tested without any shading device to find the maximum distance that can be daylit without the daylight-redirecting devices and any possibility of having overlit area. The daylighting performance of the room was measured as a function of different solar altitudes and azimuth angles. In order to assess the daylight performance, the room was divided into four equal zones, as illustrated in Figure 5.6.

First, the daylight performance of the base case, which has 25% WWR, was tested for the whole year through an annual study. The daylight performance was assessed by annual daylight metrics, namely, DA, ASE and UDI. It was found that the DA was achieved at high values at

all the daylight zones except Z4. The ASE was recorded only at Z1 by 381 hours per year. On the other hand, the UDI was extremely low at the front and the back area, Z1 and Z4. In the middle of the room at Z2 and Z3, the UDI was acceptable. Based on the annual evaluation of the base case, it was found that Z1 is overlit, Z2 is daylit, Z3 is partially daylit, and Z4 is not daylit.

In order to investigate the daylight performance during a different time of the year, the base case was assessed for each season separately. It was found that the best DA was in winter when the sun altitude is low, while the worst DA performance was in summer. On the other hand, the worst ASE was recorded in winter by 338 hours, whereas the ASE did not occur in summer. As the UDI has a minimum and maximum threshold, it gives a better assessment than the DA. It was found that the worst UDI was at Z1 and Z4 for all the seasons; however, the UDI performance was not varied among the seasons. For example, at Z2, the UDI is better when the sun altitude is higher as in summer. In contrast, at Z3, the UDI value is higher when the sun altitude is lower, as in winter.

After the annual and seasonal analysis, the sunrays behaviour was analysed at the solar noontime utilizing raytracing study for summer solstice, equinox and winter solstice. The study found that the direct sun rays only reached Z1. The worst scenario was recorded on winter solstice day as the direct sun penetrated the room by more than one meter at the work plane and two meters at the floor level. On the other hand, on the summer solstice day, the direct sun was not a challenge.

As the ray tracing considers only the direct sun components, an hourly daylight evaluation was conducted through a PIT study to investigate the daylight performance during the day. The study was between 8 am and 4 pm on 21 June, 21 September, and 21 December at 2-hour intervals. The proposed adequate illuminance level was 300 lux to 1000 lux. It was found that the desired illuminance level is achieved in the early morning at Z2 and Z3 on the three tested days. The illuminance levels exceeded the threshold at the front daylight zones whilst they were lower than the threshold at Z4.

During the time between the early morning and the late evening, particularly at 10 am, 12 pm and 2 pm, it was found that the best daylight performance was in June and September. Nevertheless, the illuminance level exceeded the threshold at the front daylight zone (Z1) for all the tested hours. At the rear daylight zone (Z4), the illuminance level was lower than the threshold for all the tested hours in June and September.

On the other hand, in December, the illuminance levels exceeded the acceptable threshold by a significant value that excessed 44,000 lux. Due to the low solar altitude angle, the direct sunlight can reach the front daylight zone, increasing the illuminance level significantly. In order to avoid the occurrence of direct sunlight, a proper daylight-redirecting system should be employed. Nevertheless, the daylight performance at Z4 was better in December. The minimum desired illuminance level was achieved at 10 am, 12 pm and 2 pm.

In order to assess the overall daylight performance, the DUWP of the total illuminance at the work plane (DUWP) was calculated for each tested hour. It was found that the DUWP dropped to 3% due to the direct sunlight occurrence at 10 am, 12 pm and 2 pm. The difference between the illuminance level at Z1 and the other daylight zones was enormous. On the other hand, in June and September, due to the absence of direct sunlight at the work plane, the DUWP was higher. The DUWP ranged from 14% to 19% in June and from 12% to 14% in September; however, these percentages are still lower than the desirable DUWP.

The daylight glare probability (DGP) was analysed for the base case. The purpose was to evaluate the visual comfort of the occupant at eye level of a seated person facing toward the window. The DGP analysis was analysed for Z1 in December, where the direct sunlight accessed the work plane. It was found that the glare comfort range was intolerable during all the tested hours, except at 8 am, which was disturbing, which still exceeds the acceptable level.

The above discussion showed that the daylight performance of the base case room with 25% WWR without shading is not adequate. The main reason for the low DUWP, as shown above, is the direct sunlight at the work plane. Furthermore, the discomfort that was shown in the DGP analysis is due to the direct sunlight that exposed the occupants. As a result, it is important to reduce the impact of direct sunlight in the front area. This objective could be reached by utilising a filtration daylighting system such as the proposed perforated solar screen (PSS).

Chapter 6. Computer modelling of the proposed daylighting system

6.1. Introduction

This chapter presents the computer simulation for the tested room with the proposed daylight system. The first phase analyse the daylight performance inside the room with a perforated solar screen (PSS) whilst the second phase assess the daylight performance after the installation of the proposed daylight redirecting system.

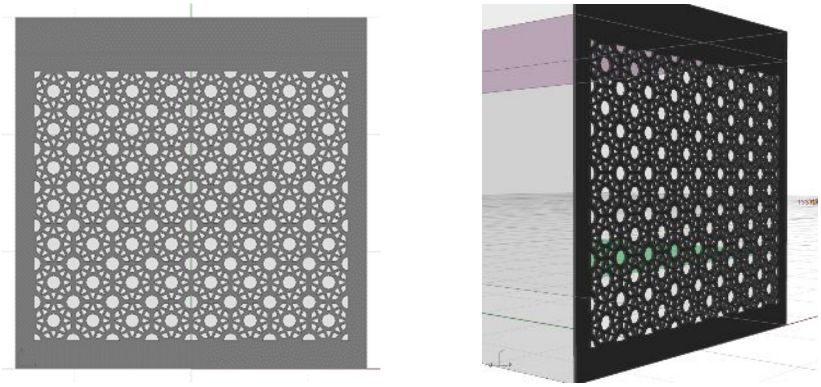
6.2. Perforated Solar Screen

The optimisation process began with the design of the perforated solar screen (PSS). The purpose of the PSS was to enhance the daylight uniformity at the workplane on the front half of the room. The performance of the PSS was assessed through raytracing to observe the behaviour of the sunrays. Later, the daylight performance was assessed through a PIT simulation for the selected hours and through an annual study for the whole year.

In order to investigate the effect of the design improvement, specific parameters have been tested. The significant parameters were selected based on the early investigation. The selected parameters were tested for both the perforated screen and the daylight-redirecting devices.

The PSS was proposed to achieve two objectives, to enhance the daylight performance at Z1 by reducing the direct illuminance to reduce the value of the ASE, and to reduce the total illuminance higher than 1000 lux to increase the value of the $UDI_{300\text{-}1000lx}$.

The proposed PSS was installed instead of the window. The first tested PSS has a perforation percentage equals to the WWR of the window, which is 25%. The WWR is determined based on the recommended window to floor ratio (WFR) found on the Saudi Building Codes-General document (SBC 201), 2018. The size of the screen is 2.7-meter width and 2.3-meter in height. The PSS was tested initially with a 25% perforation percentage, and then the perforation percentage was increased gradually by 2%. The PPS was test with six perforation percentages, namely, 25%, 27%, 29%, 31%, 33% and 35% perforation percentages. The perforation percentage was increased by 2% between each case. The impact of the perforation percentages on the annual daylight performance was investigated parametrically. The perforation percentages of the tested cases are shown in Table 6.1.



[A] [B]

Figure 6.1: Front and perspective views of case PSS5 (A) and (B), respectively

Table 6.1: Tested parameters of the Perforated Screens.

Case Name	Perforation Percentage (%)
PSS1	25
PSS2	27
PSS3	29
PSS4	31
PSS5	33
PSS6	35

The six PSS cases were tested through an annual daylight simulation, and the results were assessed for the whole year by dynamic daylight metrics that were utilised previously for the base case. Then the results were analysed and compared with the daylight performance of the base case.

Afterwards, the best PSS case was investigated through a seasonal daylight evaluation. Furthermore, a point-in-time daylight study from the annual simulation was conducted for the same case to investigate the daylight performance for specific hours. The optimum PSS was tested at 8 am, 10 am, 12 pm, 2 pm and 4 pm on 21st June (summer solstice), 21st September (equinox) and 21st December (winter solstice).

6.2.1. Overall evaluation by an annual daylight study

The daylight performance of the six PSS cases was assessed through an annual daylight study for the whole year. Then, the outputs of the annual simulation were analysed for each season individually.

6.2.1.1. Annual daylight evaluation

The effect of the perforation percentage on the daylight performance was assessed by the $ASE_{1000lux\ (250hr)}$, $UDI_{300\text{-}1000lux}$, $DA_{300lux\ (50\%)}$ and $UDI_{300\text{-}500lux}$. The results are presented in the charts from Figure 6.2 to Figure 6.9 below. The assessment starts with the annual evaluation

of direct illuminance at the work plane through the annual sunlight exposure metric. Then, the total illuminance at the work plane was assessed by the useful daylight illuminance metric.

It was found that the direct illuminance was recorded only at Z1 near the window. As shown in Figure 6.2, the ASE was increased gradually with the perforation percentage increasing. The average increase in the ASE between the cases was 29 hours. The lowest ASE was 74 hours for PSS1, whereas the highest ASE was 221 hours for PSS6.

However, the base case, which has a 25% WWR, was recorded higher ASE (381 hours), PSS1, which has a 25% perforation percentage, was recorded 74-hours ASE. Therefore, it can be demonstrated that the PSS, in general, reduces the ASE in the front area of the room, compared with the base case, even with a higher perforation percentage up to 35%.

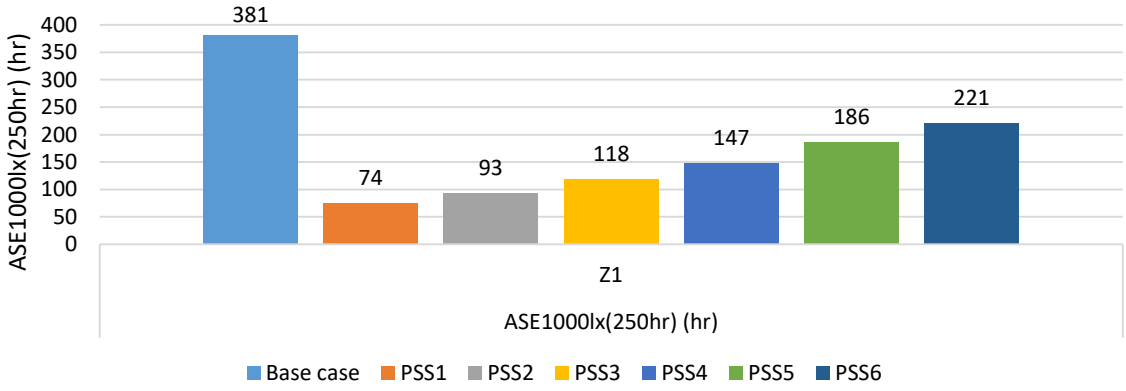


Figure 6.2: ASE at Z1 for Riyadh city

The second step was to assess the total illuminance at the work plane for each daylight zone separately. The $UDI_{300\text{-}1000\ lux}$ at the nearest zone to the window (Z1) is shown in Figure 6.3. The peak UDI among the PSS cases was 24% with PSS1, while the lowest was 2% with PSS6, which is higher than the UDI for the base case, which was 1%. The reduction in the UDI was 10%, 4%, 5%, 2% and 1% for PSS1 to PSS6, respectively.

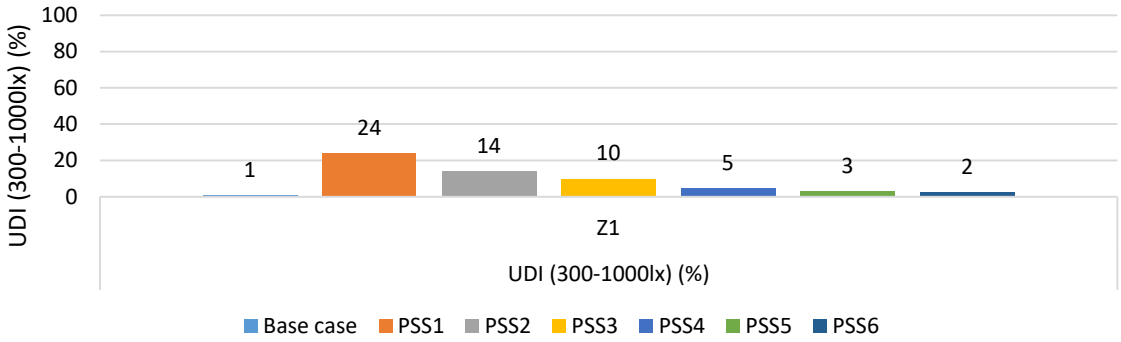


Figure 6.3: UDI at Z1 for Riyadh city

The $UDI_{300\text{-}1000\ lux}$ at Z2 was better compared to most PSS cases. The highest value was 86%, while the lowest was 46% for PSS1 and PSS6. The reduction in the UDI was 40% from PSS1 to PSS6. The reduction between the PSS cases was 4%, 3%, 17%, 5% and 11% from PSS1 to PSS6, respectively. The UDI for PSS5 was 57%, comparable to the UDI value for the base case, 58%, as shown in Figure 6.4.

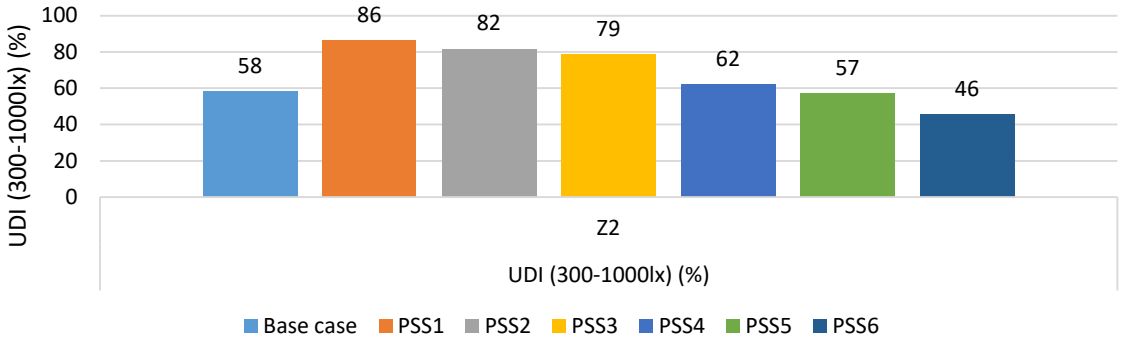


Figure 6.4: UDI at Z2 for Riyadh city

At daylight zone Z3, the UDI was better with the highest perforation percentage. The UDI was 79% for PSS6, whereas the worst case was PSS1 with a 13% UDI value. The increase in the UDI among the PSS cases was 16%, 10%, 21%, 2% and 5% from PSS1 to PSS6. The UDI at PSS5 was corresponded to the UDI for the base case, 72%, as illustrated in Figure 6.5.

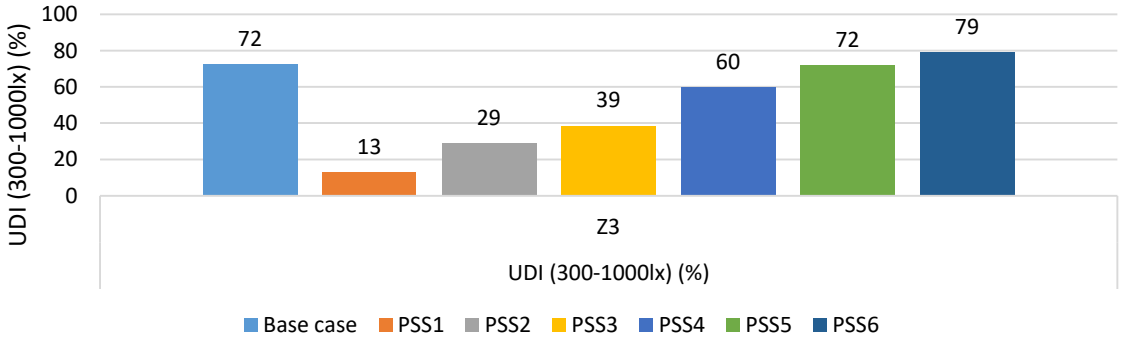


Figure 6.5: UDI at Z3 for Riyadh city

The UDI at Z4 was extremely low compared with the UDI at Z2 and Z3. It was found that the UDI for PSS1, PSS2 and PSS3 was 0%. Similarly, the UDI for the other cases was relatively low. It was 10%, 15% 19% for PSS4, PSS5 and PSS6, respectively. The increase in the UDI was 5% and 4% from PSS4 to PSS5 and from PSS5 to PSS6, sequentially. The UDI for these three cases, PSS4, PSS5 and PSS6, was higher than the UDI for the base case, which was 8%. The PSS enhanced the UDI performance by 2%, 7% and 11% with PSS4, PSS5 and PSS6, respectively, compared to the base case, as shown in Figure 6.6.

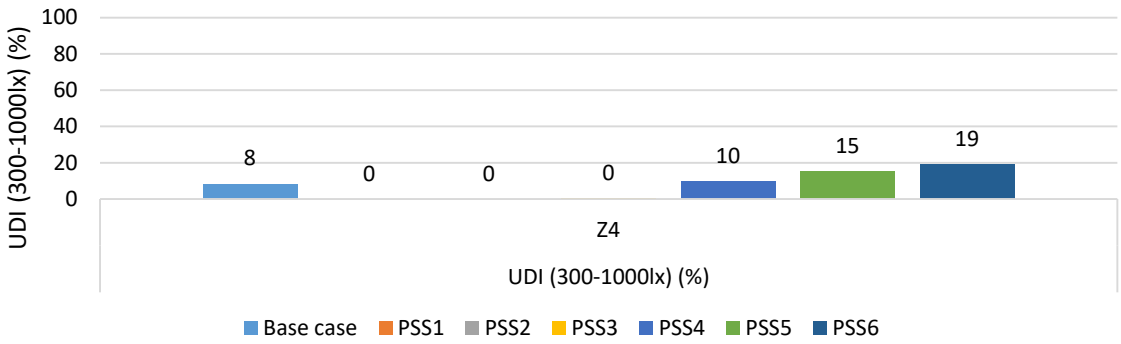


Figure 6.6: UDI at Z4 for Riyadh city

It was found that the DA was constant at Z1 and Z2; it was met for all the cases with 99 to 100 % at Z1 and with 88 to 98% at Z2. On the other hand, the DA value at Z3 was varied among the PSS cases; it was within the range from 13% to 79% from PSS1 to PSS6, respectively. The increase of the DA from PSS1 to PSS6 was 66%, and the increase between the PSS cases was 16%, 10%, 21%, 11% and 8%, from PSS1 to PSS6, respectively. Finally, at Z4, the DA was extremely low; the DA was 0% for PSS1, PSS2 and PSS3. The highest DA was 10%, 15% and 19% for PSS4, PSS5 and PSS6. However, the DA was low at Z4 for most of the PSS cases; it was higher with PSS4, PSS5 and PSS6 than the base case, which had an 8% DA value, as shown in Figure 6.7.

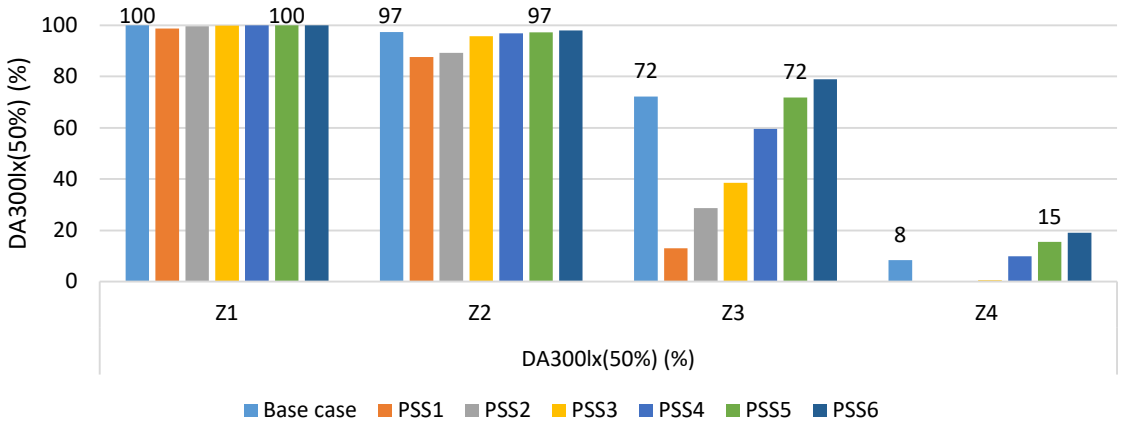


Figure 6.7: The DA for Riyadh city

The last annual daylight metric useful daylight illuminance was assessed with a lower threshold, 500 lux. The lowest values of the $UDI_{300\text{-}500\ lux}$ were at Z1 for all the cases. The highest $UDI_{300\text{-}500\ lux}$ at Z1 was 2% for PSS1 and PSS2, the lowest was 0% at PSS5 and PSS6, while it was 1% at PSS3 and PSS4. Similarly, at Z4, the $UDI_{300\text{-}500\ lux}$ was low, where the highest value was 19% for PSS6. The $UDI_{300\text{-}500\ lux}$ was 0% for PSS1, PSS2 and PSS3. The

$UDI_{300\text{-}500\ lux}$ was 10% for PSS4 and 15% for PSS5; however, the $UDI_{300\text{-}500lux}$ for these cases were higher than the UDI300-500 lux for the base case by 8%.

$UDI_{(300\text{-}500\ lux)}$ at Z2 was lower than the value of the $UDI_{(300\text{-}1000\ lux)}$ at the same zone. The highest $UDI_{(300\text{-}500\ lux)}$ was 45% for PSS1, and the lowest was 4% for PSS6. The reduction in the $UDI_{(300\text{-}500\ lux)}$ among the PSS cases was significant. It was decreased by 13%, 16%, 7%, 1%, 4% from PSS1 to PSS6, and the total reduction was 41%.

In contrast with Z1 and Z4, the difference between the $UDI_{300\text{-}500\ lux}$ and $UDI_{300\text{-}1000\ lux}$ was significant. It can be seen that the UDI values were dropped for all the cases. The value of the $UDI_{300\text{-}500\ lux}$ was lower than the $UDI_{300\text{-}1000\ lux}$ by 42%, 49%, 62%, 52%, 49% and 41% for the PSS cases from PSS1 to PSS6, respectively, and it was 49% for the base case.

The $UDI_{300\text{-}500\ lux}$ at Z3 for PSS1 and PSS2 was similar to the $UDI_{300\text{-}1000\ lux}$, 13% and 29%. On the other hand, it was different from PSS3 to PSS6 and for the base case as well. The $UDI_{300\text{-}500\ lux}$ was 33%, 45%, 51%, and 48%, respectively. It can be seen that the values were lower than the $UDI_{300\text{-}1000\ lux}$ values for all the cases; however, it was found that the value of the $UDI_{300\text{-}500\ lux}$ for PSS6 was lower than the value for PSS5, as shown in Figure 6.8 and Figure 6.9.

Form the analysis above, it was found that PSS5 can provide a desirable indirect daylight that is comparable to the base case, at the same time, it reduced the undesirable diret sunlgith that is allowed by the base case. Therefore, the PSS5 was chosen as the optimum solution and its seasonal and hourly perfroamnce were analysed.

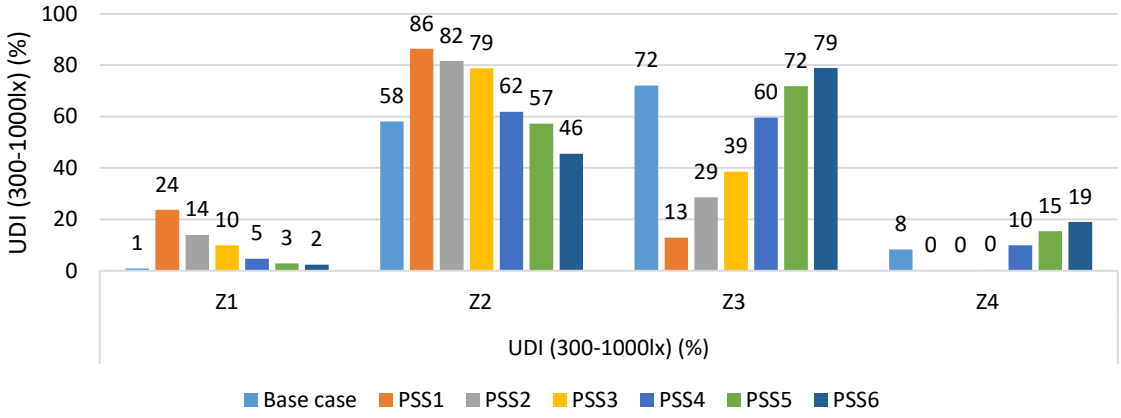


Figure 6.8: The ($UDI_{(300\text{-}1000\ lux)}$) for Riyadh city

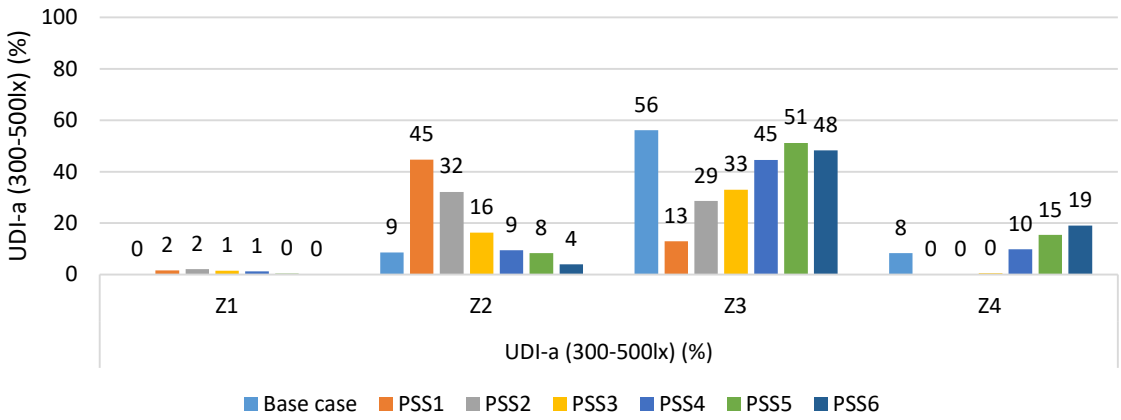


Figure 6.9: The ($UDI_{(300\text{-}500\ lux)}$) for Riyadh city

6.2.1.2. Seasonal daylight evaluation

The daylight performance of the optimum PSS case was analysed for the whole year and each season separately. From the analysis comparison of the hourly data, it was found that PSS5, which has a 33% perforation percentage, was the optimum case. Therefore, PSS5 was analysed in deep to be compared later with the base case.

As shown in Figure 6.10, the daylight autonomy was met at Z1 by high values for all seasons. It was 96%, 100%, 94%, and 90% in spring, summer, autumn, and winter. Similarly, at Z2, the DA was high for all seasons. The lowest DA was 82% in winter, whereas the highest was 90% in spring and summer, and the DA was 88% in autumn. In contrast, at Z3 and Z4, the variation between the DA values between the months was high, particularly at Z4. The difference between the peak and the lowest DA at Z3 was 21%, where the highest DA was 73% in winter while the lowest was 52% in summer. The DA at Z3 in spring and autumn was 65% and 64%, respectively. Finally, the DA at Z4 was extremely low for all the seasons with higher DA, which was 38%, in winter compared with other seasons. The DA in summer at Z4 was the worst with 0%, while in autumn and spring, it was 8% and 11%, which is still extremely low.

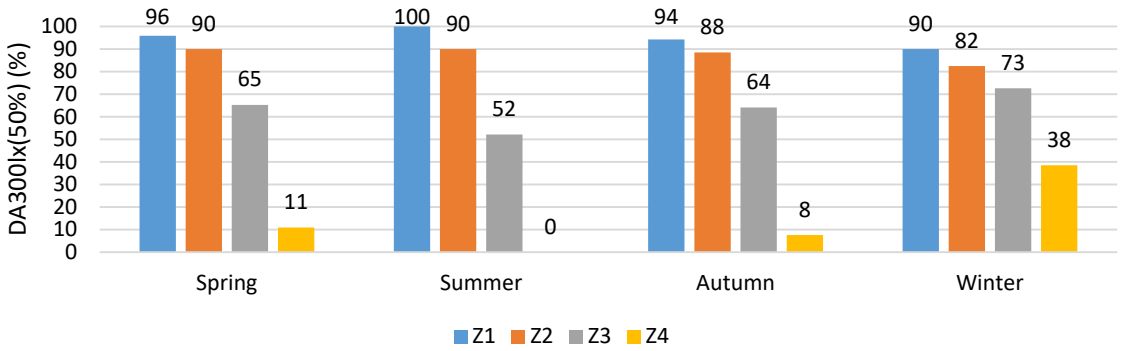


Figure 6.10: The DA during each season for case PSS5, in Riyadh

The results of the ASE after the installation of the PSS5 are shown in Figure 6.11. The ASE occurred in spring, autumn, and winter for 27 hours, 16 hours, and 129 hours, respectively. The best scenario was in summer where the ASE was not exceeding the threshold. Similarly, the ASE did occur at the rest of the daylight zones, namely, Z2, Z3 and Z4. The utilisation of PSS5 reduced the ASE at Z1 by 209 hours in winter compared with the base case, whilst it was slightly raised in spring and autumn by 7 hours 13 hours, respectively.

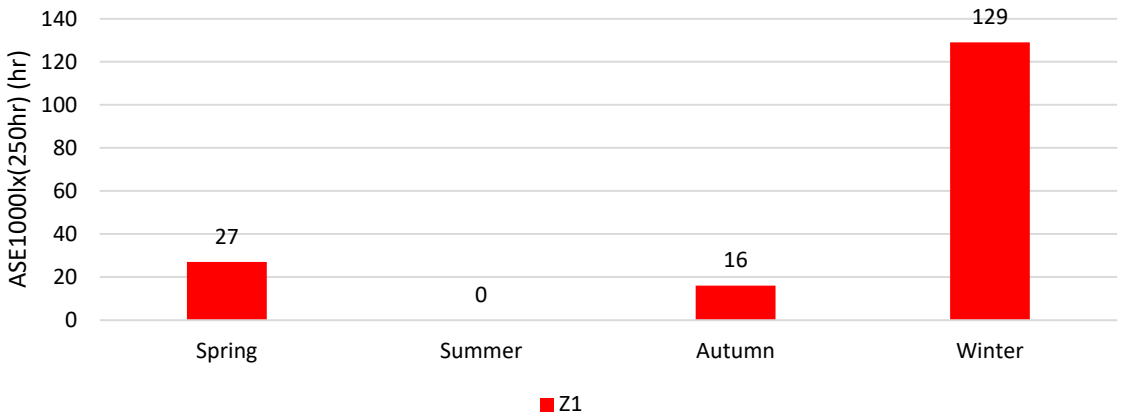


Figure 6.11: The ASE for case PSS5 in Riyadh

Like the scenario of the base case, the PSS5 has recorded a high variance of UDI values among the seasons and the daylight zones. As illustrated in Figure 6.12, it can be seen that the UDI is low at Z1 during all the season. The highest UDI was 10% in summer, and the lowest was 6% in spring. The UDI at Z2 has recorded the highest UDI in summer at 89%; however, it was low at the same zone in winter, which was 18%.

The variation among the UDI values at Z2 was 71%. On the other hand, the PSS5 performed better at Z3. It was found that the lowest variation among the seasons was 21%; however, the UDI values were between 52% and 73% in summer and winter, respectively.

In contrast, the variation between the UDI values at Z1 was extremely low, which was 4%, and similarly, the UDI values were exceptionally low during all the seasons. The highest UDI was 10 % in summer, and the lowest was 6% in spring. Finally, the rear daylight zone, which Z4, was recorded the best UDI in winter at 38%, while the worst was in summer at 0%. In spring and autumn, the UDI was 11% and 8% for the same daylight zone, respectively.

It can be seen that the PSS5 has enhanced the UDI at the nearest and furthest daylight zones, namely, Z1 and Z4. The UDI was increased by 10%, 4% and 5% at Z1 in summer, autumn and winter, respectively, compared to the base case, but it was decreased by 1.5% in spring. Similarly, the UDI at Z4 was increased; it has been raised by 11%, 8% and 20% in spring,

autumn and winter, respectively. On the other hand, at Z2 and Z3, the UDI was similar to the base case with a slight reduction.

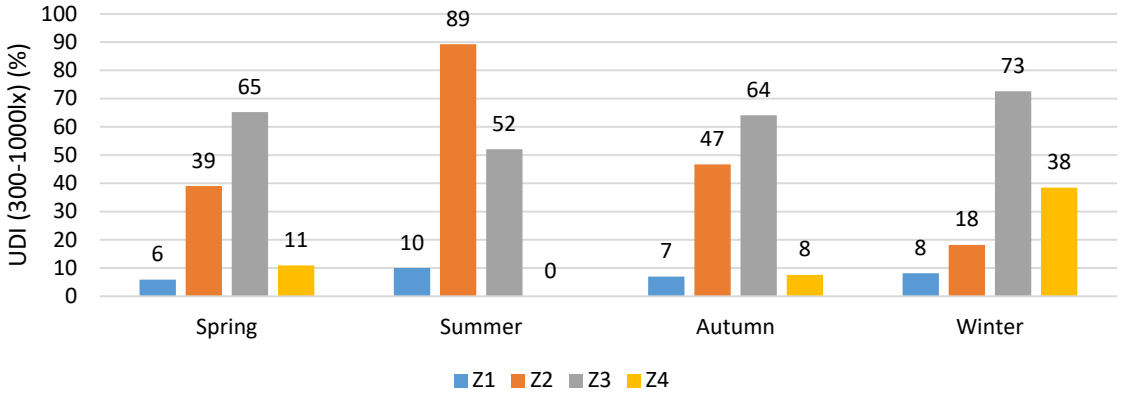


Figure 6.12: The UDI for case PSS5 in Riyadh

6.2.2. Hourly evaluation through a point-in-time daylight study

After the annual daylight analysis, the performance of the PSS5 was assessed through a point-in-time study, which extracted the data from the annual daylight simulation. The purpose was to investigate the daylight performance during the day to observe the strength and weakness of the daylight system as a function of the solar altitude and the sun azimuth.

6.2.2.1. Daylight performance during morning hours

The total illuminance values were assessed at the work plane in the morning hours, namely, at 8 am and 10 am on 21 June, 21 September and 21 December. It was recorded its peak value at Z1 on 21 December at 8 am, which was 16,061 lux. The total illuminance values at Z1 on 21 June and on 21 September was much lower; they were 1,581 lux and 2,361 lux, respectively.

The difference among the total illuminance values at Z2 was lower than Z1. The peak value was 984 lux on 21 December, while the lowest was 616 lux on 21 June, and on 21 September, it was 791 lux. The reduction in the total illuminance between the three months was 193 lux from 21 December to 21 September, and it was 175 lux from 21 September to 21 June, as shown in the charts in Figure 6.13.

Z3 and Z4 were recorded low values of total illuminance; however, the illuminance level was constant among the months. For instance, at Z3, the illuminance was decreased slightly by 58 lux and 55 lux from 21 December to 21 September and 21 September to 21 June. Similarly, at Z4, the peak value was 204 lux, 172 lux and 143 lux on 21 December, 21 September and 21 June.

In general, it can be concluded that the total illuminance value at the work plane was recorded higher values on 21 December for all the daylight zones. On the other hand, it was observed that at 8 am on 21 December, the total illuminance value was reached an excessive light intensity level.

The chart in Figure 6.14 shows the total and the direct illuminance values at 8m on 21 December. It can be seen that the total illuminance value has a 12,923-lux direct illuminance value. Therefore, the diffuse illuminance value was only 3,138 lux. The percentage of the direct illuminance value is 80% of the total illuminance at this point. From the analysis above, it can be understood that the excessive total illuminance value at 8 am on 21 December at Z1 was the direct exposure to the direct solar radiation during this hour of the year.

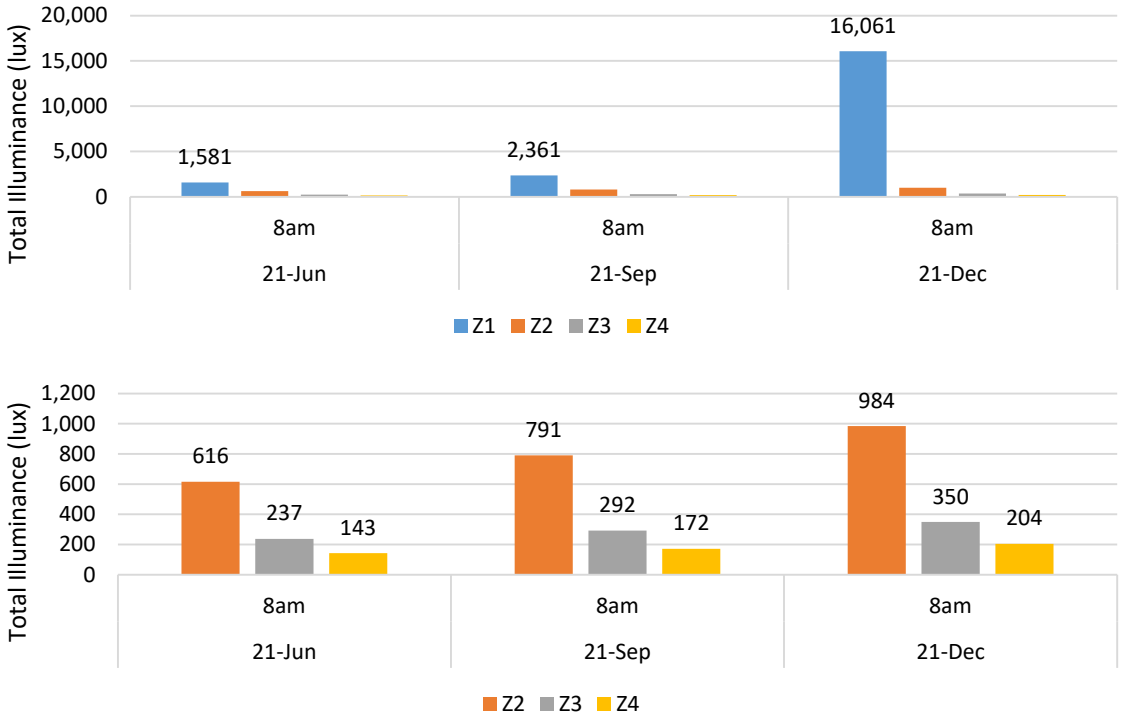


Figure 6.13: Total illuminance. Case PSS5 in Riyadh

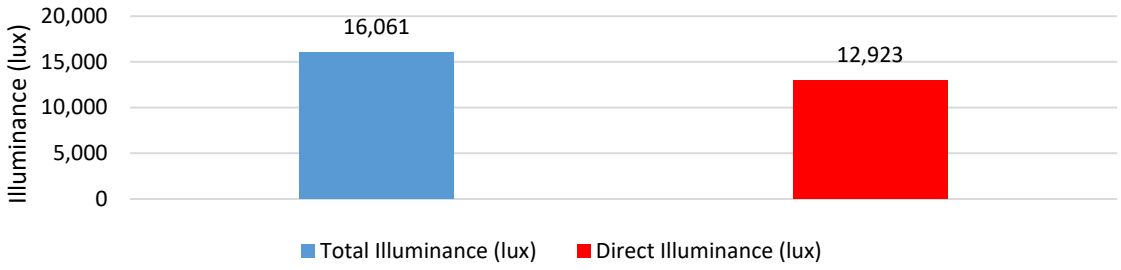


Figure 6.14: Total and direct illuminance at Z1 on 21 December at 8 am. Case PSS5, in Riyadh

Like the scenario at Z1 at 8 am on 21 December, the total illuminance value at 10 am was recorded at an exceedingly high value that reached 40,011. On 21 September and 21 June, the

total illuminance at Z1 at 10 am was 3,412 lux and 1,700 lux, as shown in Figure 6.15. At Z2, the total illuminance has a similar pattern at 8 am; the values were 1,670 lux, 1,237 lux and 723 lux on 21 December, 21 September, and 21 June, respectively.

At Z3, the total illuminance was higher than the minimum threshold (300 lux) for the three tested days. On the other hand, the values of the total illuminance were lower than the minimum threshold at Z4 on 21 September and 21 June. The total illuminance at Z4 was 366 lux, 269 lux and 219 lux on 21 December, September and 21 June.

The direct illuminance occurred at Z1 at 10 am on 21 December, as shown in Figure 6.16. The direct illuminance reached 35,405 lux, which equals 88% of the total illuminance at this point. Therefore, the diffuse illuminance was 4,606 lux. It can be concluded that the high total illuminance at this point is due to the excessive direct illuminance incidence

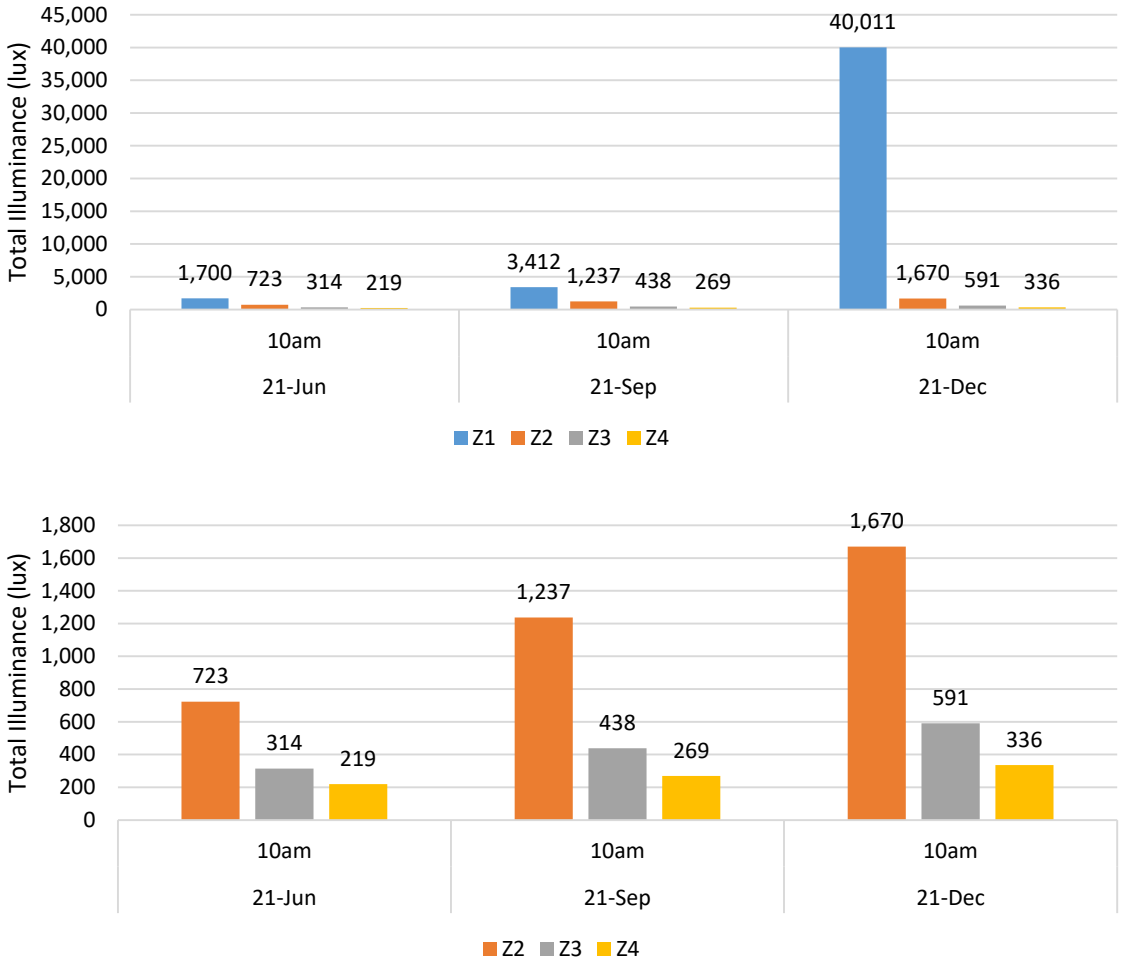


Figure 6.15: Total illuminance Case PSS5 in Riyadh

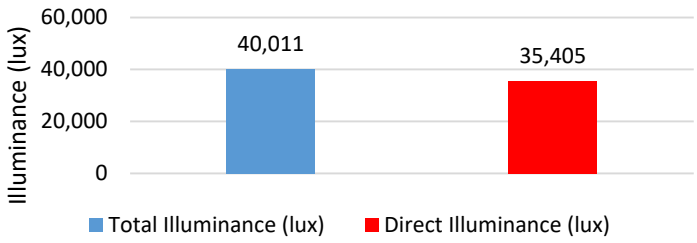


Figure 6.16: Total and direct illuminance at Z1 on 21 December at 10 am. Case PSS5, in Riyadh

6.2.2.2. Daylight performance at solar noon

The total illuminance was assessed at the solar noontime when the sun azimuth is 180 degrees and the solar altitude reaches its peak height during the day. The total illuminance at the work plane as a function of solar altitude at daylight zones Z1, Z2, Z3 and Z4 is shown in Figure 6.17.

It can be seen that the total illuminance was reduced at Z1 compared with the base case. Moreover, the total illuminance was increased relatively at Z4 for the three months. It was found that the PSS5 solved the issue of the direct illuminance at this time on 21 December compared with the base case.

Generally, the total illuminance at the work plane at the noontime comes from diffuse luminance alone, enhancing the daylight performance. The increasing pattern in the illuminance is similar to the previous scenarios at 8 am and 10 am, except at Z1 on 21 December because of the absence of the direct illuminance at noon, as was mentioned above.

The total illuminance values were higher on 21 December for the four daylight zones. It was 5,297 lux, 1,743 lux, 689 lux and 381 lux at Z1, Z2, Z3 and Z4, respectively. On 21 September, it was 3,739 lux 1,257 lux, 417lux and 241lux, and on 21 June, it was 1,874 lux, 788 lux, 291 lux and 200 lux, at Z1, Z2, Z3 and Z4, respectively.

The decrease curve of the illuminance values from 21 December to 21 June and from Z1 to Z4 was linear for all the scenarios. For example, it was decreased at Z1 by 1,558 lux and 1,865 lux, and at Z2, it was decreased by 486 lux 469 from 21 December to 21 September and from 21 September to 21 June, respectively.

The illuminance values were within the useful illuminance range (300-1000 lux) at Z2 and Z3 for all the tested dates; however, At Z3 on 21 June, the illuminance was lower than the threshold by only 9 lux. The illuminance at Z4 met the required value on 21 December but was lower than the threshold by 59 lux and 100 lux on 21 September and 21 June, respectively. On the

other hand, the illuminance at Z1 exceeded the threshold for the three dates, particularly on 21 December and 21 December.

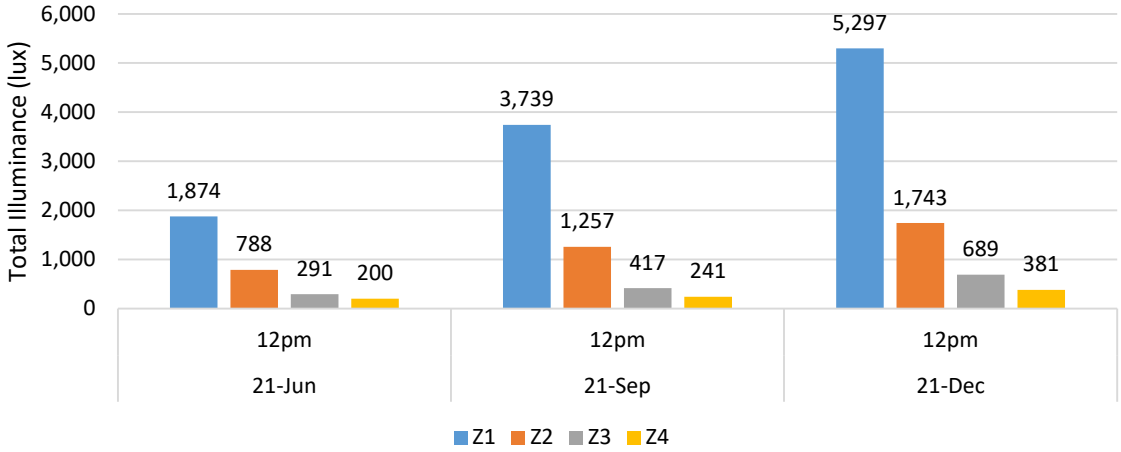


Figure 6.17: Total illuminance for case PSS5 in Riyadh City

6.2.2.3. Daylight performance during evening hours

The illuminance at 2 pm, which comes from a solar altitude lower than the noontime, has been improved after utilising the PSS5. The direct illuminance at Z1 at 2 pm on 21 December was reduced to zero compared with the base case that recorded 39,258 lux direct illuminance. The total illuminance for all the scenarios comes from diffuse daylight only.

The useful illuminance range (300-1000 lux) was met by utilising the PSS5 at Z3 for all the scenarios and Z2 except on 21 December, which exceeded the threshold by 442 lux. On the other hand, at Z4, the total illuminance was lower than the threshold for all the tested dates. In contrast, the total illuminance was higher than the threshold at Z1 for the three dates. For example, the peak value at Z1 was 3,911 lux on 21 December, while the lowest was 1,717 lux on 21 June, as shown in Figure 6.18.

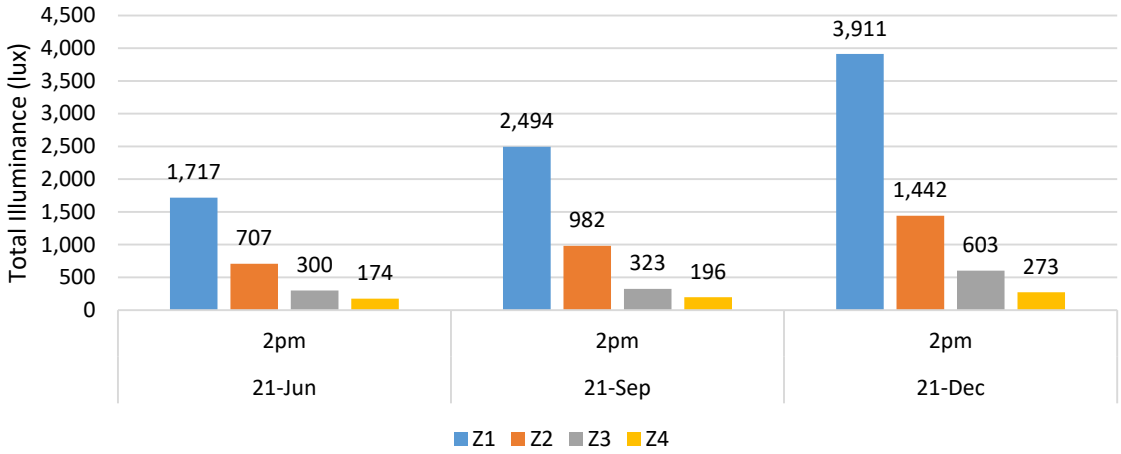


Figure 6.18: Total illuminance on 21 June, 21 September and 21 December at 2 pm. Case PSS5 in Riyadh

The total illuminance values at 4 pm on 21 June, 21 September and 21 December are shown in Figure 6.19. The increase in the total illuminance values among the three days is the opposite of the other tested hours. The highest illuminance values were recorded on 21 June, while the lowest was on 21 December. That is opposed to the other tested scenarios due to the early sunset time during winter.

The useful illuminance was met at Z2 except on 21 December, lower than the threshold, by 35 lux. At Z1, it was met only on 21 December. The total illuminance was higher than the maximum threshold at Z1 on 21 June and 21 September. On the other hand, it was lower than the 300 lux at Z3 and Z4 for all the tested scenarios.

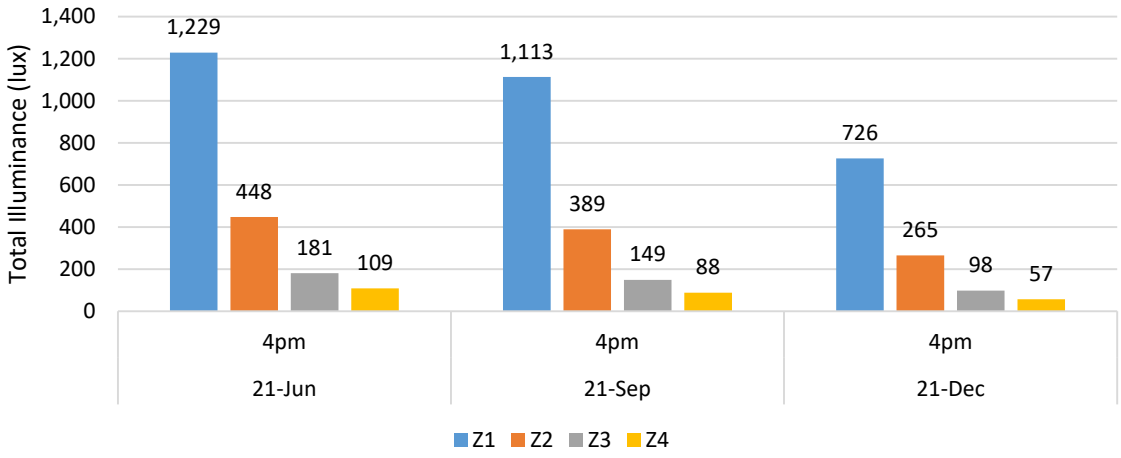


Figure 6.19: Total illuminance. Case PSS5 in Riyadh

6.2.2.4. Daylight uniformity

The analysis of the DUWP values for the optimum PSS showed that on 21 December at 8 am and 10 am, the DUWP is extremely low, which was 5% and 3%, respectively, as shown in Figure 6.20. It was found that the main reason for the low DUWP at these times was the high ASE, which is caused by the high direct illuminance. Therefore, a proposed solution was developed to minimise the ASE at these times of the year. A daylight-redirecting device (DRD) was optimised and tested for that purpose. The DRD is a compound parabolic concentrator (CPC), it is widely applied for solar energy concentration, and it was applied in some studies as a daylight-redirecting device.

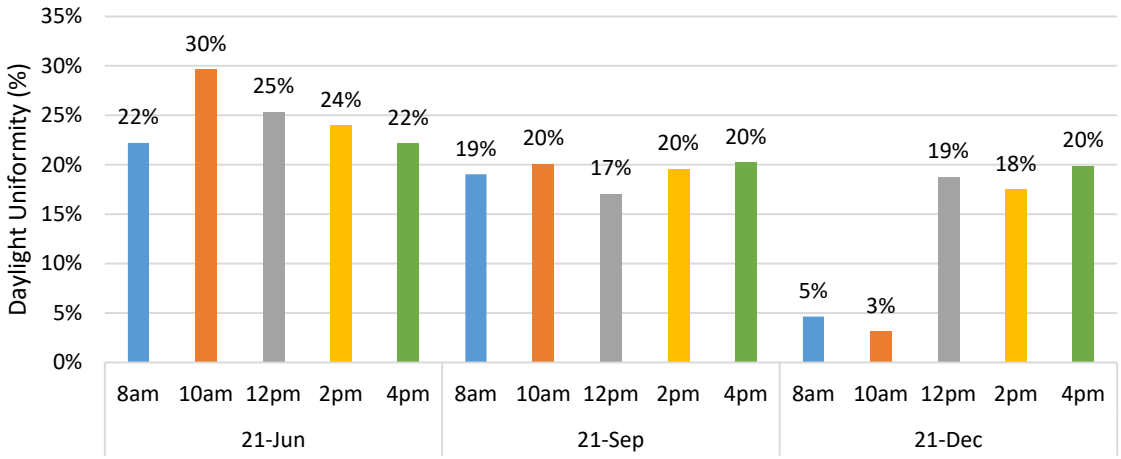


Figure 6.20: DUWP for the optimum PSS (PSS5), for Riyadh

Although the PSS5 was enhanced the daylight performance compared with the base case, the DUWP was found exceptionally low on 21 December at 8 am, and 10 am. The performance of the base case on 21 December at 8 am was 12%, which is better than the PSS5, as shown in Figure 6.21. It was found that the low DUWP is due to the high direct illuminance at the work plane during these hours. The direct illuminance at the work plane was occurred on 21 December at 8 am and 10 am with PSS5 and at 10 am, 12 pm and 2 pm for the base case.

The results of DUWP at 8 am and 10 am for PSS5 were not similar to the DUWP at 4 pm and 2 pm, respectively, because of the azimuth angle that is due to the early sunset time during this period of the year. The reason is that the direct illuminance at 8 am and 10 am was high. On the other hand, the direct illuminance does not occur at 2 pm and 4 pm on 21 December.

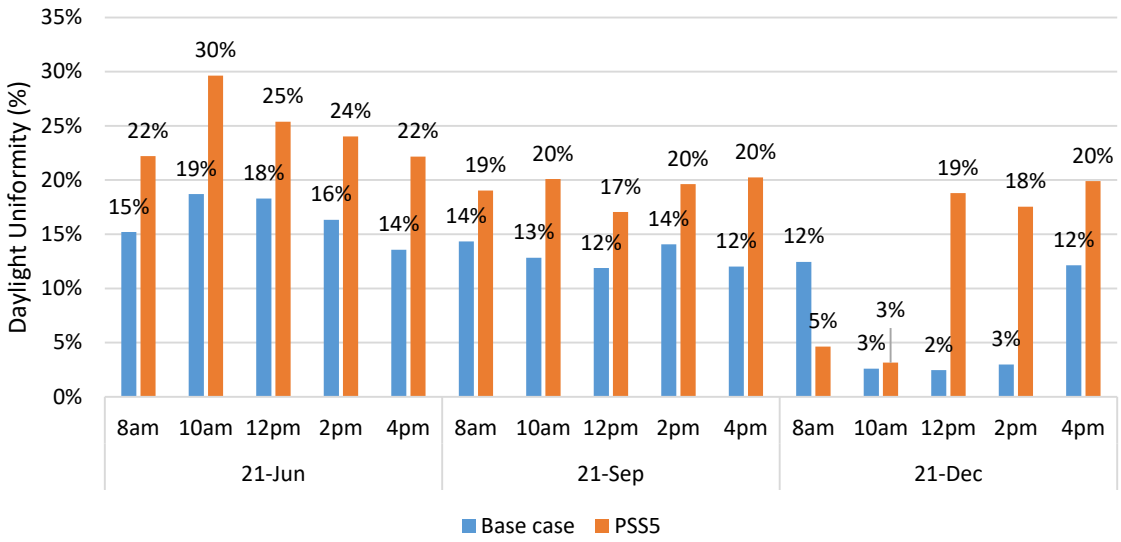


Figure 6.21: Comparison of DUWP between BCWRR25 and PSS5, for Riyadh

6.2.3. Analysis of daylight glare probability

The daylight glare probability was assessed at the worst day based on the illuminance analyses discussed previously. It was found that the 21st of December is still the worst day among the three tested days by the PIT study.

The glare comfort range, as shown in Table 6.2, was imperceptible at 8 am, intolerable at 10 am, 12 pm and 2 pm, and finally, it was perceptible at 4 pm. the DGP values were 0.34, 0.64, 0.72, 1.00 and 0.38 at 8 am, 10 am, 12 pm, 2 pm and 4 pm respectively.

It can be seen that the glare comfort range was enhanced at 8 am and at 4 pm compared with the base case. Furthermore, the DGP was reduced for all the tested hours except at 2 pm where it was increased by 0.17. The reduction on the DGP was reduced by 0.08, 0.18, 0.22 and 0.09 at 8am, 10am, 12pm, 2pm and 4pm respectively.

The luminance values for the interior of the tested room from the viewing point of the occupant for the daylight zone Z1 are shown in Figure 6.22 to Figure 6.26. The viewing point is located 1.5 meters from the façade, 1.5 height from the floor level, and the direction of the view is 180 degrees from the north

Table 6.2: Glare study results of daylight-redirecting solar screen case PSS5

Date	Time	DGP	Glare Comfort Range
21 December	8 am	0.34	Imperceptible Glare
	10 am	0.64	Intolerable Glare
	12 pm	0.72	Intolerable Glare
	2 pm	1.00	Intolerable Glare

4 pm	0.38	Perceptible Glare

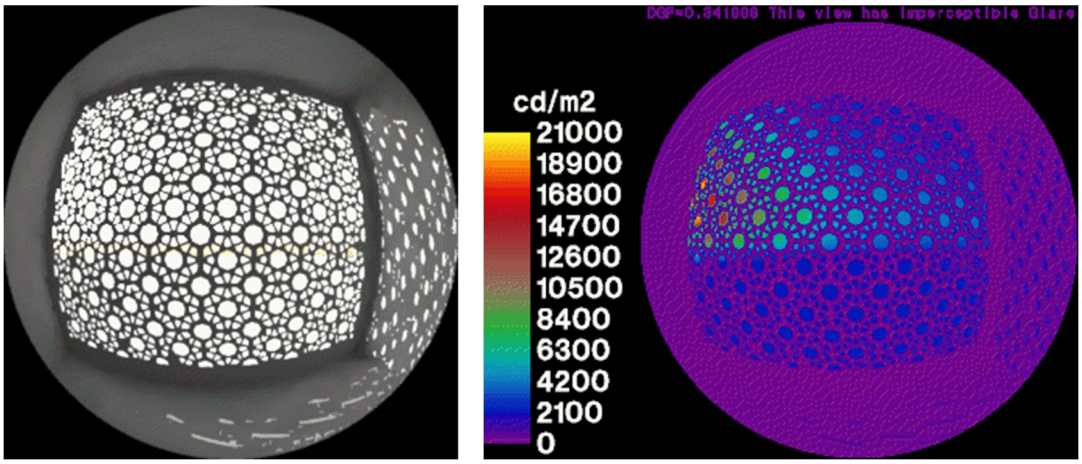


Figure 6.22: The luminance, on 21 December at 8 am, Case PSS5, Riyadh

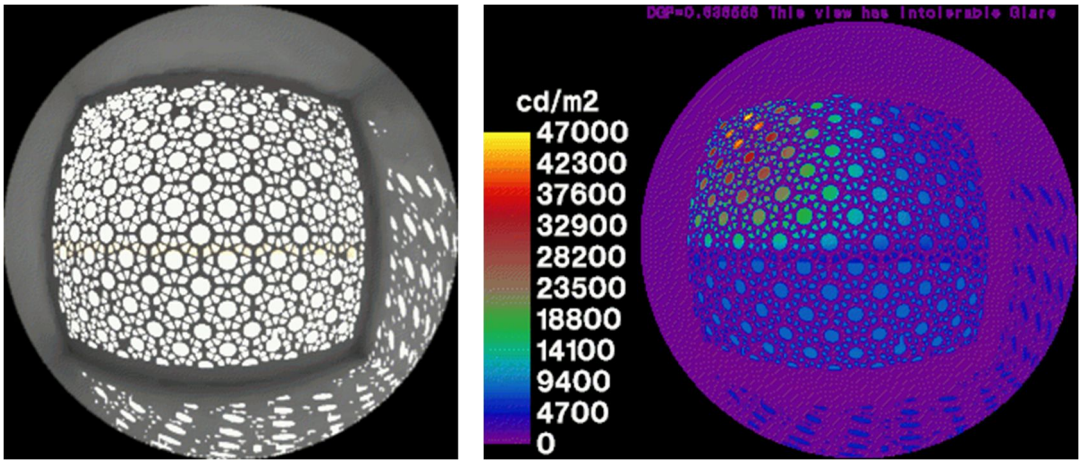


Figure 6.23: The luminance, on 21 December at 10 am, Case PSS5, Riyadh

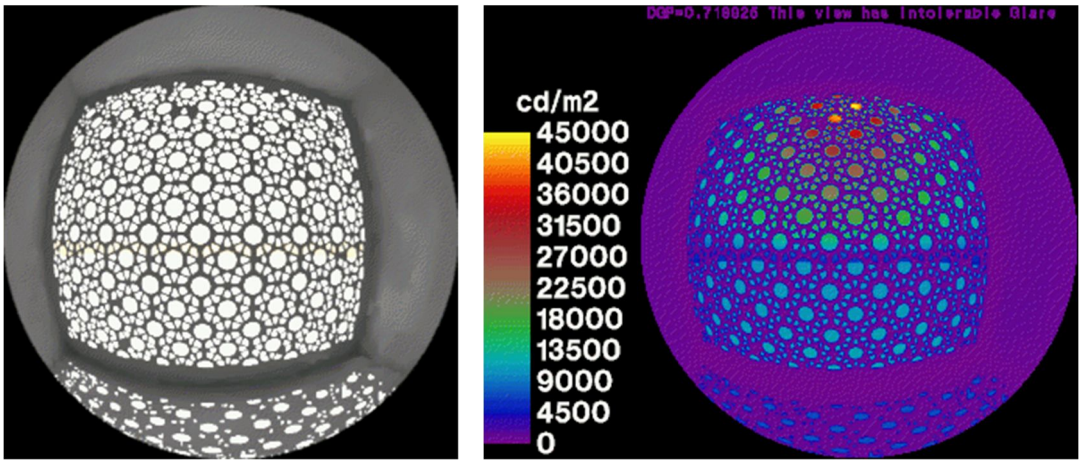


Figure 6.24: The luminance, on 21 December at 12 pm, Case PSS5, Riyadh

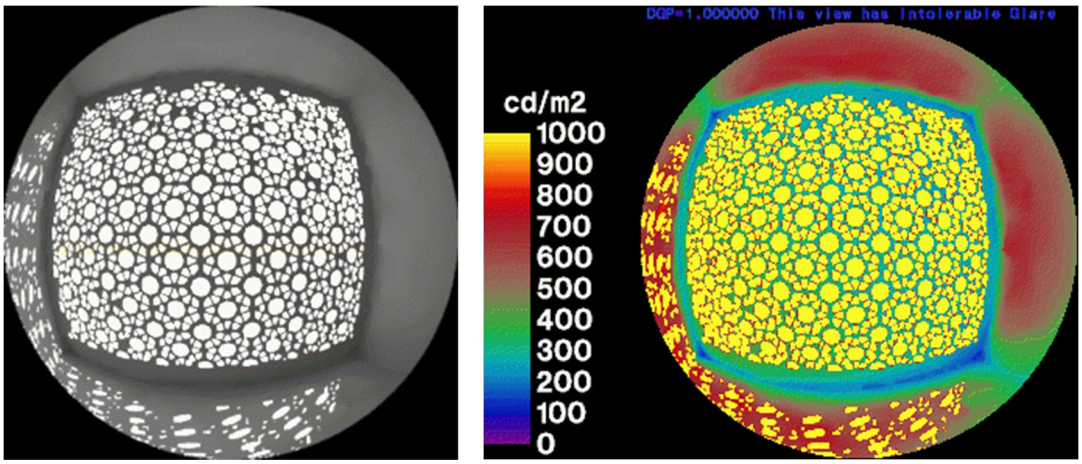


Figure 6.25: The luminance, on 21 December at 2 pm, Case PSS5, Riyadh

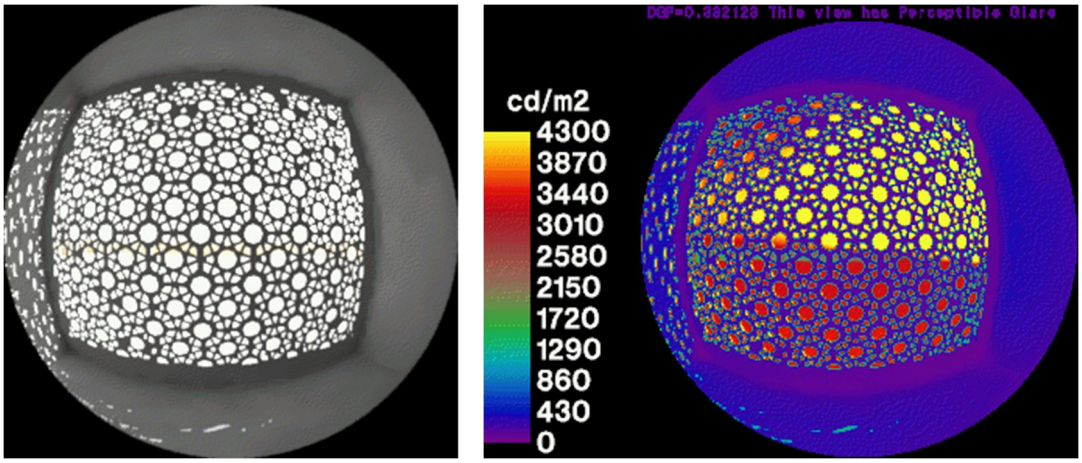
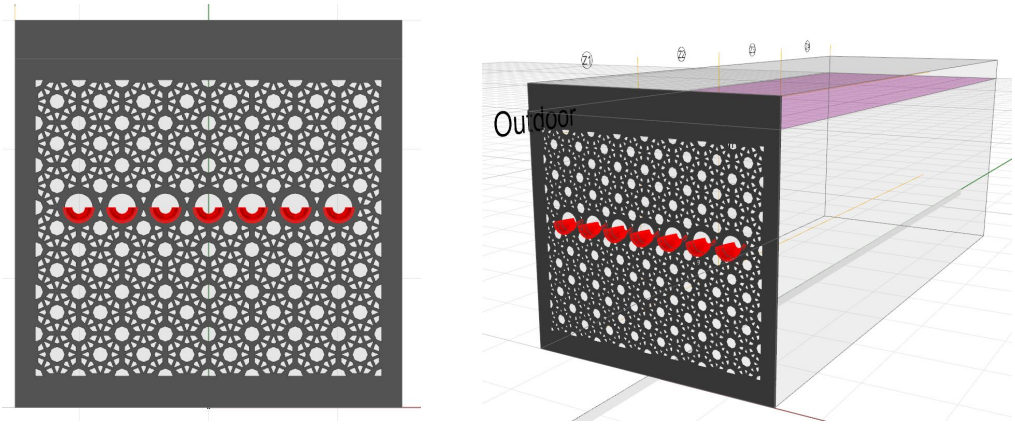


Figure 6.26: The luminance, on 21 December at 4 pm, Case PSS5, Riyadh

6.3. Daylight-redirecting device

The proposed daylight-redirecting device (DRD) (Figure 6.27) was optimised to enhance the daylight performance in the front half of the room. Then, the design of the DRD was optimised to enhance the daylight performance in the rear half of the room. The first objective of utilising the DRD was to enhance the daylight performance at Z1 by reducing the direct illuminance to reduce the ASE and increase the DUWP. The second objective was to enhance the daylight performance at Z3 and Z4 by increase the total illuminance that is lower than 300 lux at Z3 and Z4, which will increase the useful daylight illuminance value ($UDI_{300\text{-}1000lx}$).



[A] [B]

Figure 6.27: Front (A) and perspective (B) views of case PSS5

The process of the design and the optimisation of the daylight-redirecting proposed system was conducted as follows:

1. Design and model CPC in normal mode (CPC_{NM})
2. Optimisation by raytracing:
    a. Upper part
    b. Vertical position (Z-axis)
    c. Horizontal position (Y-axis)
3. Evaluation by climate-based daylight modelling (CBDM):
    a. Analyse daylight performance at 8 am, 10 am, 12 pm, 2 pm and 4 pm on 21 June, 21 September and 21 December.
    b. Analyse daylight performance during the four seasons.
    c. Analyse the overall daylight performance for the whole year.
    d. Analyse the daylight glare probability (DGP) based on the results of the ASE and UDI.

6.3.1. Design of the proposed daylight-redirecting device

The proposed DRD is a developed compound parabolic concentrator (CPC) that works in normal mode. The design based on a CPC was developed by (Vázquez-Moliní et al., 2012). The CPC was utlised as a daylight-redirecting device to enhance the performance of a horizontal daylight transporting system, as mentioned previously in Chapter 2.

The important factor in the selection of the DRD is the relation between the height of the aperture and the depth of the device. The DRD should allow most of the coming sunlight to be redirected from the interior of the DRD towards the ceiling of the room. Also, it prevents the

received sunrays from accessing the room directly towards neither the eye's level of occupant nor the work plane. The DRDs were installed above the eye level of occupant to prevent galre occurring.

The depth of the DRD is 25 centimetres, the radiation of the DRD curvature is 65 degrees, the diameter of the inlet and the outlet is 20 and 10 centimetres, respectively, as illustrated in Figure 6.28.

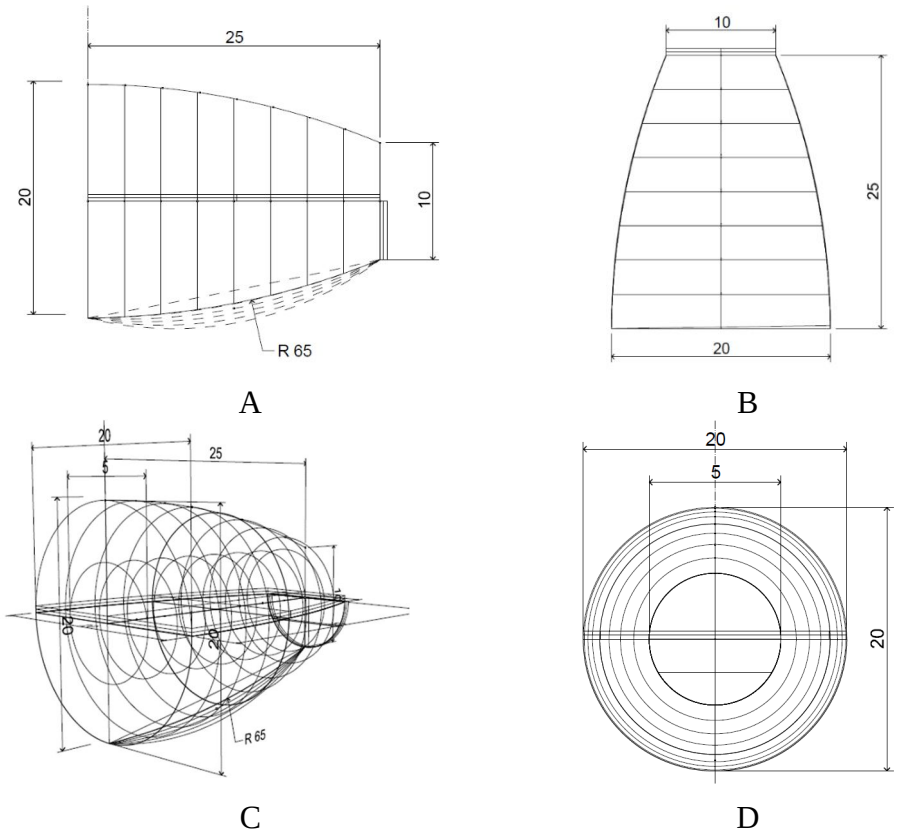


Figure 6.28: DRD views, side view (A), top view (B), 3D view (left C) and front view (D), dimensions in centimetres.

- **The integration of the DRD within the PSS**

The DRD was integrated within the proposed PSS; this integration created the novel daylight-redirecting perforated solar screen (DRSS). The DRDs were embedded into the PSS5 that has a 33% perforation percentage. The screen consists of seven DRD units aligned in one row. The vertical distance from the DRD centre point to the floor level is 1.50 meters, and from the ceiling level is 1.20 meters. The horizontal distance on X-axis between every two DRDs is 0.10 m.

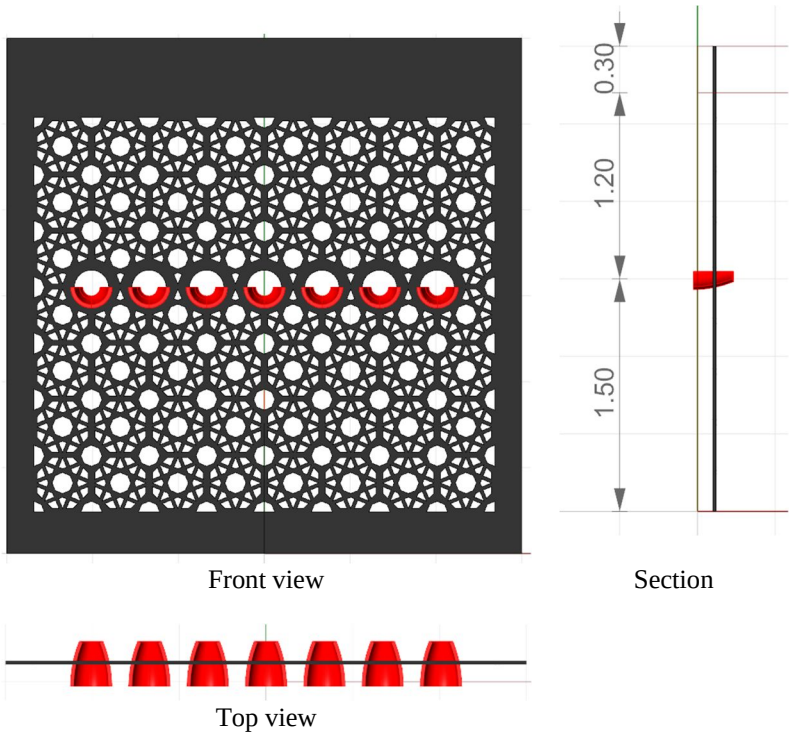


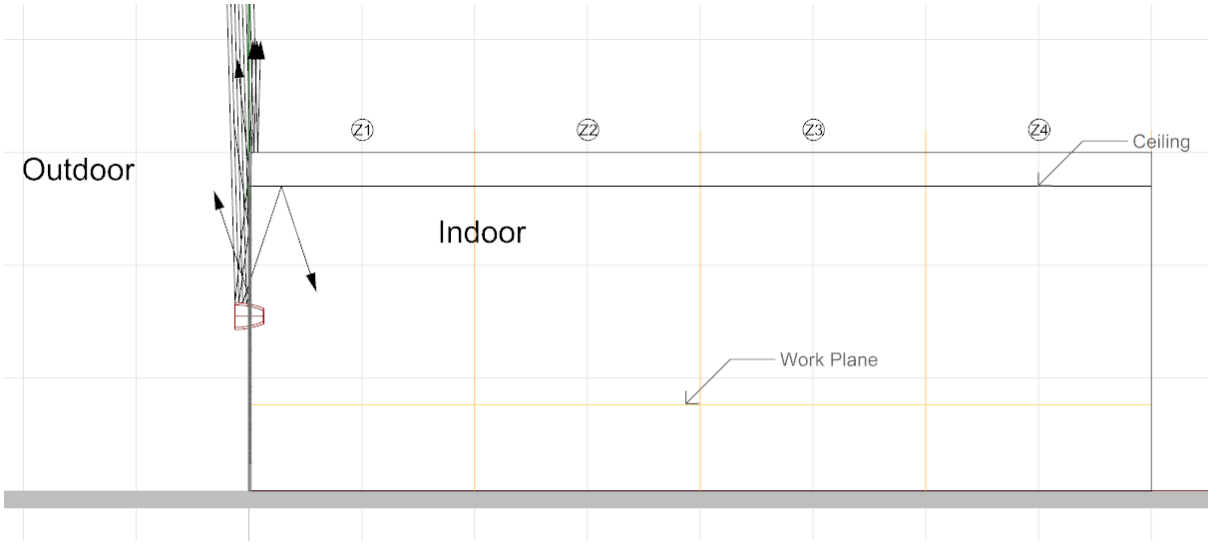
Figure 6.29: Cases DRSS. The dimensions are in meters

6.3.2. Optimisation by raytracing

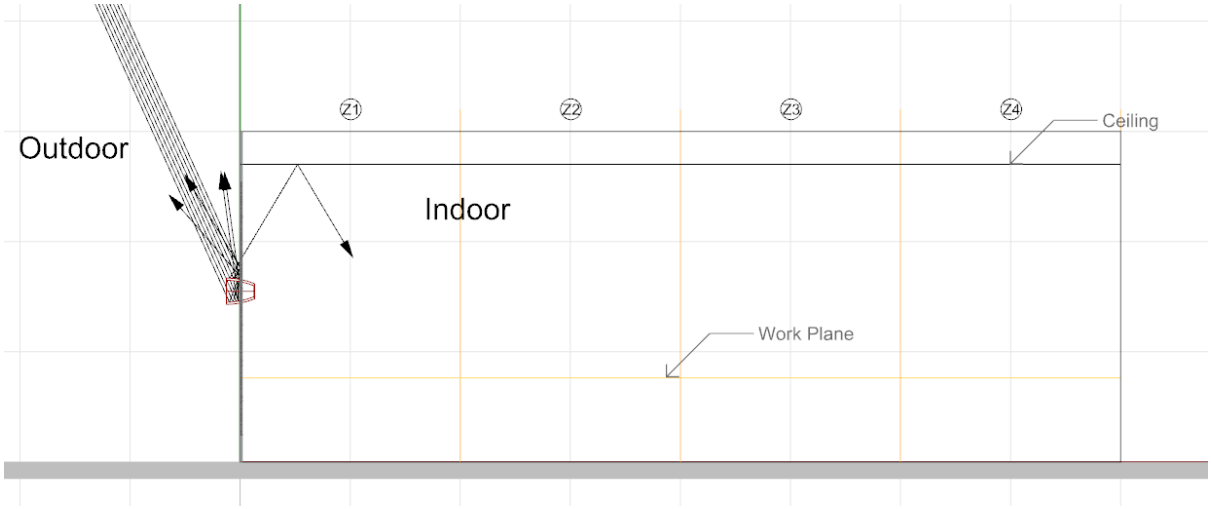
The daylight redirection performance of the DRD was investigated through a ray-tracing simulation by RADIANCE. The CPC in normal mode was tested for the worst day in terms of the visual discomfort based on the illuminance analysis at the work plane and the daylight glare probability that was conducted previously. The Worst day was 21 December where the sun altitude reached its lowest angle.

The raytracing modelling was conducted on 21 December from 8 am to 4 pm with a 2-hour interval. Next, the impact of three parameters on the performance of the DRD was investigated. The investigated parameters were the upper part of the DRD and its vertical and horizontal positions.

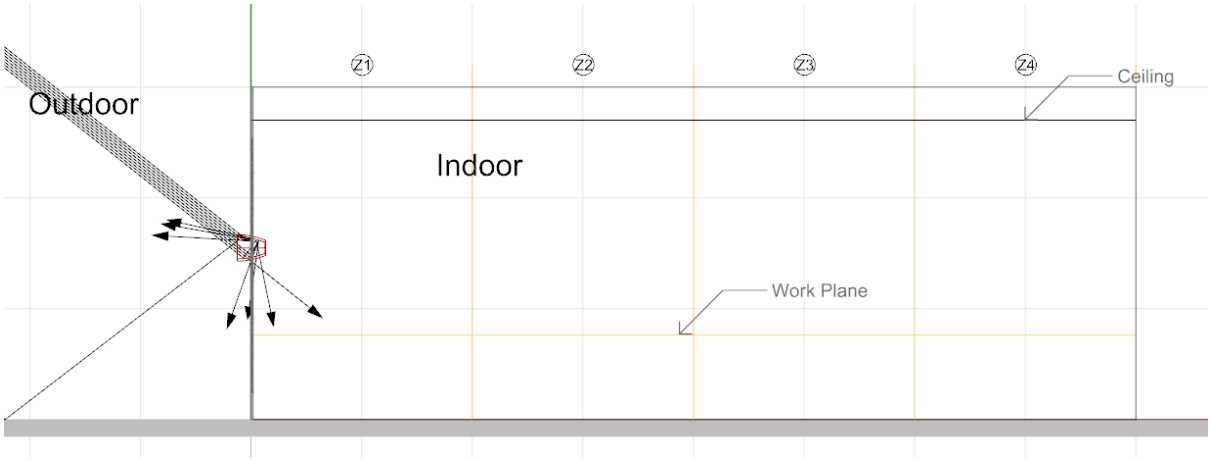
First, the impact of the DRD's upper part elimination on the redirection of the daylight was investigated. Then, the DRD was tested with three vertical positions, namely, 2.21-meter, 1.88-meter, and 1.55-meter height, from the floor level. Finally, the impact of the DRD horizontal position on the Y-axis was investigated. Three horizontal positions were tested, - 0.125 m from the façade (inward mode), 0.0 (inward and outward mode), and 0.125 (outward mode).



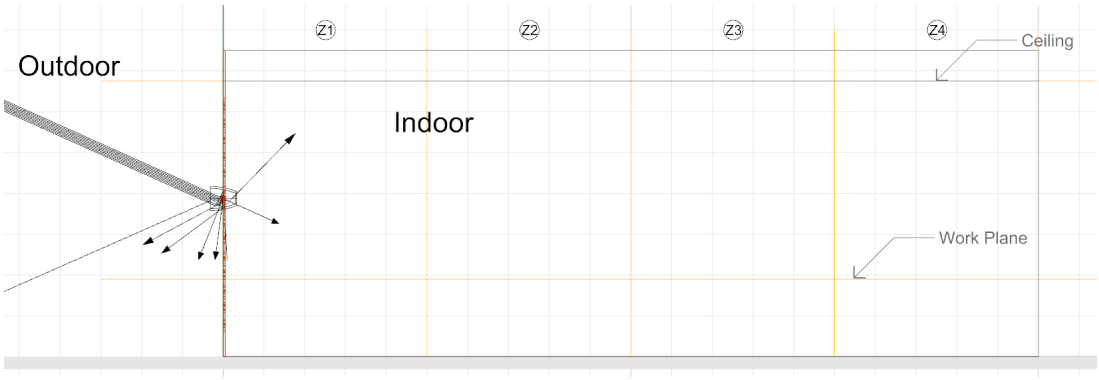
21 June at solar noon



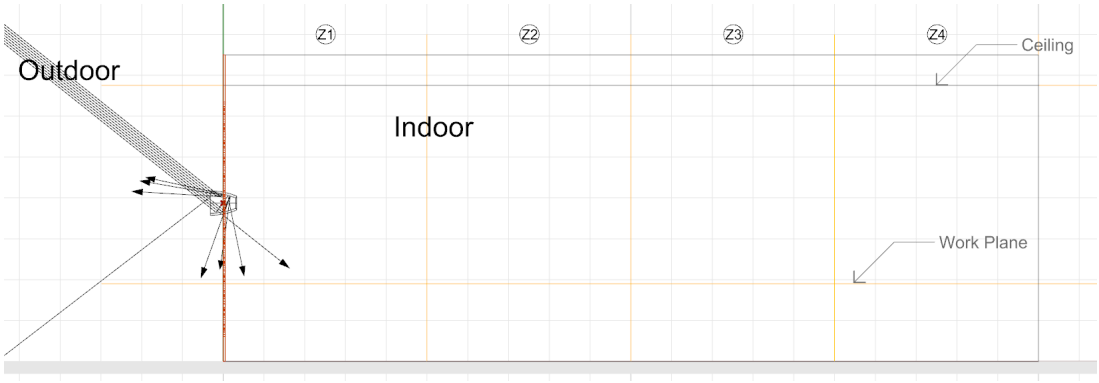
21 September at solar noon



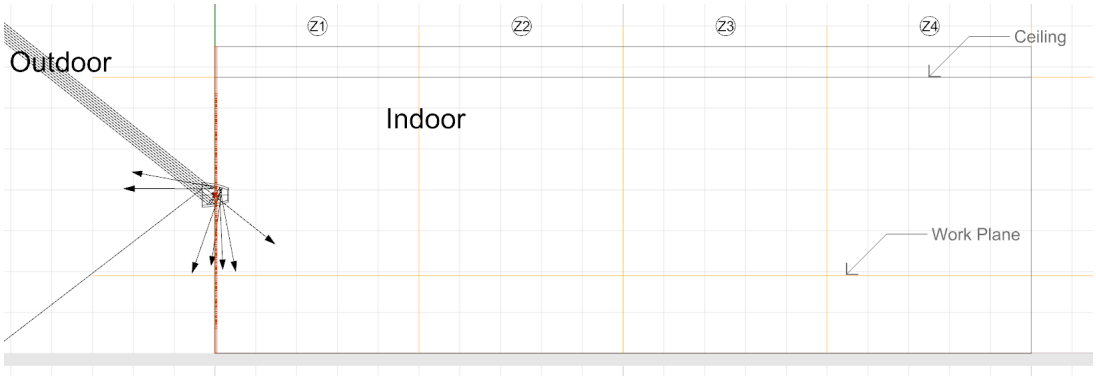
21 December at solar noon



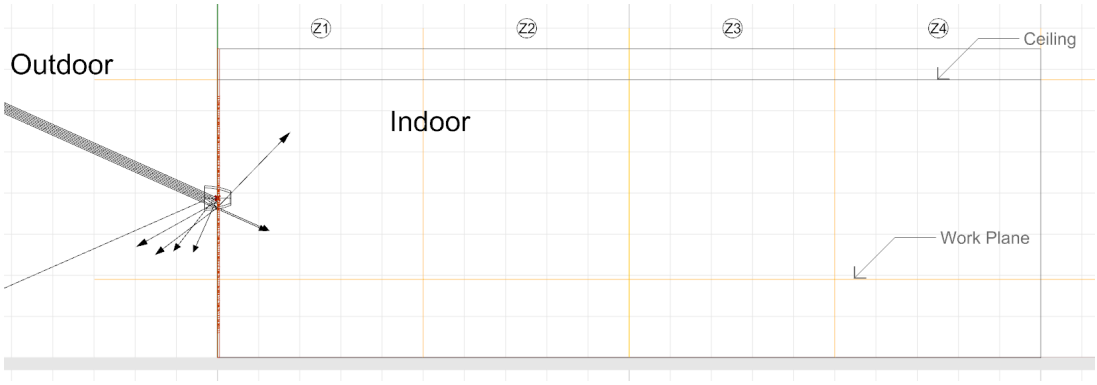
21 December at 8 am



21 December at 10 am



21 December at 2 pm



21 December at 4 pm

Figure 6.30: 21 of June, September and December at solar noon and 21 December at 8am, 10am, 2pm and 4pm [from above to below], CPC in normal mode

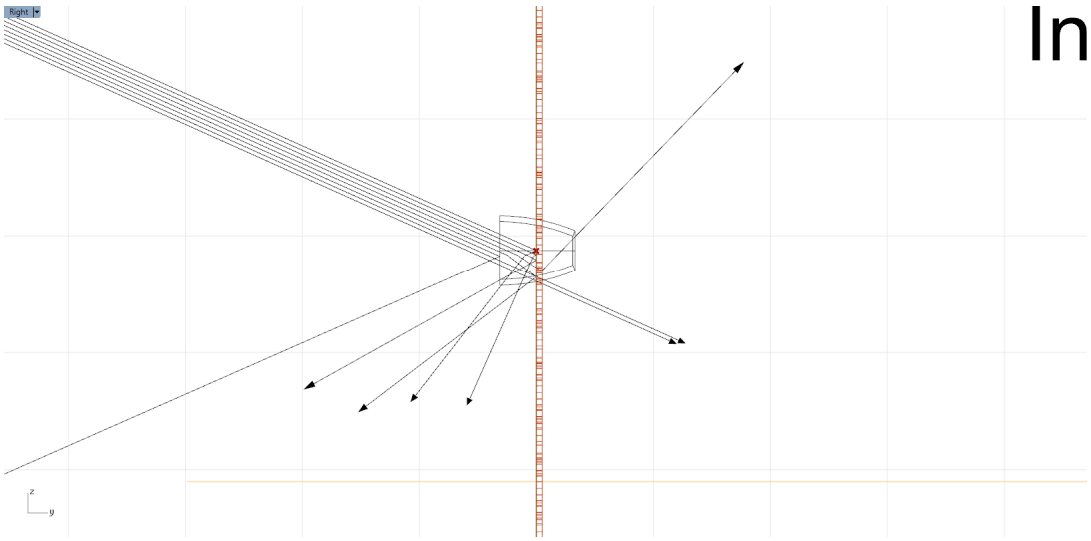


Figure 6.31: 21 December at 4 pm, CPC in normal mode

6.3.2.1. Effect of DRD upper part eliminating

In order to enhance the performance of the daylight redirection function of the DRD, the upper part of the geometry was reduced by trimming the upper half of the DRD, as illustrated in Figure 6.32. The raytracing results on 21 December at 8 am, 10 am, 12 pm, 2 pm and 4 pm are illustrated in Figure 6.36. It can be seen that the adjusted DRD has enhanced the daylight redirecting function of the device. The DRD redirects the direct-sunlight rays towards the ceiling.

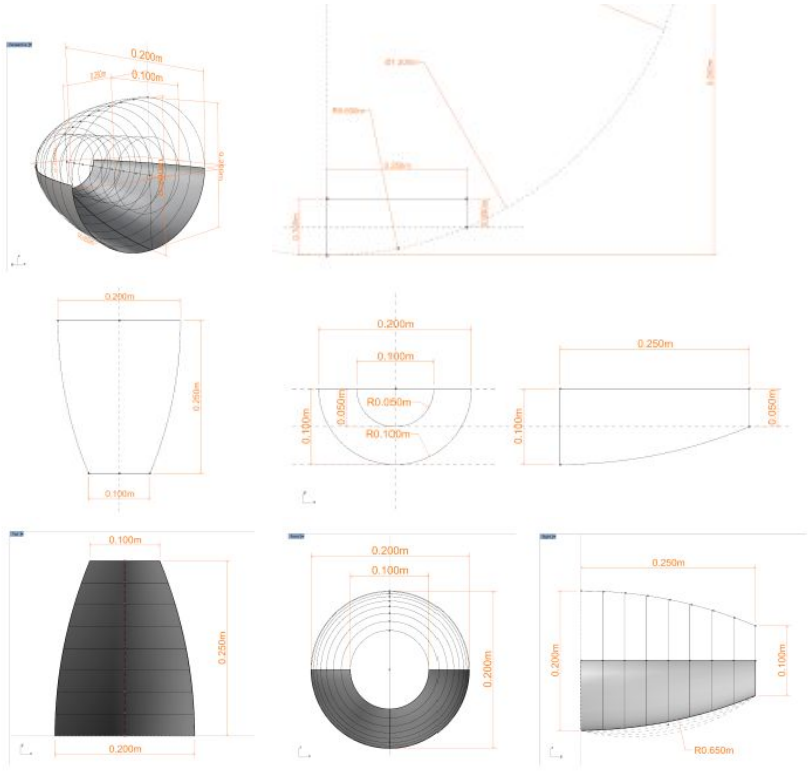
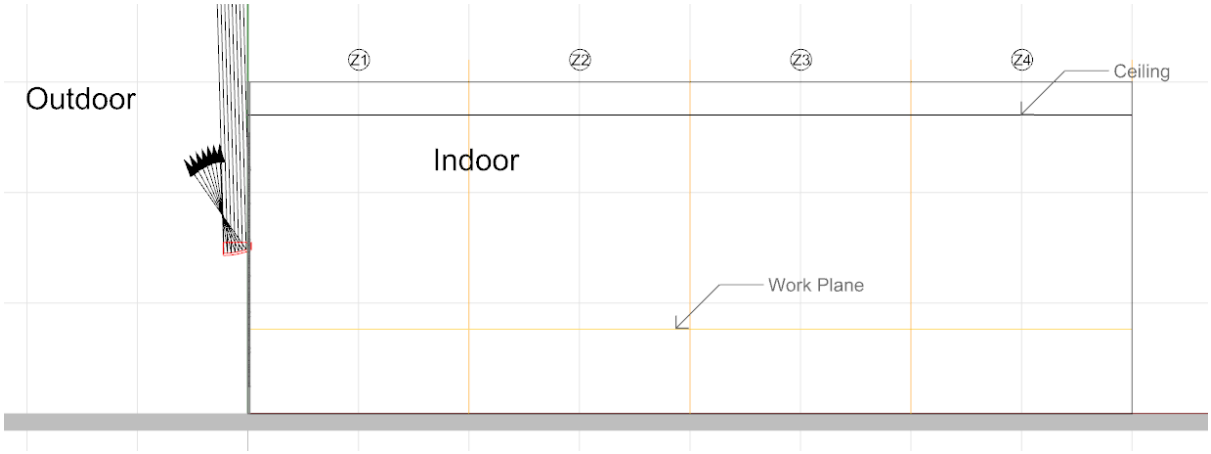


Figure 6.32: The drawings of the DRD after the elimination of the upper part

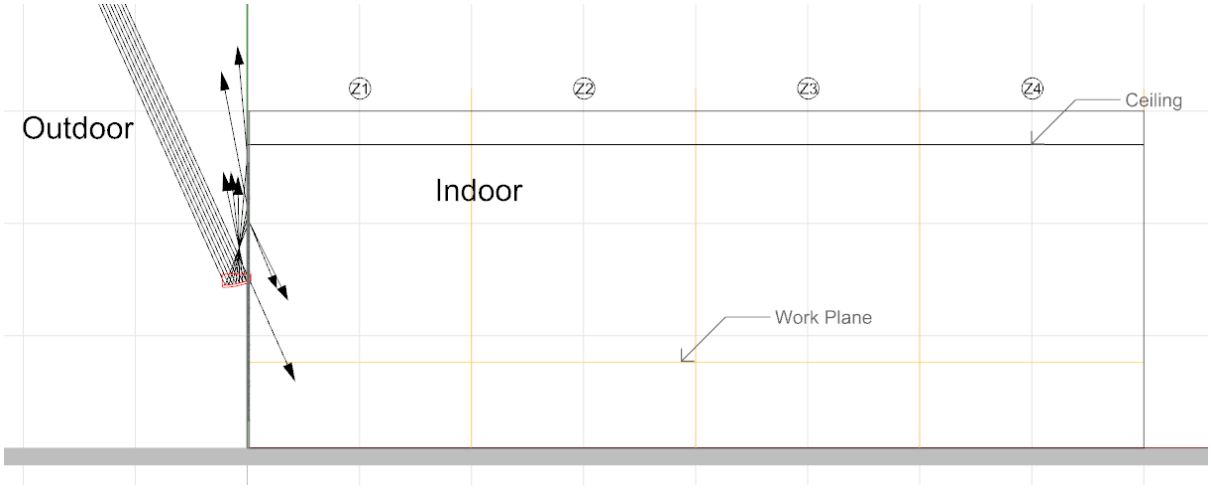
The results of the raytracing of the DRSS are shown in Figure 6.36. The results for 21 December from 8 am to 4 pm with 2-hour intervals from above to below. It was found that the elimination of the DRD upper part enhanced the daylight redirection towards the ceiling. The best performance was at 10 am, 12 pm and 2 pm, where the sun rays were reflected towards the ceiling. On the other hand, at 8 am, and 4 pm, most sunrays were obstructed by the DRD.

Half-DRD out, in and in the middle at 12 pm

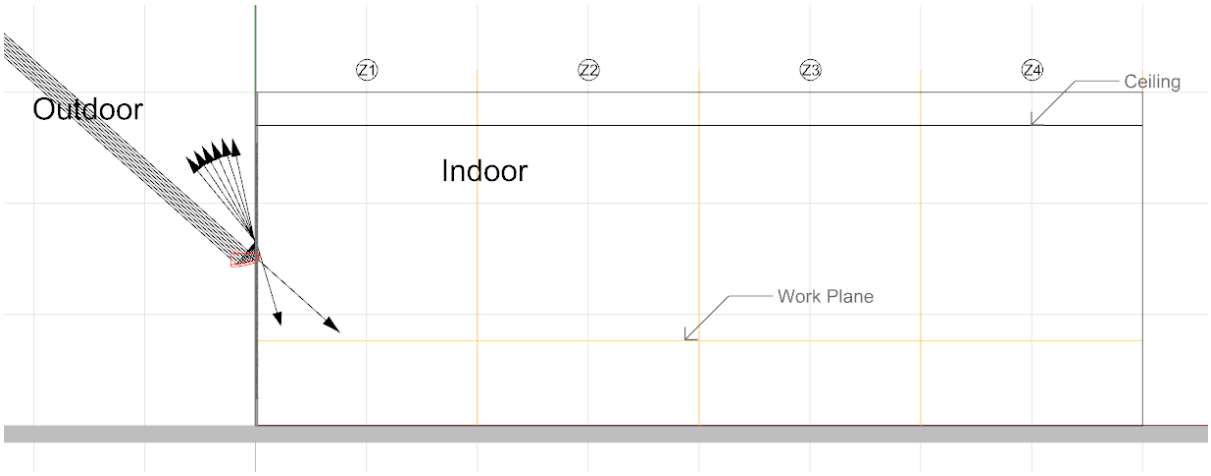
The figures below show the behavoiur of the direct sunrays when they received by the DRD. The raytracing was conducted st 12 pm on the 21st of June, September and December. Three positions of the DRD were tested, namely, inside, middle and outside.



21 June at solar noon (outside position)

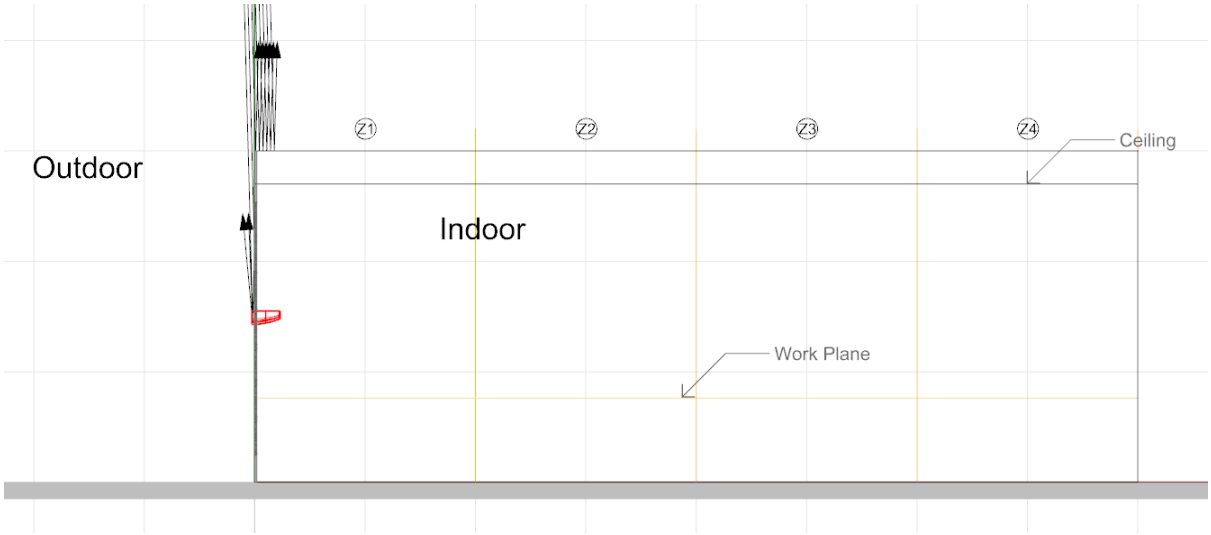


21 September at solar noon (outside position)

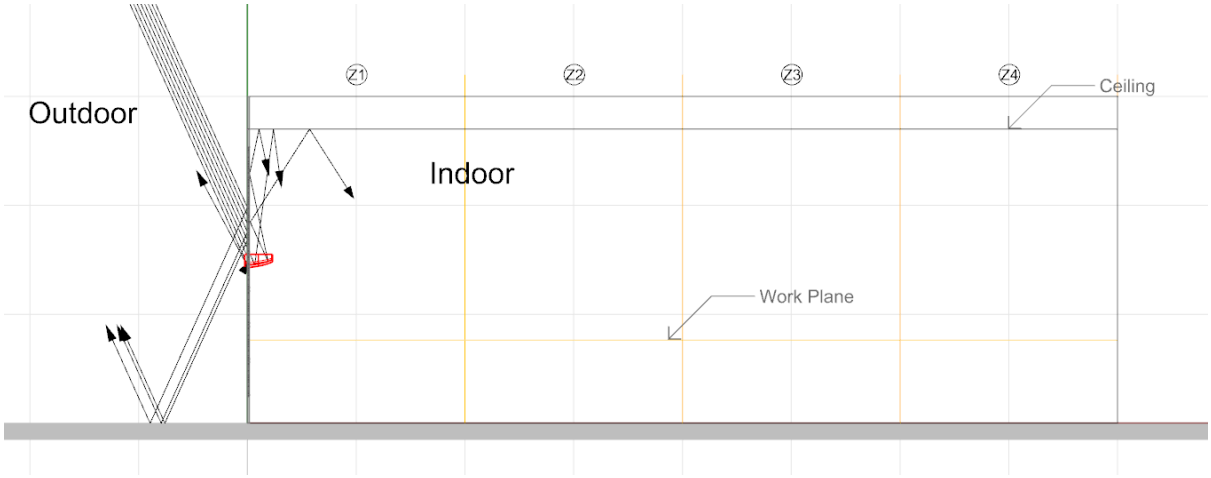


21 December at solar noon (outside position)

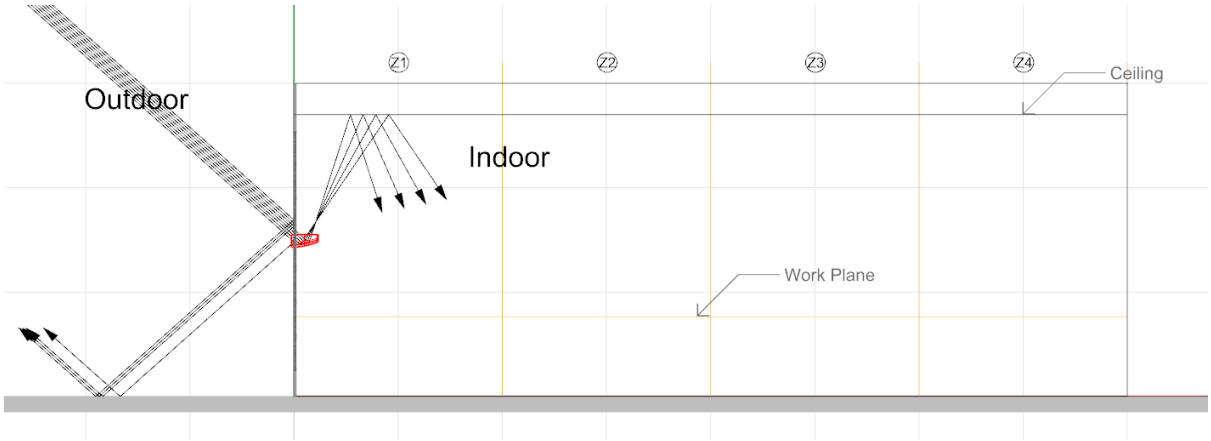
Figure 6.33: Raytracing of sun paths for developed CPC in normal mode in [out] position. At 12pm in the 21st of June, Septemberand December, [from above to below]



21 June at solar noon (inside position)



21 September at solar noon (inside position)

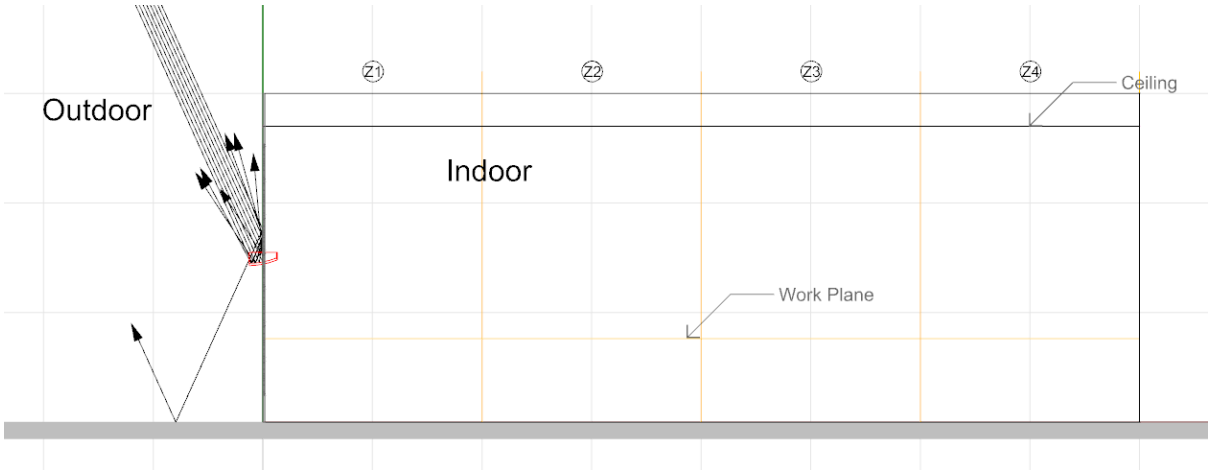


21 Decemberat solar noon (inside position)

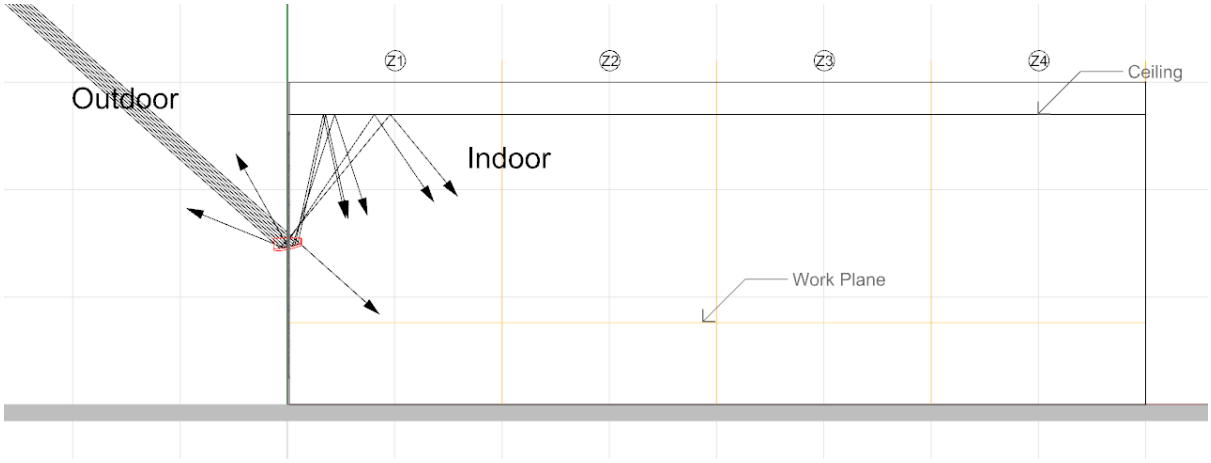
Figure 6.34: Raytracing of sun paths for developed CPC in normal mode.



21 June at solar noon (middle position)

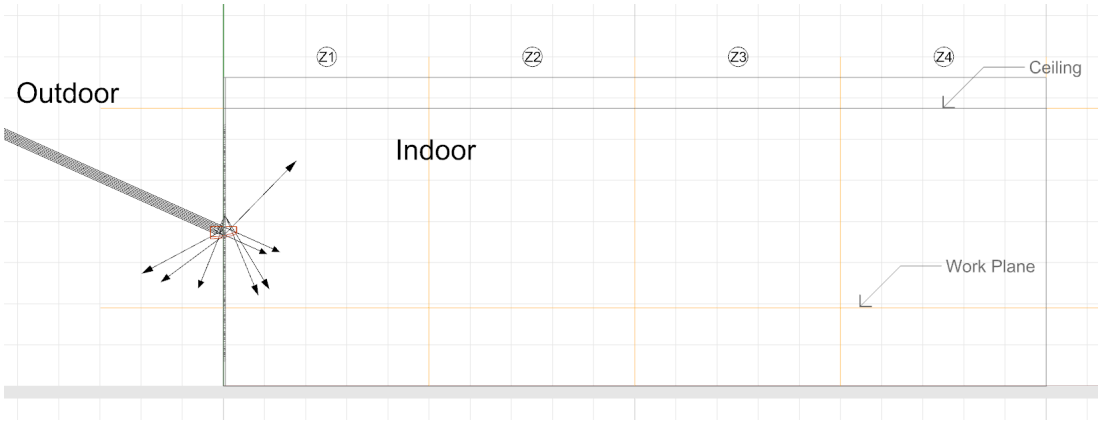


21 September at solar noon (middle position)

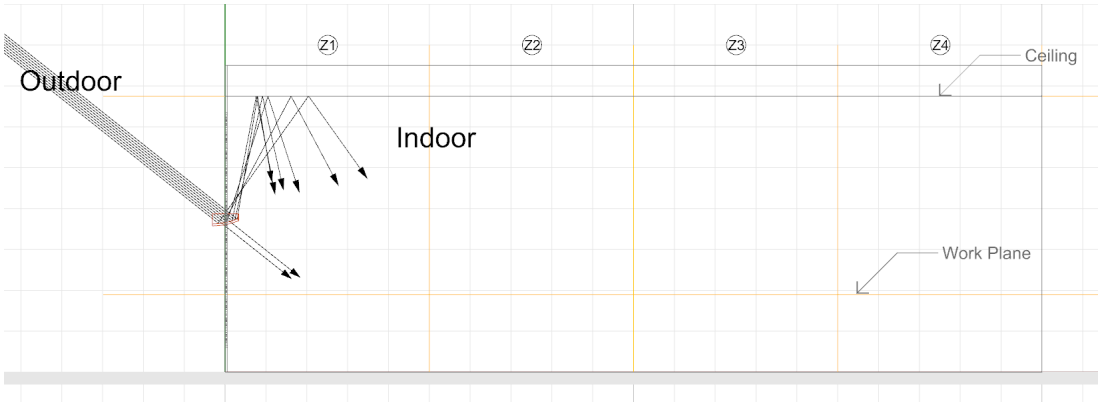


21 December at solar noon (middle position)

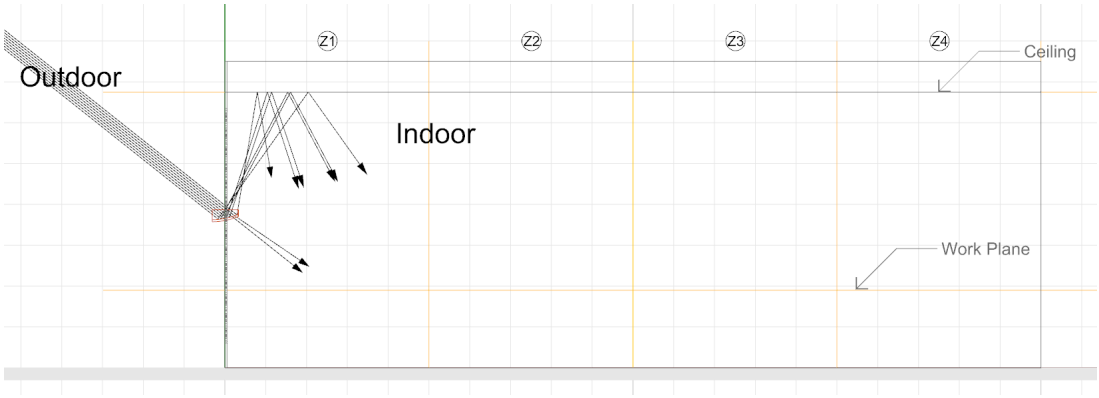
Figure 6.35: Raytracing of sun paths for developed CPC in normal mode.



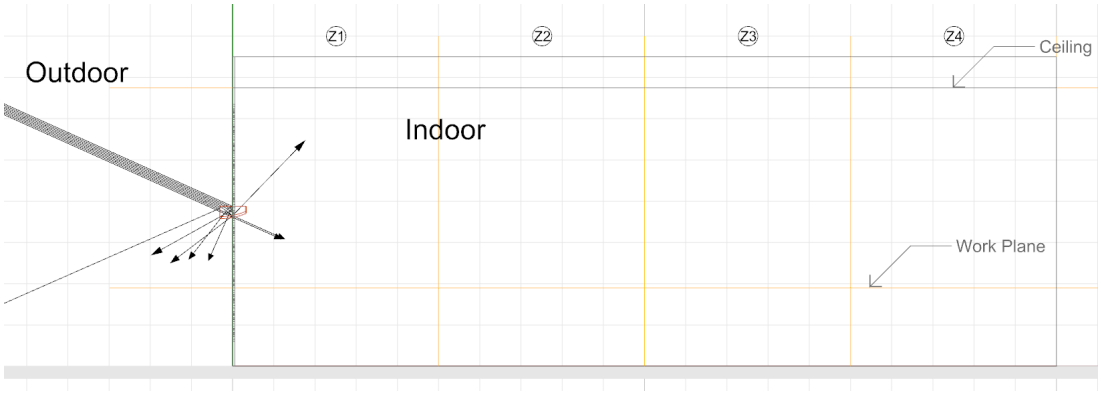
21 December at 8 am



21 December at 10 am



21 December at 2 pm



21 December at 4 pm

Figure 6.36: Raytracing of sun paths for developed CPC in normal mode. 21 December at 8am, 10am, 2pm and 4pm [from above to below]

6.3.3. Hourly evaluation through a point-in-time daylight study

The impact of the proposed DRSS system on the total illuminance level at the work plane was assessed. The daylight performance of the DRSS was analysed for summer and winter solstice and autumn equinox. It was tested at 8 am, 10 am, 12 pm, 2 pm and 4 pm on the 21st of June, September and December.

6.3.3.1. Daylight performance during morning hours

The impact of the proposed DRSS system on the total illuminance level at the work plane at the early morning hour, namely, at 8 am, was analysed. As shown in the chart in Figure 6.37, it can be seen that total illuminance was extremely high at Z1 on 21 December. On the other hand, the total illuminance at Z1 on 21 June and 21 September were significantly lower; specifically, it was 1,443 lux and 2,061 lux, respectively, as shown in Figure 6.38. In general, the total illuminance was higher on 21 December compared with other tested dates. For instance, the total illuminance values at Z2, Z3, Z4 were 904 lux, 376 lux and 204 lux on 21 December, they were 729 lux, 325 lux and 183 lux on 21 September, and finally, they were 573 lux 259 lux and 137 lux on 21 June.

Compared with the daylight performance of case PSS5, it can be seen that the total illuminance value at the front half of the room, namely at Z1, at 8 am, was reduced by 349 lux, 300 lux and 138 lux on the 21st of December, September and June, respectively. Furthermore, the total illuminance values were increased at the rear half of the room, specifically at Z3. The illuminance was raised at Z3 by 22 lux, 33 lux and 26 lux on the 21st of June, September and

December. At Z4, the illuminance level was increased by 11 lux on 21 September, and it remained the same on 21 December; however, on 21 June, it was reduced slightly by 6 lux.

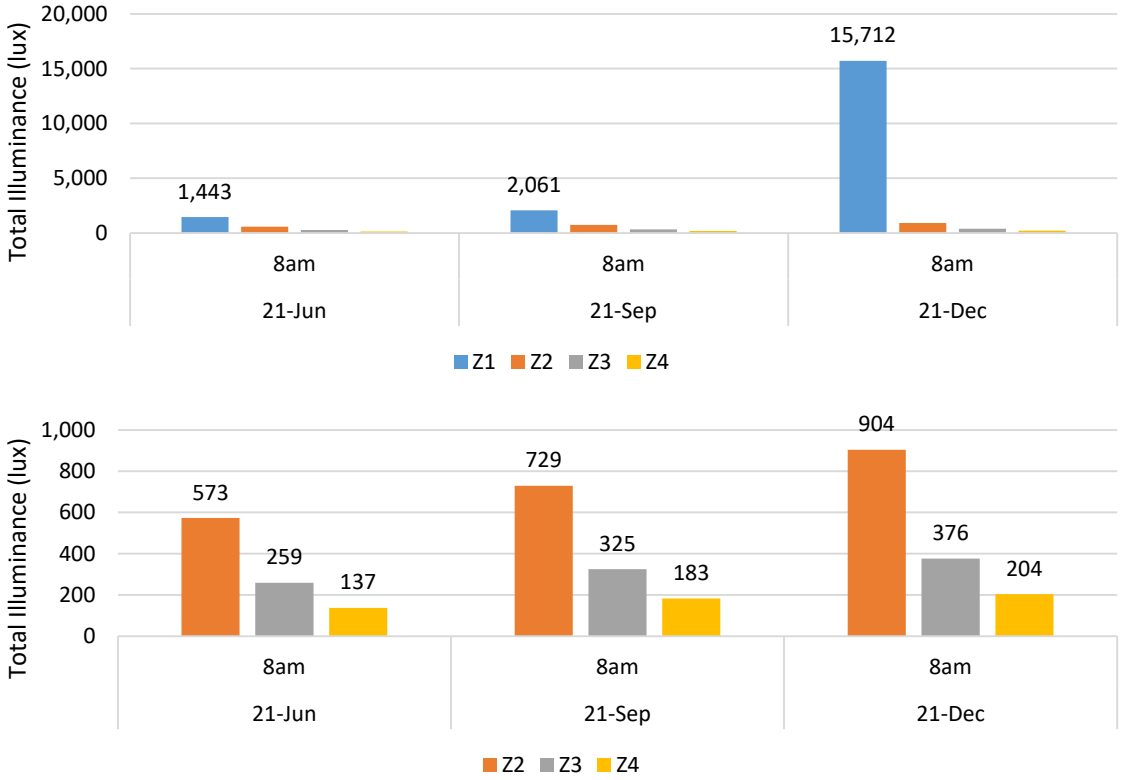


Figure 6.38: Total illuminance. Case DRSS1 in Riyadh

It was found that the direct illuminance was recorded at Z1 at 8 am on 21 December. As shown in the chart in Figure 6.39, it can be seen that the direct illuminance was reached 12,923, which is 82% of the total illuminance at this point. As a result, the diffuse illuminance at Z1 was 2,789 lux.

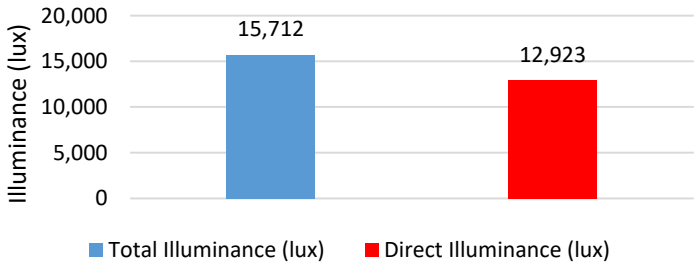


Figure 6.39: Total and direct illuminance at Z1 on 21 December at 8 am. Case DRSS1, in Riyadh

The total illuminance values at 10 am at the work plane are shown in the chart in Figure 6.40. It was found that the useful daylight illuminance (300-1000 lux) was met at Z2 and Z3 on 21 June and 21 December, while on 21 September, it was met only at Z3. The total illuminance at

Z1 was higher than the maximum threshold by 611 lux, 2,337 and 2,972 lux on the 21st of June, September and December. On the other hand, at Z4, the illuminance was lower than the minimum threshold by 124 lux and 59 lux on the 21st of June and September, respectively.

Compared with case PSS5, it can be seen that the DRSS has eliminated the direct illuminance at Z1 from 35,405 lux to zero lux. As a result, the total illuminance reduced from 40,011 lux to 3,972 lux, and the diffuse illuminance was reduced to 634 lux (from 4,606 lux to 3,972 lux). The reduction of the illuminance at Z1 on the 21st of June and September was 89 lux and 75 lux.

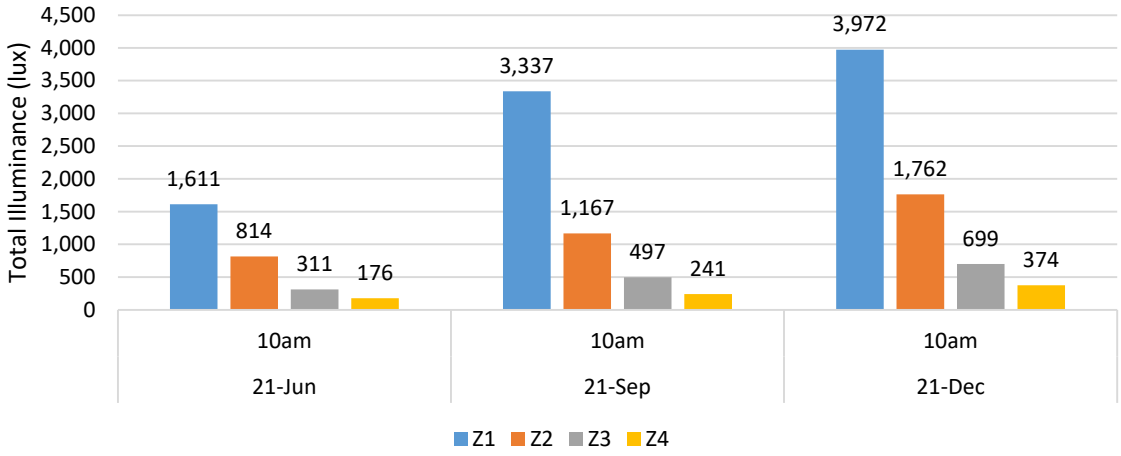


Figure 6.40: Total illuminance. Case DRSS1 in Riyadh

6.3.3.2. Daylight performance at solar noon

The daylight performance at the work plane was assessed at the solar noon when the sun azimuth is 180 degrees from the north. The total illuminance was assessed as a function of three solar altitudes, namely, 88° 68° and 42° on the 21st of June, September and December.

It was found that the illuminance is higher on 21 December, which has the lowest solar altitude. On the other hand, the lowest illuminance values were recorded on 21 June, which has the highest solar altitude. The total illuminance at all daylight zones for the three tested dates was diffuse only.

The peak illuminance was 5,129 lux at Z1 on 21 December, while the lowest was 193 lux at Z4 on 21 June. The illuminance was within the range of (300-1000 lux) at Z3 for the three tested dates. In contrast, the targeted illuminance range was not met at Z1 for the three tested

dates. At Z2, the illuminance was within the targeted range on 21 June; however, at Z4, the illuminance was above the minimum threshold only on 21 December, as shown in Figure 6.41.

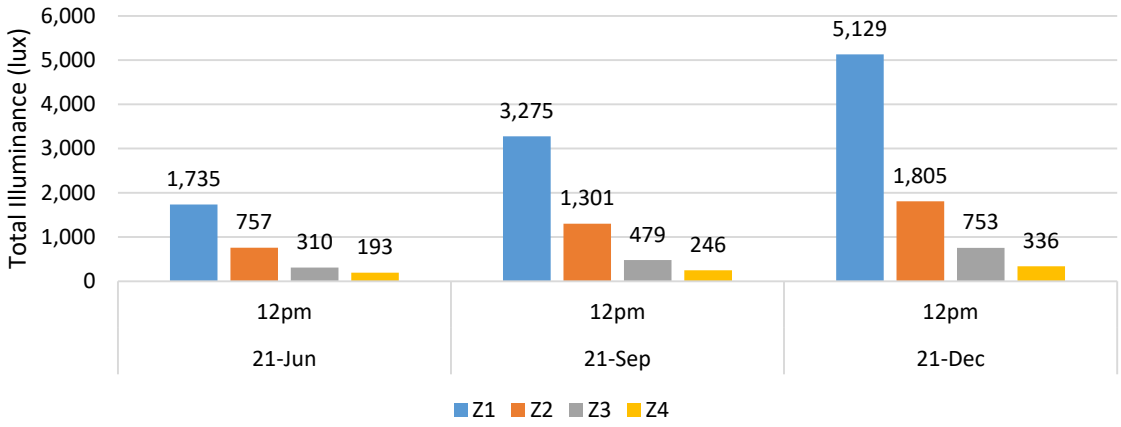


Figure 6.41: Total illuminance for case DRSS1 in Riyadh

6.3.3.3. Daylight performance during evening hours

The total illuminance at 2 pm is shown in the chart in Figure 6.42. It was found that the daylight performance is similar to the PSS5, with an insignificant increase and decrease in some zones. This is because the total illuminance consists of diffuse illuminance only, and it is higher on 21 December and lower on 21 June.

The peak illuminance at Z1 was 4,059 on 21 December, while the lowest was 1,613 lux on 21 June. The targeted illuminance range (300-1000 lux) was met at Z2 except on 21 December, which exceeded the threshold by 296 lux. The illuminance at Z3 was within the useful range for the three tested dates. Finally, at the rear zone, namely Z4, the daylight intensity at the work plane was lower than the desirable level for the three tested dates. It was lower by 147 lux, 100 lux and 49 lux on the 21st of June, September and December, respectively.

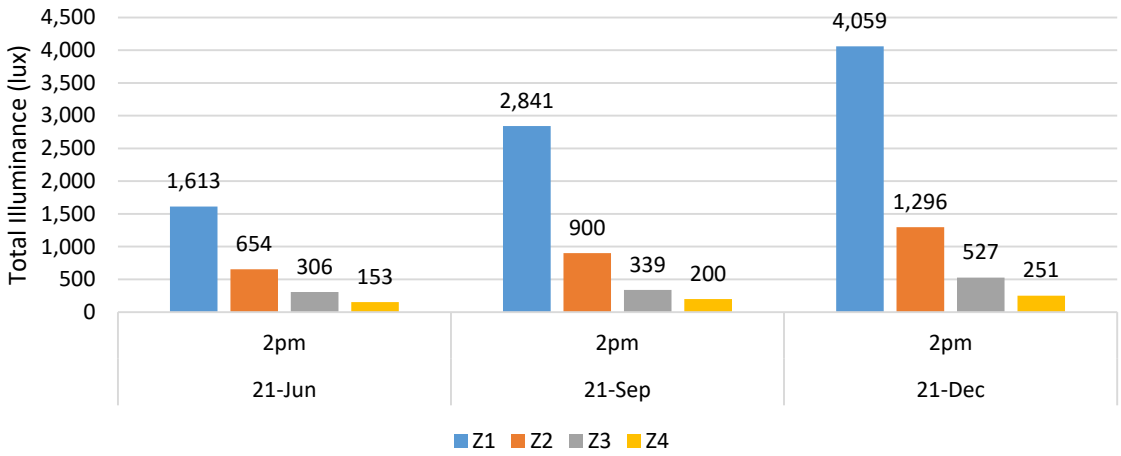


Figure 6.42: Total illuminance on 21 June, 21 September and 21 December at 2 pm. Case DRSS1 in Riyadh

The total illuminance in the late evening, specifically at 4 pm, was assessed for case DRSS. Comparable to the PSS5, it was found that no occurrence of direct illuminance at any daylight zone. Similarly, the illuminance was higher on 21 June and lowered on 21 December due to the early sunset hour in December, as described previously.

The peak illuminance values were at Z1; they were 1,118 lux, 1,030 lux and 690 lux on the 21st of June, September and December, respectively. On the other hand, the desirable illuminance level (300-1000 lux) was not met at Z3 and Z4 for the three tested dates. The lowest illuminance values were at Z4; they were 107 lux, 84 lux and 53 lux on the 21st of June, September and December, respectively. The desirable illuminance was met at Z2 except on 21 December, lower than the threshold by 51 lux, as shown in Figure 6.43.

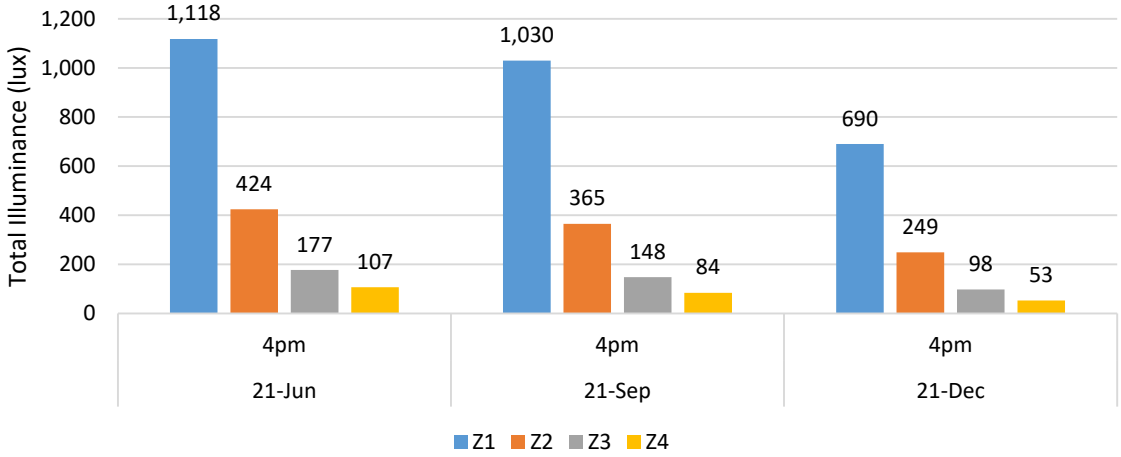


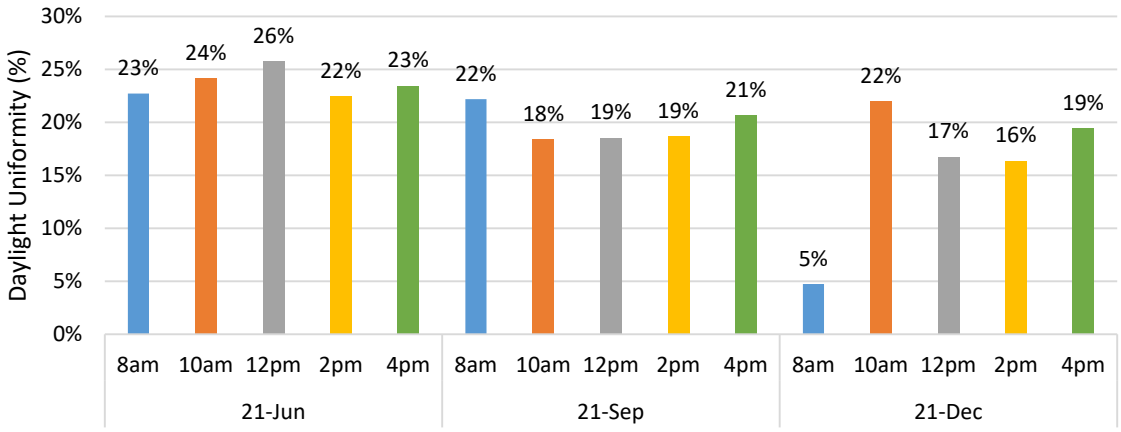
Figure 6.43: Total illuminance. Case DRSS1 in Riyadh

- **Daylight uniformity at the work plane**

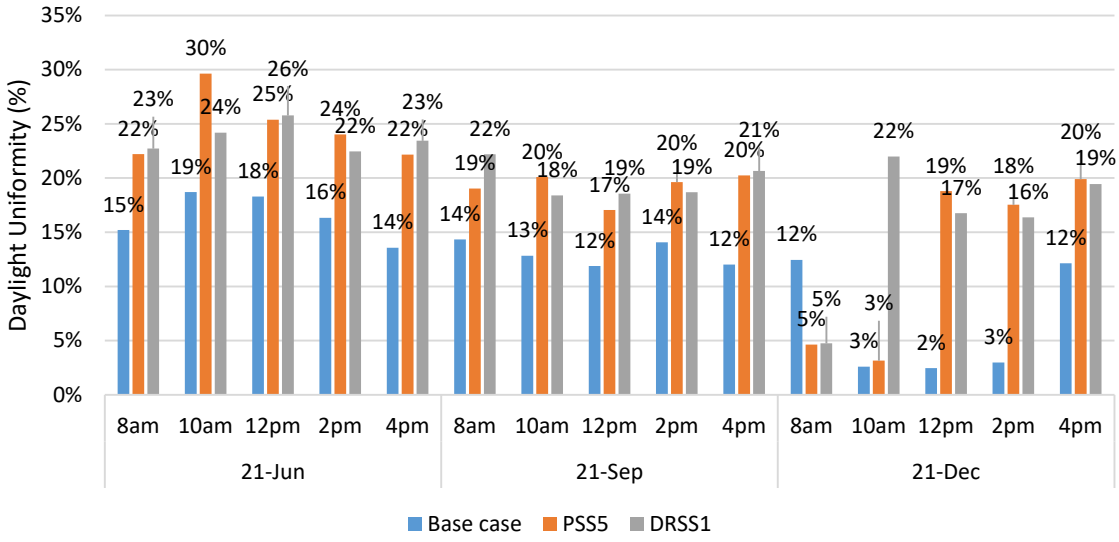
The DUWP was calculated as a function of the ratio between the minimum and the mean value of the total illuminance for the four daylight sensors. It was found that the DUWP was between 22% to 26%, 18% to 22%, and 5% to 22% on the 21st of June, September and December, respectively, as shown in Figure 6.44.

The best DUWP was recorded on 21 June, while the worst was on 21 December. The difference between the peak and the lowest DUWP was 4%, 6%, and 17% on the 21st of June, September, and December. The highest DUWP on 21 June was 26% at noon, on 21 September was 22% at 8 am and on 21 December was 22% at 10 am.

On the other hand, the worst DUWP value on 21 June was 22% at 2 pm, on 21 September was 18 at 10 am, and on 21 December was 5% at 8 am. The low DUWP at 8 am on 21 December was due to the excessive direct illuminance at Z1, increasing the total illuminance considerably. However, the DUWP at 8 am on 21 December remains with PSS5 (5%); it was found that the DUWP was enhanced significantly by utilising the DRSS at 10 am on 21 December, where it was increased from 3% to 22%.



(a)



(b)

Figure 6.44: Dayligth uniformity; (a) for Case DRSS, (b) comparison of the base case, case PSS5 and Case DRSS1 in Riyadh city.

6.3.4. Overall evaluation by an annual daylight study

The daylight performance of the DRSS was assessed by an annual daylight simulation for each season individually, namely, spring, summer, autumn and winter. Then, the daylight performance for the whole year was evaluated to observe the overall daylight enhancement. The outputs were evaluated through three dynamic daylight metrics: the ASE, DA, and the UDI. Accordingly, the daylight glare probability (DGP) was analysed for the worst day of the year.

6.3.4.1. Seasonal daylight evaluation

The seasonal daylight evaluation started with the assessment of the DA. It was found that the DA was achieved at high values at Z1 and Z2, whilst the worst DA values were at Z4. The peak value of the DA at Z1 was 100%, and the lowest was 90% in spring and winter, respectively. The DA values at Z2 were between 90% to 82% for spring and winter as well. On the other hand, the variance among the DA values at Z3 was relatively higher, 16%. The lowest DA at Z3 was 57% in summer, and the highest was 73% in winter. Finally, the rear daylight zone (Z4) has recorded the worst DA values. The difference between the peak and the lowest DA value was 44%. The highest DA value at Z4 was 44% in winter, whereas the lowest was 0% in

summer. Similarly, the DA value at Z4 in spring and autumn was significantly low, 10% and 7%, respectively, as shown in Figure 6.45.

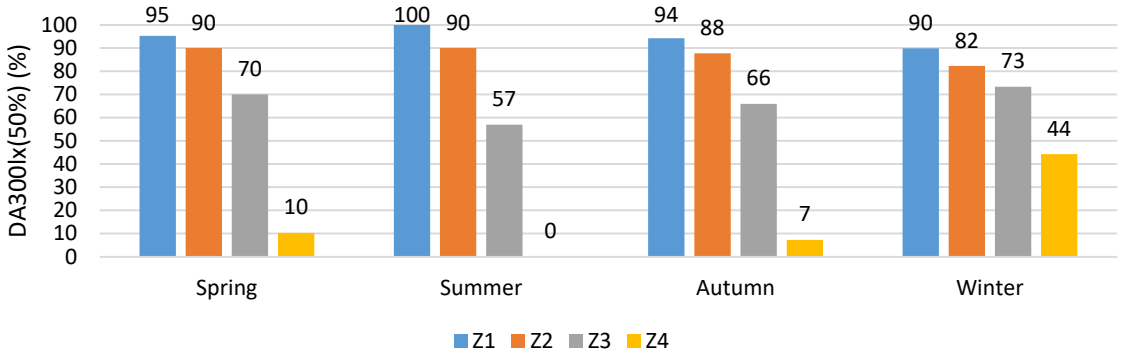


Figure 6.45: Daylight autonomy $DA_{300\ lux\ (50\%)}$ (%), case DRSS1, Riyadh

In order to assess the potentiality of the excessive direct illuminance occurrence at the work plane, the ASE was analysed for the four seasons. It was found that the worst season occurred in winter, where the sunlight exposure was exceeded the maximum threshold for 105 hours. On the other hand, the best performance was in summer, where the ASE was within the limit, which is 1000 lux for 250 hours. The ASE value was moderate in spring and autumn; it was 27 hours and 16 hours, respectively, as shown in Figure 6.46.

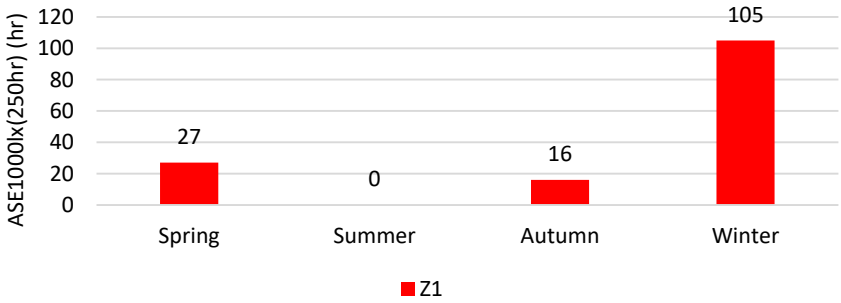


Figure 6.46: The ASE at Z1, case DRSS1, Riyadh

After assessing the DA, which has a minimum but not a maximum threshold, and after assessing ASE, which has only a maximum threshold and considers only the direct illuminance, it was important to evaluate the daylight performance by the UDI which considers the total illuminance. It has a minimum and maximum threshold, specifically, 300- 1000 lux.

It was found that the highest $UDI_{300\text{-}1000lx}$ value was 90% at Z2 in summer; however, the lowest value was 0% at Z4 in the same season. The pattern of the UDI among the daylight zones for each season was found to be variant. For instance, in autumn, the $UDI_{300\text{-}1000lx}$ at Z2 was higher than Z4, 51% and 7%, respectively. In contrast, in winter, the UDI at Z2 was lower than the

UDI at Z4, 21% and 44%, respectively, as shown in Figure 6.47. In general, it was found that Z2 and Z3 were achieved better UDI values compared with Z1 and Z4.

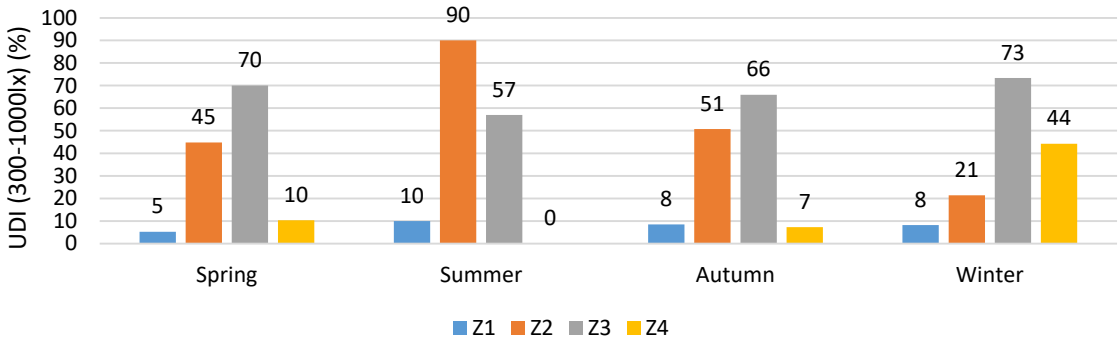


Figure 6.47: The UDI for case DRSS1 in Riyadh

6.3.4.2. Annual daylight evaluation

After investigating the seasonal daylight performance, the annual daylight performance for the whole year was evaluated. The results of the DA and the ASE are shown in the chart below in Figure 6.48. It was found that the DRSS achieved the DA by high value at Z1 and Z2 while it was moderate at Z3; however, it was exceptionally low at Z4. The DA values were 100%, 97%, 74% and only 18% at Z1, Z2, Z3 and Z4, respectively, as shown in Figure 6.48 [A].

On the other hand, as shown in the chart in Figure 6.48 [B], the daylight performance of the DRSS in terms of the sunlight exposure was optimal for all the daylight zones except Z1. The ASE at Z1 was exceeded the allowed ASE by 161 hours.

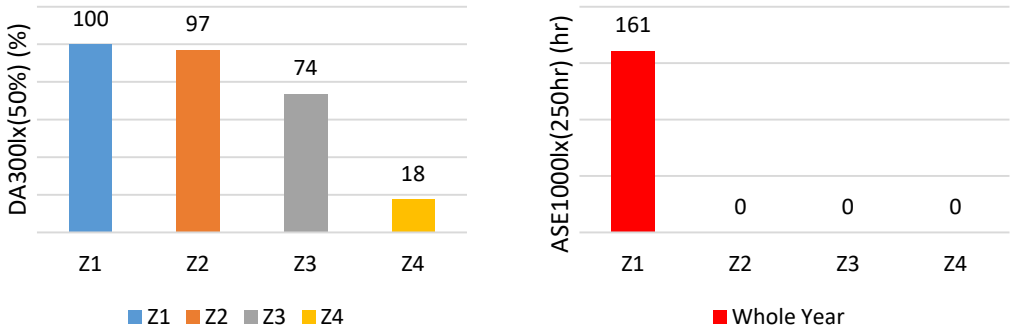
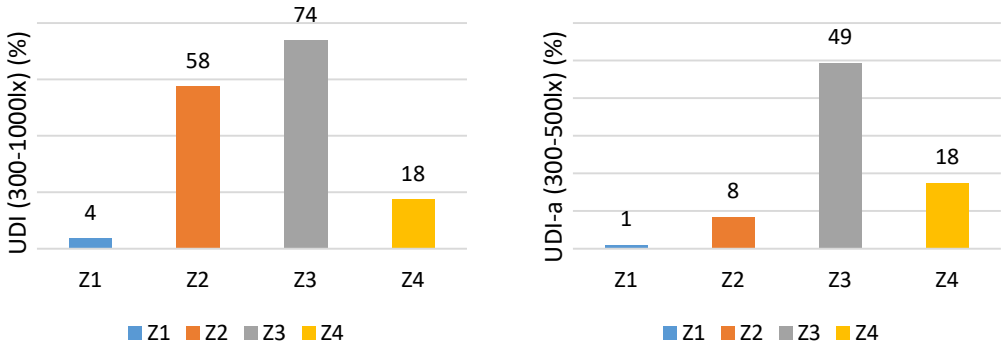


Figure 6.48: (A) the DA, and (B) the ASE for case DRSS1 in Riyadh

The useful daylight illuminance was evaluated for the whole year with two thresholds, namely 300-1000 lux and 300-500lux. The values of the $UDI_{300\text{-}1000\ lux}$ and $UDI_{300\text{-}500\ lux}$ are illustrated in the charts in Figure 6.49 [A] and [B] below. The $UDI_{300\text{-}1000\ lux}$ was met by higher values at

Z2 and Z3, which were 58% and 74%, respectively. On the other hand, it was low at Z1 and Z4, which were 4% and 18%, respectively.

The $UDI_{300\text{-}500\ lux}$ values were lower than the $UDI_{300\text{-}1000\ lux}$ values at all the daylight zones except at Z4, which remained at 18%. The heights value of the $UDI_{300\text{-}500\ lux}$ was 49% at Z3. On the other hand, it was exceptionally low at Z1 and Z2, 1% and 8%. It can be seen that the difference between the two metrics was significant at Z2, which means that the daylight level at this sensor is mostly between 500-1000 lux, which is acceptable for office tasks.



[A] [B]

Figure 6.49: (A) the $UDI_{300\text{-}1000\ lux}$, and (B) the $UDI_{300\text{-}500\ lux}$, for case DRSS1 in Riyadh

6.3.5. Analysis of daylight glare probability

In order to study the visual comfort performance of the proposed DRSS, the daylight glare probability (DGP) was analysed for 21 December at 8 am, 10 am, 12 pm and 2 pm. The DGP was analysed during the hours that was recorded an ASE value above the maximum acceptable threshold.

The DGP was analysed for the worst day of the year. It was found that the higher ASE occurred on winter solstice day, namely, 21 December. During this period, the extremely low solar altitude increases the potentiality of the daylight glare at the occupant view level. From the previous analyses, it was found that the ASE occurred only at Z1. Therefore, the DGP was assessed at test point Z1 at Z1. The distance between Z1 and the façade and its height from the floor level is 1.50 meter. The test point located 1.50 meters from the sidewall, and the view direction is 180 degrees from the north.

It was found that the glare comfort range at Z1 was Imperceptible at 8 am, and it was perceptible at 4 pm. The DGP was 0.33 and 0.38 at 8 am and 4 pm, respectively. At these two hours, the DGP was within the acceptable visual comfort zone. On the other hand, at 10 am,

12 pm, and 2 pm, the glare comfort range was intolerable, which exceeded the visual comfort zone. The DGP was 0.62, 0.71 and 1.00 at 10 am, 12 pm and 2 pm, respectively, as shown in Table 6.3. The fish-eye photos in Figure 6.50 to Figure 6.54 show the luminance value (cd/m2) inside the room from the test point described above.

Table 6.3: Glare study results of daylight-redirecting solar screen case DRSS1

Date	Time	DGP	Glare Comfort Range
21 December	8 am	0.33	Imperceptible Glare
	10 am	0.62	Intolerable Glare
	12 pm	0.71	Intolerable Glare
	2 pm	1.00	Intolerable Glare
	4 pm	0.38	Perceptible Glare

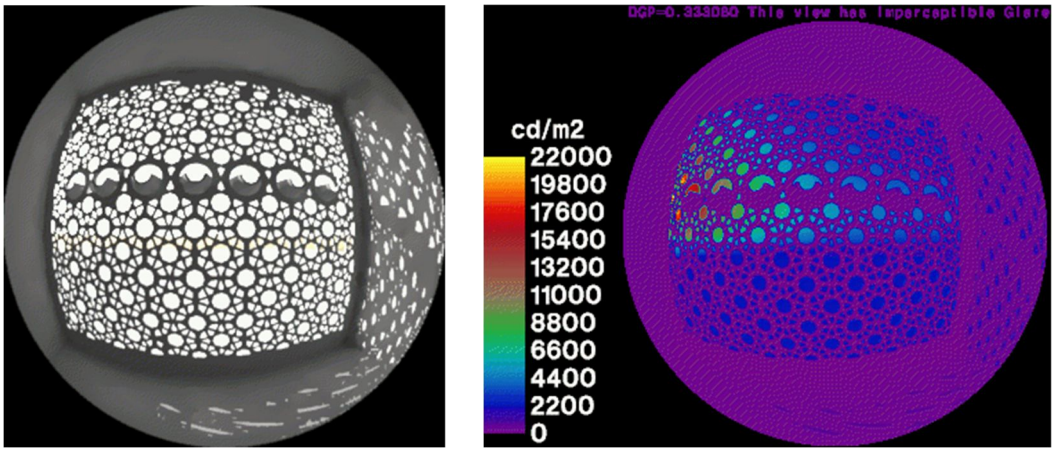


Figure 6.50: The luminance, 21 December at 8 am. Case DRSS1, Riyadh

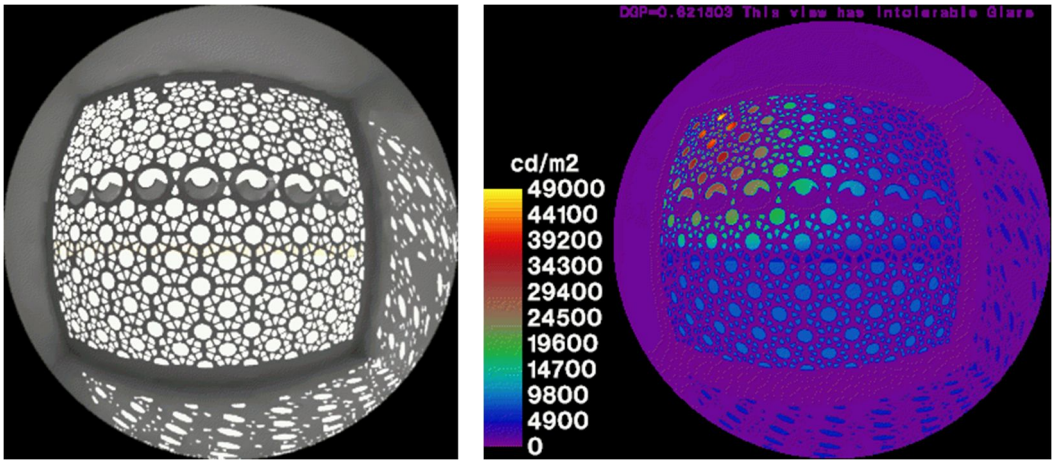


Figure 6.51: The luminance, 21 December at 10 am. Case DRSS1, Riyadh

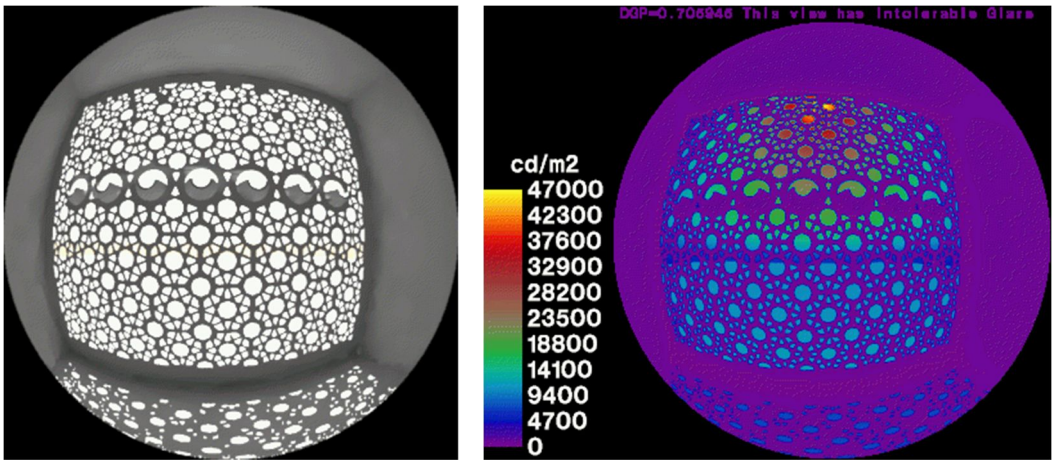


Figure 6.52: The luminance, 21 December at 12 pm. Case DRSS1, Riyadh

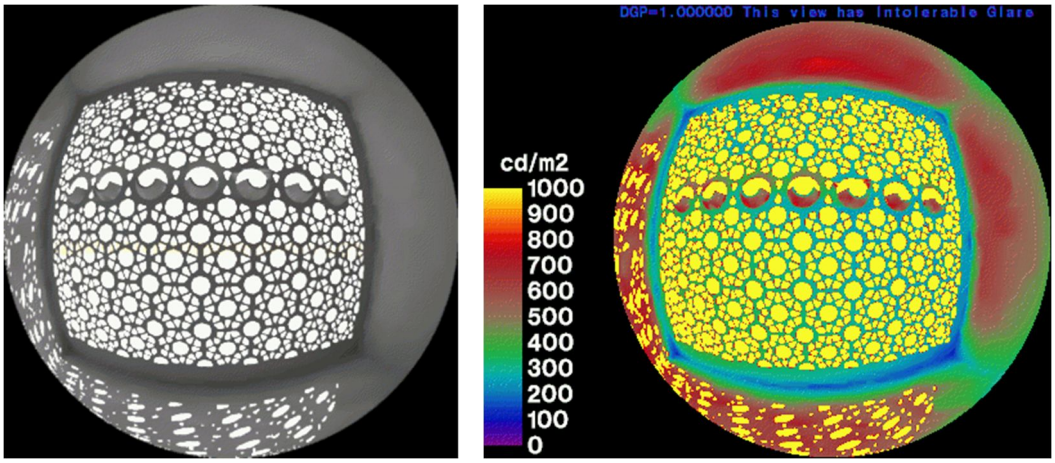


Figure 6.53: The luminance, 21 December at 2 pm. Case DRSS1, Riyadh

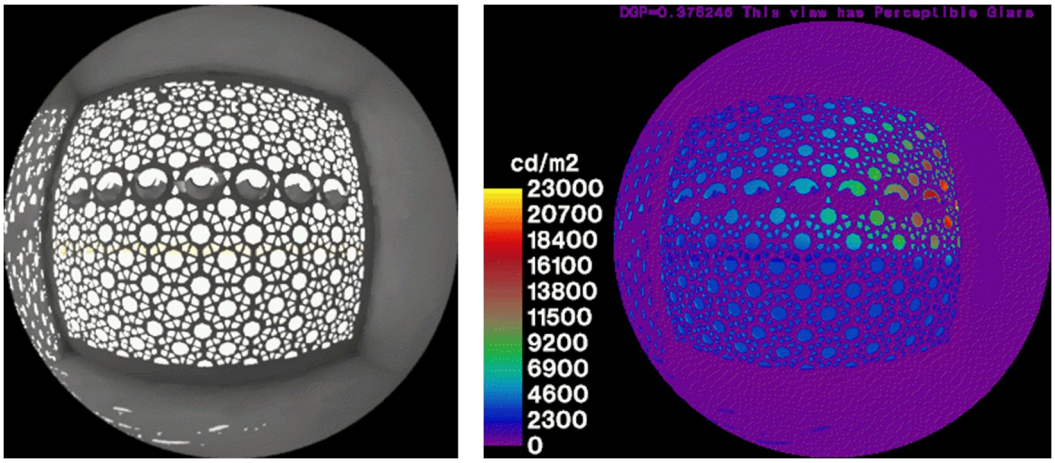


Figure 6.54: The luminance, 21 December at 4 pm. Case DRSS1, Riyadh

Comparison of the DGP for the base case, and cases PSS5 and DRSS1

A comparison of the DGP was conducted to observe the enhancement that was achieved by the proposed DRSS. The chart in Figure 6.55 shows the values of the DGP for case the base case, PSS5 (perforated screen) and the DRSS (daylight-redirecting perforated solar screen). It can be seen that the DRSS was enhanced the visual comfort by reducing the DGP compared with the two other cases, namely, the base case and case PSS5.

The DGP was reduced by from 0.42 to 0.33, 0.82 to 0.62, 0.94 to 0.71 and 0.47 to 0.38 at 8 am, 10 am, 12 pm and 4 pm. On the other hand, the proposed system increased the DGP from 0.83 to 1.00 at 2 pm. The reduction of the DGP from PSS5 to DRSS was at 8 am, 10 am and 12 pm by 0.01, 0.02 and 0.01, respectively. The DGP was the same at 2 pm and 4 pm for the two cases.

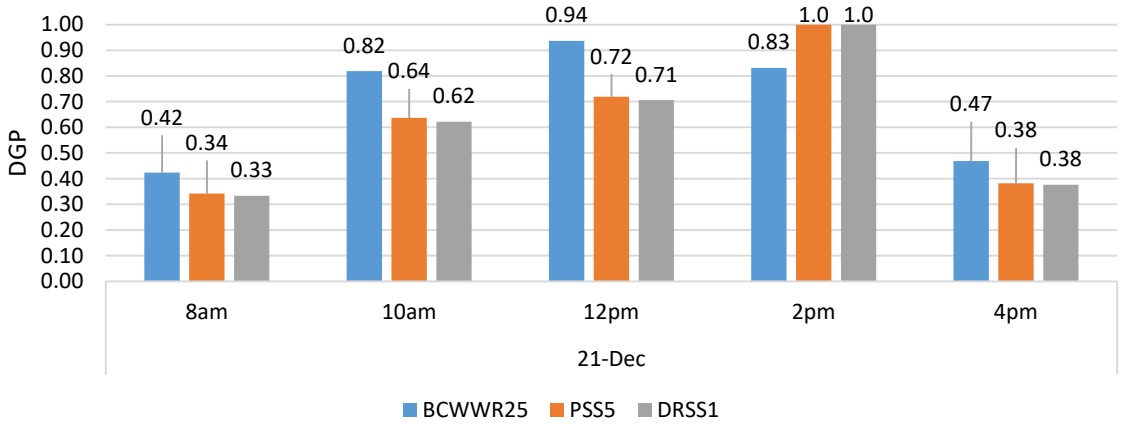


Figure 6.55: Comparison of DGP for the base case, PSS5 and DRSS1, for Riyadh

6.4. Discussion and Summary

On perforated solar screen

The PSS was assessed with six perforation percentages from 25% to 35% with 2% interval, and they have been given names PSS1 to PSs6, respectively. The daylight performance was assessed for the whole year through the annual study. The outputs were analysed for the whole year then for each season separately. Later, the daylight performance was assessed for summer solstice, equinox and winter solstice through PIT study. Finally, the DGP was assessed for the tested hours that recorded a direct sunlight occurrence on the work plane.

It was found from the analysis of the whole year outputs that the ASE occurred only at Z1. The lowest ASE value was for PSS1 (74 hours/year), whereas the highest value was for PSS6 (221 hours/year); however, it is lower than the ASE of the base case by 160 hours/year.

The analysis of the DA showed that the best performance was at Z1 and Z2 for most of the PSS cases. On the other hand, the DA at Z3 and Z4 was varied. As the DA has only a low threshold (300 lux) but does not have a higher threshold, it could highlight the overlit area at the front daylight zones. On the other hand, from the analysis of the DA at Z34 and Z4, it was found that the DA values at Z3 and Z4 were increased when the perforation percentage increased.

The UDI, which has a low and high threshold, was utilised to assess the daylight performance of the PSS cases. It was found that the PSS enhanced the UDI by 23% in the front area (one meter from the façade) compared with the base case. However, when the perforation percentage increased to 35%, the improvement was only 1%. On the other hand, at Z2, where the light sensor is 3 meters from the façade, the UDI was significantly higher than Z1. It was found that PSS1 performance exceeded the base case by 28% UDI. However, it was noticed that the increase in the perforation percentage increased the UDI value. The maximum perforation percentage to maintain the same UDI of the BS was 33% (PSS5).

In contrast, it was observed that at Z3, where the light sensor is placed five meters from the façade, the increase in the perforation percentage increased the UDI significantly. The base case and PSS5 achieved the same UDI value. The 72% UDI at Z3 achieved by the window with 25% WWR can be obtained using PSS with a 33% perforation percentage. At the very rear area (Z4), where the light sensor is placed 7 meters from the façade, it was found that the lowest acceptable perforation percentage to enhance the UDI compared with the base case is 31%. It was found that the PSS6 doubled the UDI value compared with the base case.

Finally, from the analysis of the UDI values, it was found that the optimal PSS case that can balance the daylight performance by decreasing the undesirable direct sunlight and by increasing the desirable diffuse light was PSS5. It maintained the UDI values that the base case achieved while it reduced the direct sunlight that was allowed by the base case. As a result, the PSS5 reduced the ASE from 381 hours/year to 186 hours/year.

Following the data analysis of the whole year, the optimal PSS (PSS5) daylight performance was assessed for each season separately. The best performance was recorded at Z1 and Z2 with at least 82% for all the seasons. At Z3, the change in the DA values during the season was insignificant. At Z4, the DA values were significantly varied. The highest DA was in winter (38%) due to the low solar altitude, while the lowest was in summer (0%) due to the high solar altitude.

On the other hand, the ASE has not occurred in summer, and it was low in spring (27 hours/year) and autumn (16 hours/year); however, the worst scenario was in winter, which reached 129 hours/year. The high ASE value in winter is due to the low solar altitude. As the PSS openings are parallel with the façade, they could allow the most direct sunlight at low solar altitude.

In order to assess the daylight performance of the PSS5 in the front area, it was vital to analyse the UDI as the DA does not have a high threshold, as mentioned previously. It was found that PSS5 enhanced the UDI at the front area by reducing the undesirable sunlight. Although the UDI with PSS5 at Z1 was still low (from 6% in spring to 10% in summer), it was enhanced by the double values for all the seasons, except in spring which was relatively lower than the UDI with the base case (1.6% lower).

At Z2 and Z3, the UDI was similar to the base case; however, a significant improvement was recorded in the rear area (Z4), which was increased by considerable UDI values for all the seasons. The UDI at Z4 with the base case was 0% for all the seasons except in winter, 17.7%. PSS5 increased it to 11% in spring and 8% in autumn, and 38% in winter. As the perforated solar screen openings are outspread on the whole façade area, this allows the daylight to reach a deeper area in the room compared with the window placed in the middle of the façade.

In order to understand the daylight performance of PSS5 during the day, a PIT study was conducted. It was found that the utilisation of PSS5 enhanced the overall daylight performance compared with the base case. The undesirable illuminance in the front area in June and September was reduced at the early morning hours (8 am). However, it is important to note that in December, the total illuminance level was increased at Z1 by PSS5 (from 4,610 lux to 16,061 lux). The rapid increase in the total illuminance level was due to the high value of direct illuminance (12,923 lux) at the work plane caused by the lower perforations. Therefore, it is vital to consider both the lower perforations and windowsill height as it was found to be a primary source of an overlit area in the front of the room. At 10 am, where the solar altitude is relatively high, the PSS5 was performed better than the BS. The PSS5 not just decreased the undesirable illuminance at the front area, but it increased the illuminance at the rear area. The high total illuminance at Z1 in December occurred, but it is still lower than BS (4,000 lux lower). At 12 pm and 2 pm, the direct sunlight issue at Z1 in December was solved by PSS5. As a result, the total illuminance was reduced from 48,460 lux to 5,297 lux and from 38,065 lux to 3,911 lux, respectively. For the other daylight zones, the scenario was similar to 10 am.

Although the direct sunlight did not penetrate the room with the base case, the undesirable diffuse illuminance at the front area was reduced by PSS5.

To assess the overall daylight performance, the DUWP was assessed for PSS5. Compared with the base case, it was found that the utilisation of PSS5 enhanced the DUWP at all the tested hours; however, on the winter solstice day at 8 am, the DUWP was better with BS; it was reduced from 12% to 5%. The decrease of the DUWP at this tested hour due to the direct illuminance at the work plane caused by the lower perforations. The utilisation of PSS5 increased the DUWP to 30% on 21 Jun at 10 am compared with the base case, 19%. Moreover, it increased the DUWP on 21 December at 12 pm and 2 pm to 19% and 18% compared with 2% and 3% with the base case. The improvement in these two tested hours was due to the absence of the direct illuminance at the work plane, which was occurred with the base case.

The final assessment of PSS5 was the analysis of the DGP, which was conducted on 21 December as the direct sunlight access the room during this tested date. It was found that the PSS5 reduced the DGP for the five tested hours; however, the DGP was still above the acceptable value from 10 am to 2 pm. While the direct illuminance at 8 am is higher with PSS5 than the base case, it was found that PSS5 enhanced DGP at these tested hours. The DGP was reduced from 0.42 (disturbing glare) to 0.34 (imperceptible glare). The reason is that the light sensor that measures the illuminance is placed in the work plane, while the light sensor that measures the luminance for the DGP analysis is placed at eye level. In addition, the DGP was reduced at 4 pm from 0.38 (perceptible glare) to 0.47 (intolerable glare). The distribution of the WWR to small perforations throughout the façade led to the daylight enhancement at 4 pm, which prevent the direct light from accessing the room when the solar altitude is low.

On daylight-redirecting device

As the main objective of the PSS was to reduce the overlit area in the front daylight zone in the room, it was essential to propose a solution to enhance the daylight performance in the rear area. A delight-redirecting device (DRD) was proposed and integrated within the PSS for this purpose. The integration created a novel daylight-redirecting solar screen (DRSS). Like the previous tests, the design of the DRSS was optimised by a raytracing study then the daylight performance was assessed through a PIT and an annual study.

The DRD is a CPC; it was tested in a normal mode, where the outlet is larger than the inlet aperture. It was found that the CPC reflects most of the sun rays outdoor. The best performance was found in December, when the solar altitude is low. The raytracing study found that the upper surface of the CPC obstructs the reflected sun rays. Therefore, the upper part of the CPC was eliminated. This adjustment enhanced the redirection of the sun rays towards the indoor ceiling. It was found that the upper part does not play a considerable role in the daylight redirection; nevertheless, it reduced the quantity of the redirected daylight towards the interior ceiling.

Following the ray-tracing study, which considers only the direct sun rays, an hourly evaluation of the daylight intensity was conducted by a PIT study. The enhancement in the illuminance levels was measured during the day. It was found that DRSS1 prevented the direct sun rays at Z1 in December at 10 am, which increased the DUWP from 3% to 22%. On the other hand, the problem was not solved at 8 am when the solar altitude is too low, but the total illuminance was reduced from 16,061 lux to 15,712 lux compared with PSS5. The direct sunlight in this area passed through the lower perforations, which need to be optimised to solve this challenge. However, the objective of the DRSS1 was to enhance the illuminance level in the rear area.

The daylight performance seasonal evaluation of DRSS1was presented. The results illustrated the enhancement of the illuminance levels by DRSS1 at the rear daylight zones, namely at Z3 and Z4. The DA and the UDI were increased for all the seasons, except in summer at Z4; it remained 0%. Furthermore, the ASE analysis showed the mitigation of the direct sun rays at Z1 in winter; however, the ASE was increased relatively in autumn and spring. As a result, it was vital to optimise the DRD design to minimise the negative impact of the DRD that caused the daylight redirection at the front area of the ceiling.

The annual evaluation of the whole year results illustrated the impact of the DRSS1 on the daylight performance for each daylight zone. The DRSS1 enhanced the DA and the UDI at Z4 (from 5% to 18%), and it reduced the ASE at Z1 (from 381 to 161 hours/year). Although the daylight performance was enhanced, further optimisation in the DRD was required to increase the illuminance levels at the rear area.

The final assessment step was to analyse the DGP at the worst test day, namely, 21 December. The presented results provided an understanding of the effect of the DRSS1 in visual comfort compared to PSS5. The results showed that the DGP was decreased relatively at 8 am and 10 am; however, the glare comfort ranges were not changed for all the tested hours. The worst DGPs were at 10 am, 12 pm and 2 pm. The large perforations cause the increased DGP in the lower part of the PSS. Therefore, the PSS will be optimised in a future study to minimise its negative impact when the solar altitude is low.

After the daylight assessment in phase 1, the effect of the proposed daylight system components on the daylight performance was observed. Therefore, phase two started with the integration of the DRDs within the PSS. Then, the daylight performance of the proposed system was examined as a function of different parameters. In this stage, the daylight performance was assessed for low and high latitude locations.

The first assessment was for the low latitude location, Riyadh City, which was conducted by three tools, computer modelling, under a direct solar source and a diffuse sky dome. The second location is Nottingham, which is located in high latitude regions. The second location was tested under a direct solar source, a diffuse solar source, and a real sky in Nottingham. Furthermore, it was modelled in Radiance for validation purposes.

Chapter 7. Fabrication of the rig

A prototype was created and tested inside a laboratory as well as under a real sky to observe the daylight performance in reality and to validate the computer simulation results. Furthermore, the physical model revealed the influence of the actual materials on the daylighting performance. Then, the results have been analysed and discussed and key findings and recommendations that highlighted the strengths and weaknesses of the proposed system were given.

The purpose of this chapter is to provide the reader with a description of the following points:

4. Criteria to build a prototype-scale model for daylighting studies
5. The components of the tested rig and the fabrication process
6. The daylight measurement tools that were utilised in the experiment

The main objective of building a prototype-scale model was to observe the daylight performance for a physical room and to validate the computer simulation outputs. The physical model was tested under three conditions: a direct light source, a diffuse light source, and under a real sky. The influence of four parameters of the daylight-redirecting device (DRD) was investigated, namely, the material, geometry, position and per unit area. Further investigations included, the effect of the interior finishing on enhancing the light quality at the work plane, particularly, the surface of the DRD, the ceiling, the walls and the floor.

This chapter describes the procedure of the rig fabrication. It shows the materials and the tools that have been utilised. In addition, it describes the technique and the procedure of the fabrication and assembly of each part in the rig. The fabrication procedure of the rig is divided into three main phases, the fabrication of the test room, the fabrication of the proposed system, and the installation of the measurement instruments.

7.1. Experimental design and procedure

The process of planning, developing, and analysing an experiment so that accurate and objective results can be drawn effectively and efficiently is known as experiment design (Del Vecchio, 1997) It is critical to have a thorough comprehension of the process to effectively comprehend a specified experiment. The translation of inputs into outputs is referred to as a process. Some process variables or parameters are relatively easy to regulate in real-life

scenarios, whereas others are difficult or expensive to regulate under typical production or standard circumstances (Antony, 2014).

As the available solar simulator has a limited size, the proper size of the scale model had to be determined from the beginning to reduce the bias in the outputs. According to Bodart et al. (2006), the maximum diameter of a scale model must not exceed one-fifth of the skydome diameter. This ratio is significant to control the simple parallax error (SPE). As a result, the SPE has been calculated for the solar simulator.

7.1.1. Simple parallax error (SPE)

The SPE is a significate factor; the reliability of the artificial sky and the limitation of the dimensions of the scale model is determined by the SPE (Bodart et al., 2006). The purpose of the Simple parallax error (SPE) calculations is to determine the maximum dimensions of the scale model. The dimensions of the scale model must not exceed the 5:1 rule (20% of the diameter of the skydome), which is used to control uncertainty due to parallax errors.

The accuracy of the illuminance values derived by a solar simulator is influenced by parallax errors, which are a significant factor. Bodart et al. (2006) measured the horizontal and vertical illuminance on a turntable with variable rotation and tilt angles to determine the parallax error of a single sky patch solar simulator.

The simple parallax error is described by Mardaljevic (2002) as a function of the vertical illuminance measured at the centre of the turntable (which is the origin point) and the vertical illuminance measured at the estimated error point (Bodart et al., 2006). The SPE can be calculated using the following formula:

$$SPE\ (\%) = [(V_P - V_O) / V_O] \text{ X } 100$$

Equation 13

where:

V_P: Vertical illuminance value at the point P (where the SPE will be characterized)
V_O: Vertical illuminance value at the origin (centre of the turntable)
The D-ratio (the diameter of the scale model divided by the diameter of the skydome) is linked to the low parallax error. The parallax error increases as the D-value increases (Bodart et al., 2006)

Mardaljevic (2002) analysed parallax in sky simulator domes (SSDs). His research discovered that SSDs that recreate non-uniform luminance patterns are subject to parallax errors because the luminance angular distribution is only ‘correct' for the centre point, i.e., La ≠ Lo ≠ Lb.

The difference in luminance distribution in the scale model can be caused by parallax error. A parallax error occurs when any point away from the centre perceives a luminance pattern that differs from the accurate distribution. The illustration in Figure 7.1 shows a CIE clear sky luminance pattern projected onto a dome as seen from three distinct positions along its north-south axis (Mardaljevic, 2002).

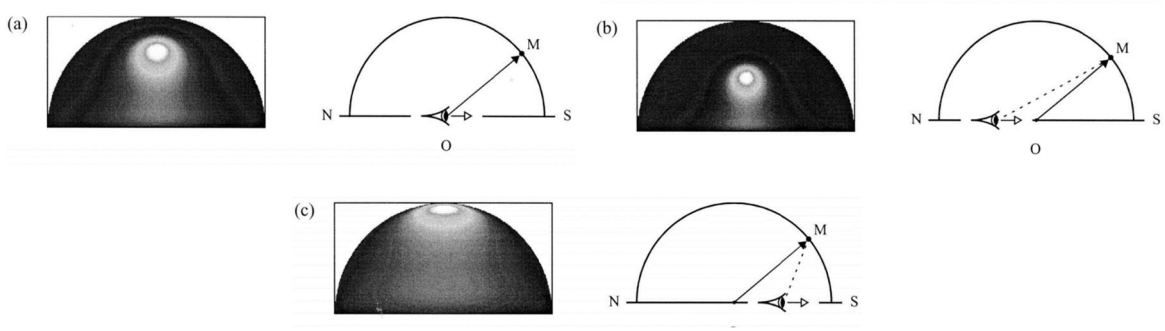


Figure 7.1: Hemispherical fish-eye views of the CIE clear sky distribution (Mardaljevic, 2002).

7.1.2. Measurements and calibrations

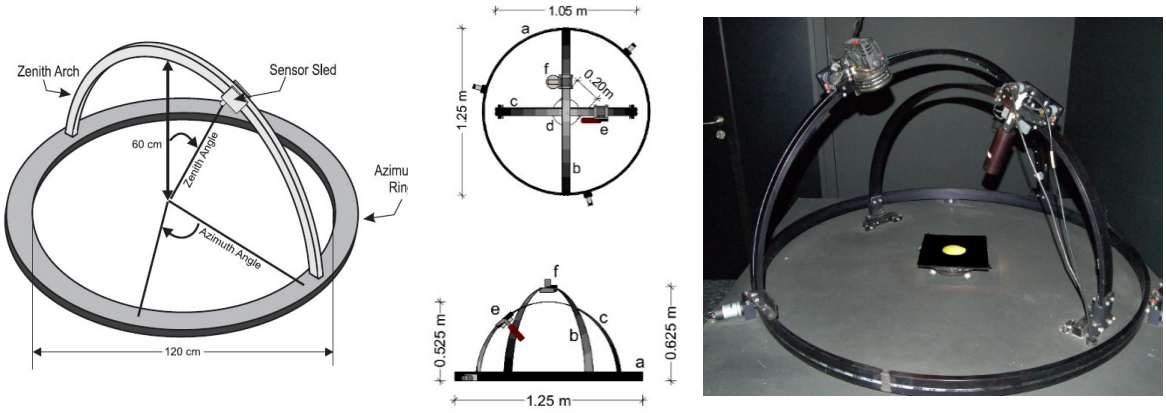
This section shows the design and fabrication procedure of a Goniophotometer (GPM) developed for three purposes. First, the GPM was utilised to calibrate the luminance meter. Second, it was utilised to measure the reflectivity of the materials that have been applied in the physical model. Third, the lux meters were calibrated by the GPM. The section starts with a description of the experimental design and procedure of the GPM fabrication. It then shows the procedure and the results of the luminance meter calibration, the materials reflectivity measurements, and finally, the lux-meter calibration.

7.1.2.1. Design and fabrication of the GPM

The primary purpose of building a GPM was to measure the reflectance value of the materials used in the experiment test to ensure that these values meet the reflectance value applied in Radiance (the computer simulation tool). Another purpose is that the GPM is an excellent tool to calibrate the luminance and illuminance meters under a constant controlled light source from a specified distance.

In order to design a reliable GPM, a literature review was conducted to determine the proper type and to understand its principles, properties, and operation methods. The design of our

GPM is a developed version of a GPM that was designed and built previously by Coburn and Peddle (2006), as illustrated in Figure 7.2 (A), and another GPM by Biliouris et al. (2007), as shown in Figure 7.2 (B and C). Then, the design was enhanced to meet the requirement and purpose of this study. The majority of goniometer systems maintain the target constant while varying the view azimuth and zenith angles. A base ring and a movable arch structure are utilised to collect data on these single-target devices. The reflectance measurements are obtained by moving the sensor along the arch to get a full set of various zenith angle measurements at a particular azimuth, and then moving the arch to capture another set of zenith measurements at the next azimuth (Coburn and Peddle, 2006).



A B C

Figure 7.2: GPM designed by [A] Coburn and Peddle (2006), and [B and C] by Biliouris et al. (2007)

The GPM used in this research consists of two arches made from aluminium perpendicular to each other. The first arch is to hold the light source, and another arch is to carry the photosensor. Each arch can be tilted from zero to 90 degrees with 15 degrees per step (12-mark divisions were engraved on the arch). Similarly, the light source position and the photosensor can be adjusted for every 15 degrees from 0 to 90 degrees.

The lightbulb is installed on the first arch. The function of the zenith angle of the first arch is to set the light source altitude angle. It can be adjusted by raising or lowering the lightbulb position over the zenith arch. The light bulb has a screw that can be loosened and tighten up to change its position. Finally, the azimuth angle of the light source can be set by changing the tilt angle of the zenith arch. Similarly, the photosensor is installed on the second arch. The same procedure of the lightbulb can set its position. The photosensor position can be adjusted by tightening up and loose the screw. The arch is divided into 12 segments, with a 15-degree step between each, as shown in Figure 7.3. A detailed drawing of the sliding support for the photosensor is illustrated in Figure 7.4.

The diameter of the GPM is 1,000 mm. The first arch is a half-circle with 500 mm radiation, which is the height of the GMP. The radiation of the second arch is 450 mm. The two arches are made from aluminium bars. The size of the platform is 200 mm in diameter, as illustrated in Figure 7.5. The GPM has a circular platform made from wood. It is marked with 48 lines, with a step of 3.75 degrees between every two marks. The purpose of degree marks is to set the azimuth angle to use the GPM as a solar simulator for illuminance measurements. A 900-lumen light bulb with a 24-degree beam angle was utilised. The details of the light bulb are shown in Figure 7.6 and Table 7.1.

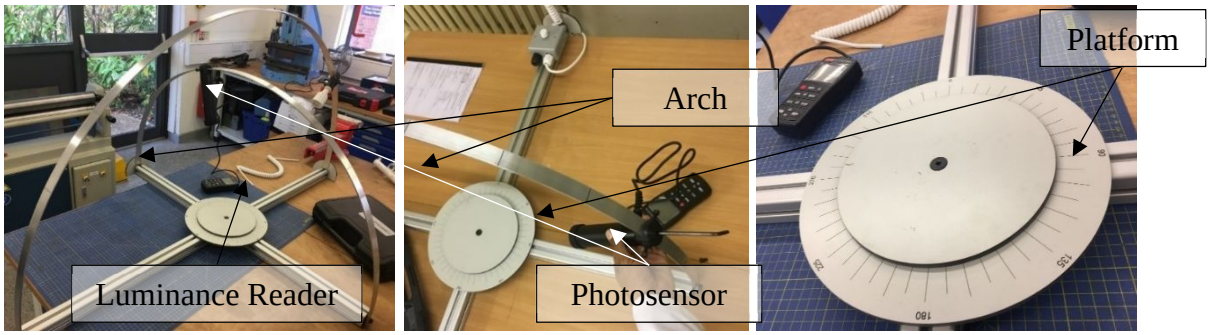


Figure 7.3: The GPM used in the research

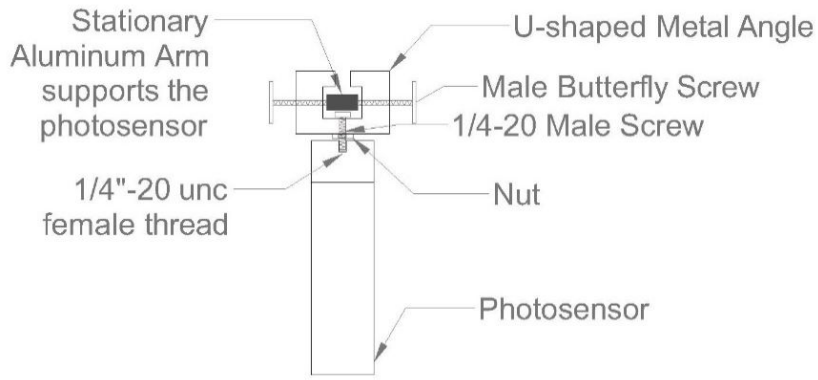


Figure 7.4: Sliding support for the photosensor

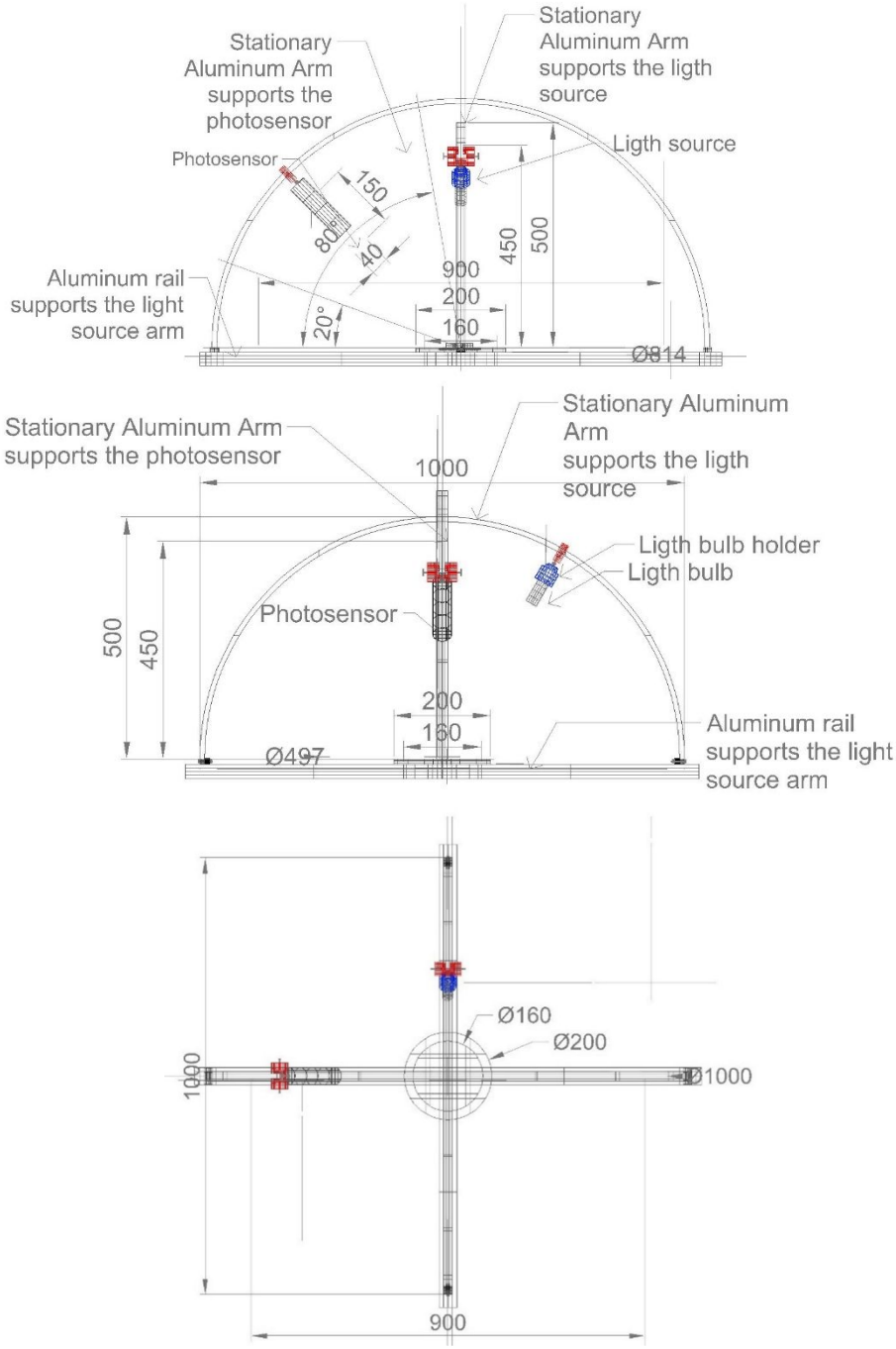


Figure 7.5: Front, side and top view of the GPM, (from above to below), dimensions in mm and degrees

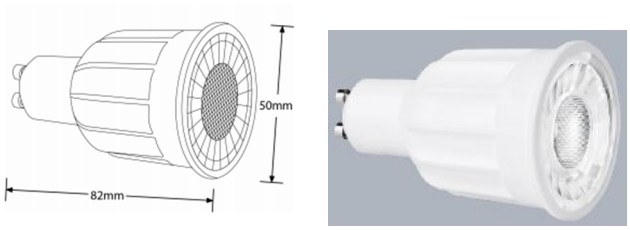


Figure 7.6: Lightbulb used in the GPM (EN-DGU1024)

Table 7.1: Specifications of the lightbulb used in the GPM.

Type	GU10
Dimmable	Yes
Maximum lumen	900 lumens
Beam angle	24 degrees
Colour	4,000 Kelvin

7.1.2.2. Calibration of the luminance meter

The experiments have been conducted inside an indoor controlled space in the Faculty of Engineering laboratories at the University of Nottingham, United Kingdom. It was ensured that uncontrollable daylight does not access the space by covering all the openings with black-matt cardboards, as shown in Figure 7.7.

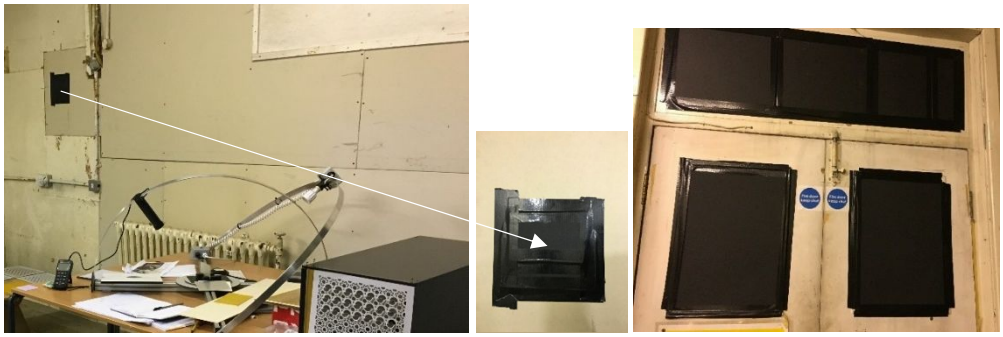


Figure 7.7: Photos inside the laboratory

With the following equation, the luminance (L) and lux (E) values are related via an ideal surface that emits all light (Ather, 2020):

$$E = L \times \pi$$

Equation 14

The luminance of a diffuse and totally reflecting surface (L) is given by:

$$L = (1/\pi) * E$$

Equation 15

A diffuse surface that reflects only a fraction R of the incident light will show the luminance (L) as:

$$L = (R/\pi) * E$$

Equation 16

where:

L is luminance, cd/m^2
E is illuminance at surface, lux
R is reflectance of surface (Rindorff et al., 1978)

The illuminance at a surface that receives constant light from a light source with known lumen can be obtained by the following equation:

$$E = \Phi / d^2$$

Equation 17

where:

E = illuminance (lux, lumen/m^2)
Φ = light emitted by a light source - luminous flux (lumen)
d = distance from the light source (meter)

The formula in Equation 17 can be utilised only if the light source is perpendicular to the surface. In other words, if the angle between the light source and the surface normal is higher than zero degree, then the Cosine law of Illumination can be utilised. The illuminance can be obtained by the following equation:

$$E = \Phi / d^2 \cos \theta$$

Equation 18

where

θ: angle between light source vertical line and surface normal (Radiance) (ToolBox, 2003)

From Equation 16 and Equation 18, the luminance (L) can be obtained as follows:

$$L = (R/\pi) * (\Phi / d^2 \cos \theta)$$

Equation 19

hence, the reflection factor (R) can be calculated by the following equation:

$$R= (L * \pi) / E = (L * \pi) / (\Phi / d^2 \cos \theta)$$

Alternatively, since the luminance of a surface can be represented mathematically as the second derivative of the luminous flux in relation to surface and solid angle with a given luminous flux function, the luminance of a light-emitting surface can be determined as:

$$L_v = d^2F / (d.A.d\Omega.\cos \theta)$$

Equation 20

where:
L_v: the surface luminance (in SI units cd/m^2)
F: the luminous flux
A: the area of the surface that emits light
θ: the angle between the surface normal and the direction from which the light comes
Ω: the solid angle (calculator.org, 2020, Riemersma, 2019)

Several calibration methods were utilised in previous studies to calibrate luminance meters. Nikolova et al. (2018) described three validate methods for luminance meter calibration:

1. Luminance calibration with a certified Lambertian diffuser reflectance standard (LRS), as illustrated in Figure 6.8
2. Luminance calibration with the use of a uniform light source, realized with opal glass, illuminated by a known level of illuminance
3. Luminance calibration with the use of a digital camera

In this study, the first method (calibration with LRS) has been utilised. The luminance meter has been calibrated using a grey card with an 18 per cent light reflectance value. The grey card was also used as a reference to find the reflectance of the materials applied for the room and the daylight proposed system. The luminance is defined by:

$$L_e = \rho_{LRS} (E_s/\pi) = \rho_{LRS} [(I_s/d^2)/ (\pi)]$$

Equation 21

where
L_e: the realized luminance, cd/m^2
ρ_{LRS}: the LRS reflectance
E_s: the illuminance at the surface, lux
I_s: the intensity from the intensity standard, cd
d: the distance between the intensity standard and the LRS, meter (Nikolova et al., 2018)

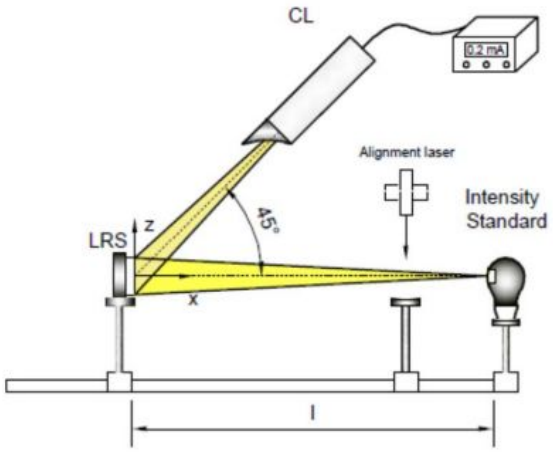


Figure 7.8: Luminance calibration setup by LRS (Nikolova et al., 2018)

Figure 7.9 shows the process of the luminance meter calibration. The luminance meter has been calibrated for two purposes. First, it was calibrated to measure the reflectance of the applied materials. Second, it was calibrated to be utilised inside the physical model to measure the luminance at the ceiling. The variation between the applied materials in the physical and computer models was achieved. The variance between the reflectance values of the applied material is significant for validation purposes.

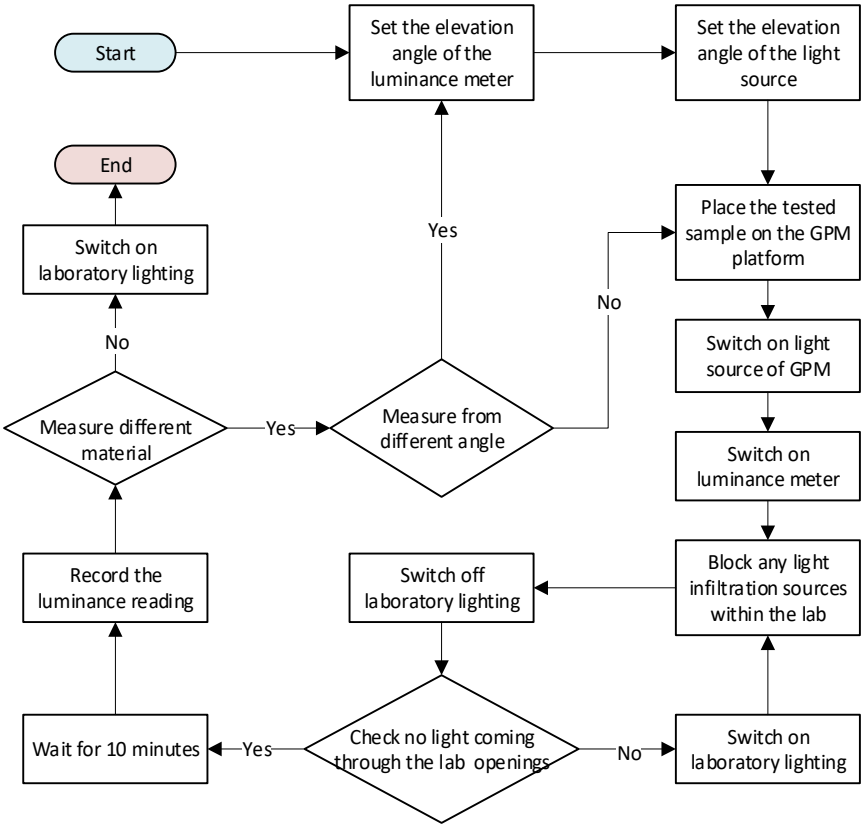


Figure 7.9: The process of the luminance meter calibration and the reflectance measurements

The calibrated luminance meter is the RS-137 Luminance Meter. The measuring angle of the luminance meter is two degrees, which is suitable to measure the luminance at a specific point accurately. The measuring ranges are 9.999, 99.99, 999.9, 9.999k, 99.99k, 999.9k and 1999k cd/m^2. The ranging can be set on an automatic mode for the seven steps based on the level of luminance are being measured. The accuracy of the luminance meter is ±3%rdg±5dgt on all ranges except 9.999, and 99.99 ranges are 10±%rdg±10dgt. The resolution of the luminance meter is 0.001 cd/m2, 0.001 fL (RS-Pro, 2017).

The 18% Grey card has been applied in previous studies to calibrate the luminance meter. The calibration was conducted following the method mentioned by (Nikolova et al., 2018) using a Grey-light calibration card with 18 per cent reflectance. The 18-Grey card was used as a reference to measure the luminance from a specific distance. Pre-known light intensity was applied; the utilised light bulb has 900 lumens. The distance between the tested surface and the light source was 0.5 meter. The angle of the light source is 24 degrees. The angle between the surface normal and the photosensor and the light source positions was 15 degrees, as illustrated in Figure 7.10.

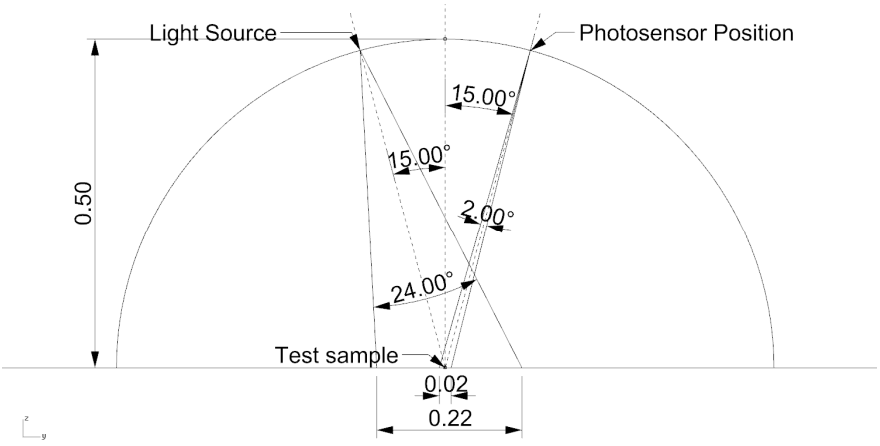


Figure 7.10: Front view shows the measuring angle (2 degrees) and the measuring area at 0.5-meter (0.0003 m^2), dimension in meter

When a light incident falls on a perfect mirror surface, the reflected light ray will be redirected with an angle of reflection that equals the angle of the incident. On the other hand, if the surface roughness is higher than zero, some of the light rays will be diffused or redirected with different angles. Figure 7.11 illustrates the law of reflection and the possible method of light reflection from a surface, which is, specular, diffuse, and spread reflection.

When measuring the reflectivity from the normal reflection angle, the angle of the photosensor must be set at the opposite angle of the light source position, as shown in Figure 7.12. The

schematic drawing in Figure 7.13 and the photographs in Figure 7.14 illustrate the setting of a light source and the photosensor with 75-degree and -75-degree altitude, respectively.

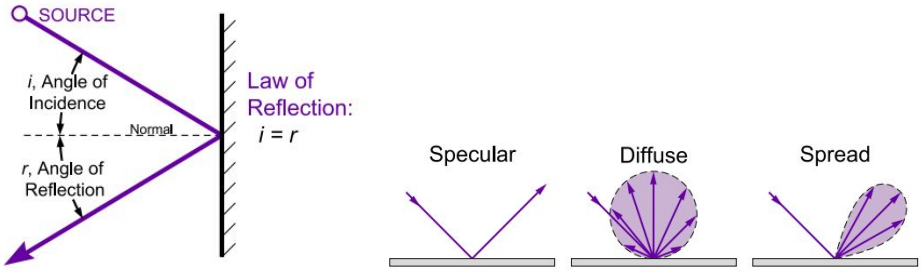


Figure 7.11: Law of reflection (left), and specular, diffuse, and spread reflection from a surface (right) (Ryer 1997) pp. 13

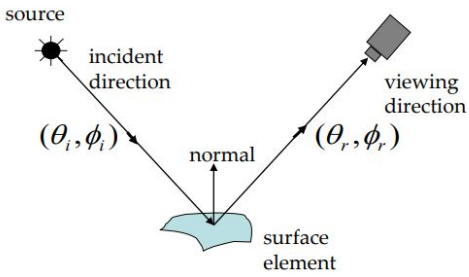


Figure 7.12: Basic principles of surface reflectance (Nayar et al., 2009)

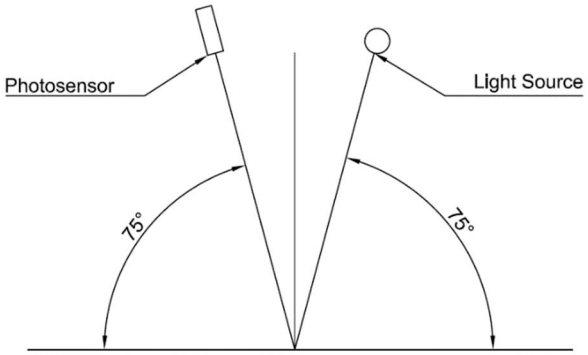


Figure 7.13: Setting of the angle between the light source and the photosensor of the GPM (Author)

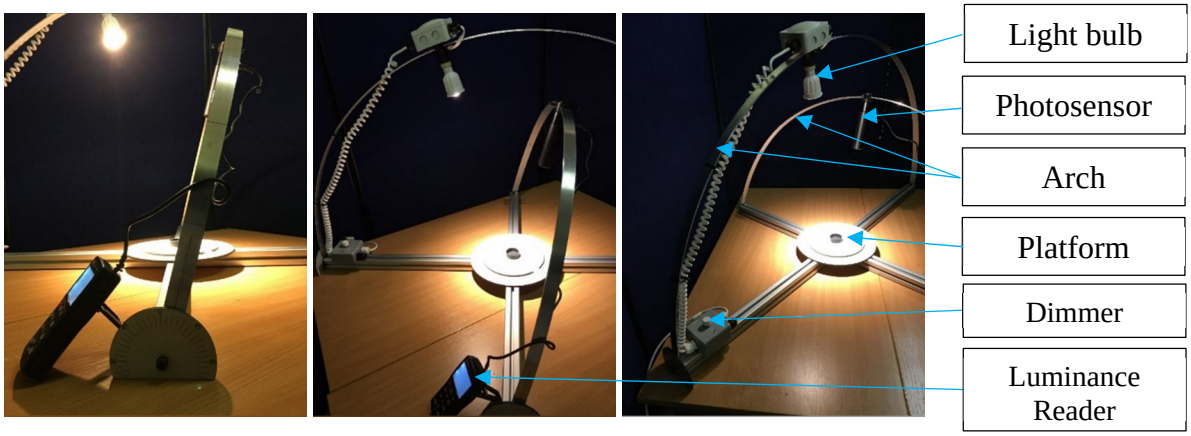


Figure 7.14: Photo of luminance measurement, the GPM is set on a 15-degree

7.1.2.3. Measurements of materials reflectance

Measurement of materials reflectance conducted in a laboratory by a goniophotometer (GPM) was designed and built for this purpose. The purpose of the reflectivity study under the GPM was to measure the reflectance values of the materials that were used in the prototype-scale model. Therefore, the outputs of the experimental tests and the computer model results can be adequately validated. It is worth mentioning that all the tested materials were applied on flat surfaces, including the materials of DRD. The materials names and their codes are shown in Table 7.2.

Table 7.2: The materials were tested utilising the Goniophotometer.

Material	Abbreviation
Goniophotometer Platform	GPF
Black light-Calibration Card	BCD
White light-Calibration Card	WCD
Grey (18%) light-Calibration Card	GCD
Black Fabric	BFC
White gloss film	WGS
White matt film	WMT
Black matt film	BMT
White HIPS	WHP
Mirror HIPS	MHP

The materials tested in this experiment include the materials of the daylight system materials, the room materials, and the materials used for calibration purposes. The daylight system was tested with two types of materials, namely, White HIPS and Mirror HIPS. The room materials include a white gloss film, a white matt film, and a black matt film. The white-gloss film was applied to the ceiling, and the white-matt film was applied to the floor and interior walls. The black matt film was then applied for the external surfaces except for the exterior ground, which had a white matt film. The purpose of applying a black matt film was to prevent the light penetration through the model except for the tested opening area.

In order to measure the reflectance of the materials, the tilt angle of the photosensor arch was set mirrored to the angle of the light source. The setting of the goniophotometer for the normal reflectance angle is shown in Figure 7.15. The set angles were 15 and -15 degrees for the light source and the photosensor, respectively. This setting provides an ideal angle to measure the amount of reflected luminance by the normal reflection angle (Nayar et al., 2009).

Furthermore, the platform was covered with black fabric to minimise the reflection of the light, which may lead to inaccurate results. That could occur due to the reflected light coming from the context surfaces. The workflow of the experimental setup for the reflectance measurements inside the laboratory was shown previously in the flow chart in Figure 7.9. It shows the experimental procedure and the necessary steps to increase the accuracy of the test results.



Figure 7.15: The setting of the goniophotometer for the normal reflectance angle

7.1.2.4. Calibration of lux meters

However, the illuminance meters were calibrated and certified by professionals from RS Components Ltd; it was worth calibrating them before conducting the daylight study. The GPM is a valuable tool to calibrate the illuminance meter because of its constant controlled light source. In addition, the distance and the angle between the light source and the test light meter can be set accurately.

Prior to the experiment of the daylight study by the prototype-scale model, four-lux meters were calibrated under the GPM, which can be considered a controlled artificial solar simulator. Each lux meter was given a name based on its position on the model, specifically, LM1 for test point-1 (Z1), LM2 for test point-2 (Z2), LM3 for test point-3 (Z3), and LM4 for test point-4 (Z4). Before the calibration, the workbench and the platform of the GPM were covered with a matt-black fabric to absorb any reflected light that may increase the reading of the illuminance.

A lux meter per test was installed in the middle of the GPM platform. It was guaranteed that all the lux meters were located on the same test point in the centre of the GPM platform. The light source was positioned perpendicular to the light sensor (elevation angle is 0 degree from the surface normal). The dimmer of the lightbulb was set to maximum, which should produce

900 lumens. The distance between the light sensor and the light source was 0.5 meter, as shown in Figure 7.10.

Based on the light source's luminous flux (lumen) and the distance between the light source and the tested surface, the illuminance at the test surface should equal 3600 lux. The accuracy of the lux meter measurement is higher with a lower measurement range; therefore, the first calibration of the lux meters was conducted at a range of 4000-lux.

Later, the lux meters were tested at another three lux ranges, namely, 40 lux, 400 lux and 40 Klux. Figure 7.16 shows the installation of the illuminance meters and the setting of the light source angle. Twenty readings of lux values have been recorded at each lux range, five readings by each meter. The mean of the five readings lux values was calculated for each lux meter. Furthermore, the standard deviation, the relative uncertainty, and the per cent uncertainty were obtained.

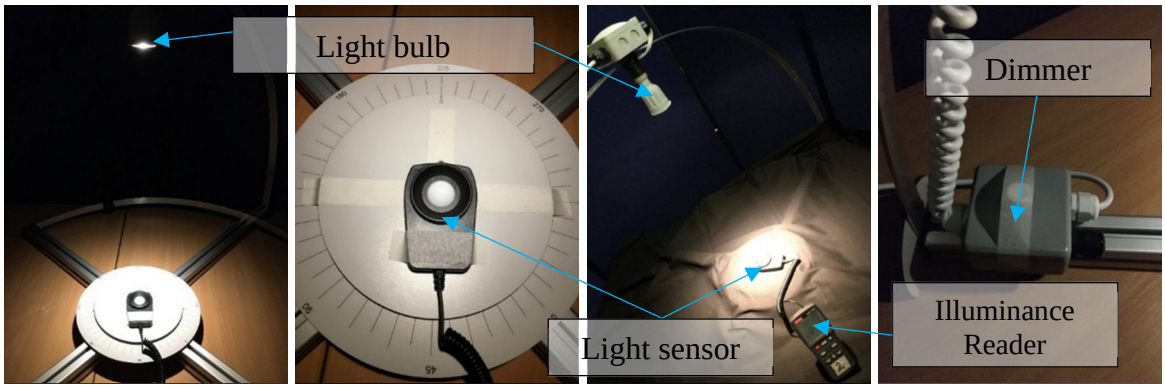


Figure 7.16: The installation of the illuminance meters and the setting of the light source angle

7.2. Results

The results of calibration and measurements are shown in the three sections below. The results include the outputs of the luminance calibration, the materials reflectance measurements and the lux meters calibration.

7.2.1. Results of luminance-meter calibration

The measurement has been recorded for ten minutes for each reading. The luminance meter can provide the average recorded value for the measurement period. The luminance value has been measured three times, and the average values of the results were calculated.

The difference between the three average luminance readings (Δ) was calculated using the following formula:

$$\Delta\,(\%)\ = \frac{(\max L - \min L) \div \ \text{mean}\ L}{100}$$

Equation 22

where L is the illuminance value

7.2.1.1. Measuring angle accuracy

In order to check the accuracy of the measuring angle of the luminance meter, which is 2 degrees, as stated in the instruction manual, the luminance was measured at a small object. The surface area of the test sample is 0.001 m^2. It has a black-matt material, as shown in Figure 7.15. Later, the luminance was measured at the GPM platform surface before adding the test sample to find the variance between the two-luminance measurements.

It was found that the luminance meter could read the luminance value with the two-degree angle. The luminance values were 1,726 cd/m^2, whereas after placing the small test sample on the centre of the platform, the luminance was only 159 cd/m^2, as shown in the chart in Figure 7.17.

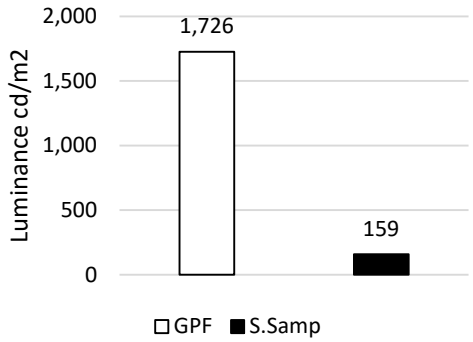


Figure 7.17: Comparison of luminance emitted by the small sample and by the GPM platform surface.

7.2.1.2. Calibration of the luminance meter by 18%-reflectance-grey card

The results of the luminance meter calibration are shown in the chart in fig. The average luminance was measured for a period of 10 minutes. The reading was done three times. The mean of the three-luminance readings was calculated. It was found that the luminance at the 18%-reflectance-grey card was ranging from 1,220 to 1,310 cd/m^2, and the average was 1,258 cd/m^2, as shown in Figure 7.18.

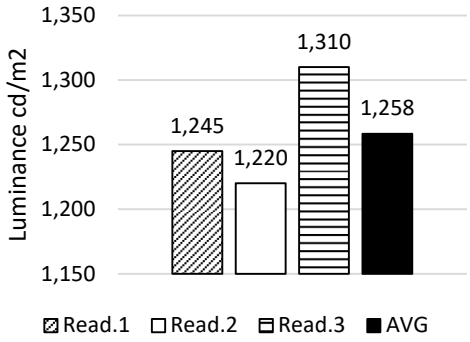


Figure 7.18: Measured luminance at the 18%-Reflectance-Grey Card

The chart in Figure 7.19 shows the typical reflectance of the 18%-reflectance-grey card, which is 0.18. It illustrates a comparison of the calculated reflectance for the same card, based on the measured luminance shown previously in Figure 7.18. It can be seen that the average of the calculated reflectance and the typical reflectance were similar.

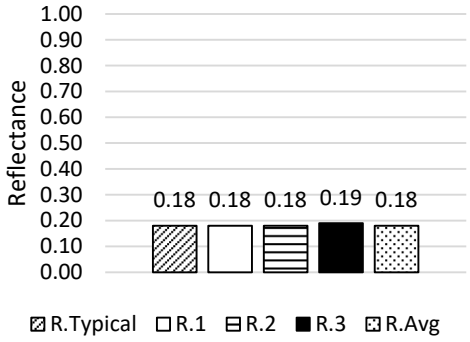


Figure 7.19: Comparison of the typical and the calculated reflectance of the 18%-Reflectance-Grey Card

7.2.1.3. The influence of the black-matt fabric on the luminance measurement

In order to reduce the light reflection from surrounding surfaces, the platform of the GPM was covered with black-matt fabric, as shown in Figure 7.15. The effect of adding the fabric is presented in the chart in Figure 7.20.

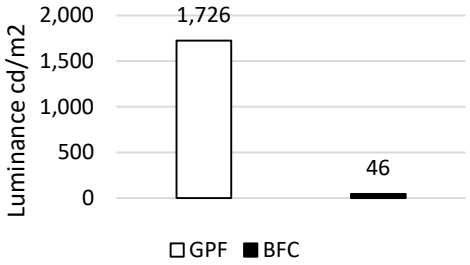


Figure 7.20: Luminance emitted by the GPM platform surface without and with the black-matt fabric

7.2.2. Results of materials reflectance measurements

The reflectance factor of the physical model materials was calculated based on the luminance measurements. The materials include the materials of the room and the materials of the daylight-redirecting devices (DRDs).

The reflectance of the applied materials in the interior and the exterior of the room were measured. Three types of materials were measured, namely, white-gloss film (WGS), white-matt film (WMT), and black-matt film (BMT). The chart in Figure 7.21 shows the luminance values for the three tested materials. It was found that the WGF emitted the highest luminance at 5,730 cd/m^{2}and the lowest was by the BMT at 1,589 cd/m^2. The luminance was increased by 64% by WMT compared to WGS and by 43% by BMT compared to WMT. The increase was 2,085 cd/m^2 and 2,058 cd/m^2, respectively.

The reflectance factor for the three materials, namely, WGS, WMT and BMT, were calculated from the measured luminance in Figure 7.21 (right) based on Equation 19. It was found that the calculated reflectance factors were 0.82, 0.53, and 0.23 for the WGS, WMT, and BMT, respectively. On the other hand, the typical reflectance factors for the applied materials, which were applied in the computer modelling, were 0.80, 0.50, and 0.20 for the WGS, WMT, and WMT, respectively. The calculated reflectance value was higher than the typical value by 2%, 3%, and 3% for the WGS, WMT, and WMT, respectively, as shown in Figure 7.21 (left).

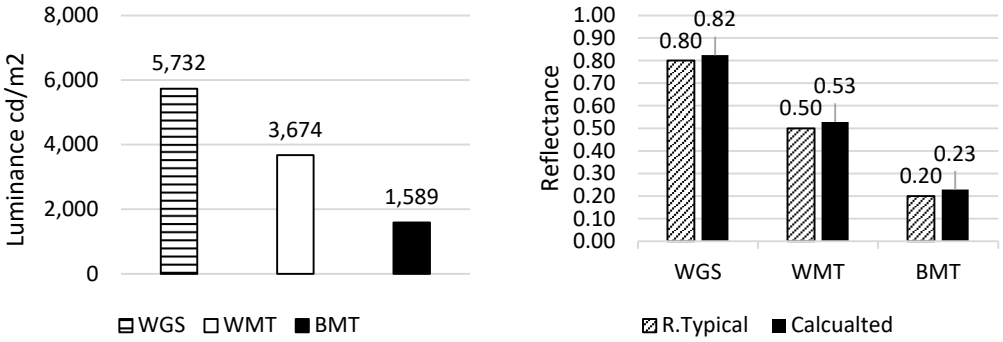


Figure 7.21: Measured luminance of room materials (left), and typical and calculated reflectance (right)

Two types of High Impact Polystyrene material (HIPS Plastic Sheets) were applied for the DRDs, namely, White-Gloss HIPS and Mirror HIPS. The luminance at the two surfaces is shown in Figure 7.22 (right).

The reflectance factor was calculated based on the measured luminance using Equation 19. The calculated reflectance values were compared with the typical reflectance value of the materials. The calculated reflectance was found to be 0.89 and 0.97, while the typical reflectance is 0.90

and 0.98 for WHP and MHP. The calculated reflectance was lower than the typical reflectance by 1% for both materials, as shown in Figure 7.22 (left).

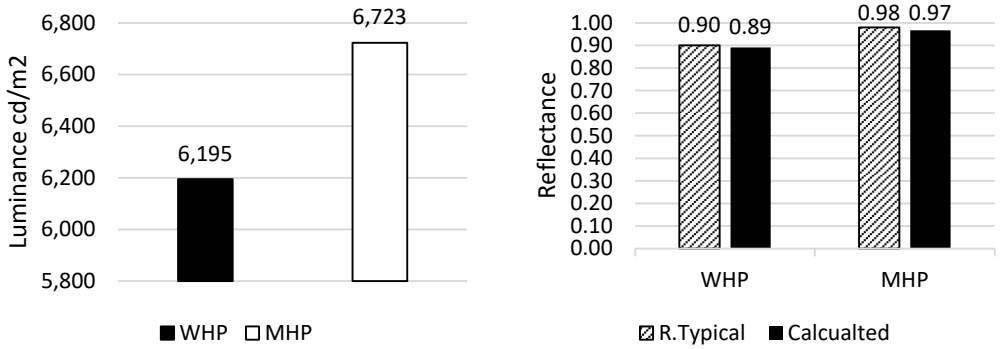


Figure 7.22: Measured luminance of DRD (left), and typical and calculated reflectance (right)

7.2.3. Results of illuminance-meters calibration

The results of the lux meter calibration by the RS Components LTD are shown in the tables from Table 7.3 to Table 7.6. The measurement uncertainty of the lux meters at range 40 lux was between ± 0.37 to ± 0.38 lux + 1 LSD. At range 400 lux, it was from ±3.2 to ±3.3 lux + 1 LSD. At a range of 4,000 lux, two values were applied. The first value was low, from 138 to 139.8 lux, while the second value was high, from 1623 to 1644 lux. The uncertainty with the low applied value was ±3.3 lux + 1 LSD. The uncertainty with the high-applied value was from ±38 to ±39 lux + 1 LSD. Finally, the uncertainty for the 40 Klux was from ±0.39 to ±0.40 Klux + 1 LSD.

Table 7.3: Calibration results of lux meter-1 (LM1) by RS Components LTD.

Serial No	Device Number	Range		Applied Value	Instrument Reading		Measurement Uncertainties	
180606976	LM1	40	lux	15.54	15.67	±	0.37	lux + 1 LSD
		400	lux	139.8	140.7	±	3.3	lux + 1 LSD
		4000	lux	139.8	151	±	3.3	lux + 1 LSD
		4000	lux	1643	1649	±	39	lux + 1 LSD
		40	Klux	16.63	16.88	±	0.40	Klux + 1 LSD

Table 7.4: Calibration results of lux meter-2 (LM2) by RS Components LTD.

Serial No	Device Number	Range		Applied Value	Instrument Reading		Measurement Uncertainties	
180607001	LM2	40	lux	15.30	15.12	±	0.37	lux + 1 LSD
		400	lux	139.0	135.7	±	3.3	lux + 1 LSD
		4000	lux	139.0	157	±	3.3	lux + 1 LSD
		4000	lux	1635	1604	±	38	lux + 1 LSD
		40	Klux	16.48	16.36	±	0.39	Klux + 1 LSD

Table 7.5: Calibration results of lux meter-3 (LM3) by RS Components LTD.

Serial No	Device Number	Range		Applied Value	Instrument Reading		Measurement Uncertainties	
180607095	LM3	40	lux	15.49	15.42	±	0.37	lux + 1 LSD
		400	lux	138.0	139.6	±	3.2	lux + 1 LSD
		4000	lux	138.0	151	±	3.3	lux + 1 LSD
		4000	lux	1644	1645	±	39	lux + 1 LSD
		40	Klux	16.51	16.37	±	0.39	Klux + 1 LSD

Table 7.6: Calibration results of lux meter-4 (LM4) by RS Components LTD.

Serial No	Device Number	Range		Applied Value	Instrument Reading		Measurement Uncertainties	
180607118	LM4	40	lux	15.67	15.47	±	0.38	lux + 1 LSD
		400	lux	138.4	138.6	±	3.2	lux + 1 LSD
		4000	lux	138.4	137	±	3.3	lux + 1 LSD
		4000	lux	1623	1633	±	38	lux + 1 LSD
		40	Klux	16.54	16.87	±	0.40	Klux + 1 LSD

Another calibration for the illuminance meters was conducted by the GPM. The lux meters were tested at four ranges: 40 lux, 400 lux, 4,000 lux and 40 Klux. The applied value of the light source was 900 lumens for the range 4,000 lux and 40 Klux. On the other hand, the lumen was reduced for the range 40 lux and 400 lux as the maximum reading range is lower than the full lumen of the light source/ as the full lumen of the light source exceeded the maximum reading range. The distance between the light sensor and light source was 50 cm and the angle between them was 90 degrees.

The outputs of the calibration tests are shown in the tables from Table 7.7 to Table 7.10. Generally, it was found that the lux meters recorded a low per cent uncertainty at all the reading ranges. The highest per cent uncertainty among the reading ranges was at range 40 Klux that ranged from 0.5 to 1.6. On the other hand, the lowest was at the range 400 lux that ranged from 0.04 to 0.27. However, at the range 40 lux, LM3 and LM4 recorded 0.0 per cent uncertainty.

Table 7.7: Calibration of the Lux meters by the GPM at range 40 lux.

	Meter 1	Meter 2	Meter 3	Meter 4
Minimum (lux)	8.78	8.83	9	9
Maximum (lux)	9.01	9.04	9	9
Mean (lux)	8.90	8.935	9	9
Standard Deviation	0.16	0.15	0.00	0.00
Standard Error	0.08	0.07	0.00	0.00
Standard Deviation	0.16	0.15	0.00	0.00
Relative Uncertainty	0.12	0.11	0.00	0.00
Percent Uncertainty	1.29	1.18	0.00	0.00

Table 7.8: Calibration of Lux meters LM2 by the GPM at range 400 lux.

	Meter 1	Meter 2	Meter 3	Meter 4
Minimum (lux)	337.5	327.6	343.2	373.3
Maximum (lux)	335.7	326.2	343.5	373.8
Mean (lux)	336.6	326.9	343.35	373.55
Standard Deviation	1.27	0.99	0.21	0.35
Standard Error	0.64	0.49	0.11	0.18
Standard Deviation	1.27	0.99	0.21	0.35
Relative Uncertainty	0.90	0.70	0.15	0.25
Percent Uncertainty	0.27	0.21	0.04	0.07

Table 7.9: Calibration of Lux meters LM2 by the GPM at range 4000 lux.

	Meter 1	Meter 2	Meter 3	Meter 4
Minimum (lux)	3451	3384	3532	3580
Maximum (lux)	3495	3424	3556	3597
Mean (lux)	3473	3404	3544	3588.5
Standard Deviation	31.11	28.28	16.97	12.02
Standard Error	15.56	14.14	8.49	6.01
Standard Deviation	31.11	28.28	16.97	12.02
Relative Uncertainty	22	20	12	9
Percent Uncertainty	0.6	0.6	0.3	0.2

Table 7.10: Calibration of Lux meters LM2 by the GPM at range 40 Klux.

	Meter 1	Meter 2	Meter 3	Meter 4
Minimum (Klux)	9.31	9.14	9.39	9.41
Maximum (Klux)	9.61	9.36	9.49	9.51
Mean (Klux)	9.46	9.25	9.44	9.46
Standard Deviation	0.21	0.16	0.07	0.07
Standard Error	0.11	0.08	0.04	0.04
Standard Deviation	0.21	0.16	0.07	0.07
Relative Uncertainty	0.15	0.11	0.05	0.05
Percent Uncertainty	1.6	1.2	0.5	0.5

7.3. Fabrication of the rig

In order to minimise the parallax error, the size of the physical model was limited to 20% of the size of the available sky simulator. The sky simulator is a half-sphere that has a 5-meter diameter. Therefore, the physical model was built on a scale of 1:10 to meet the recommendation of the physical models for lighting tests. The tested rig consists of three main parts: the room, the solar perforated screen (PSS), and the daylight-redirecting devices (DRDs). The specifications of the model elements are given in Table 7.11 and Table 7.12. The fabrication procedure of each part is explained in detail below.

7.3.1. Fabrication of the room

The drawings of the room are shown in Figure 7.23. The room elements were modelled using medium-density fibreboards (MDF) with 10 mm thickness. In order to obtain the desired

reflectivity for the interior surface, they were painted with white primer (see Figure 7.24 [A]); however, it was found that the surface roughness is relatively high; hence, the desired reflectivity was not achieved. Therefore, the interior surface was polished with sandpaper (see Figure 7.24 [B]). Then, two types of vinyl film were applied on the interior surfaces, matt-white for the walls and gloss-white for the ceiling. In addition, the exterior surfaces were improved by applying a black-matt vinyl film to prevent daylight from accessing the room through the room envelop, as shown in Figure 7.25 and Figure 7.26.

Table 7.11: Dimensions of the main elements of the model (mm)

Component	Height	Width	Depth/Thickness
Room	270	300	800
DRD	10	20	25
PSS	270	300	2

Table 7.12: Components of the model

Component	Material	Details
Floor	Wood	800 x 300 X 10 mm
Roof	Wood	800 x 300 X 10 mm
DRD	Plastic (HIPS)	2 mm thickness
Perforated screen	Wood	300 X 270 X 2 mm
Back Wall	Wood	300 x 270 X 10 mm
Side Walls	Wood	800 x 270 X 10 mm

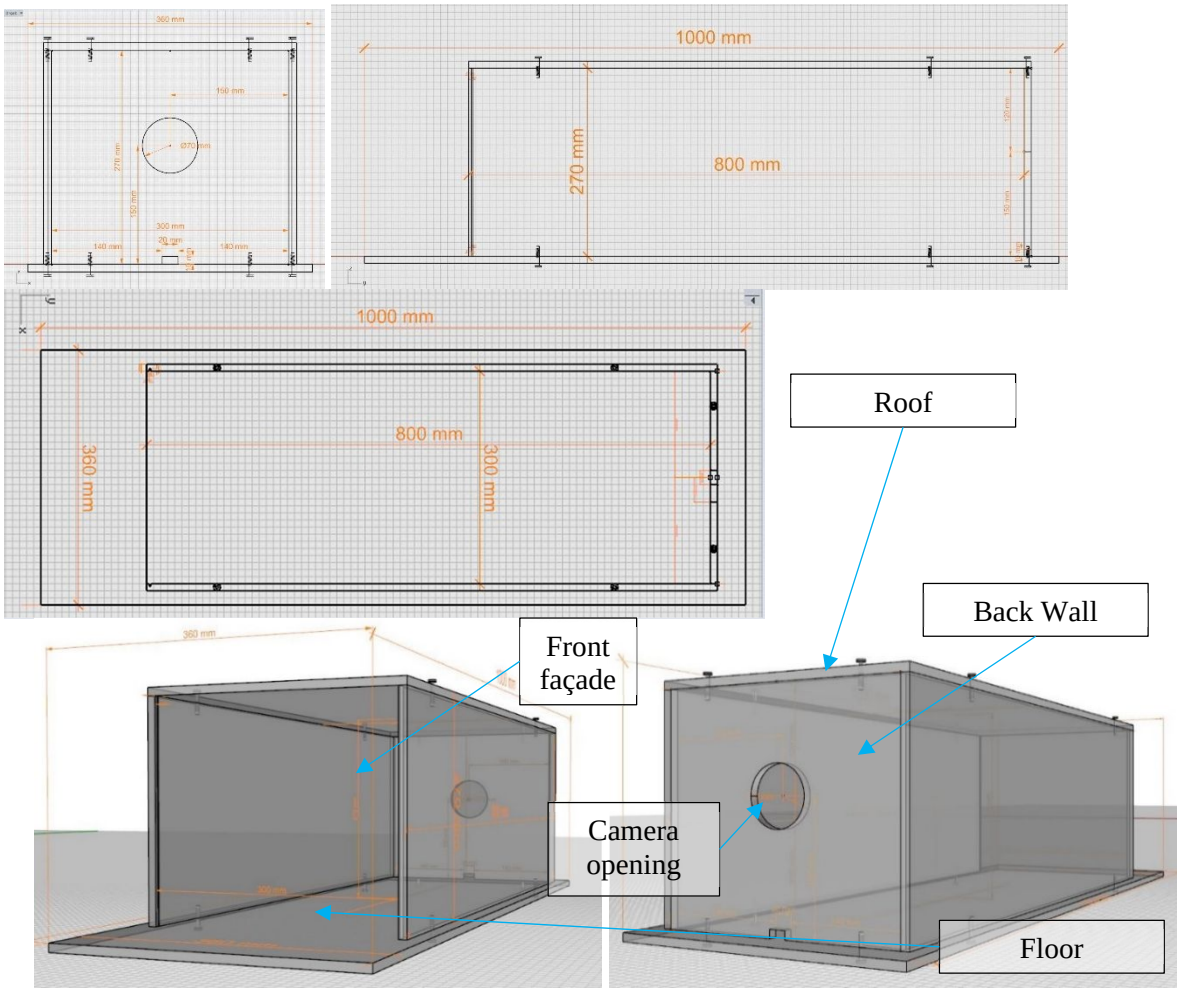
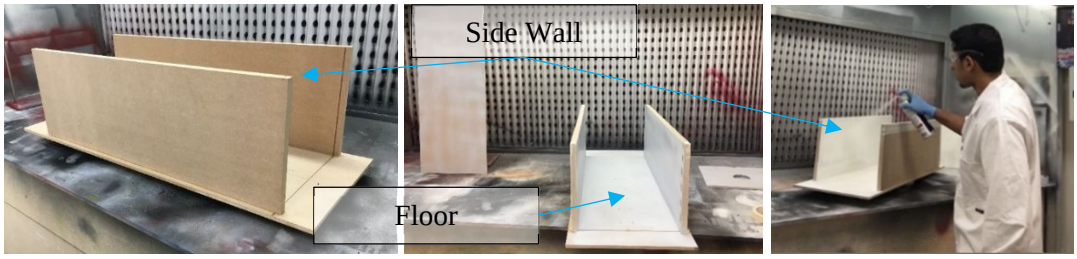


Figure 7.23: Front view (top left), side view (top right), floor plan (middle) of the room, and 3D views (below)



[A]



[B]

Figure 7.24: Coating (A) and polishing (B) of the model interior surfaces

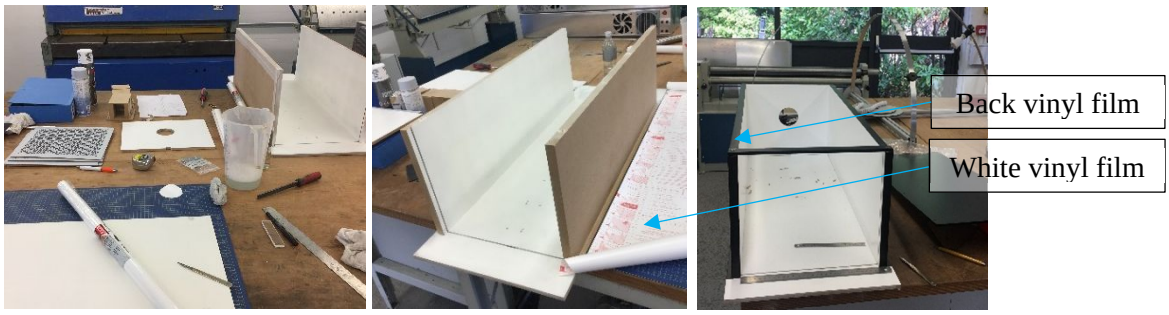


Figure 7.25: Apply vinyl film on the room surfaces

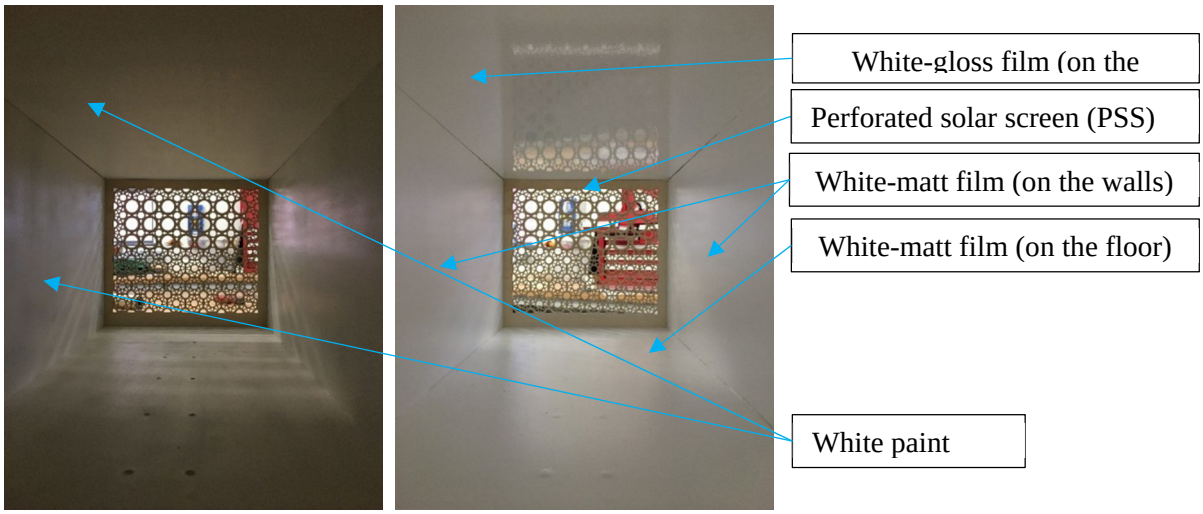


Figure 7.26: The interior of the room painted with white primer (left) and with vinyl film (right)

7.3.2. Fabrication of the PSS

The PSS is made from a 2mm thick wooden board. It was drawn in AutoCAD, and then it was cut by Hobarts laser-cut machine. This method is chosen for its accuracy and flexibility, as shown in Figure 7.27. The PSS size is 3m in width X 2.7m in height. It has painted with three layers of filler-primer paint, and then it was painted with three layers of acrylic paint. The purpose of the painting was to prevent daylight access through the PSS material, as shown in Figure 7.27. The PSS is inserted inside an engraving made in the sidewalls, the floor, and the ceiling. The purpose of the grooves was to avoid any daylight infiltration between the PSS and the room geometry, as illustrated in Figure 7.29. An exterior and interior view of the PSS are illustrated in Figure 7.30.

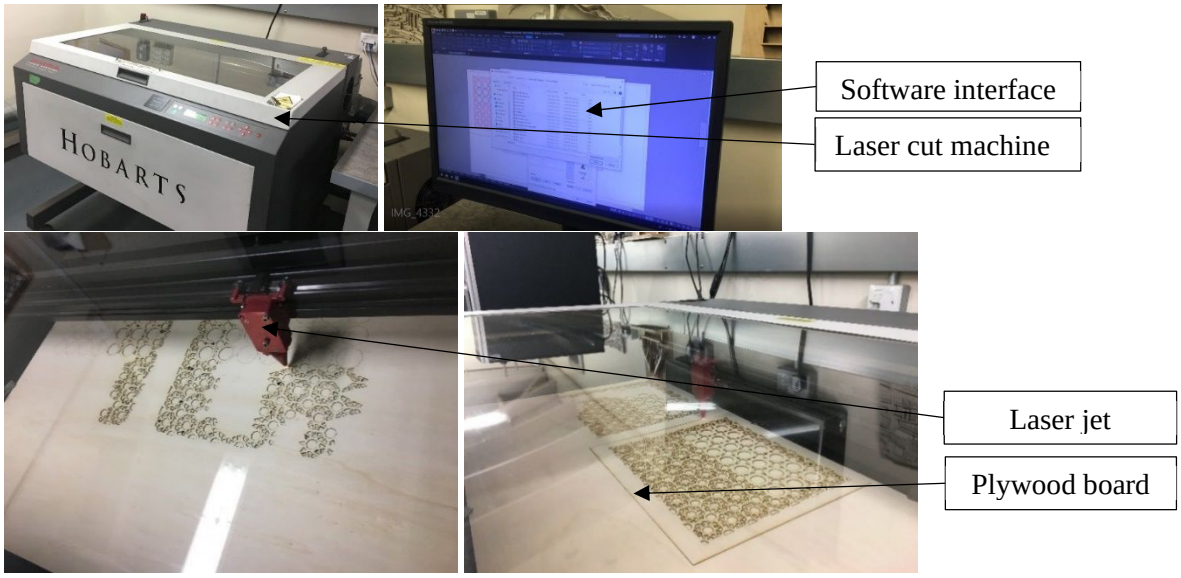


Figure 7.27: Fabrication of the PSS by a laser cut machine using AutoCAD

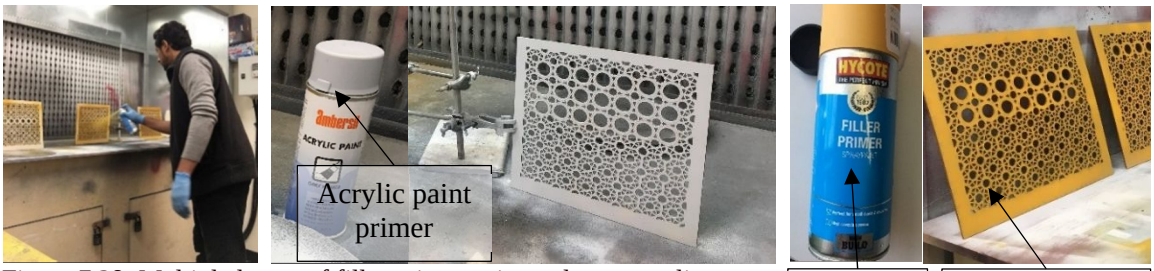


Figure 7.28: Multiple layers of filler primer paint and grey acrylic spray

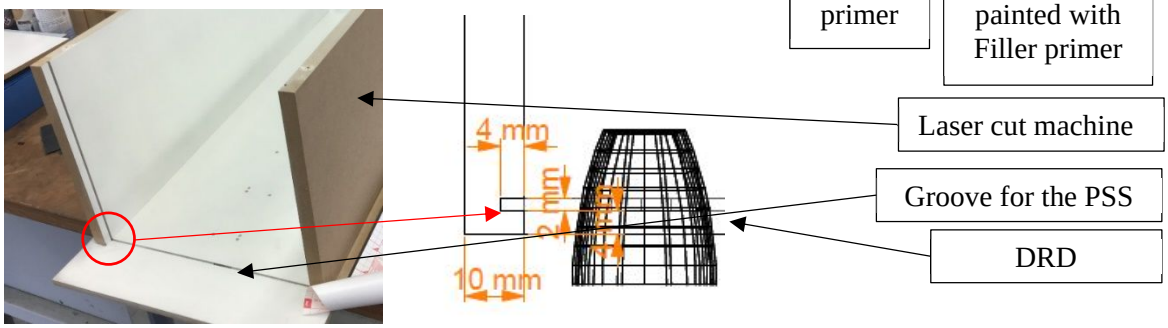


Figure 7.29: Groove in the wall to insert the PSS (bottom, left) and thickness of perforated screen (bottom, right), exterior view (left) and interior view (right)

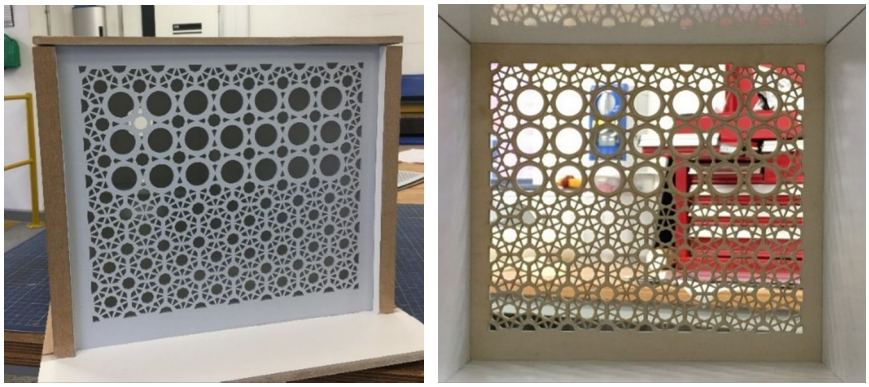


Figure 7.30: Exterior (left) and interior (right) of the PSS

7.3.3. Fabrication of the DRD

The first fabricated DRD was made of a lightweight material (Pearl white PLA material with 2.85 mm diameter) by means of a 3D printer (Ultimaker 3). This method was used to benefit from its flexibility and accuracy of modelling physical objects freely with lightweight, as shown in Figure 7.31 and Figure 7.32.

It was assumed that the surface of the 3D-printed DRD would be proper to be utilised without an additional enhancement. However, it was found that the inner surface roughness of the DRD exceeded the desirable limit. Therefore, a sanding process was made to meet the desirable roughness. Therefore, the interior of DRD was sanded with different sandpaper to reduce the surface roughness. That process was conducted to match the optical properties of the DRD material applied previously in the computer modelling.

In order to test the impact of DRD's material on the daylight performance, the DRDs were coated with a mirror-effect-spray paint. It was found that the mirror effect was achieved after the painting immediately, however, it was faded once it was dried after a short period, as presented in Figure 7.33 (A).

Thus, the second method was to apply aluminium foil paper on the interior of the DRD. However, again it was found that the optical properties of the aluminium foil were changed when it was applied on the concave surface of the DRD, as presented in Figure 7.33 (B). Consequently, to achieve the desired optical properties of the DRD inner surface, it was fabricated by the 3D printer but with an alternative method.

The proposed method was to apply a HIPs material over the negative mould of the DRD using a vacuuming machine. It was found that the resistance of the DRD was insufficient to maintain the original geometry. As a result, the formed DRD with the HIP material was bent. That was due to the insufficient resistance of the 3D-printed DRD against the heat that was applied by the vacuuming machine, as seen in Figure 7.34.

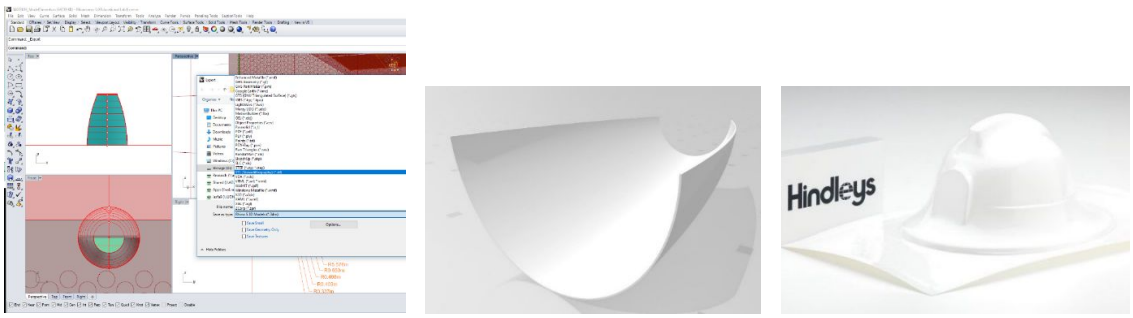


Figure 7.31: Rhinoceros interface (left), the exported STL file in Ultimaker[3] software (middle) and HIPS material (right)

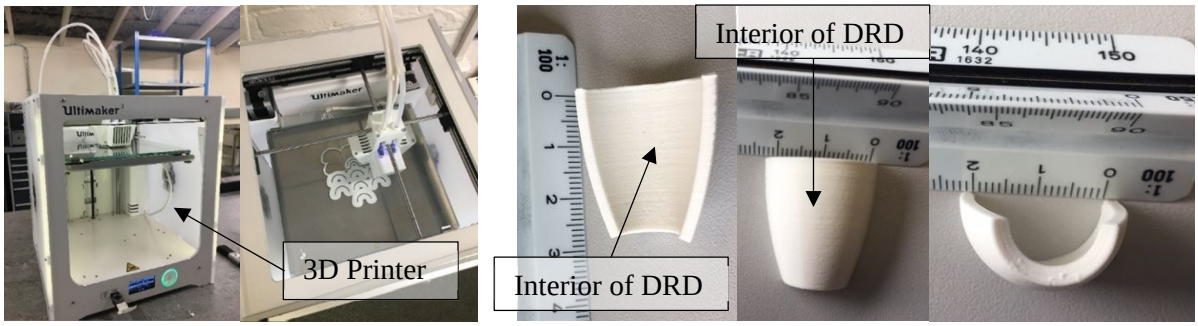
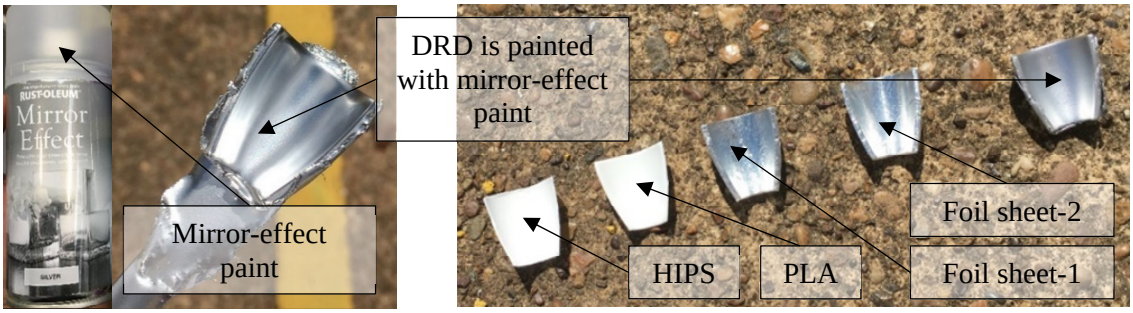


Figure 7.32: 3D-Printing process of the DRD units (left), and the fabricated DRD (right)



[A] [B]

Figure 7.33: Mirror effect paint (A), DRDs with different coatings, from left to right, HIPS, PLA, foil sheet-1, foil sheet-2, and mirror-effect paint (B)

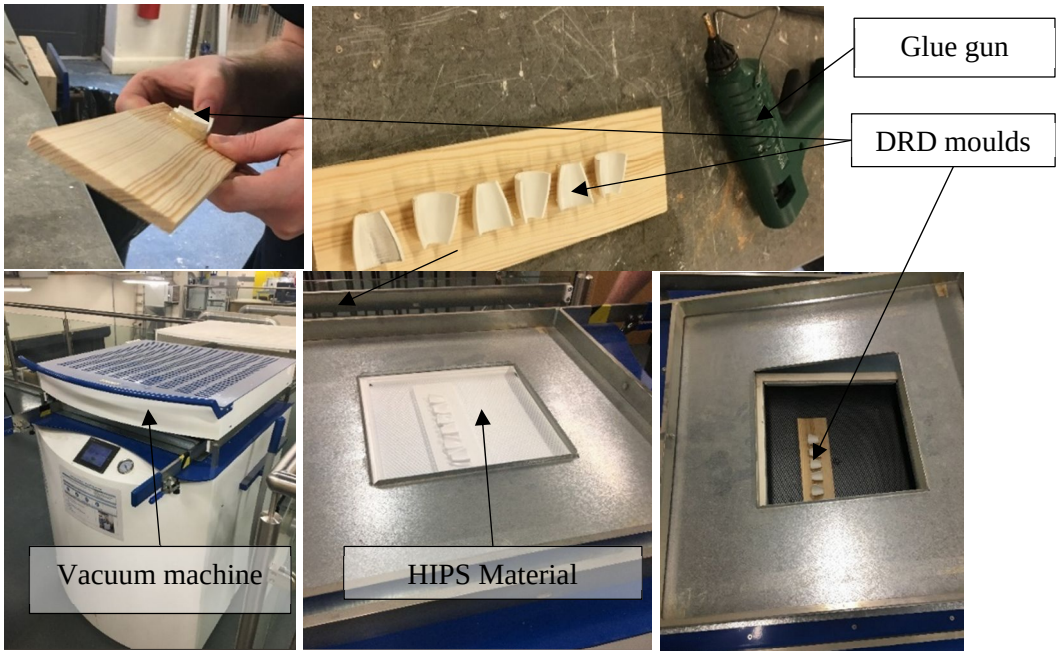


Figure 7.34: Forming HIPs on negative DRD mould by the Vacuum machine

A positive mould of the DRD interior was made by the 3D printer instead of the hollow DRD (the negative mould), as shown in Figure 7.35. Then, the DRD was formed by applying a high impact material (HIPS) inside a vacuum machine (Formech 686 Vacuum Former). This method

allowed achieving the desirable reflectance by applying a HIPS material with the required optical properties.

It was found that the HIPs material was bent at the end of the DRD mould, which changes the final product of the DRD geometry. Therefore, the positive DRD mould was improved by adding an extra length, as shown in Figure 7.36. The extra material aims to ensure that the HIPs sheet is formed precisely overall the DRD. Later, the extra parts of the HIP material were removed.

In order to enhance the interior surface of the DRD, the mould was painted with three layers of filler primer, as shown in Figure 7.36. The purpose was to reduce the roughness of the mould as the 3D printer produces relatively high rough surfaces. The vacuuming process and the formed DRD devices are shown in Figure 7.37.



Figure 7.35: Positive moulds of DRD made by the 3D printer (left). DRD sanding before the vacuuming (right)

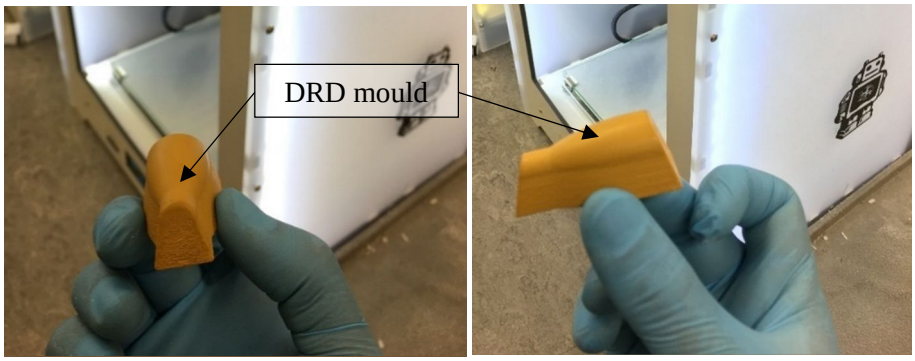


Figure 7.36: The enhanced positive DRD mould

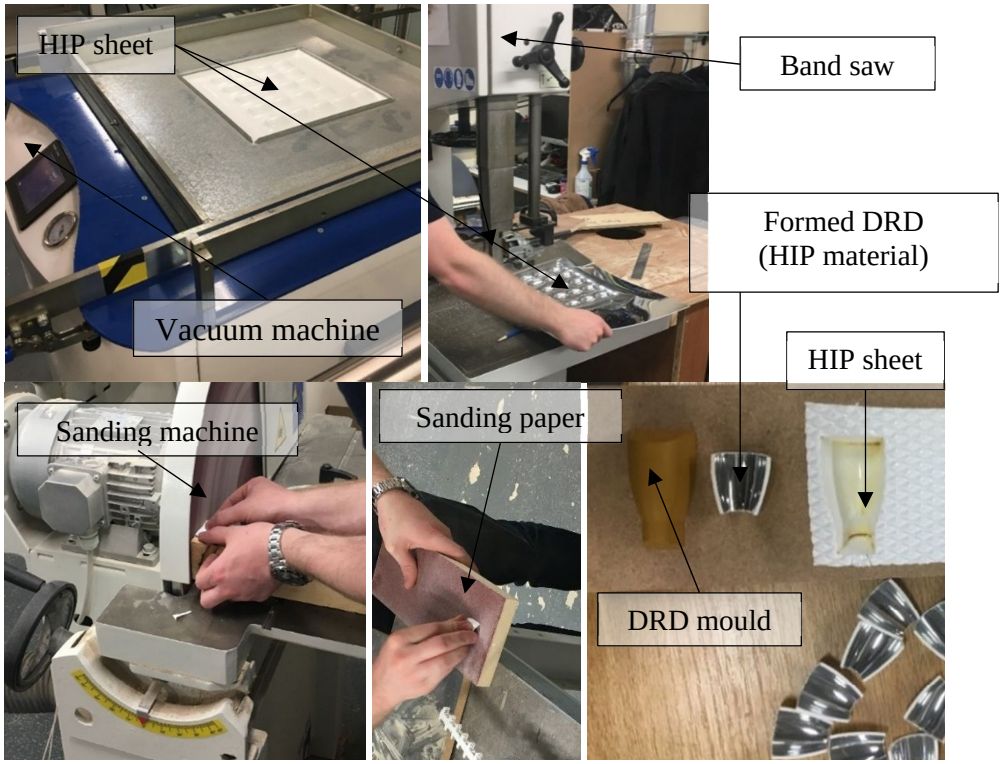


Figure 7.37: Vacuuming and finishing of the HIP sheet on the positive mould of the DRD

In order to ensure that the DRDs are positioned accurately within the PSS, flat objects were placed, as shown in Figure 7.38. The PSS was flipped where the DRDs face downwards. The wooden blocks have a height equals to the distance between the DRDs upper-row and the PSS upper-edge. The installation of the DRDs in the PSS was conducted in three stages. For each stage, the wooden objects were increased based on the height of the DRDs row.

Finally, the prismatic lenses were produced by applying a prismatic film (3M Daylight-redirecting Film) on an acrylic sheet. Then, the acrylic sheet was cut by a laser cut machine, as shown in Figure 7.39. Afterwards, the prismatic lenses were integrated into the DRD.

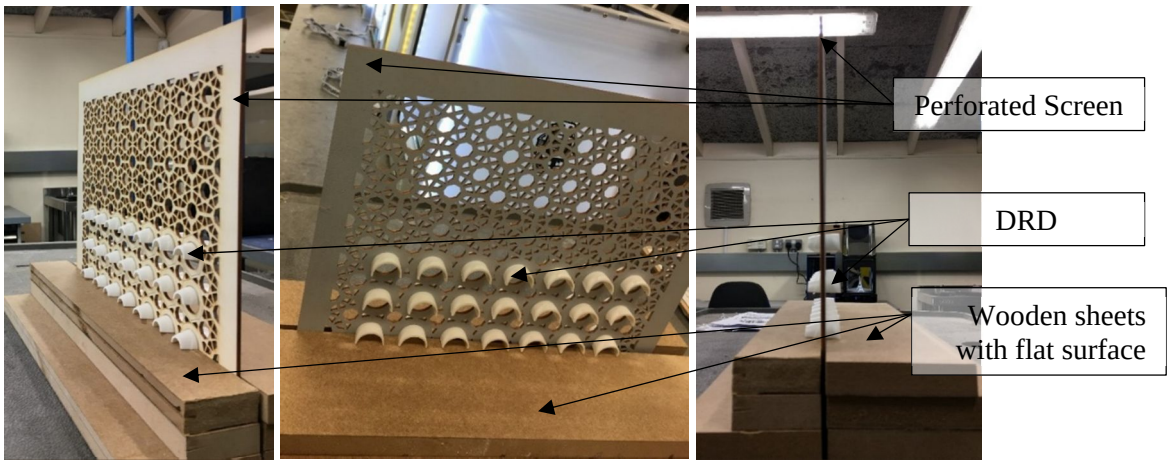


Figure 7.38: The installation of the DRDs within the PSS

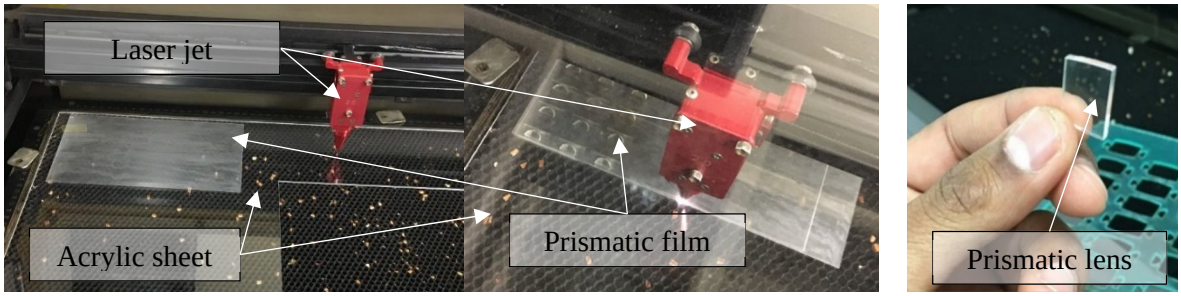


Figure 7.39: The cutting process by the laser-cut machine (left) and prism lens (right)

7.4. Daylight measurement tools

Four single-point Illuminance meters (RS PRO ILM1335 Light Meter [Calibrated]) were utilised to measure the illuminance level at the work plane. The illuminance meter that was used in the experiment is shown in Figure 7.40. A luminance meter (Commercial name) was used to measure the luminance value at the ceiling level in the middle of the room. The meters are calibrated and come with a calibration certificate, as mentioned previously in this chapter.



Figure 7.40: Single-point illuminance meter (uk.rs-online.com)

The connection sequence of the lux measurement is shown in Figure 7.41. When the light falls on the light sensor, it records the lux value and transfers it to the lux meter-reading screen through cable. Later, the data was transferred to the computer. The light sensors were installed as described previously in section 5.2.3 on page 95 above. The distance between each sensor is 2 meters. The distance from the façade and Z1 is one meter as well as between Z4 and the rear wall, as illustrated in Figure 7.42.

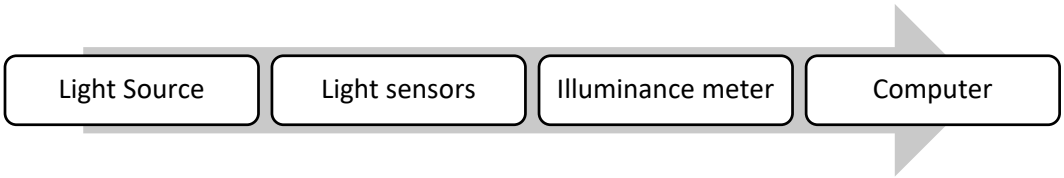


Figure 7.41: Connection sequence of the measurement equipment

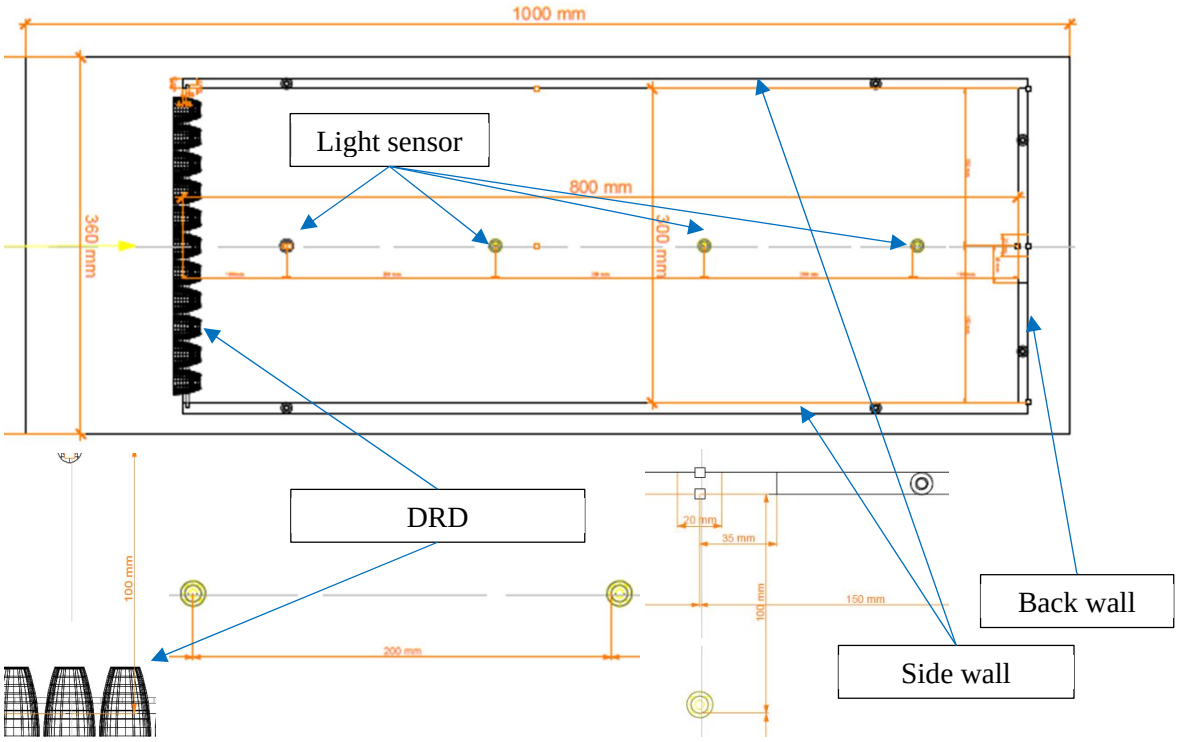


Figure 7.42: Floor plan (top) and details drawing (below) of the model show the light sensors position

Four wooden bases were fabricated that represent the office desks. The height of the desk is 0.76 m from the floor level. The light sensors of the lux meters were installed on these desks. Each desk has a hole to install the light sensor above it, stabilised by a screw. The stabilisation of the light sensor position is critical to ensure that all the illuminance readings are taken from the same point. The photos in Figure 7.43 illustrate the procedure of the light sensor installation. The desks were painted with black-matt paint to reduce the reflectance of their surfaces. On the other hand, the photosensor of the luminance meter was installed at the floor level by a screw from the bottom of the model.

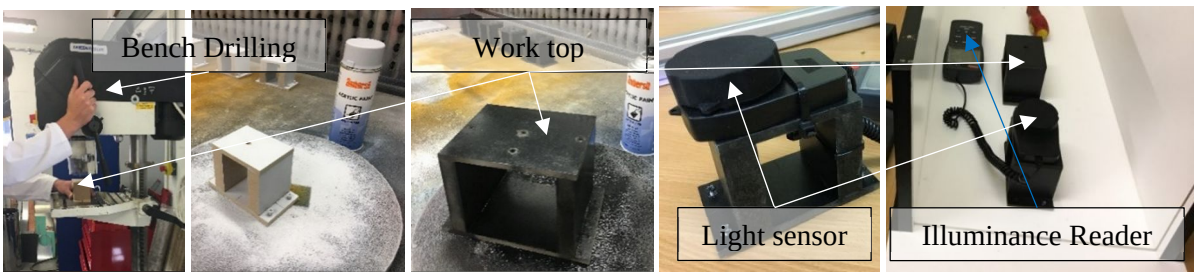


Figure 7.43: Installation of light sensors inside the model

The daylight performance inside the physical prototype was tested through three methods: under a direct-light simulator (DRLS), a diffuse-light simulator (DFLS), and a real sky (RSK). The flowchart in 7.44 shows the proposed procedure that was followed during these tests. The outputs of the tests are presented in Chapters 8 to 10.

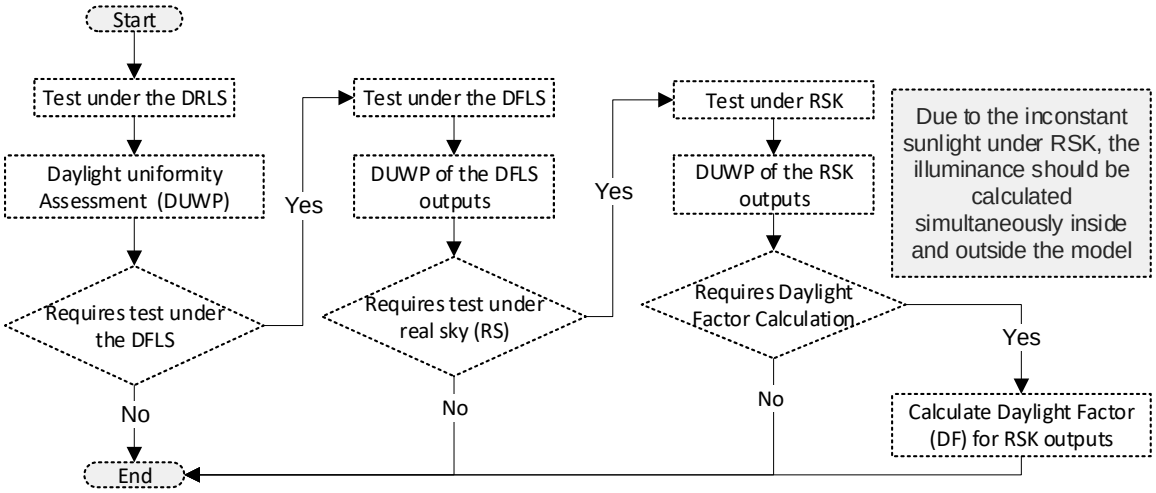


Figure 7.44: Flowchart of DRLS, DFLS and RSK daylight tests

Chapter 8. Test under the direct-light simulator

This chapter describes the procedure followed for the daylight experimental arrangement which was performed inside a laboratory at the Faculty of Engineering, the University of Nottingham, United Kingdom. It is conducted under a direct-light solar simulator (DRLS) that consists of four light bulbs arranged in grid order.

The purpose of the experimental study was to assess the effect of a number of parameters on the daylight performance inside the prototype-scale model under direct sunlight. The experiment was conducted for two locations in two different days of the year. The first location was Riyadh city, Saudi Arabia, and the second location was Nottingham city, UK. The two locations represent the low and the high latitude regions.

8.1. Procedure

8.1.1. Location and time

The first location (Riyadh city) was described previously in Chapter 5. The second location, Nottingham city, United Kingdom, has a latitude of 52.95 north and a longitude of 1.15 west. The highest sun altitude at solar noon in Nottingham is 60.50 degrees in summer solstice (21 June), and the lowest is 13.68 degrees in winter solstice (21 December) while it is 37.58 degrees in the equinoxes (21 September and 21st March).

The tests were conducted at conditions simulating solar noon for both locations, where the sun azimuth is 180 degrees on the south façade. Riyadh city test was conducted on 21 June, where the solar altitude is 88 degrees, while the Nottingham city test was conducted on 21 October, where the solar altitude is 26^{o}.

8.1.2. Test Process

The flowchart in Figure 8.1 shows the procedure of the daylight test. The test starts by setting up the tilt angle of the solar simulator and the turntable to meet the desirable solar altitude. Then, the orientation of the turntable is set for the required azimuth angle. Later, the model is placed above the turntable and the sample screen is inserted. The environment of the laboratory is well controlled so it prevents any other light source infiltration.

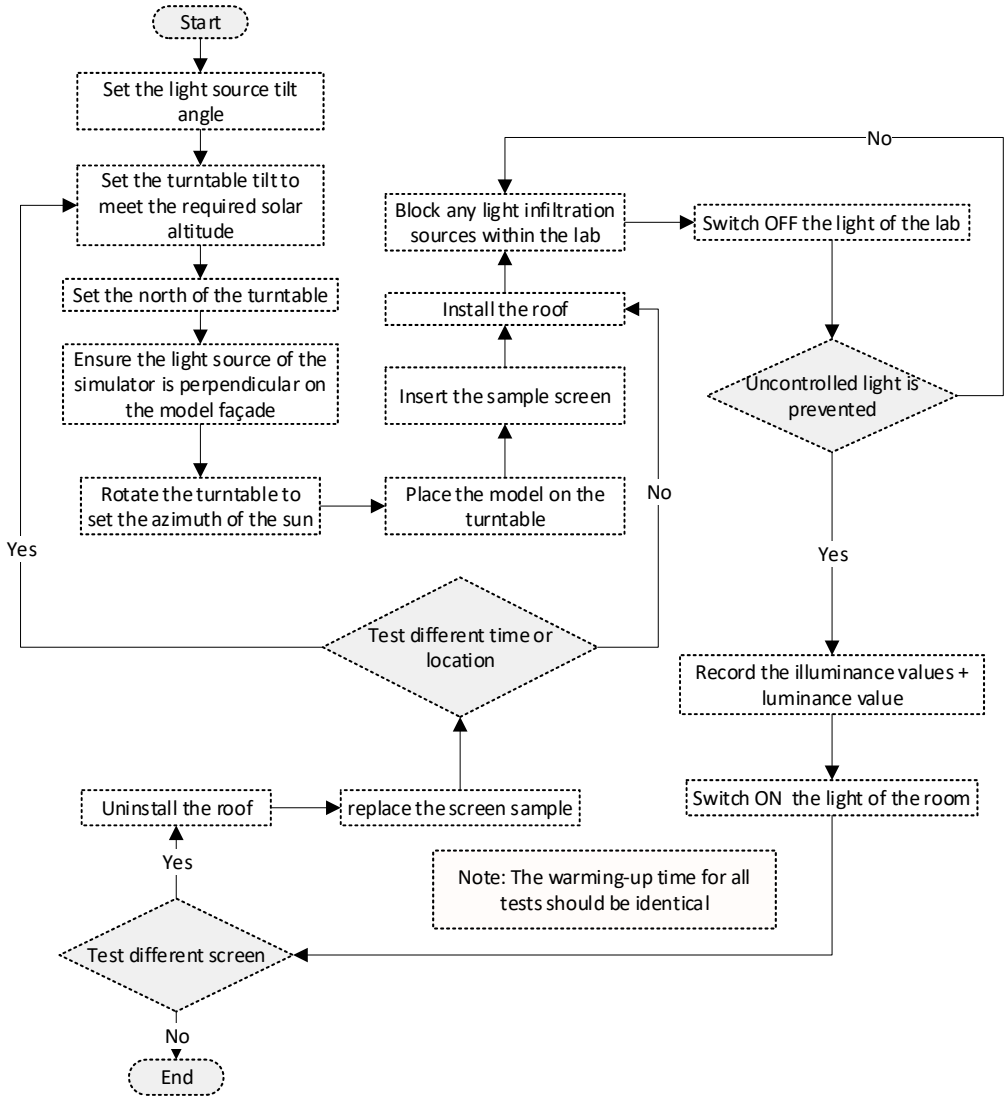


Figure 8.1**:** Flowchart of the daylight tests procedure

8.1.3. The uniformity of the light source

The simulator uses a light bulb that produces an 18,000 lumen with 8500-Kelvin colour temperature as presented in Table 8.1 and Figure 8.2. In order to achieve a uniform light source, the distance between the solar simulator and the prototype-scale model was determined based on the 1:5 rule. According to Bodart et al. (2006), to minimise the parallax error, the maximum dimension of the prototype-scale model must not exceed one-fifth of the sky dome diameter. Since the dimensions of the prototype-scale model are 300 mm × 300 mm 800 ×mm, the sky dome diameter should be at least 4,000 mm, five times the longest side of the model. As a result, the distance between the centre of the model and the light source must be at least 2,000 mm.

The sky dome diameter can be obtained as follows:

$$\text{Sky dome diameter (D)} \geq 5 \times \text{Longest side of the model}$$

Equation 23

$$D \geq 5 \times 800 \text{ mm}$$

$$D \geq 4{,}000 \text{ mm}$$

The horizontal distance (H) between the centre of the model and the light source

$$H = \text{Sky dome diameter (D)} / 2$$

Equation 24

$$H = 4{,}000 \text{ mm}/2$$

$$H = 2{,}000 \text{ mm}$$

Table 8.1: The specifications of the light bulb used for the DRLS (Lamp, 2018)

Power	250 Watt
Base	GY9.5 (2-Pin Prefocus)
Colour temperature	8500 Kelvin
Light output	18,000 Lumens
Type	MSD 250/2 30H



Figure 8.2: The light bulb used for the DRLS

8.1.4. The setting of the solar altitude and azimuth

To simplify the process and the fabrication cost, a turntable was utilised to set up the tilt of the model in order to set up the solar altitude for the high altitude location (Riyadh city), as shown in Figure 8.3 to Figure 8.6. On the other hand, for Nottingham city, the turntable was not utilised as the solar altitude was set up by adjusting the tilt of the solar simulator. The interior and the exterior of the model are shown in Figure 8.7. While the test was limited to two locations, this procedure was appropriate.

This test utilised a single light source that was positioned at the position of the sun for the test hour at the designated location. The 1:5 ratio rule mentioned previously was applied. However, it was found that the uniformity of the light was relatively uneven. Therefore, the distance

between the light source and the model was increased to enhance the light uniformity. Then, the tilt of the light source was adjusted to achieve the desired solar altitude.

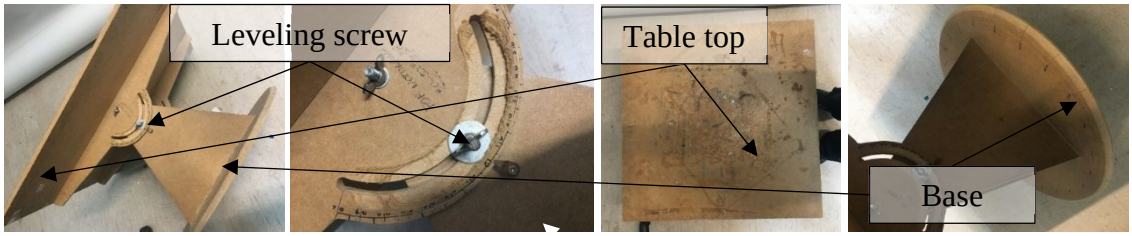


Figure 8.3: Turntable used for Riyadh city test

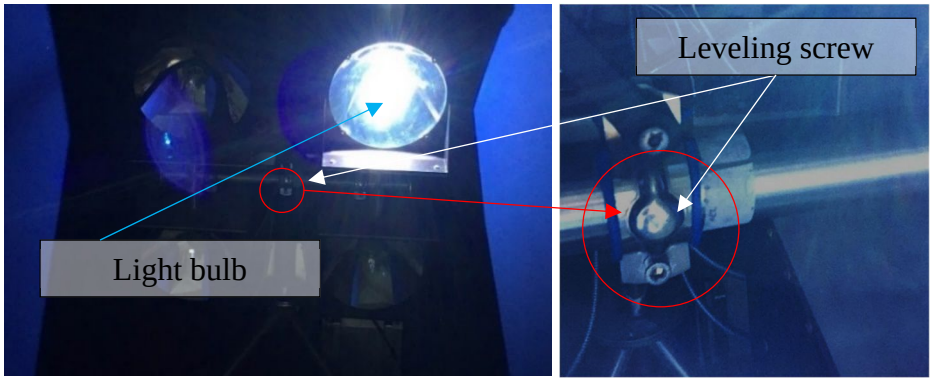


Figure 8.4: DRLS (left) and adjustable tilt angle (right)

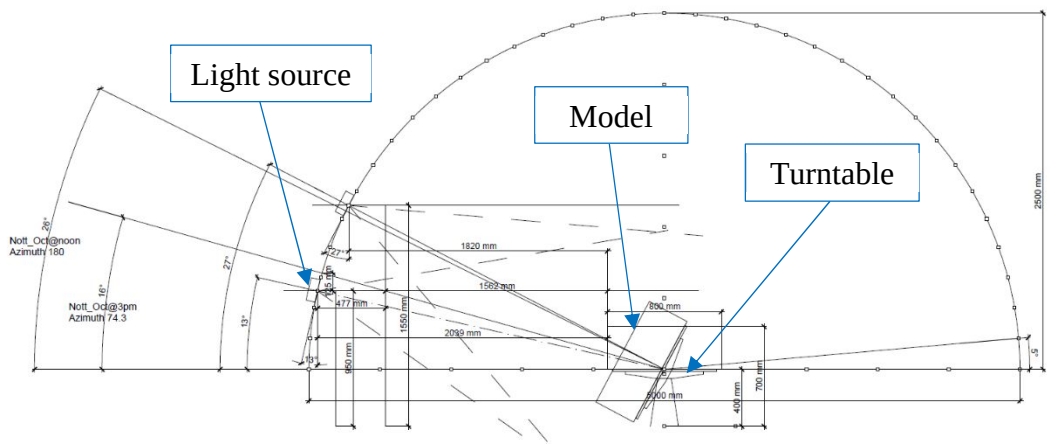


Figure 8.5: Model and sun position setup

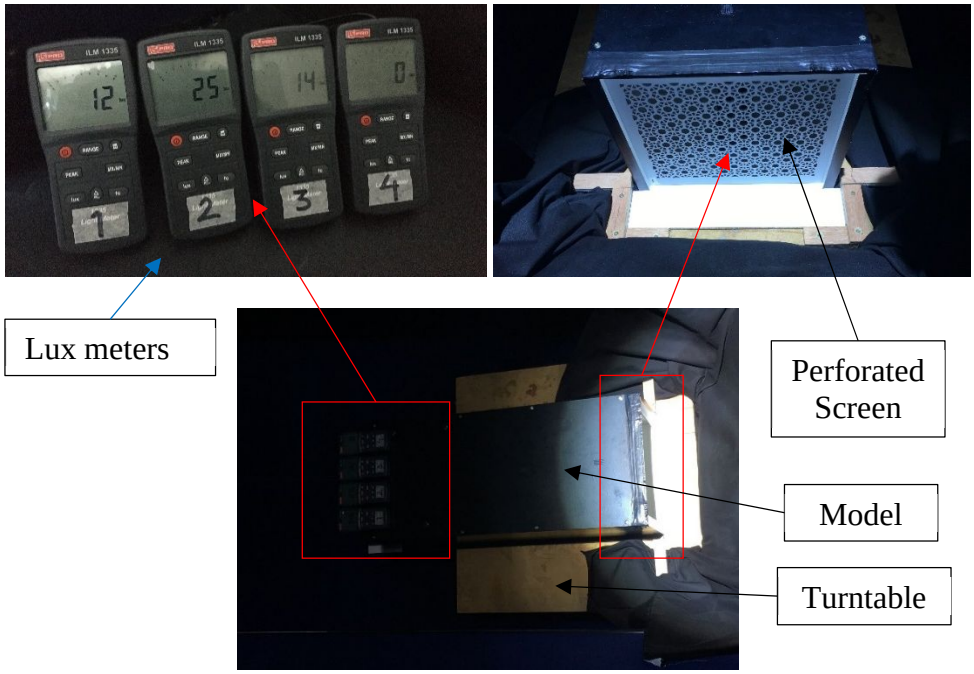


Figure 8.6: Model was set for Riyadh 21st June at solar noon

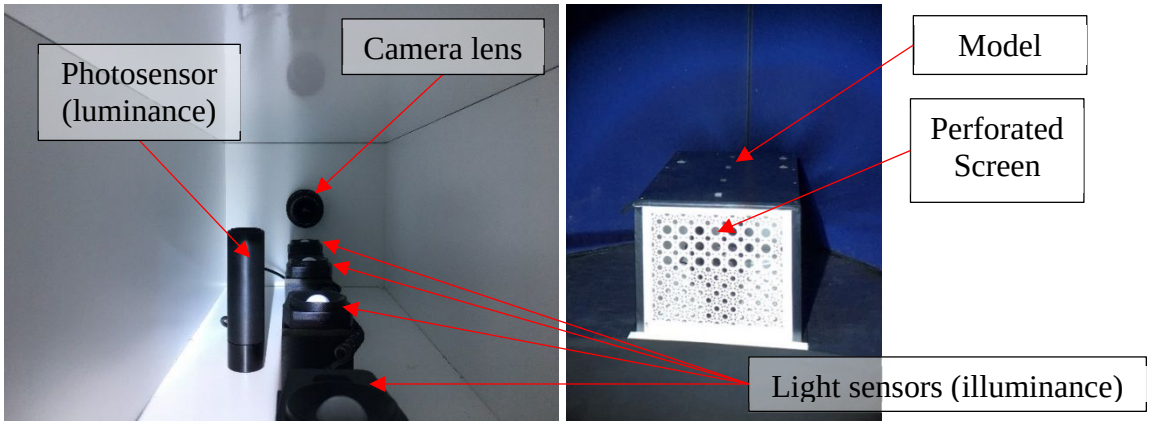


Figure 8.7: The interior (left) and the exterior (right) of the model, for Nottingham, 21 October at 12 pm

8.1.5. Elimination of the external light reflection

The effect of the light reflected by the camera lens on the illuminance was investigated. A calibration aimed to find the effect of light reflection from the lens of the camera on the illuminance level was conducted. The test was made at point 3 and it was found that the illuminance was relatively decreased by 0.07% (from 835 lux to 773 lux), as shown in Figure 8.8.

In addition, the daylight tests were conducted inside a well-controlled laboratory environment, as previously mentioned in Chapter 7. Furthermore, a matt-black fabric was applied in the ground in front of the prototype-scale model to reduce any light reflection, as shown in Figure 8.9.

Table 8.2: Conditions of the DRLS test, the dimensions in mm and degree

Distance from the light source to the prototype	Height	Lumen applied	Azimuth	Altitude
3,400	1,550	18,000	180	26

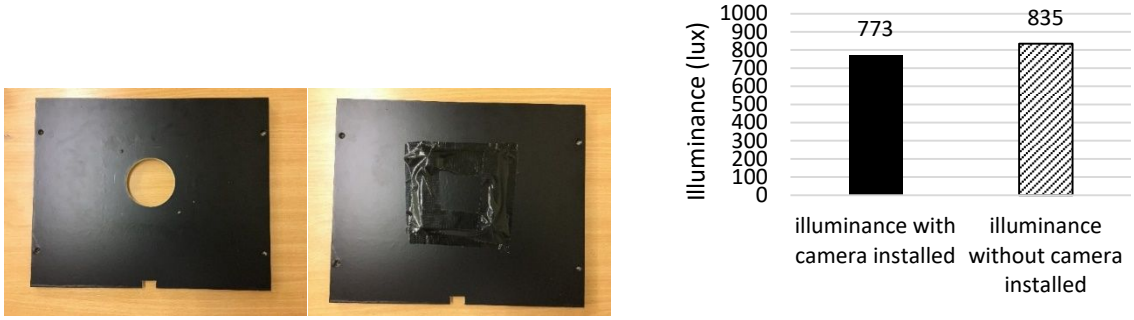


Figure 8.8: Opening for the camera (left) and the illuminance with and without the camera (right)

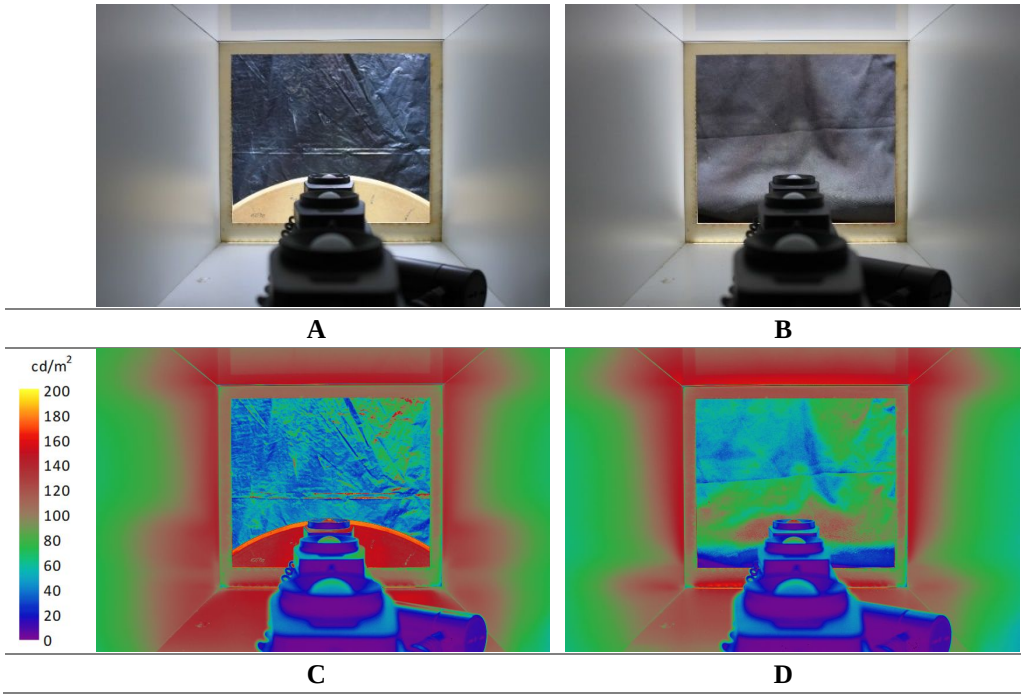


Figure 8.9: The external ground with black plastic (A) and with matt-black fabric (B), and luminance levels (C and D), for Riyadh on 21Jun at 12 pm

8.2. Investigation of daylight performance

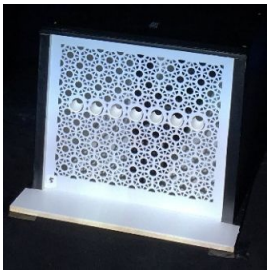
The daylight performance of the optimum perforated solar screen (PSS5) and daylight-redirection solar screen (DRSS1) were compared. Later, the effect of significant parameters of the DRD on daylight performance was investigated. The illuminance at the work plane was measured at the four daylight zones at test points Z1, Z2, Z3 and Z4. Then the DUWP was calculated based on Equation 4.

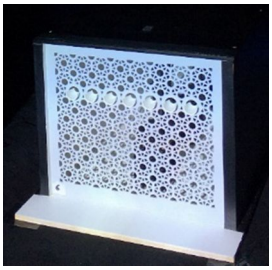
The effect of four main parameters on the daylight performance at the work plane was investigated under the direct-solar simulator. The study was conducted at solar noon for high (88º) and low (26º) solar latitudes, namely, Riyadh city and Nottingham city. The tested parameters are shown in Table 8.3, which include the vertical position of the DRDs, the DRD unit per façade area ratio, the material of the DRDs, and finally, the geometry of the DRD. Exterior views of the tested cases are shown in Figure 8.10.

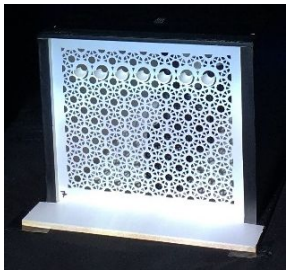
Table 8.3: Main parameters and their properties

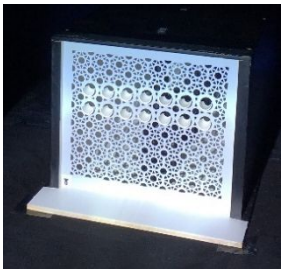
	Parameter	**Properties**	**Case**
1	Position	Low	DRSS1
		Medium	DRSS2
		High	DRSS3
2	Unit per area ratio	7 per $9m^2$	DRSS1
		14 per $9m^2$	DRSS4
		21 per $9m^2$	DRSS5
3A	Material [Parabolic]	White-Gloss HIPs	DRSS5
		Mirror HIPs	DRSS6
3B	Material [Flat]	White-Gloss HIPs	DRSS7
		Mirror HIPs	DRSS8
4A	Geometry [White-Gloss HIPs]	Parabolic	DRSS5
		Flat	DRSS7
4B	Geometry [Mirror HIPs]	Parabolic	DRSS6
		Flat	DRSS8

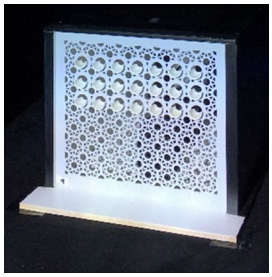

PSS5

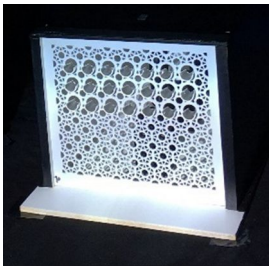

DRSS1

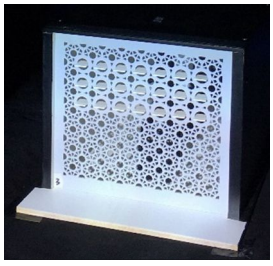

DRSS2

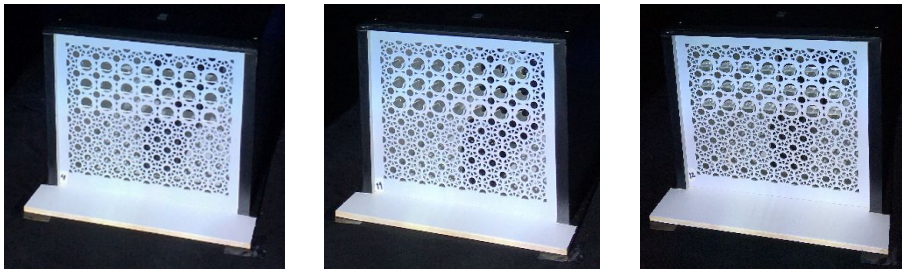

DRSS3


DRSS4


DRSS5


DRSS6


DRSS7



DRSS8 DRSS9 DRSS10

Figure 8.10: Exterior view of tested cases

8.2.1. Effect of position

The effect of the DRDs position on the daylight performance was assessed at the work plane. Three cases were tested, namely, DRSS1, DRSS2 and DRSS3. The DRDs had three height levels: low (1.55 m), middle (1.88 m), and high (2.21 m). Figure 8.11 shows the front view, top view and section of the cases.

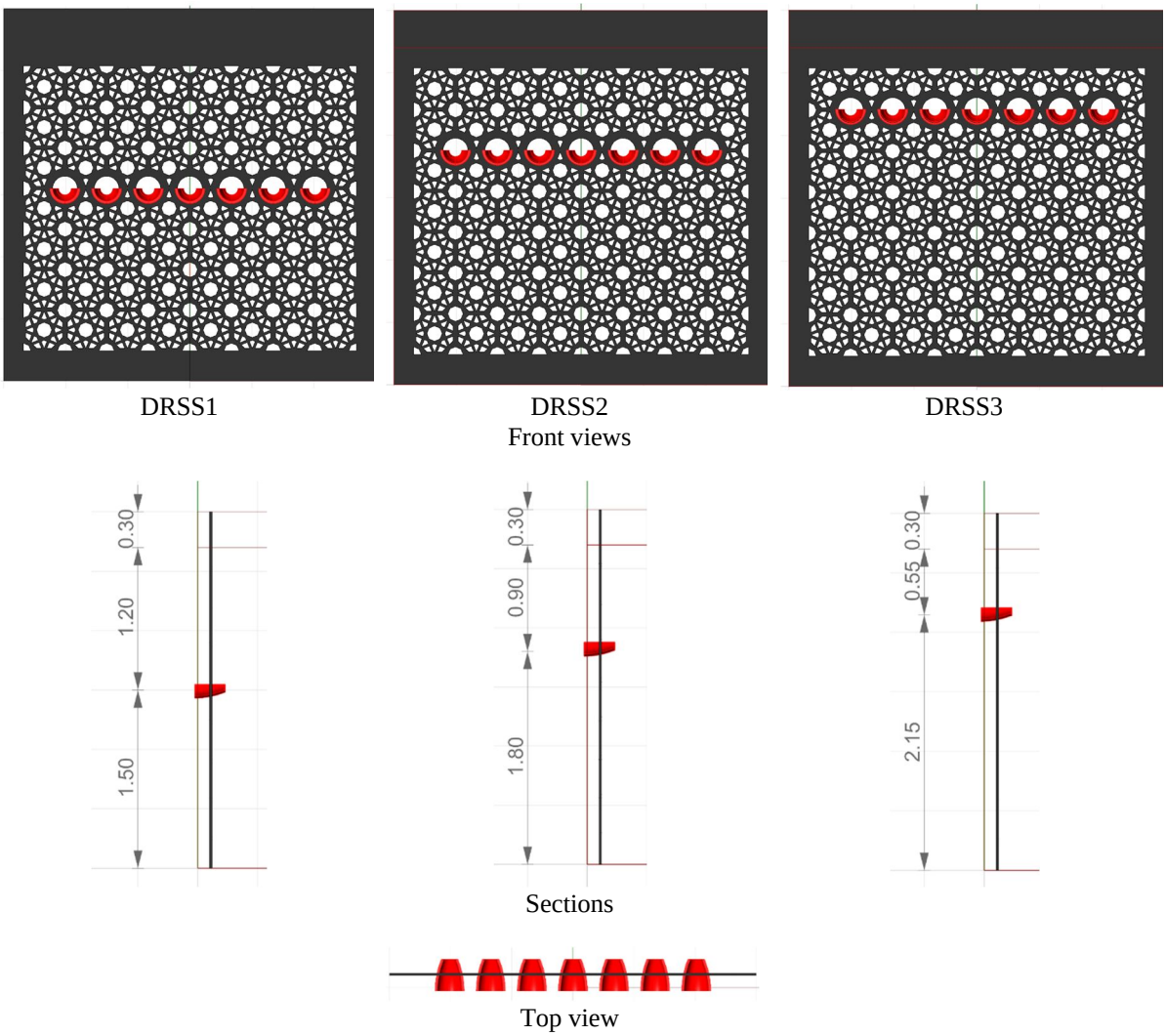


Figure 8.11: Drawings of cases DRSS1, DRSS2 and DRSS3, dimensions are in meters.

8.2.2. Effect of unit per area ratio

The effect of the DRD units per area ratio was investigated. Three cases were tested, namely DRSS1, DRSS4 and DRSS5. The tested ratios were 7-unit/8.1 m^2, 14-unit/8.1 m^2, and 21-unit/8.1 m^2. The drawings of the tested cases are shown in Figure 8.12.

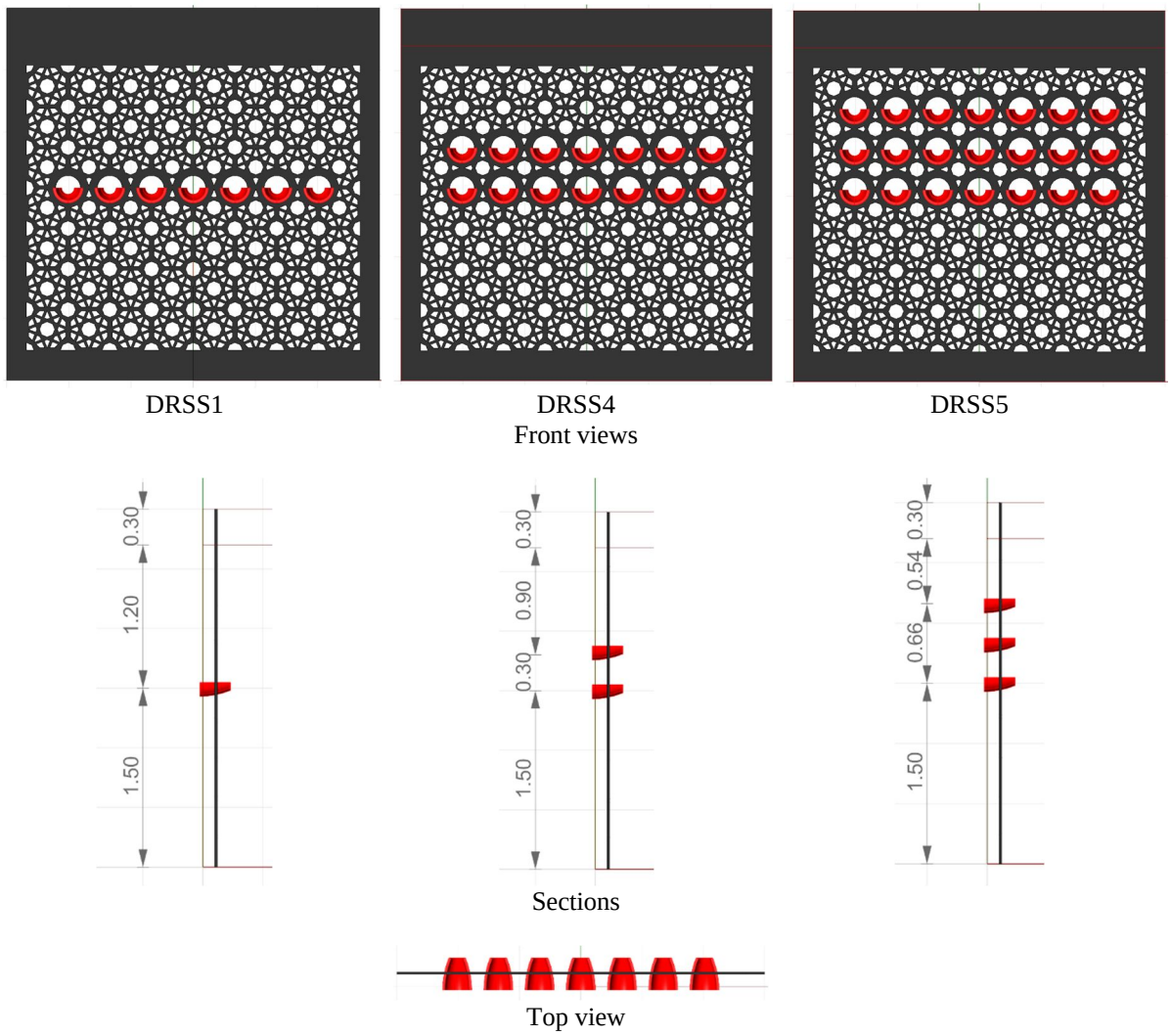


Figure 8.12: Cases DRSS1, DRSS4 and DRSS5, dimensions are in meters

8.2.3. Effect of material

The effect of the DRD interior material on daylight performance was investigated. It was tested with the proposed concave device and with a flat surface. Two types of materials were tested: white-gloss HIPS (DRSS5) and mirror HIPS (DRSS6). The daylight performance of the two cases was compared with PSS5. In addition, the same materials were applied on a flat surface and their effect on the daylight performance was investigated.

8.2.4. Effect of geometry

The effect of the DRDs geometry on the daylight performance was tested for four cases. Case DRSS5 and DRSS7 are made of gloss-white HIPS, while DRSS6 and DRSS8 are made of mirror HIPS. DRSS5 and DRSS6 have parabolic surfaces, whereas DRSS7 and DRSS8 have flat surfaces. The comparison of the daylight performance was conducted for the DRSS5 with DRSS7 and for the DRSS6 with DRSS8. The drawings of the tested cases are illustrated in Figure 8.13.

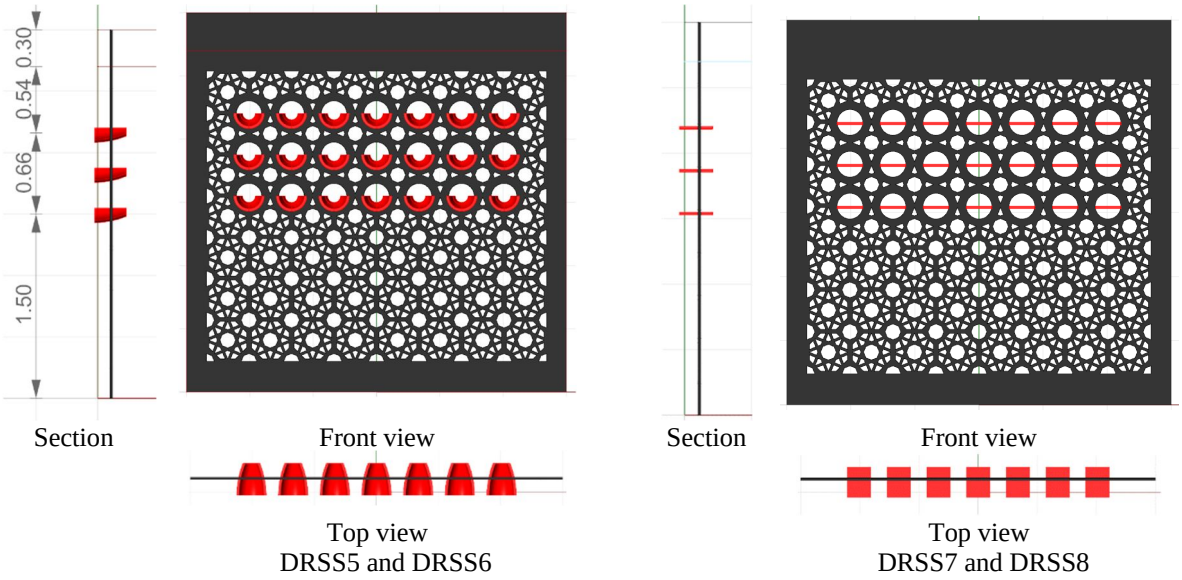


Figure 8.13: Case DRSS5, DRSS6, DRSS7, and DRSS8, dimensions are in meters

8.2.5. Effect of truncation

In order to enhance the design of the DRD, the inlet and the outlet of the device were truncated. The effect of the truncation on the illuminance level and the DUWP was investigated. The performance of the truncated DRD (DRSS9) was compared with that of the DRSS8.

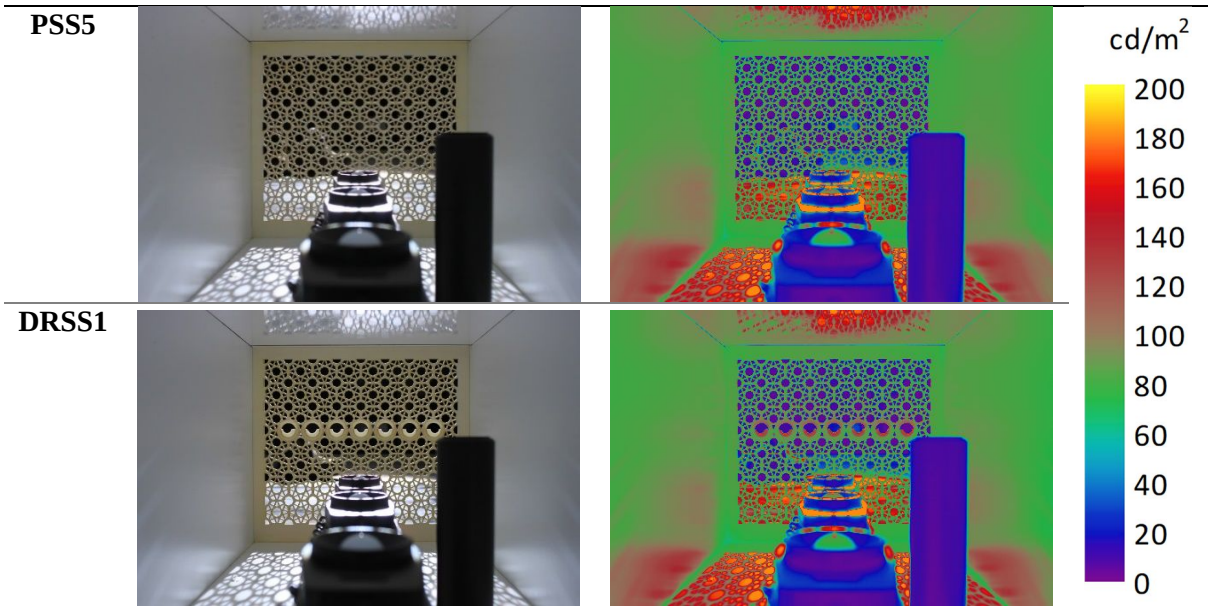
8.2.6. Effect of prismatic lens

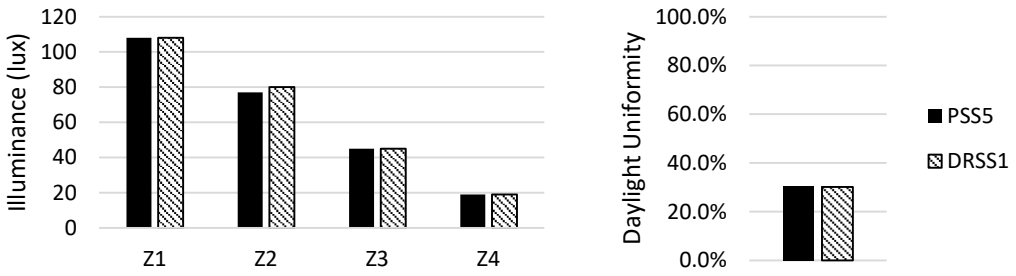
The last parameter investigated under the artificial sky dome was the effect of the prismatic lens on daylight performance. Two prismatic lenses were integrated with the DRD. The performance of the perforated screen with prismatic DRDs (case DRSS10) was compared against case DRSS9.

8.3. Results

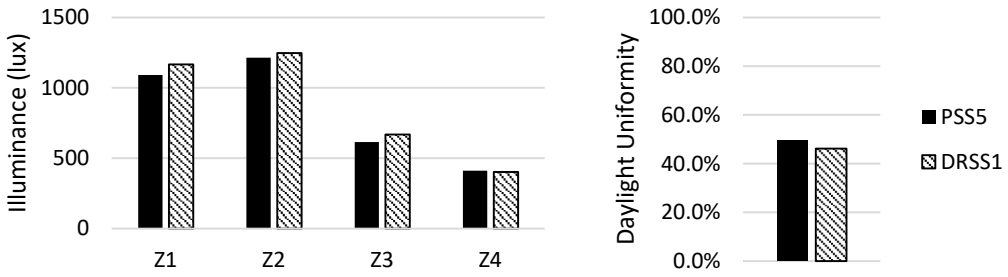
8.3.1. Comparison of PSS5 and DRSS1

It was found that the illuminance at the work plane was increased by the DRSS1 only at Z2 by 4%, for Riyadh city on 21 June at solar noon (solar altitude is 88 degrees). The DUWP was decreased from 30.5% to 30.2%. On the other hand, in Nottingham city on 21 October at solar noon (solar altitude is 26 degrees), the illuminance was increased by the DRSS1 by 7%, 3%, 9% at Z1, Z2 and Z3, while it was decreased by 2% at Z4. The DUWP was decreased from 49.4% to 46.2%, as shown in Figure 8.14.





[Riyadh city on 21 June]



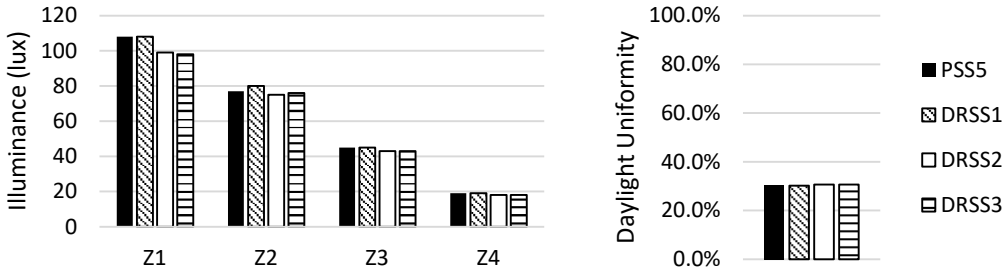
[Nottingham city on 21 October]

Figure 8.14: Illuminance (left) and DUWP (right) under DRLS at solar noon

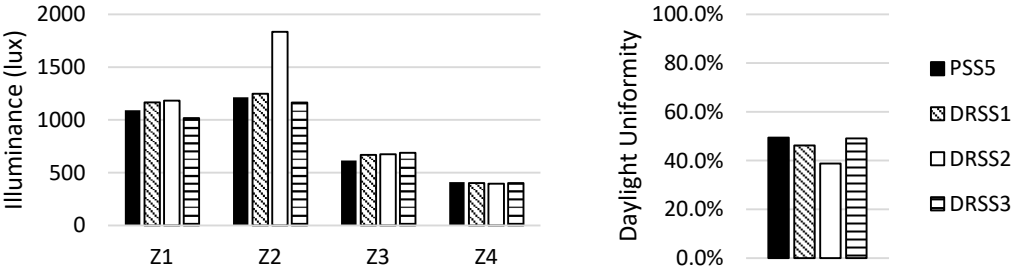
8.3.2. Test effect of significant parameters of DRDs

8.3.2.1. Effect of position

It was found that for the Riyadh city test, the illuminance at the work plane decreased by 8%, 3%, 4% and 5% at Z1, Z2, Z3 and Z4 compared with PSS5. The DUWP increased from 30.5% to 30.6% for DRSS2 and DRSS3 compared with PSS5. On the other hand, for the Nottingham city test, the illuminance increased by DRSS2 compared with PSS5 by 8%, 51% and 10% at Z1, Z2 and Z3, but it decreased by 4% at Z4. For DRSS3, the illuminance was decreased compared with PSS5 by 7%, 4% and 2% at Z1, Z2 and Z4, while it was increased at Z3 by 12%. The DUWP was decreased from 49.4% to 46.0%, 38.8% and 49.1% for DRSS1, DRSS2 and DRSS3, respectively, as shown in Figure 8.15.



[Riyadh city on 21 June]



[Nottingham city on 21 October]

Figure 8.15: Illuminance (left) and DUWP (right) under DRLS at solar noon

8.3.2.2. Effect of unit per area ratio

For Riyadh city, it was found that DRSS4 decreased and increased the illuminance at the work plane by 3% at Z1 and Z2, respectively; however, at Z3 and Z4, it remains as it was with PSS5. On the other hand, DRSS5 increased the illuminance compared with PSS5 by 5% at Z2 and Z4, 2% at Z3, and it decreased it at Z1 by 5%. As a result, the DUWP increased from 30.5% (PSS5) and 30.2% (DRSS1) to 30.6 for DRSS4 and 32.0% for DRSS5.

For Nottingham city, the illuminance was increased at Z1, Z2 and Z3 for DRSS1, DRSS4 and DRSS5 compared with PSS5. The increase in the illuminance was by 7%, 12% and 6% at Z1, and by 3%, 54% and 37% at Z2, and by 9%, 10% and 11% at Z3. On the other hand, it was decreased by 2%, 5% and 7% at Z4, for DRSS1, DRSS4 and DRSS5, respectively. As a result, the DUWP decreased from 49.4% (PSS5) to 46.2% for DRSS1, to 37.7% for DRSS4 and 39.4% for DRSS5, as shown in Figure 8.16.

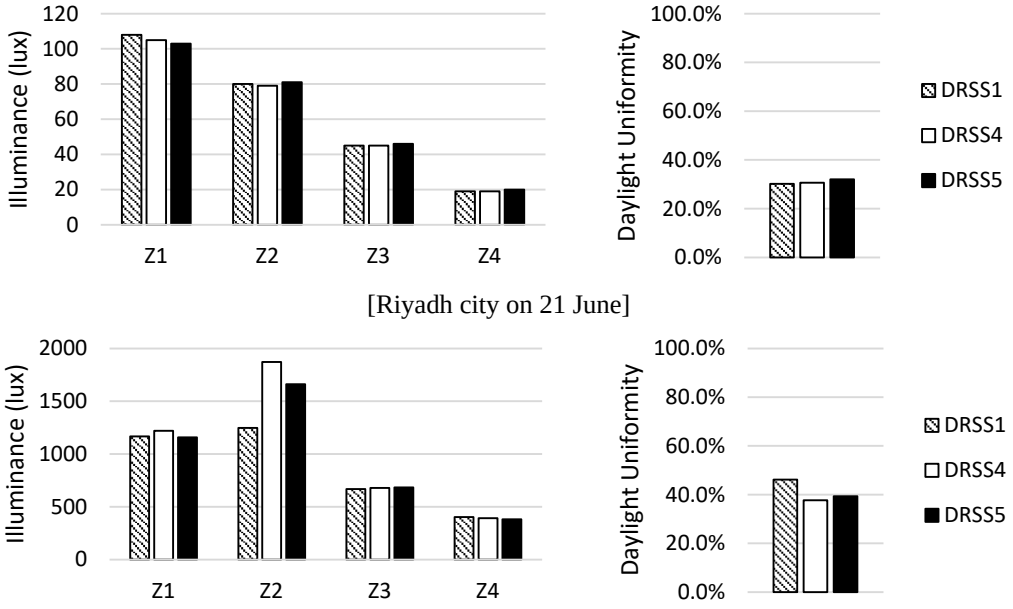


Figure 8.16: Illuminance (left) and DUWP (right) under DRLS at solar noon

8.3.2.3. Effect of material

a) Effect of material with parabolic surface

For the Riyadh city test, it was found that the illuminance at the work plane was decreased by 5% and 7% at Z1, while it was increased by 5% and 1% at Z2 for DRSS5 and DRSS6. At Z3, the illuminance was increased by 2% for DRSS5, while it was decreased by 2% for DRSS6.

At Z4, the illuminance was increased by 5% for DRSS5. The DUWP was increased to 32.0 % for DRSS5 and 31.5% for DRSS6.

On the other hand, for the Nottingham city test, the illuminance at the work plane compared with PSS5 was increased by DRSS5 and DRSS6 at Z1, Z2 and Z3 by 6% and 13%, 37% and 101%, and 11% and 42%, respectively. At Z4, the illuminance was decreased by DRSS5 by 7%, while it was increased by 3% by DRSS6. As a result, the DUWP was decreased by the DRSS5 and DRSS6 to 39.4% and 34.1%, respectively, as shown in Figure 8.17.

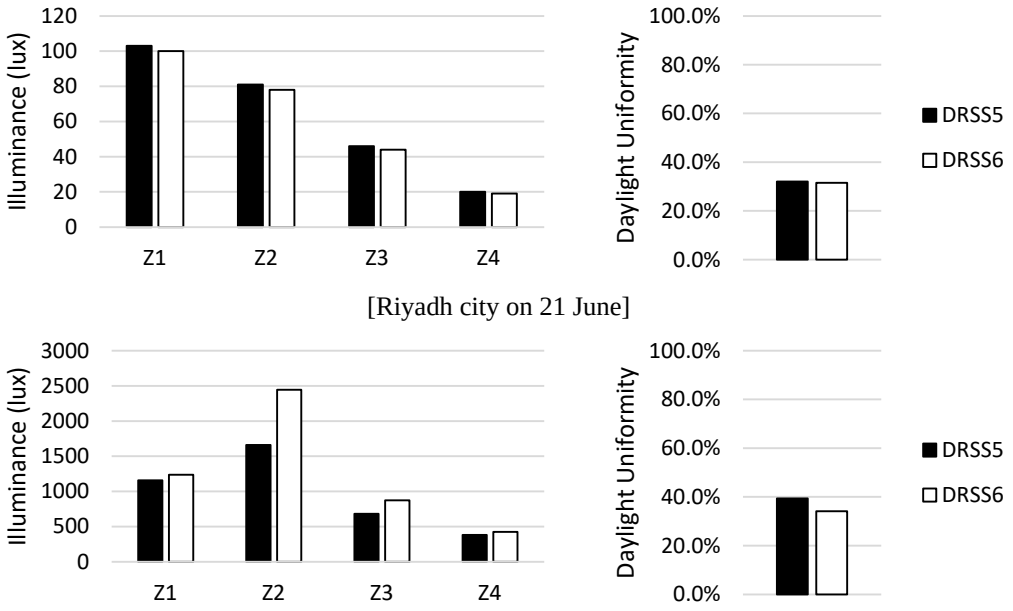


Figure 8.17: Illuminance (left) and DUWP (right) under DRLS at solar noon

b) Effect of material with a flat surface

For the Riyadh test, the illuminance was increased by DRSS7 by 3%, 4%, 2% and 5% at Z1, Z2, Z3 and Z4, respectively, compared with PSS5. In contrast, DRSS8 decreased the illuminance by 5%, 1% and 2% at Z1, Z2 and Z3, respectively. As a result, the daylight performance was increased by the DRSS7 and DRSS8 to 31.1% and 31.4%, respectively.

For the Nottingham city test, the illuminance was increased at Z2 by 11% and 12%, and at Z3 by 10% and 11% for DRSS7 and DRSS8. At Z1, the illuminance was increased by 2%, and it was decreased by 1% for DRSS7 and DRSS8. In contrast, DRSS8 increased the illuminance at Z4 by 12%, while DRSS7 decreased it by 7%. As a result, DRSS7 decreased the DUWP from 49.4% (PSS5) to 43.7%. However, DRSS8 increased the DUWP to 51.5%, as shown in Figure 8.18.

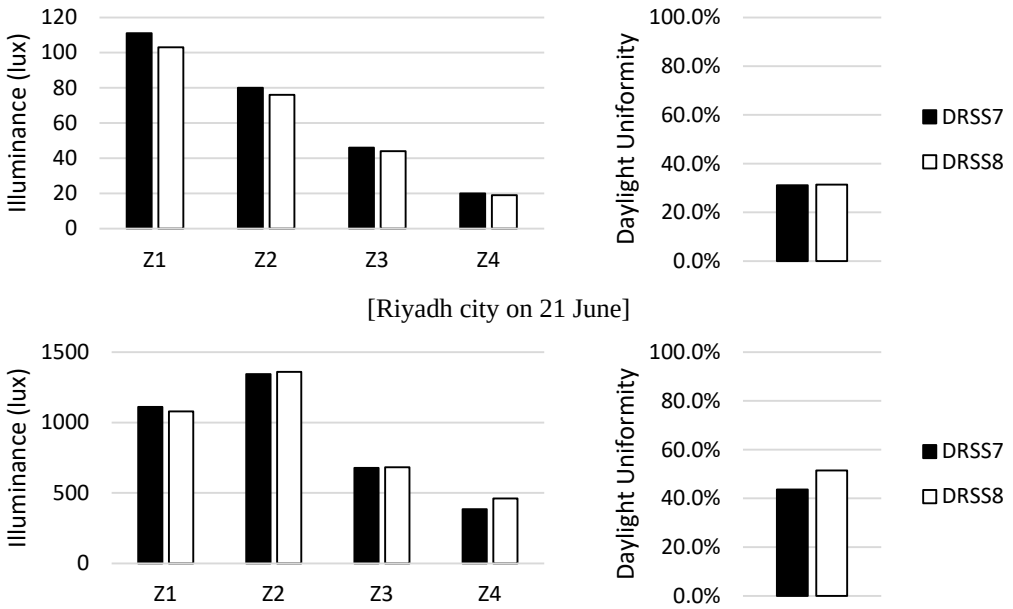


Figure 8.18: Illuminance (left) and DUWP (right) under DRLS at solar noon

8.3.2.4. Effect of geometry

a) Effect of geometry with gloss-white HIPS

Illuminance levels were measured on the work plane for high and low solar altitude (Riyadh and Nottingham) at solar noon for cases DRSS5 and DRSS7. The effect of the DRD geometry on the daylight performance was assessed for the mirror HIPS material. The performance of Case DRSS6 (Parabolic with mirror HIPS) and case DRSS8 (Flat with mirror HIPS) were analysed.

The illuminance levels at the high solar altitude at Z1 were higher with DRSS7 than DRSS5 by 8%, while it was lower by 1% at Z2. The illuminance levels at Z3 and Z4 were equalled. The DUWP was decreased from 32.0% (by DRSS5) to 31.1% (by DRSS7).

At the low solar altitude, the illuminance levels were decreased by the DRSS7 by 4%, 19%, 1%, while they were increased by 1% at Z1, Z2, Z3 and Z4, respectively compared with DRSS5. The DUWP was increased from 39.4% at DRSS5 to 51.5% with DRSS7. The measured illuminance and the calculated DUWP for DRSS5 and DRSS7 are illustrated in Figure 8.19.

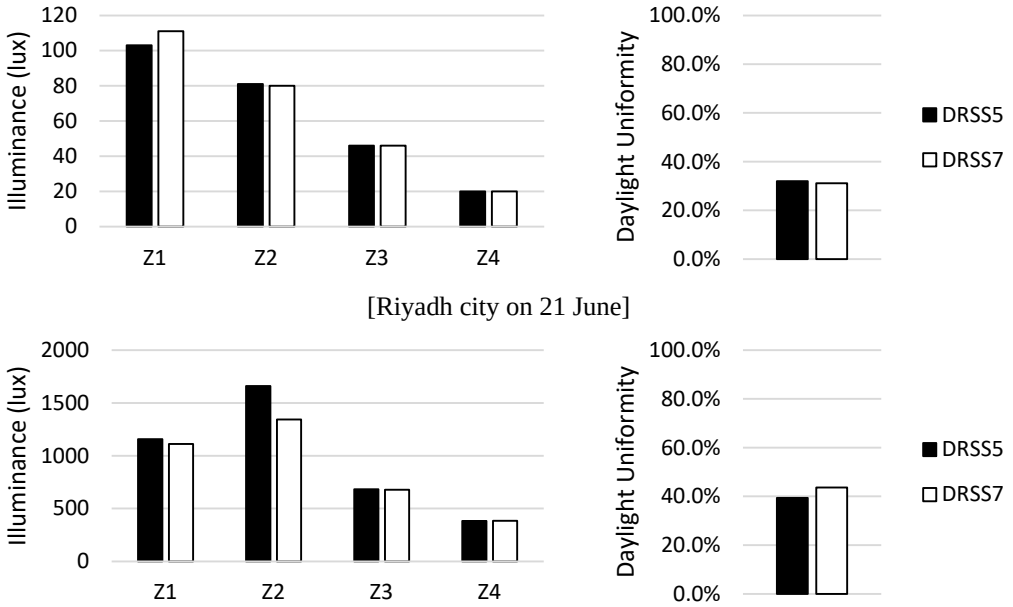


Figure 8.19: Illuminance (left) and DUWP (right) under DRLS at solar noon

b) Effect of geometry with mirror HIPS

It was found that at the high solar altitude, DRSS8 increased the illuminance by 3% at Z1 while it decreased it at Z2 by 3% compared with DRSS6. The illuminance levels at Z3 and Z4 were equalled. The DUWP was decreased from DRSS6 to DRSS8 by 0.1%.

On the other hand, at the low solar altitude, the illuminance was decreased by DRSS8 by 13%, 44% and 22% at Z1, Z2 and Z3, while it was increased by 8% at Z4, compared with DRSS6. As a result, the DUWP was increased by the DRSS8 to 51.5%, as shown in Figure 8.20.

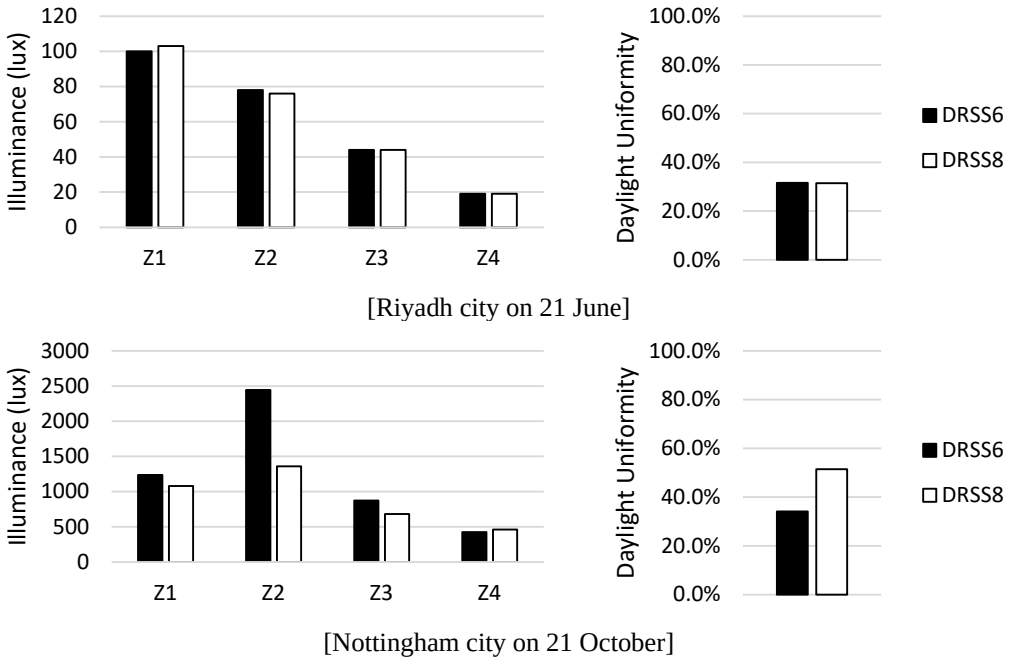
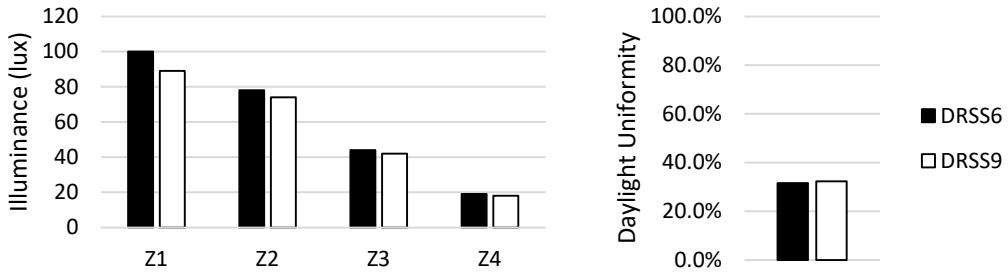


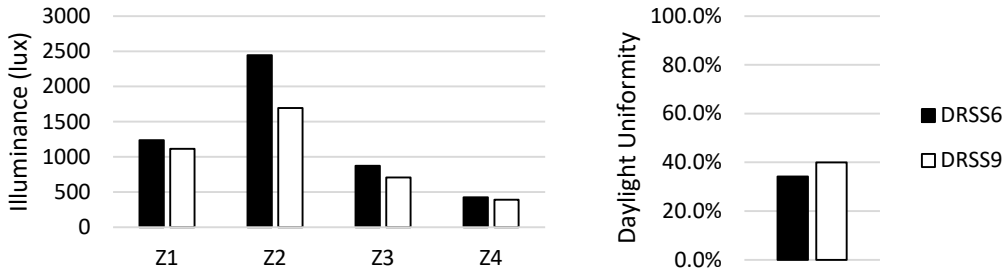
Figure 8.20: Illuminance (left) and DUWP (right) under DRLS at solar noon

8.3.2.5. Effect of truncation

The effect of the truncation on the daylight performance is shown in Figure 8.21. The illuminance and the DUWP were compared for case DRSS9 against DRSS6. It was found that the illuminance levels for Riyadh city on 21 June were decreased at all the test points. They were reduced by 11% at Z1 and by 5% at the other test points. However, the DUWP was relatively increased from 31.5% to 32.3%. Similarly, for Nottingham city on 21 October, the illuminance levels were decreased at the four test points. The highest increase was 31% at Z2. The decrease was 10%, 19% and 8% at Z1, Z3 and Z4. Nevertheless, the DUWP was increased from 34.1% to 39.9%.



[Riyadh city on 21 June]



[Nottingham city on 21 October]

Figure 8.21: Illuminance (left) and DUWP (right) under DRLS at solar noon

8.3.2.6. Effect of prismatic lens

The influence of the prismatic lens (case DRSS10) on the daylight performance was investigated. The illuminance and the DUWP were compared for DRSS9 against DRSS10, as shown in Figure 8.22. It can be seen that the illuminance levels for Riyadh city on 21 June were decreased relatively by DRSS10 at Z1 and Z4 by 2% and 6%. Similarly, the DUWP was relatively reduced from 32.3% to 30.9%. On the other hand, the test for Nottingham city shows that the illuminance level was increased by DRSS10 at Z1 by 8% while it was decreased at Z2 by 20% and by 5% at Z3 and Z4. However, the DUWP was relatively increased from 39.9% to 41.4%.

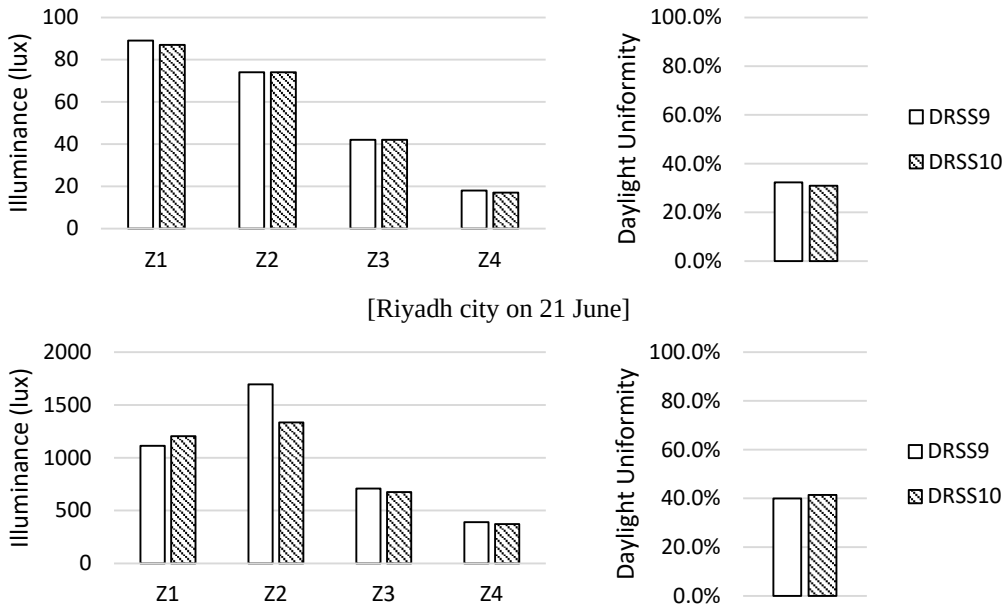


Figure 8.22: Illuminance (left) and DUWP (right) under DRLS at solar noon

8.4. Discussion and Conclusions

The results of the physical model test under the DRLS simulator were presented. The impact of the direct sun component on daylight performance was analysed. Eleven cases were tested at solar noon under high and low solar altitudes, namely, 88 degrees (21 June in Riyadh city) and 26 degrees (21 October in Nottingham city). The outputs of PSS5 and DRSS1 were compared then the effect of four main parameters on the daylight performance was investigated, namely, the position, unit per area ratio, material, and the geometry of the DRD.

The results showed that the impact of the DRSS1 at 88-degree solar altitude was insignificant. On the other hand, at a 26-degree solar altitude, the illuminance was relatively increased; however, the DUWP was reduced by 3.2%.

The investigation of DRD's position effect showed that the highest illuminance was recorded with DRSS1 (low DRD position) at high solar altitude and with DRSS2 (mid-DRD position) at low solar altitude. The DUWP was higher with DRSS3 (high DRD position) at low solar altitude, while at high solar altitude, the change in the DUWP was insignificant.

The effect of DRD's unit per area ratio was investigated. It was found that the highest ratio increased the illuminance level relatively at the high solar altitude except at Z1. The high ratio of DRD plays a key role in reducing direct sunrays to reach the front area at the work plane. The best DUWP at high solar altitude was relatively higher with DRSS5. The illuminance at

low solar altitude was increased significantly at Z2 by DRSS4 and DRSS5; therefore, the best DUWP was with DRSS1.

The effect of two types of DRD's materials, namely, white-gloss HIPS and mirror HIPS, was assessed. The two materials were tested with the proposed DRD geometry, DRSS5 and DRSS6, respectively. Later, the two materials were tested with flat surfaces. It was found that the mirror HIPS material lost some of its reflectance properties due to the heat that was applied during the vacuuming process. Furthermore, the bending process of the material has affected the material optical properties due to the stretching process. Therefore, the daylight performance of the white-gloss HIPS and the Mirror HIPs were compared with a flat surface to investigate the effect of each material on their original optical properties. DRSS7 has a flat surface made from white-gloss HIPS, while DRSS8 has a flat surface, and it is made of mirror HIPS.

The mirror material (DRSS6) relatively decreased the illuminance with the high solar altitude, but it increased it with the low solar altitude, particularly with a high increase at Z2. The test of the flat surfaces showed that the variation in the results compared with the concave surface was not significant except with low solar altitude at Z2, where the increase in the illuminance was relatively low.

Finally, the proposed DRD was compared with a flat surface that has the same material. Similar to the above, the effect of the geometry was investigated with gloss-white and mirror materials. It was found that with high solar altitude, the flat geometry increased the illuminance level at the work plane for both materials. On the other hand, the concave geometry with the low solar altitude increased the illuminance levels, particularly at the front areas. Therefore, the tilt angle of the DRDs should be optimised to reach the optimal performance of the proposed system.

Due to the absence of the diffuse sky element in the DRLS simulator, number of limitations were determined during the test. The sky component, which produces diffuse daylight, was not considered. The light bulb produces direct daylight alone. The error could be more significant for the Nottingham test because the diffuse daylight for Riyadh on 21st Jun was exceptionally low, compared to direct daylight.

For the Riyadh city test, the model was faced to the floor because of the extreme tilt of the turntable, which is necessary to obtain the required solar altitude (88 degrees). The solar altitude angle was the sum of the DRLS and the turntable tilt angles.

As a result, it was necessary to find a validated artificial sky simulator to conduct the test under its reliable conditions. Artificial sky simulators are one of the assessment tools to measure the

lighting quality of buildings. The best artificial sky simulator in the UK at the time of the study was the Bartlett Lighting Simulator (BLS) at the UCL Institute for Environmental Design and Engineering (IEDE) in London.

Chapter 9. Test under the diffuse-light sky dome

In addition to tests carried out under direct daylight, presented in Chapter 8, the proposed system has also been tested under a diffuse-light simulator, which is a validated artificial sky dome. The test was carried out at the UCL Institute for Environmental Design and Engineering (IEDE), The Bartlett, UCL, Faculty of the Built Environment in London.

The purpose was to investigate the influence of diffuse light on the daylight performance at the work plane (DPWP). The tested cases include case PSS5, DRSS1, DRSS2, DRSS3, DRSS4, DRSS5, DRSS6, DRSS7, DRSS8, DRSS9, and DRSS10. The illuminance was measured at the four test points, namely, Z1, Z2, Z3 and Z4, as shown in Figure 9.1. Later, the DUWP was calculated for each test.



Figure 9.1: The interior of the prototype

The prototype was tested under diffuse light that is produced by the sky patches of the sky dome (DFLS). The purpose of the study was to investigate the effect of diffuse daylight on the daylight performance of the proposed system. The aim of this experimental study was achieved through the following objectives:

1. To test the effect of the tested parameters on the illuminance level and the daylight uniformity at the work plane. The investigated parameters were presented previously in Chapter 8, table 8.3.
2. To validate the outputs of the computer simulation against the experimental tests

In order to mitigate the uncertainty in the validation study, the following conditions were applied with identical inputs in the computer simulation and the physical prototype: test location, date and time (to determine the sun and sky position), sky type, and model orientation and materials properties.

9.1. Test Procedure

9.1.1. Location and time

The daylight experimental study was conducted for three different solar altitudes, namely, 88 degrees, 42 degrees, and 26 degrees. The location and the date of the tested scenarios were Riyadh city on 21st of June, Riyadh city on the 21st of December, and finally Nottingham city on the 21st of October. The tested hours were given three names as following, scenario-1, scenario-2 and scenario-3, respectively. Table 9.1 displays the properties of the three skies. The ISO classification of the skies was a clear sky with low turbidity, the test hour was solar noon, and the azimuth was180 degrees.

Table 9.1: The properties of the tested scenarios

Sky Name	Location	Date	Solar Altitude	Average device intensity
Scenario-1	Riyadh	21 June	88 degree	12 %
Scenario-2	Riyadh	21 December	42 degree	9 %
Scenario-3	Nottingham	21 October	26 degree	6 %

9.1.2. The sky dome

The prototype has been tested under a validated sky simulator at the Institute for Environmental Design and Engineering (IEDE) in UCL, London, as shown in Figure 9.2. The diameter of the sky dome is five meters, and the height is 2.5 meters. It consists of 810 light sources. This number of light sources provides a uniform light source. The sky dome is operated through a computer programme developed at the IEDE (UCL, 2019).

The sky simulator is setup through computer software connected with light bulbs through networking and electricity cables. Three inputs are required to set the sky simulator. They include the location, the time and the sky type. The location is provided as latitude and longitude values. The sky applied the standard ISO CIE skies shown in Table 9.2. (See Appendix 2 for the full list of the standard parameters).

In order to identify the sun and sky elements, a full mathematical model of the sky distribution was prepared. Then, the location (latitude and longitude) of the test, the test time and the sky type were provided to the sky dome software.

Table 9.2: Standard parameters of the CIE Standard Clear Sky (ISO, 2004)

Type	Gradation group	Indicatrix group	a	b	c	d	e	Description of luminance distribution
12	V	4	-1.0	-0.32	10	-3.0	0.45	CIE Standard Clear Sky, low illuminance turbidity

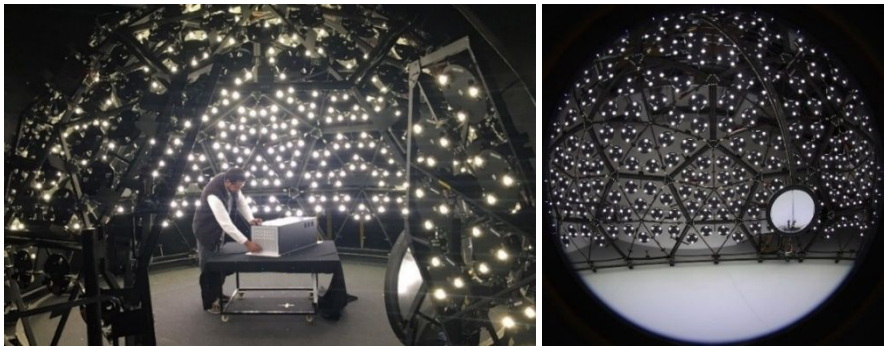


Figure 9.2: The interior of the sky dome at the IEDE

9.1.3. The position of the sun and sky elements

The most significant data for daylighting design practice is daylight distribution. In order to evaluate the luminance of a sky element, the description of luminance distributions is necessary. A full mathematical model is required to generate the general function. Series of similar functions are provided by “ISO 15469:2004, Spatial distribution of daylight - CIE standard general sky”. The mathematical models for artificial sky dome can be defined by studying the distribution of daylight in the sky vault (Souza et al., 2016).

According to ISO 15469:2004, "The position of an arbitrary sky element is defined by its zenith angle, Z, and by the azimuth difference between the element and the sun, [α - α_s]. If Z_s is the zenith angle of the sun, the angular distance between the element and the sun is”: The graph in Figure 9.3 shows the zenith, azimuths (y_s and y), and the altitudes (a_s and a) of the sun and its sky elements, respectively.

$$x = \arccos\left(\cos Zs * \cos Z + \sin Zs * \sin Z * \cos\left|\alpha - \alpha s\right|\right.$$

Equation 25

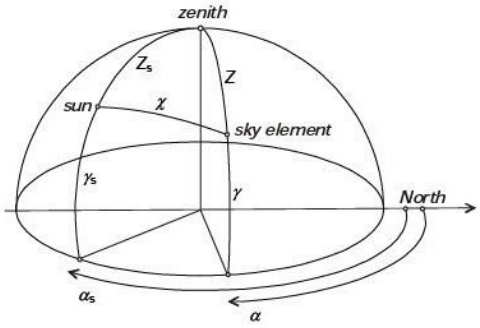


Figure 9.3: Sun and sky elements positions and the angular distance (x) between them

The azimuth and the altitude/elevation of the sun can be obtained by using the *LadyBug_SunPath* component in Ladybug in Grasshopper. The *LadyBug_SkyDome* component can visualize the sky element for a particular hour. Then, it can be presented by Rhino. The location and the time were provided to the software.

By obtaining the centre point of the sky patches and the centre of the sky dome, the altitude and the azimuth of the sky patches can be obtained in Rhinoceros software. The method is to draw straight lines from the centre of the dome to the centre of the sky patch, as shown in Figure 8.3. Extended explanation examples of the sky luminance calculation were presented by Darula and Kittler (2009).

The position of the sky element on the summer solstice (21st June) at solar noon in Riyadh (latitude = 24.7136° N, longitude = 46.6753° E) can be obtained as follows:

If:

Z_s = 0.02 (rad), α_s = 3.14 (rad), γ_s = 1.55 (rad), Z = 0.12 (rad), α = 1.57 (rad), γ = 1.46 (rad)

The angular distance between the sun position and the sky element position x can be obtained by:

$$x = \arccos\left(\cos Zs * \cos Z + \sin Zs * \sin Z * \cos|\alpha - \alpha s|\right)$$

$$x = \arccos\left(\cos 0.02 * \cos 0.12 + \sin 0.02 * \sin 0.12 * \cos|1.57 - 3.14|\right)$$
$$x = 0.12\ (\text{rad})$$

where:

Zs is the zenith of the sun at solar noon [rad]
αs is the azimuth of the sun (clockwise from north)[rad]
γs is the angle of elevation of the Sun above the horizon [rad]
Z is the zenith of the sky element at solar noon [rad].
α is the azimuth of the sky element (clockwise from north)[rad].
γ is the angle of elevation of the sky element above the horizon [rad].

The position of the sky element on the winter solstice (21st December) at solar noon in Riyadh (latitude = 24.7136° N, longitude = 46.6753° E) can be obtained as follows:

If:

Z_s= 0.84 (rad), α_s= 3.14 (rad), γ_s= 0.73 (rad), Z= 0.86 (rad), α = 3.01 (rad), γ = 0.71 (rad).

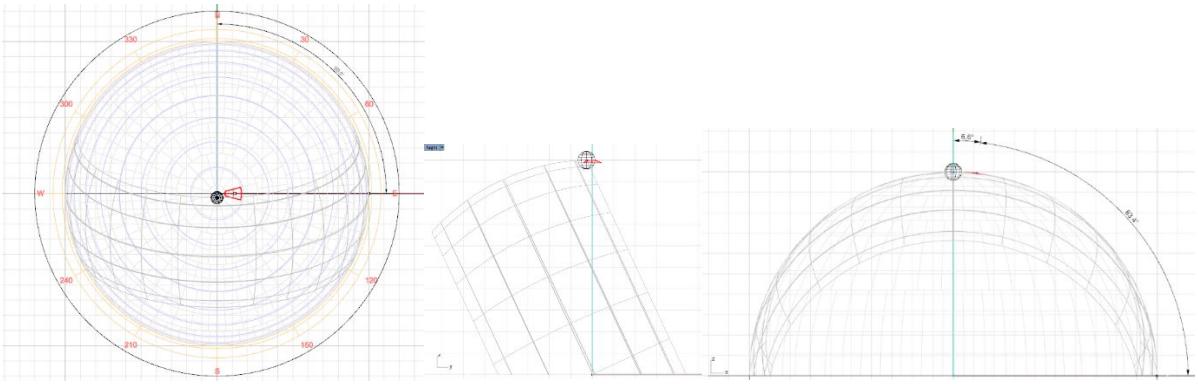
The angular distance x can be obtained by:

$$x = \arccos\left(\cos Zs * \cos Z + \sin Zs * \sin Z * \cos|\alpha - \alpha s|\right)$$

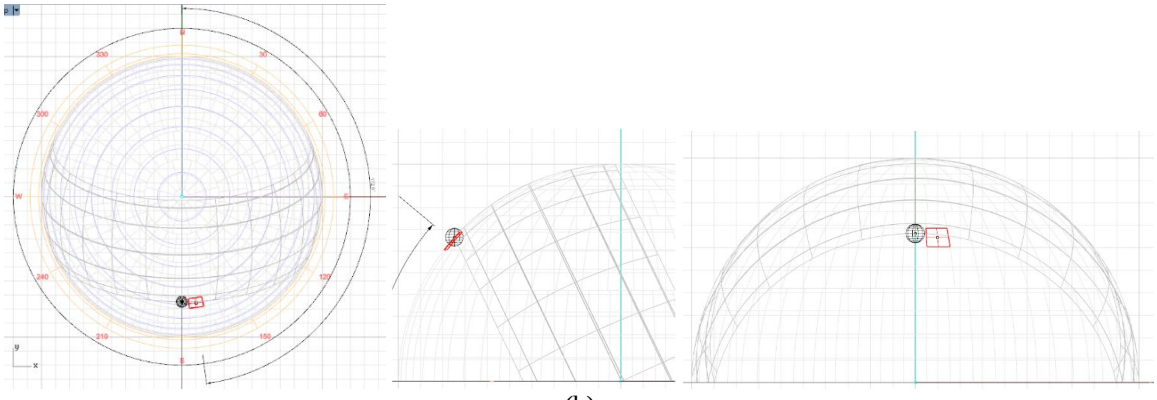
$$x = \arccos\left(\cos 0.84 * \cos 0.86 + \sin 0.84 * \sin 0.86 * \cos|3.01 - 3.14|\right)$$
$$x = 0.10\ (\text{rad})$$

where:

Z_s is the zenith of the sun at solar noon [rad].
α_s is the azimuth of the sun (clockwise from north)[rad].
γ_s is the angle of elevation of the Sun above the horizon [rad].
Z is the zenith of the sky element at solar noon [rad].
α is the azimuth of the sky element (clockwise from north) [rad].
γ is the angle of elevation of the sky element above the horizon [rad].



(a)



(b)

Figure 9.4**:** Sun and sky element position at solar noon in Riyadh; (a) on the 21 June; (b) 21 December

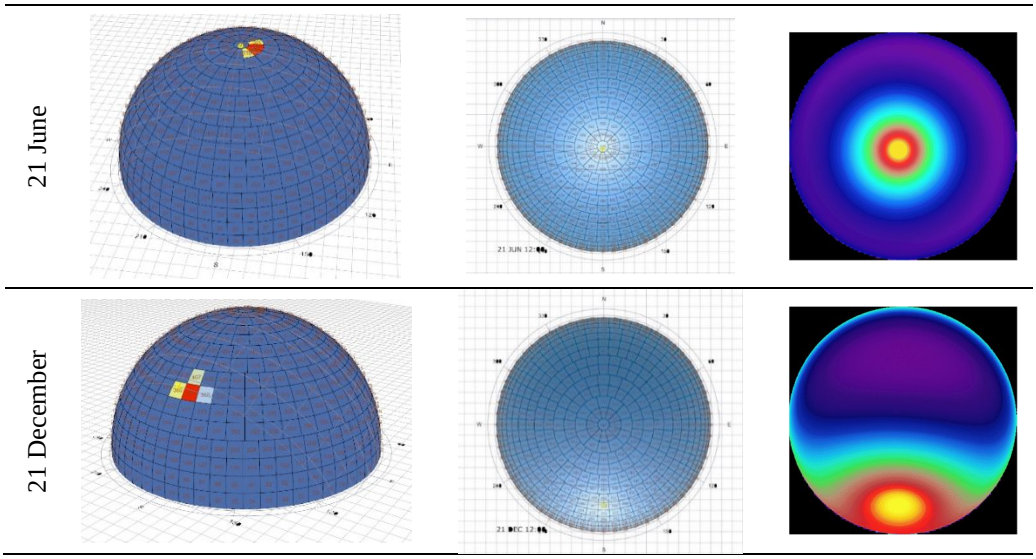


Figure 9.5: The sun and sky positions at solar noon in Riyadh

9.1.4. Tests process

The experimental study was set through the following steps that are shown in the flowchart in Figure 9.6 below:

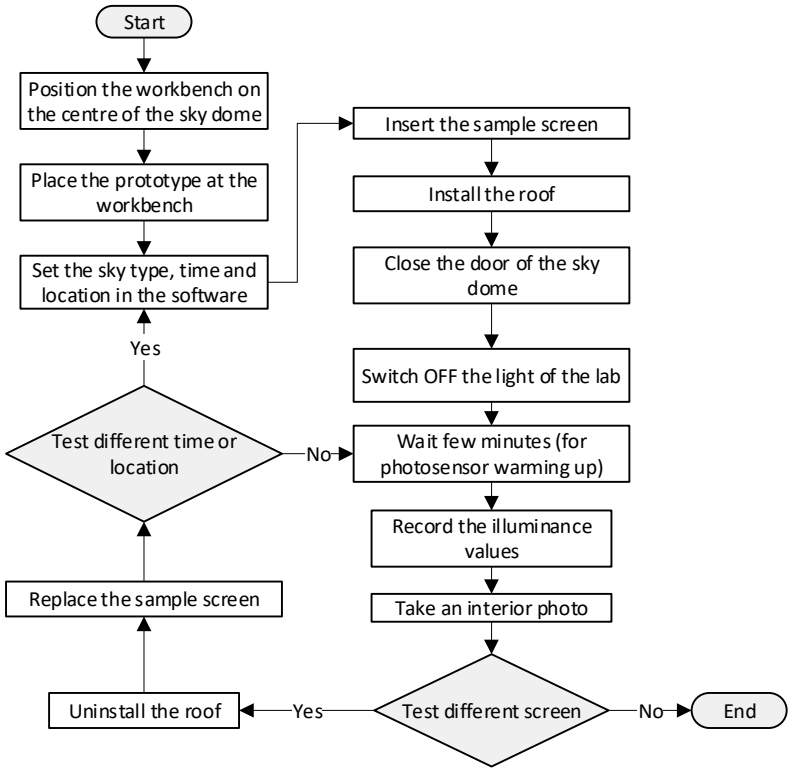


Figure 9.6: Flowchart of the test process

The photographs in Figure 9.7 show the setting equipment and the software interface that was used to set the light intensity of the sky dome. In addition, the method to install the sample solar screen is shown in Figure 9.8. The screen is inserted inside engraved edges that were made within the floor, roof and internal sidewalls. This method was employed to prevent any light infiltration.

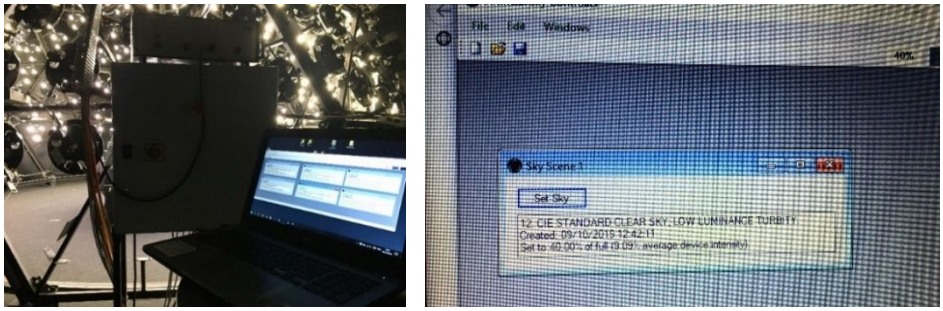


Figure 9.7: The DFLS setting



Figure 9.8: The installation of the sample screen

9.2. Results

The outputs of the daylight experiment under the diffuse sky simulator are shown below. They start with a comparison of the daylight performance of case PSS5 and case DRSS1. Then, the effect of the tested parameters of DRD was illustrated and analysed. The tested parameters were the position, the unit per area ratio, the material, the geometry, the truncation, and the prismatic lens.

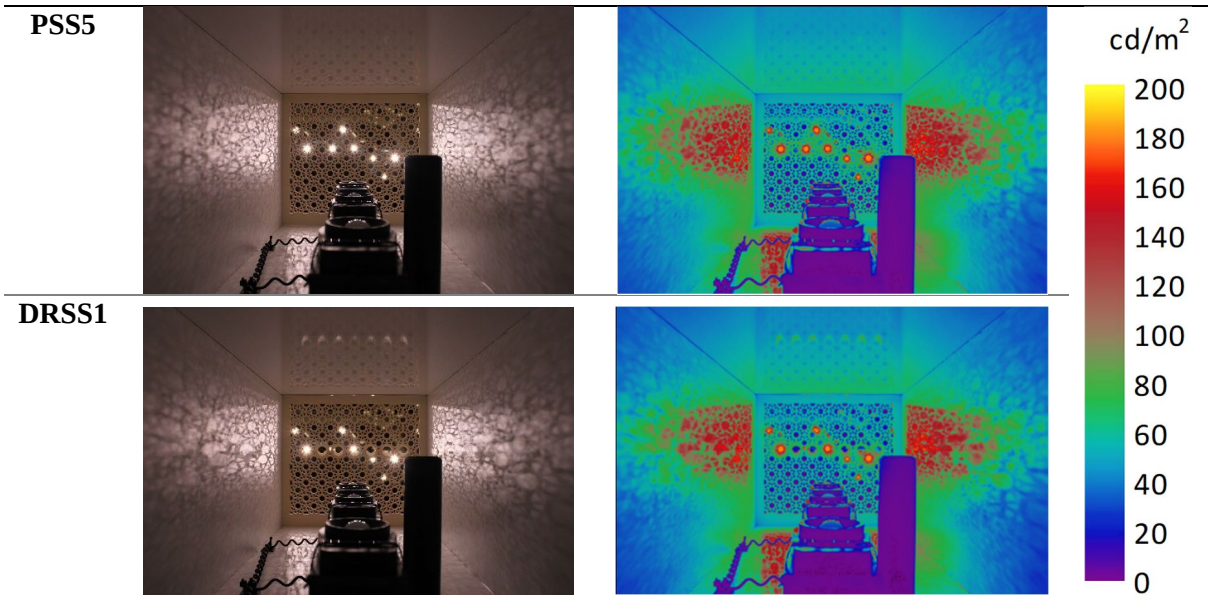
The illuminance levels at the work plane for the tested cases are shown below. The test was conducted at solar noon, where the sun azimuth is 180 degrees on the south façade. The test was conducted for three different solar altitudes: 88 degrees (Scenario-1), 42 degrees (Scenario-2), and 26 degrees (Scenario-3). The location and the date of the three tests were Riyadh city on 21st of June, Riyadh city on the 21st of December, and finally Nottingham city on the 21st of October.

9.2.1. Comparison of PSS5 and DRSS1

The illuminance levels at the work plane for case PSS5 and case DRSS1 are shown in Figure 9.9. It was found that at the highest solar altitude, namely, 88 degrees, the change in the illuminance level was insignificant between the two cases. At Z1, Z2 and Z3, the illuminance was increased by 2.5%, 1%, and 3.2%, while at Z4, the illuminance was not changed. As a result, the DUWP was decreased by 0.8%.

Similarly, at a 42-degree solar altitude, the change in the illuminance was insignificant. The illuminance increased at Z2 and Z3 by 1.9% and 4.2%, while it decreased at Z1 and Z4 by 0.8% and 1.5%. The DUWP decreased by 1%.

Finally, at the lower solar altitude, namely, 26 degrees, the illuminance level increased by 7.2% at Z3, while the increase at Z2 was only 0.8%. On the other hand, it decreased by 4.1% at Z1, and the DUWP increased by only 0.1%.



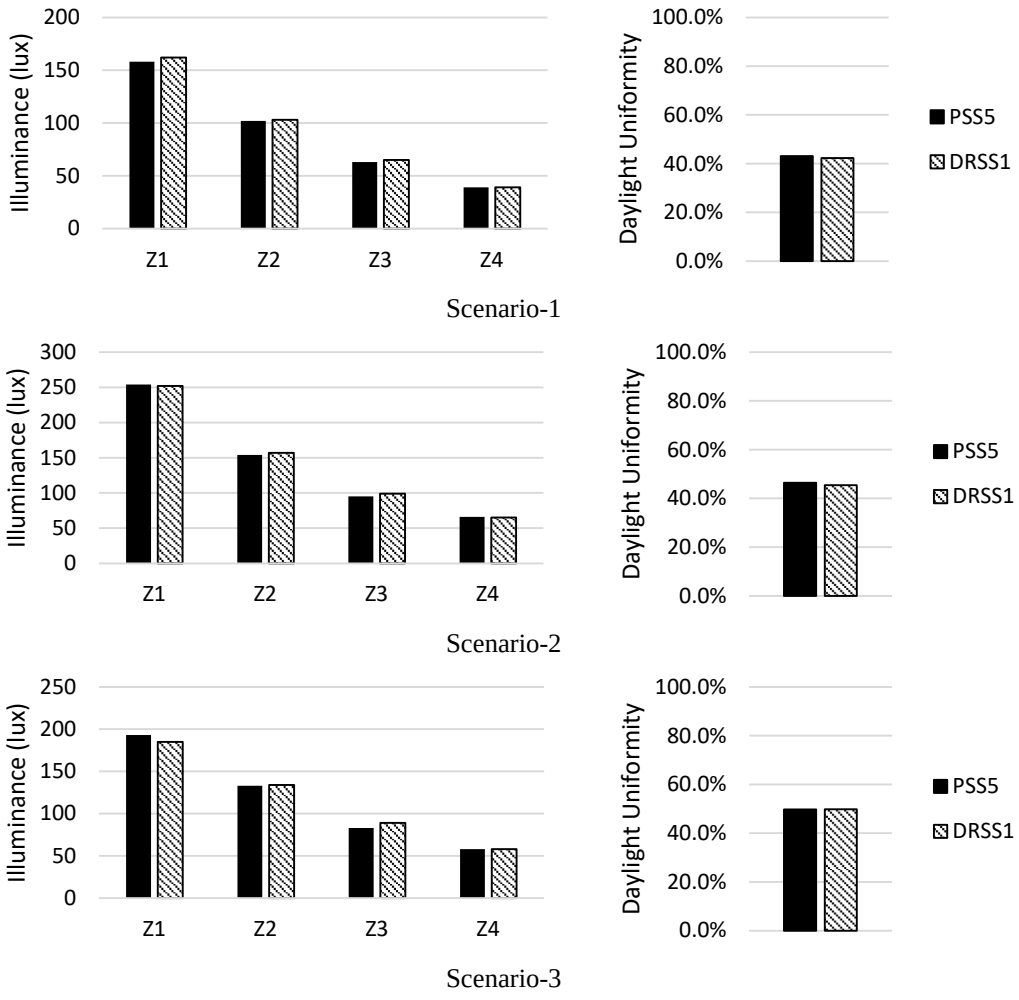


Figure 9.9: The illuminance (left) and DUWP (right) under the DFLS

9.2.2. Effect of position

The effect of changing the DRD's position on the daylight performance was investigated. The charts in Figure 9.10 show the measured illuminance levels and the calculated DUWP for cases DRSS1, DRSS2 and DRSS3. The cases were tested for scenario-1, scenario-2 and scenario-3. Then, the three cases were compared with case PSS5.

For scenario 1, it was found that the highest increase in the illuminance level was at Z1 by 2.5% by case DRSS1 while the highest decrease at the same point was 5.1% by DRSS2. At Z2, the change in the illuminance was from -2% to 1% by DRSS3 and DRSS1, respectively. The change in illuminance at the rear-half of the room was from -4.8% to 3.25% at Z3, and it was from -5.1% to 0%, by DRSS3 and DRSS1, respectively. The change in the DUWP was varied from -1.4% to 0.3% by DRSS3 and DRSS2.

For scenario 2, it was found that, at the front area, namely at Z1 and Z2, the change in the illuminance ranged from -5.95% to 1.6% by DRSS2 and DRSS3, and from -2.6% to 1.9% by

DRSS3 and DRSS1, respectively. At the rear half of the room, the illuminance change ranged from -6.3% to 4.2% by DRSS2 and DRSS1, and from -6.1% (by DRSS2 and DRSS3) to -1.5% (by DRSS1). The change in the DUWP was ranging from -0.65 to -2.1% by DRSS2 and DRSS3.

For scenario 3, the change in the illuminance at Z1 and Z2 was from -1% to 4.1% by DRSS3 and DRSS1, and from -3.8% to 1.5% by DRSS3 and DRSS2. At the back of the room, at Z3, the lowest decrease was by -3.6% by DRSS3, while the highest increase was by 7.2% by DRSS1. At Z4, the illuminance was decreased by 3.4% by DRSS2 and DRSS3, while it was not changed by DRSS1. The change in the DUWP was an increase from -1.2% to 0.1% by DRSS3 and DRSS1.

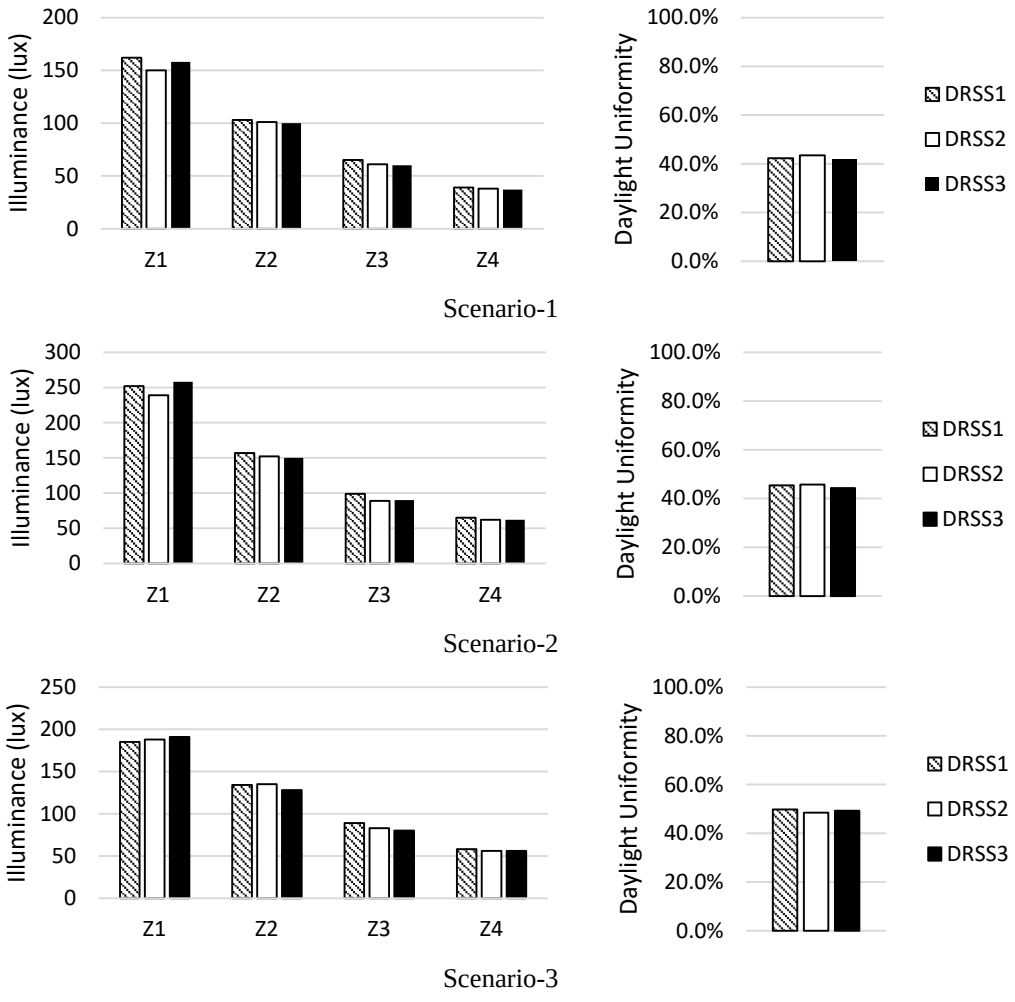


Figure 9.10: The illuminance (left) and DUWP (right) under the DFLS

9.2.3. Effect of unit per area ratio

The effect of the DRD's units per area on the daylight performance was investigated. Three cases were tested, namely DRSS1 (7unit/8.1m^2), DRSS4 (14unit/8.1m^2) and DRSS5 (21unit/8.1m^2), as shown in Figure 8.10. The measured illuminance levels and the calculated DUWP are shown in the charts in Figure 9.11 below.

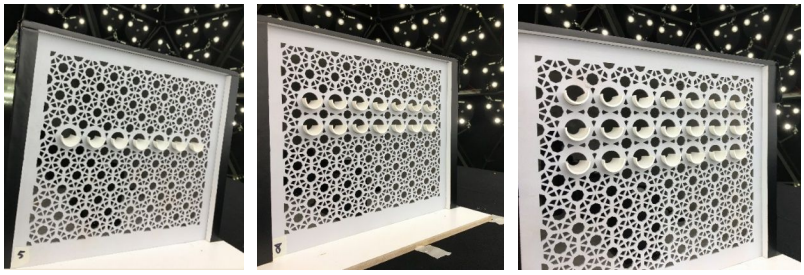


Figure 9.11: Case DRSS1, DRSS4 and DRSS5, from left to right

For scenario-1, the change in the illuminance was from -7% to 2.5% at Z1 by DRSS5 and DRSS1. At Z2, it was 0% to 2%, at Z3 it was from -1.6% to 3.2%, at Z4 it was -5.1% to 0%. The change in the DUWP was from -0.8% to -0.3%.

For scenario-2, it can be seen that the illuminance has decreased at Z1 for the three cases compared to case PSS5. The highest decrease was 10.6% by DRSS5. At Z2, the illuminance has decreased by DRSS5 by 1.9%; however, it has increased by DRSS1 by 1.9%. On the other hand, at the end of the room, namely, at Z4, the illuminance was decreased by the three cases by 1.5%, 6.1% and 7.6%, by DRSS1, DRSS4 and DRSS5, respectively. The DUWP was decreased by the three cases as well. The reduction was 1%, 0.3% and 0.4%, by DRSS1, DRSS4 and DRSS5, respectively.

For scenario-3, the change in the illuminance at Z1 was from - 6.2% to - 4.1% by DRSS4 and DRSS5, and DRSS1, respectively. At Z2, the change range was from -0.8% to 2.3% by DRSS5 and DRSS4. At Z3, the highest increase was by 7.2% by DRSS1, while the lowest reduction was by 1.2% by DRSS5. Finally, at Z4, the illuminance was not changed by DRSS1 and DRSS4; however, it was decreased by 3.4% by DRSS5. The change in the DUWP was from 0.1% to 0.4% by DRSS1 and DRSS4; it was not changed by DRSS5, as presented in Figure 9.12.

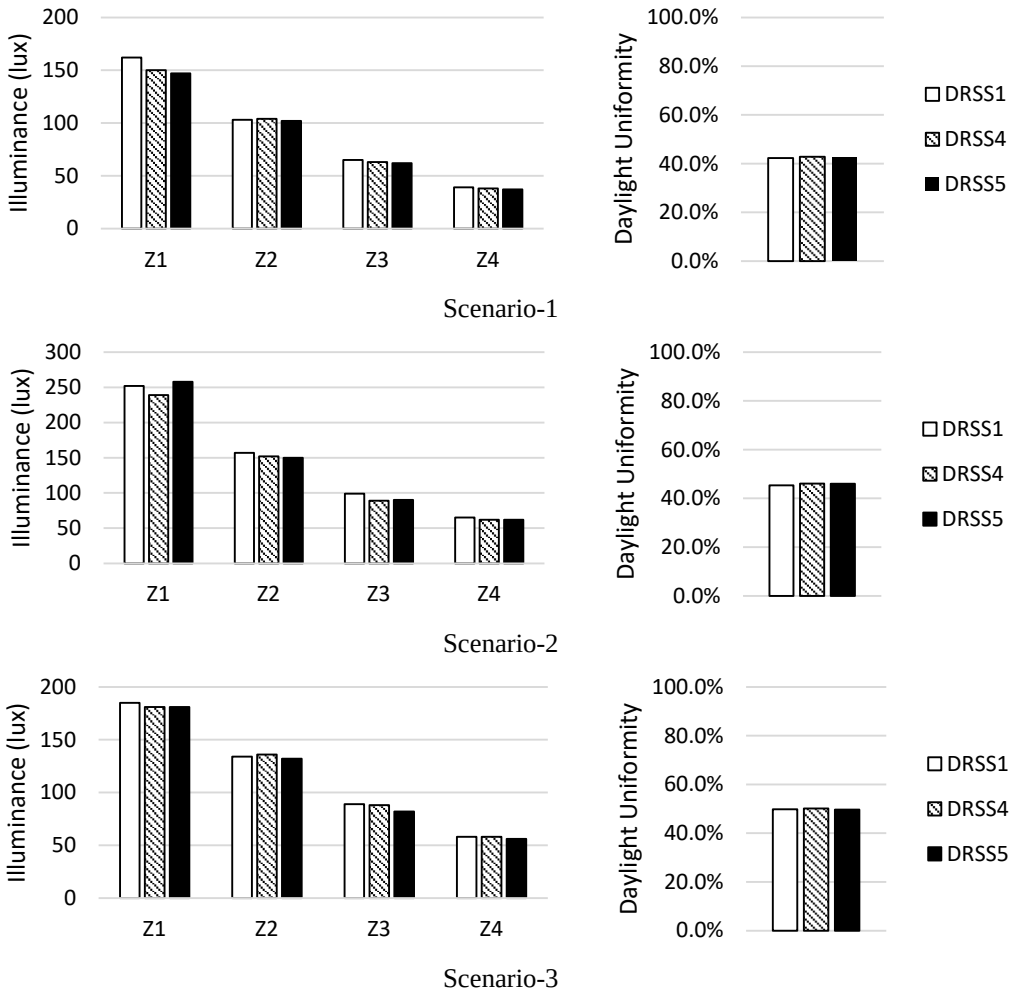


Figure 9.12: The illuminance (left) and DUWP (right) under the DFLS

9.2.4. Effect of material

The effect of the DRD material on daylight performance was investigated. The effect of the material was tested with a parabolic and a flat surface. The purpose was to investigate the effect of the material with its original optical properties, as mentioned in Chapter 8. As was described previously, it was found that the optical properties of the DRD material were changed due to the applied heat by the vacuum machine. Furthermore, the stretching of the material has changed the reflectivity of the DRD inner surface as well.

Effect of material with parabolic surface

First, the effect of the material was tested with the proposed parabolic surface (DRD). The DRDs were made of a white-gloss HIPS and a mirror HIPS for cases DRSS5 and DRSS6, respectively. The outputs of the illuminance measurements and the calculated DUWP for the three scenarios are shown in the charts in Figure 9.13.

In general, it can be seen that the illuminance levels were higher at 42-degree solar altitude while the lower illuminance was at 88-degree solar altitude. The peak DUWP with DRSS5 was 49.7% at scenario-3 while the lowest was 42.5% at scenario-1. The highest DUWP with DRSS6 was 49.9% at scenario-3 while the lowest was 43.4% at scenario-1. The DRSS6 increased the DUWP value by 0.9% and by 0.2% at scenario-1 and scenario-3 compared with DRSS5. Compared with PSS5, the DUWP was increased by 0.3% and 0.2% by DRSS6 at scenario-1 and scenario-3.

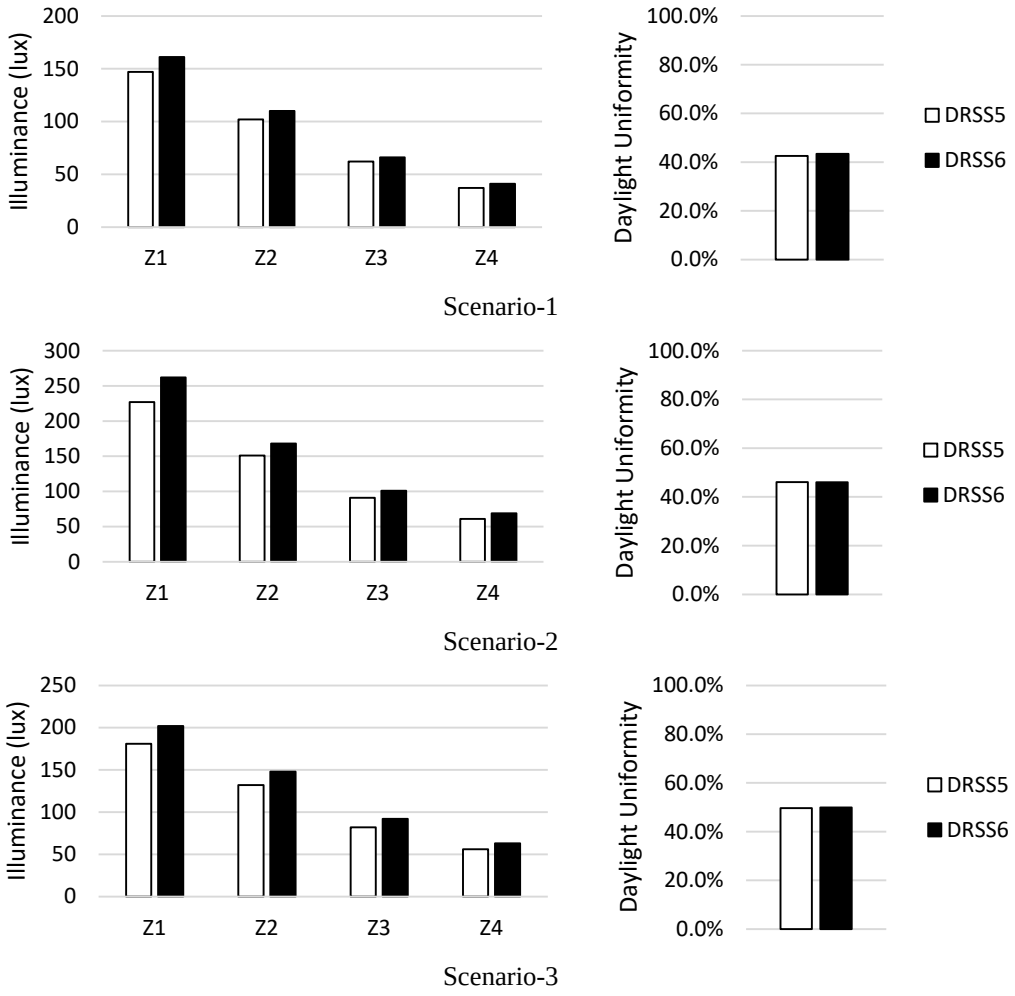


Figure 9.13: The illuminance (left) and DUWP (right) under the DFLS

Effect of material with a flat surface

The effect of the DRDs material on the daylight performance was investigated with a flat surface. The two cases, DRSS7 (white-gloss HIPS) and case DRSS8 (mirror HIPS) are shown in Figure 9.14. The illuminance levels for the four test points and the DUWP are shown in the charts in Figure 8.14 below.

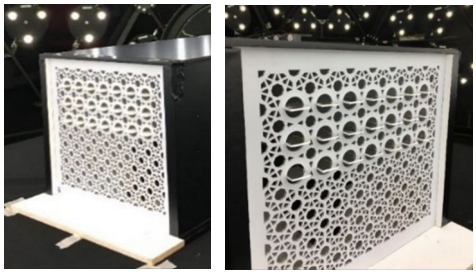


Figure 9.14: External photographs show the used material for the proposed system. White gloss HIPS material on the left and Mirror HIPS material on the right

The charts in Figure 9.15 show that the illuminance was higher at the lowest solar altitude (88 degrees); however, the illuminance at 42-degree solar altitude was higher than the illuminance at 26-degree solar altitude. The DUWP between the two cases was relatively higher with DRSS8 (by 0.5%) at an 88-degree solar altitude. In contrast, the DUWP was relatively higher with DRSS7; it was higher than DRSS8 by 0.3% and 0.4% at 42 degree and 26-degree solar latitudes.

Compared with case PSS5, the range of the change in the illuminance levels were from -7% and -6.3% at Z1 to 0% and 2.6% at Z4, by DRSS7 and DRSS8 at 88-degree solar altitude, respectively. The DUWP was increased by 1.7% and 2.2% with DRSS7 and DRSS8, respectively. At 42-degree solar altitude, the peak change in the illuminance was at Z1 by -13.4% and -11.4, and the lowest was at Z4 by -3% and -1.5%, for DRSS7 and DRSS8, respectively. DUWP was increased by 2.8% and 2.5% by DRSS7 and DRSS8, respectively.

For Nottingham on the 21st of October (26-degree solar altitude), the highest illuminance reduction was at Z1 by 9.8% and 6.7%, while the peak increase was at Z4 by 1.7% and 5.2%, by DRSS7 and DRSS8, respectively. The DUWP was increased by 4.1% and 3.7% by DRSS7 and DRSS8, respectively.

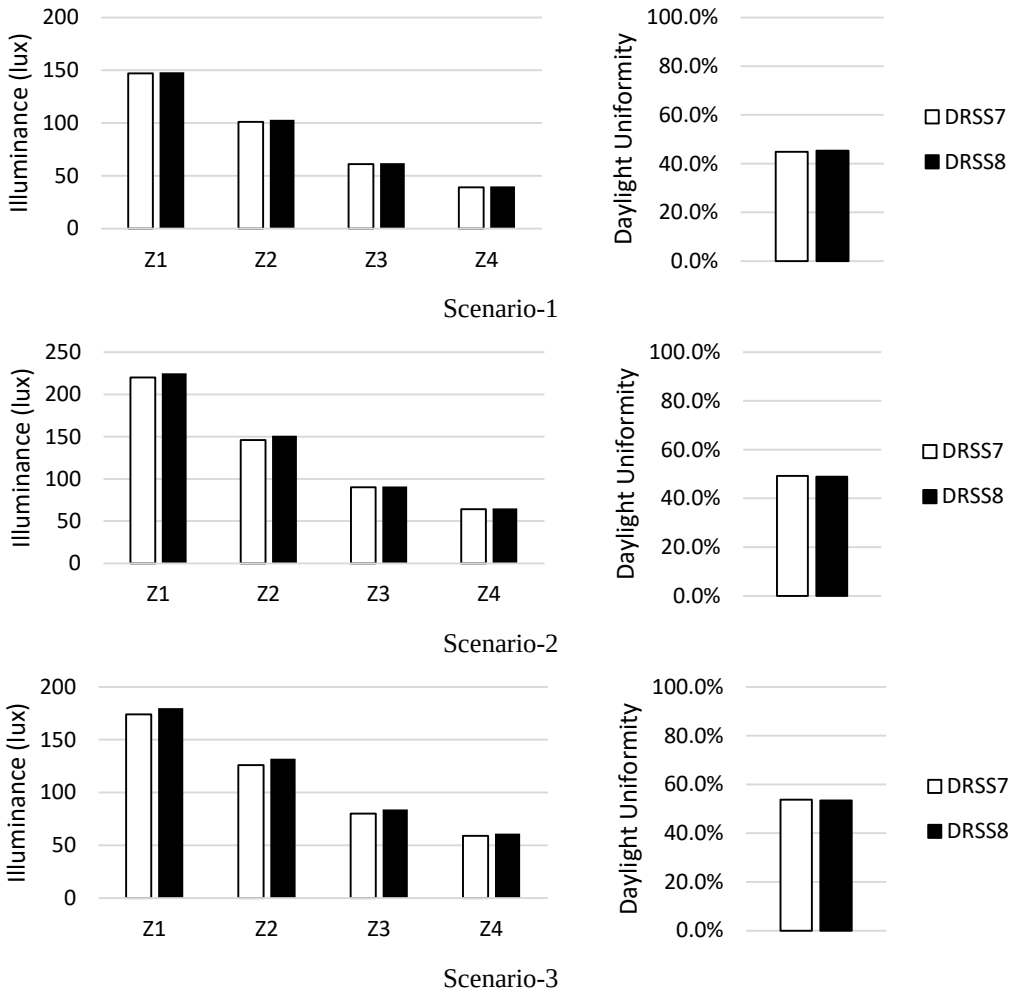


Figure 9.15: The illuminance (left) and DUWP (right) under the DFLS

9.2.5. Effect of geometry

After investigating the DRD material effect on daylight performance, the effect of the DRDs geometry was investigated. The daylight tests were conducted for the proposed parabolic device and a flat surface. The first comparison was between cases DRSS5 and DRSS7, which were made of white-gloss HIPS. The second comparison was between DRSS6 and DRSS8, which are made of mirror HIPS. The illuminance measurements and the DUWP of the cases are shown in Figure 9.17.

Effect of geometry with gloss-white HIPS

First, the daylight study was conducted for cases DRSS5 and DRSS7. As displayed in the charts in fig, it was found that the highest illuminance was recorded at a 42-degree solar altitude. On the other hand, the lowest illuminance values were recorded at an 88-degree solar altitude. In general, DRSS5 has recorded higher illuminance values than DRSS7, particularly at Z1 and Z2. However, the illuminance at Z4 was higher with DRSS7 for the three solar altitudes.

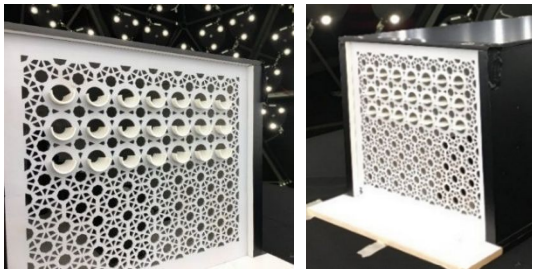


Figure 9.16: External photographs of DRSS5 (left) and DRSS7 (right)

In terms of the DUWP, DRSS7 has recorded relatively higher DUWP than DRSS5. It was higher by 2.3%, 3.2% and 4.1% at 88-degree, 42-degree and 26-degree solar altitudes, respectively.

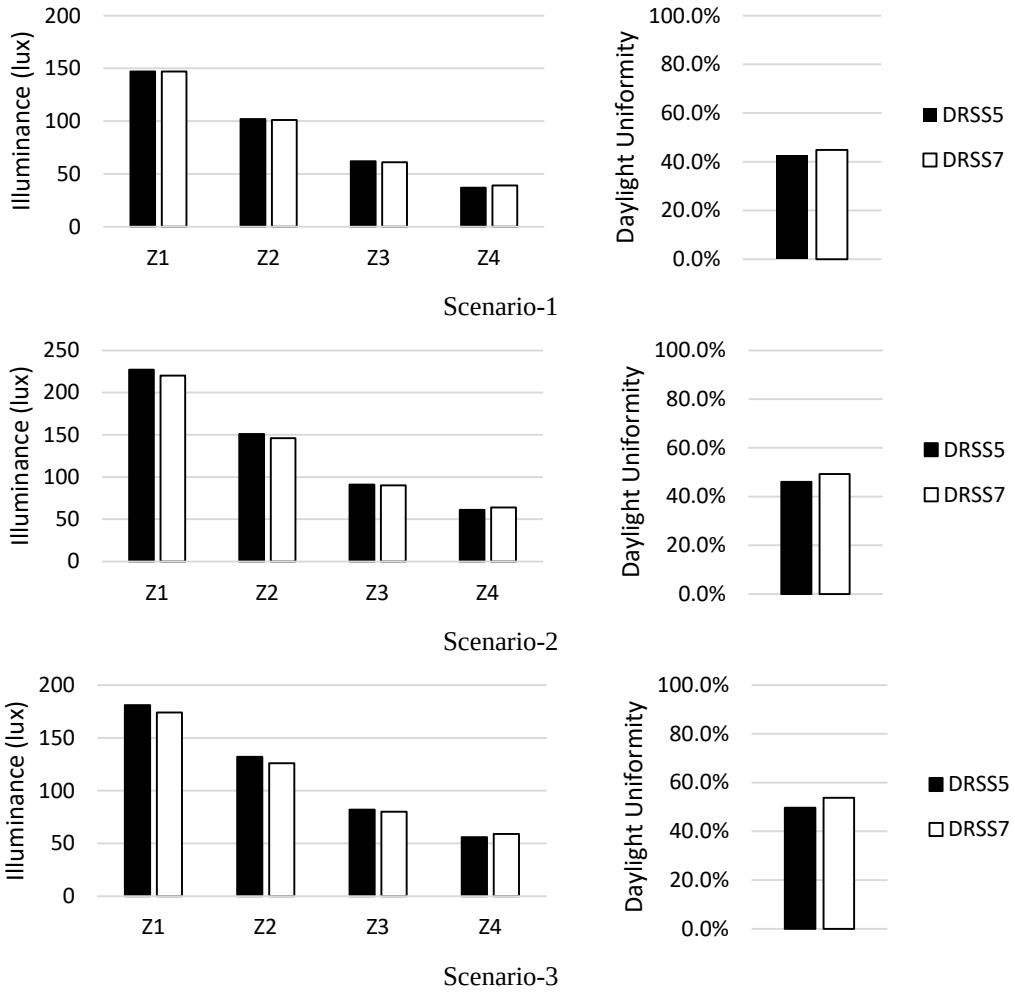


Figure 9.17: The illuminance (left) and DUWP (right) under the DFLS

Effect of geometry with mirror HIPS

A comparison was conducted between the daylight performance with the proposed parabolic device (DRSS6) and a flat surface (DRSS8). The two cases are made of mirror HIPS material. The outputs of the illuminance measurements and the DUWP are shown in Figure 9.18.

It can be seen from the charts below that illuminance was higher at 42-degree solar altitude while the lowest was at 88-degree solar altitude. The highest DUWP was at 26-degree solar altitude, while the lowest was at 88-degree solar altitude.

It was found that the DRSS8 was recorded lower illuminance levels at the four test points at the three solar altitudes. The illuminance was reduced by 8.1%, 6.4%, 6.1% and 2.4% at 88-degree solar altitude, and by 14.1%, 10.1%, 9.9% and 5.8% at 42-degree solar altitude, and by 10.9%, 10.8%, 8.7% and 3.2% at 26-degree solar altitude at Z1, Z2, Z3 and Z4, respectively.

In contrast, the DUWP with DRSS8 was higher than the DRSS6 for the three solar altitudes. The DUWP was higher with DRSS8 by 1.9%, 2.9% and 3.5% at 88-degree, 42-degree, and 26-degree solar altitudes.

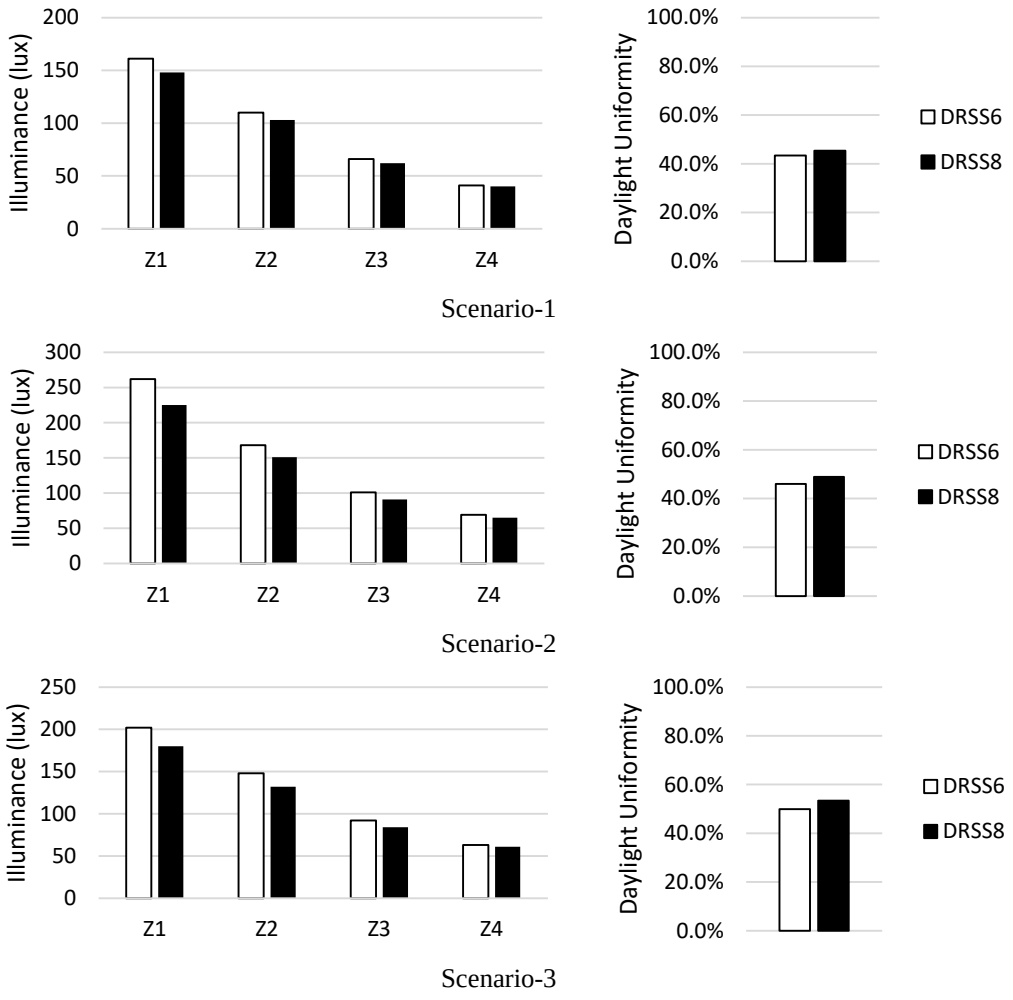


Figure 9.18: The illuminance (left) and DUWP (right) under the DFLS

9.2.6. Effect of truncation

The measured illuminance and the calculated DUWP are shown in the charts in Figure 9.19.

In general, it was found that the DRSS9 increased the illuminance level compared with DRSS8; however, the DUWP was decreased. The illuminance was increased by 7.6%, 6.0% and 4.4% at 42-degree solar altitude, and by 3.9%, 4.5%, and 1.2% at 26-degree solar altitude at Z1, Z2 and Z3, respectively.

In contrast, the illuminance was decreased at Z4 by 5%, 1.5% and 4.9% at 88-degree, 42-degree, and 26-degree solar altitudes, respectively. Similarly, the DUWP was decreased by 2.1%, 3.3% and 3.8%, at 88-degree, 42-degree, and 26-degree solar altitudes, respectively. On the other hand, compared with PSS5, it was found that DRSS9 was not enhanced the daylight performance significantly.

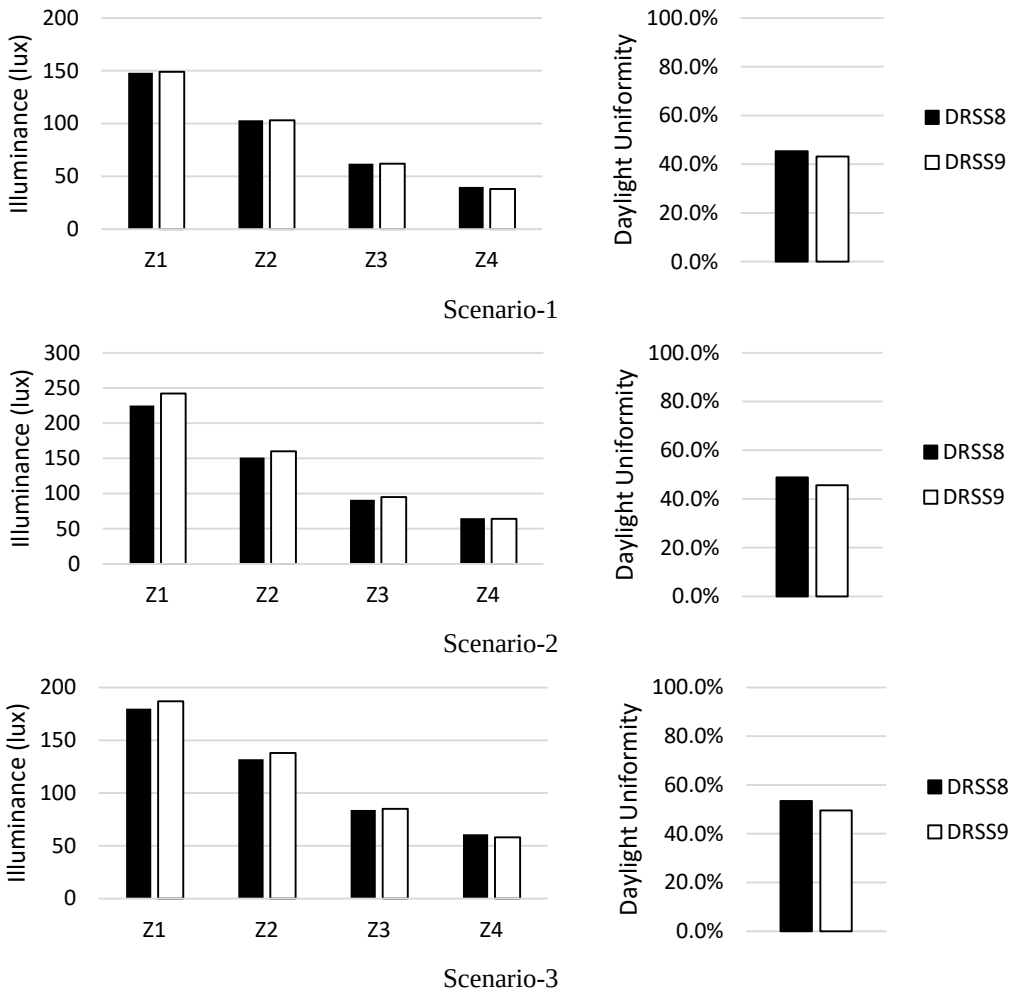


Figure 9.19: The illuminance (left) and DUWP (right) under the DFLS

9.2.7. Effect of prismatic lens

It was found that the daylight performance of DRSS10 was not like what was predicted. The change in the DUWP was insignificant compared with DRSS9 and with PSS5. The DUWP was decreased by 0.1% to 0.8% and by 0.4% to 0.9% compared with DRSS9 and PSS5, respectively.

Similarly, the illuminance levels were decreased by DRSS10. As it is displayed on the charts below, it can be seen that the illuminance was decreased at the four light sensors at all the solar altitudes. The range of the change in the illuminance at 88-degree solar altitude was from 5.4% to 7.9%, at 42-degree solar altitude, it was from 5.4% to 9.5%, and finally, at 26-degree solar altitude, it was from 4.8% to 10.9%. The outputs of the illuminance measurements and the calculated DUWP for the three solar altitudes, namely, 88 degrees, 42 degrees and 26 degrees, are shown in the charts in Figure 9.20. Interior views of the prototype and high dynamic range images (HDR) are presented in Figure 9.21.

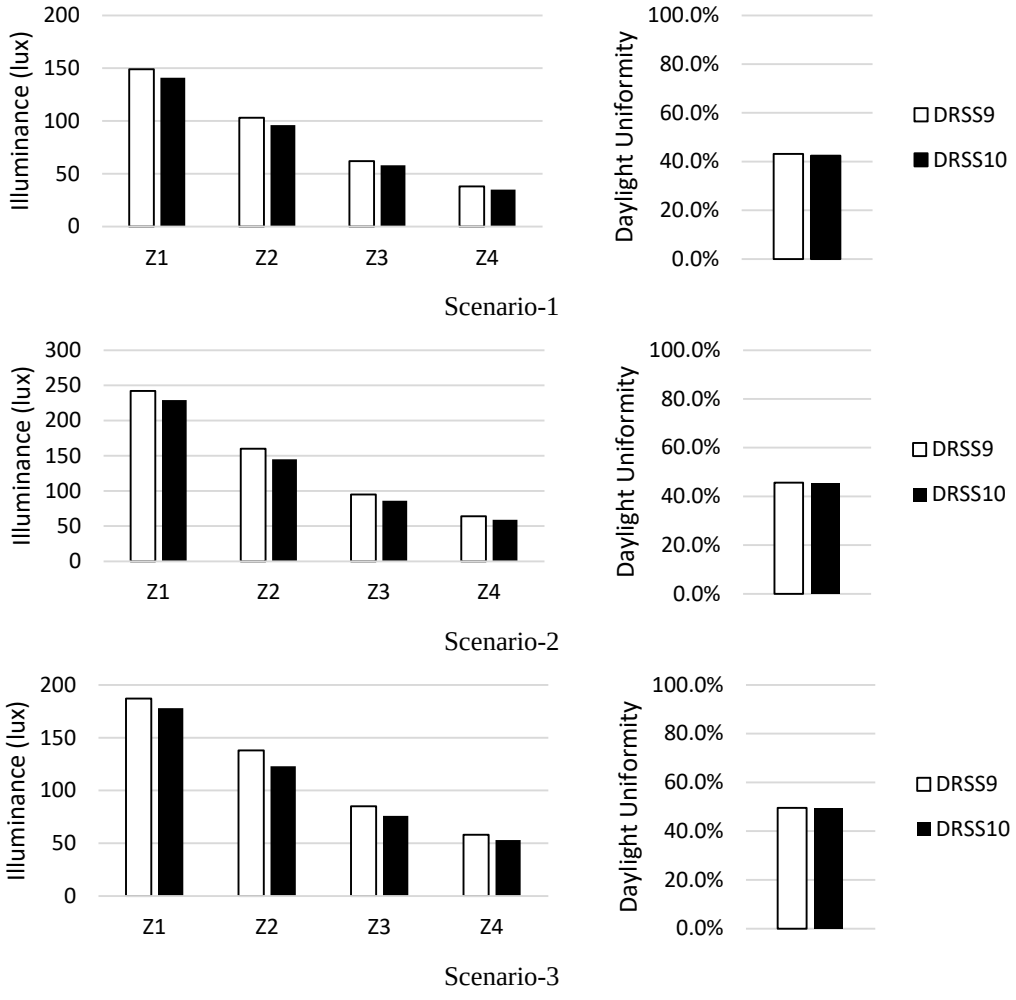


Figure 9.20: The illuminance (left) and DUWP (right) under the DFLS

9.3. Discussion and Conclusions

This chapter presented the measured illuminance values at the work plane by the means of four calibrated light meters. Twelve cases have been tested under the ISO sky conditions as described in (ISO, 2004). The sky that was utilised in this test was the CIE Standard Clear Sky with low luminance turbidity. The test was conducted for solar noon for three solar altitudes, namely, 88-degree (scenario-1), 42 degrees (scenario-2) and 26 degrees (scenario-3). The dates and the location of the tests were Riyadh city on 21st June and 21st December, and Nottingham city on 21st October. The DUWP for each case has been calculated to assess the daylight performance. The study has investigated several DRD parameters: position, unit per area, material, geometry, truncation, and prismatic lens.

The previous test under the DRLS that was presented in chapter 7 was conducted under a simulated direct sun component. Therefore, the purpose of the daylight test in this chapter was to investigate the daylight performance of the proposed system under a diffuse sun component. The diffuse sun component is the sky patches that reflect the sunlight that produces by the sun.

Although the sky dome at the IEDE has both the direct sun component and the sky patches (diffuse light component), the direct sun component was not utilised in this test. It was found that the direct light component of the sky dome does not represent the accurate light intensity for the direct sun component. Although it can be located in the correct position obtained by the given location, the intensity of the light was extremely low compare to the change in the sky patches component. As a result, it was recommended to use the sky component alone.

The results provided a good understanding of the daylight performance of the proposed system under a diffuse sky with three different solar altitudes. The comparison of cases PSS5 and DRSS1 showed that the change in the illuminance levels was less with 88-degree and 42-degree compared with 26-degree solar altitude.

The investigations of the influence of the DRD position showed that the maximum change in the DUWP was recorded with the lower DRD position (DRSS1) at 88-degree solar altitude by 2%. The illuminance levels were higher at a 42-degree altitude for the three cases. The findings showed that when the DRD position raises and the solar altitude decrease, the illuminance at the front area increased. As a result, the lower DRD position is better to redirect the daylight to a deeper area towards the ceiling. The effect of the unit per area ratio was investigated. The findings showed that the DUWP increased when the solar altitude decreased. For example, the DUWP for DRSS4 was 42.8% at 88-degree altitude, while it was 50.1% at 42-degree altitude.

The investigation of the material effect showed that the mirror HIPS increased the illuminance levels at the work plane for all the daylight zones and all tested solar altitudes. The impact of the mirror material was higher with the parabolic surface compared with the flat surface. Nevertheless, it is important to mention that the mirror HIPS has lost some of its reflectivity during the forming process. As a result, it can be expected that a perfect parabolic mirror surface could redirect a more significant amount of daylight towards the ceiling.

The impact of the DRD truncation was found to be effective to increase the illuminance levels, particularly at the 42-degree and 26-degree solar altitudes. In contrast, the DUWP was relatively decreased due to increased illuminance at the front areas. The integration of the prismatic lens has reduced the illuminance levels at the front area, but the DUWP was not increased.

The objective of this chapter was to test the proposed system under the diffuse sky, a solar simulator with sky components. Furthermore, the objective of the previous test under the direct-light simulator was to test the proposed system under a direct light solar simulator. Therefore, it was essential to test the model under real sky conditions with both daylight components, namely, the sun component (direct sunlight) and the sky component (diffuse daylight).

Chapter 10. Test under real sky

10.1. Introduction

The physical model was tested under a real sky in Nottingham city, United Kingdom. Nottingham has N 52° latitude and W 1° longitude. The test was conducted at noon (solar time) on the 21st of October 2020. The model orientation was towards the south. The solar altitude and the azimuth angles were 26 degrees and 180 degrees, respectively.

10.2. Purpose of the experiment

The test was conducted for two main purposes. First, it was conducted to observe and investigate the effect of the tested parameters under a real sky with sun and sky components, as this was not available in the two previous experiments. As mentioned previously, the direct-light simulator represents only the direct sun components. Similarly, the diffuse sky dome represents only the sky elements. Therefore, it was necessary to conduct the daylight test under a real sky with the two mean components of the daylight source.

The second purpose of the experiment was to determine the uncertainty between the outputs of the computer simulation and the test under the real sky conditions. A daylight study was conducted by computer simulation in Radiance under the same conditions of the sky and the same properties of the model. The variance between the outputs was investigated and discussed.

10.3. Experiment setup and procedure

In order to assess the daylight performance inside the tested room, the daylight factor was obtained at the front area of the room and the back of the room. The illuminance level was measured at Z1 and Z4, which represent daylight zone Z1 and Z4. Another two lux-meter were placed above the roof, as a simultaneous illuminance reading is necessary to calculate the daylight factor under such an inconstant daylight source.

The orientation of the model was set up towards the south by a compass. As the azimuth angle at solar noon on the south is 180, it was possible to ensure that the orientation and test time were accurate, as shown in Figure 10.1. The solar time was obtained from (Agafonkin, 2020) and by Ladybug Tools software. It was found that the 12 pm solar time was 11:50 am local time.

The daylight factor has been calculated for each point as well. The daylight factor was calculated by dividing the internal illuminance value of each test point on the illuminance value at the exact location above the roof of the room. The calculation was conducted based on Equation 1. The tested cases are shown in Figure 10.2 and Table 10.1.

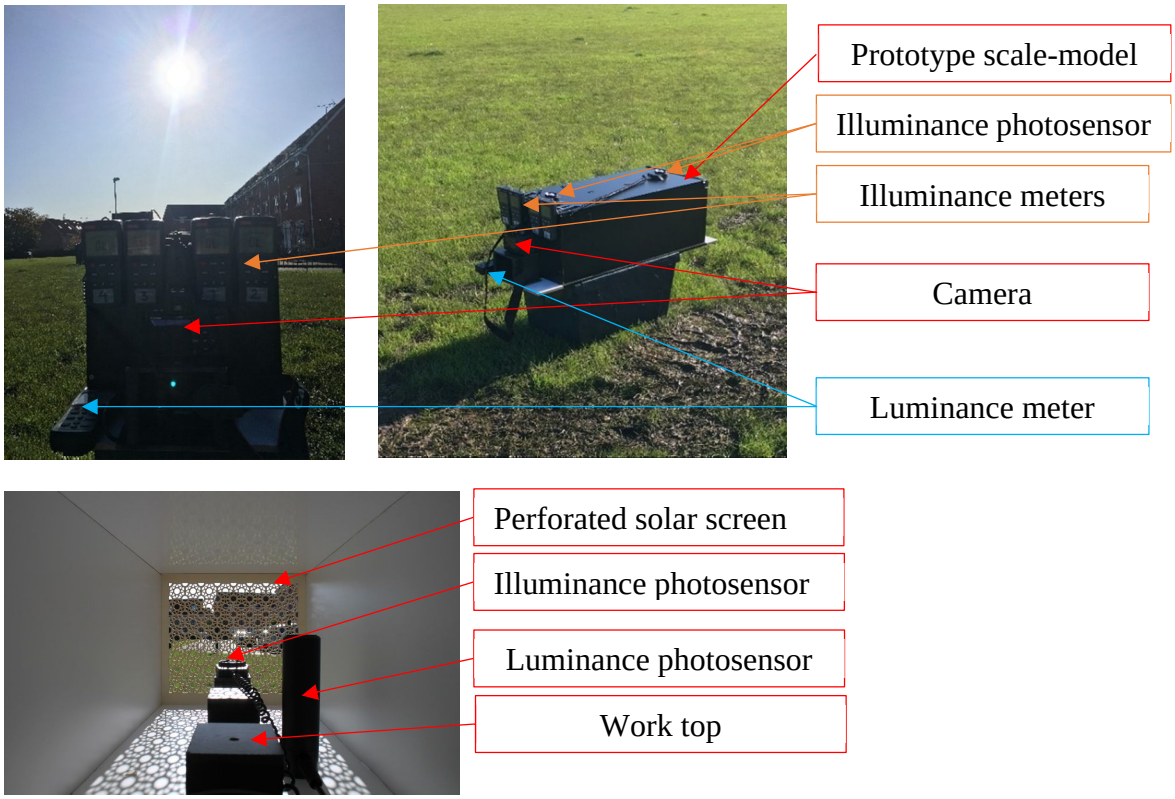


Figure 10.1: The sun azimuth was 180 degrees from the north. A clear sunny day in Nottingham on 21 st Oct at solar noon

Table 10.1: Main parameters and their properties

	Parameter	**Properties**	**Case**
1	Position	Low	DRSS1
		Medium	DRSS2
		High	DRSS3
2	Per unit area ratio	7 per 9m^2	DRSS1
		14 per 9m^2	DRSS4
		21 per 9m^2	DRSS5
3A	Material [Parabolic]	White-Gloss HIPs	DRSS5
		Mirror HIPs	DRSS6
3B	Material [Flat]	White-Gloss HIPs	DRSS7
		Mirror HIPs	DRSS8
4A	Geometry [White-Gloss HIPs]	Parabolic	DRSS5
		Flat	DRSS7
4B	Geometry [Mirror HIPs]	Parabolic	DRSS6
		Flat	DRSS8

5	Truncation	Parabolic	DRSS9
6	Prism	Parabolic	DRSS10

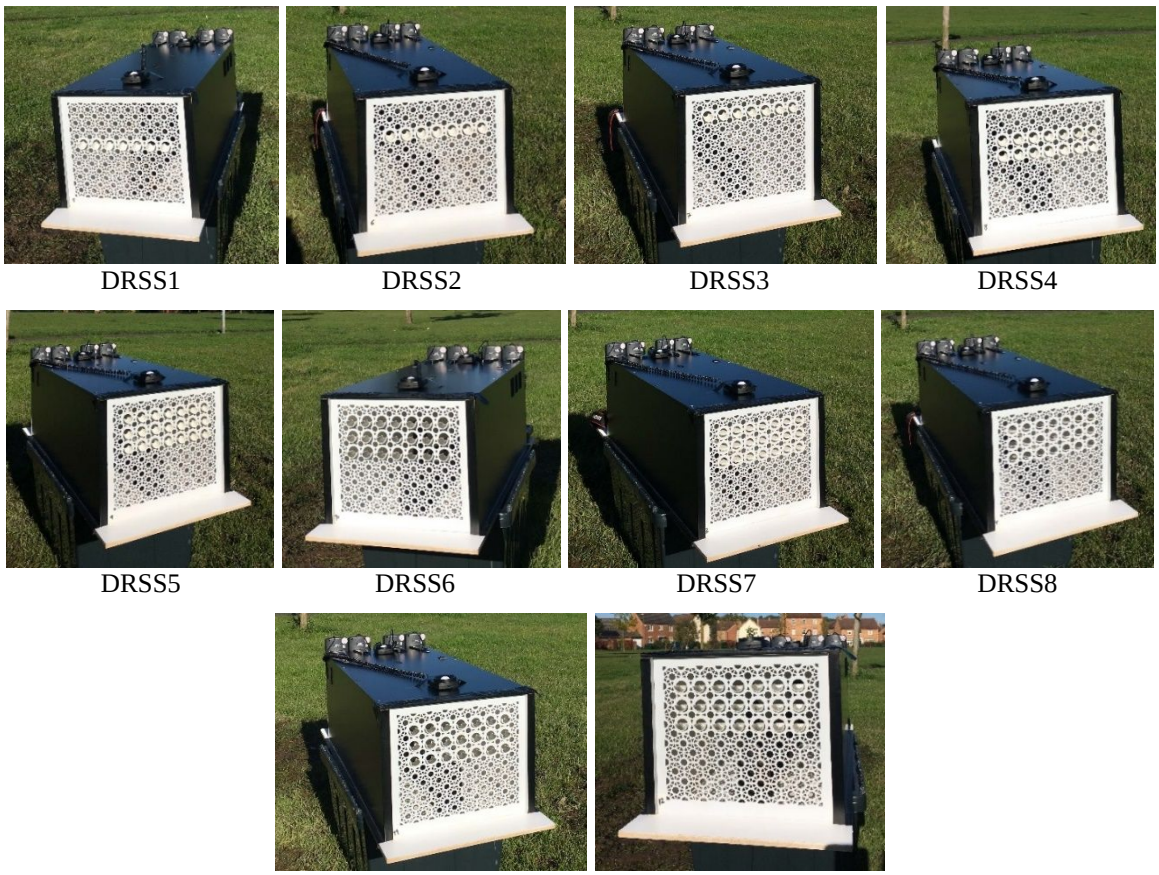


Figure 10.2: Exterior view of the model under the real sky in Nottingham on 21 October at solar noon

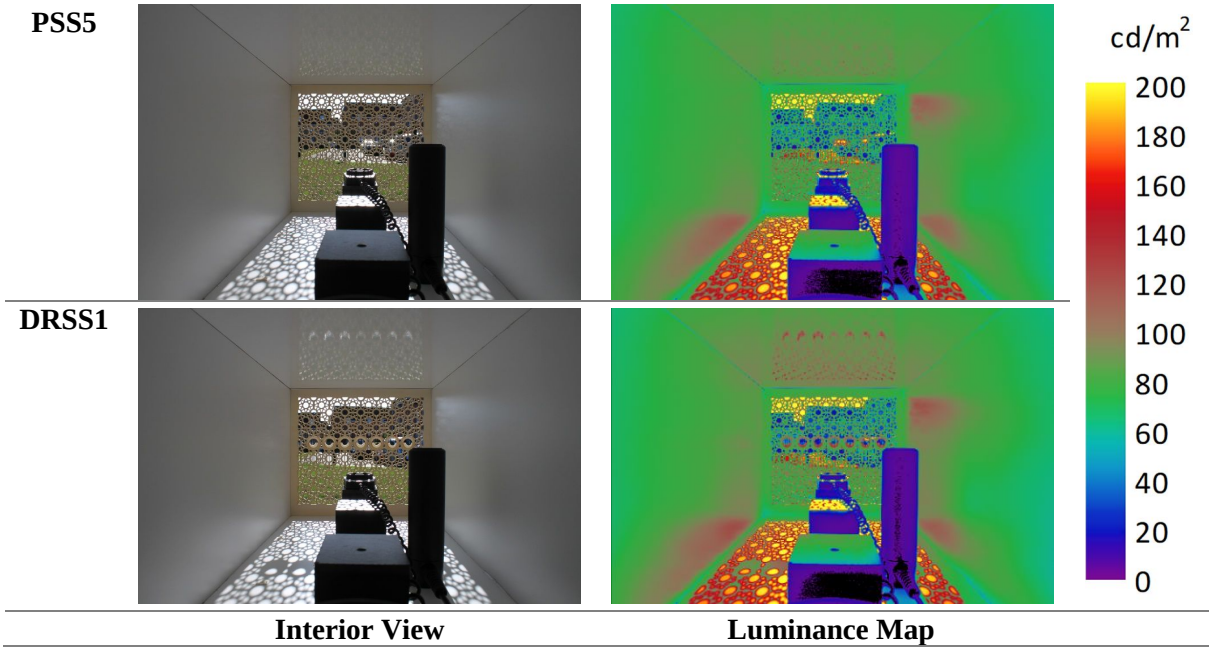
10.4. Results

The daylight was assessed by the daylight factor (DF) at Z1 and Z4. Later, the relationship between the luminance at the ceiling (cd/m2) and the illuminance level at the work plane (lux) was investigated. Then, the luminance at the interior surfaces was obtained and discussed.

10.4.1. Comparison of PSS5 and DRSS1

The daylight factor was calculated at Z1 and Z2 for the perforated solar screen with a 33% perforation ratio (PSS5) and the proposed integrated daylight-redirecting solar screen (DRSS1), which has seven DRD units at 1.55-meter height from the floor. As it is displayed in the chart in Figure 10.3, it was found that the DF at Z1 was significantly high for the two cases.

On the other hand, the DF at Z4 was low compared with DF at Z1. The DF was reduced by DRSS1 at the front area by 6.9% and the rear area by 0.3% compared with PSS5.



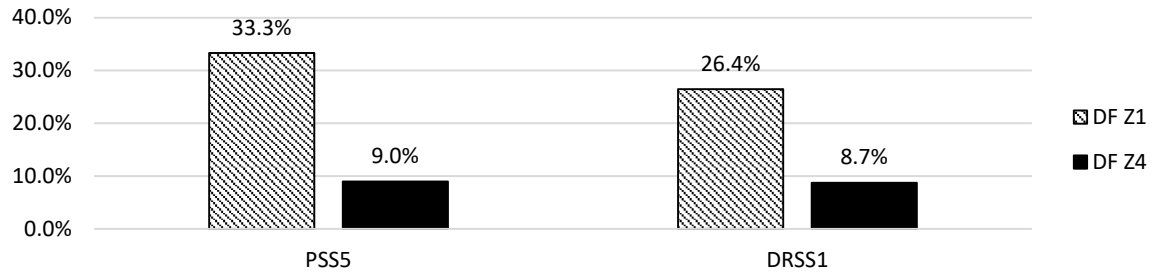


Figure 10.3: Daylight factor (%) at light sensor Z1 and Z2 for Case PSS5 and DRSS1

10.4.2. Effect of position

The effect of the DRD devices position on the daylight performance at the work plane was investigated. Three cases were compared; each case has seven DRD units aligned in one row. The height of the DRD devices was 1.55-meter, 1.88 meters and 2.1 meters for DRSS1, DRSS2 and DRSS3, respectively, as shown previously in Figure 8.11. The daylight factor at the first and the second half of the room was calculated and compared for DRSS1, DRSS2 and DRSS3.

It was found that the DF at Z1 was increased when the DRD devices height was raised. The DF at Z1 was increased by 5% and 7.4% by DRSS2 and DRSS3, respectively, compared with DRSS1. On the other hand, the DF at Z4 was decreased relatively with a higher DRD devises position. It was reduced by 0.2% and 0.4% by DRSS2 and DRSS3 compared with DRSS1, as shown in the chart in Figure 10.4.

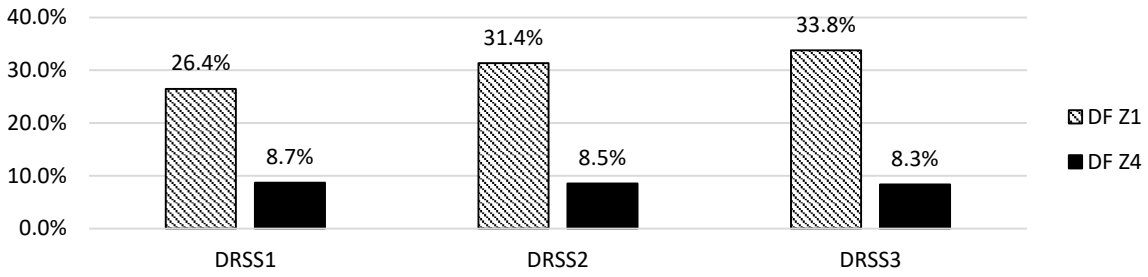


Figure 10.4: Daylight factor at light sensor Z1 and Z2

10.4.3. Effect of unit per area ratio

The effect of the ratio of the DRD units per façade area on the daylight performance was assessed. Three ratios were tested, 7-unit per area, 14-unit per area, and 21-unit per area. The names of the cases are DRSS1, DRSS4 and DRSS5. The cases were illustrated previously in Figure 8.12.

As it is shown in the chart in Figure 10.5., it can be seen that the DF at Z1 was higher for DRSS4. The DF was increased at Z1 by 4.2% by increasing the DRD units from 7 units to 14 units. In contrast, the increase of the units from 7 units to 21 units has reduced the DF relatively at Z1 by 1.2 compare with DRSS1. On the other hand, at Z4, the change in the DF was insignificant. It was decreased by 0.2% and 0.5% by DRSS4 and DRSS5 compared with DRSS1.

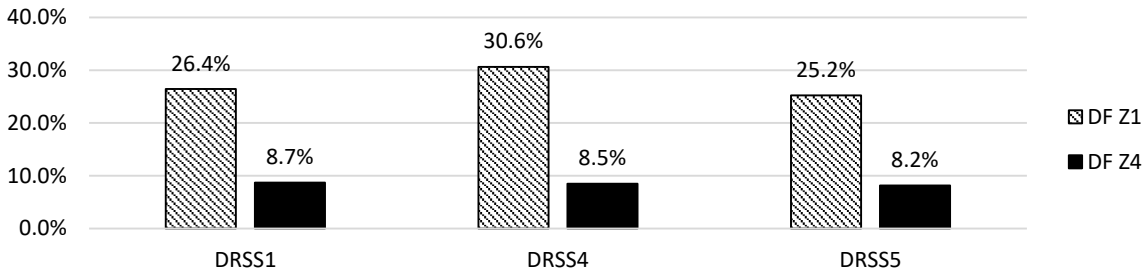


Figure 10.5: Daylight factor at light sensor Z1 and Z2

10.4.4. Effect of material

The effect of DRD devices material on the daylight performance was investigated. The effect of the material was assessed for the parabolic proposed daylight-redirecting devices and with a flat surface. As mentioned previously, some of the optical properties of the material have been changed after the fabrication of the DRD devices. Therefore, the material was tested on a flat surface. The purpose was to investigate the effect of the material on its original optical properties.

The daylight factor at Z1 and Z4 for cases DRSS5 and DRSS6 are illustrated in the chart in Figure 10.6 [A]. The DRD devices for DRSS5 are made of white-gloss HIPS material, while DRSS6 consists of DRD devices made of mirror HIPS material. It can be seen that the DF was increased at Z1 by 5.6% by DRSS6 compared with DRSS5. Similarly, the DF was relatively increased by DRSS6 by 0.9%.

In contrast with the effect of the material with the parabolic devices, it was found that the effect of the material with a flat surface was insignificant. As shown in the chart in Figure 9.6 [B], the DF was increased only by 1% at Z1 and by 0.4% at Z4 by using the mirror HIPS material.

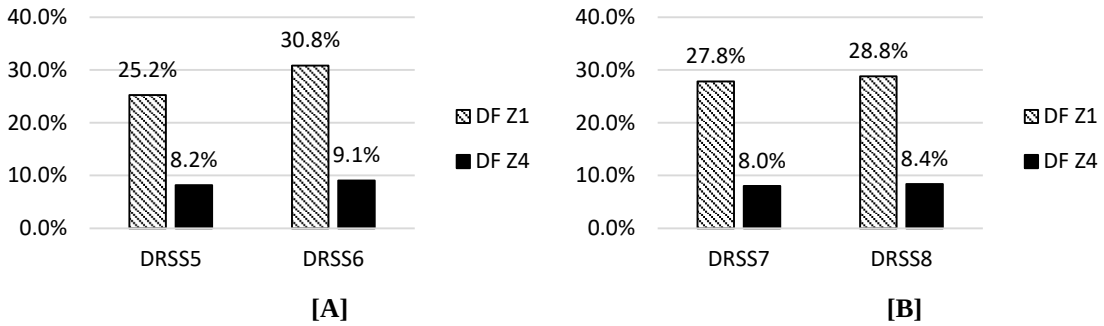


Figure 10.6: Daylight factor at light sensor Z1 and Z2

10.4.5. Effect of geometry

The effect of the DRD devices geometry on the daylight performance was investigated. The proposed parabolic geometry was compared with a flat surface. The comparison was conducted for daylight-redirecting devices made of white-gloss HIPS and others made of mirror HIPS.

The DF values of the parabolic and flat white-gloss HIPS devices are presented in the chart in Figure 10.7 [A]. The DF was increased at Z1 by 2.6%, while it was decreased by 0.2% at Z4 utilising the flat devices (DRSS7) compared with parabolic devices (DRSS5). In contrast, for the mirror HIPS devices, the flat daylight-redirecting devices (DRRS8) reduced the DF at Z1 and Z4 by 2% and 0.7%, respectively, as shown in the chart in Figure 10.7 [B].

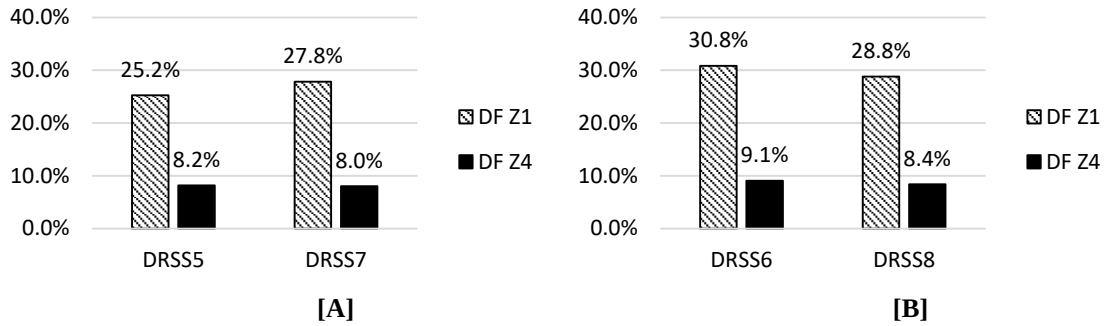


Figure 10.7: Daylight factor at light sensor Z1 and Z2

10.4.6. Effect of truncation

The truncation of DRD devices inlet and outlet on the daylight performance was investigated. It was found that the truncated DRDs (case DRSS9) reduced the DF from 30.8% to 26.1% i.e.; by 4.7% at the front area and from 9.1% to 8.55 i.e.; by 0.6% at the deep area compared with DRSS6, as shown in the chart below in Figure 10.8.

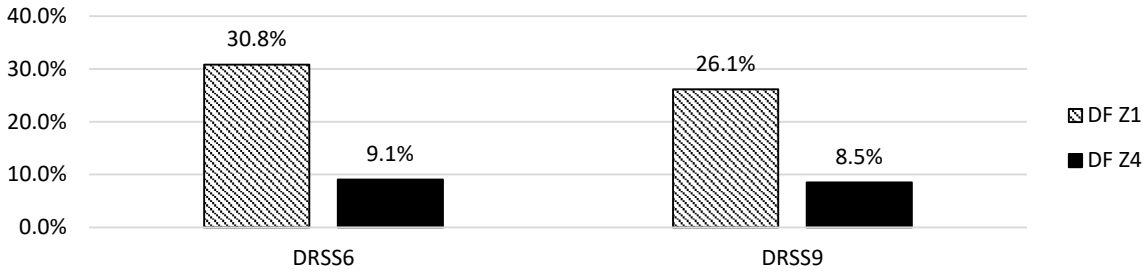


Figure 10.8: Daylight factor at light sensor Z1 and Z2

10.4.7. Effect of prismatic lens

A prismatic lens was integrated with the DRD devices to enhance the daylight performance inside the room. The effect of the prismatic lens was assessed through the comparison of DF values at Z1 and Z4. It can be seen in the chart in Figure 10.9 below that the prismatic lens (case DRSS10) has increased the DF from 26.1% to 28.6% i.e.; by 2.5% at Z1; however, the DF at Z4 was reduced relatively from 8.5% to 8.1% i.e.; by 0.4%, compared with DRSS9.

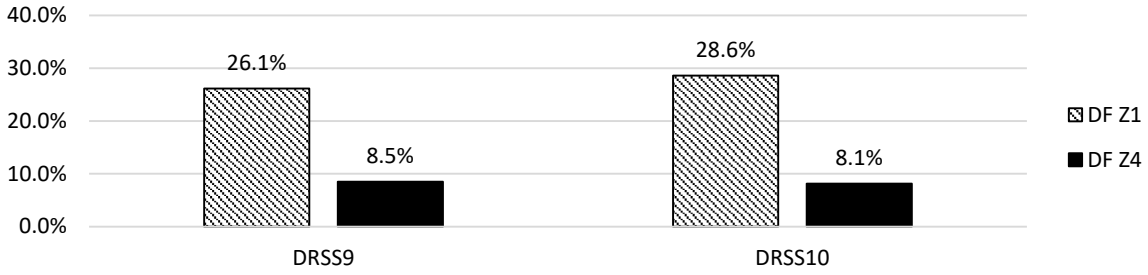


Figure 10.9: Daylight factor at light sensor Z1 and Z2

10.5. Validation of the simulation model

The results of the daylight assessment that were obtained by the computer simulation in RADIANCE were validated against the outputs that were obtained for the prototype scale-model under the real sky condition of Nottingham city, UK. The test was conducted on 21 October at solar noon, see Figure 10.10. The daylight factor (DF) and daylight uniformity indicators were utilised to compare the outputs. The illuminance levels were measured at four light sensors, namely, Z1, Z2, Z3 and Z4.

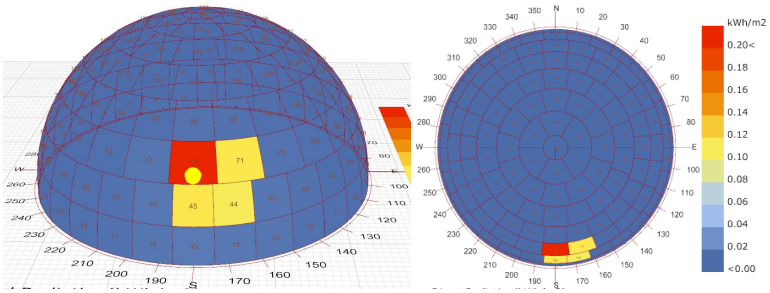


Figure 10.10: Luminance distribution and Sky patch and sun position for Nottingham city, 21st October at solar noon. Tregenza sky division.

Scale models have been utilised for centuries by architects to study the daylight performance of buildings. Scale models can be tested either under a real sky or under an artificial solar simulator. The variation of the outputs of the scale model tested under the real sky can be significant due to the change in the solar radiation over a short period, such as a minute or even shorter. Therefore, daylight factor (DF) was utilised widely to assess the scale model due to the inconstant light intensity of the real sky (Tregenza and Mardaljevic, 2018).

The results of the simulation for case DRSS5 were compared to the outputs that were obtained under the real sky. The chart in Figure 10.11 below shows the daylight factor values (DF). It was found that the DF values were higher under the real sky compared to the simulation at the same test points. The variation among the DF values was ranging from 5% at Z4 to 10% at Z2; however, the change was linear.

In addition, the daylight uniformity values were compared under the two test conditions. Similarly, it was found that the daylight uniformity value under the real sky was higher than the simulation by 17%. The daylight uniformity was 46% and 29% under the real sky and in the simulation, respectively, as displayed in Figure 10.12. The increase in the daylight intensity

inside the prototype-scale model compared with the simulation modelling can be due to the scale effect, as the ratio between the two models is 1:10.

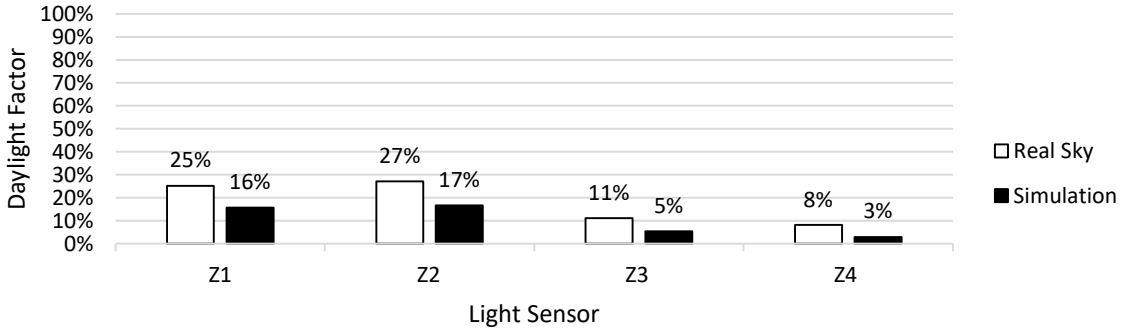


Figure 10.11: Daylight factor values of case DRSS5 in Nottingham on 21st October at solar noon

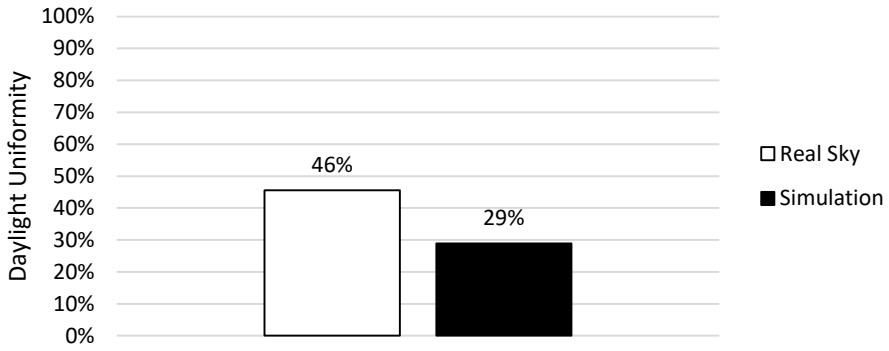


Figure 10.12: Daylight uniformity values of case DRSS5 in Nottingham on 21st October at solar noon

10.6. Discussion and Conclusions

The proposed daylight-redirecting system was tested under a real sky in Nottingham city on 21 October at solar noon. The daylight performance was assessed through the analysis of the DF values. First, the performance of DRSS1 was compared with PSS5. Then, the tested effect of the tested parameters was investigated. The parameters are the DRD position, unit per area ratio, material, geometry, truncation, and the prismatic lens.

The comparison of the DRSS1 and the PSS5 showed that the DF was enhanced by the integration of DRD. The DF reduced in the front area from 33.3% to 26.4%. The DRD plays a vital role in reducing the direct sunlight that could access through the perforation of the PSS. Simultaneously, the DF in the rear area was reduced only from 9.0% to 8.7%, which was not significantly reduced. Nevertheless, it is higher than the minimum recommended DF for an office building, which is 4%. According to BREEAM (2016), at least 80% of the area should

have a 4% average daylight factor at offices within single-story buildings and a 3% average daylight factor within multi-story buildings.

The analysis of the DRD position effect showed that the DF increased at the front area when the DRD position increased. In contrast, the DF relatively decreased in the rear area when the DRD position increased. Therefore, the lower DRD position performed better in reducing the illuminance level at the front area and increasing it at the rear area of the room. Nevertheless, this finding may differ if the solar altitude has changed.

The effect of the unit per area ratio was not parallel at the front area (Z1) as the DRD position. For instance, DRSS4, which has 14 units, recorded a higher DF value at Z1 than DRSS1 (7 units) and DRSS5 (21 units). On the other hand, the DF value was relatively increased when the DRD units increased. However, DRSS5 performance was better because it reduced the difference between the DF values at the front and the rear area of the room.

The effect of DRD material was tested with parabolic and flat surfaces. The findings showed that the mirror material increased the DF value at the front and the rear area of the room. The impact of the mirror material was higher with the parabolic geometry. It increased the DF at Z1 from 25.2% to 30.8%; however, at Z4, it increased only from 8.2% to 9.1%. Therefore, it can be noticed that the DRD redirect a large amount of sunlight in the front area of the ceiling compared with the rear area. As mentioned previously in chapter 8, the mirror surface has lost some of its reflectivity during the forming process. As a result, a different method to produce a DRD with an interior mirror surface will be followed in future work.

The DRD inlet was truncated to allow the sunlight to reach the lower rows of DRDs. The findings showed that the DF was reduced at both Z1 and Z4; however, the gap between the DF values was reduced. Later, the truncated DRDs were integrated with a prismatic lens to increase the depth of the redirected sunlight at the ceiling. The findings showed that the prismatic lens increased the DF at Z1 and decreased it relatively at Z4. It was noticed that the transparency of the prismatic lens was decreased. The dust on the lens could be the reason that it reduced its daylight-redirecting properties.

The results of the daylight assessment of case DRSS5 obtained by the simulation were validated against the outputs of the prototype under a real sky in Nottingham city, UK. The variation in the daylight factor values for each light sensor was measured. It was found that the difference between the DF values was ranging from 5% to 10%. Afterwards, the daylight uniformity was calculated, and the variation among the daylight tests was calculated. The

analysis of the daylight uniformity showed that the variation between the outputs under the real sky and the simulation results was 17%.

Chapter 11. Alternative DRD design and further investigation

11.1. Introduction

After the completion of the experimental tests and the validation study, an alternative DRD design was proposed and developed. This has investigated the potential of enhancing the daylight performance through the utilisation of the daylight-redirecting device (DRD) in a reverse mode. In addition, the impact of the geometry and the tilt angle of the DRD weretested. Furthermore, the effect of integrating innovative glazing within the DRD was investigated. A prismatic lens was applied to enhance the redirecting functionality of the device.

The daylight assessment of the design was achieved through a raytracing study at solar noontime. Then, the illuminance levels and the daylight uniformity at the work plane (DUWP) were assessed for the summer solstice, autumn equinox, and winter solstice days. The assessment was conduct at 8 am, 10 am, 12 pm, 2 pm and 4 pm, solar time. The tests in this stage were conducted for Riyadh city latitude in Saudi Arabia. The daylight analysis was achieved through a point-in-time daylight study (PIT).

In addition, an annual daylight study was conducted for the whole year. Furthermore, the daylight performance was evaluated for each season. Three daylight metrics were utilised for this purpose, daylight autonomy (DA), annual sunlight exposure (ASE), and useful daylight illuminance (UDI). Finally, the daylight performance of the optimal proposed systems and the base case were compared. The comparison was conducted through an assessment of the DUWP for the tested hours and through an annual daylight performance.

11.2. Optimisation process

First, as it was mentioned in Chapter 4, the proposed DRD was created based on a design of a compound parabolic concentrator (CPC). While the effect of the CPC in a normal mode was assessed in the previous chapters, in this phase, the influence of the CPC in a reverse mode was investigated. The CPC in the normal mode has a large inlet and smaller outlet; on the other hand, in the reverse mode, the inlet is smaller than the outlet. As a result, the curvature of the CPC in the reverse mode may increase the depth of the redirected sunbeams on the ceiling. The assessment of the CPC performance in the normal mode showed that most of the sunbeams

were redirected near the front area of the ceiling. On the other hand, the curvature of the CPC in the reverse mode should increase the distance of the redirected sunbeams on the ceiling.

Therefore, CPC units in a reverse mode were applied as DRD units with a 7-unit/area ratio. Next, the daylight redirection function of the DRD units was analysed using a raytracing study. Later, the geometry of the original CPC unit was optimised. Afterwards, the daylight redirection function of the developed CPC has been analysed through a raytracing study.

Subsequently, the developed CPC was applied as DRD units with a 21-unit/area ratio (case DRSS11). The daylight performance of case DRSS11 was assessed through raytracing and climate-based daylight modelling methods. Hourly evaluations for the summer solstice, autumn equinox, and winter solstice days were conducted. In addition, a seasonal daylight assessment was conducted for spring, summer, autumn and winter.

Second, the performance of the DRDs was assessed at the highest solar altitude using a raytracing method for 7 tilt angles from 0 to 30 degrees with a 5-degree interval, as shown in Table 11.1. The enhancement in the daylight redirection function was measured and discussed. Afterwards, hourly assessments for the daylight intensity were conducted for the 7 tested cases, namely, cases DRSS11-A to DRSS11-G. Later, a seasonal daylight analysis was conducted for the optimal case.

Table 11.1: Cases names and tilt angles in degree

Case	**DRSS11-A**	**DRSS11-B**	**DRSS11-C**	**DRSS11-D**	**DRSS11-E**	**DRSS11-F**	**DRSS11-G**
Tilt	0	5	10	15	20	25	30

The effect of integrating a prismatic lens was investigated (case DRSS12). A prismatic lens was integrated within case DRSS11-B, which was optimal among the other tested cases. The prismatic lens was installed vertically on the DRD outlet, as shown in Figure 11.1. The function of the lens was to redirect the daylight that is received from low soar altitudes, for instance, during the early morning and the late evening and in winter. The illuminance level at the work plane was assessed through PIT and annual daylight studies.

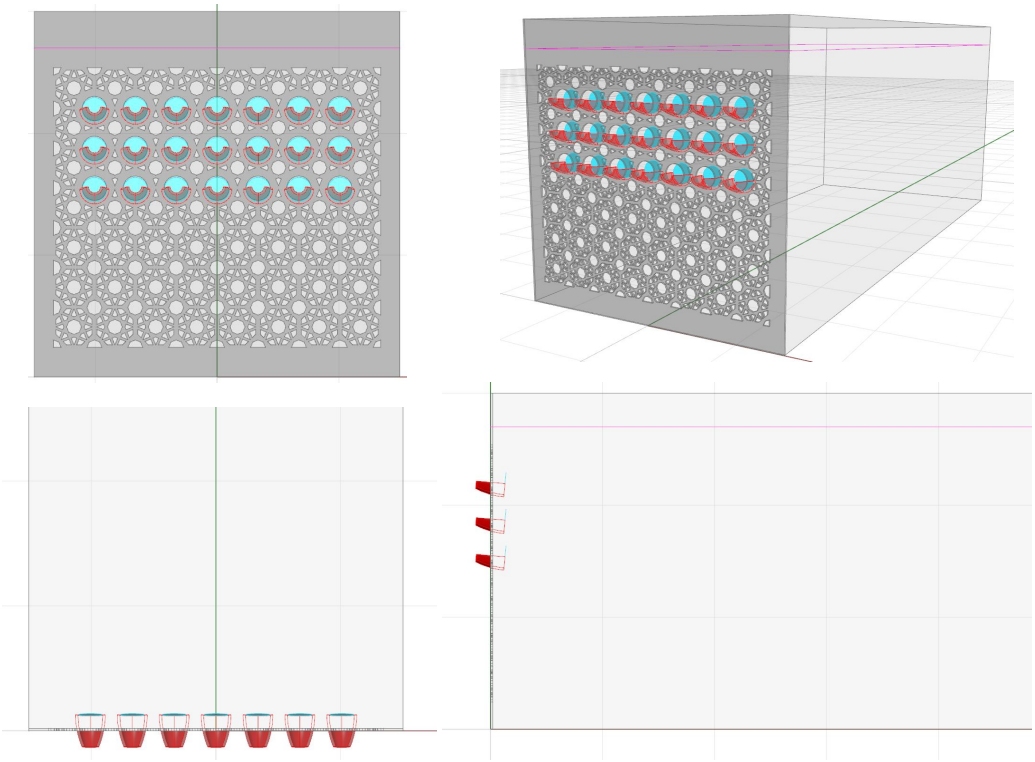


Figure 11.1: Integration of prismatic lens within the DRD units

11.3. Results

11.3.1. Further investigationof the geometry

11.3.1.1. Raytracing study

The performance of the original CPC units in a reverse mode was investigated. Figure 11.2 illustrates the sun paths behaviour of the direct light beams. The raytracing study was conducted for solar noon on the summer solstice, autumn equinox, and winter solstice. It was found that direct sunlight could not access the interior surface of the CPC on the summer solstice. It can be seen that all the direct sunlight is redirected outdoor. On the other hand, on the autumn equinox, the CPC unit can redirect the direct sunlight towards the ceiling. The maximum depth of the redirected light beam can reach 2.64 meters from the external façade.

Nevertheless, the CPC redirected the sunlight to further distance on the ceiling on the winter solstice day. It was found that the redirected beams reached 4.12 meters from the façade. However, it was noticed that some of the redirected beams could be redirected at low vertical levels, which may reach the eye level of a standing person. Therefore, a glare study was conducted to investigate the possibility of visual discomfort occurrence.

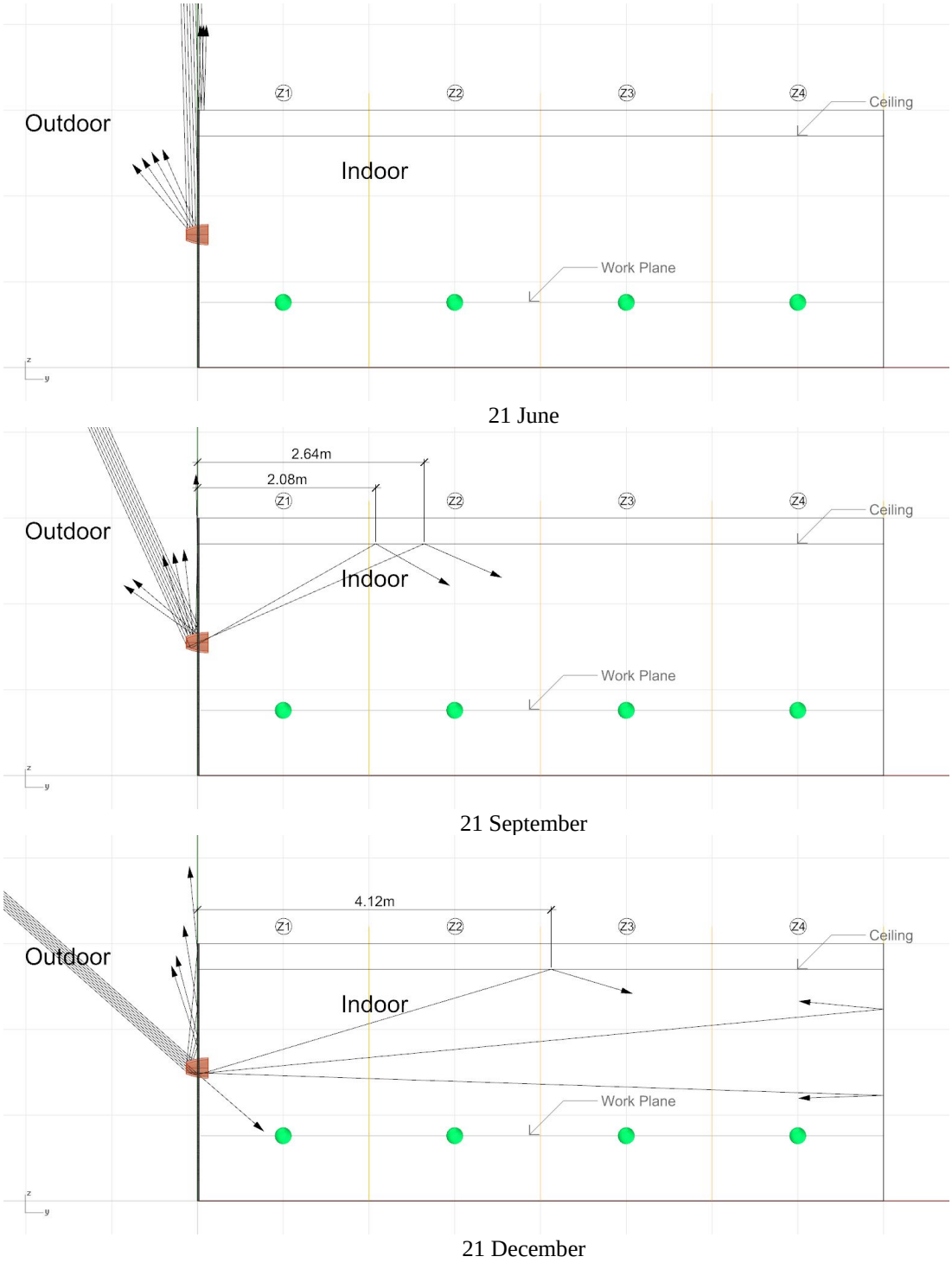


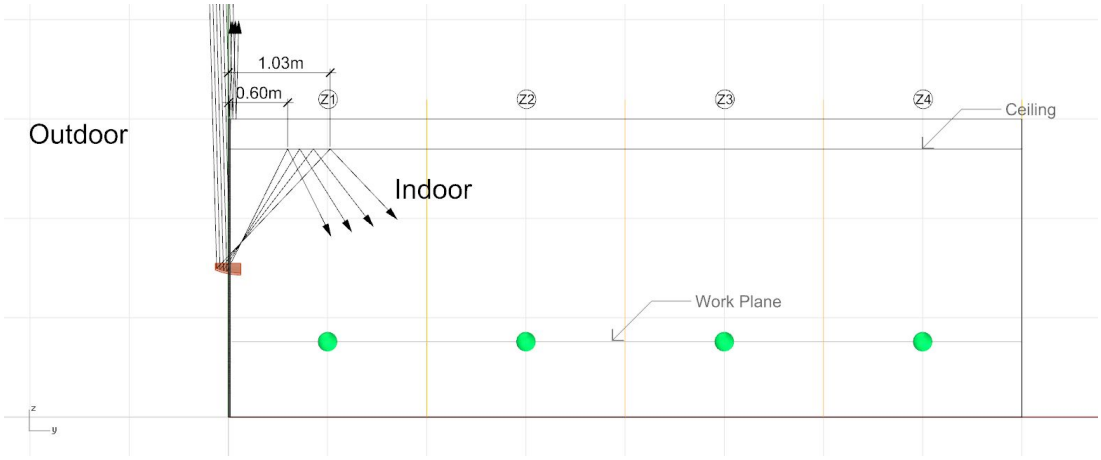
Figure 11.2: Sun rays reflection with the initial CPC in a reverse mode, Riyadh at 12 pm

Developed CPC unit

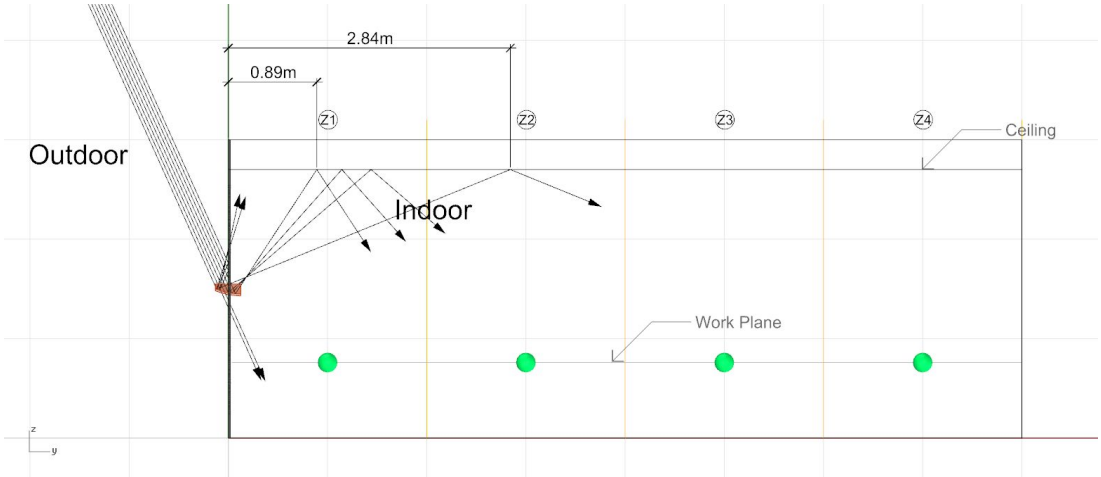
The CPC unit was assessed through a raytracing study at the solar noon on the summer solstice, autumn equinox, and winter solstice. The results of the raytracing study are shown in the sections in Figure 11.3 below. From the analysis of the sun paths behaviour of the initial CPC units, it was found that the upper part could reduce the functionality of the CPC unit in terms

of the daylight redirection, particularly on the summer solstice day. As a result, the upper part was mitigated, and the sun paths were retraced.

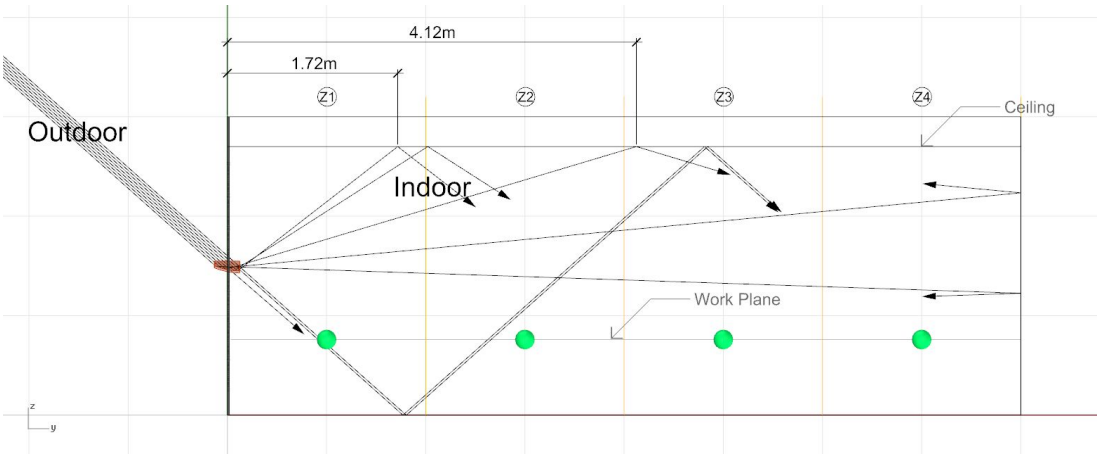
From the section in Figure 11.3 below, it can be seen that the redirection of the sunlight was improved on the summer solstice day. The direct sunbeams can be redirected towards the ceiling up to 1.03 meters. On autumn equinox, the sunlight can reach a further point on the ceiling, precisely 2.84 meters. The redirection of the sunlight was increased by 0.62 meters compared with the initial CPC unit. However, the developed CPC unit increased the direct sunlight at the workplane on the winter solstice. Therefore, more investigation is required to observe its effect on the daylight performance at the work plane.



21 June



21 September



21 December

Figure 11.3: Sun rays reflection with the developed CPC in a reverse mode, Riyadh at 12 pm

11.3.1.2. PIT daylight study

The daylight performance of case DRSS11, which is a perforated solar screen that consists of 21 units of developed CPC units, was assessed through a PIT daylight study. The tests were conducted on the 21st of June, September and December at five test hours, namely, 8 am, 10 am, 12 pm, 2 pm and 4 pm. Later, an evaluation of the daylight performance was assessed for spring, summer, winter and autumn.

Hourly daylight assessment

The total illuminance at the work plane was evaluated for case DRSS11. It was found that the peak total illuminance at 8 am was 15,241 lux at Z1 on 21 December. On the other hand, the lowest total illuminance at Z1 was 1,108 lux on 21 June, which was lower than 21 September by 545 lux, as shown in Figure 11.3.

At daylight zone Z2, the illuminance was 535 lux, 739 lux and 894 lux on 21 June, 21 September and 21 December, respectively. At Z3, the illuminance was decreased by 294 lux on 21 June and 447 lux on 21 September and 539 lux on 21 December, respectively, compared with Z2. The lowest illuminance was at Z4; it was 137 lux, 155 lux and 176 lux on 21 June, 21 September and 21 December, respectively, as shown in Figure 11.4 and Figure 11.5.

In order to investigate the reason for the excessive total illuminance at the work plane at 8 am on 21 December, the direct illuminance and the diffuse illuminance was analysed for the five tested hours for the three tested days. It was found that the direct illuminance occurred only at 8 am on 21 December. As illustrated in Figure 11.6 below, the direct illuminance was 12,923

lux while the diffuse illuminance was 2,369. In other words, the direct illuminance equals around 85% of the total illuminance at this point.

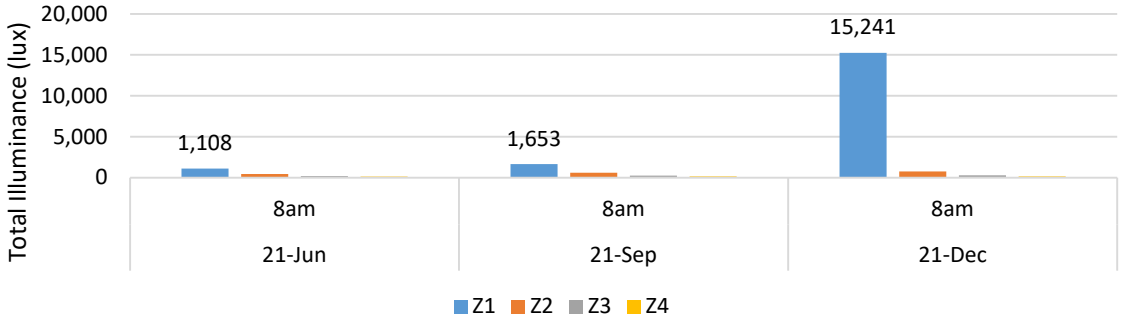


Figure 11.4: Total illuminance for case DRSS11

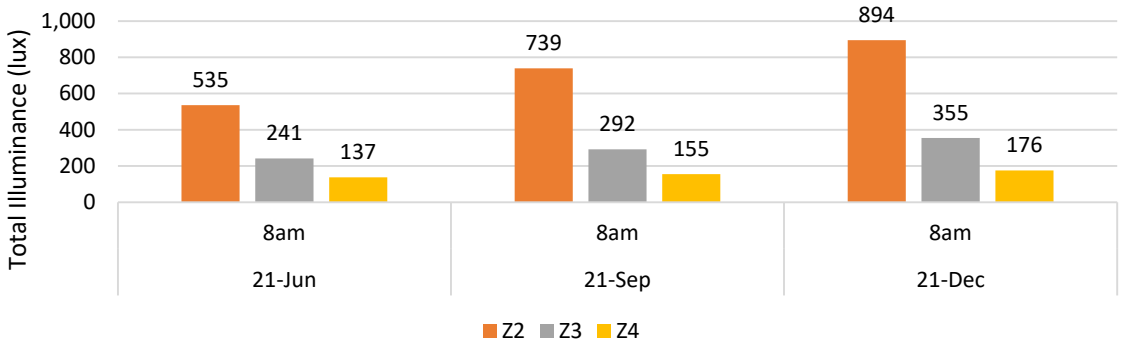


Figure 11.5: Total illuminance for case DRSS11

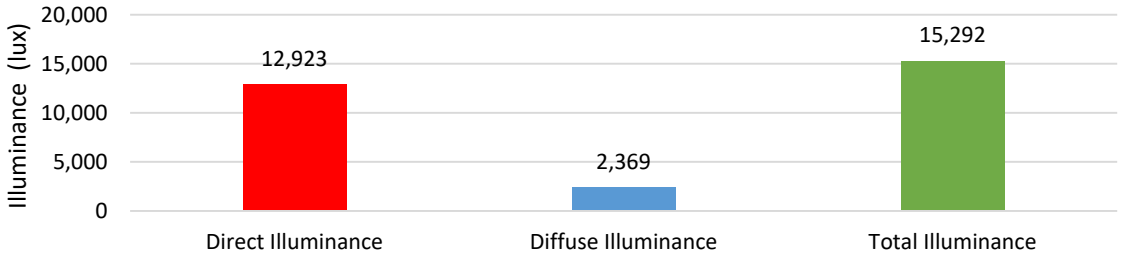


Figure 11.6: Direct illuminance, diffuse illuminance, and total illuminance at Z1 on 21 December at 8 am

The illuminance at the work plane at 10 am was higher on 21 September and 21 December. The peak illuminance was at Z1 for the three tested dates. The illuminance was 3,642 lux and 3227 lux on the 21st of December and September; however, on 21 June, the illuminance was lower than 21 December by 2,174 lux.

At Z2, the illuminance was decreased by higher than 50% compared with Z1 for the three tested dates. Similarly, the illuminance was decreased by about 50% from Z2 to Z3 and from Z3 to Z4. The illuminance was 680 lux, 1,112 lux and 1,462 lux at Z2, and it was 304 lux, 441 lux, and 607 lux at Z3, and it was 174 lux, 244 lux and 321 lux at Z4, on the summer solstice, autumn equinox and winter solstice, respectively, as shown in Figure 11.7.

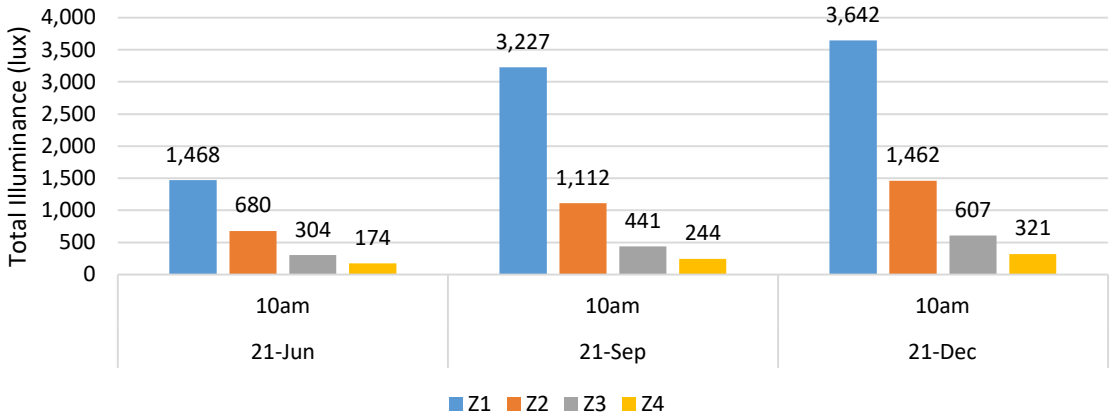


Figure 11.7: Total illuminance for case DRSS11

The daylight performance of DRSS11 at noon was found similar to its performance at 10 am. The lowest illuminance levels were recorded on 21 June whiles the highest was on 21 September and 21 December. The peak illuminance at Z1 was 3,917 lux in December, while the lowest was 1,532 lux on 21 June. The illuminance exceeded the high threshold at Z1 on 21 June by 532 lux, 21 September by 2, 311 lux, and 21 December by 2,917 lux.

On the other hand, the lowest illuminance levels were at Z4. The lowest illuminance level was 195 lux on 21 June, while the highest was 339 lux on 21 December. The illuminance at Z4 was higher than the lower threshold on 21 June by 105 lux and 31 lux on 21 September. At Z2 and Z3, the illuminance levels were within the desired illuminance level for the three tested dates, as illustrated in Figure 11.8.

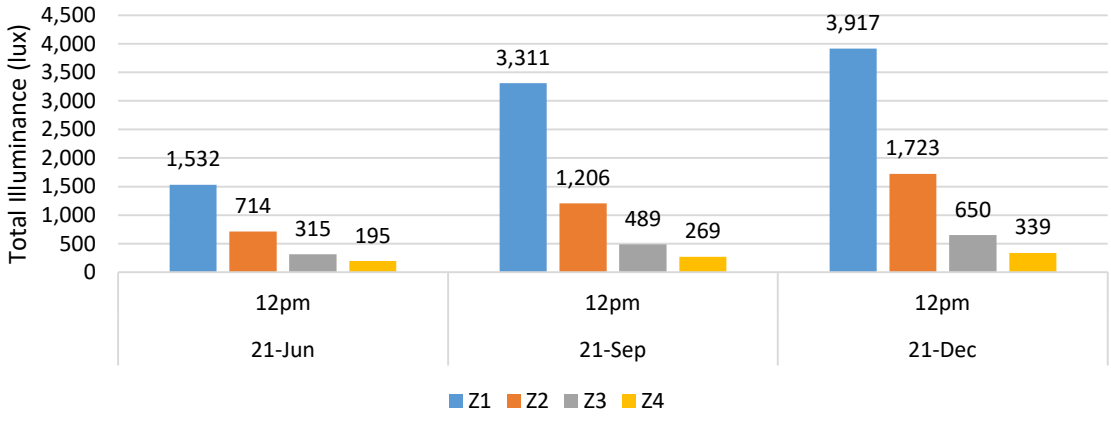


Figure 11.8: Total illuminance for case DRSS11

The daylight performance of case DRSS11 at 2 pm was changed compared with the previous test at 10 am and at solar noon. The difference in the illuminance level between 21 June and 21 September was decreased. The illuminance level was 1,424 lux, 2,545 lux, and 3,177 lux

on 21 June, 21 September and 21 December. The illuminance level exceeded the high threshold at Z1 by 424 lux, by 1,545 lux and 2,177 lux on 21 June, 21 September and 21 December.

The illuminance levels at Z2 were within the desired level at the three test dates, except on 21 December, which was higher by 355 lux. The highest illuminance was 1,355 lux on 21 December, while the lowest was 627 on 21 June. Similarly, the illuminance levels at Z3 were between 300 lux to 1000 lux, except on 21 June, which was lower than the low threshold by only 8 lux.

On the other hand, the illuminance levels at Z4 were lower than the threshold for the three tested dates. The worst scenario was on 21 June, which was 166 lux, while the best was on 21 December, which was 281 lux, as shown in Figure 11.9.

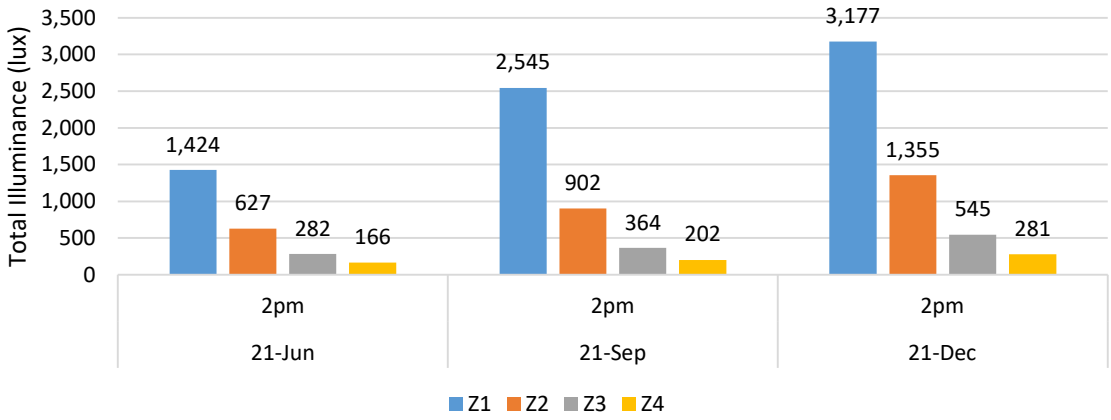


Figure 11.9: Total illuminance for case DRSS11

In contrast to the previous scenarios from 8 am to 2 pm, the daylight performance of case DRSS11 at 4 pm was higher on 21 June while it was lower on 21 December. The illuminance levels were within the desirable range at Z1 for the three tested dates. It was ranging from 981 lux on 21 June to 631 lux on 21 December. The illuminance at Z1 on 21 September was lower than 21 June by only 30 lux. The illuminance level was 177 lux and 96 on 21 June at Z3 and Z4, respectively. On 21 September, the illuminance levels were 148 lux and 89 lux at Z3 and Z4.

At daylight zone Z2, the illuminance level was lower than the threshold only on 21 December by 63 lux. At daylight zone Z3 and Z4, the minimum illuminance level was not achieved. The worst scenario was on 21 December. It was lower than the threshold by 199 lux and 244 lux at Z3 and Z4, respectively, as shown in Figure 11.10.

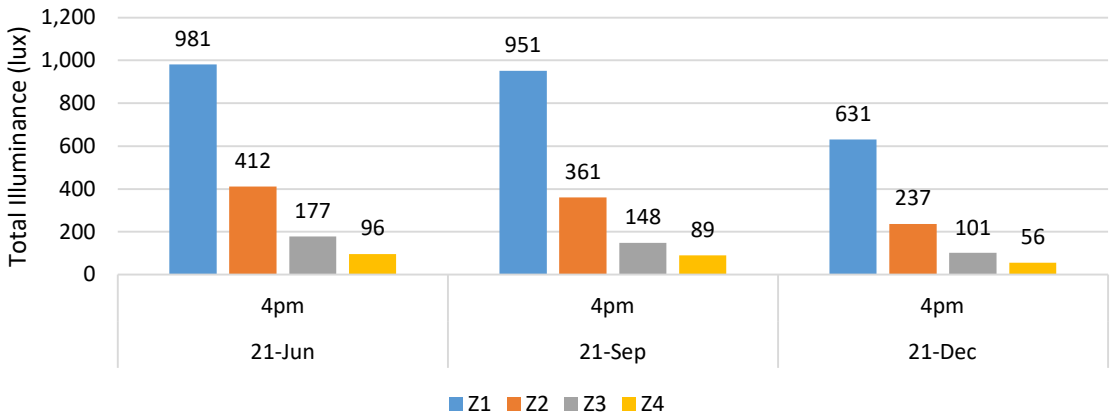


Figure 11.10: Total illuminance for case DRSS11

In order to assess the overall quality of daylight performance at the work plane, the daylight uniformity (DUWP) was calculated for the four test points. The chart in Figure 11.11 below shows the DUWP for the 15 tested hours. The DUWP values ranged from 19.4% to 28.3%, excluding the very low DUWP at 8 am on 21 December. The lowest DUWP was on 21 September at 10 am, while the highest was at noon on 21 June. It can be seen that there is a clear drop in the DUWP on 21 December at 8 am. The DUWP was 4%, and that was due to the excessive direct illuminance on the test point at that time as described previously.

The highest DUWP was on 21 June; it ranged from 23.1% at 4 pm to 28.3% at 12 pm. on 21 September, the DUWP was higher at 4 pm, which was 23%, while the lowest was 19.4% at 10 am. On 21 December, the highest DUWP was 21.7% at 4 pm, while the lowest was 4.2% at 8 am.

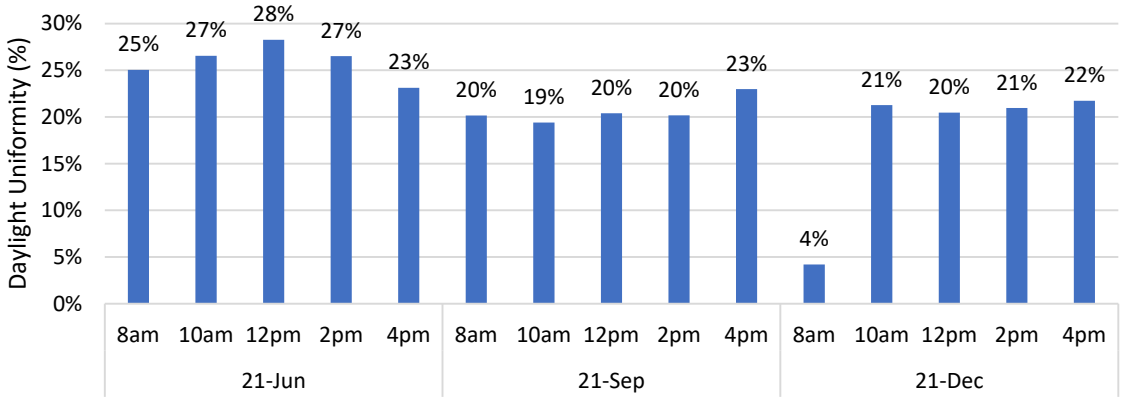


Figure 11.11: DUWP for case DRSS11

Seasonal daylight assessment

The seasonal daylight performance was assessed for case DRSS11. Three daylight metrics were utilised to evaluate the performance, namely, daylight autonomy (DA), annual sunlight

exposure (ASE), and useful daylight illuminance (UDI). The performance was assessed for spring, summer, autumn and winter, for daylight zones Z1, Z2, Z3 and Z4.

The results of the DA are shown in Figure 11.12. It can be seen that the DA was achieved by a high percentage at Z1 and Z2, where the lowest DA at Z1 was 90% and at Z2 was 82%. On the other hand, at Z3, the DA was lower, particularly in summer, which was 33%. The worst DA values were at Z4, which dropped to 0% in summer.

The DA at Z1 was from 90% in winter to 100% in summer. At Z2, it was from 82% in winter to 90% in spring and summer. The difference between the DA values at Z1 and Z2 during the four seasons was insignificant. It was 5% at Z1, and it was 6% at Z2. In contrast, the values of the DA at Z3 and Z4 were varied. The difference between the DA values at Z3 among the seasons was 38%. The variation in the DA values at Z4 was significant as well. The difference between the DA values reached 30%.

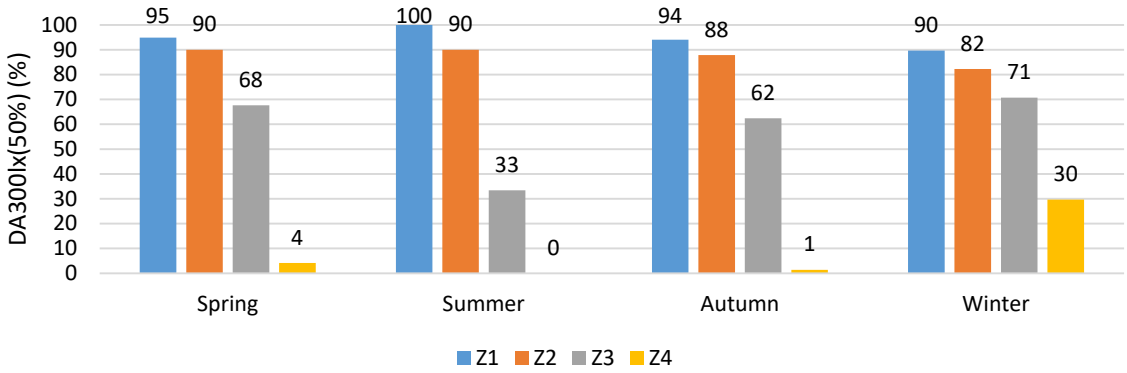


Figure 11.12: The daylight autonomy for case DRSS11

The ASE was analysed at the work plane for the four daylight zones. As it is illustrated in the chart in Figure 11.13 below, it can be seen that the worst scenario was in winter while the best scenario was in summer. The ASE reached 84 hours in winter, 12 hours in spring. In summer, the ASE did not occur; similarly, in autumn, the ASE was insignificant, which was 7 hours.

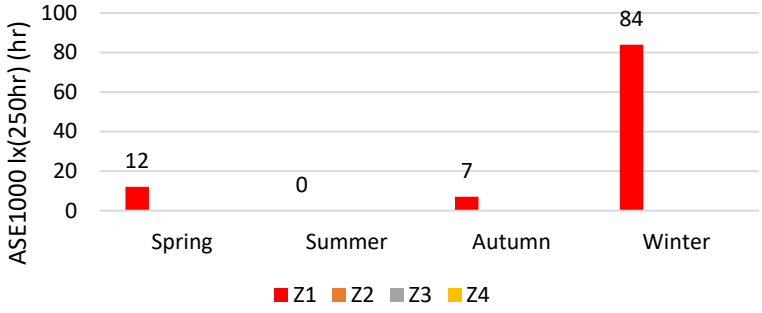


Figure 11.13: Annual sunlight exposure for case DRSS11

After the analysis of the DA and the ASE, the $UDI_{300\text{-}1000lx}$ was assessed for each season. It was found that the peak $UDI_{300\text{-}1000lx}$ was achieved at Z2 in summer while the lowest UDI was at Z4 in the same season, as illustrated in the chart in Figure 11.14. The UDI at Z1 was varied from 22% in winter to 90% in summer. The variation of the UDI at Z3 was lower than Z1. The highest UDI at Z3 was 71% in winter, and the lowest was 33% in summer. The UDI in the front and back areas, namely, at Z1 and Z4, was low. The highest UDI at Z1 was 15% in summer, and the lowest was 7% in spring. The UDI at Z4 recorded the best performance in winter, which reached 30%. However, in spring, summer and autumn, they were significantly low; it was 4%, 0% and 1%, respectively.

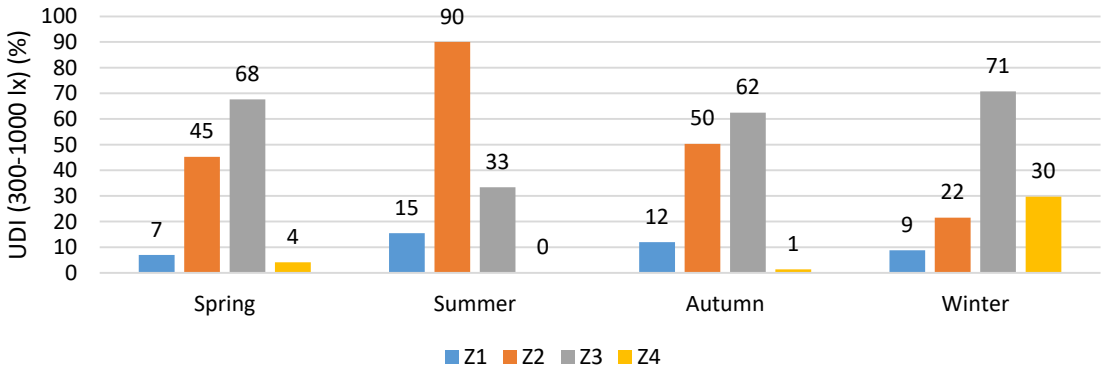


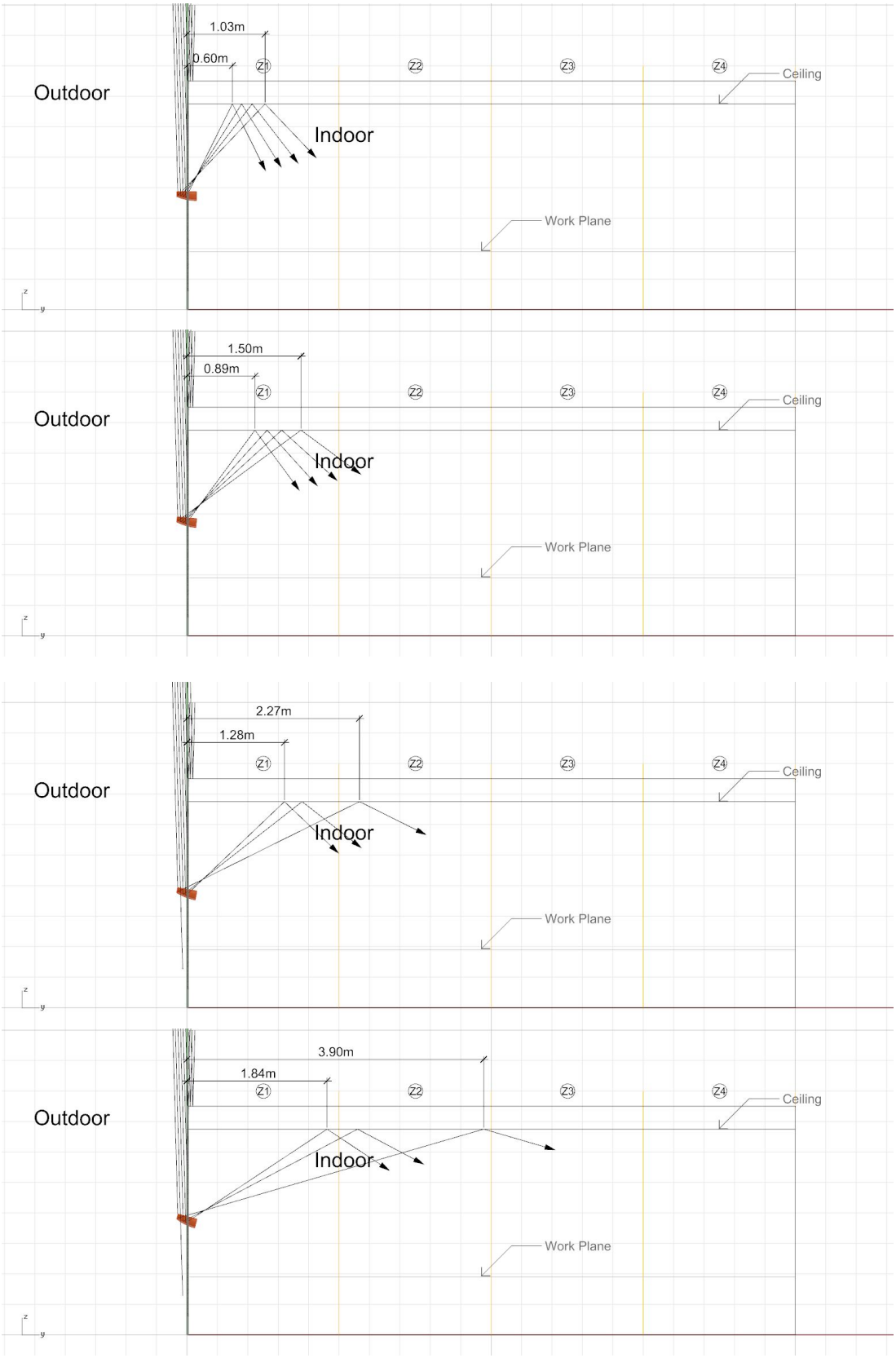
Figure 11.14: Useful daylight illuminance for case DRSS11

11.3.2. Optimisation of the tilt angle

11.3.2.1. Raytracing study

The results of the ray-tracing study for the case from case DRSS11-A to DRSS11-G are illustrated in the drawings in Figure 11.15 below. The depth of the redirected sunlight was 1.03-meter, 1.50-meter, 2.27-meter, 3.90-meter, 5.37-meter, 3.57 meter, and 7.84 meters for tilt angles 0, 5, 10, 15, 20, 25, and 30 degrees, respectively.

It was found that a tilt angle greater than 20 degrees could redirect the sunlight towards the walls or the viewing level. In order to assess the daylight performance at the work plane for the cases DRSS11-A to DRSS11-G, a PIT daylight study was conducted. The illuminance levels at the work plane were analysed at the four daylight zones for summer solstice, autumn equinox, and winter solstice.


1.03m
0.60m
Z1
Z2
Z3
Z4
Ceiling
Outdoor
Indoor
Work Plane
1.50m
0.89m
Z1
Z2
Z3
Z4
Ceiling
Outdoor
Indoor
Work Plane
2.27m
1.28m
Z1
Z2
Z3
Z4
Ceiling
Outdoor
Indoor
Work Plane
3.90m
1.84m
Z1
Z2
Z3
Z4
Ceiling
Outdoor
Indoor
Work Plane

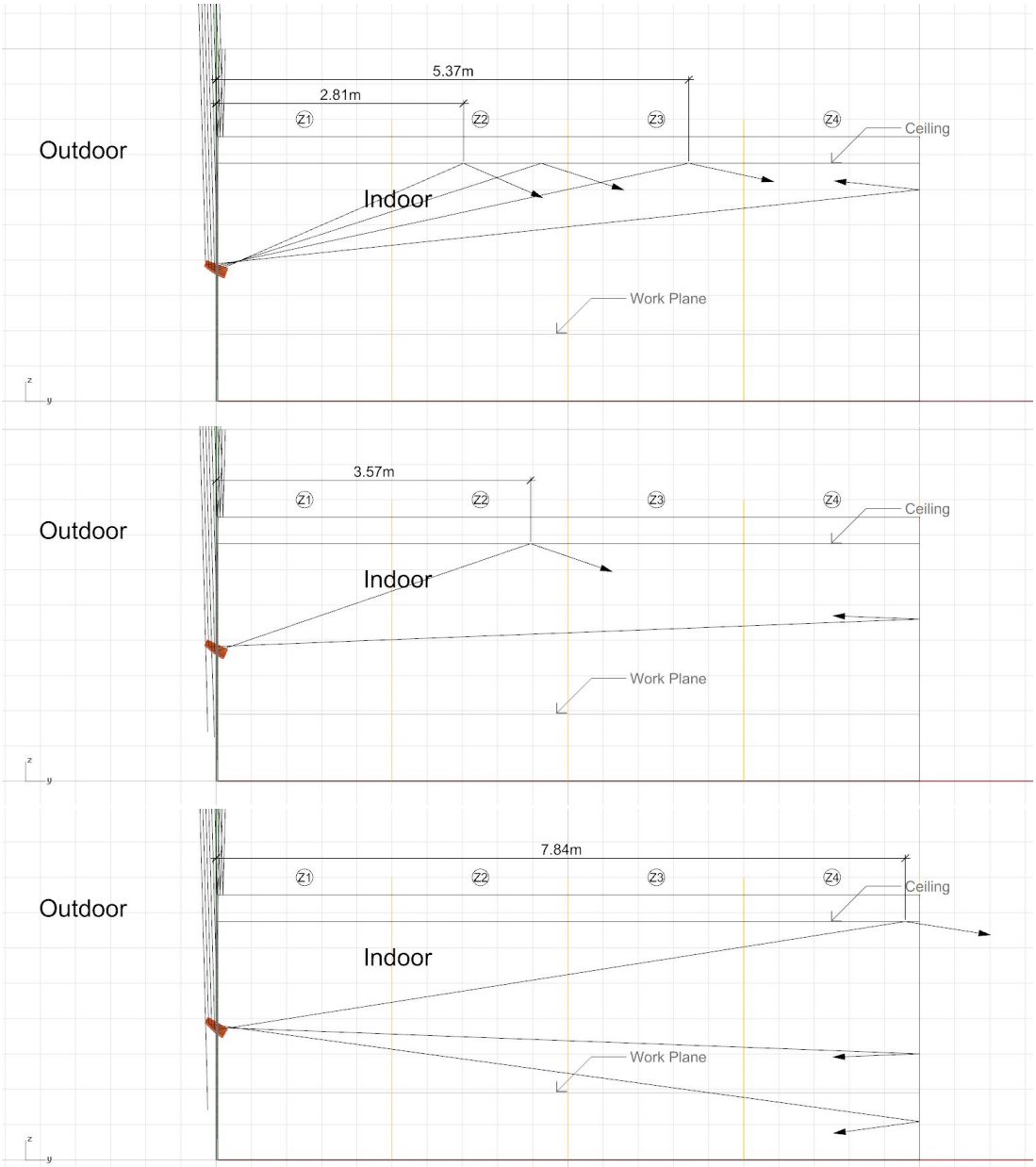


Figure 11.15: Raytracing of sun paths at solar noon on 21st June, from above to below, the tilt angle of the DRD is 0, 5, 10, 15, 20, 25 and 30 degrees

11.3.2.2. PIT daylight study

Hourly daylight assessment

From the analysis of the previous cases, it was found that the lowest daylight level was at Z4. As a result, the optimisation of the DRD tilt angle aimed to increase the depth of the redirected sunlight at the ceiling to increase the illuminance level at the work plane in the deep daylight zone, particularly at Z4.

The PIT study analysed the effect of the DRD tilt angle on the daylight performance at Z4. Table 11.2 below shows the illuminance levels at the work plane at daylight zone Z4 for the 15 tested hours for the cases DRSS11-A to DRSS11-G. It was found that the best tilt angle to increase the illuminance at Z4 was a 5-degree tilt angle; on the other hand, a 30-degree tilt angle was the worst.

Table 11.2: Total illuminance levels angle at the work plane at Z4 as a function of DRDs tilt angle.

		Tilt angle (deg.)						
		0	5	10	15	20	25	30
21-Jun	8am	137	135	133	127	127	125	124
	10am	174	186	182	186	189	180	171
	12pm	195	220	193	187	180	184	181
	2pm	166	180	165	157	157	172	146
	4pm	96	104	102	102	92	102	90
21-Sep	8am	155	170	168	160	154	148	155
	10am	244	254	262	242	244	242	231
	12pm	269	263	270	291	248	275	243
	2pm	202	222	214	197	206	210	184
	4pm	89	88	83	85	81	83	71
21-Dec	8am	176	189	190	188	181	177	167
	10am	321	352	355	353	295	318	297
	12pm	339	336	341	336	311	362	298
	2pm	281	290	298	282	273	266	231
	4pm	56	56	54	58	53	50	46

The illuminance levels at Z4 at 8 am for the tested cases are illustrated in the chart in Figure 11.16. In general, the illuminance levels are higher on 21 December and lower on 21 June. The highest illuminance level on 21 June was 137 lux with a zero-degree tilt angle, while the lowest was 124 lux with a 30-degree tilt angle. On 21 September, the peak illuminance value was 170 lux with a 5-degree tilt, while the lowest illuminance was 148 lux with a 25-degree tilt angle. The highest illuminance level on 21 December was 190 lux with a 10-degree tilt, and the lowest illuminance was 167 lux with a 30-degree tilt angle.

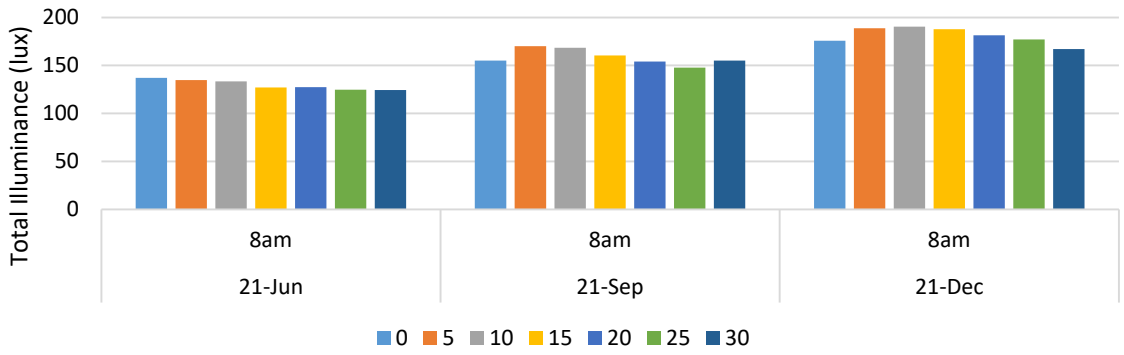


Figure 11.16: Total illuminance at Z4 as a function of DRDs tilt angle from zero to 30 degrees with a 5-degree step

The illuminance levels for the cases DRSS11-A to DRSS11-G are shown in the chart in Figure 11.17 below. Similar to the scenario at 8 am, the highest illuminance levels were recorded on 21 December, while the lowest was on 21 June for all the tested cases. The peak illuminance level on 21 June was 189 lux with a 20-degree tilt, while the lowest was 171 lux with a 30-degree tilt. The highest illuminance value on 21 September was 262 with a 10-degree tilt, and the lowest was 231 lux with a 30-degree tilt. Finally, on 21 December, the peak illuminance level was 355 lux with a 10-degree tilt, and the lowest was 295 lux with a 20-degree tilt angle.

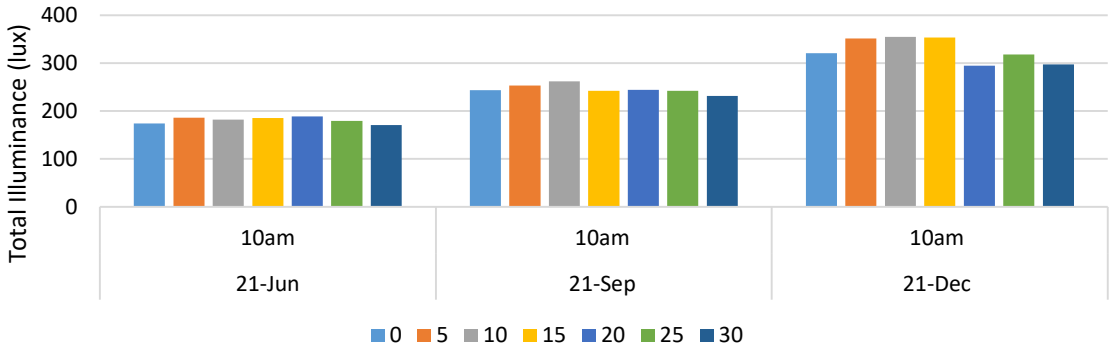


Figure 11.17: Total illuminance at Z4 as a function of DRDs tilt angle from zero to 30 degrees with a 5-degree step

The illuminance levels at Z4 at solar noontime are illustrated in the chart in Figure 11.18. The highest illuminances for the seven tested cases were recorded on 21 December, and the lowest was on 21 June. The peak illuminance value on 21 June was 220 lux with a 5-degree tilt, while the lowest illuminance was 180 lux with a 20-degree tilt. On 21 September, the highest illuminance was 291 lux, and the lowest was 248 lux with 15-degree and 20-degree tilt angles, respectively. On 21 December, the peak illuminance value was 362 lux, while the lowest was 298 lux with 25-degree and 30-degree tilt angles.

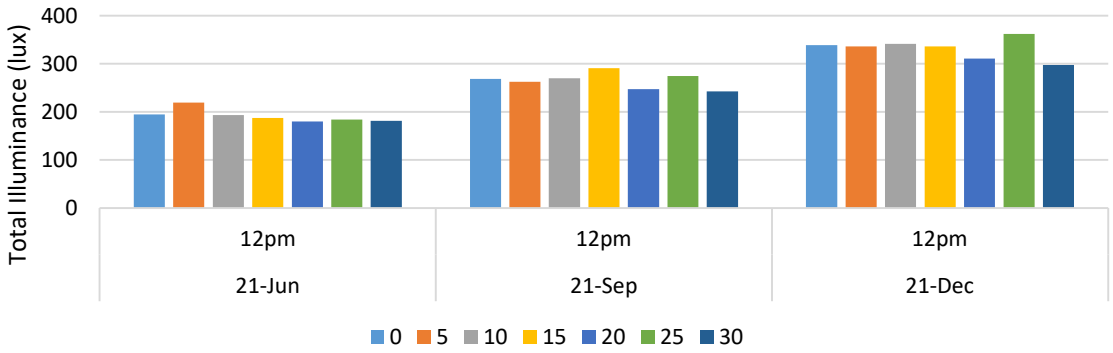


Figure 11.18: Total illuminance at the work plane at Z4 as a function of DRDs tilt angle from zero to 30 degrees with a 5-degree step

The illuminance levels at the work plane at Z4 at 2 pm are shown in the chart in Figure 11.19 below. It can be seen that the illuminance levels were higher on 21 December and lower on 21 September, while the lowest was on 21 June for all the tested cases. The highest illuminance on 21 June and 21 September was recorded with a 5-degree tilt at 180 lux and 222 lux. On 21 December, the peak illuminance was recorded with a 10-degree tilt at 298 lux. On the other hand, the worst scenarios were with a 30-degree tilt angle for the three tested dates. It was 146 lux, 184 lux, and 231 lux on the 21st of June, September, and December.

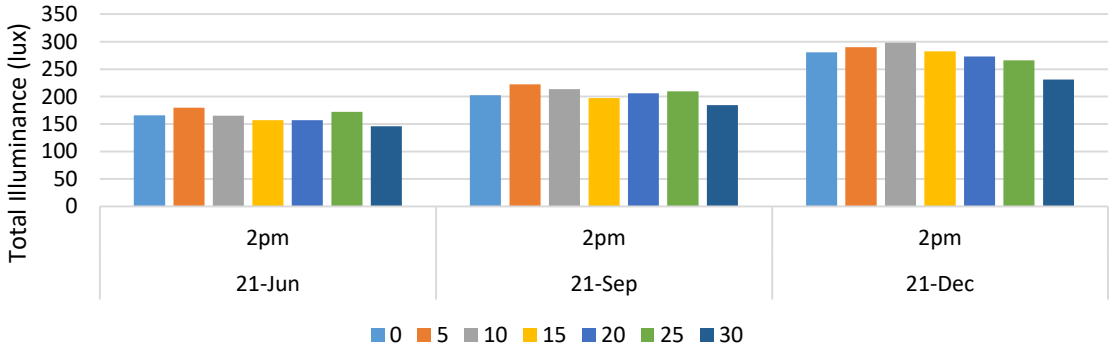


Figure 11.19: Total illuminance at the work plane at Z4 as a function of DRDs tilt angle from zero to 30 degrees with a 5-degree step

The illuminance levels at the work plane at daylight zone Z4 are illustrated in the chart below in Figure 11.20. It can be seen that illuminance levels on 21 June were the highest, while the lowest illuminance was on 21 December for all the tested tilt angles. The peak illuminance value on 21 June was 104 lux, while the lowest was 90 lux with 5-degree and 30-degree tilt, respectively. On 21 September, the highest illuminance was 89 lux, and the lowest was 71 lux with 0-degree and 30-degree tilt, respectively. The highest illuminance on 21 December was 58 lux, and the lowest was 46 lux with 15-degree and 46-degree tilt, respectively.

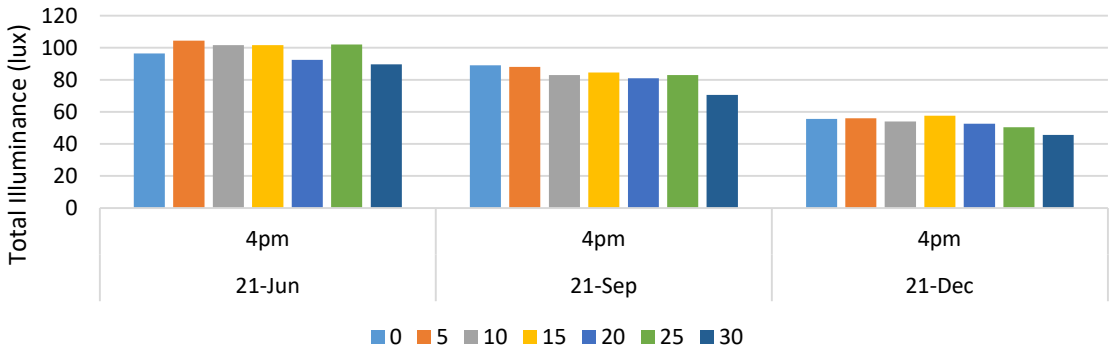


Figure 11.20: Total illuminance at the work plane at Z4 as a function of DRDs tilt angle from zero to 30 degrees with a 5-degree step

Evaluation of the DUWP

The DUWP for the cases DRSS11-A to DRSS11-G is shown in Table 11.3. The DUWP was calculated for each tested hour for the three tested dates. It was found that the highest DUWP was achieved with a 5-degree tilt angle. The DUWP range was from 4.5% to 28.5% at 8 am on 21 December and 2 pm on 21 June, respectively. On the other hand, the lowest DUWP was with a 30-degree tilt angle. The highest DUWP was 26.6% at 10 am on 21 June, while the lowest was 4% at 8 am on 21 December.

Table 11.3: DUWP at the work plane as a function of DRDs tilt angle

		Tilt angle (deg.)						
		0	5	10	15	20	25	30
21-Jun	8am	25.0%	24.7%	24.6%	23.4%	23.1%	22.6%	22.9%
	10am	26.5%	28.0%	28.0%	27.6%	28.0%	26.7%	26.6%
	12pm	28.3%	32.2%	28.0%	26.8%	26.1%	26.6%	26.8%
	2pm	26.5%	28.5%	26.1%	24.8%	24.6%	27.2%	23.3%
	4pm	23.1%	25.1%	24.5%	24.6%	21.9%	24.0%	21.6%
21-Sep	8am	20.2%	21.5%	21.8%	20.1%	19.0%	18.6%	20.1%
	10am	19.4%	21.1%	20.2%	20.0%	19.5%	21.2%	19.2%
	12pm	20.4%	21.1%	21.1%	21.6%	18.1%	19.6%	18.9%
	2pm	20.2%	22.8%	21.3%	19.4%	19.9%	21.0%	17.8%
	4pm	23.0%	22.9%	21.6%	21.9%	20.9%	21.0%	18.4%
21-Dec	8am	4.2%	4.5%	4.5%	4.4%	4.2%	4.2%	4.0%
	10am	21.3%	22.4%	23.5%	22.0%	18.4%	19.9%	19.7%
	12pm	20.5%	21.0%	19.8%	20.5%	19.5%	20.0%	19.2%
	2pm	21.0%	21.9%	21.7%	21.5%	20.2%	21.0%	18.2%
	4pm	21.7%	21.6%	21.4%	22.1%	20.7%	20.1%	18.3%

The chart in Figure 11.21 below shows the DUWP at 8 am on the 21st of June, September and December. It was found that the DUWP was higher in June and September. It ranged from 22.6% to 25% in June and 18.6% to 21.8% in September. In June, the highest DUWP was obtained by a 0-degree tilt angle, while the lowest was with a 25-degree tilt angle. In September, the best DUWP was obtained with a 10-degree tilt angle, while the worst was with a 25-degree tilt angle. On the other hand, the DUWP was extremely low in December. The highest DUWP was 4.5%, with a 5- and 10-degree tilt angle.

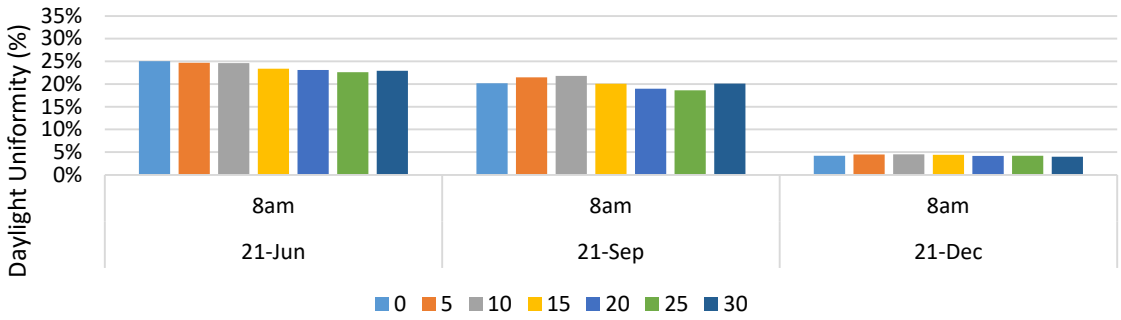


Figure 11.21: DUWP as a function of DRDs tilt-angle from zero to 30 degrees with a 5-degree step

The DUWP at 10 am is shown in the chart below in Figure 11.22. It was noticed that the DUWP was increased on December 10 am compared with 8 am. In addition, the results showed that the DUWP was higher in December compared with September with a tilt angle from 0 to 5-degree. Although the DUWP was higher in June, the reduction in the DUWP in September and December was about 10% DUWP. The highest DUWP in June was 28% by 5- and 10-degree tilt angle, while the lowest was 26.5% by 0-degree tilt degree. In September, the highest DUWP was 21.2% by 25-degree tilt, while the lowest was 19.2% by 30-degree tilt. In December, the best DUWP was 23.5% by 10-degree tilt, and the worst was 18.4% by 20-degree tilt.

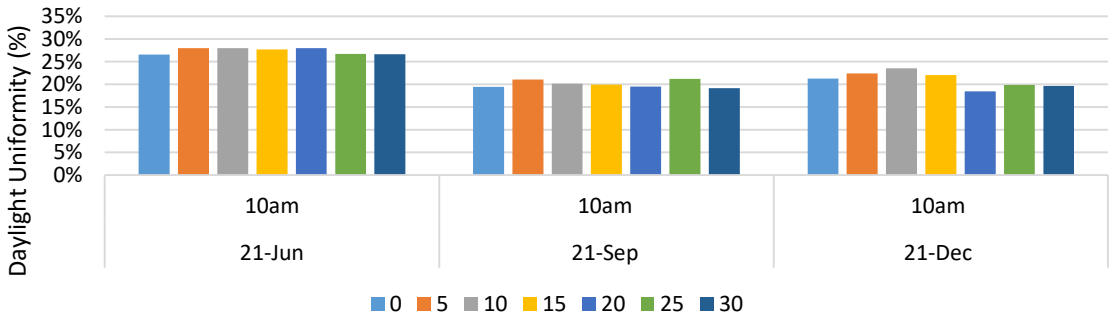


Figure 11.22: DUWP as a function of DRDs tilt-angle from zero to 30 degrees with a 5-degree step

The DUWP values at solar noon are shown in the chart in Figure 11.23 below. It was found that the DUWP is still higher in June. The best daylight performance in June was achieved by 5-degree tilt (32.2%), and the worst was by 20-degree tilt (26.1%). In September, the best

DUWP was 21.6%, and the worst was 18.1% by 15-degree and 20-degree, respectively. In December, the highest DUWP was 21% by 5-degree title, and the lowest was 19.2% by 30-degree tilt.

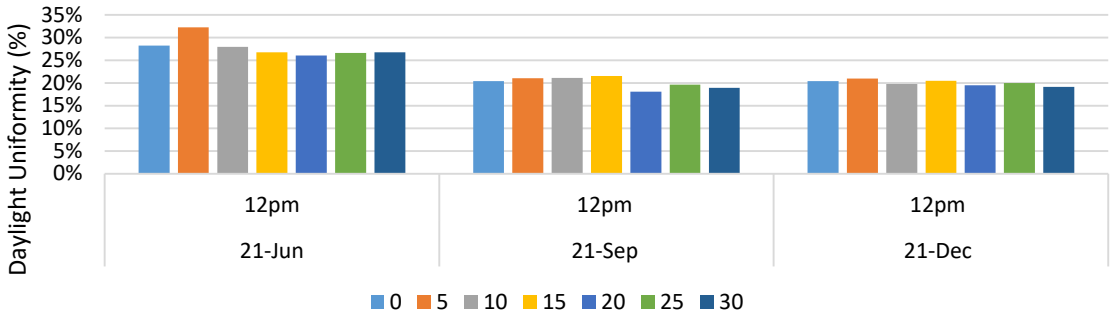


Figure 11.23: DUWP as a function of DRDs tilt-angle from zero to 30 degrees with a 5-degree step

The chart in Figure 11.24 below illustrates the DUWP at 2 pm on the 21st of June, September and December. It was noticed that the difference in the DUWP among the three tested days was decreased. The DUWP is still better in June, with a high DUWP of 28.5% obtained by a 5-degree tilt. In September and December, the best tilt angle was 5-degree as well, which provided 22.8% and 21.9% DUWP, respectively. In contrast, the worst performance for the three months was by 30-degree tilt. The worst DUWP was 23.3%, 17.8%, and 18.2% in June, September, and December.

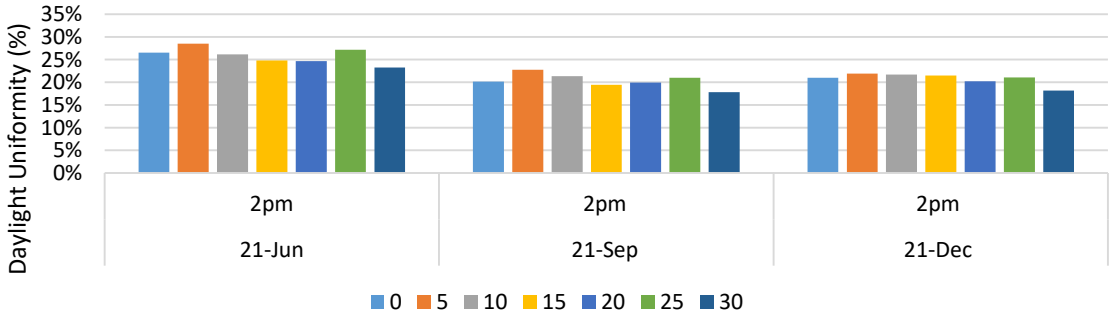


Figure 11.24: DUWP as a function of DRDs tilt-angle from zero to 30 degrees with a 5-degree step

The DUWP at 4 pm among the three test dates was similar; however, it was relatively higher in June. As shown in the chart in Figure 11.25 below, the difference in the DUWP among the three months was insignificant. The highest DUWP was 25.1%, 23%, and 22.1% in June, September, and December. On the other hand, the lowest DUWP was 21.6%, 18.4%, and 18.3% in June, September, and December. The best DUWP in Jun, September and December was obtained by 5-degree, 0-degree and 15-degree tilt. On the other hand, the worst DUWP on the three tested dates was obtained by 30-degree tilt.

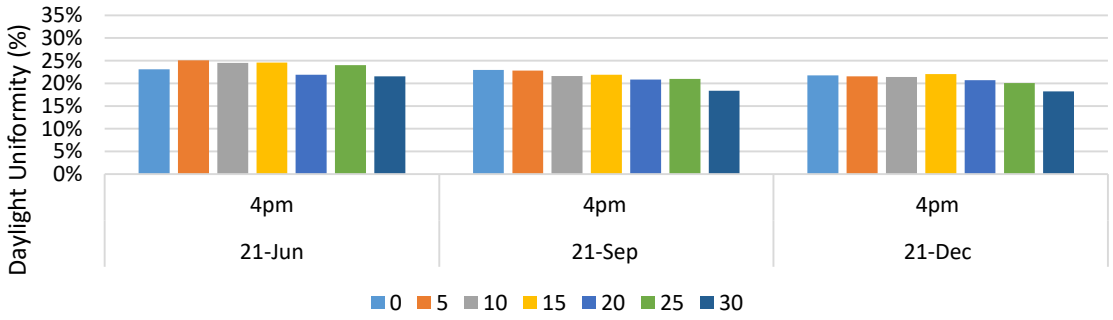


Figure 11.25: DUWP as a function of DRDs tilt-angle from zero to 30 degrees with a 5-degree step

11.3.2.3. Daylight assessment of case DRSS11-B

It was found from the analysis of the tested cases above that the optimum tilt angle for the DRDs is 5-degree inwards, which is named DRSS11-B. Therefore, further investigation was conducted to analyse the performance of DRSS11-B in order to conduct a deep analysis of its performance. First, the DUWP of DRSS11-B was compared with the performance of DRSS11. It was found that DRSS11-B increased the DUWP for all the tested hours except at 8 am on 21 June, which was relatively lower (by 0.3% DUWP), as shown in the chart in Figure 11.26 below. It was found that the worst hour was at 8 am on 21 December for both cases. Therefore, the direct and diffuse illuminance were analysed for this tested hour separately.

The analysis of the total illuminance level at 8m on 21 December is shown in the chart in Figure 11.27 below. It was found that the direct illuminance was 12,923 lux while the diffuse illuminance was only 2,547 lux. In other words, the direct illuminance was about 84% of the total illuminance at this light sensor.

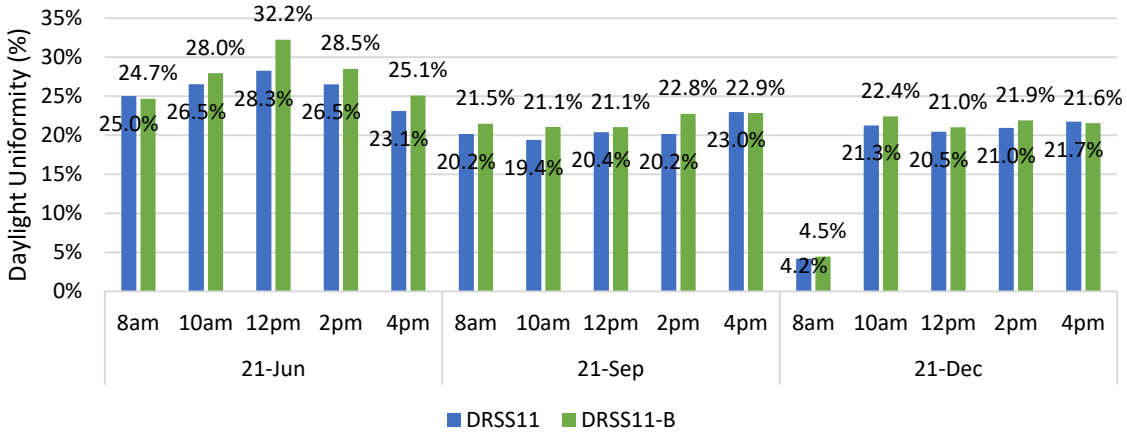


Figure 11.26: Comparison of DUWP between case DRSS11 and DRSS11-B

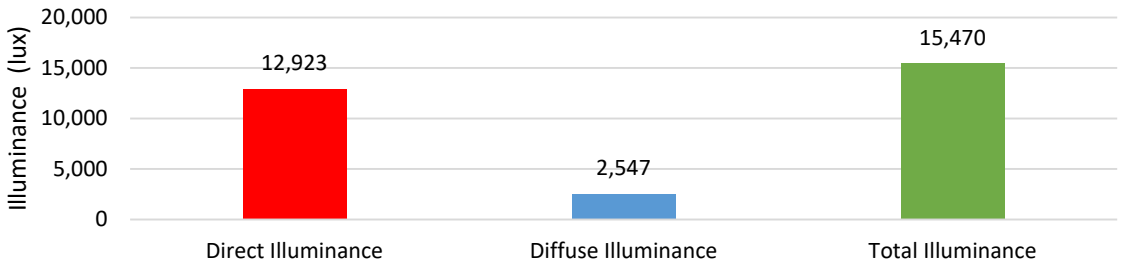


Figure 11.27: Direct illuminance, diffuse illuminance, and total illuminance at Z1 on 21 December at 8 am for case DRSS1-B

Seasonal daylight assessment

The daylight performance of case DRSS1-B was analysed for each season to investigate the overall seasonal enhancement. The chart in Figure 11.28 below shows the DA for each daylight zone. It can be seen that DA at Z1 and Z2 was adequate. The best DA at Z1 was 100% in summer, and the lowest was 90% in winter. The highest DA at Z2 was 90% in spring and summer, while the lowest was 82% in winter.

In contrast, the DA at Z3 was varied, where the best DA was achieved in winter at 74% while the worst was 36% in summer. Similarly, at Z4, the DA was exceptionally low most of the year except in winter. The DA was 11% in spring, 0% in summer, 9% in autumn and 40% in winter.

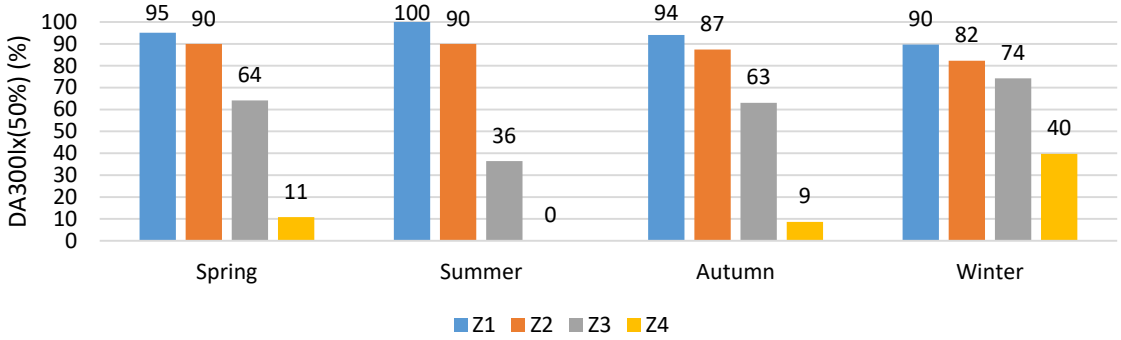


Figure 11.28: The DA for case DRSS11-B (5-deg. tilt)

The ASE was assessed at the work plane for DRSS1-B to investigate the direct sunlight occurrence during each season. It was found that the worst scenario was in winter as the ASE reached 90 hours. On the other hand, the ASE in summer did not occur. The performance in spring and autumn was acceptable as the ASE was only 14 hours and 8 hours, respectively, as shown in Figure 11.29 below.

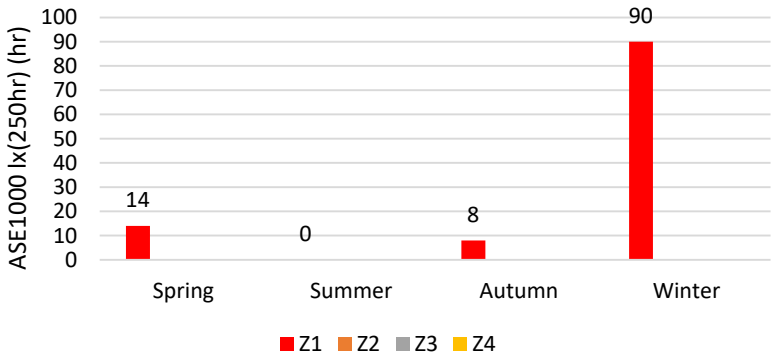


Figure 11.29: Annual sunlight exposure for case DRSS11-B

The chart in Figure 11.30 below illustrates the UDI for DRSS1-B for each season. The UDI was analysed to measure the improvement in the daylight performance, particularly at the front and rear areas of the room. It was found that the UDI at Z1 was extremely low for all the seasons. It ranged from 6% in spring to 12% in summer. At Z2, the UDI was adequate in summer, which reached 90%; however, it dropped to 22% in winter. The UDI at Z3 was relatively balanced among the seasons. It ranged from 36% in summer to 74% in winter, and it was 64% and 63% in spring and autumn. On the other hand, the UDI at the rear area (Z4) was not met in summer (0%). Furthermore, the highest UDI at Z4 was 40% in winter.

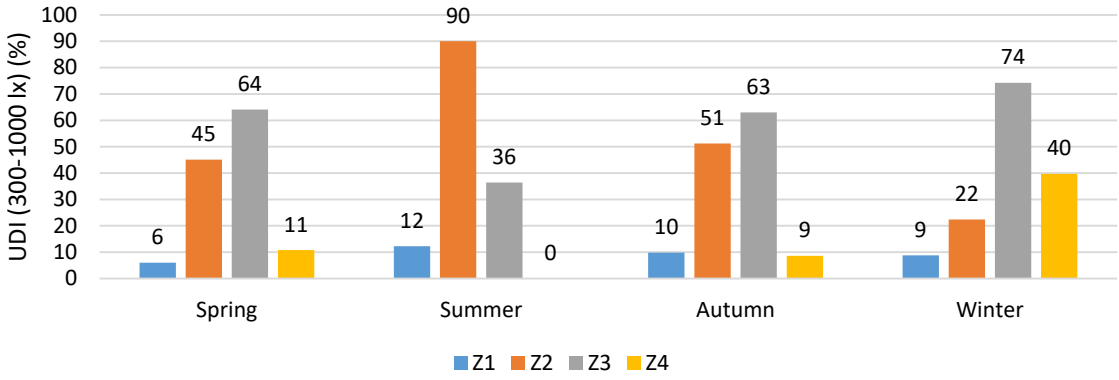


Figure 11.30: Useful daylight illuminance for case DRSS11-B

11.3.3. Integration of the prismatic lens

The impact of an integration of a prismatic lens with the DRD on the daylight performance was investigated. Case DRSS12 is a developed daylight-redirecting system with a prismatic lens in the inlet and outlet of the DRD. The daylight performance of DRSS12 was assessed through a PIT study for the three important days in the year. Later, an annual study was conducted for each season separately. Finally, the overall performance was assessed for the whole year.

11.3.3.1. PIT daylight study

Hourly daylight assessment

The performance of DRSS12 was assessed through a PIT study for the summer solstice day, equinox day, and winter solstice day at 8 am, 10 am, 12 pm, 2 pm and 4 pm. The illuminance levels at the work plane and DUWP were analysed.

The total illuminance values at 8 am on the 21st of June, September and December are shown in the charts in Figure 11.31and Figure 11.32 below. It can be seen that the total illuminance on 21 December at Z1 was excessive, which reached 15,241 lux. On 21 June and 21 September, the total illuminance was 1,108 lux and 1,653, respectively. The illuminance levels at Z2 were within the desired threshold. The maximum illuminance was 749 lux in December, and the minimum was 445 lux in June. On the other hand, at Z4, the illuminance was 120 lux, 141 lux and 150 lux in June, September and December.

The excessive total illuminance value on 21 December at Z1 at 8 am was analysed. The chart in Figure 11.32 below shows that direct illuminance at the work plane was 12,923 lux. On the other hand, the diffuse illuminance was only 2,318 lux. The percentage of the direct illuminance to the total illuminance was about 85%.

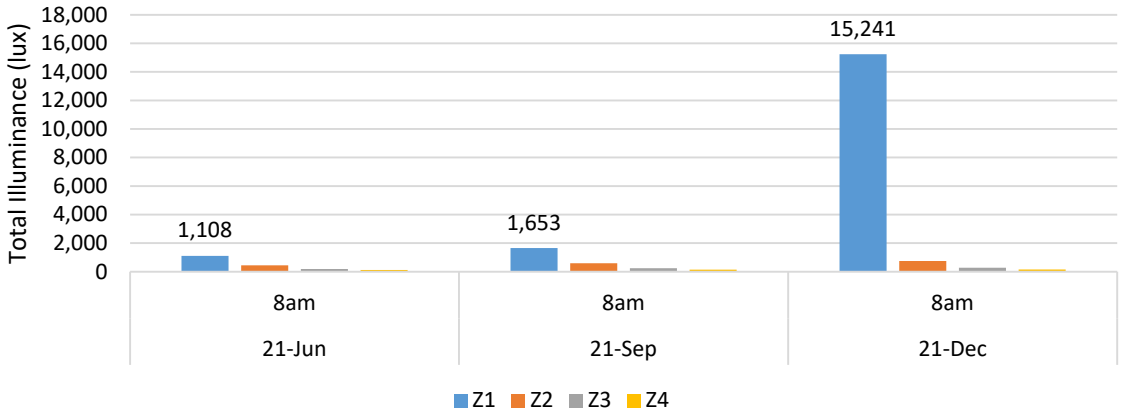


Figure 11.31: Total illuminance at Z1, Z2, Z3 and Z4 for case DRSS12

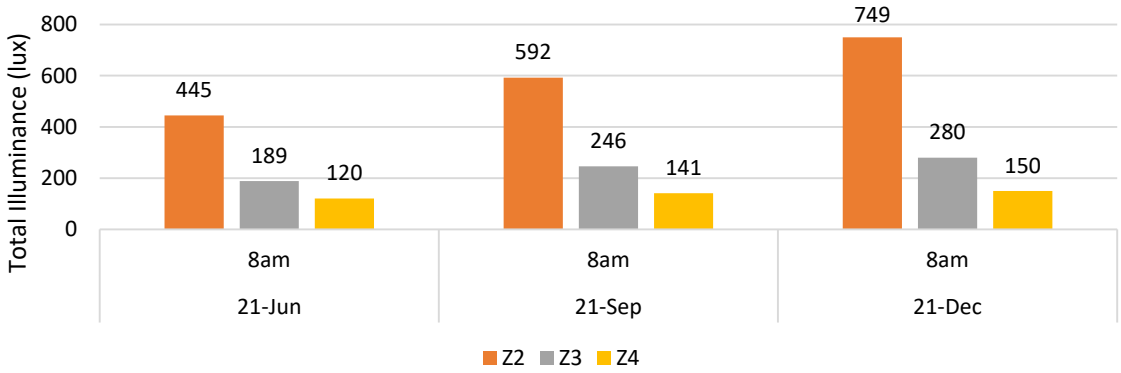


Figure 11.32: Total illuminance at Z2, Z3 and Z4 for case DRSS12

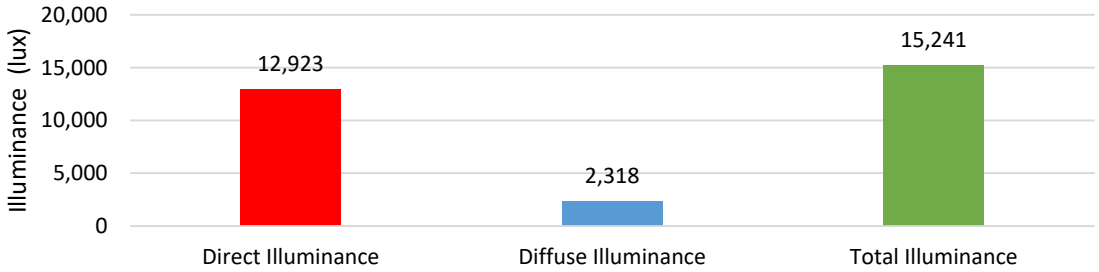


Figure 11.33: Direct illuminance, diffuse illuminance, and total illuminance at Z1 on 21 December at 8 am, case DRSS12

The chart in Figure 11.34 shows the total illuminance at 10 am. It was found that the highest illuminance occurred on 21 December while the lowest was on 21 June. Among the daylight zones, the illuminance at Z1 was higher than Z2 by about 300%. The illuminance at Z1 was 1,304 lux, 2,579 lux and 3,598 lux, on the other hand, at Z2 was 555 lux, 1,002 lux, and 1,413 lux in June, September, and December. The illuminance levels at Z3 were within the desired range in September and December, while it was relatively lower in June. The illuminance values were 244 lux, 381 lux and 518 lux in June, September and December. Finally, the illuminance at the rear zone ranged from 150 lux in June to 274 lux in December.

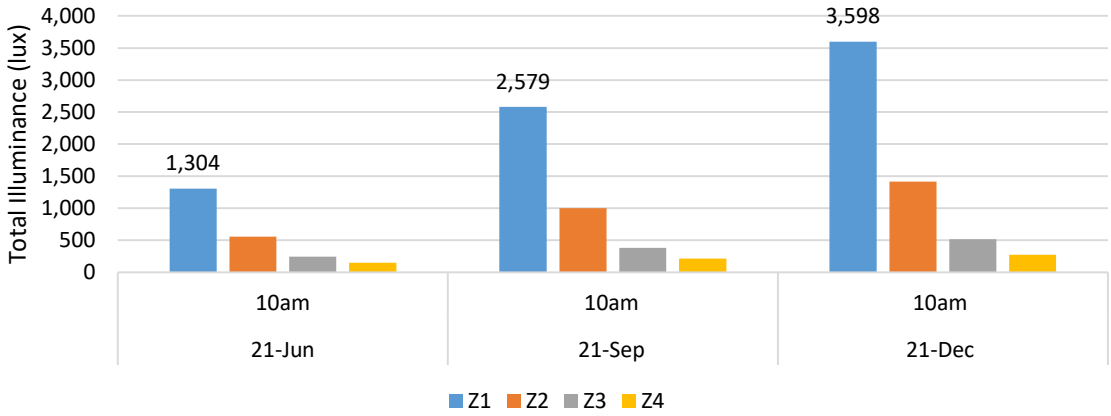


Figure 11.34: Total illuminance for case DRSS12

Similarly, at noon, the illuminance had the same scenario at 10 am. The illuminance levels are given in the chart in Figure 11.35 below. It was found that the illuminance values were increased relatively at all daylight zones. For example, it was increased by 14%, 16% and 13% at Z1 and by 13%, 14% and 13% at Z4 in June, September and December, respectively. The illuminance at the front area (Z1) ranged from 1,354 lux in June to 3,708 lux in December. At Z2, the highest illuminance level was 1436 lux in December, and the lowest was 630 lux in June. At the rear area (Z3), the illuminance was within the desired level except in June, which was lower by only 54 lux. At Z4, the worst illuminance was 154 lux in June; however, the illuminance in December was lower than the threshold by only 17 lux.

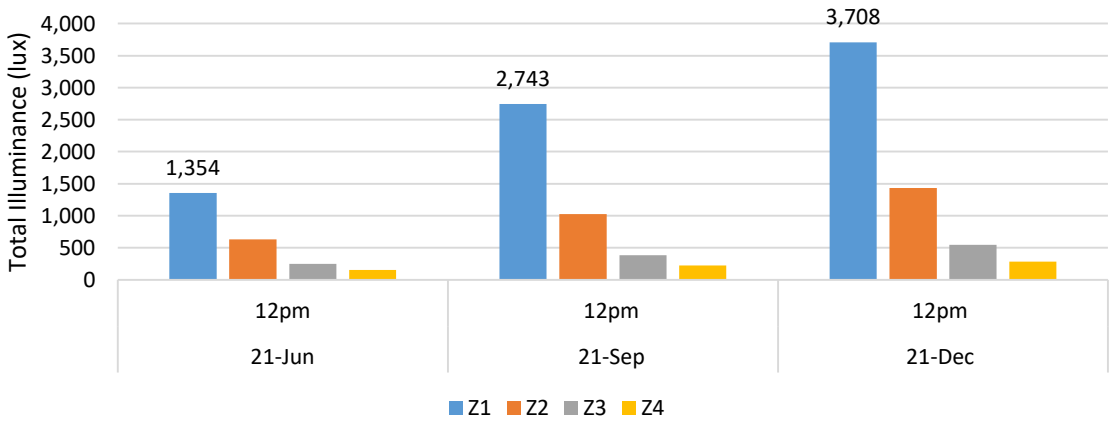


Figure 11.35: Total illuminance for case DRSS12



Figure 11.36: Interior view of the room at solar noon on 21 June, case DRSS12

The illuminance levels at 2 pm are shown in the chart in Figure 11.37 below. It can be seen that the illuminance levels were relatively reduced compared with noontime; however, the curve of the illuminance reduction is similar. The illuminance at Z1 reached 2,855 in December, and the lowest was 1,280 lux in June. On the other hand, the highest illuminance at Z4 was 221 lux in December, and the lowest was 136 lux in June. At Z3 and Z4, the illuminance

levels were within the desired range. However, there was an insignificant increase at Z2 in December by 158 lux and a decrease at Z3 in June by 77 lux.

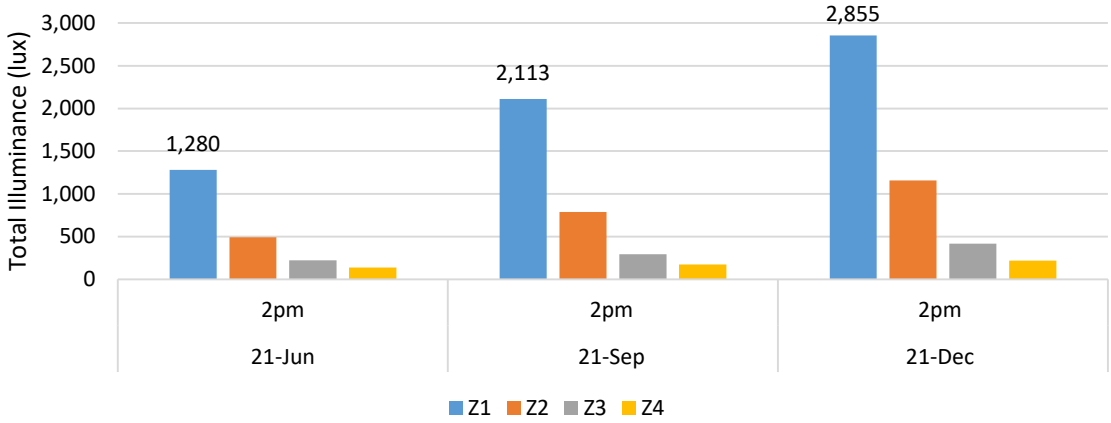


Figure 11.37: Total illuminance for case DRSS12

The illuminance levels at 4 pm are shown in the chart in Figure 11.38 below. It can be seen that the illuminance levels decreased in December while they increased in June. The illuminance at Z1 was 885 lux, 823 lux, and 568 lux in June, September, and December. At Z2, the illuminance was acceptable; however, it was relatively lower in December than the threshold by 96. On the other hand, at Z3 and Z4, the illuminance levels at all the tested hours were lower than the threshold.

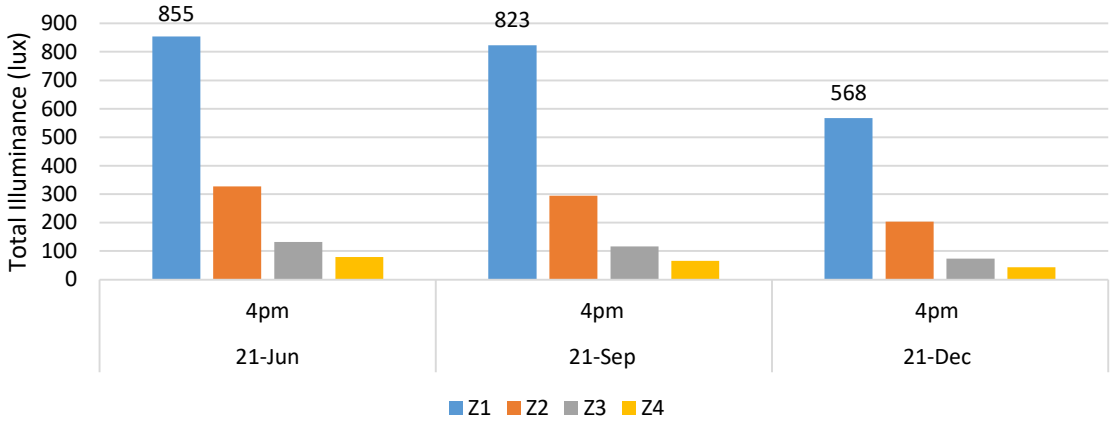


Figure 11.38: Total illuminance for case DRSS12

The DUWP is given for the 15 tested hours in the chart in Figure 11.39 below. It was found that the DUWP was higher on 21 June; it ranged from 22.8% at 4 pm to 26.6% at 10 am. The highest DUWP on 21 September was 21.5% at 8 am, and the lowest was 20.1% at 4 pm. On the other hand, on 21 December at 8 am, the DUWP was exceptionally low, which was 3.7%. However, from 10 am to 4 pm, the DUWP ranged from 18.9% to 19.5%.

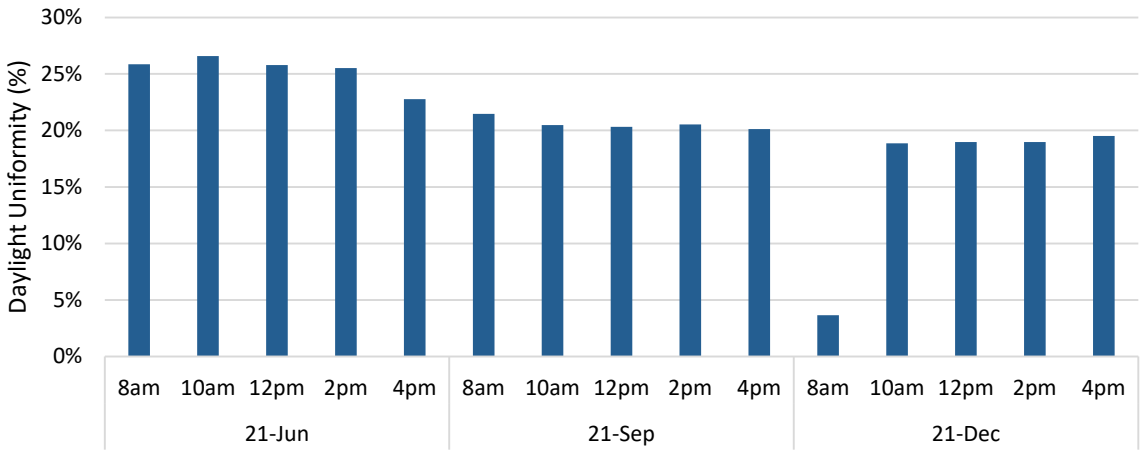


Figure 11.39: DUWP for case DRSS12

11.3.3.2. Annual daylight study

Seasonal daylight assessment

The daylight performance of case DRSS12 was assessed through the DA, ASE and UDI metrics. The DA values are shown in the chart in Figure 11.40 below. It can be seen that the DA was adequate at Z1 and Z2 for the whole year; however, it was varied at Z3 and Z4. The best DA values at the rear daylight zones were recorded in winter.

The DA at Z1 ranged from 90% in winter to 100% in summer. Similarly, at Z2, it was 81% in winter and 85% in summer. On the other hand, the highest DA at Z3 was 66% in winter, and the lowest was 20% in summer. Finally, the best DA at Z4 was 14% in winter while 0% in summer.

The ASE values for case DRSS12 are given in the chart in Figure 11.41 below. It was found that the worst ASE value was 68 hours in winter. In summer, the ASE did not occur, and in spring and autumn, the ASE was adequate as the values were 7 and 2 hours, respectively.

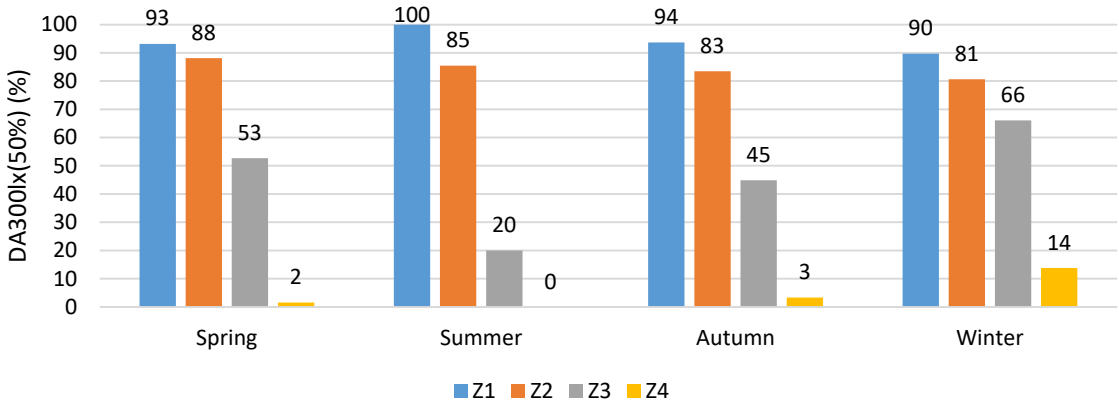


Figure 11.40: Daylight autonomy for case DRSS12

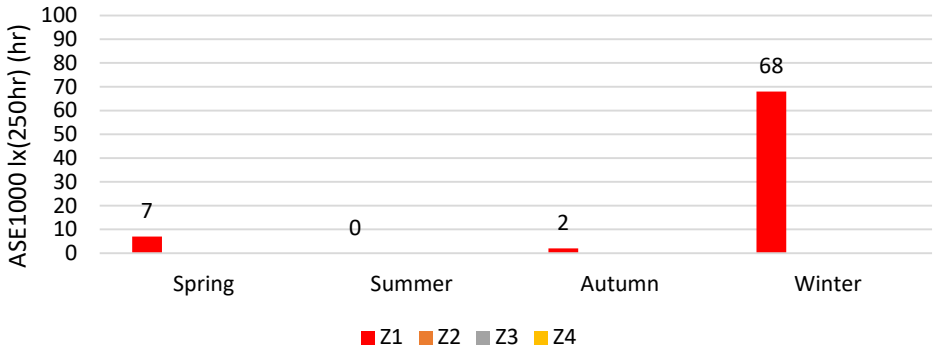


Figure 11.41: Annual sunlight exposure for case DRSS12

The $UDI_{300\text{-}1000lux}$ values for case DRSS12 are shown in the chart in fig below. It was found that UDI values were higher at Z2 and Z3, while the lowest UDI values were at Z1 and Z4. The best UDI at Z1 was 20% in summer, and the worst was 9% in spring. In contrast, the worst UDI value at Z4 was 0% in summer, and the best UDI was 14% in winter.

The UDI values at Z2 ranged from 34% in winter to 85% in summer. On the other hand, at Z3, the highest UDI value was 66% in winter, and the lowest was 20% in summer. In spring and autumn, the UDI values were similar. The UDI values in spring and autumn at Z1 was 9% and 14%, at Z2 was 67% and 68%, at Z3 was 53% and 45%, and at Z4 was 2% and 3%, as shown in Figure 11.42.

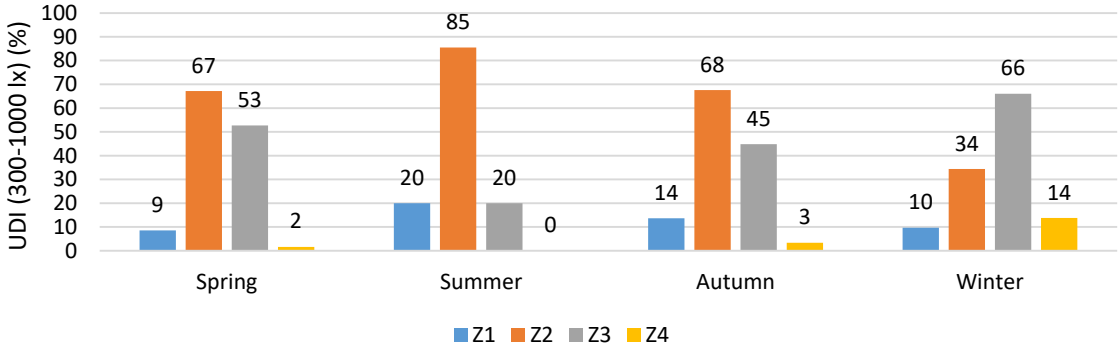


Figure 11.42: Useful daylight illuminance for case DRSS12

Annual daylight assessment

In order to draw a clear understanding of the overall daylight performance for the whole year, the DRSS12 annual daylight performance was assessed. The DA and the ASE values are shown in the charts in Figure 11.43 below. The DA values show that at Z1 and Z2, the DA was adequate, which was 100% and 93%, respectively. On the other hand, it decreased to 51% at Z3 and dropped to 5% at Z4. The ASE was occurred only at Z1 by 86 hours/year.

The UDI was analysed for DRSS12 with two high thresholds, namely 1000 lux and 500 lux. The UDI values are illustrated in the chart in Figure 11.44 below. It can be seen that the best $UDI_{300\text{-}1000lx}$ was achieved at Z2 and Z3 by 70% and 51%, respectively. At Z1, the $UDI_{300\text{-}1000lx}$ was 10%, while it was 5.3% at Z4.

In addition, the $UDI_{300\text{-}500lx}$ was analysed. It was found that the best values were obtained at Z3 by 43%. The $UDI_{300\text{-}1000lx}$ at Z1 and Z4 was extremely low, which was 1.4% and 5.3%, respectively. At Z2, the $UDI_{300\text{-}1000lx}$ was relatively higher than Z1 and Z4, which was 17%.

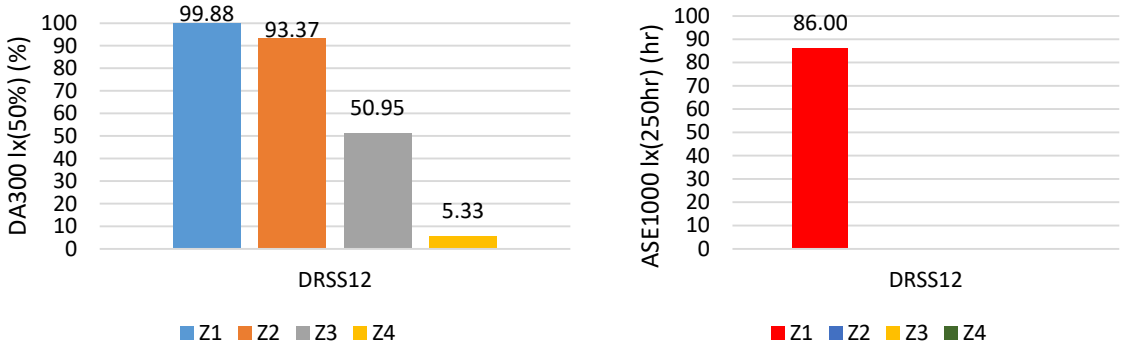


Figure 11.43: DA (left) and ASE (right) for the whole year for case DRSS12

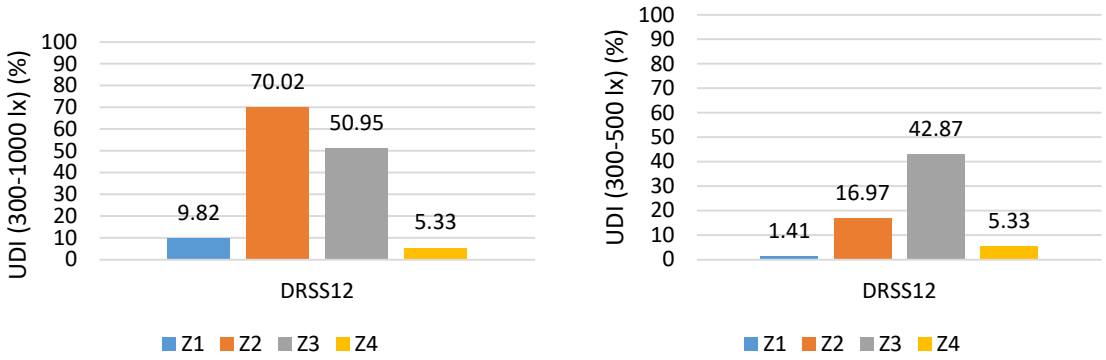


Figure 11.44: $UDI_{300\text{-}1000lx}$ (left) and $UDI_{300\text{-}500lx}$ (right) for the whole year for case DRSS12

11.4. Comparison of case DRSS11-B performance with the base case and PSS5

Figure 11.45 shows the daylight uniformity for the base case, case PSS5 and case DRSS11-B. It was found that the daylight uniformity was enhanced by case DRSS11-B for most of the tested hours compared to the base case and case PSS5. The highest daylight uniformity, in general, was recorded on 21 June for the three cases. The best uniformity was 32% at 12 pm by DRSS11-B whereas the lowest value was 14% at 4 pm by the base case. On the other hand, the worst daylight uniformity was recorded on 21 December. The lowest uniformity was 2% at 12 pm by the base case whereas the highest uniformity was 22% at 10 am by case DRSS11-B.

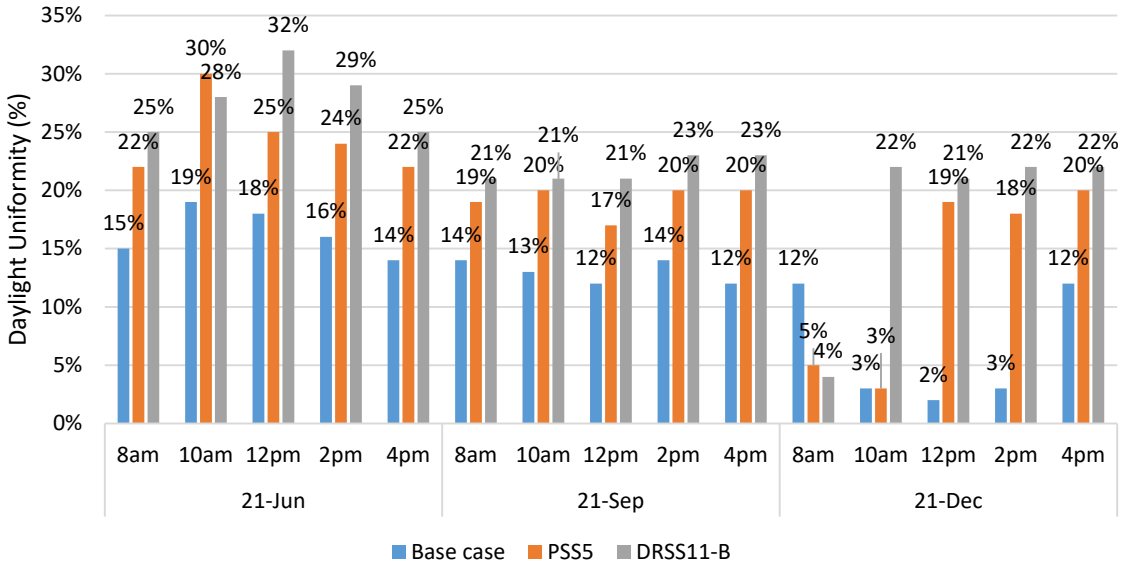


Figure 11.45: Comparison of the daylight uniformity

The annual analysis of the daylight performance indicates that the proposed system reduce the negative impact of the direct sunlight where the ASE was reduced from 381 hours with the base case to 121 hours with case DRSS11-B and to 186 hours with case PSS5, as shown in Figure 11.46. On the other hand, the DA values showed that at daylight zone Z1 and Z2 the performance was similar for the base case, case PSS5 and case DRSS11-B. The DA value was 100% at Z1 and 97 to 98% at Z2. However, the DA values at Z3 the highest DA was 72% with case PSS5 with an increase of 3% and 6% compared to the base case and case DRSS11-B, respectively, as presented in Figure 11.47. Nevertheless, the UDI values revealed that the at daylight zones Z1 and Z4, case DRSS11-B increased the UDI values from 1% and 3% to 5% at Z1, and 5% and 15% to 17% compared to the base case and case PSS5, respectively, as shown in Figure 11.48.

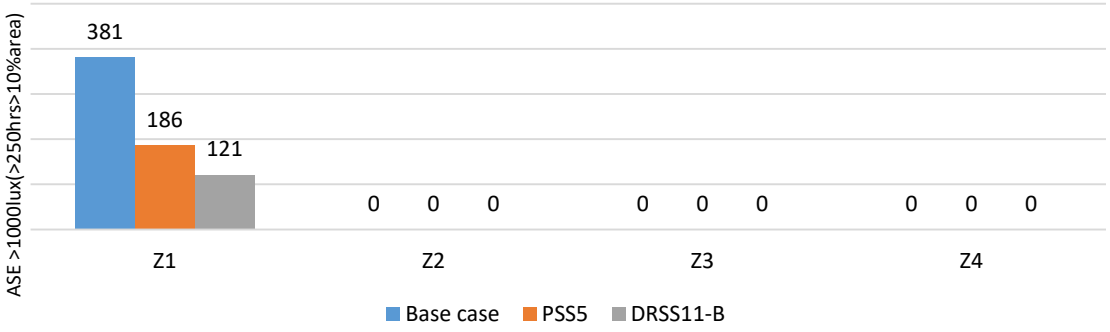


Figure 11.46: Comparison of annual sunlight exposure (ASE)

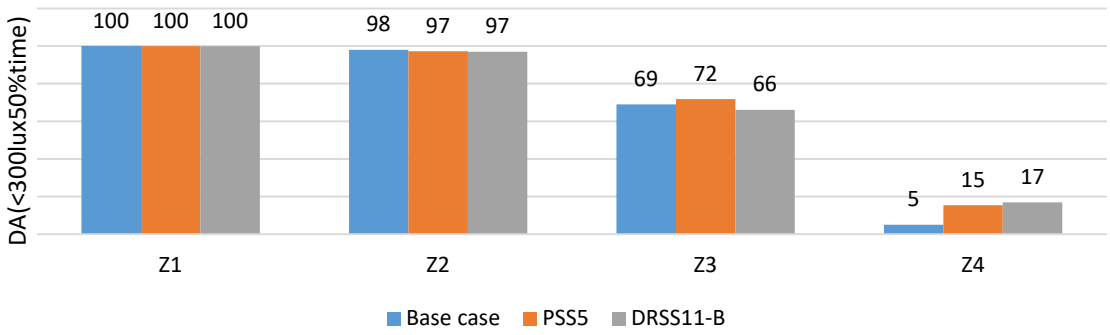


Figure 11.47: Comparison of daylight autonomy (DA)

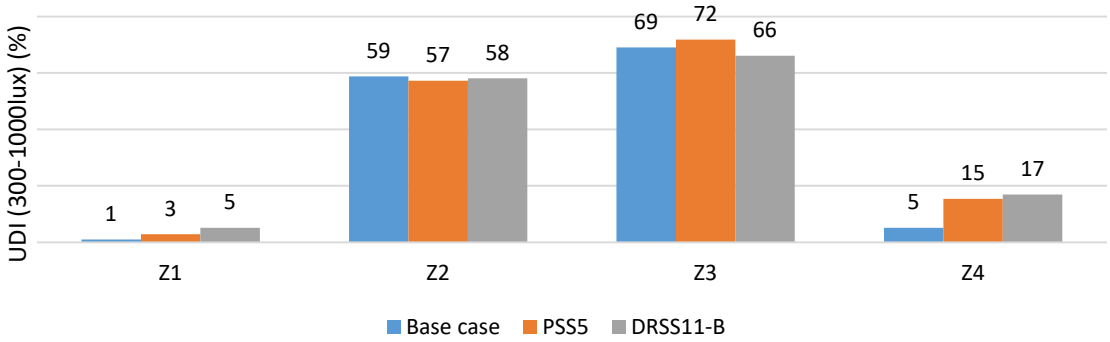


Figure 11.48: Comparison of useful daylight illuminance (UDI)

11.5. Discussion and Conclusions

Although the performance of the daylight-redirection device (DRD) was optimised, it was found that most of the sunrays were reflected at the front area of the ceiling. Therefore, the compound parabolic concentrator (CPC) was applied in a reverse mode, where the inlet aperture is smaller than the outlet. It was found that the curvature of the DRD inner surface plays a significant role in the daylight-redirection process.

First, a raytracing study was conducted at solar noon on summer solstice day, equinox day and winter solstice day for a whole CPC in a reverse mode. It was found that the CPC redirected the sunrays to further distance inside the ceiling compared with the same CPC in a normal mode. The maximum redirecting depth was achieved in December by 4.12 meters. On the other hand, in summer, the sunrays were not reached the interior surface of the CPC. It was found that the external upper part of the CPC redirected the sunrays towards outdoor in June. Nevertheless, the performance was better in September, which reached 2.64 meters; however, most of the sunrays were blocked by the upper part of the CPC.

Therefore, the geometry of the initial CPC was developed by eliminating its upper part. It was found that the developed CPC allowed more sunbeams to be redirected towards the ceiling. It

was observed that the lower part of the CPC plays the main role in the redirection function of the sunrays. The redirection of the sunrays in June was enhanced where it reached 1.03 meters at the ceiling. However, it was found that in December direct sunrays could access the work plan through the CPC.

While the raytracing study is useful to analyse the direct sunrays behaviour, the point-in-time (PIT) and the annual daylight studies are necessary to evaluate the daylight intensity for both the direct and diffuse daylight components. Therefore, the proposed system was assessed through a daylight simulation to investigate its performance.

The hourly evaluation of case DRSS1 showed that at extremely low solar altitude (at 8 am on 21 December), the direct sunrays access the room through the lower perforations. Nevertheless, the excessive total illuminance at this test hour was reduced by 420 lux compared with DRSS1.

It was found that DRSS11 enhanced the daylight performance at solar noon compared with DRSS1 (half CPC in normal mode). The illuminance levels were reduced in the front daylight zones, namely at Z1 and Z2, while they were increased in the rear daylight zones, namely at Z3 and Z4. The illuminance level at Z1 in June was reduced from 1,735 lux to 1,532 (a decrease of 11.7%). In September, the illuminance at Z4 was increased from 246 lux to 269 lux (an increase of 9.6%). Similarly, at 2 pm, the illuminance was decreased at Z1 while it was increased at other daylight zones. In the late evening, at 4 pm, the illuminance levels were increased at Z1 and Z2. However, the increase at Z3 and Z4 was insignificant. The above enactment in the illuminance levels increased the DUWP by DRSS11 compared with DRSS1. The DUWP was increased by 2% to 5% for most of the test hours.

The annual daylight performance of DRSS11 and DRSS1 showed that the ASE at Z1 was reduced for all the seasons. It was reduced by 15, 9 and 21 hours in spring, autumn and winter, respectively. On the other hand, the $UDI_{300\text{-}1000lx}$ was relatively decreased at Z3 and Z4. Its maximum decrease was 24 lux at Z3 in summer and 14 lux at Z4 in winter. Therefore, the tilt angle of the DRDs for case DRSS11 was optimised.

The investigation of six tilt angles (from 5 to 30 degrees with a 5-degree step) was analysed. The investigation started with raytracing for the highest solar altitude, which occurs at the solar noon on the summer solstice day. It was found that the direct sunrays could be redirected towards the ceiling up to 7.84 meters by 30-degree tilt compared with 1.03-meter by 0-degree tilt angle. However, the simulation of the daylight intensity showed that the best daylight performance was obtained by a 5-degree tilt angle. Therefore, it is important to mention that

the raytracing study is useful to observe the behaviour of the sun paths. However, the daylight simulation for the light intensity is required to assess the final daylight performance.

It was found that the impact of the tilt angle on the daylight-redirection functionality is significant. When the tilt angle increases inwards, the sunlight can reach a deeper area on the ceiling. However, the tilt angle should be adjusted sensibly to prevent the sunrays from reaching the work plane directly.

The DUWP was increased by the optimised tilt angle (5-degree inwards). The best enhancement was at the highest solar altitude on June 21 at solar noon. The DWUP was increased from 28% to 32%. On the other hand, the low DUWP value at the lowest solar altitude on December 21 at 8 am was not enhanced. The DUWP was increased relatively from 4.2% to 4.5%. The seasonal evaluation showed that case DRSS11-B increased the $UDI_{300\text{-}1000lx}$ value only at Z4 in winter from 30% to 40%. Therefore, a prismatic lens was applied (case DRSS12) to investigate the effect of the lens on the enhancement of daylight performance.

The ASE was reduced by DRSS12 compared with DRSS11-B from 90 hours to 68 hours in winter, 14 hours to 7 hours in spring, and 8 hours to 2 hours in autumn. In contrast, the DRSS12 reduced the $UDI_{300\text{-}1000lx}$ at daylight zones except for Z1, which was slightly increased. Therefore, the prismatic lens impact was not enhanced the daylit performance as was predicted. Additional investigations will be conducted in future work to investigate the unpredicted performance of the prismatic lens. The study will include the method of the simulation and optimisation of the prismatic lens properties. The most significant property of the prism is the redirection angle of the lens.

Chapter 12. Conclusions

12.1. Summary

The potential of optimising the daylighting performance for an office building by means of a passive daylighting system was assessed. A novel integrated daylight-redirecting solar screen (DRSS) was proposed for this purpose. The proposed system is an integration of daylight filtration and daylight redirection systems. First, a perforated solar screen (PSS) was developed and optimised. Afterwards, daylight-redirecting devices (DRDs) were integrated within it. Later, the DRD was developed by adding a prismatic lens.

The thesis was conducted in four phases; each phase has a particular objective;

- To study the daylight performance for the current base case
- To design a novel daylighting system and to evaluate its performance
- To validate the outputs of the daylighting assessment study
- To optimise the final design of the proposed system and to assess its performance

The daylight performance of the proposed system was assessed under four conditions:

- Computer simulation (a Raytracing and Climate-based daylighting modelling)
- Under an artificial direct-light
- Under an artificial sky dome (diffuse-light)
- Under a real sky

The study began with an evaluation of the daylighting performance for the base case. A typical office with a rectangular plan that has one external façade facing south was modelled in RHINOCEROS 3D and GRASSHOPPER software. Then, the daylight modelling was prepared inside GRASSHOPPER by means of LADYBUG and HONEYBEE software. Later, the simulation of the daylight modelling was run in RADIANCE software.

The results of the daylight assessment for the base case showed that the daylight performance was inadequate, therefore, a perforated solar screen (PSS) was utilised. The perforation percentage of the PSS was optimised and the daylighting performance was assessed. Although the PSS enhanced the daylighting performance at the front area of the room compared to the base case, the performance at the deep area was not improved. As a result, daylight-redirecting devices (DRDs) were integrated into the PSS and the daylighting performance was assessed.

The daylight performance of the base case was assessed by means of raytracing study at solar noontime for the summer solstice, autumn equinox and winter solstice days. Then, a daylight simulation study was conducted for the same days from 8 am to 4 pm with a 2-hour interval. The hourly simulation aimed to assess the daylight performance during the day. Furthermore, the annual daylight performance was evaluated for the whole year and each season separately. Similarly, the performance of the PSS and DRSS was evaluated. The PSS was assessed with six perforation percentages from 25% to 35% with a 2% interval, and they have been given names PSS1 to PSS6, respectively.

The daylight performance was evaluated using the illuminance levels at the work plane and the daylight uniformity for the hourly assessment. On the other hand, dynamic daylight metrics were utilised for the annual daylight assessment. They are the daylight autonomy (DA), the annual sunlight exposure (ASE) and the useful daylight illuminance (UDI). In addition, the visual discomfort was evaluated by the measurements of the daylight glare probability (DGP).

The effect of four parameters of the DRD was investigated. They are the position, unit per area ratio, geometry and material of the DRD. Later, the tilt angle of the DRD was optimised. Furthermore, the truncation angle of the DRD and integration of a prismatic lens on the daylight performance was analysed.

The daylight uniformity was enhanced by the proposed system compared to the base and the perforated solar screen for most of the tested hours. A significant enhancement was achieved on winter solstice day. The daylight uniformity was increased to 22% while it was 2% for the base case. Furthermore, on the summer solstice and the autumn equinox days, the uniformity reached 32% whereas the highest uniformity was19 % and 28% with the base case and the PSS, respectively.

In addition, the analysis of the annual daylight performance revealed that the negative impact of direct sunlight was reduced by the utilisation of the proposed system. The ASE was decreased to 121 by case DRSS11-B, and 186 hours with case PSS5 while it was 381 hours with the base case. On the other hand, the DA values showed that at daylight zone Z1 and Z2 the performance was similar for the base case, case PSS5 and case DRSS11-B. The DA value was 100% at Z1 and 97 to 98% at Z2. However, the DA values at Z3 the highest DA was 72% with case PSS5 with an increase of 3% and 6% compared to the base case and case DRSS11-B, respectively. Nevertheless, the UDI values revealed that the at daylight zones Z1 and Z4,

case DRSS11-B increased the UDI values from 1% and 3% to 5% at Z1, and 5% and 15% to 17% compared to the base case and case PSS5, respectively.

12.2. Key findings

Base case performance

The evaluation of the base case revealed that the daylight level was overlit, daylit, partially daylit and not adequately daylit at Z1, Z2, Z3 and Z4, respectively. The direct sunbeams reached only daylight zone Z1. The worst scenario was recorded on winter solstice day as the direct sunbeams penetrated the room by more than one meter at the working level, and by two meters at the floor level. On the other hand, the direct sunbeams were not a challenge on the summer solstice day. The DA values were sufficient at all the daylight zones except at Z4 (rear zone). The best DA value was recorded in winter when the sun altitude is low, whereas the worst was recorded in summer. The ASE was occurred only at Z1 (front zone) by 381 hours per year. The worst ASE value was recorded in winter by 338 hours; however, the ASE did not occur in summer. The worst UDI value was at Z1 and Z4 during all the seasons. The UDI values were extremely low at both the front and rear zones, and they were acceptable in the middle of the room.

The desired illuminance level was achieved in the early morning at daylight zones Z2 and Z3 on the three tested days. The illuminance levels on the other hand exceeded the threshold at the front daylight zone (Z1) whilst they were lower than the threshold at the rear daylight zone (Z4) for all the tested hours in June and September. The best daylight performance, in general, was recorded in June and September, particularly at 10 am, 12 pm and 2 pm. The illuminance levels exceeded the acceptable threshold in December by a significant value that exceeded 44,000 lux. The main reason was due to the low solar altitude in winter. Since the direct sunbeams can reach the front daylight zone that could lead to a significant increase in the illuminance level. In addition, the daylight uniformity dropped to 3%. However, the daylight performance at Z4 was better in December. The minimum desired illuminance level was achieved at 10 am, 12 pm and 2 pm. The difference between the illuminance level at Z1 and the other daylight zones was significant. In June and September, the daylight uniformity was higher due to the absence of direct sunlight at the work plane. The daylight uniformity ranged from 14% to 19% in June and from 12% to 14% in September; however, these percentages are still lower than the desirable daylight uniformity level.

It was found that the glare comfort range at Z1 in December was intolerable during all the tested hours in December, except at 8 am it was disturbing, which still exceeds the acceptable level. The findings above revealed that the daylight performance of the base case without additional daylighting devices was not adequate. The main reason for the low daylight uniformity was the direct sunlight at the work plane. Furthermore, the discomfort that was shown in the DGP analysis was due to the direct sunlight that exposed the occupants. As a result, it was important to reduce the impact of direct sunlight in the front area of the room. This objective was achieved by utilising a filtration daylighting system, which is a perforated solar screen (PSS).

The performance of the perforated solar screen (PSS)

The best DA performance was recorded at Z1 and Z2 for most of the PSS cases. The DA values at Z3 and Z4 increased when the perforation percentage increased. The ASE has occurred only at Z1. The lowest ASE value was recorded with case PSS1 (74 hours/year), whereas the highest value was with case PSS6 (221 hours/year). The perforated screen reduced the ASE value by 117 to 264 hours/year compared to the base case. The lowest acceptable perforation percentage to enhance the UDI at Z4 compared with the base case was 31%. The sufficient perforation percentage to maintain a balanced daylight performance that decreases undesirable direct sunlight and increase desirable diffuse light was 33% (case PSS5). Case PSS5 maintained the UDI values that the base case achieved while it reduced the direct sunlight that is allowed by the base case. For instance, the UDI at zone Z3 was 72% for both cases. As a result, the PSS5 reduced the ASE from 381 hours/year to 186 hours/year.

The performance of Case PSS5

The utilisation of PSS5 enhanced the overall daylighting performance compared with the base case. The best DA value was recorded at Z1 and Z2 with at least 82% during all the seasons. On the other hand, the DA values at Z4 were significantly varied. The highest DA value was in winter (38%), whereas the lowest was in summer (0%), due to the low and high solar altitude, respectively. The ASE has not occurred in summer, and it was low in spring (27 hours/year) and autumn (16 hours/year); however, the worst scenario was in winter, which reached 129 hours/year. Since the perforations within the solar screen are parallel with the façade, they allow the most direct sunlight at low solar altitude to reach the work plane.

Although the UDI at the front area was enhanced by case PSS5, it was lower than the desirable level. It ranged from 6% in spring to 10% in summer. Nevertheless, it was increased by two

times for all the seasons compared with the base case, except in spring, which was relatively lower than the base case by 1.6%. At zones Z2 and Z3, the UDI was similar to the base case; however, a significant improvement was recorded in the rear area (Z4), which was increased by considerable UDI values for all the seasons. While the UDI at Z4 for the base case was 0% during all the seasons except in winter, which was17.7%, it was increased by PSS5 to 11% in spring, 8% in autumn and 38% in winter. Since the perforations within the solar screen are outspread on the whole area of the façade, this allowed the daylight to reach a deeper area in the room compared with the base case, as the window is placed in the middle of the façade.

The undesirable illuminance in the front area in June and September was reduced in the early morning (8 am), however, the total illuminance was increased in December from 4,610 lux to 16,061 lux. The rapid increase in the total illuminance level was due to the high value of direct illuminance (12,923 lux) at the work plane caused by the perforations in the lower third part of the solar screen. On the other hand, a significant enhancement was achieved by reducing the direct sunlight at 12 pm and 2 pm at Z1 in December, the total illuminance was reduced from 48,460 lux to 5,297 lux and from 38,065 lux to 3,911 lux, respectively. The daylight uniformity was enhanced at most of the tested hours compared with the base case. It was increased from 19% to 30% at 10 am on 21 Jun, and from 2% and 3% to 19% and 18% at 12 pm and 2 pm, respectively. However, it was reduced at 8 am on the winter solstice day at 8 am from 12% to 5%.

The visual comfort was enhanced by case PSS5 for all the tested hours; however, from 10 am to 2 pm the DGP values were still higher than the acceptable levels. The DGP was reduced from 0.42 (disturbing glare) to 0.34 (imperceptible glare) at 8 am, and from 0.47 (perceptible glare) to 0.38 (intolerable glare) at 4 pm. The distribution of the WWR to small perforations throughout the façade led to a daylight enhancement at 4 pm, as it prevented the direct light from accessing the room when the solar altitude is extremely low. It is vital to consider both the perforations positions and the windowsill height when designing a building façade as it was found to be a primary source of over lighting particularly in the front area of the room.

The performance of case DRSS1 (normal mode)

The best performance was in December when the solar altitude is low. Most of the sunrays were reflected towards outdoor by the DRD. The upper part of the DRD did not play a considerable role in the daylight redirection; nevertheless, it reduced the quantity of the redirected daylight towards the interior ceiling. The upper surface of the DRD obstructs the

redirected sunrays, therefore, it was eliminated. As a result, the redirection of the sunrays towards the indoor ceiling was enhanced. The undesirable direct sunrays were prevented by case DRSS1 at 10 am at zone Z1 in December, which increased the daylight uniformity from 3% to 22%. The annual evaluation of the whole year revealed the impact of case DRSS1 on the daylighting performance. Case DRSS1 increased the UDI values at Z4 from 5% to 18%, and it reduced the ASE value at Z1 from 381 to 161 hours/year. Also, the overall DA and the UDI values were increased for all the seasons.

The visual comfort was analysed for the worst scenario when the direct sunlight reached the work plane, specifically on 21 December. The glare comfort ranges at 8 am and 4 pm were enhanced compared to the base case. They were changed from disturbing to imperceptible glare and from intolerable to perceptible glare, respectively. Although the glare comfort range was not changed at 10 am and 12 pm, the DGP values were decreased from 0.82 to 0.62 and from 0.94 to 0.71. The DGP values were decreased relatively compared to PSS5 at 8 am, 10 am and 12 pm; however, the glare comfort ranges were not changed. The worst DGP values were recorded at 10 am, 12 pm and 2 pm. The large perforation openings in the lower part within the PSS caused the increase in the DGP values.

Experimental tests

The highest illuminance level was recorded at 88-degree solar altitude with case DRSS1 (DRDs at low position) and at 26-degree altitude with case DRSS2 (DRD at mid position). The DRD unit's ratio per area plays a key role in reducing direct sunrays at the work plane in the front area. The illuminance at 26-degree solar altitude was increased significantly at Z2 by cases DRSS4 and DRSS5 [add values]. The mirror-HIPS material (case DRSS6) decreased the illuminance level relatively at the high solar altitude, but it increased it at the low solar altitude, specifically at daylight zone Z2. The flat geometry increased the illuminance levels at the work plane for both materials at 88-degree solar altitude. On the other hand, the concave geometry increased the illuminance levels at 26-degree solar altitude, particularly at the front areas. The tilt angle of the DRD should be optimised to reach the optimal performance of the proposed system.

Test under diffuse-light simulator

The comparison of cases PSS5 and DRSS1 showed that the change in the illuminance levels was less with 88-degree and 42-degree compared with 26-degree solar altitude. The illuminance levels were higher at a 42-degree altitude for the three cases. The increase of the

DRD position and the decrease of the solar altitude increased the illuminance level at the front area. As a result, the sunbeams can be redirected to a deeper area by utilising the lower DRD position. The daylight uniformity was increased when the solar altitude was decreased. The mirror HIPS material increased the illuminance levels for all the daylight zones and tested solar altitudes. The impact of the mirror material was higher with the parabolic surface compared with the flat surface. The truncation of the DRD increased the illuminance levels at the front zones, particularly at the 42-degree and 26-degree solar altitudes. The integration of the prismatic lens reduced the illuminance levels at the front area.

Test under real sky

The daylight factor (DF) was enhanced by the integration of the DRD. The DF value was reduced in the front area from 33.3% to 26.4%. The lower DRD position performed better in reducing the illuminance level at the front area and increasing it at the rear area of the room, however, this may differ due to the change of the solar altitude. On the other hand, the increase of the DRD position increased the DF value at the front zones while it decreased it at the rear zones. The mirror material increased the DF value at the front and rear areas of the room. The impact of the mirror material was higher with the parabolic geometry. It increased the DF at test point Z1 from 25.2% to 30.8%; however, at Z4, it increased only from 8.2% to 9.1%. The truncated DRD reduced the DF values at both Z1 and Z4; however, the variation between the DF values was reduced. The prismatic lens increased the DF value at Z1 and decreased it relatively at Z4.

Final simulation

The inner surface curvature of the DRD plays a significant role in the daylight-redirection process. The DRD redirected the sunrays to further distance at the ceiling level compared with the same DRD in a normal mode. The maximum redirection depth was achieved in December by 4.12 meters. On the other hand, in June, the sunrays did not reach the interior surface of the DRD. It was found that the external upper part of the DRD redirected the sunrays towards the outdoor. Similarly, in September most of the sunrays were blocked, however, they reached 2.64 meters.

The developed DRD allowed more sunbeams to be redirected towards the ceiling. The lower part of the DRD plays the main role in the redirection function of the sunrays. The redirection of the sunrays in June was enhanced where it reached 1.03 meters at the ceiling. The direct

sunbeams reached the work plane through the lower part of the façade through the perforations. The daylight uniformity was increased by 2% to 5% for most of the test hours.

The ASE value at Z1 was reduced for all the seasons. It was reduced by 15, 9 and 21 hours in spring, autumn and winter, respectively. The direct sunbeams could be redirected towards the ceiling up to 7.84 meters by 30-degree tilt compared with 1.03-meter by 0-degree tilt angle. However, the daylight simulation of the light intensity showed that the best daylight performance was obtained by a 5-degree tilt angle.

The impact of the tilt angle on the daylight-redirection functionality is significant. When the tilt angle increases inwards, the sunlight can reach a deeper area on the ceiling. However, the tilt angle should be adjusted sensibly to prevent the sunrays from reaching the work plane directly. The daylight uniformity was increased by the optimised tilt angle (5-degree inwards). The best enhancement was at the highest solar altitude on June 21 at solar noon. The daylight uniformity was increased from 28% to 32%. Case DRSS11-B increased the UDI300-1000lx value at Z4 in winter from 30% to 40%. The ASE value was reduced by DRSS12 compared with DRSS11-B from 90 hours to 68 hours in winter, 14 hours to 7 hours in spring, and 8 hours to 2 hours in autumn.

12.3. Limitations

In order to reduce the uncertainty, some limitations can be resolved in future work. The prototype scale-model was constructed at scale 1:10, it was found that the illuminance inside the prototype compared to the simulation model gave a good correlation. The illuminance level at the prototype-scale model was approximately higher by ten times. However, an experimental test at a scale of 1:1 could reduce the uncertainty among the outputs.

The current study investigated only the south façade. Other orientations require further investigations. In addition, the urban context was not included in the study. The purpose was to investigate the effect of the optimisation of the tested parameters.

The outputs of the experimental tests under the DRLS (Chapter 8) are limited to direct sunlight. On the other hand, the outputs obtained under the DFLS (Chapter 9) are limited to the diffuse-light components, which represent the sky patches. The test under the real sky (Chapter 10) is limited to high latitude regions, further tests will be conducted under a real sky in Riyadh city, Saudi Arabia.

Due to the technical limitations, the fabrication of the DRD with a mirror-effect material was influenced. The reflectivity of the surface was reduced due to the vacuuming process. That was due to the applied heat and the bending of the material. In addition, the transparency of the prismatic film was influenced by the adhesive material that was applied to install the film on the lens. It was noticed that the transparency of some lenses was impacted.

12.4. Future works

The study highlighted the importance of the daylight-redirecting system for better daylighting performance; however, further works will be conducted to investigate the influence of the proposed system on other aspects as follows:

- Calculation of the annual lighting profile
- Investigation of the impact of the proposed system on the thermal comfort and cooling loads
- Investigation of the daylight performance for different building orientations
- Test the system under a real sky in Riyadh city, Saudi Arabia.

The annual lighting profile will be calculated to measure the efficiency of the proposed system in energy saving. It assumed that the increase of the illuminance levels at the rear area of the room should decrease the usage of artificial lighting. Furthermore, the reduction of ASE value and the illuminance levels at the front area may reduce the heat gain and hence the cooling loads of the room.

Although the proposed system enhanced the daylighting performance for the south façade, further investigations are required for other building orientations. While the geometry of the DRD is parabolic, the sunbeams at the east and west façades may need different processing. Therefore, the effect of the DRD rotation angles on the daylighting performance will be investigated. Finally, the proposed system will be tested at a scale of 1:1 under a real sky in Riyadh city, Saudi Arabia.

References

AGAFONKIN, V. 2020. *SunCalc sun position and sunlight phases calculator* [Online]. Available: http://suncalc.net/#/52.9068,-1.2441,20/2020.10.21/12:47 [Accessed October 15, 2020].

AIZENBERG, J. B. 2013. Hollow light guides: 50 years of research, development, manufacture and application-a retrospective and looking to the future. *Light & Engineering,* 21.

AIZIEWOOD, M. E. 1993. Innovative daylighting systems: An experimental evaluation. *International Journal of Lighting Research and Technology,* 25**,** 141-152.

AL-OBAIDI, K. M., ISMAIL, M. & ABDUL RAHMAN, A. M. 2014. A study of the impact of environmental loads that penetrate a passive skylight roofing system in Malaysian buildings. *Frontiers of Architectural Research,* 3**,** 178-191.

AL-OBAIDI, K. M., MUNAAIM, M. A. C., ISMAIL, M. A. & ABDUL RAHMAN, A. M. 2017. Designing an integrated daylighting system for deep-plan spaces in Malaysian low-rise buildings. *Solar Energy,* 149**,** 85-101.

ALAWADHI, E. M. 2012. Using phase change materials in window shutter to reduce the solar heat gain. *Energy and Buildings,* 47**,** 421-429.

ALRUBAIH, M. S., ZAIN, M. F. M., ALGHOUL, M. A., IBRAHIM, N. L. N., SHAMERI, M. A. & ELAYEB, O. 2013. Research and development on aspects of daylighting fundamentals. *Renewable and Sustainable Energy Reviews,* 21**,** 494-505.

ALTAN, H. & ALSHAREEF, H. F. 2015. An Evaluation of the Total Energy Consumption of Educational Buildings Prototype Case Studies in Saudi Arabia.

ANSTEAD, K. & FRANTA, G. Ecovillage-Striving for Sustainability Near Our Nation's Capital. PROCEEDINGS OF THE NATIONAL PASSIVE SOLAR CONFERENCE, 1994. AMERICAN SOLAR ENERGY SOCIETY INC, 304-304.

ANTONY, J. 2014. 2 - Fundamentals of Design of Experiments. *In:* ANTONY, J. (ed.) *Design of Experiments for Engineers and Scientists (Second Edition).* Oxford: Elsevier.

APPELFELD, D., MCNEIL, A. & SVENDSEN, S. 2012. An hourly based performance comparison of an integrated micro-structural perforated shading screen with standard shading systems. *Energy and Buildings,* 50**,** 166-176.

ASCIONE, F. 2017. Energy conservation and renewable technologies for buildings to face the impact of the climate change and minimize the use of cooling. *Solar Energy*.

ATHER, H. 2020. *How to Calculate Lux Levels* [Online]. Available: https://sciencing.com/calculate-lux-levels-6953934.html [Accessed 15 January 2021].

AWS, A. W. S. 2015. *U-VALUE & SHGC EXPLAINED* [Online]. Available: http://www.awsaustralia.com.au/vantage/u-value-shgc-explained [Accessed Augest 4 2017].

BAETENS, R., JELLE, B. P. & GUSTAVSEN, A. 2010. Properties, requirements and possibilities of smart windows for dynamic daylight and solar energy control in buildings: A state-of-the-art review. *Solar Energy Materials and Solar Cells,* 94**,** 87-105.

BAETENS, R., JELLE, B. P. & GUSTAVSEN, A. 2011. Aerogel insulation for building applications: A state-of-the-art review. *Energy and Buildings,* 43**,** 761-769.

BAHAJ, A. S., JAMES, P. A. B. & JENTSCH, M. F. 2008. Potential of emerging glazing technologies for highly glazed buildings in hot arid climates. *Energy and Buildings,* 40**,** 720-731.

BAKER, N. & STEEMERS, K. 2014. *Daylight design of buildings: a handbook for architects and engineers*, Routledge.

BAKKER, L. G., HOES-VAN OEFFELEN, E. C. M., LOONEN, R. C. G. M. & HENSEN, J. L. M. 2014. User satisfaction and interaction with automated dynamic facades: A pilot study. *Building and Environment,* 78**,** 44-52.

BARRIOS, D., VERGAZ, R., SÁNCHEZ-PENA, J. M., GARCÍA-CÁMARA, B., GRANQVIST, C. G. & NIKLASSON, G. A. 2015. Simulation of the thickness dependence of the optical properties of suspended particle devices. *Solar Energy Materials and Solar Cells,* 143**,** 613-622.

BHUSAL, P., ZAHND, A., ELOHOLMA, M. & HALONEN, L. 2007. Replacing fuel based lighting with light emitting diodes in developing countries: energy and lighting in rural Nepali homes. *Leukos,* 3**,** 277-291.

BILIOURIS, D., VERSTRAETEN, W. W., DUTRÉ, P., VAN AARDT, A. N. J., MUYS, B. & COPPIN, P. 2007. A Compact Laboratory Spectro-Goniometer (CLabSpeG) to Assess the BRDF of Materials. Presentation, Calibration and Implementation on Fagus sylvatica L. Leaves. *Sensors,* 7.

BLANCO, J. M., BURUAGA, A., ROJÍ, E., CUADRADO, J. & PELAZ, B. 2016. Energy assessment and optimization of perforated metal sheet double skin façades through Design Builder; A case study in Spain. *Energy and Buildings,* 111**,** 326-336.

BODART, M., DENEYER, A., DE HERDE, A. & WOUTERS, P. 2006. Design of a new single-patch sky and sun simulator. *Lighting Research & Technology,* 38**,** 73-87.

BOUBEKRI, M. 2008. *Daylighting, architecture and health : building design strategies / Mohamed Boubekri,* Oxford, Oxford : Architectural Press.

BOUBEKRI, M. 2014. *Daylighting Design: Planning Strategies and Best Practice Solutions*, Birkhäuser.

BOURGEOIS, D., REINHART, C. F. & WARD, G. 2008. Standard daylight coefficient model for dynamic daylighting simulations. *Building Research & Information,* 36**,** 68-82.

BOYANO, A., HERNANDEZ, P. & WOLF, O. 2013. Energy demands and potential savings in European office buildings: Case studies based on EnergyPlus simulations. *Energy and Buildings,* 65**,** 19-28.

BREEAM. 2016. *5.0 Health and Wellbeing > Hea 01 Visual comfort* [Online]. UK. Available: https://www.breeam.com/BREEAMUK2014SchemeDocument/content/05_health/hea01_nc.htm [Accessed 5.0 SD5076].

BREMBILLA, E. 2017. *Applicability of Climate-Based Daylight Modelling.* PhD, Loughborough University.

BULLOCK, J. N., BECHINGER, C., BENSON, D. K. & BRANZ, H. M. 1996. Semi-transparent a-SiC:H solar cells for self-powered photovoltaic-electrochromic devices. *Journal of Non-Crystalline Solids,* 198-200**,** 1163-1167.

BURATTI, C. & MORETTI, E. 2012. Glazing systems with silica aerogel for energy savings in buildings. *Applied Energy,* 98**,** 396-403.

CALCULATOR.ORG. 2020. *luminance - calculator.org* [Online]. Available: https://www.calculator.org/properties/luminance.html [Accessed 25 March 2020].

CALLOW, J. M. & SHAO, L. 2003. Air-clad optical rod daylighting system. *Lighting Research & Technology,* 35**,** 31-38.

CAPROS, P., MANTZOS, L., PAPANDREOU, V. & TASIOS, N. 2008. European energy and transport. *Trends to,* 2030.

CASINI, M. 2016. 10 - Energy-generating glazing. *In:* CASINI, M. (ed.) *Smart Buildings.* Woodhead Publishing.

CEIC DATA, A. I. E. M. G. C. 2020. *Saudi Arabia Electricity: Consumption* [Online]. London. Available: https://www.ceicdata.com/en/saudi-arabia/electricity-statistics/electricity-consumption#:~:text=Saudi%20Arabia's%20Electricity%3A%20Consumption%20data,to%202018%2C%20with%2019%20observations. [Accessed 26 November 2020].

CHABANE, I. J. & BENSALEM, R. 2006. Tinted Glass Curtain Wall and its Implications on the Occupants' Health–Case Study of a Tight Office Building in Algiers.

CHAVES, J. 2015. *Introduction to nonimaging optics*, CRC press.

CHOW, T. T., LI, C. Y. & LIN, Z. 2010. Innovative solar windows for cooling-demand climate. *Solar Energy Materials and Solar Cells,* 94**,** 212-220.

CHRISTOFFERSEN, J. 1995. *Daylight utilisation in office buildings*, SBI forlag.

CIE. 2012. *Tubular Daylight Guidance Systems* [Online]. Available: http://www.cie.co.at/index.php/index.php?i_ca_id=899 [Accessed May 9 2017].

COBURN, C. A. & PEDDLE, D. R. 2006. A low-cost field and laboratory goniometer system for estimating hyperspectral bidirectional reflectance. *Canadian Journal of Remote Sensing,* 32**,** 244-253.

COLLINS, B. L. 1975. Windows and people: A literature survey. Psychological reaction to environments with and without windows. National Bureau of Standards, Washington, DC (USA); US Dept. of Commerce, National Bureau of Standards, Institute for Applied Technology, Washington, DC 20234.

CRAWLEY, D. B., HAND, J. W., KUMMERT, M. & GRIFFITH, B. T. 2008. Contrasting the capabilities of building energy performance simulation programs. *Building and environment,* 43**,** 661-673.

CUCE, E. & CUCE, P. M. 2016. Vacuum glazing for highly insulating windows: Recent developments and future prospects. *Renewable and Sustainable Energy Reviews,* 54**,** 1345-1357.

CUCE, E. & RIFFAT, S. B. 2015. A state-of-the-art review on innovative glazing technologies. *Renewable and Sustainable Energy Reviews,* 41**,** 695-714.

DARULA, S. & KITTLER, R. 2009. Standard sky calculations for daylighting design and energy performance purposes. *Fizyka Budowli w Teorii i Praktyce,* 4**,** 23-28.

DAY, M. 2010. 2000-2010. Rhino Grasshopper, AEC Magazine, X3DMedia.

DEL VECCHIO, R. J. 1997. Understanding design of experiments: a primer for technologists. Hanser. Gardner Publications, Cincinnati.

DOE, U. 2005. Annual Energy Review. *In:* ENERGY EFFICIENCY AND RENEWABLE ENERGY, D. E.-. (ed.).

DREAM GLASS GROUP. 2017. *DreamGlass® Switchable Glass Operation* [Online]. Available: http://www.dreamglassgroup.com/privacy-glass/# [Accessed 21 April 2017].

DUBOIS, M., BISEGNA, F., GENTILE, N., KNOOP, M. & MATUSIAK, B. 2016. Daylighting and lighting retrofit to reduce energy use in non-residential buildings: A literature review.

EDMONDS, I. 2005. Daylighting high-density residential buildings with light redirecting panels. *Lighting Research & Technology,* 37**,** 73-84.

EDMONDS, I. R. & GREENUP, P. J. 2002. Daylighting in the tropics. *Solar Energy,* 73**,** 111-121.

EDWARDS, L. & TORCELLINI, P. 2002. Literature Review of the Effects of Natural Light on Building Occupants. National Renewable Energy Lab., Golden, CO.(US).

EMAMI, N. & GILES, H. 2016. Geometric Patterns, Light and Shade: Quantifying Aperture Ratio and Pattern Resolution in the Performance of Shading Screens. *Nexus Network Journal,* 18**,** 197-222.

FASI, M. A. & BUDAIWI, I. M. 2015. Energy performance of windows in office buildings considering daylight integration and visual comfort in hot climates. *Energy and Buildings,* 108**,** 307-316.

FERNANDES, L. L., LEE, E. S., MCNEIL, A., JONSSON, J. C., NOUIDUI, T., PANG, X. & HOFFMANN, S. 2015. Angular selective window systems: Assessment of technical potential for energy savings. *Energy and Buildings,* 90**,** 188-206.

FINNEGAN, M. C. & SOLOMON, L. Z. 1981. Work attitudes in windowed vs. windowless environments. *The Journal of Social Psychology,* 115**,** 291-292.

FREEWAN, A. A., SHAO, L. & RIFFAT, S. 2009. Interactions between louvers and ceiling geometry for maximum daylighting performance. *Renewable Energy,* 34**,** 223-232.

GALATIOTO, A. & BECCALI, M. 2016. Aspects and issues of daylighting assessment: A review study. *Renewable and Sustainable Energy Reviews,* 66**,** 852-860.

GESIMAT. 2017. *Electrochromic Laminated Glass.pdf* [Online]. Available: https://www.berlin-innovation.de/uploads/tx_innodb/product_information_gesimat.pdf [Accessed April 12 2017].

GHOSH, A. & NORTON, B. 2017. Interior colour rendering of daylight transmitted through a suspended particle device switchable glazing. *Solar Energy Materials and Solar Cells,* 163**,** 218-223.

GHOSH, A., NORTON, B. & DUFFY, A. 2015. Measured overall heat transfer coefficient of a suspended particle device switchable glazing. *Applied Energy,* 159**,** 362-369.

GHOSH, A., NORTON, B. & DUFFY, A. 2016. First outdoor characterisation of a PV powered suspended particle device switchable glazing. *Solar Energy Materials and Solar Cells,* 157**,** 1-9.

GIOVANNINI, L., VERSO, V. R. M. L., KARAMATA, B. & ANDERSEN, M. 2015. Lighting and Energy Performance of an Adaptive Shading and Daylighting System for Arid Climates. *Energy Procedia,* 78**,** 370-375.

GOIA, F., PERINO, M. & HAASE, M. 2012. A numerical model to evaluate the thermal behaviour of PCM glazing system configurations. *Energy and Buildings,* 54**,** 141-153.

GRANQVIST, C. G. 1995. Chapter 4 - Tungsten Oxide Films: Preparation, Structure, and Composition of Sputter-Deposited Films. *Handbook of Inorganic Electrochromic Materials.* Amsterdam: Elsevier Science B.V.

GUTH, S. K. 1963. A method for the evaluation of discomfort glare. *Illuminating Engineering,* 58**,** 351-364.

HAMMAD, F. & ABU-HIJLEH, B. 2010. The energy savings potential of using dynamic external louvers in an office building. *Energy and Buildings,* 42**,** 1888-1895.

HEE, W. J., ALGHOUL, M. A., BAKHTYAR, B., ELAYEB, O., SHAMERI, M. A., ALRUBAIH, M. S. & SOPIAN, K. 2015. The role of window glazing on daylighting and energy saving in buildings. *Renewable and Sustainable Energy Reviews,* 42**,** 323-343.

HOFFMANN, S., LEE, E. S., MCNEIL, A., FERNANDES, L., VIDANOVIC, D. & THANACHAREONKIT, A. 2016. Balancing daylight, glare, and energy-efficiency goals: An evaluation of exterior coplanar shading systems using complex fenestration modeling tools. *Energy and Buildings,* 112**,** 279-298.

HOWARD, T. C., PLACE, W., ANDERSON, B. & COUTIERS, P. Variable-area, Light Reflecting Assemblies (VALRA). Proceedings of the 2nd International Daylighting Conference, 1986 Long Beach.

HUANG, Y., NIU, J.-L. & CHUNG, T.-M. 2014. Comprehensive analysis on thermal and daylighting performance of glazing and shading designs on office building envelope in cooling-dominant climates. *Applied Energy,* 134**,** 215-228.

HÜSING, N. & SCHUBERT, U. 1998. Aerogels - Airy Materials: Chemistry, Structure, and Properties. *Angewandte Chemie - International Edition,* 37**,** 22-45.

INNOVATIVE GLASS CORPORATION. 2017. *LC Privacy Glass* [Online]. Available: http://www.innovativeglasscorp.com/lc-privacy [Accessed 21 April 2017].

INOUE, T., ICHINOSE, M. & ICHIKAWA, N. 2008. Thermotropic glass with active dimming control for solar shading and daylighting. *Energy and Buildings,* 40**,** 385-393.

ISO, B. 2004. British Standard. *Spatial distribution of daylight. CIE standard general sky.* London.

JAKUBIEC, A. & REINHART, C. 2010. The Use of Glare Metrics in the Design of Daylit Spaces: Recommendations for Practice. *9th International Radiance Workshop.* Freiburg, Germany: Harvard Design School.

JANDA, K. 2009. Worldwide status of energy standards for buildings: a 2009 update. *Proceedings of the ECEEE Summer Study, June***,** 1-6.

JELLE, B. P., HYND, A., GUSTAVSEN, A., ARASTEH, D., GOUDEY, H. & HART, R. 2012. Fenestration of today and tomorrow: A state-of-the-art review and future research opportunities. *Solar Energy Materials and Solar Cells,* 96**,** 1-28.

JOMOAH, I. M., AL-ABDULAZIZ, A. U. M. & KUMAR, R. S. Energy management in the buildings of a university campus in Saudi Arabia — A case study. 4th International Conference on Power Engineering, Energy and Electrical Drives, 13-17 May 2013 2013. 659-663.

KALAGI, S. S., MALI, S. S., DALAVI, D. S., INAMDAR, A. I., IM, H. & PATIL, P. S. 2011. Limitations of dual and complementary inorganic–organic electrochromic device for smart window application and its colorimetric analysis. *Synthetic Metals,* 161**,** 1105-1112.

KIM, Y., JUNG, D., JEONG, S., KIM, K., CHOI, W. & SEO, Y. 2015. Optical properties and optimized conditions for polymer dispersed liquid crystal containing UV curable polymer and nematic liquid crystal. *Current Applied Physics,* 15**,** 292-297.

KISTLER, S. S. 1931. Coherent expanded aerogels and jellies [5]. *Nature,* 127**,** 741.

KLAMMT, S., NEYER, A. & MÜLLER, H. F. O. 2012. Redirection of sunlight by microstructured components – Simulation, fabrication and experimental results. *Solar Energy,* 86**,** 1660-1666.

KNOOP, M., AKTUNA, B., BUENO, B., DARULA, S., DENEYER, A., DIAKITE, A., FUHRMANN, P., GEISLER-MORODER, D., HUBSCHNEIDER, C. & JOHNSEN, K. 2016. Daylighting and electric lighting retrofit solutions. Universitätsverlag der TU Berlin.

KONIS, K. & LEE, E. S. 2015. Measured daylighting potential of a static optical louver system under real sun and sky conditions. *Building and Environment,* 92**,** 347-359.

KONSTANTOGLOU, M. & TSANGRASSOULIS, A. 2016. Dynamic operation of daylighting and shading systems: A literature review. *Renewable and Sustainable Energy Reviews,* 60**,** 268-283.

KONSTANTZOS, I., TZEMPELIKOS, A. & CHAN, Y.-C. 2015. Experimental and simulation analysis of daylight glare probability in offices with dynamic window shades. *Building and Environment,* 87**,** 244-254.

KOTA, S., HABERL, J. S., CLAYTON, M. J. & YAN, W. 2014. Building Information Modeling (BIM)-based daylighting simulation and analysis. *Energy & Buildings,* 81**,** 391-403.

LAAR, M. & GRIMME, F. W. 2002. German developments in guidance systems: an overview daylight. *Building Research & Information,* 30**,** 282-301.

LAMP, P. 2018. *Philips MSD250/2 Lamp* [Online]. Available: https://www.thomann.de/gb/philips_msd250_2.htm [Accessed October 20 2018].

LAOUADI, A., REINHART, C. F. & BOURGEOIS, D. 2008. Efficient calculation of daylight coefficients for rooms with dissimilar complex fenestration systems. *Journal of Building Performance Simulation,* 1**,** 3-15.

LARSON, G. W. & SHAKESPEARE, R. 1998. *Rendering with Radiance: The Art and Science of Lighting Visualization,* San Francisco, Morgan Kaufmann.

LARSON, G. W. & SHAKESPEARE, R. 2021. *Rendering with Radiance: The Art and Science of Lighting Visualization*, Gumroad.

LAVIN, C. & FIORITO, F. 2017. Optimization of an external perforated screen for improved daylighting and thermal performance of an office space.

LEE, E. S. & DIBARTOLOMEO, D. L. 2002. Application issues for large-area electrochromic windows in commercial buildings. *Solar Energy Materials and Solar Cells,* 71**,** 465-491.

LEE, E. S., DIBARTOLOMEO, D. L. & SELKOWITZ, S. E. 2006. Daylighting control performance of a thin-film ceramic electrochromic window: Field study results. *Energy and Buildings,* 38**,** 30-44.

LEE, E. S., PANG, X. F., HOFFMANN, S., GOUDEY, H. & THANACHAREONKIT, A. 2013. An empirical study of a full-scale polymer thermochromic window and its implications on material science development objectives. *Solar Energy Materials and Solar Cells,* 116**,** 14-26.

LEE, H., KIM, K., SEO, J. & KIM, Y. 2017. Effectiveness of a perforated light shelf for energy saving. *Energy and Buildings,* 144**,** 144-151.

LITTLEFAIR, P. 1996. *Designing with innovative daylighting,* Watford, Building Research Establishment , Construction Research Communications Ltd Report.

LITTLEFAIR, P. J., AIZLEWOOD, M. E. & BIRTLES, A. B. 1994. The performance of innovative daylighting systems. *Renewable Energy,* 5**,** 920-934.

LIU, J.-H., LIU, H.-T. & CHENG, Y.-B. 1998. Preparation and characterization of gradient refractive index polymer optical rods. *Polymer,* 39**,** 5549-5552.

LONG, L. & YE, H. 2014a. How to be smart and energy efficient: a general discussion on thermochromic windows. *Sci Rep,* 4**,** 6427.

LONG, L. S. & YE, H. 2014b. Discussion of the performance improvement of thermochromic smart glazing applied in passive buildings. *Solar Energy,* 107**,** 236-244.

LUCKIESH, M. & GUTH, S. K. 1949. Brightness in visual field at borderline between comfort and discomfort (BCD). *Illuminating engineering,* 44**,** 650-670.

MAININI, A. G., POLI, T., ZINZI, M. & SPERONI, A. 2014. Spectral Light Transmission Measure of Metal Screens for Glass Façades and Assessment of their Shading Potential. *Energy Procedia,* 48**,** 1292-1301.

MAININI, A. G., POLI, T., ZINZI, M. & SPERONI, A. 2015. Metal Mesh as Shading Devices and Thermal Response of an Office Building: Parametric Analysis. *Energy Procedia,* 78**,** 103-109.

MANNING, M. A. 2006. An Experimental Evaluation and Comparison of Four Daylighting Strategies for Schools in North Carolina.

MARDALJEVIC, J. 1999. *Daylight Simulation _ Validation, Sky Models and Daylight Coefficients _ 1999 mardaljevic_chap1.* PhD, De Montfort University.

MARDALJEVIC, J. 2002. Quantification of parallax errors in sky simulator domes for clear sky conditions. *Lighting Research & Technology,* 34**,** 313-327.

MARDALJEVIC, J., HESCHONG, L. & LEE, E. 2009. Daylight metrics and energy savings. *Lighting Research & Technology,* 41**,** 261-283.

MASHALY, I. A., NASSAR, K., EL-HENAWY, S. I., MOHAMED, M. W. N., GALAL, O., DARWISH, A., HASSAN, O. N. & SAFWAT, A. M. E. 2017. A prismatic daylight redirecting fenestration system for southern skies. *Renewable Energy,* 109**,** 202-212.

MAYHOUB, M. S. & LABIB, R. 2015. Towards a solution for the inevitable use of glazed facades in the arid regions via a parametric design approach. *28th CIE Session.*

MCNEIL, A., LEE, E. S. & JONSSON, J. C. 2017. Daylight performance of a microstructured prismatic window film in deep open plan offices. *Building and Environment,* 113**,** 280-297.

MEHLING, H. 2004. Strategic project "Innovative PCM-Technology"—results and future perspectives. *8th expert meeting and work shop.* Kizkalesi, Turkey.

MICHEL, L. 1998. Scale model daylighting systems evaluation. *IEA SHC Task,* 21.

MILLS, E. 2005. The specter of fuel-based lighting. *Science,* 308**,** 1263-1264.

MOECK, M., LEE, E. S., RUBIN, M. D., SULLIVAN, R. T. & SELKOWITZ, S. E. 1998. Visual quality assessment of electrochromic and conventional glazings. *Solar Energy Materials and Solar Cells,* 54**,** 157-164.

MOHAMMED, M. A. & BUDAIWI, I. M. 2013. Strategies for reducing energy consumption in a student cafeteria in a hot-humid climate: A case study. *Journal of Sustainable Development of Energy, Water and Environment Systems,* 1**,** 14-26.

MOHELNIKOVA, J. Chromogenic glazings. proceedings of the 9th international conference on modern building materials, structures and techniques, Vilnius, 2007.

MORENO, I. 2010. <Illumination uniformity assessment based on human vision.pdf>.

MOTAMEDI, S. & LIEDL, P. 2017. Integrative algorithm to optimize skylights considering fully impacts of daylight on energy. *Energy and Buildings,* 138**,** 655-665.

NABIL, A. & MARDALJEVIC, J. 2005. Useful daylight illuminance: a new paradigm for assessing daylight in buildings. *Lighting Research & Technology,* 37**,** 41-57.

NABIL, A. & MARDALJEVIC, J. 2006. Useful daylight illuminances: A replacement for daylight factors. *Energy and Buildings,* 38**,** 905-913.

NASA. 2011. *Catching Comet Dust With Aerogel* [Online]. Available: https://www.nasa.gov/topics/technology/features/aerogels.html [Accessed April 26 2017].

NAYAR, S., RAMAMOORTHI, R. & HANRAHAN, P. 2009. *Basic Principles of Surface Reflectance* [Online]. Available: https://www.cs.cmu.edu/afs/cs/academic/class/15462-f09/www/lec/lec8.pdf [Accessed 15 December 2019].

NIKOLOVA, K., PAVLOV, D. & NENOVA, M. Uncertainty Budget for Calibration of Luminance Meters for Measurement of Photopic Adaptation Luminance of Road Tunnels. 2018 Seventh Balkan Conference on Lighting (BalkanLight), 20-22 Sept. 2018 2018. 1-5.

NITZ, P. & HARTWIG, H. 2005. Solar control with thermotropic layers. *Solar Energy,* 79**,** 573-582.

OMIDFAR, A. 2011. A methodology for designing contemporary high performance shading screen-the integration of 'form'and the DIVA simulation tool. *12th Conference of International Building Performance Simulation Association.* Sydney, Australia.

OSTERHAUS, W. K. E. 2005. Discomfort glare assessment and prevention for daylight applications in office environments. *Solar Energy,* 79**,** 140-158.

PALMERO-MARRERO, A. I. & OLIVEIRA, A. C. 2010. Effect of louver shading devices on building energy requirements. *Applied Energy,* 87**,** 2040-2049.

PARK, H. K. & KIM, H. 2015. Acoustic insulation performance of improved airtight windows. *Construction and Building Materials,* 93**,** 542-550.

PARKIN, I. P., BINIONS, R., PICCIRILLO, C., BLACKMAN, C. S. & MANNING, T. D. 2008. Thermochromic Coatings for Intelligent Architectural Glazing. *Journal of Nano Research,* 2**,** 1-20.

PÉREZ-LOMBARD, L., ORTIZ, J. & POUT, C. 2008. A review on buildings energy consumption information. *Energy and Buildings,* 40**,** 394-398.

PETERMANN, N. 2008. The Efficient Windows Collaborative: Research Tool Dissemination to Increase Energy Efficient. Alliance to Save Energy

PICCOLO, A., PENNISI, A. & SIMONE, F. 2009. Daylighting performance of an electrochromic window in a small scale test-cell. *Solar Energy,* 83**,** 832-844.

PRASAD, D. K. & HALL, M. 2005. *The construction challenge: sustainability in developing countries*, RICS.

REIM, M., KÖRNER, W., MANARA, J., KORDER, S., ARDUINI-SCHUSTER, M., EBERT, H. P. & FRICKE, J. 2005. Silica aerogel granulate material for thermal insulation and daylighting. *Solar Energy,* 79**,** 131-139.

REINHART, C. 2014. *Daylighting handbook I : fundamentals : designing with the sun / Christoph Reinhart,* United States], United States : Christoph Reinhart.

REINHART, C. & FITZ, A. 2006. Findings from a survey on the current use of daylight simulations in building design. *Energy and Buildings,* 38**,** 824-835.

REINHART, C. F. 2010. Tutorial on the Use of Daysim Simulations for

Sustainable Design.

REINHART, C. F. & WALKENHORST, O. 2001. Validation of dynamic RADIANCE-based daylight simulations for a test office with external blinds. *Energy and Buildings,* 33**,** 683-697.

REZAEI, S. D., SHANNIGRAHI, S. & RAMAKRISHNA, S. 2017. A review of conventional, advanced, and smart glazing technologies and materials for improving indoor environment. *Solar Energy Materials and Solar Cells,* 159**,** 26-51.

RIEMERSMA, T. 2019. *Candela, Lumen, Lux: the equations* [Online]. Compuphase.com. Available: https://www.compuphase.com/electronics/candela_lumen.htm [Accessed 15 May 2019].

RINDORFF, H. J., BRÜEL & KJÆR 1978. Luminance Reflectance: Explanation and calculation of contrast. B&K Instruments, Inc.

ROBERTSON, K. 2003. *Daylighting guide for Buildings*, Canada Mortgage and Housing Corporation.

ROGERS, Z. 2006. Daylighting metric development using daylight autonomy calculations in the sensor placement optimization tool. *Boulder, Colorado, USA: Architectural Energy Corporation: http://www. archenergy. com/SPOT/SPOT_Daylight% 20Autonomy% 20Report. pdf*.

ROUDSARI, M. S. 2018. *Honeybee - Honeybee - Component for Grasshopper | Grasshopper Docs* [Online]. Available: https://grasshopperdocs.com/components/honeybee/honeybee.html [Accessed April 20 2019].

ROUDSARI, M. S. & PAK, M. 2013. <LADYBUG_A PARAMETRIC ENVIRONMENTAL PLUGIN FOR GRASSHOPPER TO HELP DESIGNERS CREATE AN ENVIRONMENTALLY-CONSCIOUS DESIGN.pdf>.

RS-PRO 2017. Instruction Manual: RS-137, 146-4653 Luminance Meter. *In:* PRO, R. (ed.).

RUCK, N., ASCHEHOUG, O., AYDINLI, S., CHRISTOFFERSEN, J., EDMONDS, I., JAKOBIAK, R., KISCHKOWEIT-LOPIN, M., KLINGER, M., LEE, E. & COURRET, G. 2000. Daylight in Buildings: A source book on daylighting systems and components. Berkeley (USA): International Energy Agency, Lawrence Berkeley National Laboratory.

SADINENI, S. B., MADALA, S. & BOEHM, R. F. 2011. Passive building energy savings: A review of building envelope components. *Renewable and Sustainable Energy Reviews,* 15**,** 3617-3631.

SBAR, N. L., PODBELSKI, L., YANG, H. M. & PEASE, B. 2012. Electrochromic dynamic windows for office buildings. *International Journal of Sustainable Built Environment,* 1**,** 125-139.

SCHILER, M. Examples of Glare Remediation Techniques. Passive and Low Energy Architecture Conference, Quebec City, Canada, 2009.

SEC, S. E. C. 2015. Electrical Data in Saudi Arabia from 2000 to 2014

SHARMA, A., TYAGI, V. V., CHEN, C. R. & BUDDHI, D. 2009. Review on thermal energy storage with phase change materials and applications. *Renewable & Sustainable Energy Reviews,* 13**,** 318-345.

SHERIF, A., EL-ZAFARANY, A. & ARAFA, R. 2012a. External perforated window Solar Screens: The effect of screen depth and perforation ratio on energy performance in extreme desert environments. *Energy and Buildings,* 52**,** 1-10.

SHERIF, A., SABRY, H. & RAKHA, T. 2012b. External perforated Solar Screens for daylighting in residential desert buildings: Identification of minimum perforation percentages. *Solar Energy,* 86**,** 1929-1940.

SHERIF, A., ZAFARANY, A. E. & ARAFA, R. 2014. Energy Efficient Shading Strategies for Windows of Hospital ICUs in the Desert. *World Academy of Science, Engineering and Technology*

International Journal of Civil, Environmental, Structural, Construction and Architectural Engineering, 8.

SHERIF, A. H., SABRY, H. M. & GADELHAK, M. I. 2012c. The impact of changing solar screen rotation angle and its opening aspect ratios on Daylight Availability in residential desert buildings. *Solar Energy,* 86**,** 3353-3363.

SHI, L. & CHEW, M. Y. L. 2012. A review on sustainable design of renewable energy systems. *Renewable and Sustainable Energy Reviews,* 16**,** 192-207.

SILVA, T., VICENTE, R. & RODRIGUES, F. 2016. Literature review on the use of phase change materials in glazing and shading solutions. *Renewable and Sustainable Energy Reviews,* 53**,** 515-535.

SISSON, B. & VAN AERSCHOT, C. 2007. Energy Efficiency in Buildings: Business Realities and Opportunities; Summary Report. *World Business Council Sustainable Development (WBCSD)*.

SOUZA, D. F., SCARAZZATO, P. S. & PEDRINI, H. 2016. Classifying skies from images: A multidimensional approach to detecting high dynamic range imaging attributes. *Lighting Research & Technology,* 48**,** 559-572.

SPYROPOULOS, G. N. & BALARAS, C. A. 2011. Energy consumption and the potential of energy savings in Hellenic office buildings used as bank branches—a case study. *Energy and Buildings,* 43**,** 770-778.

STERNER, C. 2017. *Measuring Daylight: Dynamic Daylighting Metrics & What They Mean for Designers* [Online]. Available: https://blog.sketchup.com/article/measuring-daylight-dynamic-daylighting-metrics-what-they-mean-designers#:~:text=Annual%20Sun%20Exposure%20(ASE)%20describes,250%20occupied%20hours%20per%20year.) [Accessed May 20 2017].

SUBRAMANIAM, S. 2018. *PARAMETRIC MODELING STRATEGIES FOR EFFICIENT ANNUAL ANALYSIS OF DAYLIGHT IN BUILDINGS.* Architectural Engineering.

SZOKOLAY, S. V. 2014. *Introduction to architectural science: the basis of sustainable design*, Routledge.

TOOLBOX, E. 2003. *Optical Distance Law* [Online]. Available: https://www.engineeringtoolbox.com/optical-distance-law-d_353.html [Accessed 20 March 2019].

TREGENZA, P. & MARDALJEVIC, J. 2018. Daylighting buildings: Standards and the needs of the designer. *Lighting Research & Technology,* 50**,** 63-79.

TYAGI, V. V. & BUDDHI, D. 2007. PCM thermal storage in buildings: A state of art. *Renewable & Sustainable Energy Reviews,* 11**,** 1146-1166.

UCL. 2019. *Our resources* [Online]. Available: https://www.ucl.ac.uk/bartlett/about-us/our-resources [Accessed 10 April 2019].

VÁZQUEZ-MOLINÍ, D., FERNÁNDEZ-BALBUENA, A. Á. & GARCÍA-FERNÁNDEZ, B. 2012. Natural lighting systems based on dielectric prismatic film. *Dielectric Material.* InTech.

VÁZQUEZ-MOLINÍ, D., GONZÁLEZ-MONTES, M., ÁLVAREZ FERNÁNDEZ-BALBUENA, A., GARCÍA-BOTELLA, Á., POHL, W., GALAN, T. & BERNABÉU, E. 2013. Horizontal daylighting system for office buildings. *Energy and Buildings,* 67**,** 525-530.

VERGAZ, R., SÁNCHEZ-PENA, J.-M., BARRIOS, D., VÁZQUEZ, C. & CONTRERAS-LALLANA, P. 2008. Modelling and electro-optical testing of suspended particle devices. *Solar Energy Materials and Solar Cells,* 92**,** 1483-1487.

WARD, G., MISTRICK, R., LEE, E. S., MCNEIL, A. & JONSSON, J. 2011. Simulating the Daylight Performance of Complex Fenestration Systems Using Bidirectional Scattering Distribution Functions within Radiance. *LEUKOS,* 7**,** 241-261.

WEINLADER, H., BECK, A. & FRICKE, J. 2005. PCM-facade-panel for daylighting and room heating. *Solar Energy,* 78**,** 177-186.

WIENOLD, J. *Daylight Glare analysis and metrics* [Online]. EPFL, Lausanne, Switzerland. [Accessed].

WITTWER, V., DATZ, M., ELL, I., GEORG, A., GRAF, W. & WALZE, G. 2004. Gasochromic windows. *Solar Energy Materials and Solar Cells,* 84**,** 305-314.

WONG, I. L. 2017. A review of daylighting design and implementation in buildings. *Renewable and Sustainable Energy Reviews,* 74**,** 959-968.

YAMAGUCHI, R. & TAKASU, T. 2015. Hybrid aligned nematic liquid crystal smart glass with asymmetrical daylight controls. *Journal of the Society for Information Display,* 23**,** 365-370.

YU, X. & SU, Y. 2015. A discussion of inner south projection angle for performance analysis of dielectric compound parabolic concentrator. *Solar Energy,* 113**,** 101-113.

YU, X., SU, Y., ZHENG, H. & RIFFAT, S. 2014. A study on use of miniature dielectric compound parabolic concentrator (dCPC) for daylighting control application. *Building and Environment,* 74**,** 75-85.

Appendices

Appendix 1: Energy Consumption in Saudi Arabia

Year / Details	2000	2001	2002	2003	2004	2005	2006	2007	2008	2009	2010	2011	2012	2013	2014	Growth Rate during period (%)	Average annual growth rate (%)
Residential	56,063	61,340	65,460	70,373	73,365	78,304	86,028	89,903	96,687	100,832	108,627	109,261	120,246	125,678	135,908	142.4	6.5
Commercial	9,969	11,147	11,112	14,315	14,301	15,580	17,074	19,440	21,367	23,605	29,310	33,007	39,809	39,500	42,855	329.9	11.0
Governmental	13,896	15,457	15,330	16,131	16,772	16,675	18,005	19,802	20,457	22,248	24,514	23,921	26,089	27,384	30,011	116.0	5.7
Industrial	27,657	28,232	29,319	33,383	31,975	33,801	32,549	30,634	32,421	34,654	38,569	42,129	41,711	51,080	51,499	86.2	4.5
Agricultural	2,265	2,380	2,640	2,666	2,920	3,164	3,380	3,168	3,461	5,062	3,620	3,786	4,191	4,290	4,577	102.1	5.2
Others * *	4,311	4,388	4,768	5,326	5,052	5,760	6,115	6,833	6,705	7,071	7,623	7,557	8,242	8,756	9,653	123.9	5.9
Total of Energy Sold	114,161	122,944	128,629	142,194	144,385	153,284	163,151	169,780	181,098	193,472	212,263	219,661	240,288	256,688	274,502	140.5	6.5

* Since 2014, Sold Energy doesn't contain transferred energy for companies subjected to weeling agreement.
** Others: include (streets lighting, mosques, hospitals and charities)

Sold Energy by Consumption Types (GWh), ESC 2014: Electrical data Saudi Arabia 2000-2014 (SEC, 2015)

Year / Details	2000	2001	2002	2003	2004	2005	2006	2007	2008	2009	2010	2011	2012	2013	2014	Growth Rate during period	Average annual growth rate (%)
Residential	2,991,161	3,122,282	3,340,417	3,511,431	3,700,161	3,897,916	4,083,830	4,262,494	4,456,755	4,675,554	4,892,271	5,023,038	5,335,563	5,672,965	5,933,614	98.4	5.0
Commercial	459,593	489,761	497,271	534,274	577,797	609,423	641,092	679,641	709,751	756,919	830,107	1,035,177	1,097,812	1,154,871	1,329,778	189.3	7.9
Governmental	79,227	81,363	85,744	88,231	91,188	95,563	100,358	103,196	110,874	118,506	118,942	117,970	123,747	131,333	141,687	78.8	4.2
Industrial	5,179	5,753	6,180	5,943	6,791	6,154	6,273	6,697	6,967	7,289	7,489	7,646	8,166	8,471	9,218	78.0	4.2
Agricultural	36,595	39,780	42,875	47,021	51,788	51,787	54,553	56,422	57,870	59,503	61,334	63,527	67,453	72,022	75,915	107.4	5.4
Others *	50,636	53,271	56,832	59,998	63,992	66,528	69,800	74,089	78,593	83,745	87,410	93,667	98,258	103,154	112,067	121.3	5.8
Total	3,622,391	3,792,210	4,029,319	4,246,898	4,491,717	4,727,371	4,955,906	5,182,539	5,420,810	5,701,516	5,997,553	6,341,025	6,730,999	7,142,816	7,602,279	109.9	5.4
Electrified Communities	7,610	8,295	9,249	9,864	10,160	10,385	10,713	10,953	11,405	11,782	11,990	12,256	12,450	12,644	12,772	67.8	3.8

* Others: include (streets lighting, mosques, hospitals and charities)

Number of Customers by Consumption Types, ESC 2014: Electrical data Saudi Arabia 2000-2014 (SEC, 2015).

Appendix 2: Standard parameters of the CIE skies

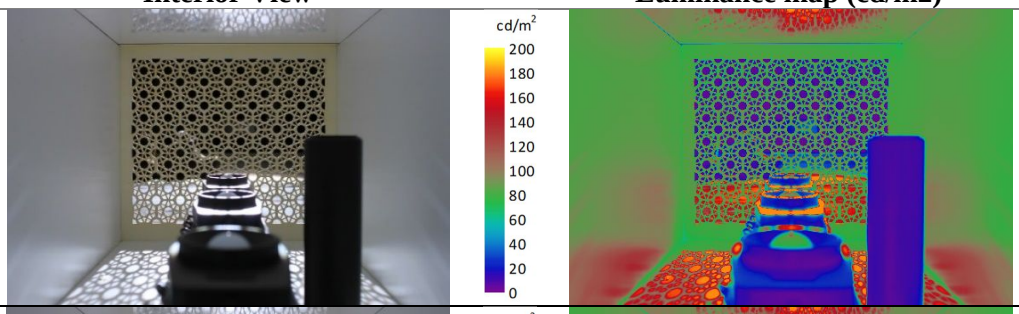
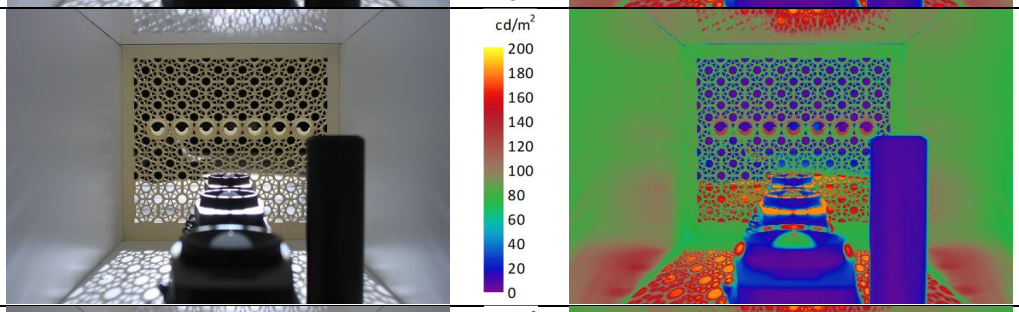
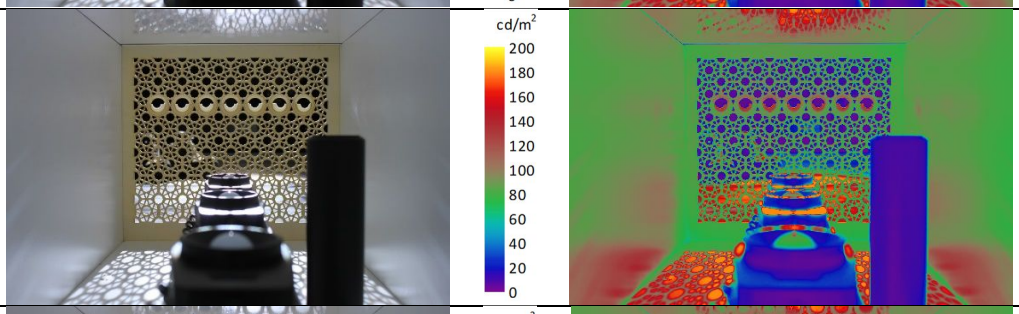
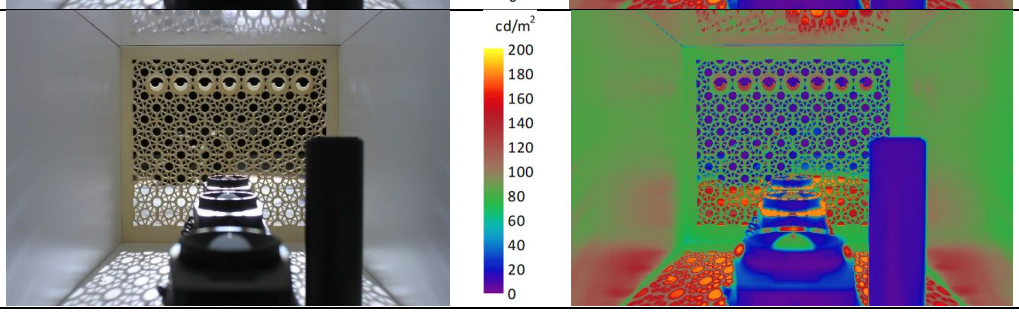
Standard parameters in BS ISO 15469:2004 (ISO, 2004).

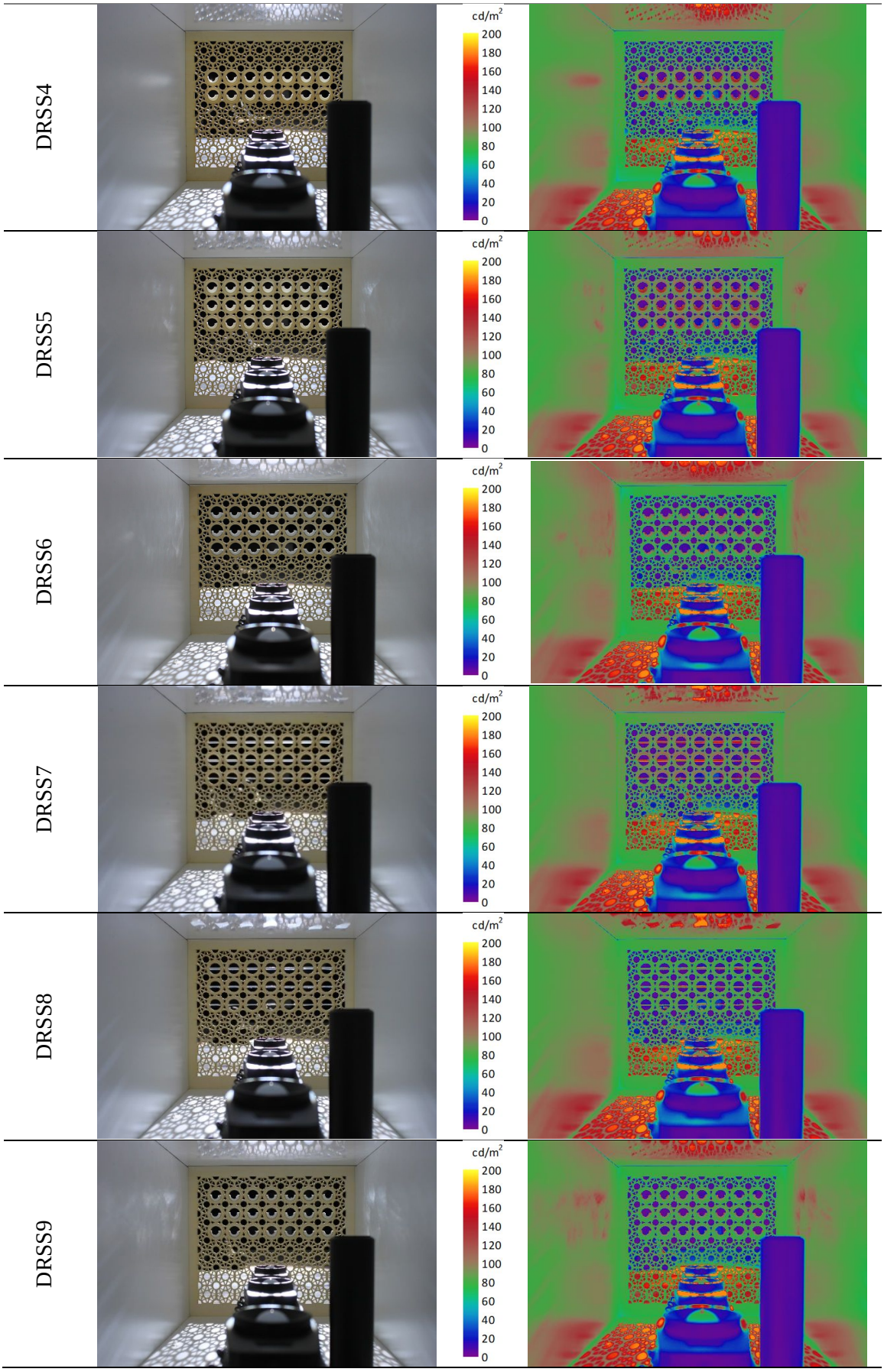
Type	*Grada-tion group*	*Indica-trix group*	*a*	*b*	*c*	*d*	*e*	*Description of luminance distribution*
1	I	1	4,0	-0,70	0	-1,0	0	**CIE Standard Overcast Sky,** Steep luminance gradation towards zenith, azimuthal uniformity
2	I	2	4,0	-0,70	2	-1,5	0,15	Overcast, with steep luminance gradation and slight brightening towards the sun
3	II	1	1,1	-0,8	0	-1,0	0	Overcast, moderately graded with azimuthal uniformity
4	II	2	1,1	-0,8	2	-1,5	0,15	Overcast, moderately graded and slight brightening towards the sun
5	III	1	0	-1,0	0	-1,0	0	**Sky of uniform luminance**
6	III	2	0	-1,0	2	-1,5	0,15	Partly cloudy sky, no gradation towards zenith, slight brightening towards the sun
7	III	3	0	-1,0	5	-2,5	0,30	Partly cloudy sky, no gradation towards zenith, brighter circumsolar region
8	III	4	0	-1,0	10	-3,0	0,45	Partly cloudy sky, no gradation towards zenith, distinct solar corona
9	IV	2	-1,0	-0,55	2	-1,5	0,15	Partly cloudy, with the obscured sun
10	IV	3	-1,0	-0,55	5	-2,5	0,30	Partly cloudy, with brighter circumsolar region
11	IV	4	-1,0	-0,55	10	-3,0	0,45	White-blue sky with distinct solar corona
12	V	4	-1,0	-0,32	10	-3,0	0,45	**CIE Standard Clear Sky, low luminance turbidity**
13	V	5	-1,0	-0,32	16	-3,0	0,30	**CIE Standard Clear Sky, polluted atmosphere**
14	VI	5	-1,0	-0,15	16	-3,0	0,30	Cloudless turbid sky with broad solar corona
15	VI	6	-1,0	-0,15	24	-2,8	0,15	White-blue turbid sky with broad solar corona

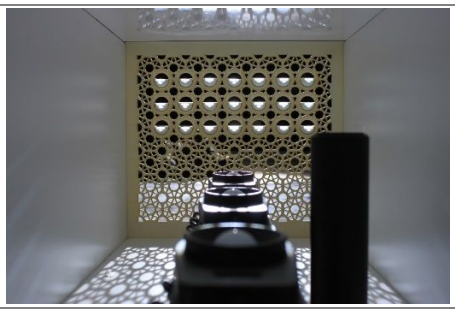
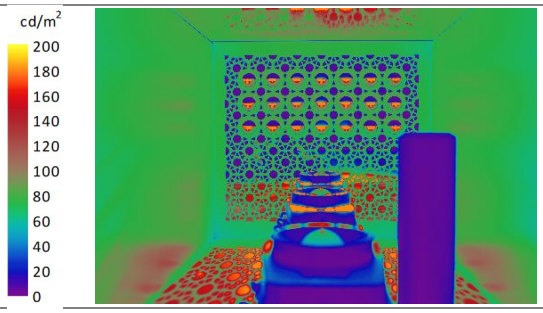
Appendix 3: Luminance Values

The luminance maps (cd/m^2) for the tested cases were obtained by HDR images. The photographs were converted to HDR images then the luminance maps were produced by Radiance software through the Ladybug Tools software. The luminance maps for Riyadh city on 21 June and for Nottingham city on 21 October are illustrated below.

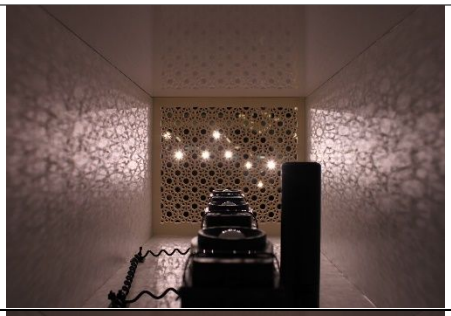
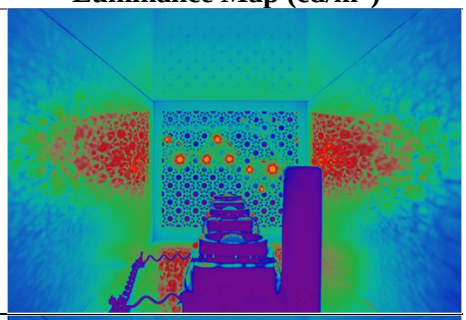
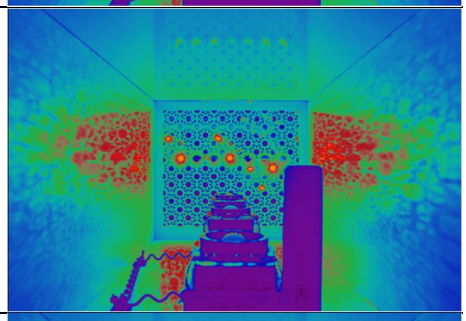
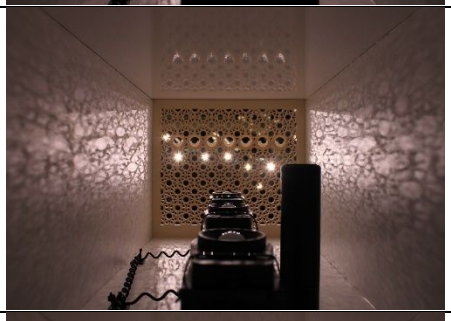
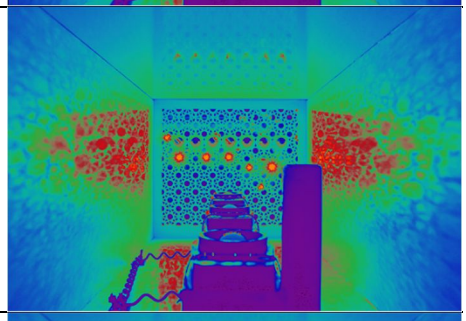
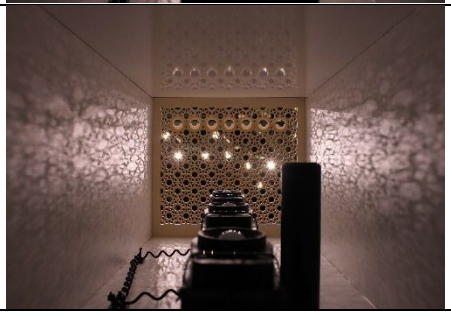
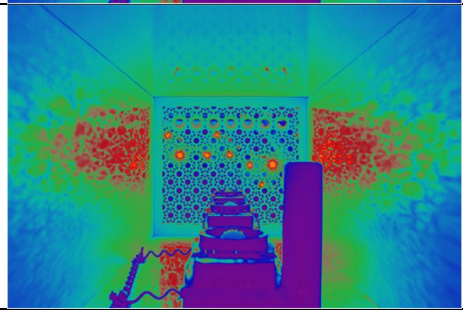
Interior view (left) and luminance map (right) under the DRLS for Nottingham on 21 October at 12 pm

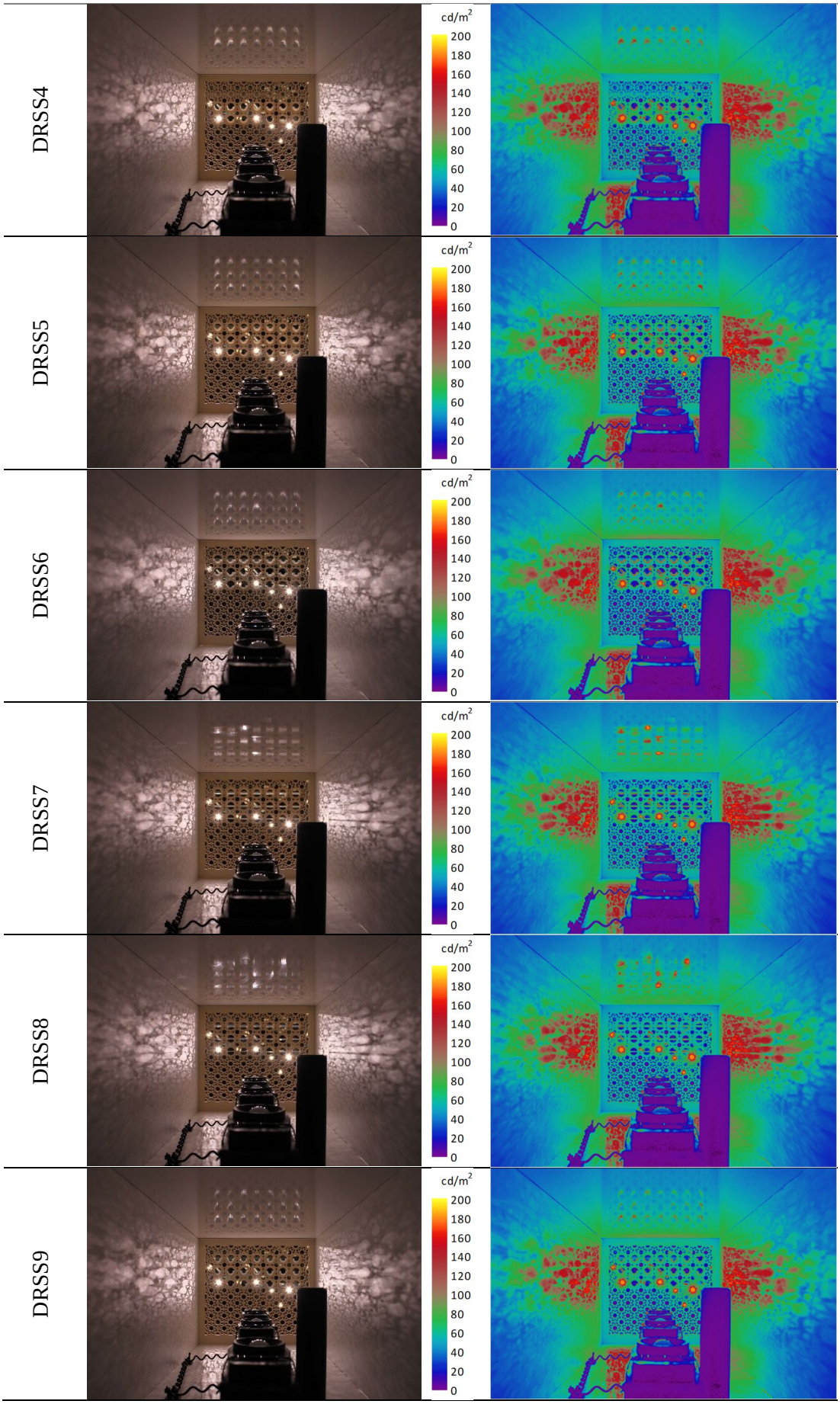
Case	Interior View	Luminance map (cd/m2)
PSS5		
DRSS1		
DRSS2		
DRSS3		

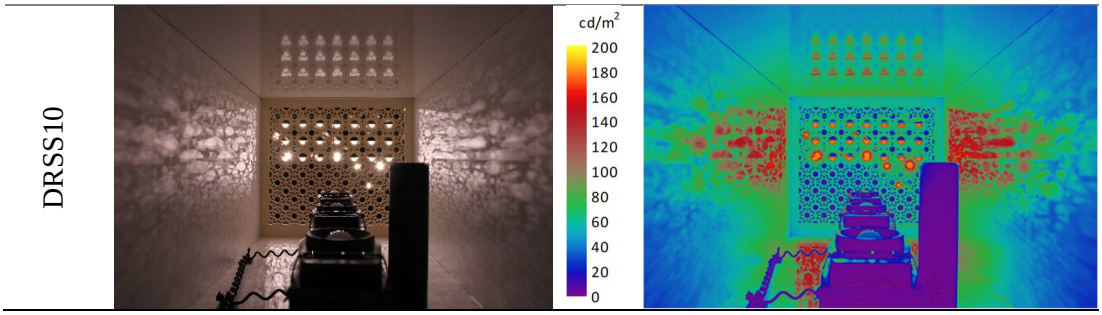

DRSS4
DRSS5
DRSS6
DRSS7
DRSS8
DRSS9
cd/m²
200
180
160
140
120
100
80
60
40
20
0

DRSS10			

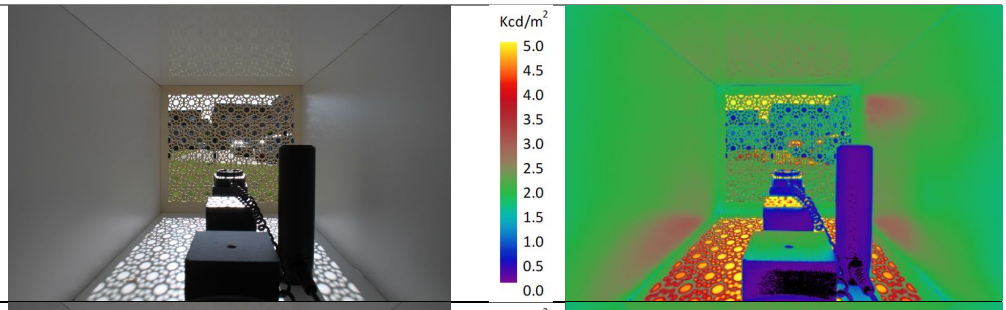
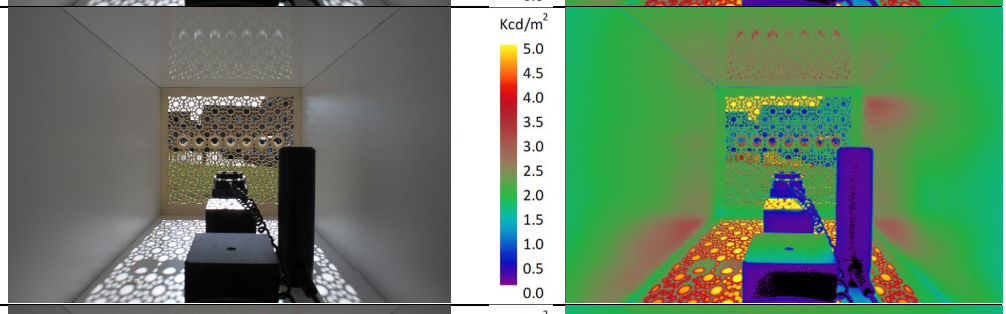
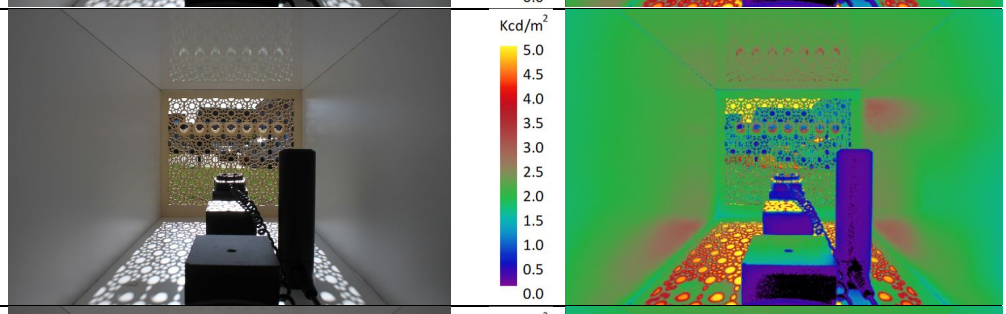
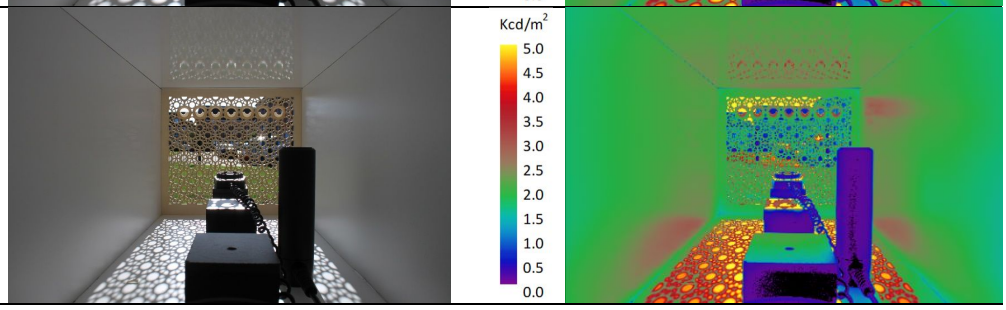
Interior view (left) and luminance levels (right) under the DFLS for Scenario-3

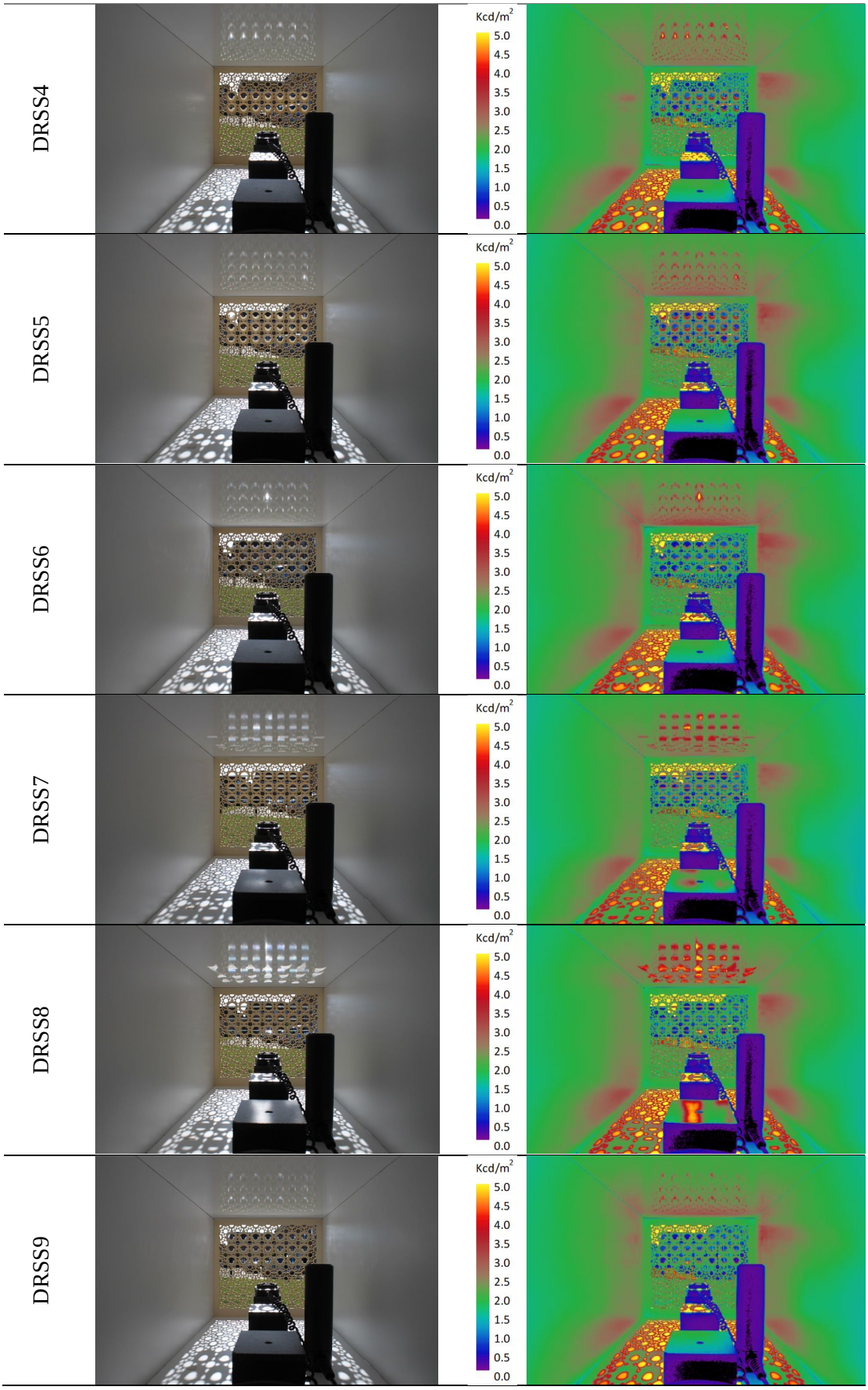
Case	Interior View	Luminance Map (cd/m^2)
PSS5		
DRSS1		
DRSS2		
DRSS3		


DRSS4
DRSS5
DRSS6
DRSS7
DRSS8
DRSS9
cd/m2
200
180
160
140
120
100
80
60
40
20
0



Interior [left] and exterior [right] of the model under the real sky conditions in Nottingham on 21 October at 12 pm, solar altitude is 26-degree, sun azimuth is 180 degree

Case	Interior View	Luminance Map (cd/m^2)
PSS5		
DRSS1		
DRSS2		
DRSS3		


DRSS4
DRSS5
DRSS6
DRSS7
DRSS8
DRSS9
Kcd/m²
5.0
4.5
4.0
3.5
3.0
2.5
2.0
1.5
1.0
0.5
0.0

DRSS10		